THE UNIVERSITY OF CHICAGO

HARNESSING AU(I) CATALYSIS IN THE PURSUIT OF ALKALOID AND TERPENE NATURAL PRODUCTS

A DISSERTATION SUBMITTED TO

THE FACULTY OF THE DIVISION OF THE PHYSICAL SCIENCES

IN CANDIDACY FOR THE DEGREE OF

DOCTOR OF PHILOSOPHY

DEPARTMENT OF CHEMISTRY

BY

PHILIPP MICHAEL GEMMEL

CHICAGO, ILLINOIS

DECEMBER 2022

Ganz nebenbei oder Das Derivat des Fortschritts

Indes sie forschten, röntgen, filmten, funkten,
entstand von selbst die köstlichste Erfindung:
der Umweg als die kürzeste Verbindung
zwischen zwei Punkten.

—Erich Kästner (1899-1974)

TABLE OF CONTENTS

LIST OF SCHEMES

LIST OF FIGURES

LIST OF TABLES

List of Abbreviations

1,2-DCE	1,2-dichloroethane
9-BBN	9-borabicyclo[3.3.1]nonane
Ac	acetyl
acac	acetylacetonate
AIBN	azobisisobutyronitrile
Ar	aryl
Ar_F	tetrakis[3,5-bis(trifluoromethyl)phenyl]
BDE	bond dissociation energy
BDSB	bromodiethylsulfonium bromopentachloroantimonate
BHT	butylated hydroxytoluene, 2,6-di-*tert*-butyl-4-methylphenol
BINOL	1,1'-bi-2-naphthol
Bn	benzyl
Boc	*tert*-butyloxycarbonyl
bpy	2,2'-bipyridyl
brsm	based on recovered starting material
Bu	butyl
Bz	benzoyl
cap	caprolactam
cod	1,5-cyclooctadiene
coll	2,4,6-collidine, 2,4,6-trimethylpyridine
CSA	camphorsulfonic acid
Cy	cyclohexyl

d.r.	diastereomeric ratio
DBU	1,8-diazabicyclo[5.4.0]undec-7-ene
DEAD	diethylazodicarboxylate
DIAD	diisopropylazodicarboxylate
DIBAL-H	diisobutylaluminum hydride
DIPT	diisopropyl tartrate
DMAPP	dimethylallylpyrophosphate
DMF	*N*,*N*-dimethyl formamide
DMP	Dess–Martin periodinane,
DMPU	*N*,*N'*-dimethylpropyleneurea
DMSO	dimethyl sulfoxide
DNs	2,4-dinitrobenzenesulfonyl
dpm	dipivaloylmethane, 2,2,6,6-tetramethylheptanedione
ee	enantiomeric excess
esp	α,α,α',α'-tetramethyl-1,3-benzenedipropionic acid
Et	ethyl
FPP	farnesylpyrophosphate
GGPP	geranylgeranylpyrophosphate
HAT	hydrogen atom transfer
HMDS	hexamethyldisilazane
HMPA	hexamethylphosphoramide
*i*amyl	isoamyl
IBX	2-iodoxybenzoic acid

imid.	imidazole
IPP	isopentenylpyrophosphate
IPr	1,3-bis(2,6-diisopropylphenyl)imidazol-2-ylidene
*i*Pr	isopropyl
KHMDS	potassium bis(trimethylsilyl)amide
LDA	lithium diisopropylamide
LiHMDS	lithium bis(trimethylsilyl)amide
LUMO	lowest unoccupied molecular orbital
*m*CPBA	*meta*-chloroperoxybenzoic acid
Me	methyl
Mes	mesityl, 2,4,6-trimethylphenyl
Ms	methanesulfonyl
MS	molecular sieves
NaHMDS	sodium bis(trimethylsilyl)amide
NBS	*N*-bromosuccinimide
NCS	*N*-chlorosuccinimide
NHPI	*N*-hydroxyphthalimide
NIS	*N*-iodosuccinimide
NMO	*N*-methylmorpholine *N*-oxide
NMR	nuclear magnetic resonance
nOe	nuclear Overhauser effect
Ns	*p*-nitrobenzenesulfonyl
Nu	nucleophile

o-Ns	*o*-nitrobenzenesulfonyl
PCC	pyridinium chlorochromate
PDC	pyridinium dichromate
PG	protecting group
Ph	phenyl
phen	1,10-phenanthroline
PMB	*para*-methoxybenzyl
PMP	*para*-methoxyphenyl
PPTS	pyridinium *p*-toluenesulfonate
Pr	propyl
p-Ts	*para*-toluenesulfonyl
py	pyridine
pyr.	pyridine
TBDPS	*tert*-butyldiphenylsilyl
TBS	*tert*-butyldimethylsilyl
*t*Bu	*tert*-butyl
TEMPO	(2,2,6,6-tetramethylpiperidin-1-yl)oxyl
TES	triethylsilyl
Tf	trifluoromethanesulfonyl
TFA	2,2,2-trifluoroacetic acid
THF	tetrahydrofuran
TIPS	triisopropylsilyl
TMS	trimethylsilyl

TPAP	tetrapropylammonium perruthenate
Tr	trityl, triphenylmethyl
Troc	2,2,2-trichloroethoxycarbonyl

ACKNOWLEDGMENTS

As I reflected on my five years as a graduate student at the University of Chicago, it occurred to me that beyond working towards the completion of this dissertation and becoming a better organic chemist, my time here was filled with a myriad of experiences, opportunities, and friendships that have shaped me into the scientist and person I am today. Below, I would like to take the time to thank the people who have been great mentors, co-workers, and friends and have contributed to this work.

First and foremost, I would like to thank my research advisor Prof. Scott Snyder for taking me into in research group and having served as a mentor in my time here. He gave me the freedom to explore my passions both in research and in teaching. Hands-off, yet maintaining high expectations, Prof. Snyder has taught me to think like a scientist and stepped to offer advice and direction in difficult moments. I am grateful for the unwavering support and generosity he has given me in my time at the University of Chicago and hope that many more generations of graduate students get to benefit from his teaching, his mentoring, and his vast knowledge of natural product total synthesis.

In addition to Prof. Snyder, I am also indebted to my dissertation committee members Prof. Guangbin Dong and Prof. Mark Levin. I have gotten to know Prof. Dong as an excellent lecturer in two of my graduate classes and have already appreciated his thoughtful questions and advice during my candidacy examination. Prof. Levin has been a great addition to the Department of Chemistry in my time at the University of Chicago and I would like to thank him for taking the time to offering advice and support for future opportunities as a teacher-scholar. I am also grateful for the thought-provoking and challenging questions all three of my dissertation committee members asked during my defense.

When I decided on which graduate school to join for my doctoral studies, my decision primarily focused on the research I would be able to conduct. As I will elaborate further down in this section, I was interested in pursuing natural product total synthesis from the start and found Prof. Snyder's research program to be perfectly suited. In graduate school it helpful to be passionate about the research one will be doing for a little more than half a decade, however, in my experience, it was more important work with people whose company I enjoyed.

I would like to thank my first research mentor in the Snyder lab, Dr. Lilia Fuentes Morales for her wisdom, for teaching me laboratory techniques, and especially for her friendship and infinite patience with me. In addition, working with Dr. Zhiyao Zhou on the harziane diterpene natural products (Chapter III) and getting to learn from his vast literature knowledge and way of thinking has been a privilege and I am grateful for his help in becoming a confident organic chemist. Sohee Kim, who joined the harziane diterpene project after Dr. Zhou graduated, has also made invaluable contributions to the project and it has been a great journey of sharing the successes and failures we have had while working towards these natural products.

For her friendship inside and outside of the lab, I would like to thank Dr. Tessa Lynch-Colameta. The many fun lunches, afternoon chats in lab, and evening shenanigans helped create a much-needed diversion from graduate school. Though the pandemic has disrupted so many aspects of our lives, I am grateful for my friendship with Dr. Cooper Taylor and Russell Kielawa that took the edge off of the shift work and social distancing. I cherish the memories of our social bubble that allowed me to unwind from tough weeks in lab and the general uncertainty of the times. Having become friends with Julia Noel in the past year, it is sad that we did not overlap more during our time at the University of Chicago. I am grateful for all the memories we have had in this short time, from fostering cats from PAWS to our regular instrument room chats.

I would also like to thank Dr. Jonathan Keim, Prof. Hyung Min Chi, Prof. Pengfei Hu, Dr. Yu-An Zhang, Dr. Vladislav Lisnyak, Cheng Peng, Bryan Reynolds, Justin Bossenbroek, Noel Cercizi, Prof. Ming Yang, Justin Ngai, Seth Freedman, and other Snyder lab members who have been a great part of my becoming a better scientist by providing insight, advice, and making the Snyder lab a great place to work.

Keeping the research in the Department of Chemistry running smoothly is no small feat. As such, I would like to thank Dr. Antoni Jurkiewicz and Dr. Josh Kurutz for their support in the NMR facilities, Dr. Alex Filatov, Dr. Andrew McNeece, Dr. Kate Jesse, and Sophie Anferov for their help with single-crystal X-ray diffraction, and Dr. Jin Qin for training in mass spectrometry. I am grateful for Mike Reedy and Laura Luburich for their tireless work in making sure the facilities are taken care of and in supporting departmental events. In addition, I would also like to thank Dr. Melinda Moore, Debrah Morgan, Laura Baker, and Trudy Beaubrun for their support during graduate school.

During my time at the University of Chicago, I have also had the privilege to work in a variety of teaching positions. I would like to thank Prof. Britni Ratliff for her having taught me so much about teaching, pedagogy, and mentorship when I worked with her in the Collaborative Learning program. The opportunities that I have had in this program have been transformative for me as a teacher-scholar. I would also like to thank Prof. Valerie Keller for her support in the Organic Chemistry teaching labs and her insight into how to improve student learning in the Collaborative Learning program. In addition, I am also incredibly thankful for Prof. Vera Dragisich, who has given me the opportunity to be involved in TA training and for being a voice of support and a sounding board in difficult situations. I would also like to thank my fellow DoGSIs of 2020/2021, Dr. Adam Antoszewski, Dr. Matthew Zajac, and Sarah Willson for the great time

we had throwing remote events for the department community during the pandemic and for being great friends after our tenure.

My time at the University of Chicago is not isolated within my path to defending the dissertation herein. As such, it is important to me to acknowledge friends, mentors, and family that have made this journey possible. I serendipitously found my passion for scientific research and Organic Chemistry at Grinnell College. I would like to thank Prof. Iris Levin for piquing my interest in scientific inquiry and forming hypotheses and Prof. Kathryn Jacobson for taking a chance on a first-year student to work in her laboratory for a year. Kathy's mentoring style, discussing research ideas in fungal biology and her unwavering support even in difficult times have been a major reason why I was able to pursue science as a career. I owe my passion for organic chemistry to Prof. Erick Leggans' Advanced Organic Chemistry. The focus on discussing natural product total syntheses has stuck with me ever since. I am also grateful to Jordan Compton who as a tutor infected me with her excitement about Organic Chemistry and teaching. In addition, I would like to thank my chemistry advisor, Prof. Elaine Marzluff, my political science advisor, Prof. Eliza Willis, Rachel Bly, Minna Mahlab, and the Rev. Deanna Shorb for their advice and help in my time at Grinnell. Thank you to Prof. Christopher Douglas, Dr. Constance Anderson, Dr. Steven Underwood, and Dr. Nicholas Serratore at the University of Minnesota for mentoring me during my summer REU.

Thank you to so many friends I made along the way, who have made this journey so much more enjoyable: Emily McClure, Amal Dadi, William Foster, Raul Reynoso, Briannah Wilson, Dr. Megan Treichel, Ian Windham, Elizabeth Eason, Tanvi Varadhachary, Anna and Alexander Andres.

In this last section, I would like to extend my gratitude to the people who are most important in my life. Thank you to my parents, Martin Gemmel and Ute Becker-Gemmel, for always supporting me in any and all of my endeavors, no matter how crazy they may seem. I am grateful that you have raised me to be the independent and compassionate person I have become. I also want to thank my sister Miriam Gemmel for being a source of happiness and pride to me, as well as an inspiration as she pursues a law degree in Germany.

Last and absolutely not the least, my gratitude goes to Dr. Charles Cole. It was a challenge to decide where to mention his contributions in my graduate career, as he has been a fixture in all aspects of my life. I met Charles on my first day at the University of Chicago and soon after worked with him on the total synthesis toward koumine (Chapter II). I am indebted to Charles, as he has also proofread and provided his suggestions to each chapter of this dissertation. Over the past years, I have learned so much about chemistry from him and am grateful for the many engaging discussions we have had on science. In addition to being a partner in lab, Charles also is a partner in life for almost five years. His wisdom, his wit, his compassion, and his support continue to enrich my life more than I could have imagined. I look forward to our future together, to many more of our long debates, to exploring new places, and to spending time with our cats.

ABSTRACT

A persistent challenge in the field of natural product total synthesis is the ability to rapidly establish complex carbon frameworks in mild and selective manner. Over the past decades, the development of Au^{I}-catalyzed alkyne cyclization reactions enabled organic chemists to forge such complex ring systems in the pursuit of the total synthesis of terpene and alkaloid natural products. In this dissertation, I will review several such reactions, their application to total synthesis, and the synthetic efforts toward the total synthesis of the indole alkaloid koumine, as well as the harziane diterpenoid natural product family.

In Chapter 1, I review the reactivity of Au^{I} species and provide an overview of the application of Au^{I}-catalyzed cyclization reactions. Three distinct reaction types will be discussed: (1) Au^{I}-catalyzed Conia-ene reactions between an activated carbonyl and a pendant alkyne, (2) Cyclization reactions of indoles onto alkynes activated by a Au^{I} catalyst, and (3) Au^{I}-catalyzed cycloisomerization reactions of 1,*n*-enynes to form several rings in one synthetic step.

Chapter 2 will focus on two synthetic efforts toward the total synthesis of koumine. Following a review of the biosynthetic pathway in the producing organism, *Gelsemium elegans* Benth., we will review previous total and formal syntheses of koumine and discuss the synthetic strategies taken therein. We first attempted to access the framework of koumine via an inverse electron-demand pyridone Diels–Alder reaction and then pivoted to a Au^{I}/Ag^{I}-mediated cyclization to obtain an intermediate spiroindolenine. Though we were unable to complete the total synthesis of koumine, we have gained insight into the reactivity of the complex frameworks of our synthetic intermediates.

Lastly, in Chapter 3, I will focus on our successful total synthesis of harziandione. First, we will review the biosynthesis of the harziane diterpene natural product family and prior synthetic approaches. Then, we will discuss the development of our synthetic strategy, involving a key Au^{I}-catalyzed cycloisomerization and a ring contraction event. We will discuss the progression of synthetic approaches taken, discuss undesired results, and summarize the ultimately successful route.

CHAPTER I:

APPLICATION OF Au^{I}-CATALYZED REACTIONS IN NATURAL PRODUCT SYNTHESIS

SECTION 1.1: INTRODUCTION

Over the past century, organic chemists have sought to synthesize plant and microbe secondary metabolites for a variety of reasons. The chief purpose of laboratory synthesis aids in affording sufficient quantities of such a metabolite, often scarcely produced by nature, so as to enable extensive biological testing or even commercialization as in the pacific yew bark-derived natural product taxol (**1**). Additionally, laboratory synthesis allows chemists to strategically deploy their ever-expanding arsenal of organic reactions to expand scope and utility to complex molecular frameworks. Such efforts have led to some of the most elegant and concise synthetic approaches and further illuminate our understanding of the scope of organic transformations.

While organic chemists have had the knowledge and tools to pursue total synthesis over little more than a century, nature has had several billion years of evolutionary experience in synthesizing complex molecules. Simple amino acids, such as glycine are hypothesized to have formed in the primordial soup and have slowly led to the assembly of living organism that evolved to produce ever more complex metabolites.[1] The intricately assembled biosynthetic machinery of microbes, plants, and animals produces a vast array of small molecules to communicate with, attract, or deter other organisms, with some of these compounds either leading to or serving as inspiration for antibiotics, anti-tumor agents, or over the counter non-steroidal anti-inflammatory drugs (NSAIDs). Representative structures include linear and cyclic oligopeptides (**2** and **3**), polyketides (**4** and **5**), terpenes (**1** and **6**), and alkaloids (**7** and **8**), all of which have unique features and activities (Figure 1.1).

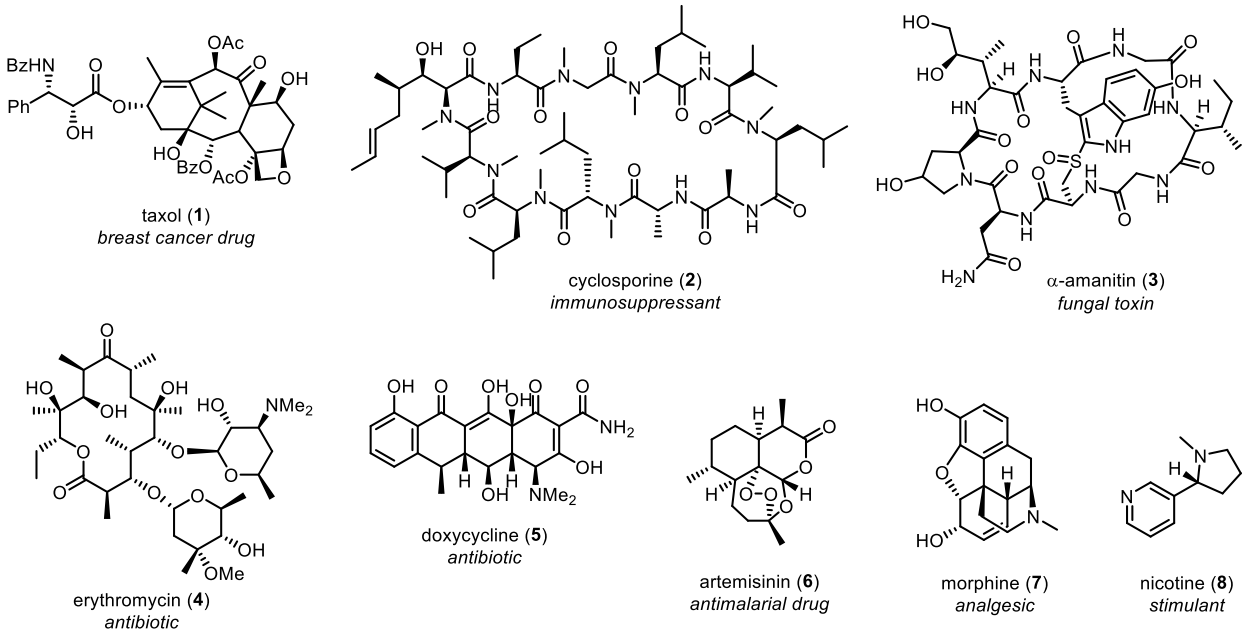

Figure 1.1. Examples of the diverse groups of natural products and their bioactivity

The creativity that natural products inspire in synthetic chemists has not dissipated despite the realization that if given enough time and resources, any molecule can be created in the laboratory.[2] In fact, organic chemists have continued to develop new ways of envisioning bond disconnections as new methods become available to shorten synthetic routes or to develop greener syntheses. One aspect of natural products that has continued to excite organic chemists is their diverse structural complexity. In particular, the highly congested, sometimes even cage-shaped frameworks of alkaloids and terpenes have spurned the most innovative and daring synthetic strategies, leading to a whole range of classic total syntheses.[3,4]

Within the wide range of approaches developed over the past years, Au^{I}-catalyzed cyclization reactions have been central to the Snyder groups' efforts to accelerate the generation of molecular complexity. Au^{I}-catalysis has enabled formation of a diversity of ring sizes and ring systems, as well as shown the ability to tame otherwise highly unstable and strained intermediates.[5–7] The versatile reactivity patterns and relatively mild conditions employed in these

reactions make them particularly attractive for the sometimes sterically congested or densely functionalized scaffolds found in natural products. In this opening chapter, I will review the reactivity of Au^I species and provide a survey of natural product syntheses aided by Au^I-catalyzed cyclization reactions.[8–12]

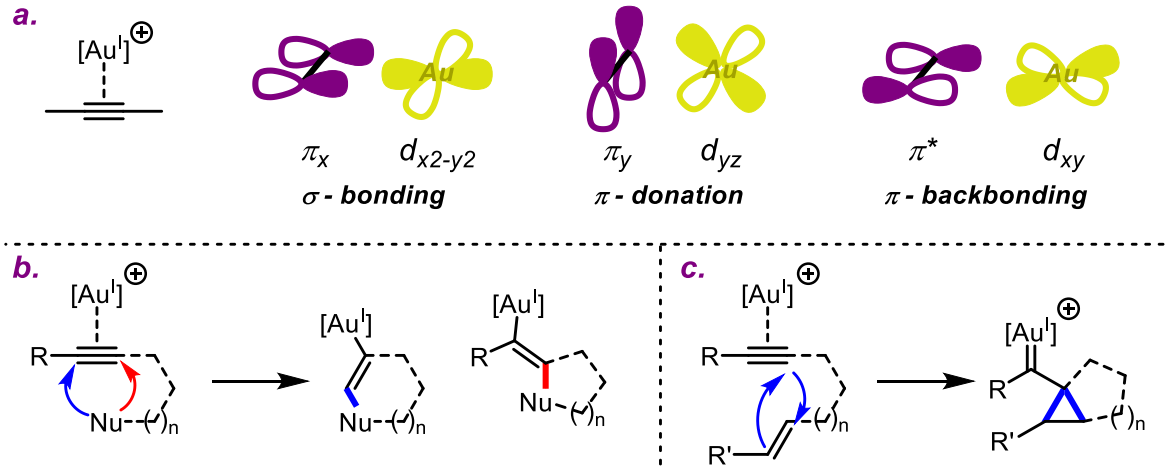

Scheme 1.1. a. Modes of metal-alkyne bonding relevant to Au^I-catalyzed reactions, b. Nucleophilic additons of nucleophiles to alkynes activated by Au^I, c. Reactions between alkenes and alkynes activated by Au^I, leading to cyclopropanation and formation of Au^I-carbene.

As illustrated in Scheme 1.1, cationic Au^I species can not only serve as powerful π-acids, activating alkynes through σ-bonding, π-backbonding, and π-donation, but also stabilize cationic intermediates.[13,14] Alkenes are similarly activated to nucleophilic addition reactions, but this has not unlocked the same degree of synthetic utility as the activation of alkynes has. One major factor that has been discussed as the origin of the reactivity of Au^I species is the contraction of the *6s* orbital, when taking into account relativistic effects.[15] This has been postulated to lower the LUMO at the metal center, increasing the Lewis acidity. Coupled with the relatively low charge density on the large gold atom, Au^I species are soft Lewis acids, thus preferentially activating soft electrophiles such as olefins and alkynes. The metal-alkyne orbital interactions allow alkynes to readily serve as electrophiles for nitrogen, oxygen, or carbon nucleophiles, both inter- and

intramolecularly.[16,17] In the case of heteroatom nucleophiles, intramolecular cyclizations have allowed for the facile formation of heterocycles in various natural products, such the cyclic ether within cephalosporolide H (**11**), or the nitrogen-containing heterocycle found in quinocarcin (**14**, Scheme 1.2).[18,19]

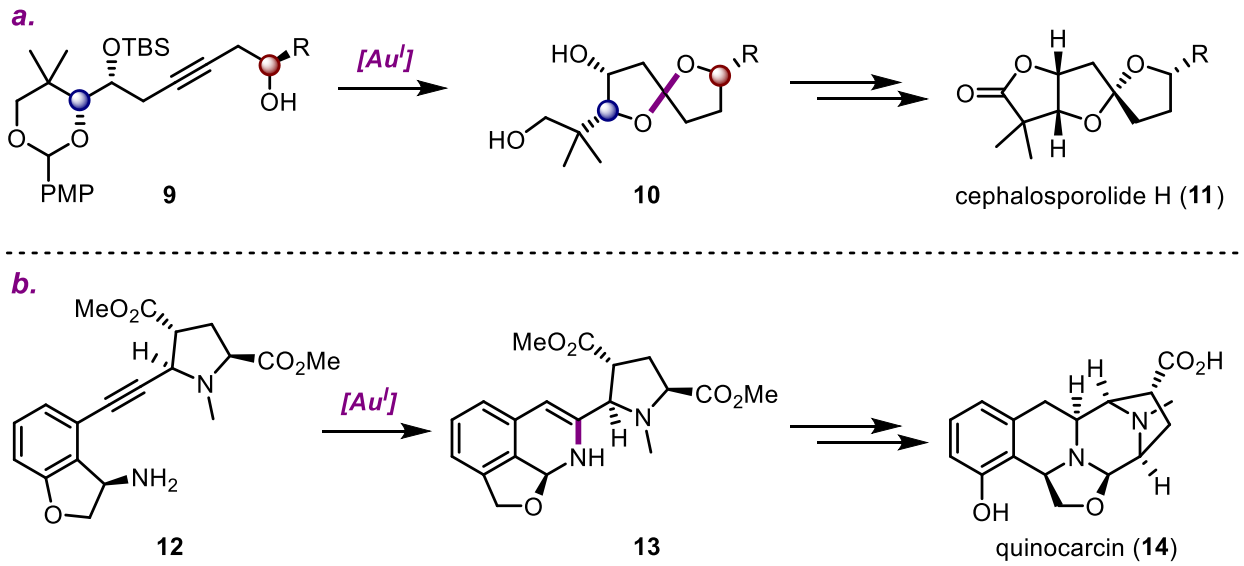

Scheme 1.2. a. Dudley's total synthesis of cephalosporolide H (**11**), b. Fujii and Ohno's total synthesis of quinocarcin (**14**)

Carbon nucleophiles, often less reactive than their heteroatom counterparts, present an intriguing opportunity for addition into alkynes, as they allow the often challenging formation of one or more fused or bridged carbocycles in one synthetic operation.[13,20,21] Given this powerful reactivity as well as the scope of the work presented herein, this chapter will focus on the application of Au^{I}-catalyzed cyclization reactions with carbon nucleophiles in natural product total synthesis. The discussion will be divided into three distinct parts: a. Au^{I}-catalyzed Conia-ene cyclization reactions, b. Au^{I}-catalyzed formation of bridged indole bicycles, and c. Au^{I}-catalyzed cycloisomerization cascades of tethered enynes (Scheme 1.3).

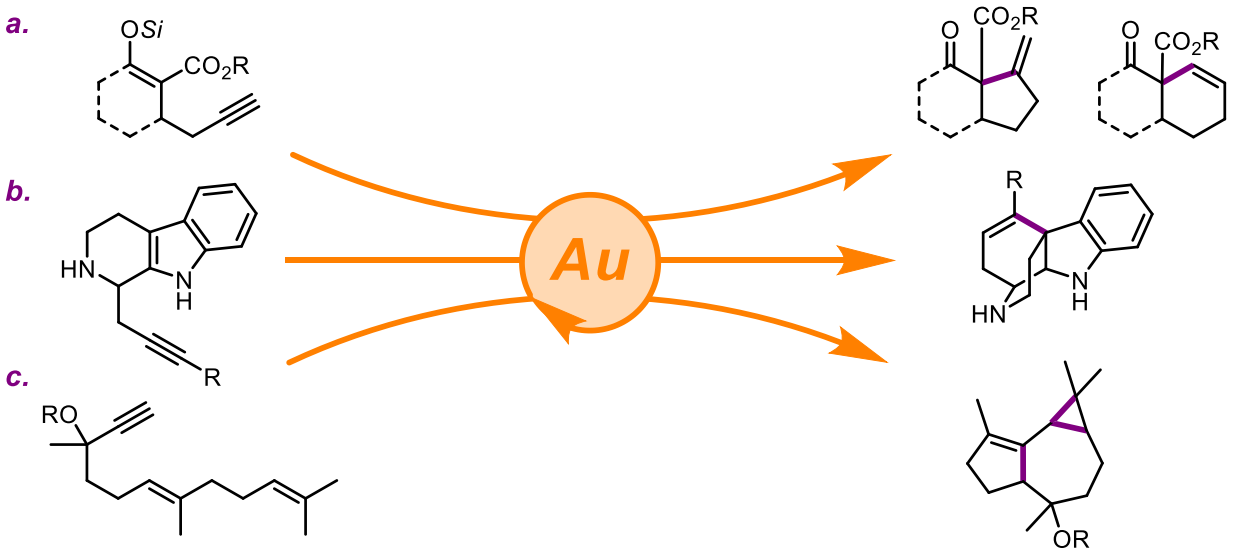

Scheme 1.3. Summary of the types of Au^{I}-catalyzed reactions in natural product total synthesis covered in this chapter.

SECTION 1.2.1: AU^{I}-CATALYZED CONIA-ENE REACTIONS IN NATURAL PRODUCT TOTAL SYNTHESIS

Traditionally, the Conia-ene cyclization reaction is an intramolecular variation of the carbonyl-ene reaction, first reported by Jean-Marie Conia.[22] The general reaction proceeds via a six-membered transition state, where the enol within **16** attacks the pendant olefin or alkyne, which in turn abstracts a proton from the enol (Scheme 1.4). While this reaction is a powerful method to establish functionalized carbocycles, traditional conditions and substrates require exceedingly forcing conditions, with temperatures above 300 °C being necessary to form the desired product.

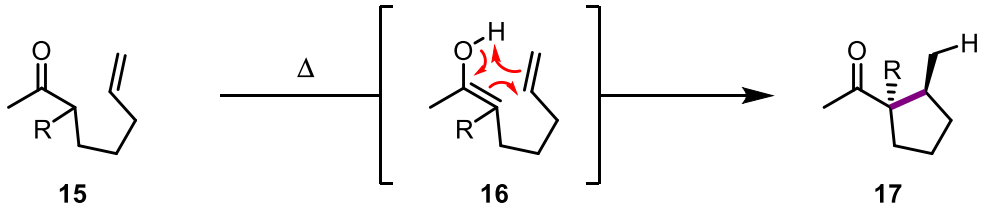

Scheme 1.4. Classic Conia-ene reaction reported by Conia, requiring high reaction temperatures.

This limits the broader applicability of the reaction in organic synthesis, as many functional groups and advanced frameworks are sensitive to such harsh conditions. In the past decades, a

number of approaches have been developed to allow for milder reaction conditions, including the *in situ* formation of enolates or their analogues, and activation of the olefin or alkyne with electron-poor transition metals or Lewis acids. One such approach that has found wide application in natural product total synthesis is the use of catalytic amounts of π-acidic Au^I species, which activate the alkyne and allow for reactions to proceed often at ambient temperature, even with catalyst loadings as low 1 mol%.[23]

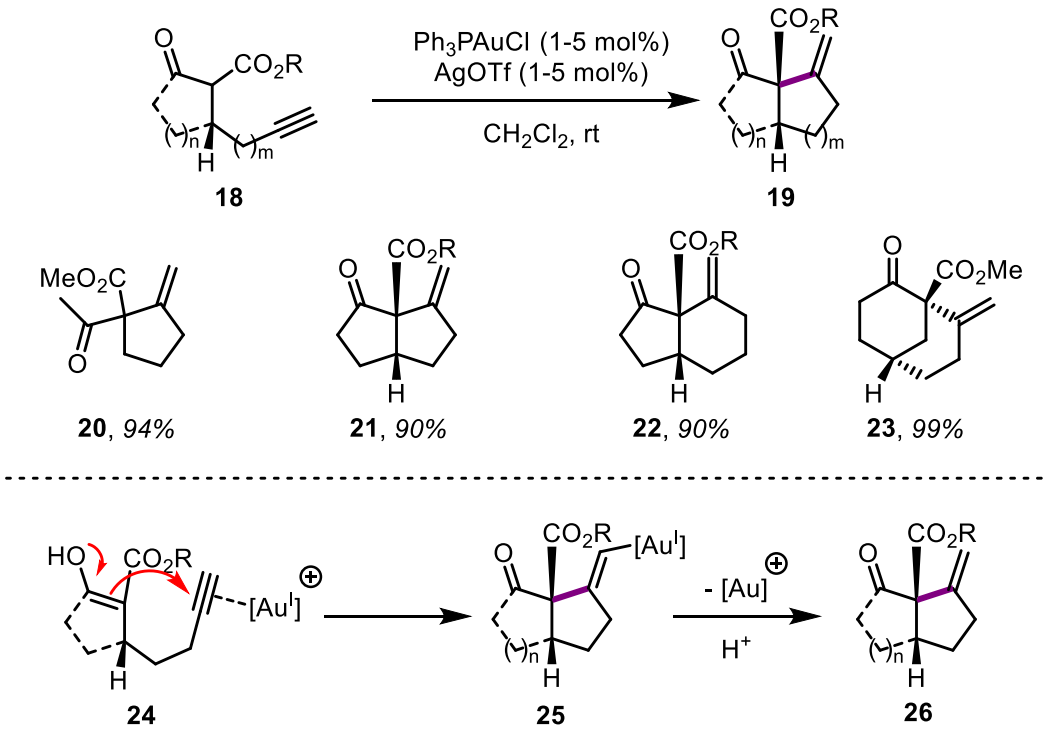

Scheme 1.5. Toste's report of the Au^I-catalyzed Conia-ene reaction of β-ketoesters.

The Toste group, who pioneered this approach with unactivated tethered alkynes and β-ketoesters (Scheme 1.5), has applied this method to the total synthesis of a variety of natural products. The total synthesis of fawcettimine (**29**) is an early example of an extension of this method, as it features a key Au^I-catalyzed Conia-ene cyclization reaction between a silyl enol ether and an alkynyl iodide (**27**, Scheme 1.6).[24] Conjugate addition of allenyl stannane **31** to enone **30** is followed by *in situ* trapping of the tin enolate with TBSCl. Subsequent iodination of the alkyne

proceeds via the silver acetylide, delivering the Conia-ene precursor **27**. Treatment with catalytic Ph_3PAuCl and $AgBF_4$ at 40 °C efficiently formed the *cis*-hydrindane within vinyl iodide **28**.

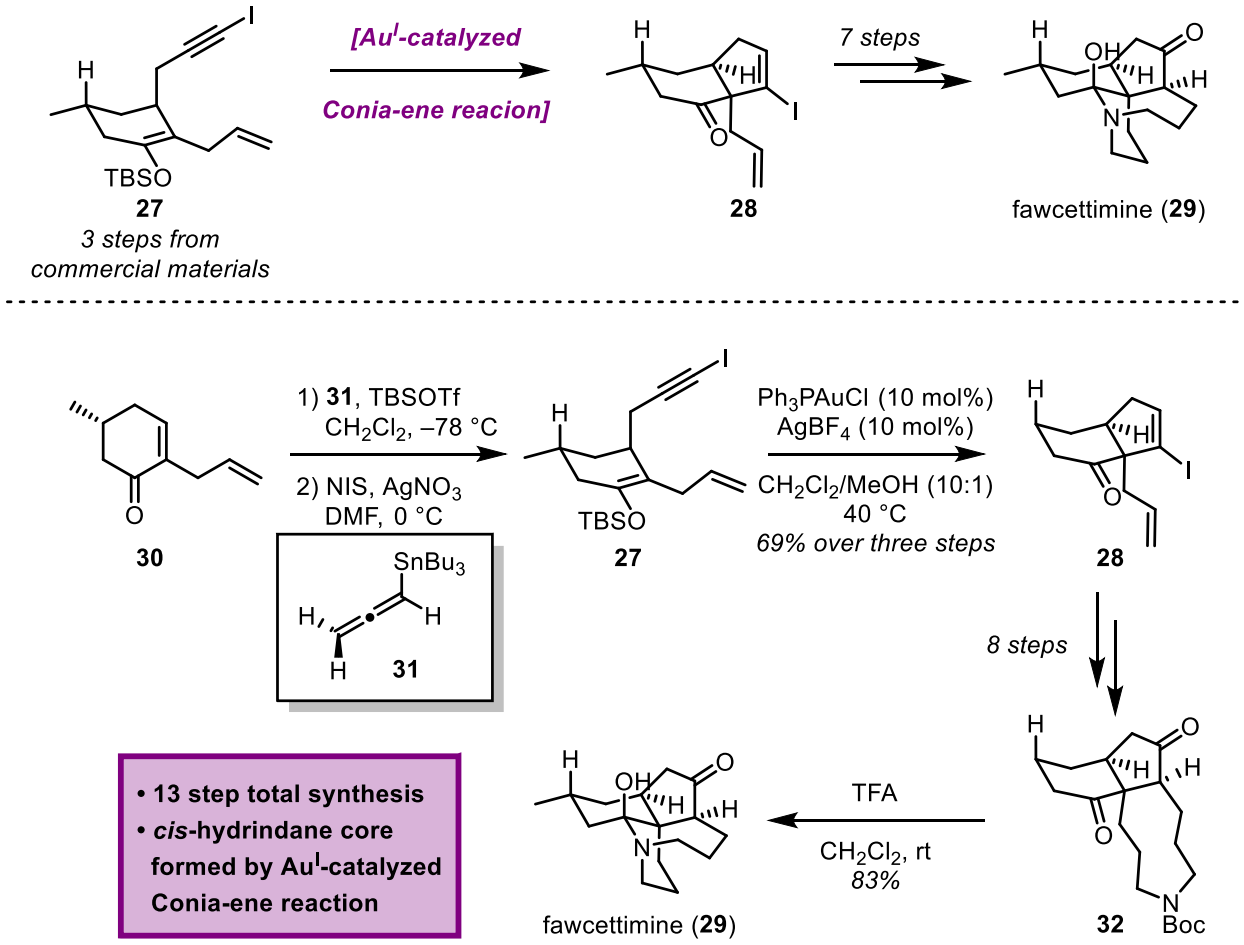

Scheme 1.6. Toste's total synthesis of the alkaloid fawcettimine (**29**)

This vinyl iodide serves a functional handle for introduction of an amine side chain needed to complete the natural product. Following an 8-step sequence that led to the formation of the 9-membered *N*-Boc protected secondary amine **32**, the total synthesis of fawcettimine (**29**) is completed by a TFA-mediated Boc deprotection and hemiaminal formation. This 13-step synthesis is an early, yet powerful example of strategically utilizing the Au^I-catalyzed Conia-ene reaction in

natural product total synthesis, as it rapidly introduces a key feature of the carbocyclic core under mild reaction conditions.

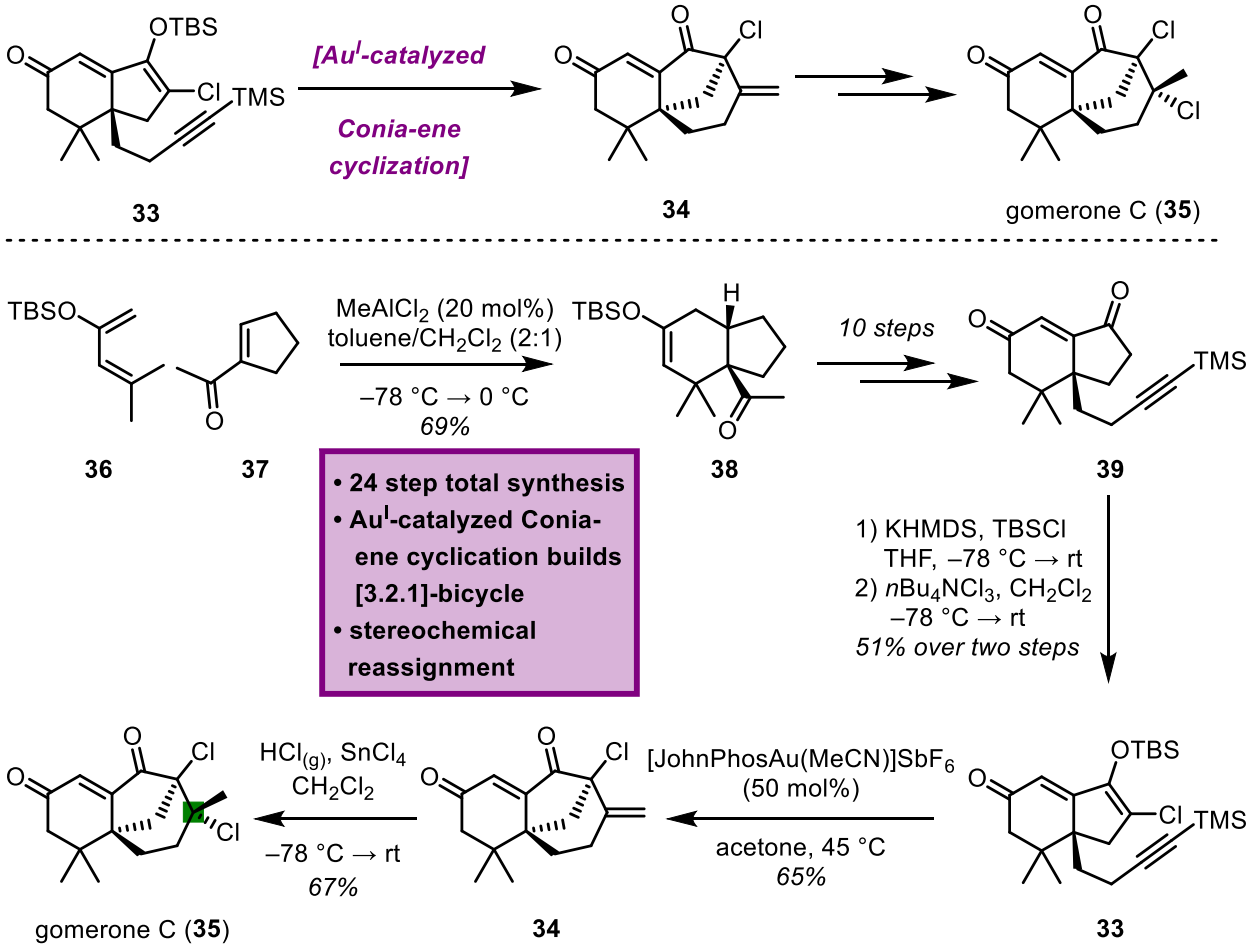

Scheme 1.7. Carreira's total synthesis of gomerone C (**35**)

Such Au-promoted Conia-ene reactions have continued to find their way into the total syntheses of various natural product types and frameworks. An intriguing example is the total synthesis of the chlorinated natural product gomerone C (**35**) by Carreira and co-workers (Scheme 1.7).[25] In particular, the late-stage formation of the sterically encumbered [3.2.1]-bicycle highlights the synthetic utility of the Conia-ene cyclization. An initial Diels–Alder reaction of the activated pentadiene **36** with acetylcyclopentene (**37**) establishes the congested hydrindane within **38**, which

features two vicinal all-carbon quaternary centers. Oxidative manipulations and introduction of the pendant alkyne via the methyl ketone delivers dienone **39**.

Silyl enol ether formation and electrophilic α-chlorination utilizing Mioskowski's reagent[26] are followed by treatment with [JohnPhosAu(MeCN)]SbF_6 to furnish the [3.2.1]-bicyclic dienone **34**. Of note, 50 mol% of the Au^I catalyst was required to achieve full conversion of the halogenated silyl enol ether **33**. Despite this minor issue, Carreira *et al.* argue that such a transformation had not previously been known producing bridgehead halides such as that found within **33**. Subsequent chlorination of 1,1-disubstituted olefin delivered gomerone C (**35**) in 24 steps, with the stereochemistry of the newly formed tertiary chloride apparently misassigned by the isolation team.

While the Carreira synthesis of gomerone C (**35**) features a late-stage Conia-ene cyclization, the Li synthesis of the complex *Daphniphyllum* alkaloid daphenylline (**42**) builds the four remaining rings of the natural product around the initial Conia-ene product **41** (Scheme 1.8).[27] This work once again underscores the concise fashion by which an otherwise challenging bicyclic system can be established via a Conia-ene cyclization, giving an explanation for the overall popularity of the strategy. In fact, the Au-promoted cyclizations of propargylic amines like **40** to prepare such bridged systems has featured prominently in the synthesis of a number of alkaloid natural products from a variety of groups. Starting from the enantiomerically enriched enone **43**, a Mitsunobu inversion with *N*-(2-butynyl)sulfonamide **44** yields the Conia-ene cyclization precursor. Following the formation of a silyl enol ether, treatment with Ph_3PAuCl (20 mol%) and AgOTf (30 mol%) effects the cyclization onto the amine-tethered alkyne at ambient temperature to furnish the desired [3.3.1]-azabicycle **41**.

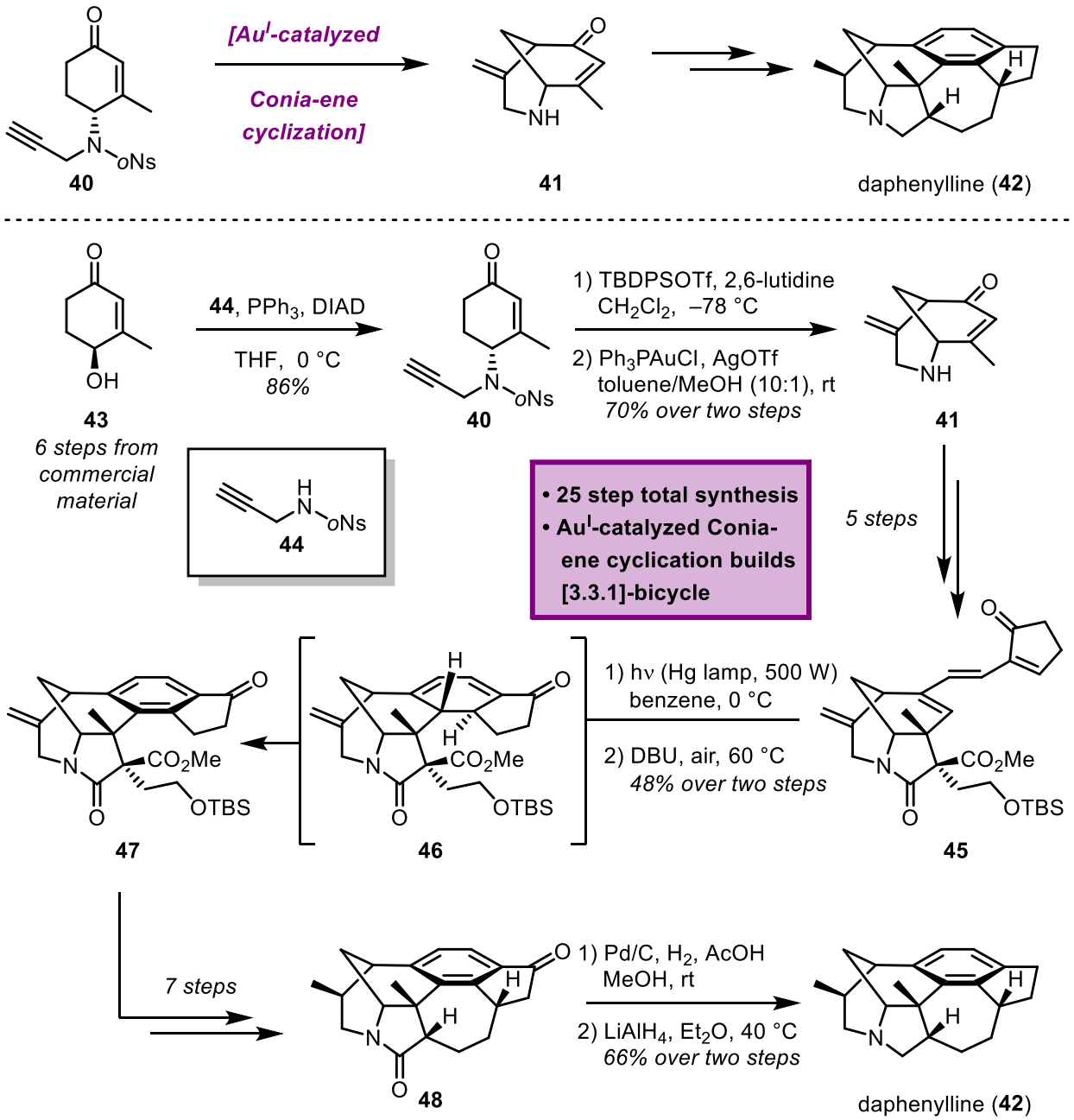

Scheme 1.8. Li's total synthesis of daphenylline (**42**)

Subsequent formation of γ-lactam and installation of the triene within **45** sets the stage for the 6π-electrocyclization to install the arene found in the natural product. With pentacycle **47** in hand, Li and co-workers complete the total synthesis of daphenylline (**42**) in nine further steps. This constitutes the first total synthesis of **42** in a total of 25 steps, an effort significantly

accelerated by the initial formation of the bicyclic enone **41** via a Au^{I}-catalyzed Conia-ene reaction. Bicylic enone **41** was similarly utilized as a starting point by Garg and co-workers in their total synthesis of the methanoquinolidine-containing indole alkaloid strictamine (**XX**).[28]

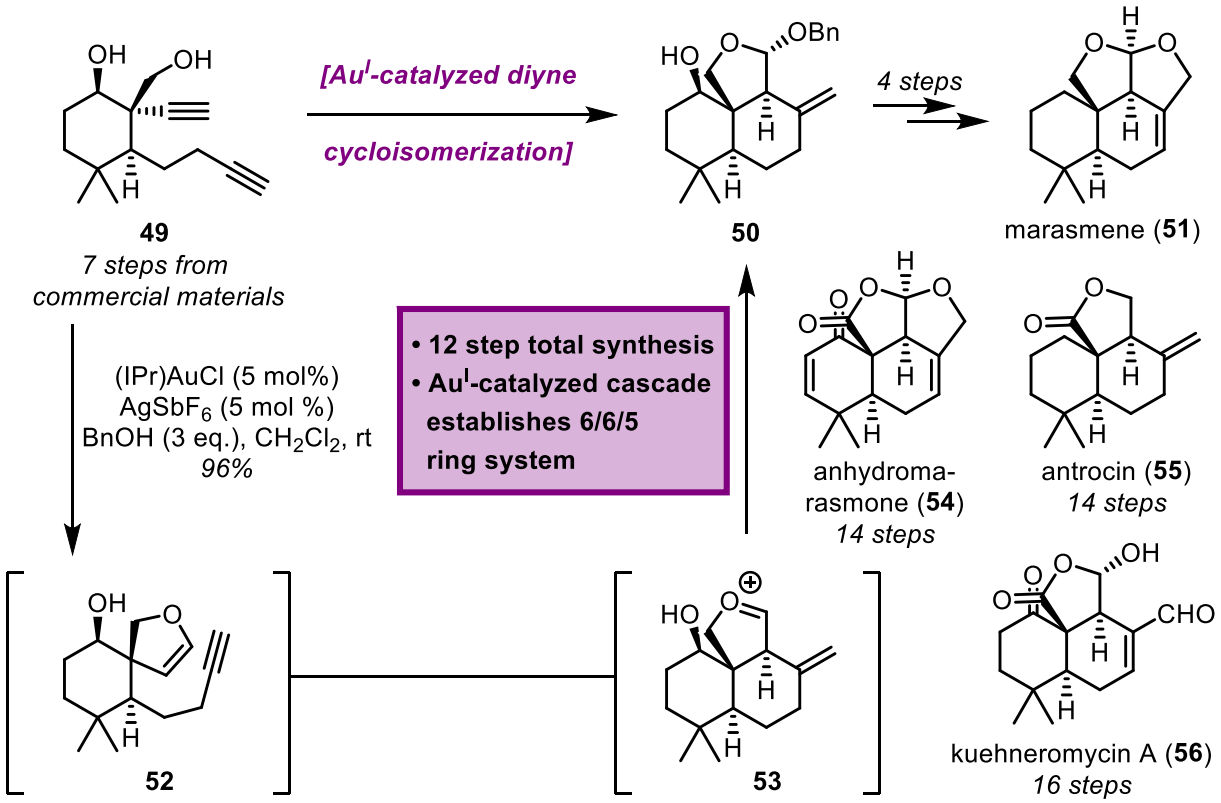

Scheme 1.9. Yang's total synthesis of marasmene (**51**) and related natural products.

While not a classical Conia-ene cyclization, the next example does feature a close analogue to the strategy discussed in this section. In their total synthesis of the drimane-type sesquiterpenoids marasmene (**51**), anhydromarasmone (**54**), antrocin (**55**), and kuehneromycin A (**56**), Yang and co-workers apply a Au^{I}-catalyzed cascade to furnish the common tricyclic core of the closely related natural products (Scheme 1.9).[29] Treating the precursor diyne (**49**) with (IPr)AuCl and $AgSbF_6$ triggers an initial nucleophilic attack of the primary alcohol on the Au^{I}-activated akyne, followed by a nucleophilic attack of the cyclic enol ether **52** at the distal alkyne. This strategy delivers the core of these four natural products in short order.

The Conia-ene reaction has also featured prominently in several recent total syntheses by the Snyder group. The first total synthesis of the highly complex polyphenolic chalcitrin (**59**), isolated from the fungus *Calciporus piperatus*, featured an approach orthogonal to the putative biosynthetic origin (Scheme 1.10).[30] Instead of the proposed dimerization of a polyphenolic precursor, the Snyder group employed a Conia-ene reaction strategy that established the nested 5/6/6 tricyclic core with suitable functional group handles that would allow later installation of the polyphenolic side chains. Concise decoration of commercially available cyclopentenone delivered the Conia-ene reaction precursor, silyl enol ether **57**, in four steps.

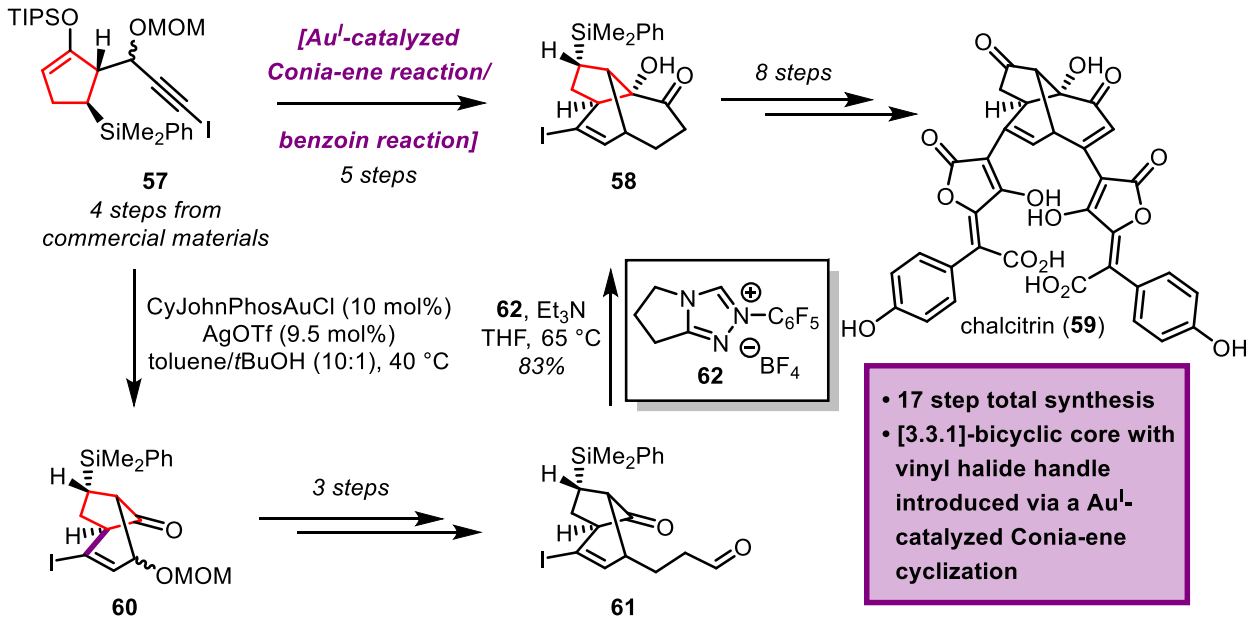

Scheme 1.10. Snyder's total synthesis of chalcitrin (**59**)

A Au^{I}-catalyzed Conia-ene cyclization formed the initial [3.2.1]-bicyclic vinyl iodide **60** followed by a three-step, three-carbon homologation at the protected alcohol to yield aldehyde **61**. This set the stage for completion of the tricyclic core of chalcitrin (**59**) via a triazolium-catalyzed benzoin condensation. With tricyclic ketone **58** in hand, the Snyder group proceeded to install a

second vinyl halide handle to enable the coupling of the polyphenolic side chains *en route* to the completion of the total synthesis of **59** in 17 steps.

It is worth noting that most of the entries relied on Au^{I}-catalysis, though where cyclization proved impossible, alternative alkyne-activating metal salts were employed. One such example is the formation of the decorated decalin core of the scaparvins (Scheme 1.11).[31] An In^{III}-mediated Conia-ene cyclization of the β-ketoester within **63** onto the terminal alkyne efficiently delivered the fused bicycle **64**, setting the stage for the formation of the highly congested natural product scaparvin B (**65**, 24 steps total) and two of its close congeners. Here, $InCl_3$ activates the alkyne for nucleophilic attack owing to its Lewis acidity.

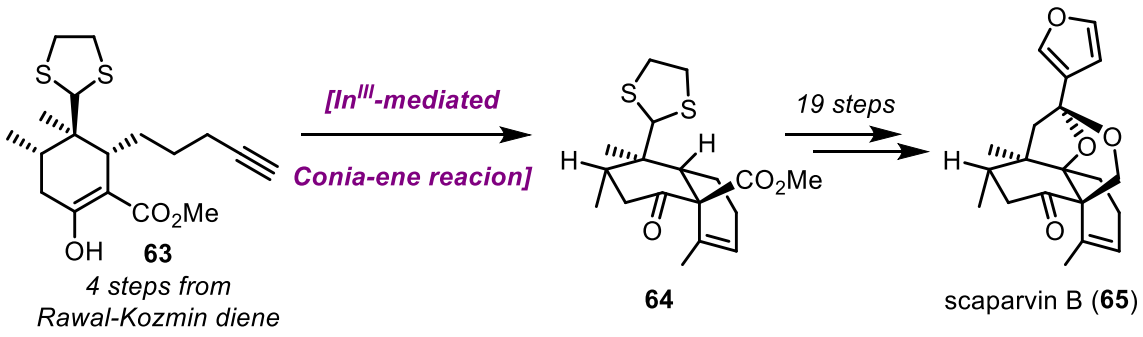

Scheme 1.11. Snyder's total synthesis of scaparvin B (**66**)

The examples covered in this brief review have so far included molecules with a varying amount of functionalization. We have seen that the Au^{I}-catalyzed Conia-ene cyclization reaction is relatively functional group tolerant, as evidenced by the cyclization of alkynyl halides as seen in the total syntheses of gomerone C (**35**) and chalcitrin (**59**) and in the presence of a protected amine as in daphenylline (**42**). Densely functionalized molecules often pose significant challenges due to incompatible reaction conditions. In turn, the synthesis of scarcely functionalized molecules can be equally as daunting for the lack of functional group handles that allow for desired reactions to take place.

In this context, the Snyder group's synthesis of the essentially non-functionalized, highly congested angular triquinane-containing terpene waihoensene (**68**) employs a Au^{I}-catalyzed Conia-ene cyclization in order to establish the *cis*-hydrindane starting from the cyclopentanone **66** (Scheme 1.12).[32] Of note, the Yang group's 15-step asymmetric total synthesis of **68** takes a similar approach, starting from a substituted cyclohexanone forming the *cis*-hydrindane via a base-mediated Conia-ene cyclization.[33]

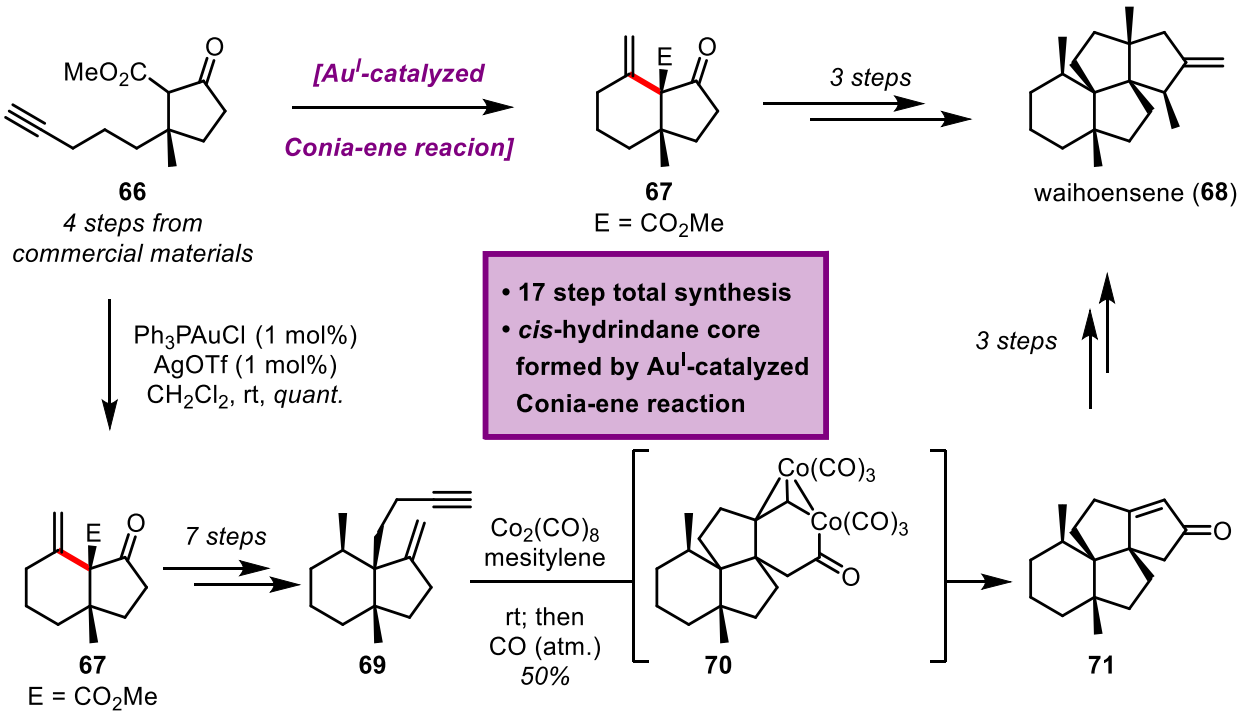

Scheme 1.12. Snyder's total synthesis of waihoensene (**68**)

Snyder and co-workers commenced their synthesis with the decoration of cyclopentanedione to obtain their Conia-ene reaction precursor, β-ketoester **66**, in four steps. Treatment with 1 mol% of each Ph_3PAuCl and AgOTf at ambient temperature formed the desired hydrindane **67** in quantitative yield. Subsequent functionalization of the α-quaternary methyl ester to the homologated alkyne in **69** over seven steps set up a Pauson-Khand reaction that furnishes

the angular triquinane framework. A three-step sequence starting from enone **71**, completes the 17-step total synthesis of waihoensene (**68**).

One last example of how a Conia-ene cyclization reaction accelerated the investigations toward the total synthesis of structurally complex and sterically encumbered natural products is the unified total synthesis of the *Lycopodium* alkaloid natural product family of the annotinolides by the Snyder group (Scheme 1.13).[34] The natural products targeted in that study, annotinolides C (**77**), D (**74**), and E (**78**) all share a cage-shaped tetracyclic framework. The strategic Conia-ene cyclization reaction is designed to form the central [3.2.1]-bicycle, elegantly setting up the final three cyclization events in short order. TBS enol ether **72** is synthesized in seven steps from commercially available 1-pent-4-ynol. Upon treatment of **72** with 30 mol% of Echavarren's catalyst in refluxing CH_2Cl_2 with *i*PrOH as cosolvent, the bicyclic carbon framework of **73** is formed in moderate yield.

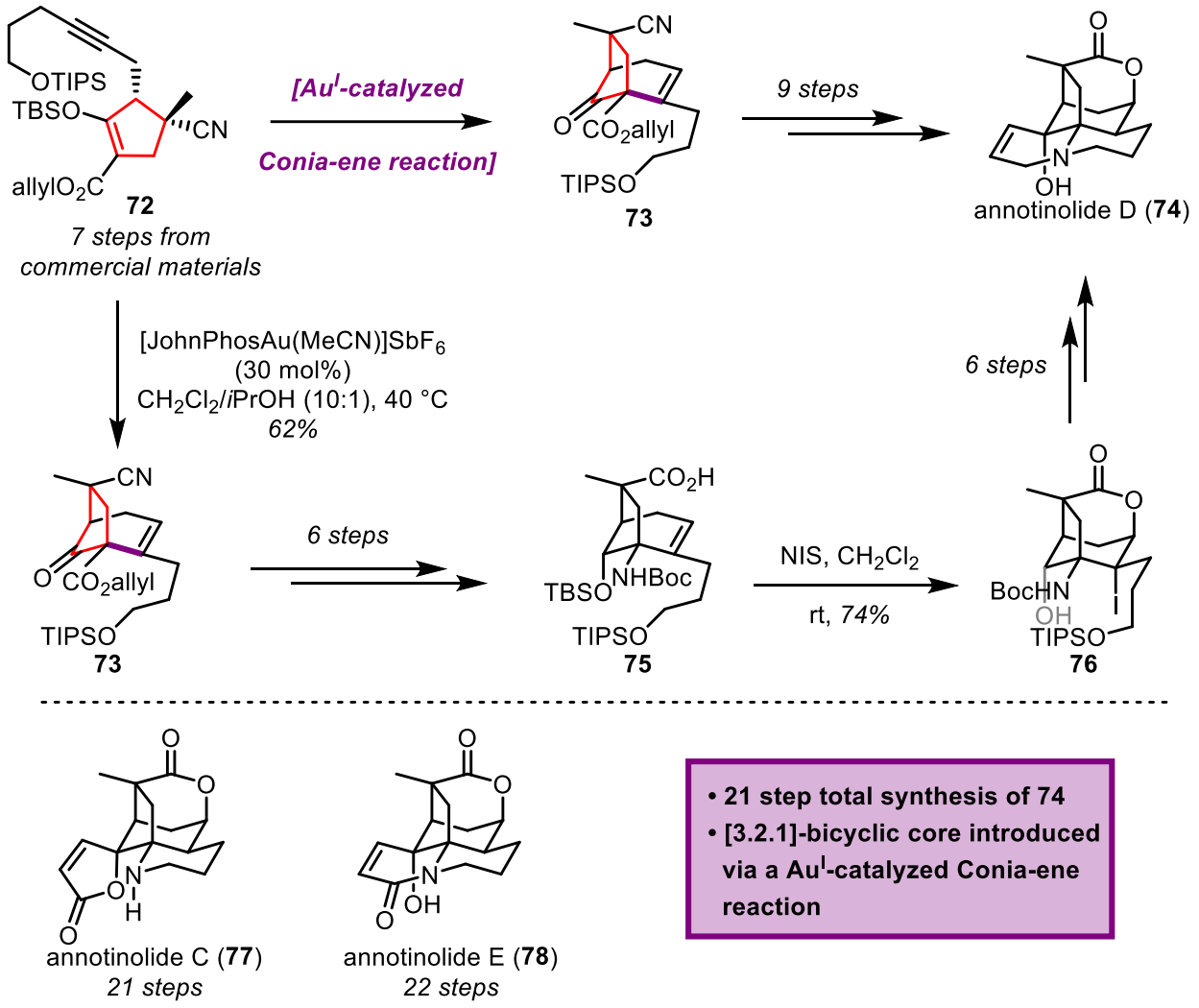

Scheme 1.13. Snyder's total synthesis of annotinolide C, D, and E (**77**, **74**, and **78**)

A short order of functional group interconversions over six steps prepares the next cyclization event. Notably, the allyl ester moiety within the Conia-ene precursor **72** not only aids in the Conia-ene reaction, but is also introduced strategically, to serve as the source of the *N*-Boc protected amine group within **75** via a Curtius rearrangement of the corresponding acyl azide, followed by trapping the resultant isocyanate with *t*BuOK (not shown). Carboxylic acid **75**, in turn, undergoes iodolactonization upon introduction of *N*-iodosuccinimide to furnish lactone **76**. The final rings in the annotinolide natural products are formed by nucleophilic substitution reactions of the amine located at the bridgehead in **76**, leading to the total synthesis of annotinolide

D (**74**) in a total of 21 steps, with modified reaction sequences leading to the formation of **77** and **78**.

In conclusion, the Au^{I}-catalyzed Conia-ene cyclization reaction has been widely applied in natural product total synthesis and proved to be a powerful strategy to construct fused or bridged bicycles in short order.

Section 1.2.2: Au^{I}-catalyzed cyclization reactions in the total synthesis of indole alkaloids

Organic chemists throughout the last century have continued to be fascinated by indole alkaloid natural products, many of which have either desirable bioactivity or intriguing heteroatom-rich molecular scaffolds (cf. Chapter 2). Some indole alkaloid natural products have a sterically demanding cage-shaped core, posing a significant synthetic challenge. The Snyder group has, in the past years successfully applied Au^{I}-catalyzed intramolecular alkyne cyclization reactions to quaternize the C-3 carbon of indole substrates in the pursuit of akuammiline natural products. This reaction is similar to the Conia-ene cyclization, as it is an intramolecular cyclization of a carbon nucleophile, in this case an indole, onto an activated alkyne. This section of the review will cover the Snyder group's syntheses of strictamine (**81**) and arborisidine (**86**).[35,36]

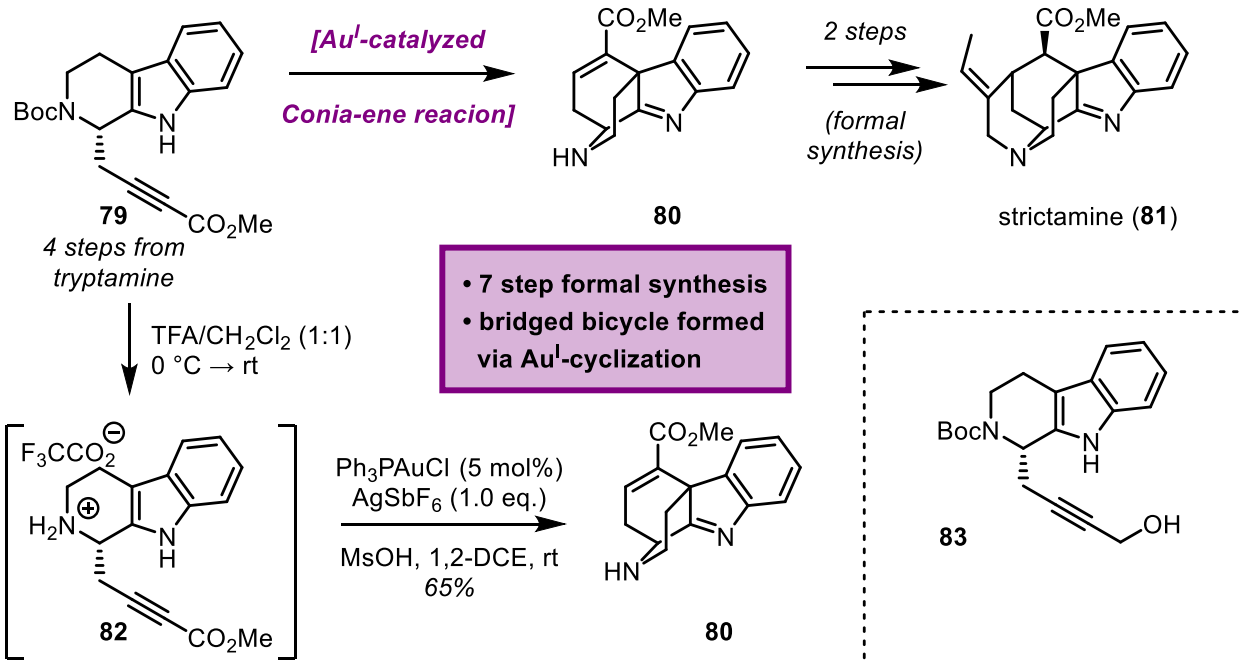

Scheme 1.14. Snyder's total synthesis of strictamine (**81**)

The formal total synthesis of strictamine (**81**) starts with a four-step reaction sequence featuring an asymmetric propargylation and Pd-mediated carbonylation reaction to furnish β-carboline **79** (Scheme 1.14).[35] This species sets the stage for the key Au^{I}-catalyzed 6-*endo*-dig cyclization that furnishes the bridged bicycle in α,β-unsaturated ester **80**. It is notable that this cyclization takes place in a non-canonical fashion, whereby the carbon nucleophile attacks the a-position of the pendant ynoate affording the desired a,b-unsaturated ester. This result, though at odds with the traditional reactivity of these two functionalities, is explained by the π-acidic activation of the ynoate by Au^{I}. This quaternization step intercepts an intermediate in the previously reported total synthesis of **81** by Zhu and co-workers and as such, this approach is a formal synthesis, wherein the key Au^{I}-cyclization step enables the rapid formation of a highly congested tetracyclic ring system in the form of **80**. Of note, an additional synthesis by Fujii and

Ohno takes a similar approach, yet requiring a total of 20 steps for the formal synthesis of strictamine (**81**).[37]

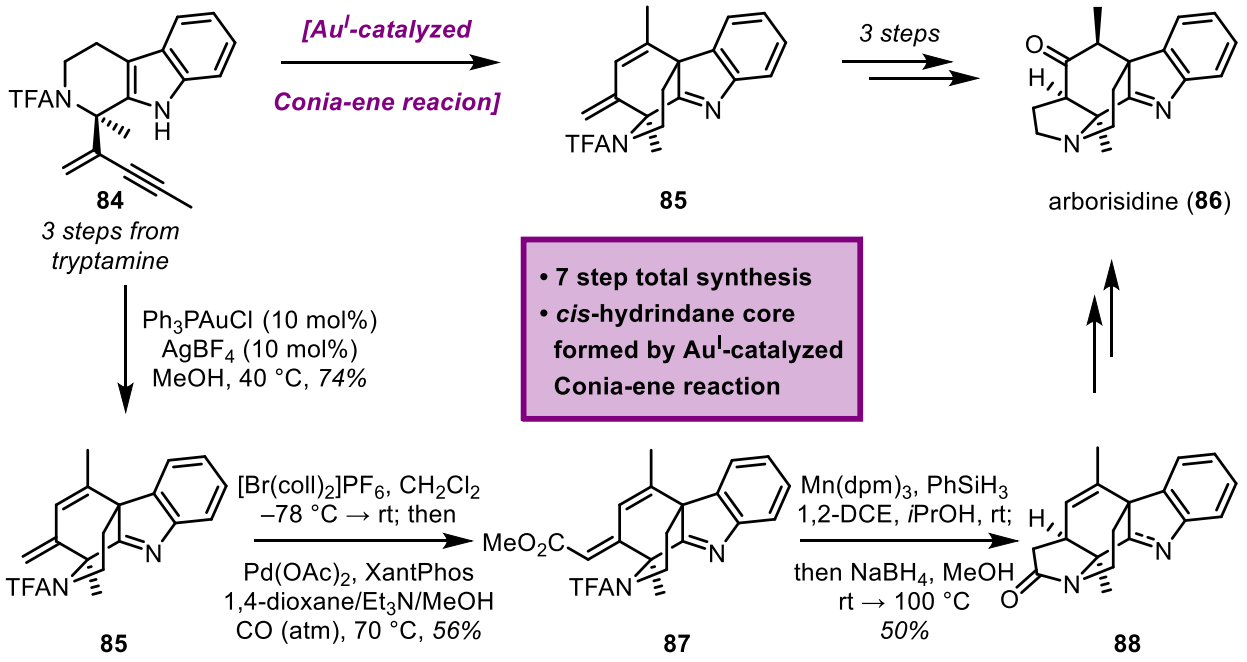

Scheme 1.15. Snyder's total synthesis of arborisidine (**86**)

In addition to strictamine (**81**), the Snyder group has studied the indole alkaloid arborisidine (**86**), a natural product featuring a similar [3.3.1]-bicyclic core, yet with a different overall ring system (Scheme 1.15).[38] The synthetic approach resembles that discussed for the formal synthesis of strictamine (**81**), with formation of **84** in a concise fashion from tryptamine via a Pictet–Spengler reaction. Au^{I}-catalyzed cyclization of the indole into the alkyne, efficiently furnishes indolenine **85**. The final ring is completed in a short three step sequence, each of which features a number of elegantly combined transformations. First, bromination at the 1,1-disubstituted alkene followed by carbonylation forms methyl dienoate **87**. Selective hydrogen atom-transfer (HAT) at the β-carbon and *in situ* lactam formation then affords **88**. The seven-step

total synthesis of arborisidine (**86**) is concluded by a one-pot reaction involving several redox state adjustments.

SECTION 1.2.3: AU^{I}-CATALYZED CYCLOISOMERIZATION REACTIONS OF ENYNES IN NATURAL PRODUCT TOTAL SYNTHESIS

The final category of Au^{I}-catalyzed reactions applied in natural product synthesis discussed in this chapter is the cycloisomerization of 1,*n*-enynes.[20,21,39,40] These reactions proceed via initial addition of the olefin reaction partner to the alkyne, forming a cyclopropyl intermediate with a pendant Au^{I}-carbene. Such carbenes may undergo further strain-promoted rearrangements or simple protodeauration to release the reaction product.

Over the past 20 years, the area of Au^{I} catalysis has flourished, with many research groups making significant contributions to the field. In particular, methods utilizing cycloisomerizations of 1,*n*-enynes have enabled the formation of numerous complex molecular architectures as found in countless natural products.

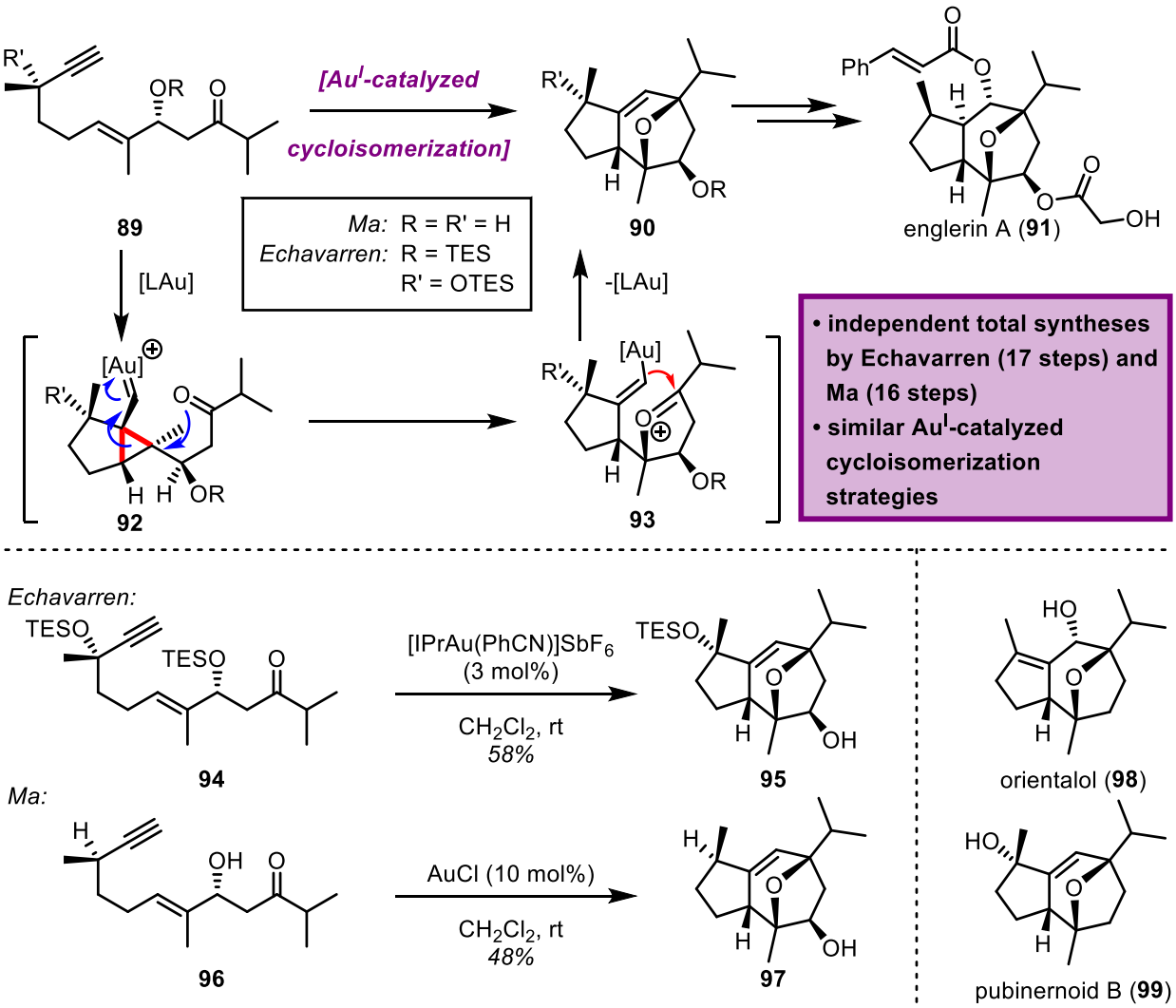

Scheme 1.16. Echavarren and Ma's total synthesis of englerin A (**91**)

The Echavarren group has applied their Au^{I}-catalyzed cycloisomerization chemistry to concisely establish natural product frameworks to a number of molecules, one being englerin A (**91**, Scheme 1.16).[41] A contemporary approach closely resembling this work by the Ma group is discussed as well.[42] Among the numerous syntheses of englerin A (**91**) published in the literature, this approach manages to construct the entire carbocyclic framework from a substituted linear 1,6-enyne. First applied on the related, yet less functionalized natural products orientalol (**98**) and pubinernoid B (**99**), the Echavarren and Ma syntheses commence by independent synthesis of the cyclization precursor **89**.[43]

Treatment with a suitable Au^I-catalyst triggers the initial electrophilic cyclopropanation at the olefin which forges the five-membered ring. Subsequent attack at the cyclopropane by the ketone within **92** forms the cyclic oxonium ion which is part of the second ring. Finally, attack of the Au^I-carbene at the oxonium completes the englerin A (**91**) carbocyclic core following protodeauration. A varying number of functional group interconversions and *O*-alkylations deliver englerin A (**91**) in a total of 17 (Echavarren) and 16 steps (Ma), respectively.

In a later publication of the total synthesis of the natural products epiglobulol (**101**) and (−)-4α,7α-aromadendranediol (**102**), Echavarren and co-workers liken the Au^I-catalyst in their cascade to an "artificial cyclase," which emulates "the action of terpene cyclases forming polycyclic skeletons."[44] As pointed out by Willot and Christmann, it is notable that the proposed biosynthesis of englerin A (**91**) and related natural products, starting from farnesylpyrophosphate (FPP), forms only the 5/7 fused bicycle, leaving oxidative transformations and formation of the bridging ether to a separate enzyme.[41] The remarkable Au^I-catalyzed cycloisomerization that leads to the efficient formation of the entire skeleton of englerin A (**91**) in a single cascade reaction is enabled by the highly engineered nature of the cyclization precursor ketoenyne **94**.

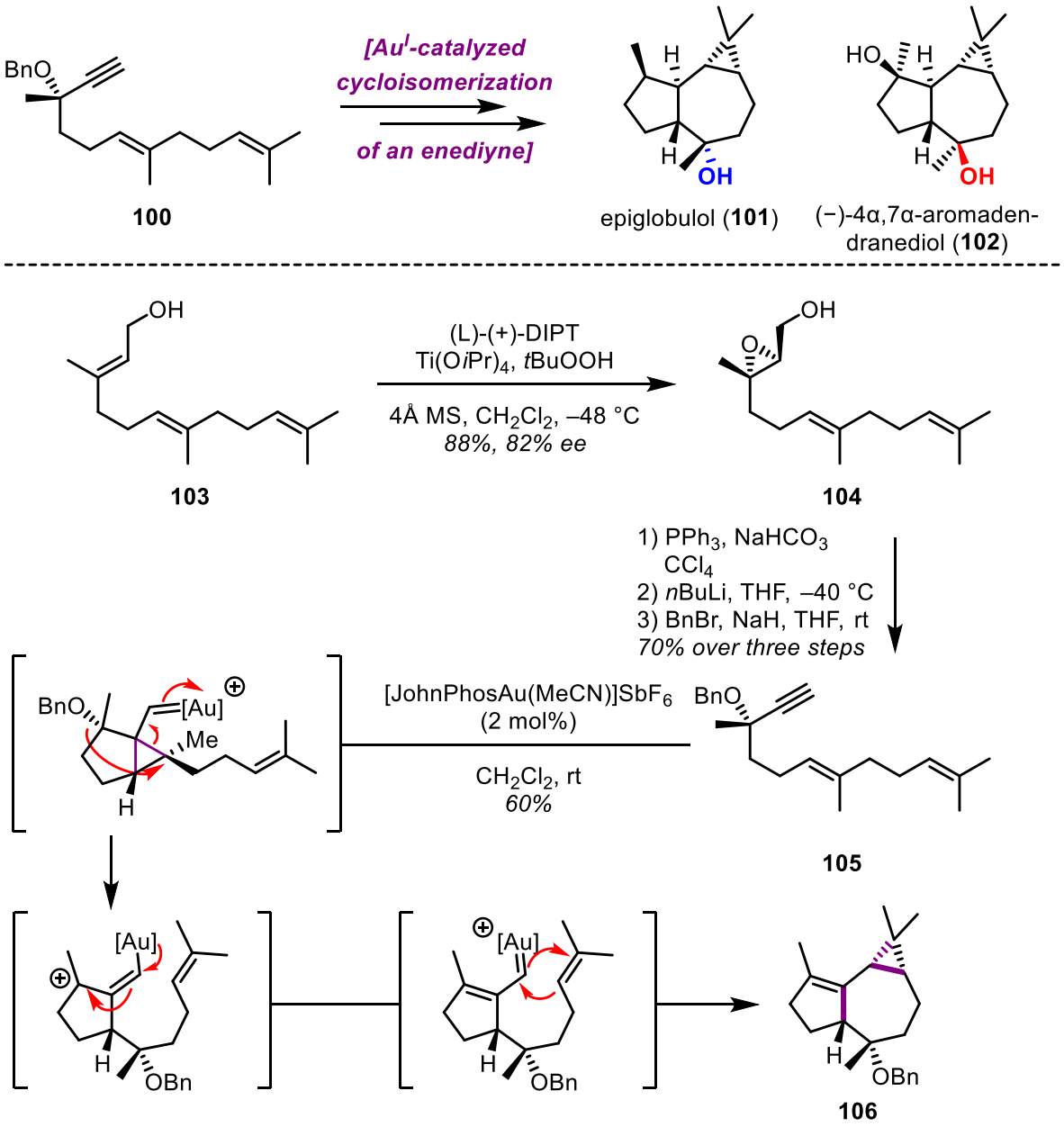

Scheme 1.17. Echavarren's total synthesis of epiglobulol (**101**)

In a continued pursuit of harnessing the power of their so-called artificial cyclase, the Echavarren group reported the total synthesis of epiglobulol (**101**) and (−)-4α,7α-aromadendranediol (**102**, Scheme 1.17).[44] The 5/7/3 tricyclic core was envisioned to be formed in a single Au^I-catalyzed cycloisomerization cascade of dienyne **105**. The synthesis commenced with the Sharpless asymmetric epoxidation of farnesol (**103**), followed by an Appel reaction. Double

elimination and protection of the resultant tertiary alcohol yields cycloisomerization precursor **105**. Upon treatment with Echavarren's catalyst, initial electrophilic cyclopropanation occurs, as described above in the total synthesis of englerin A (**91**). In contrast to their prior efforts, there is no pendant nucleophile that is available to attack the activated cyclopropane species. Instead, the tertiary benzyloxy group migrates. The subsequent second cyclopropanation with the distal olefin completes the ring system of epiglobulol (**101**). The natural product is then completed following a short redox manipulation sequence and in a total of eight steps.

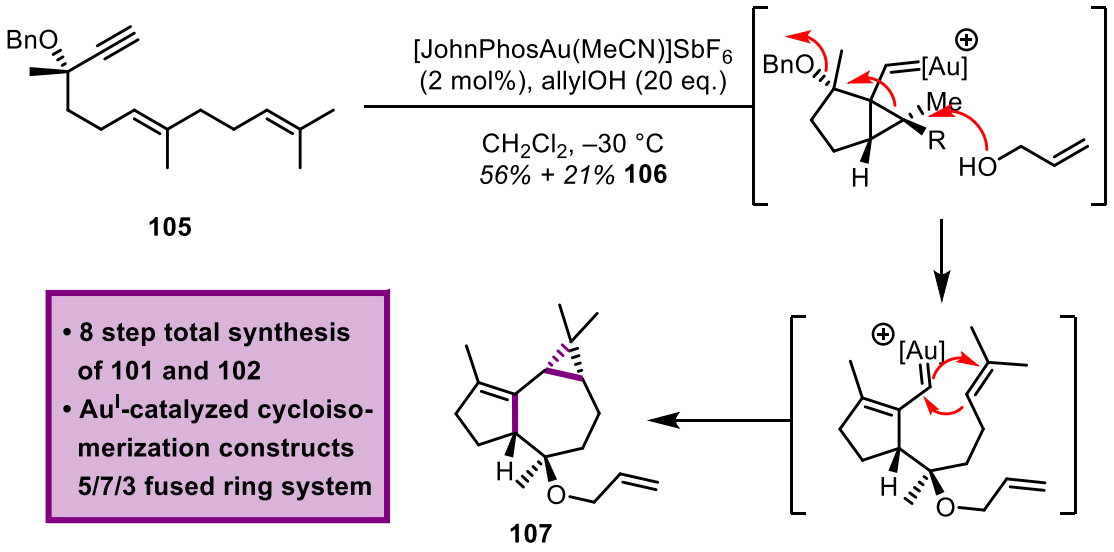

Scheme 1.18. Echavarren's total synthesis (−)-4α,7α-aromadendranediol (**102**)

While the commercially available (*E*,*E*)-farnesol utilized in this reaction allowed for the efficient formation of epiglobulol (**101**) due to the predetermined facial approach of the migrating benzyloxy group, synthesis of (−)-4α,7α-aromadendranediol (**102**) proved to be more challenging (Scheme 1.18). The key tertiary alcohol stereocenter in the tricyclic core is inverted, which led the Echavarren group to a creative solution, instead managing to trap the activated cyclopropane species with an external nucleophile. Given the efficiency of the intramolecular transfer of the benzyloxy group as shown above, this intermolecular trapping with allyl alcohol was not able to

fully suppress the undesired pathway, delivering the desired allyl ether **107** in moderate yield alongside notable amounts of **106**.

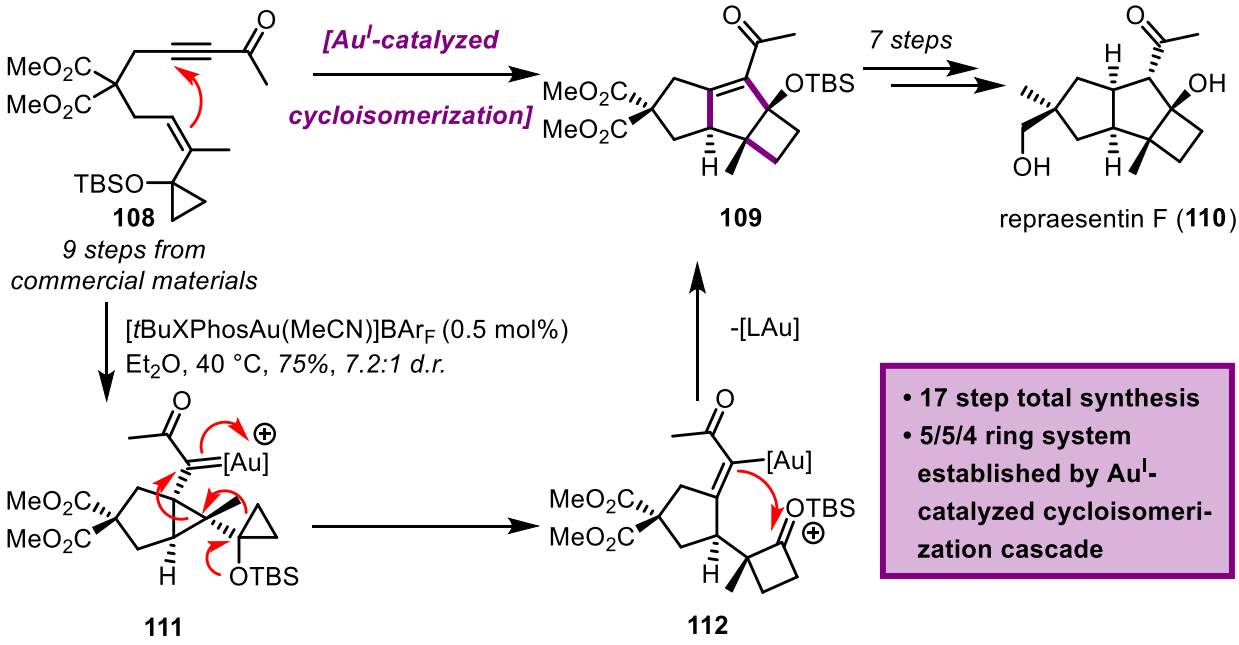

Scheme 1.19. Echavarren's total synthesis of repraesentin F (**110**)

In their total synthesis of repraesentin F (**110**), the Echavarren group once again demonstrated the versatility of their cycloisomerization approach to rapidly forge 5/5/4 fused ring systems (Scheme 1.19).[45] After their previous entries featuring cyclopropane trapping with carbonyl or olefin nucleophiles, this synthesis relies on a semi-pinacol-type ring expansion strategy. The cycloisomerization precursor enyne (**108**) was prepared in nine steps and contains a distal TBS-protected cyclopropyl alcohol. Upon treatment with the Au^{I} catalyst, initial cyclopropanation is intercepted by semi-pinacol-type rearrangement of the cyclopropyl silyl ether. Subsequent addition into the oxonium furnishes the carbocyclic skeleton of repraesentin F (**110**), which is completed in another seven steps.

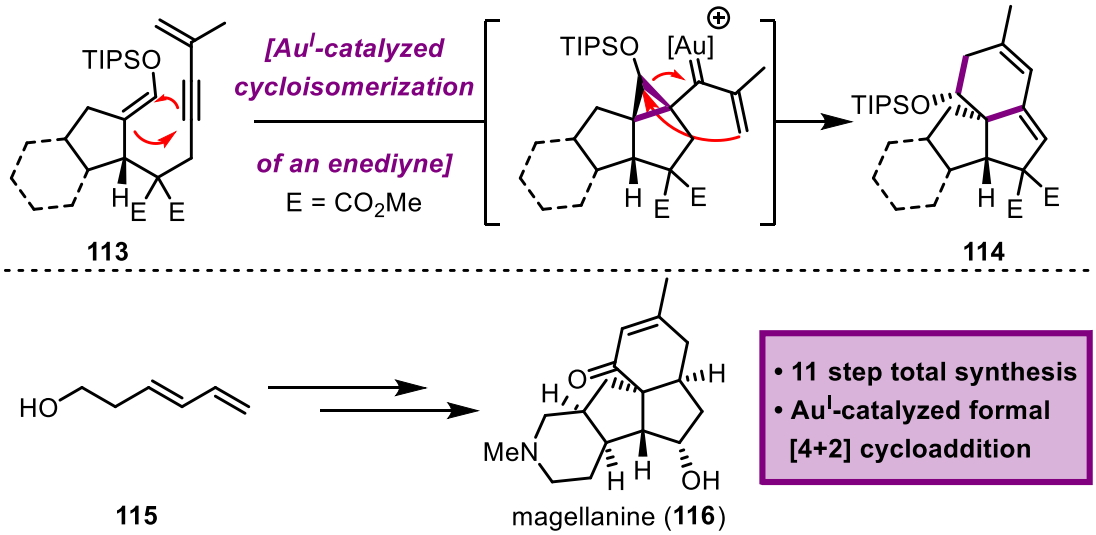

Scheme 1.20. Barriault's Au^{I}- catalyzed cycloisomerization reaction and application to the total synthesis of magellanine (**116**)

Barriault and co-workers developed a Au^{I}-catalyzed formal [4+2] cycloaddition reaction, which features a substrate scope with a number of different ring systems, leading to the formation of a highly congested angular 5/5/6 ring system (Scheme 1.20).[46] It takes advantage of an initial cyclopropanation event, which is then opened in a rearrangement reaction the authors describe as a formal [4+2] cycloaddition. This cycloisomerization cascade was utilized as the key step in the total synthesis of magellanine (**116**).

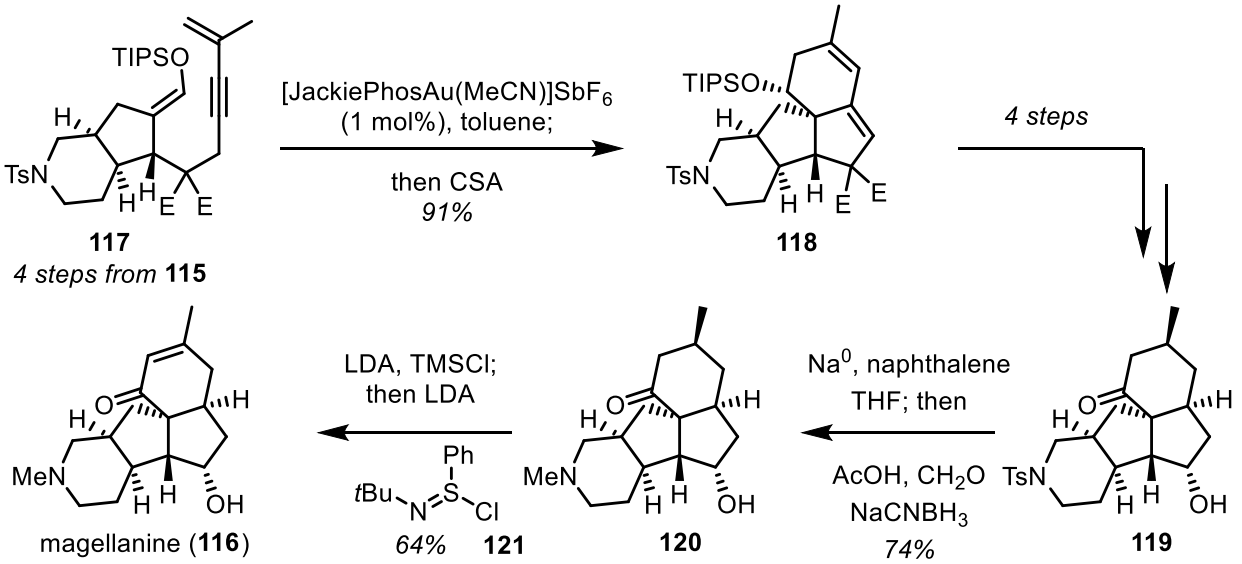

Scheme 1.21. Barriault's total synthesis of magellanine (**116**)

The synthetic route toward magellanine (**116**) commences from 3,5-hexadien-1-ol (**115**) with a four-step sequence to form cycloisomerization precursor **117**. Treatment of dienyne **117** with [JackiePhos(MeCN)]SbF_6 and subsequent addition of acid led to the formation of the highly congested silyl ether (Scheme 1.21). Subsequent oxidative decarboxylation of the geminal diester forged alcohol **119**. The synthesis concludes with a deprotection and *N*-methylation, followed by desaturation of the ketone within **120** with Mukaiyama salt **121** in a total of 11 steps. While the latter steps of the synthesis revolve around the adjustment of oxidation states and protecting group manipulations, the Au-cascade is key in establishing a significant portion of the target framework.

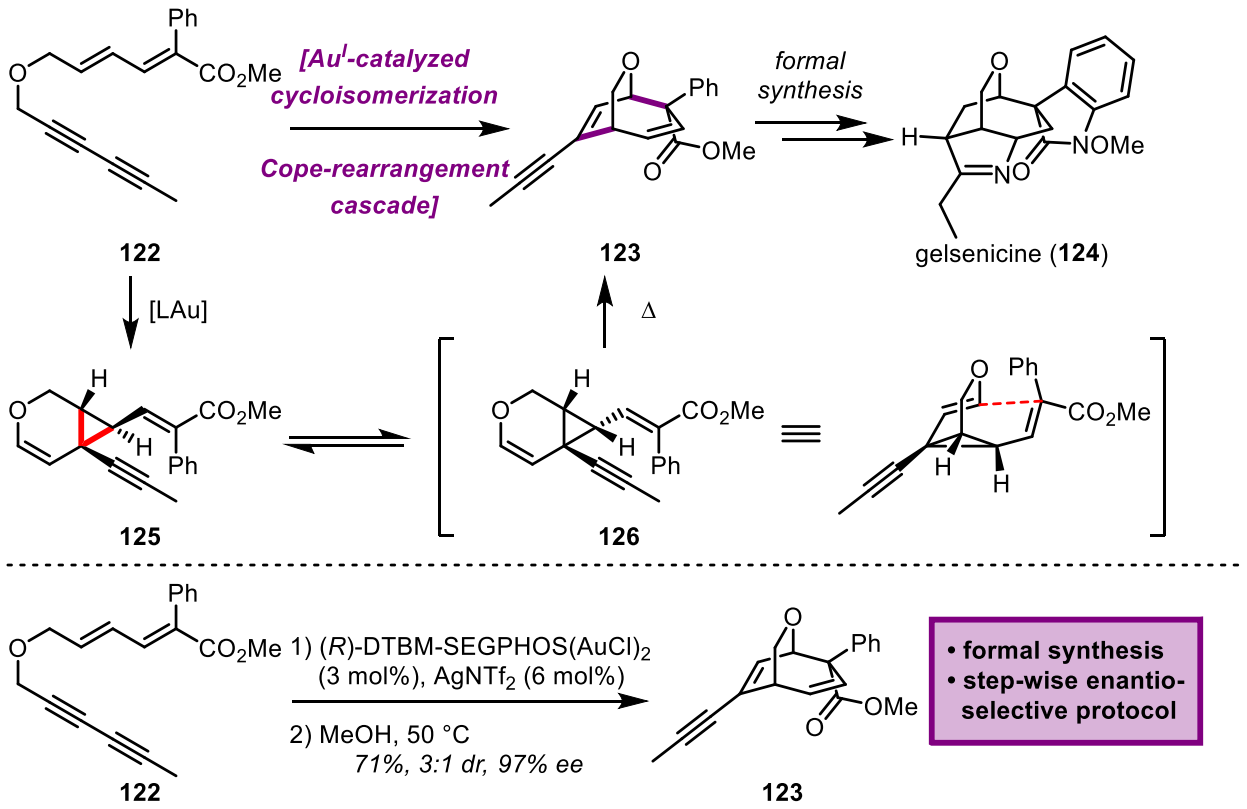

Scheme 1.22. Ferreira's formal total synthesis of gelsenicine (**124**)

A more recent example of the application of Au^{I}-catalyzed cycloisomerization in total synthesis is the incorporation into the domino reactions as in the formation the bridged bicyclic ether within gelsenicine (**124**, Scheme 1.22).[47] Such a transformation is particularly notable, as most Au-catalyzed cyclization reactions often result in the formation of fused ring systems as opposed to bridged ether shown above. The formal synthesis by the Ferreira group is adapted from their previous Pt^{II}-catalyzed cycloisomerization reaction in the total synthesis of **124**.[48] The key advantage of the reaction discussed herein is the formation of intermediate **123** with excellent *ee* from cycloisomerization precursor ether **122** by use of a chiral ligand. The cyclopropane intermediate **125** formed in this reaction is able to isomerize and undergo a Cope-type rearrangement to furnish the desired oxa[3.2.2]bicycle **123**, notably in high enantiomeric excess.

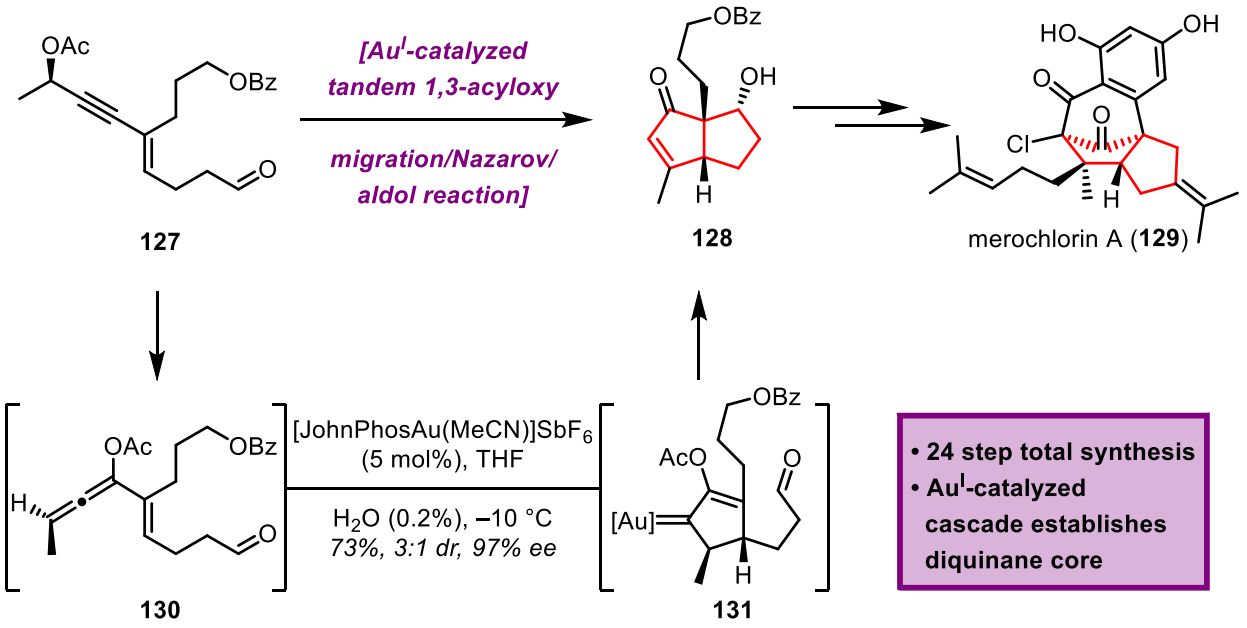

Scheme 1.23. Summary of Carreira's total synthesis of merochlorin A (**129**)

The Carreira group has also made a number of contributions to the field of natural product total synthesis while exploiting the synthetic power of Au^{I}-catalyzed cycloisomerizations. In their total synthesis of merochlorin A (**129**), they employ an elegant cascade to forge the central diquinane, starting from the branched enyne acetate **127** (Scheme 1.23).[49] Exposure to Echavarren's catalyst effects a 1,3-acyloxy rearrangement, a variation of a Meyer-Schuster rearrangement, to allenyl acetate **130**, which in turn undergoes a Nazarov cyclization, owing to the sufficient Lewis acidity of the Au^{I} catalyst. After protodeauration of **128** and aldol addition into the pendant aldehyde, the 5/5 fused ring system is completed in a total of seven steps. Notably, the enantioenriched acetate **127** undergoes chirality transfer, conserving an impressive 97% *ee*.

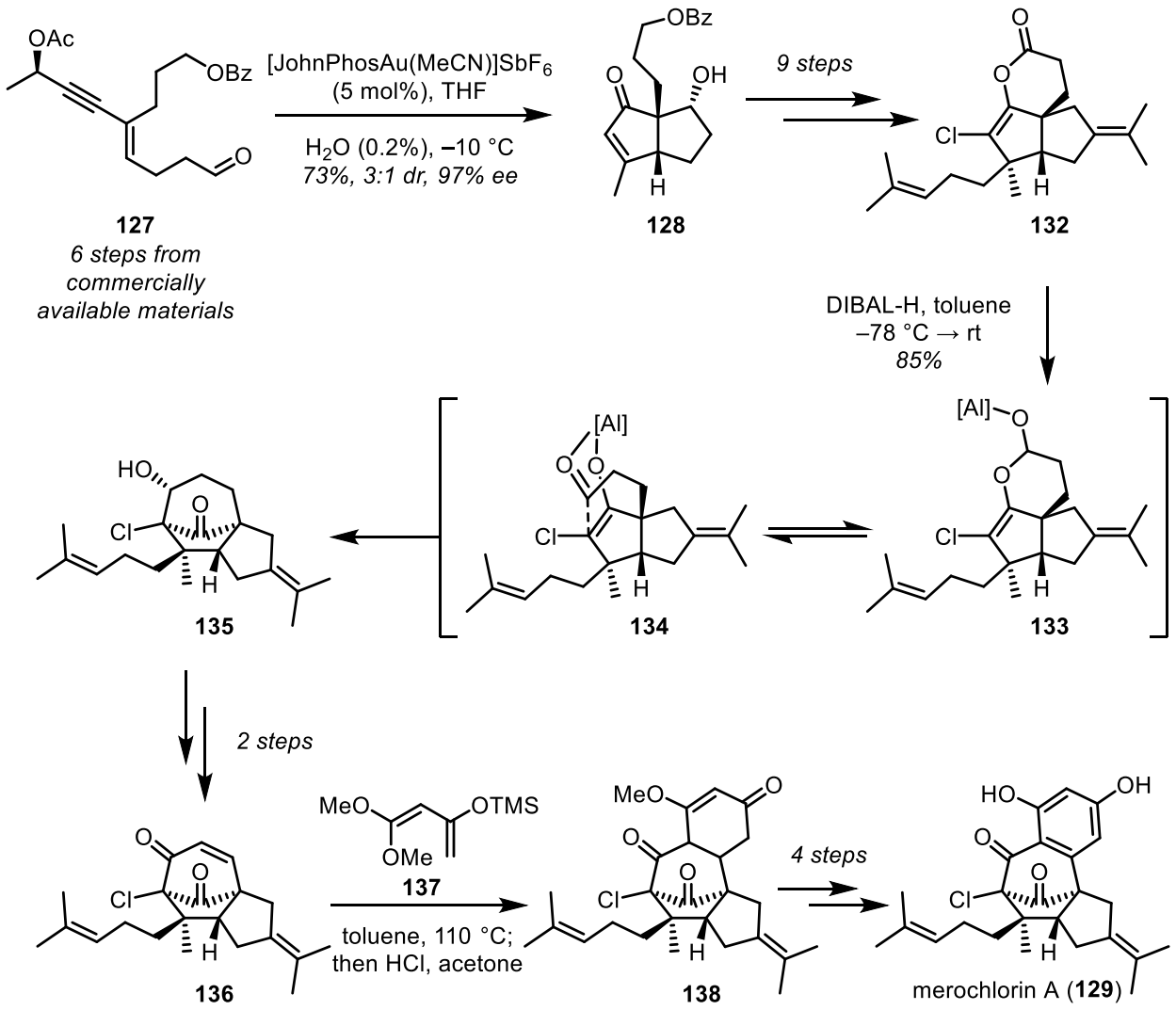

Scheme 1.24. Carreira's total synthesis of merochlorin A (**129**)

The remaining rings of merochlorin A (**129**) are formed in an additional 17 steps, starting with a nine-step sequence to install lactone **132** (Scheme 1.24). Careful treatment of the lactone with DIBAL-H triggers an impressive reductive rearrangement to furnish the bridged [3.2.1]-bicycle within **135**. Desaturation to enone **136** is followed by the installation of the final six-membered ring via a Diels–Alder reaction and aromatization to complete the total synthesis of merochlorin A (**129**) in a total of 24 steps. This synthesis highlights the ability of Au^{I} catalysts to not only activate alkynes to nucleophilic attack, but also trigger rearrangements that in carefully

designed systems, such as the one presented here, lead to further cyclization events. In addition, it showcases the ability to furnish ubiquitous structures found within natural products such as diquinanes with several functional group handles from linear precursors.

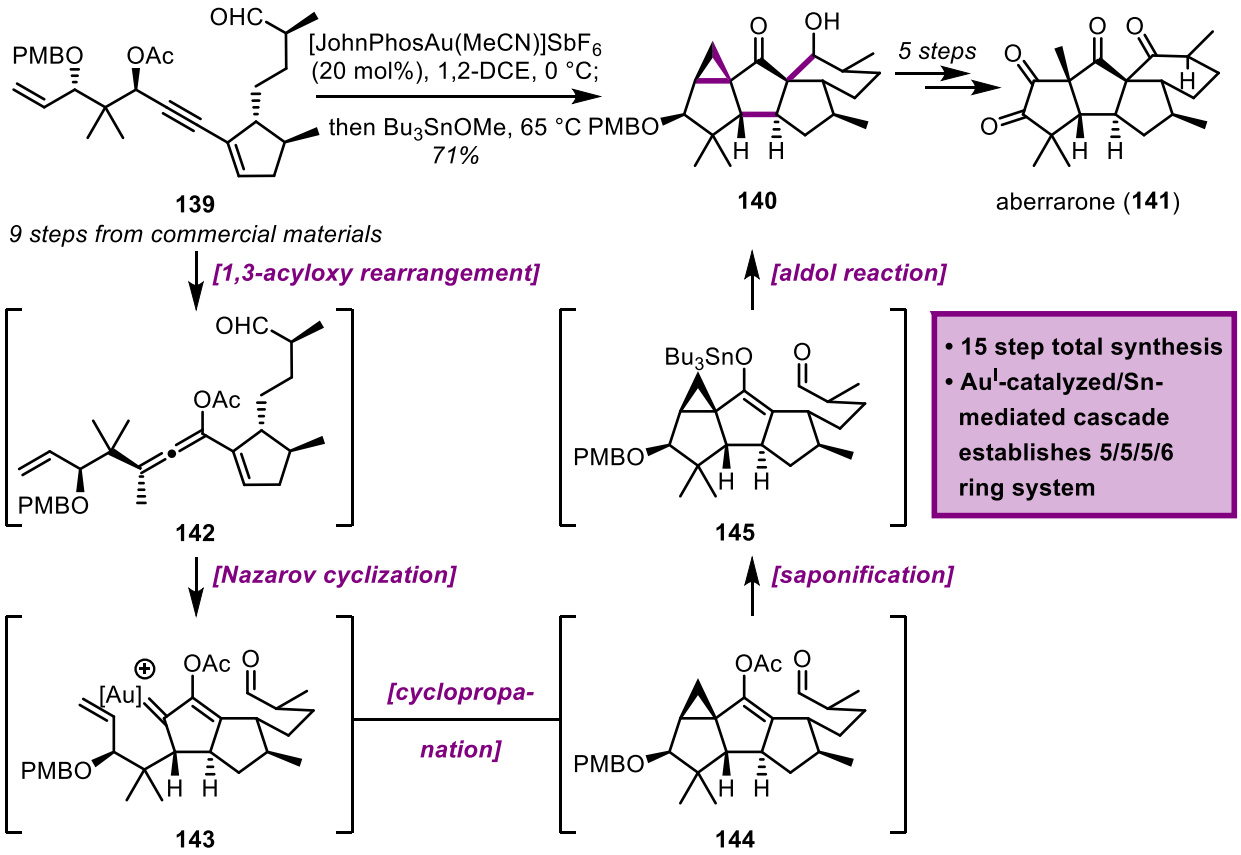

Scheme 1.25. Carreira's total synthesis of aberrarone (**141**)

In an extension of the strategy employed in the total synthesis of merochlorin A (**129**) is the Carreira group's approach to the diterpenoid natural product aberrarone (**141**, Scheme 1.25).[50] It once again showcases the how far the concept of Au^{I} catalysts serving as artificial terpene cyclases can be pushed. Starting from the cyclization precursor, propargyl acetate **139**, treatment with Echavarren's catalyst triggers a Meyer-Schuster rearrangement to allenyl acetate **142**. The subsequent Nazarov cyclization forges the first five-membered ring, the second being formed via cyclopropanation onto the terminal olefin. Addition of Bu_3SnOMe to the reaction leads to

saponification of the acetate group within **144** and subsequent aldol reaction into the pendant aldehyde to furnish the pentacyclic ketone **140**. An additional five steps are needed to complete the concise total synthesis of aberrarone (**141**), with the Au-cascade serving to construct four of the five rings found within the final target.

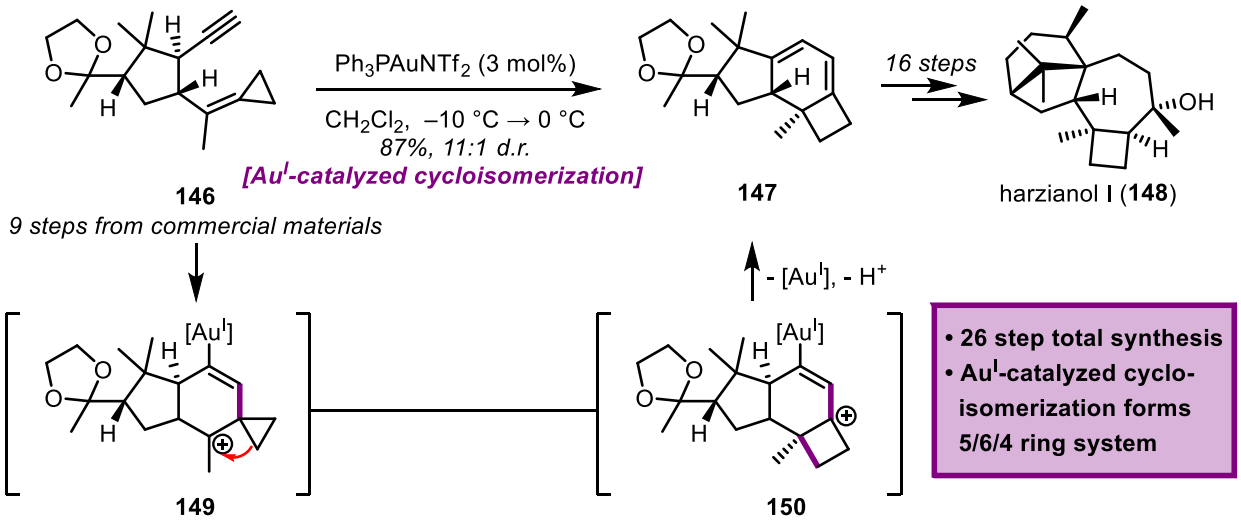

Scheme 1.26. Carreira's total synthesis of harzianol I (**148**)

A further foray by the Carreira group into applying Au^{I}-catalyzed cycloisomerizations to natural product synthesis is the total synthesis of harzianol I (**148**, Scheme 1.26).[51] The strategy here is to build a 5/6/4 tricyclic scaffold, which is later elaborated into the 6/5/7/4 ring system of harzianol I (**148**). Alkylidenecyclopropane **146** serves as the cycloisomerization precursor, prepared in nine steps from commercially available materials. Upon treatment with $Ph_3PAuNTf_2$, the olefin attacks the alkyne, followed by ring-opening of the cyclopropane in **146**. The stabilized carbocation **149** then undergoes elimination and protodeauration to furnish the desired tricyclic diene **150**. The remaining 16 steps and further details to this synthesis are discussed in Chapter 3.

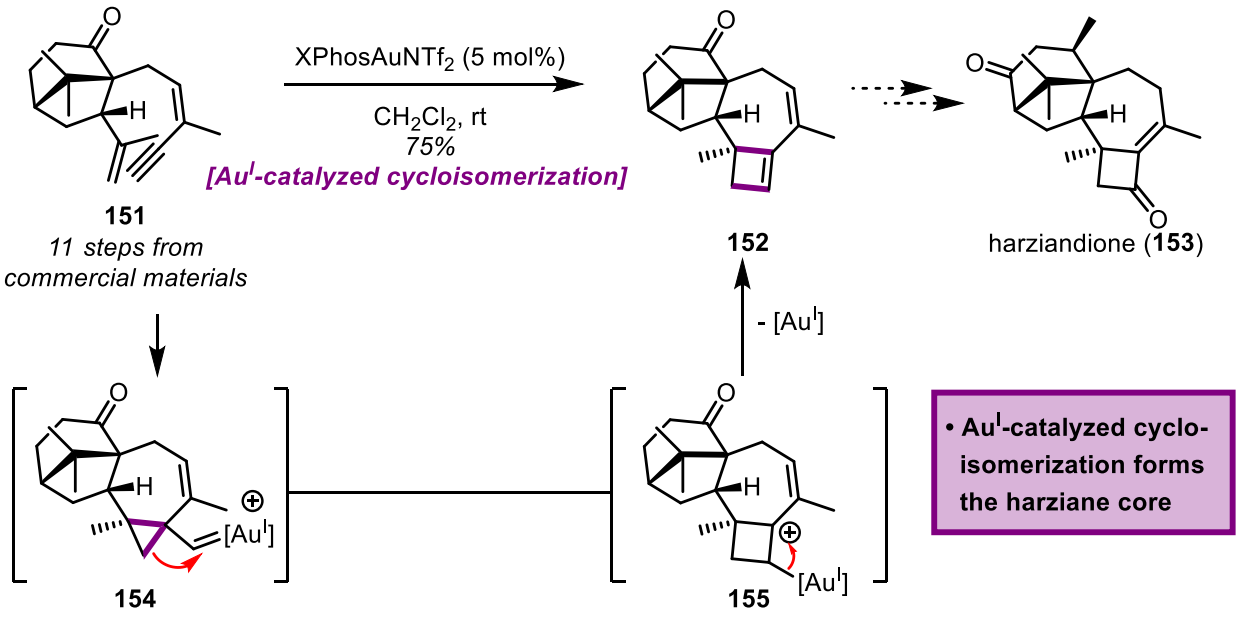

Scheme 1.27. Yang's studies toward the total synthesis of harziandione (**153**)

A related approach to the harziane diterpenes has been published by the Yang group (Scheme 1.27).[52] In their studies toward the total synthesis of harziandione (**153**), they apply a cycloisomerization reaction published by Gagosz and co-workers. Initial cyclopropanation of the olefin in 1,8-enyne **151** is followed by strain-promoted ring opening into the Au^{I}-carbene. Protodeauration then delivers ketone **152**, which constitutes the carbon skeleton of the harziane diterpens, however, the Yang group was unable to complete the total synthesis of this natural products. This synthesis and our group's successful total synthesis of harziandione (**153**) utilizing a similar approach are covered in depth in Chapter 3.

SECTION 1.3: REFERENCES:

(1) Miller, S. L. *Science* **1953**, *117*, 528–529.

(2) Baran, P. S. *J. Am. Chem. Soc.* **2018**, *140*, 4751–4755.

(3) Nicolaou, K. C.; Sorensen, E. J. *Classics in Total Synthesis: Targets, Strategies, Methods*; Wiley-VCH, 1996.

(4) Nicolaou, K. C.; Snyder, S. A. *Classics in Total Synthesis II : More Targets, Strategies, Methods*; Wiley-VCH, 2003.

(5) Li, D.; Zang, W.; Bird, M. J.; Hyland, C. J. T.; Shi, M. *Chem. Rev.* **2021**, *121*, 8685–8755.

(6) Mato, M.; Franchino, A.; García-Morales, C.; Echavarren, A. M. *Chem. Rev.* **2021**, *121*, 8613–8684.

(7) Xu, Y.; Conner, M. L.; Brown, M. K. *Angew. Chemie Int. Ed.* **2015**, *54*, 11918–11928.

(8) Hashmi, A. S. K.; Rudolph, M. *Chem. Soc. Rev.* **2008**, *37*, 1766–1775.

(9) Pflästerer, D.; Hashmi, A. S. K. *Chem. Soc. Rev.* **2016**, *45*, 1331–1367.

(10) Silva, C.; Faza, O. N.; Luna, M. M. *Front. Chem.* **2019**, *7*, 296.

(11) Sugimoto, K.; Matsuya, Y. *Tetrahedron Lett.* **2017**, *58*, 4420–4426.

(12) Zhang, Y.; Luo, T.; Yang, Z. *Nat. Prod. Rep.* **2014**, *31*, 489–503.

(13) Fürstner, A. *Chem. Soc. Rev.* **2009**, *38*, 3208–3221.

(14) Fürstner, A. *Acc. Chem. Res.* **2014**, *47*, 925–938.

(15) Gorin, D. J.; Toste, F. D. *Nat. 2007 4467134* **2007**, *446*, 395–403.

(16) Teles, J. H.; Brode, S.; Chabanas, M. *Angew. Chem. Int. Ed* **1998**, *37*.

(17) Brenzovich, W. E. *Angew. Chemie - Int. Ed.* **2012**, *51*, 8933–8935.

(18) Tlais, S. F.; Dudley, G. B. *Org. Lett.* **2010**, *12*, 4698–4701.

(19) Chiba, H.; Oishi, S.; Fujii, N.; Ohno, H.; Chiba, H.; Oishi, S.; Fujii, N.; Ohno, H. *Angew. Chemie Int. Ed.* **2012**, *51*, 9169–9172.

(20) Jiménez-Núñez, E.; Echavarren, A. M. *Chem. Rev.* **2008**, *108*, 3326–3350.

(21) Fürstner, A.; Davies, P. W.; Fürstner, A.; Davies, P. W. *Angew. Chemie Int. Ed.* **2007**, *46*, 3410–3449.

(22) Conia, J. M.; Le Perchec, P. *Synthesis (Germany)*. Georg Thieme Verlag January 1, 1975, pp 1–19.

(23) Kennedy-Smith, J. J.; Staben, S. T.; Toste, F. D. *J. Am. Chem. Soc.* **2004**, *126*, 4526–4527.

(24) Linghu, X.; Kennedy-Smith, J. J.; Toste, F. D. *Angew. Chemie Int. Ed.* **2007**, *46*, 7671–

7673.

(25) Huwyler, N.; Carreira, E. M. *Angew. Chemie Int. Ed.* **2012**, *51*, 13066–13069.

(26) Schlama, T.; Gabriel, K.; Gouverneur, V.; Mioskowski, C. *Angew. Chemie Int. Ed. English* **1997**, *36*, 2342–2344.

(27) Lu, Z.; Li, Y.; Deng, J.; Li, A. *Nat. Chem.* **2013**, *5*, 679–684.

(28) Picazo, E.; Morrill, L. A.; Susick, R. B.; Moreno, J.; Smith, J. M.; Garg, N. K. *J. Am. Chem. Soc.* **2018**, *140*, 6483–6492.

(29) Shi, H.; Fang, L.; Tan, C.; Shi, L.; Zhang, W.; Li, C. C.; Luo, T.; Yang, Z. *J. Am. Chem. Soc.* **2011**, *133*, 14944–14947.

(30) Yang, M.; Yin, F.; Fujino, H.; Snyder, S. A. *J. Am. Chem. Soc.* **2019**.

(31) Ye, Q.; Qu, P.; Snyder, S. A. *J. Am. Chem. Soc.* **2017**, *139*, 18428–18431.

(32) Peng, C.; Arya, P.; Zhou, Z.; Snyder, S. A. *Angew. Chemie Int. Ed.* **2020**.

(33) Qu, Y.; Wang, Z.; Zhang, Z.; Zhang, W.; Huang, J.; Yang, Z. *J. Am. Chem. Soc.* **2020**, *142*, 6511–6515.

(34) Qu, P.; Snyder, S. A. *J. Am. Chem. Soc.* **2021**, *143*, 11951–11956.

(35) Smith, M. W.; Zhou, Z.; Gao, A. X.; Shimbayashi, T.; Snyder, S. A. *Org. Lett.* **2017**, *19*, 1004–1007.

(36) Zhou, Z.; Gao, A. X.; Snyder, S. A. *J. Am. Chem. Soc.* **2019**, *141*, 7715–7720.

(37) Nishiyama, D.; Ohara, A.; Chiba, H.; Kumagai, H.; Oishi, S.; Fujii, N.; Ohno, H. *Org. Lett.* **2016**, *18*, 1670–1673.

(38) Zhou, Z.; Gao, A. X.; Snyder, S. A. *J. Am. Chem. Soc.* **2019**, *141*, 7715–7720.

(39) Obradors, C.; Echavarren, A. M. *Acc. Chem. Res.* **2014**, *47*, 902–912.

(40) Obradors, C.; Echavarren, A. M. *Chem. Commun.* **2014**, *50*, 16–28.

(41) Willot, M.; Christmann, M. *Nat. Chem.* **2010**, *2*, 519–520.

(42) Zhou, Q.; Chen, X.; Ma, D.; Zhou, Q.; Chen, X.; Ma, D. *Angew. Chemie Int. Ed.* **2010**, *49*, 3513–3516.

(43) Jiménez-Núñez, E.; Molawi, K.; Echavarren, A. M. *Chem. Commun.* **2009**, *0*, 7327–7329.

(44) Carreras, J.; Livendahl, M.; McGonigal, P. R.; Echavarren, A. M. *Angew. Chemie Int. Ed.* **2014**, *53*, 4896–4899.

(45) Ferrer, S.; Echavarren, A. M. *Org. Lett.* **2018**, *20*, 5784–5788.

(46) McGee, P.; Bétournay, G.; Barabé, F.; Barriault, L. *Angew. Chemie Int. Ed.* **2017**, *56*, 6280–6283.

(47) Knutson, P. C.; Ji, H.; Harrington, C. M.; Ke, Y. T.; Ferreira, E. M. *Org. Lett.* **2022**, *24*,

4971–4976.

(48) Newcomb, E. T.; Knutson, P. C.; Pedersen, B. A.; Ferreira, E. M. *J. Am. Chem. Soc.* **2016**, *138*, 108–111.

(49) Brandstätter, M.; Freis, M.; Huwyler, N.; Carreira, E. M. *Angew. Chemie Int. Ed.* **2019**, *58*, 2490–2494.

(50) Amberg, W. M.; Carreira, E. M. *J. Am. Chem. Soc.* **2022**, *144*, 15475–15479.

(51) Hönig, M.; Carreira, E. M. *Angew. Chemie Int. Ed.* **2020**, *59*, 1192–1196.

(52) Tu, Q.; Wang, Z.; Zhang, Z.; Huang, J.; Yang, Z. *Org. Lett.* **2021**, *23*, 4088–4093.

CHAPTER II:

SYNTHETIC STUDIES TOWARD THE TOTAL SYNTHESIS OF KOUMINE

SECTION 2.1: INTRODUCTION

The alkaloids isolated from the *Gelsemium* species, a family of East Asian shrubs, have for several decades been a popular target for synthetic chemists due to their promising biological activities and structural complexity.[1] Many of the more than 120 reported *Gelsemium* alkaloids have anti-tumor, anti-inflammatory, analgesic, and anxiolytic effects.[2] Isolated in 1931 from *Gelsemium elegans* Benth., the indole alkaloid koumine (**1**) had long resisted structural confirmation and total synthesis.[1,3–6] With its structure established in 1981, it is a unique caged indole alkaloid, containing two contiguous all-carbon quaternary centers, a central azabicyclo[2.2.2]octane ring, and a pyran ring, a feature observed in many other *Gelsemium* alkaloids (Scheme 1). Koumine (**1**) has been shown to exhibit anti-inflammatory properties, however its complex cage-shaped structure was the motivation for our synthetic study.[7]

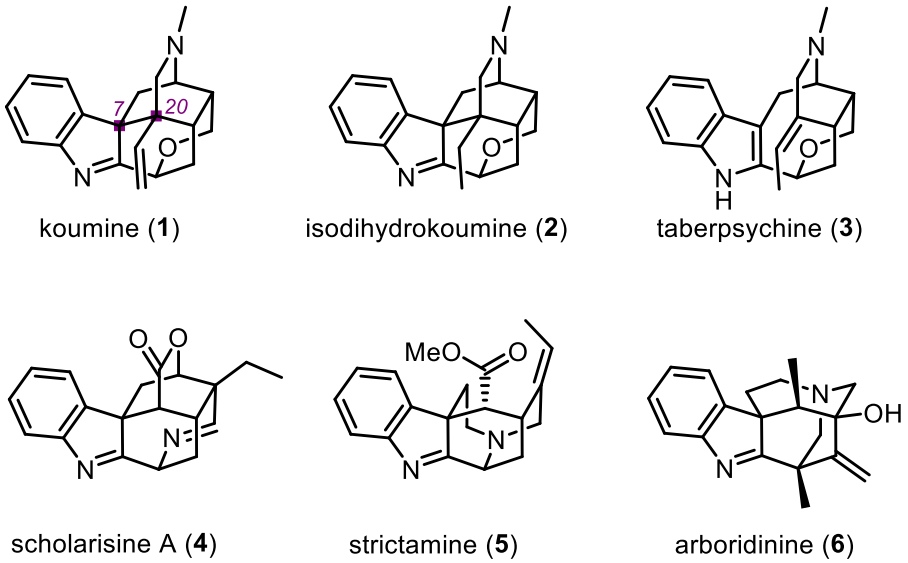

Figure 2.1. Structure of koumine (**1**) and other indole alkaloids sharing its structural motifs

Koumine is part of a number of highly complex indole alkaloids targeted by our group, among them scholarisine A (**4**), strictamine (**5**), and arboridinine (**6**).[8–10] As was custom with our

work towards the aforementioned completed targets, our goal with this molecule was to rapidly introduce molecular complexity, in order to identify new ways of synthesizing and modifying cage-shaped molecules. Below we present several previously reported successful approaches that have allowed for access to koumine (**1**) and closely related compounds. As the majority of these approaches are biomimetic, we will also outline the proposed biosynthetic origin of koumine (**1**) and its precursors. We will then describe the rationales behind the two synthetic routes that we proposed and lay out the progress we were able to make and the challenges that remain to be solved.

*Section 2.1.1: Proposed Biosynthetic Pathway for Koumine (**1**) and Related Natural Products*

Despite the incredible diversity of monoterpene indole alkaloid natural products, which span many natural product families and are produced by a myriad of plants, there seems to be a relatively conserved biosynthetic logic for many of these compounds. Over the past six decades, isotope labeling studies, feeding studies with synthetic intermediates, and more recently the more targeted identification of the key genes and enzymes, have identified the biosynthetic machinery and pathways involved in the biosynthesis of these targets.[11] A complicating factor for identifying the biosynthetic pathways of natural products in plants is that unlike in bacteria and fungi, enzyme-encoding genes are not typically located in gene clusters, but are distributed throughout the genome.[12,13] Natural products such as those discussed in Figure 2.1 above, as well as other indole alkaloids, such as the *Gelsemium*-derived gelsemine (**9**), sarpagine (**10**), vinorine (**11**), and the highly toxic strychnine (**12**), have all shown to ultimately derive from tryptamine (**7**), and the monoterpenoid, secologanin (**8**). Secologanin (**8**) can, in turn, be traced back to isoprene building blocks ubiquitous in terpene biosynthesis. Of note, many of the early studies discussed herein had

not yet focused on elucidating the biosynthesis of koumine (**1**), as the structure had yet to be determined at that time.

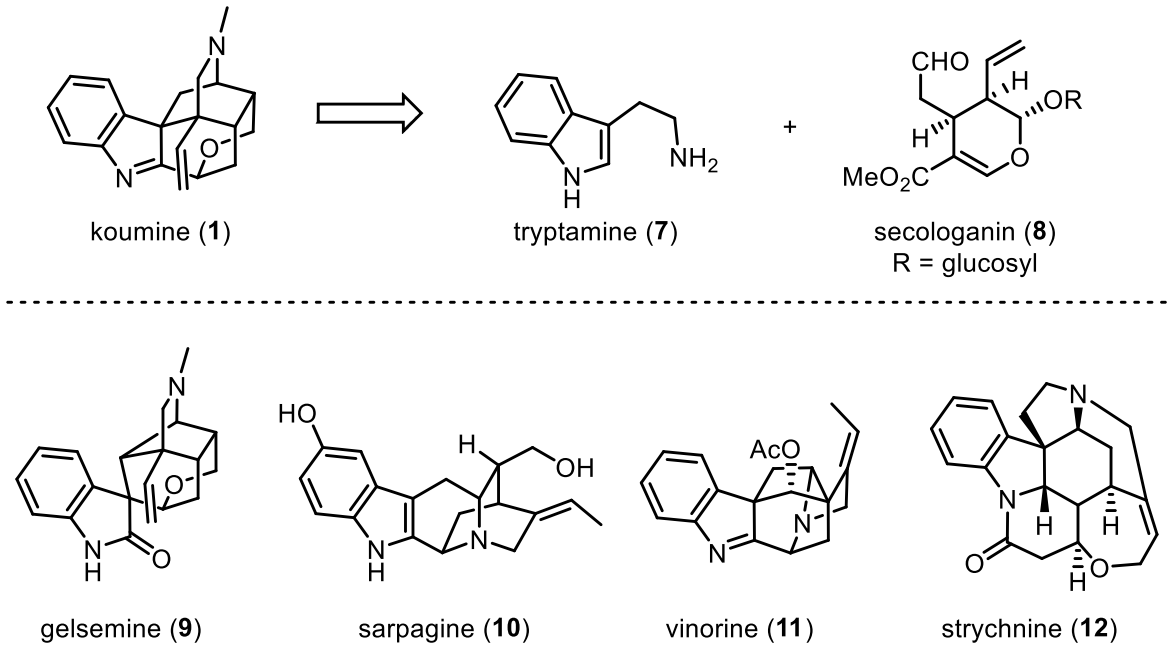

Scheme 2.1. Biosynthetic origin of koumine (**1**) and related indole alkaloids generated via the same intermediates

In the late 1960's, pioneering work by Battersby and Smith established that a condensation, mediated by strictosidine synthase (**SS**) and reminiscent of a Pictet–Spengler reaction, between secologanin (**8** and tryptamine (**7**) forms the key intermediate strictosidine (**13**, Scheme 2.2).[14] **13** is subsequently deglucosylated by strictosidine glucosidase (SGD) to its aglycon **14**. At this point another key intermediate for monoterpene indole alkaloid biosynthesis, geissoschizine (**16**), is formed by condensation of the lactol within strictosidine aglycon (**14**) onto the secondary amine within the β-carboline framework and a subsequent reduction of the imine by geissoschizine synthase (**GS**).

O'Connor and Courdavault have recently identified the enzymes in the biosynthetic pathways of **12**. There, geissoschizine (**16**) undergoes a complex oxidative carbon framework

rearrangement, ultimately leading to *Strychnos* alkaloids such as (**12**).[15] Although the activity of the P450 enzyme involved had been discovered previously, this work identified the genes encoding the enzyme and shed light on the mechanism. In a similar fashion, the conversion of geissoschizine (**16**) to the quinuclidine-containing species **18** had been known.[16] O'Connor *et al*. then identified the relevant genes and characterized the enzymes involved in this process.[17] The reaction proceeds via a formal intramolecular oxidative Mannich reaction, catalyzed by sarpagan bridge enzyme (**SBE**), and forms the polyneuridine aldehyde **18**, which not only bears the skeleton of natural products like sarpagine (**10**), but is also elaborated to ajmalan-type alkaloids like vinorine (**11**).

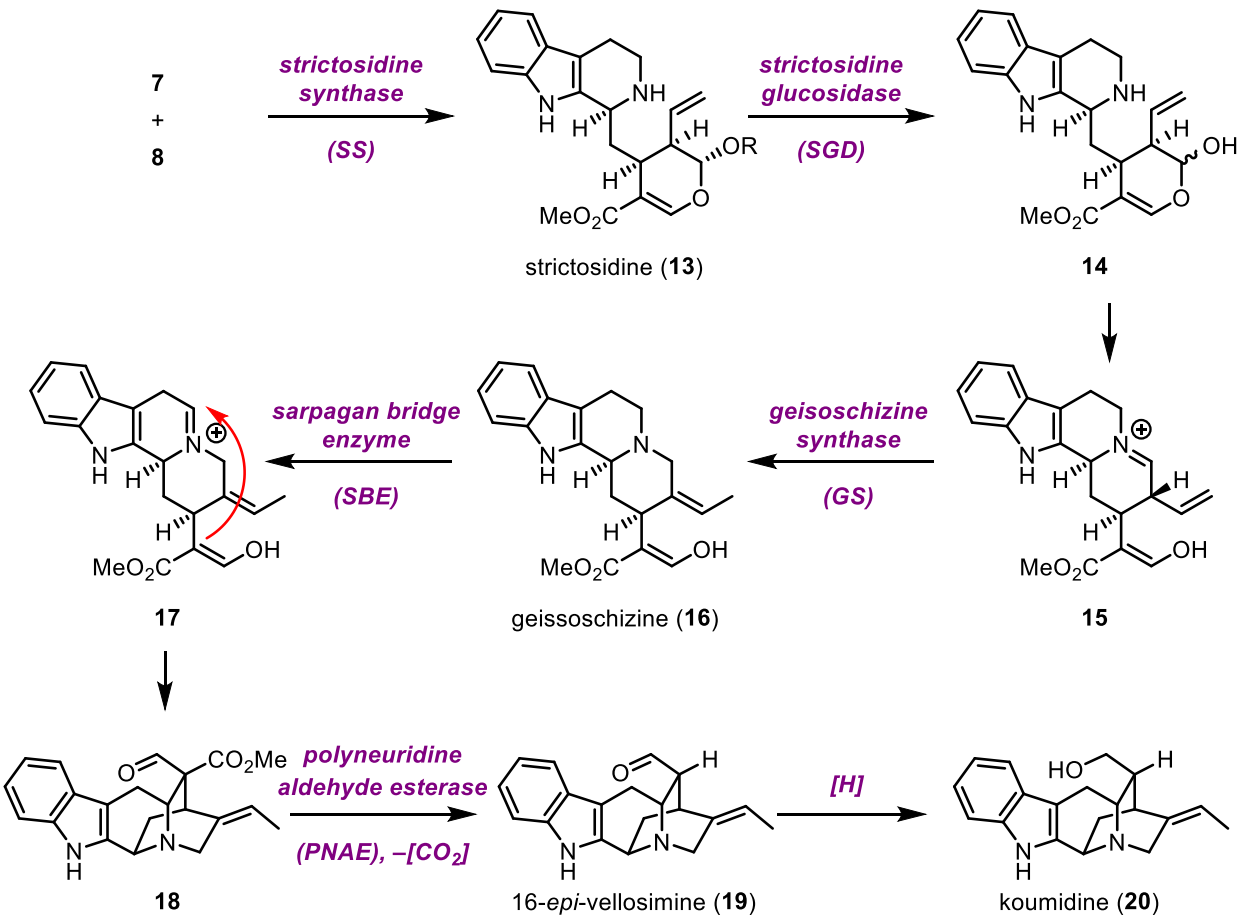

Scheme 2.2. Biosynthetic pathway of many indole alkaloids starting from strictosidine (**13**) formation

Though there have not been any recent studies that conclusively established an enzymatic link between **18** and the *Gelsemium* alkaloids gelsemine (**9**) and koumine (**1**), such a connection has been suggested by researchers, and is bolstered by a range of biomimetic total syntheses, some of which are discussed in Section 2.1.2. It has been shown that 16-*epi*-vellosimine (**19**) arises from **18** via a polyneuridine aldehyde esterase (PNAE)-promoted decarboxylation.[18] Though no definite connection has been identified to date, it seems plausible that koumidine (**20**) can arise from **19** via simple reduction. Soon after the structural elucidation of koumine (**1**), Lounasmaa proposed a *N*-methylation-induced rearrangement (Scheme 2.3) of the carbon skeleton of koumidine (**20**) to koumine (**1**).[19] It is unclear whether the quinuclidine ring is opened by an intermolecular process or oxidation, as suggested by Lounasmaa, or by an intramolecular nucleophilic substitution by the primary alcohol to form the ether within **23**, as suggested by biomimetic laboratory synthetic efforts and shown here (Scheme 2.3). Other groups have put forward similar proposals naming **20** as a key intermediate.[20,21] The biosynthesis of koumine (**1**) concludes with an intramolecular S_N2'-type cyclization, forming the highly caged hexacyclic framework.

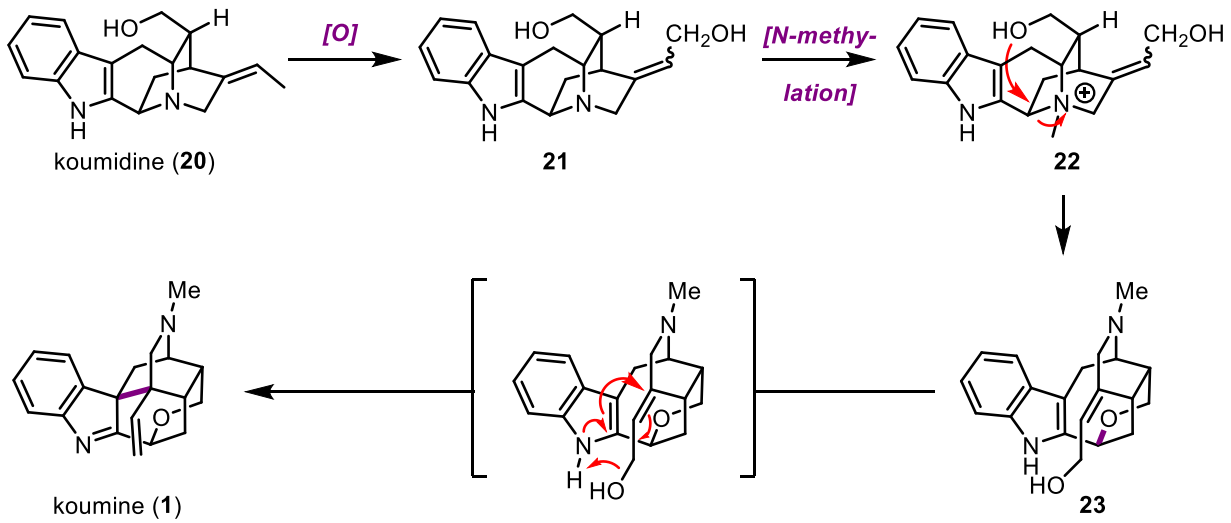

Scheme 2.3. Proposed biosynthetic transformation of 16-*epi*-normacusine B (**20**) to koumine (**1**) via a quinuclidine rearrangement cascade

Recent work to identify and characterize the genes and enzymes involved in the biosynthesis of *Strychnos* and ajmaline-like alkaloids has produced fascinating insight into how plants forge these highly complex monoterpene indole alkaloids. With the rapid advances made in the past decade, it is only a question of time until the scientific community shines a light on the processes connecting the skeleton of the sarpagine-like alkaloids to those of the *Gelsemium* alkaloids.

*Section 2.1.2: Prior Total Syntheses of Koumine (**1**) and Related Natural Products*

To date, there are four published total syntheses of koumine (**1**), as well as a total synthesis of its structural congener, isodihydrokoumine (**2**).[1,6,22–27] While some of the total syntheses have taken a biomimetic approach, following the biosynthetic proposal put forth by Lounasmaa, a recent total synthesis bypassed the key rearrangement of a quinuclidine-containing *aza*-bicycle. With this quinuclidine species itself being close congeners to the sarpagan alkaloids, the biomimetic total syntheses of **1** also report total syntheses of several other sarpagan-type natural products. In this section, we will discuss the various reports, starting with a total synthesis achieved by Magnus and co-workers, which was disclosed less than a decade after the structure of koumine (**1**) was published.[22,23]

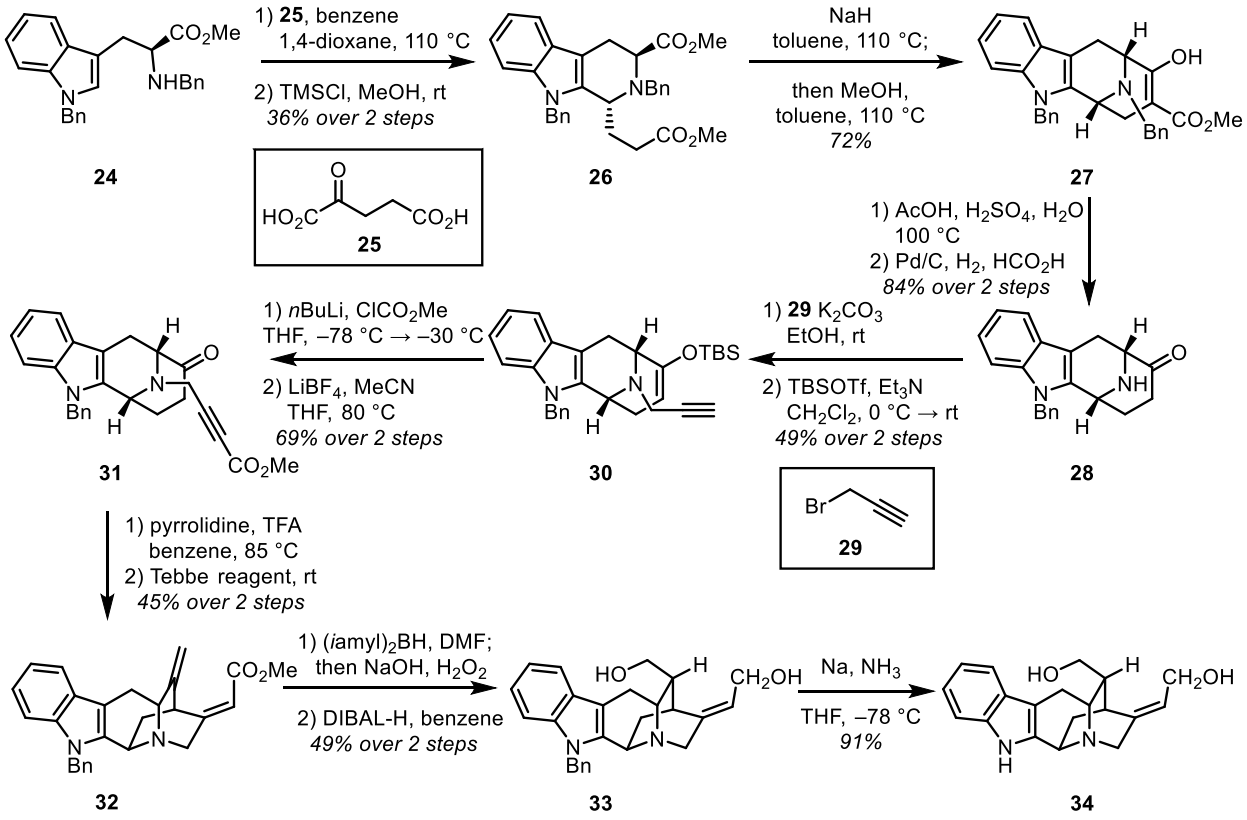

Scheme 2.4. Initial phase of the Magnus group's total synthesis of koumine (**1**) leading to the biomimetic rearrangement precursor **34.**

The synthesis commenced with a Pictet–Spengler reaction of doubly benzyl-protected tryptophan (**24**) with ketoglutaric acid (**25**), followed by esterification to afford β-carboline **26**. A subsequent Dieckmann condensation allows concise access to the [3.3.1]-*aza*-bicycle **27**. At this stage, Magnus *et al*. set up a sequence of reactions to complete the quinuclidine core needed for the biomimetic rearrangement discussed above. Hydrolysis and decarboxylation of the 1,3-dicarbonyl in **27** is followed by debenzylation of the bridging amine to afford **28**. A four-step sequence consisting of *N*-alkylation with propargyl bromide (**29**), ketone protection as its silyl enol ether **30**, alkyne carbonylation, and ketone deprotection yielded the cyclization precursor ynoate **31**. An intramolecular Michael addition into the ynoate within **31** is followed by methylenation of the ketone to quinuclidine-containing enoate **32**. With the quinuclidine species in hand, the

Magnus group closed in on their biomimetic rearrangement cascade via a hydroboration/oxidation of the 1,1-disubstituted alkene and DIBAL-H reduction of the methyl ester. *N*-debenzylation of **33** then afforded key diol **34**, in a total of 18 steps from tryptophan.

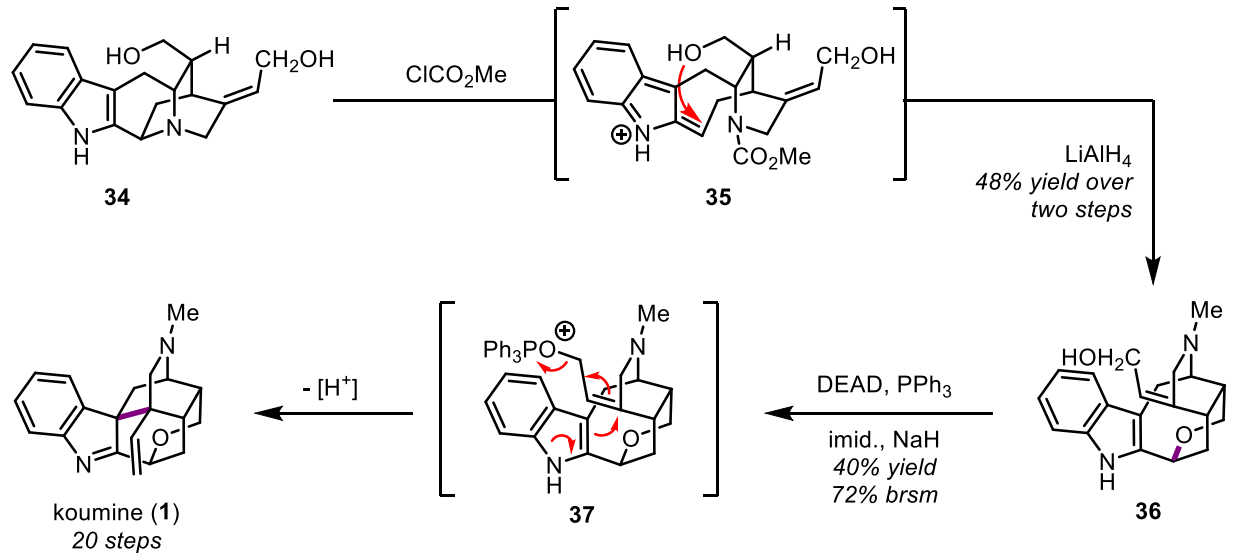

Scheme 2.5. Completion of the Magnus group's total synthesis of koumine (**1**) via a late-stage biomimetic rearrangement to the koumine framework.

The last two steps of the total synthesis of koumine (**1**) include the biomimetic rearrangement and an intramolecular Mitsunobu reaction. The biomimetic rearrangement is triggered by formation of methyl carbamate **35**, with concomitant cleavage of the quinuclidine by the electron-rich indole. The pendant alcohol then forms the pyran found within **36**, followed by reduction of the carbamate to the *N*-methyl group. The first total synthesis is completed by an intramolecular Mitsunobu reaction, a transformation that also mimics the biosynthetic proposal by Lounasmaa, to furnish koumine (**1**) in a total of 20 steps.

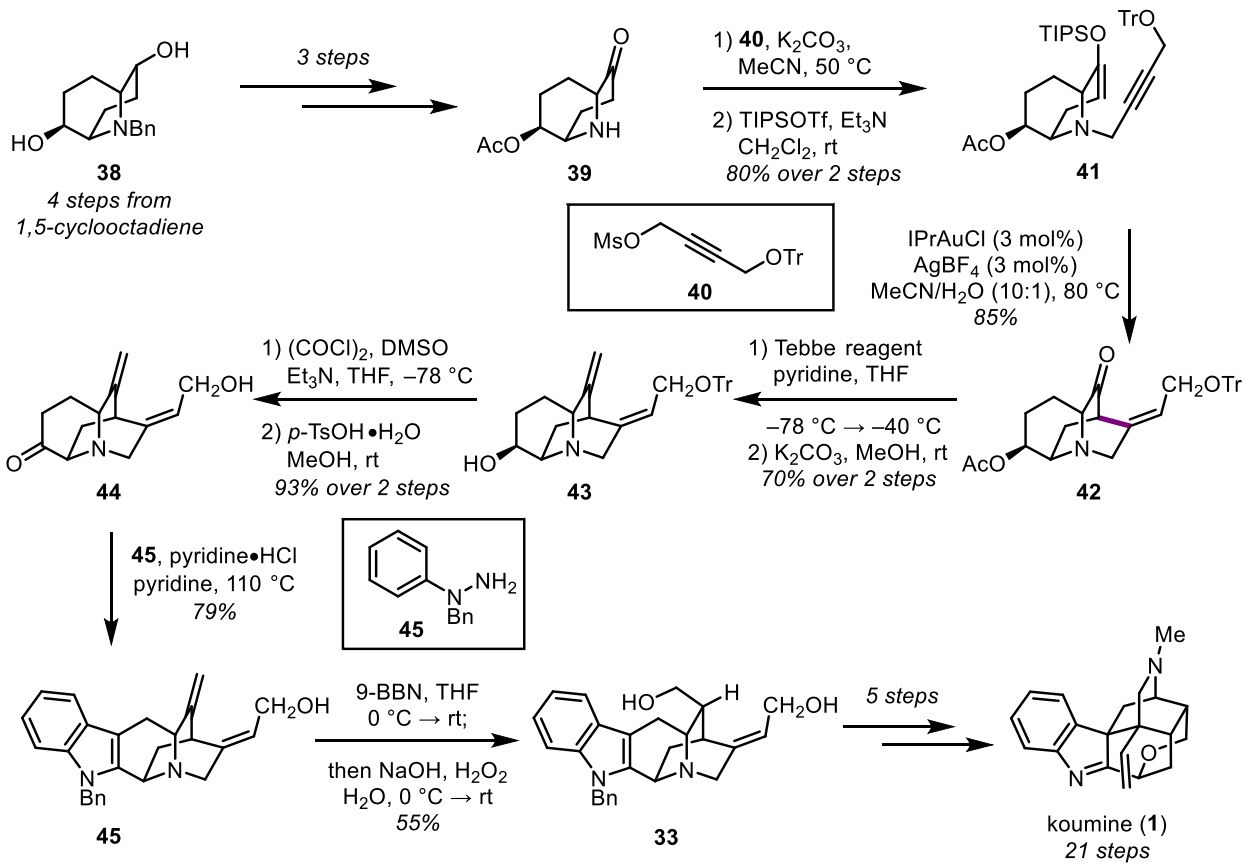

Scheme 2.6. Takayama *et* al's total synthesis of koumine (**1**).

More recently, Takayama *et al*. published a total synthesis of koumine (**1**).[24] In this approach, which intercepts the Magnus intermediate diol **33**, a previously reported four-step synthesis provided [3.3.1]-*aza*-bicycle **38** from 1,5-cyclooctadiene.[28] Three further synthetic operations form acetate **39**, which in turn is alkylated by 1,4-butynediol-derived mesylate **40**. The ketone is protected as its silyl enol ether to set up the formation of quinuclidine **42**. A Au^{I}-catalyzed Conia-ene cyclization of the silyl enol ether within **41** onto the tethered alkyne affords quinuclidine **42**. In a four-step sequence ketone **44** prepared, which is subjected to a Fischer indole synthesis. A hydroboration/oxidation reaction of resultant indole **45** then intercepts a key intermediate in the Magnus route. As such, the final steps in this approach mirror those in the original total synthesis,

including a palladium-catalyzed intramolecular Tsuji–Trost reaction to close the final ring, akin to Magnus' Mitsunobu approach.

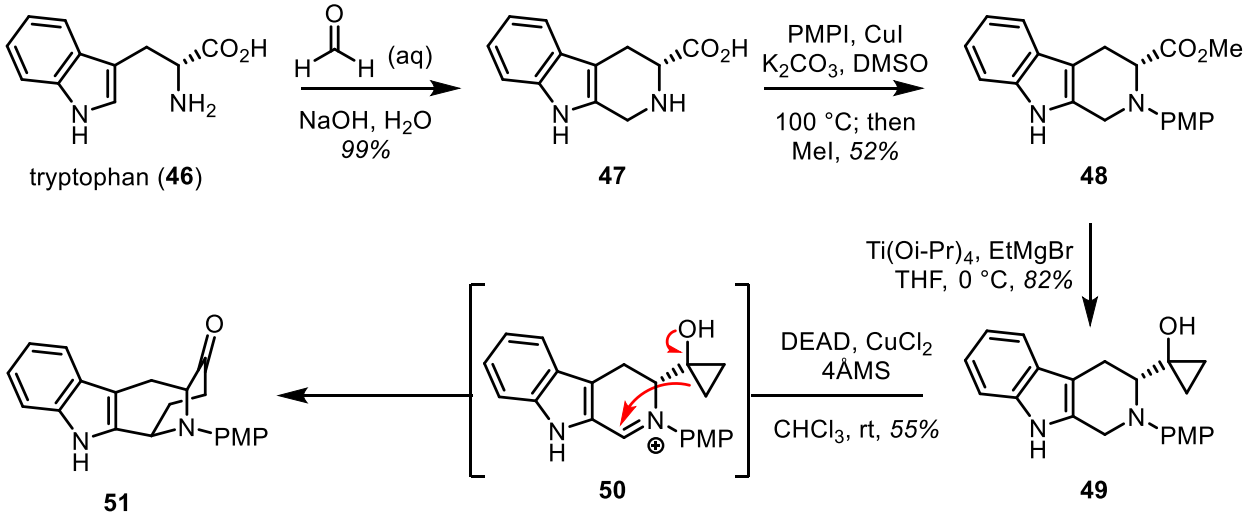

Scheme 2.7. Zhang *et al.*'s total synthesis of koumine (**1**) features formation of tetracyclic ketone **51** via a Kulinkovich cyclopropanation and semi-pinacol rearrangement

In addition to the approaches published by Magnus and Takayama, which rely on a biomimetic cascade of the sarpagan framework, Zhang *et al.* have reported their entry into biomimetic total syntheses of koumine (**1**).[26] While the approach still features a similar rearrangement, the manner of quinuclidine construction and the mode of the final intramolecular cyclization differs. This route commences with a Pictet–Spengler reaction of tryptophan to construct the tetrahydro-β-carboline within **47**. Subsequent amine protection and esterification affords ester **48**, which in the next step is transformed to the cyclopropyl alcohol **49** through a Kulinkovich cyclopropanation. This sets up an elegant oxidative ring expansion, wherein the amine is first oxidized to its iminium species **50** followed by alkyl migration via a semi-pinacol rearrangement, leading to tetracyclic ketone **51**.

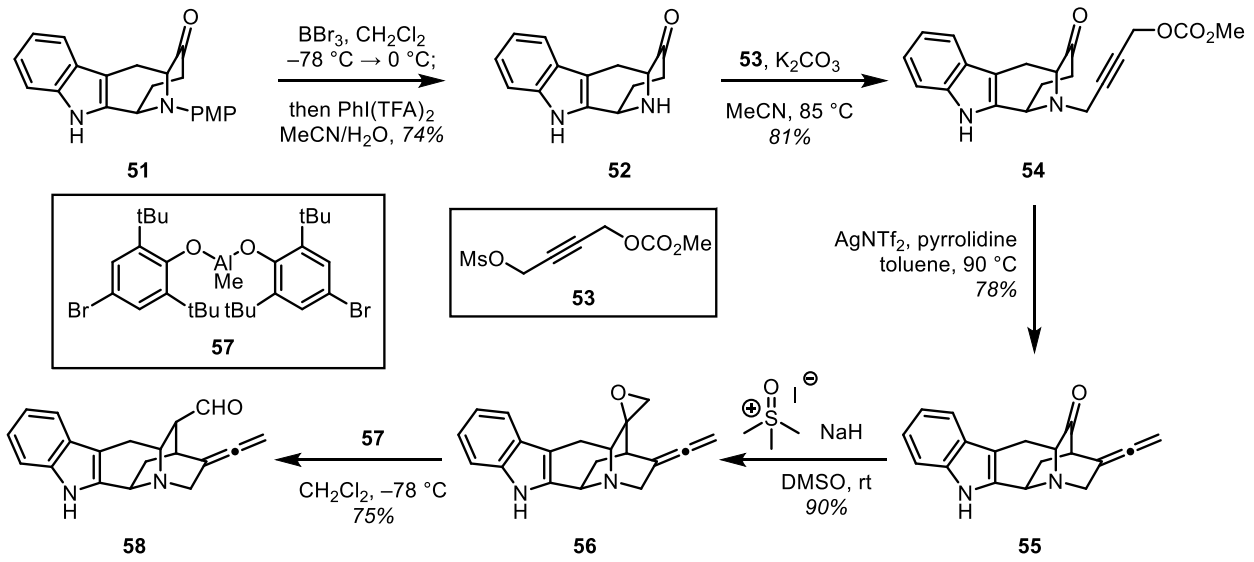

Scheme 2.8. Aldehyde **58** is formed as a biomimetic rearrangement precursor *en route* to koumine (**1**).

With ketone **51** in hand, Zhang and co-workers perform a deprotection and alkylation sequence with a 1,4-butynediol-derived mesylate **53** to form the propargyl amine within **54**, which closely resembles the tetracyclic intermediates by Magnus and Takayama. In an approach slightly diverging from its precedents, Ag^{I}-mediated cyclization onto the alkyne leads to allene **55**, which is further elaborated, first to epoxide **56** by a Corey-Chaykovsky reaction, then to aldehyde **58** via a Lewis acid-mediated Meinwald rearrangement. At this stage, Zhang *et al*. also report the total syntheses of several sarpagan-type natural products by a variety of synthetic operations at the carbonyl within **58**.

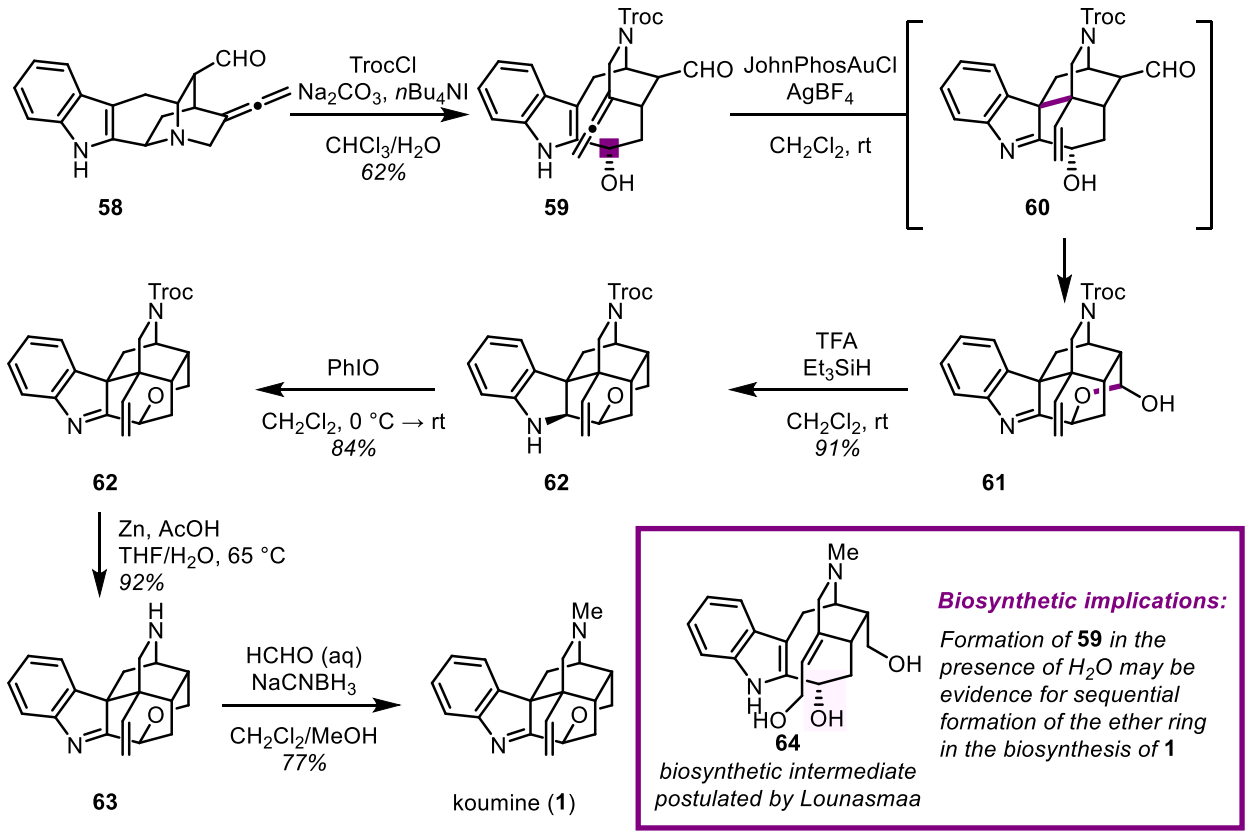

Scheme 2.9. Zhang *et al.*'s total synthesis of koumine (**1**) is completed by initial *aza*-bicycle formation, followed by the cyclic ether to complete the koumine skeleton.

The biomimetic cascade of quinuclidine **58** is triggered by Troc carbamate. The resultant aldehyde **59** is formed by trapping of the intermediate carbocation with H_2O at the carbon indicated in purple. This compound could serve as evidence for the intermediate **64** postulated by Lounasmaa, who proposed a similar trapping event, instead of a direct intramolecular etherification. It is clear that there is no pendant alcohol present within **59** that would readily form the cyclic ether, however, it is still significant to see that such trapping of a cationic intermediate at the same position can occur. The next step in the Zhang synthesis of koumine (**1**) involves a Au^I-catalyzed intramolecular Conia-ene-type cyclization in which the indole in **59** attacks the activated allene, followed by epimerization of the pendant aldehyde, which is trapped as its corresponding lactol. The lactol is subsequently reduced to the ether, with concomitant reduction

of the indolenine. Oxidation with iodosobenzene and reductive carbamate deprotection affords **62**, which is converted into koumine (**1**) by reductive amination. This total synthesis relies on the same biomimetic strategy as the syntheses discussed previously, yet utilizes the rearrangement with a different set of pendant functional groups, thus alternating the order of bond formation toward the koumine framework.

The final total synthesis of a *Gelsemium* alkaloid natural product to be discussed in this chapter is that of isodihydrokoumine (**2**) reported by Kerr in 2018.[25] This synthesis takes an entirely different approach to generating the carbocyclic framework of **1**, leading to an elegant cascade that still follows a similar bond-forming logic seen in the proposed biosynthesis. In a sense, it is fitting that the synthesis commences with construction of what will be elaborated into the *aza*-bicycle, only later introducing the indole moiety. A Pd^0-catalyzed hydrostannylation of propargyl alcohol (**65**) is followed by an *in situ* formation of palladium black, which catalyzes a Stille coupling with vinyl iodide **66**, leading to the formation of δ-lactone **67**. Conjugate addition at the β-position of the lactone with vinyl cuprate is followed by reduction to diol **69**. A chemoselective Mitsunobu reaction at the allylic alcohol with bis-carbamate protected hydroxylamine afforded alcohol **70**. Acid-mediated deprotection and nitrone-formation by addition of indoline-containing aldehyde **71** sets up the key [3+2] cycloaddition. Upon heating, nitrone **72** undergoes a cycloaddition to give isoxazolidine **73**. A subsequent three-step sequence including deprotection of the *p*-toluenesulfonamide, oxidative aromatization, and *N*–O ring cleavage leads to acetal **74**, which serves as a cyclization precursor to the koumine skeleton.

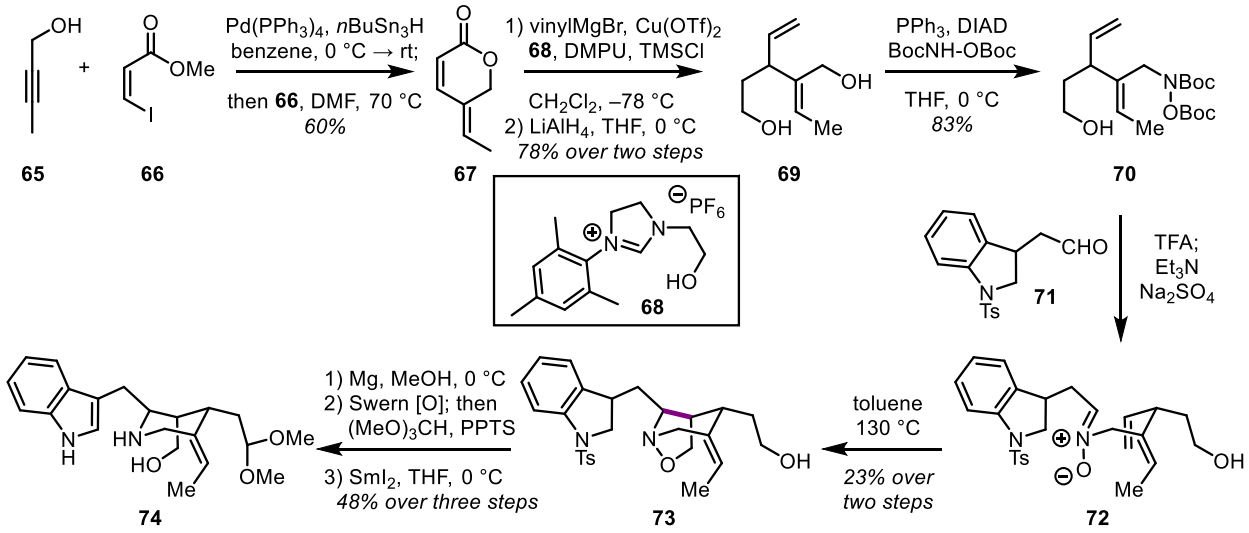

Scheme 2.10. The initial stage of Kerr's total synthesis of isodihydrokoumine (**2**) produces piperidine **74** via an intramolecular nitrone [3+2] cyclization.

Impressively, the Kerr team was then able to forge the remaining three rings in one synthetic operation. In this event, using *in situ*-generated TMSI as a Lewis acid, the alcohol within **74** condensed onto the acetal, forming a cyclic oxonium ion **75** which then underwent a Friedel–Crafts reaction with the C-2 position of the indole. After rearomatization, an ene-reaction generates the two remaining all-carbon quaternary centers and the synthesis is completed through installation of the *N*-methyl group to afford isodihydrokoumine (**2**) in 11 steps. By employing BF_3•OEt_2 as an alternative Lewis acid, intermediate **76** could be generated, which allowed for a formal synthesis of koumine (**1**).[21] This total synthesis managed to combine both the biomimetic origami-like molecular folding cascade that elegantly transforms the cyclization precursor **74** into the highly cage-shaped **77** in a single synthetic step, with an overall strategic application of modern organic chemistry to complete the concise total synthesis of isodihydrokoumine (**2**).

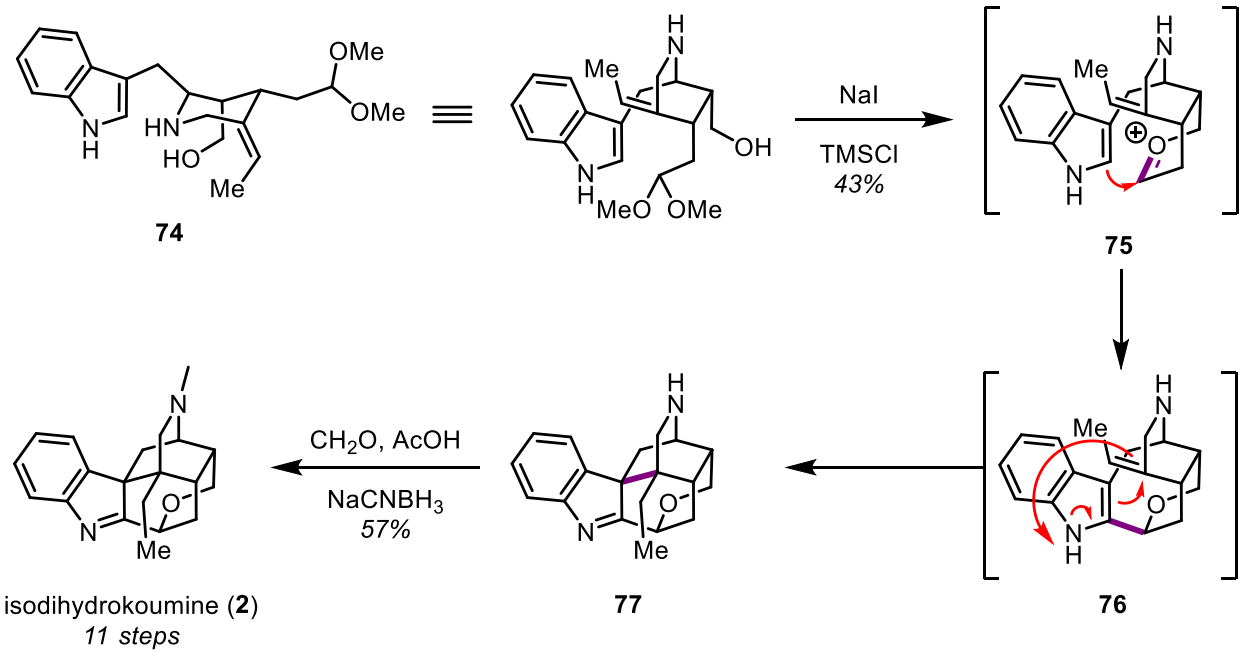

Scheme 2.11. The Kerr group completes the total synthesis of isodihydrokoumine (**2**) with a Lewis acid-mediated cascade.

Overall, the currently reported total syntheses of koumine (**1**) have all relied on a similar strategy of cage-shaped framework construction, following the biosynthetic proposal.[29] Nevertheless, there is some amount of variety within these approaches, as each approach employs unique tactics in either construction of the quinuclidine rearrangement precursor, or in choosing the entry point into the biomimetic rearrangement cascade. Common to each approach is the key connection between C-7 and C-20 of koumine (**1**, cf. Figure 2.1) triggered by nucleophilic attack of the indole. In our synthetic design, we attempted to counter this paradigm by forming this bond relatively early, and as such move away from the biomimetic strategy predominating the literature thus far.

*Section 2.2: Development of a Non-Biomimetic Strategy Toward the Total Synthesis of Koumine (**1**)*

Our prime inspiration came from the total synthesis of scholarisine A (**4**) by our group.[30] Here, they achieved a concise 15-step synthesis of this structurally related akuammiline natural product. Central to their approach was a rapid formation of the tetracyclic cage-shaped core of scholarisine A (**4**) via an enantiospecific pyrone Diels–Alder reaction. Starting from methyl coumalate (**74**) and serine-derived vinyl ketone (**75**), they forged the [2.2.2]-bicyclic lactone **76** with moderate d.r. A subsequent acetonide deprotection and Appel reaction at the resultant primary alcohol afforded bromide **77**, which underwent an intramolecular Giese-type radical cyclization into the enoate within **77**. The tertiary radical formed during this cyclization was trapped through a Keck-type allylation with allyltri-*n*-butylstannane (**78**) to afford tricyclic **79** in a stereoselective manner. It is notable that radical trapping only occurred from the less sterically encumbered *re*-face to form the *endo* ester. The cage-shaped core of scholarisine A (**4**) is completed by a two-step inversion sequence of the secondary amine to *syn*-aminoalcohol **81**, followed by lactam formation, oxidation of the secondary alcohol, and condensation of 2-iodoaniline (**82**) to yield tetracyclic imine **83**.

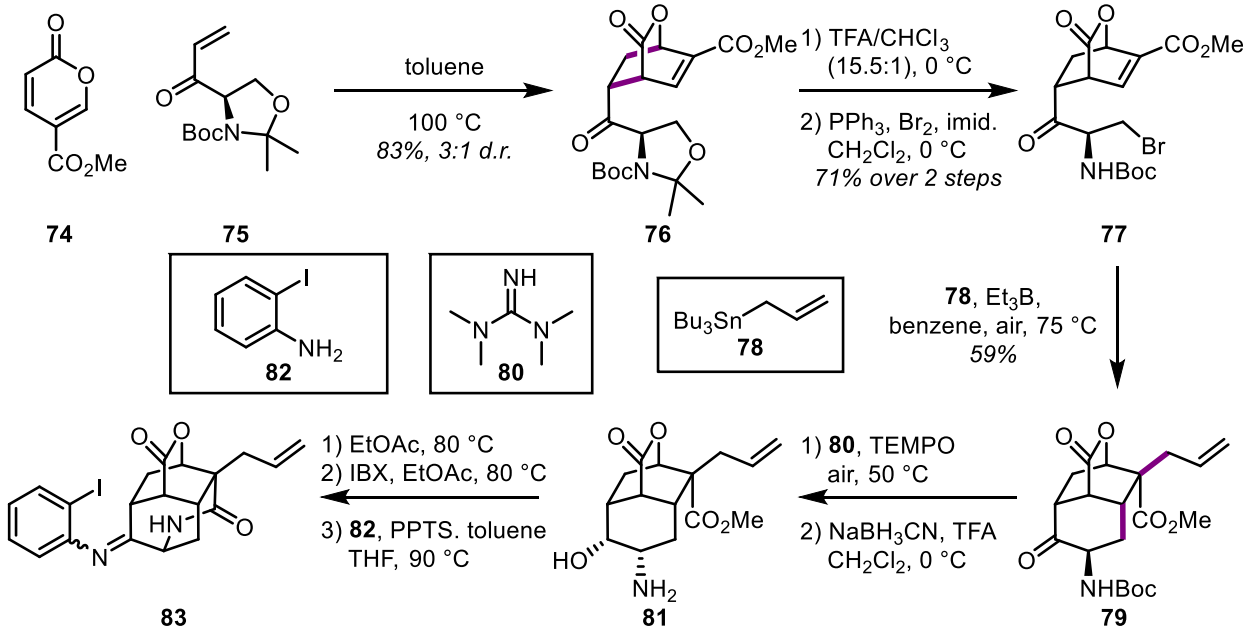

Scheme 2.12. Our group's total synthesis of scholarisine A (**4**) showcases an effective strategy to rapidly construct the cage-shaped tetracyclic core in **83**.

At this stage, three objectives remained in the total synthesis of scholarisine A (**4**): (1) formation of the indolenine moiety, (2) reductive dehomologation of the allyl group to an ethyl chain, and (3) reduction of the amide moiety to the cyclic imine. The first problem was elegantly solved with a strategically-designed radical-mediated C–H functionalization to form the indolenine. Treatment of imine **83** with *n*Bu_3SnH and the radical initiator **84** led to formation of a tin radical, which abstracted the aryl iodide within **83**. A subsequent 1,5-HAT forms the tertiary radical species **86**, which in turn undergoes a 5-*exo*-trig addition into the arene. Oxidative rearomatization of the resultant radical intermediate affords the now hexacyclic lactone **87**, thus completing the carbocyclic framework of scholarisine A (**4**). The solution to the second and third objectives discussed above were taken up in tandem. Ozonolysis and reductive work-up of the allyl group in lactone **87** is followed by treatment with Lawesson's reagent to form the thioimidate **88** via thiation of the lactam and dehydration. Desulfurization of **88** affords the desired imine and ethyl moieties found in the natural product. A final oxidation of the indoline to the indolenine,

which was reduced during the ozonolysis step, completes the total synthesis of scholarisine A (**4**) in a total of 15 steps.

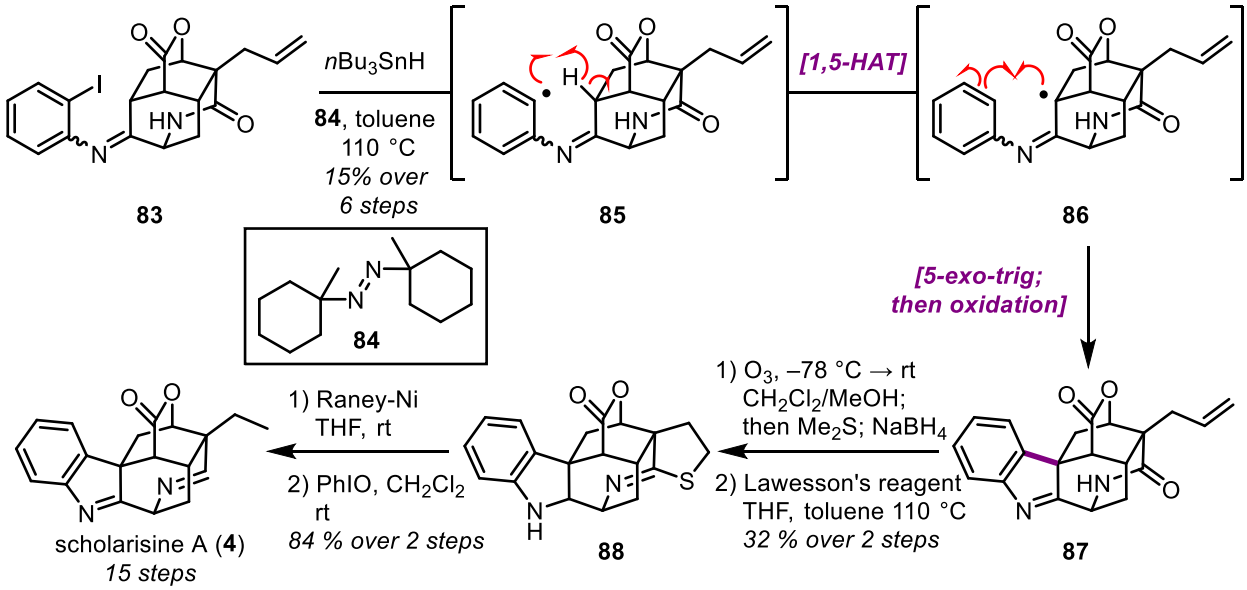

Scheme 2.13. The total synthesis of scholarisine A (**4**) is completed by an intramolecular C–H functionalization

With the similar hexacyclic core also found in koumine (**1**), scholarisine A (**4**) was a precedent that we sought to build on. As such, our key disconnections in our retrosynthetic analysis closely mirrored those of scholarisine A (**4**), with formation of the cyclic ether and the indolenine moiety at a late stage of our proposed synthesis (Scheme 2.14). Enone **90** can be traced back to the tricyclic lactam **91**, which in turn is envisioned to arise from a radical cyclization of pyridone Diels–Alder product **92**. The required starting material for this cycloaddition, pyridone **93**, can be accessed in a short sequence of operations from 6-hydroxynicotinic acid methyl ester (**XX**).

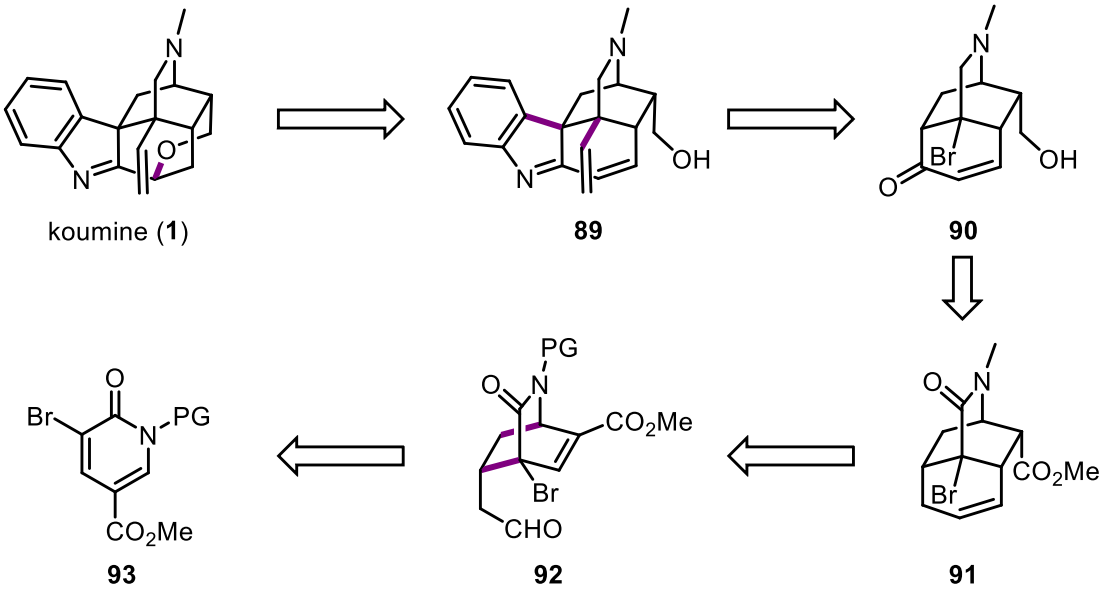

Scheme 2.14. Retrosynthetic analysis of a pyridone Diels–Alder reaction approach toward the total synthesis of koumine (**1**).

This synthetic approach utilizing an inverse electron-demand pyridone Diels–Alder reaction was encouraged by recent efforts within the group leading to the development of an enantioselective, dienamine-catalyzed, inverse electron-demand pyrone Diels–Alder reaction (Scheme 2.15).[31,32] This method uses the Hayashi–Jørgensen proline-derived catalyst **95**, which forms dienamine **97** upon condensation onto α,β-unsaturated aldehyde **94**.[33] A subsequent [4+2] cycloaddition using the β,γ-position of the dienamine as the electron-rich dienophile partner forges the bicyclic lactone **96** in an asymmetric fashion. With our retrosynthetic analysis of koumine (**1**) centering around the azabicyclo-[2.2.2]-octane ring, we set out to develop a method that could access this framework via an analogous inverse electron-demand pyridone Diels–Alder reaction. If successful, this approach would be, to the best of our knowledge, the first application of an enantioselective inverse electron-demand pyridone Diels–Alder reaction to natural product total synthesis. In addition, what sets this approach apart from the previous total syntheses is that, as

discussed above, it allows for accessing koumine (**1**) in a manner orthogonal to the biosynthetic proposal.

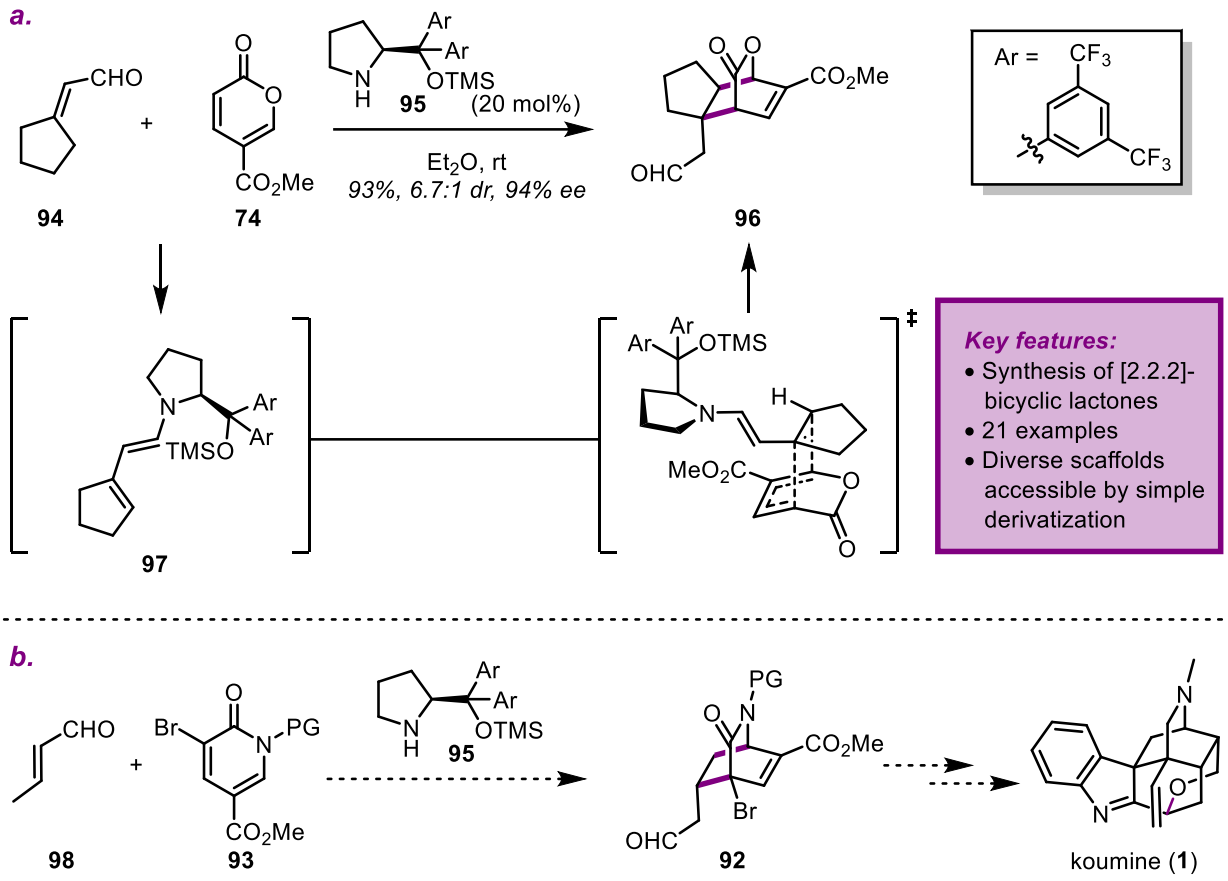

Scheme 2.15. *a.* Asymmetric inverse electron-demand pyrone Diels–Alder reaction developed in our group *b.* Proposed analogous inverse electron-demand pyridone Diels–Alder reaction.

Though much rarer than the pyrone Diels–Alder reaction, owing to the increased aromatic character of the pyridone system relative to the pyrone, there are a variety of examples showing pyridone Diels–Alder cycloadditions forming both fused and bridged bicyclic systems.[34,35] The only asymmetric pyridone Diels–Alder reaction reported to date is an enantioselective normal electron-demand pyridone Diels–Alder reaction to produce bridged bicyclic systems (Scheme 2.16).[36] Unfortunately, this method is limited in scope for both of the reaction partners. In particular, the electron rich 5-hydroxypyridones does not produce the structural motif required to

access the koumine core and results in a bridgehead hydroxyl group whose further elaboration is not facile. Prior work by the Posner group showed that the electron poor pyridone sulfonamide **103** can undergo a racemic IEDDA in the presence of alkyl vinyl ethers to form bicyclic lactam **105** (Scheme 2.16).[37]

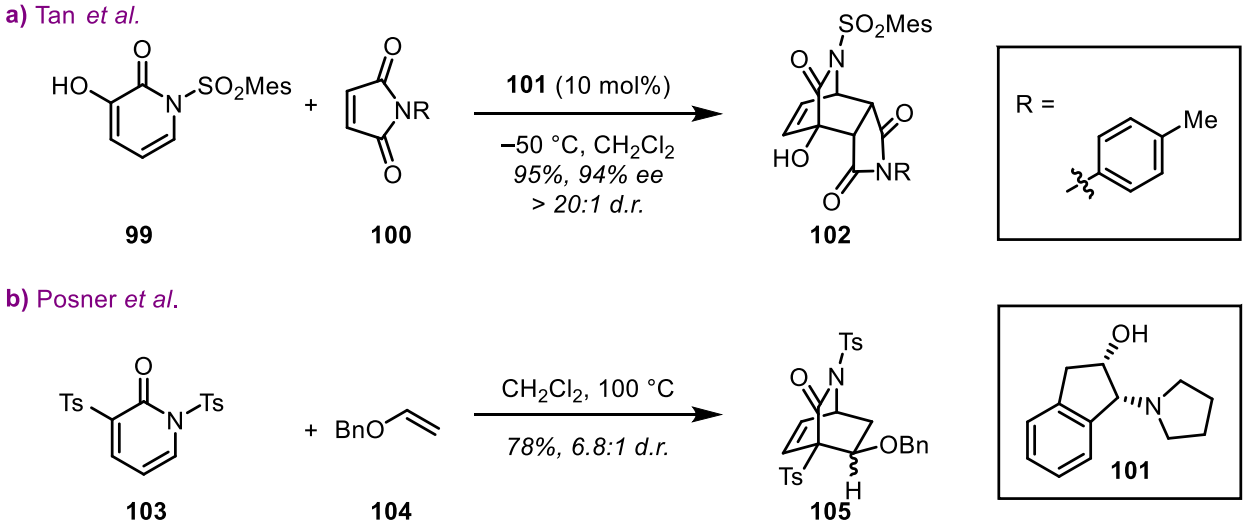

Scheme 2.16. Previous examples of normal and inverse electron-demand Diels–Alder reactions.

While this system gave us a good starting point in understanding reactivity patterns and the necessity of an electron-deficient pyridone ring, we found that **105** did not map onto the koumine scaffold in such a way that it could allow for any real synthetic expediency. We noticed, however, that by analogy to the previously reported pyrone Diels–Alder work, the inverse electron-demand pyridone Diels–Alder reaction product between protected methyl 5-bromonicotinate (**93**) and crotonaldehyde (**98**) should give bridged lactam **92** with substitution patterns matching the core structure of koumine (**1**). Thus, working around this central transformation, we envisioned the first disconnection to be the formation of the pyran ring within **1** via a previously reported intramolecular hydroalkoxylation.[38,39] Late-stage radical-mediated bridgehead functionalization would then be used to install the vinyl group.[40] In turn, alcohol **89** could be obtained from the C–

H arylation strategy applied to scholarisine A (**4**), which would arise from a 1,5-type radical ring closure of a homologated halide derivative of aldehyde **92**. What sets this approach apart from the previous work is that it allows for accessing koumine (**1**) in an asymmetric fashion.

Section 2.3: Studies Toward the Total Synthesis of Koumine (1) via a Pyridone Diels–Alder Reaction

With the inverse electron-demand pyridone Diels–Alder reaction being a centerpiece to our proposed total synthesis of koumine (**1**), we decided to initially probe the efficiency of such a reaction. With the knowledge that pyridones were expected to be more resistant to react in the desired mode, we synthesized a series of pyridones that would allow us to screen for desired reactivity. Starting from 6-hydroxynicotinic acid methyl ester (**106**), we first undertook a standard bromination reaction to afford **107** in good yield. Subsequent deprotonation and addition of a range of arylsulfonyl chlorides led to a small variety of pyridone Diels–Alder reaction precursors. Strongly electron-withdrawing protecting groups that worked for the Posner group, such as *p*-toluene- (Ts), *p*-nitrobenzene- (Ns), and 2,4-dinitrobenzene- (DNs) sulfonamides performed best in forging the desired bridged bicycle. In our search for more step-economical protecting groups that could later be reduced to give the desired *N*-methyl amine in one step, we found that groups such as Boc, methylcarbamate, or Cbz were not electron withdrawing enough to undergo the dienamine-catalyzed cycloaddition. In addition, as Posner has observed previously, these carbonyl-based protecting groups suffer from N vs. O selectivity during protection, initially adding to the more nucleophilic nitrogen atom, yet over time migrating to form protected hydroxypyridine species.

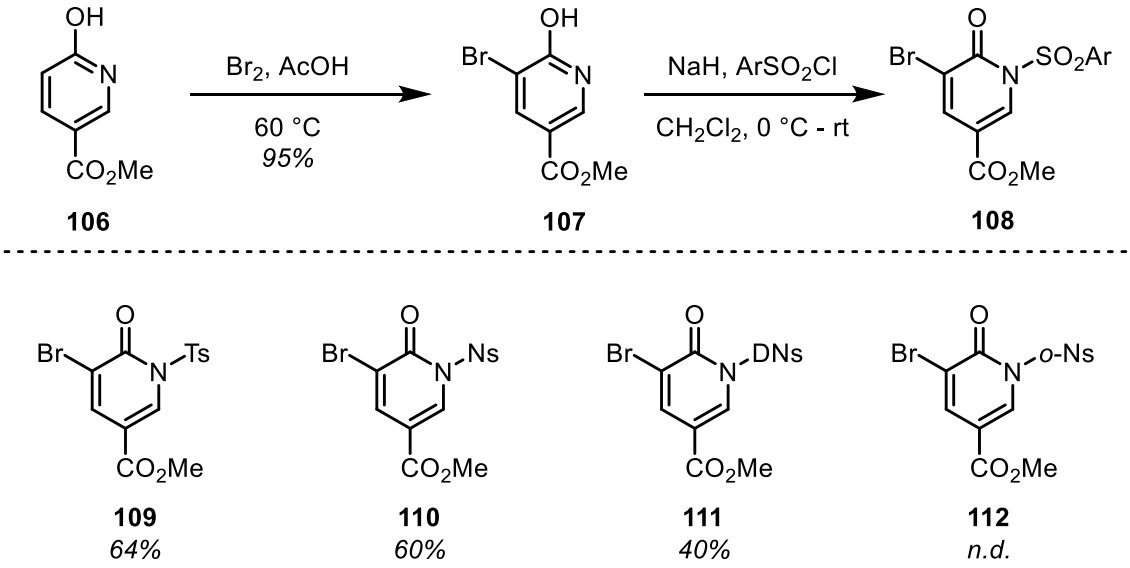

Scheme 2.17. Synthesis of pyridone Diels–Alder reaction precursors.

Using *p*-nitrobenzenesulfonyl pyridone **110** as our diene partner in the initial stages of our exploration, we screened a variety of enals and secondary amine catalysts in hopes of obtaining the desired *aza*-bicycle (Scheme 2.18). We were delighted to find that the reaction of **110** with crotonaldehyde (**98**) and a catalytic amount of TMS-protected prolinol **95** proceeded smoothly at room temperature, forming **115** in 68% yield and moderate *ee*. This result was promising, as such an asymmetric, inverse electron-demand Diels–Alder reaction has not, to the best of our knowledge, been previously reported.

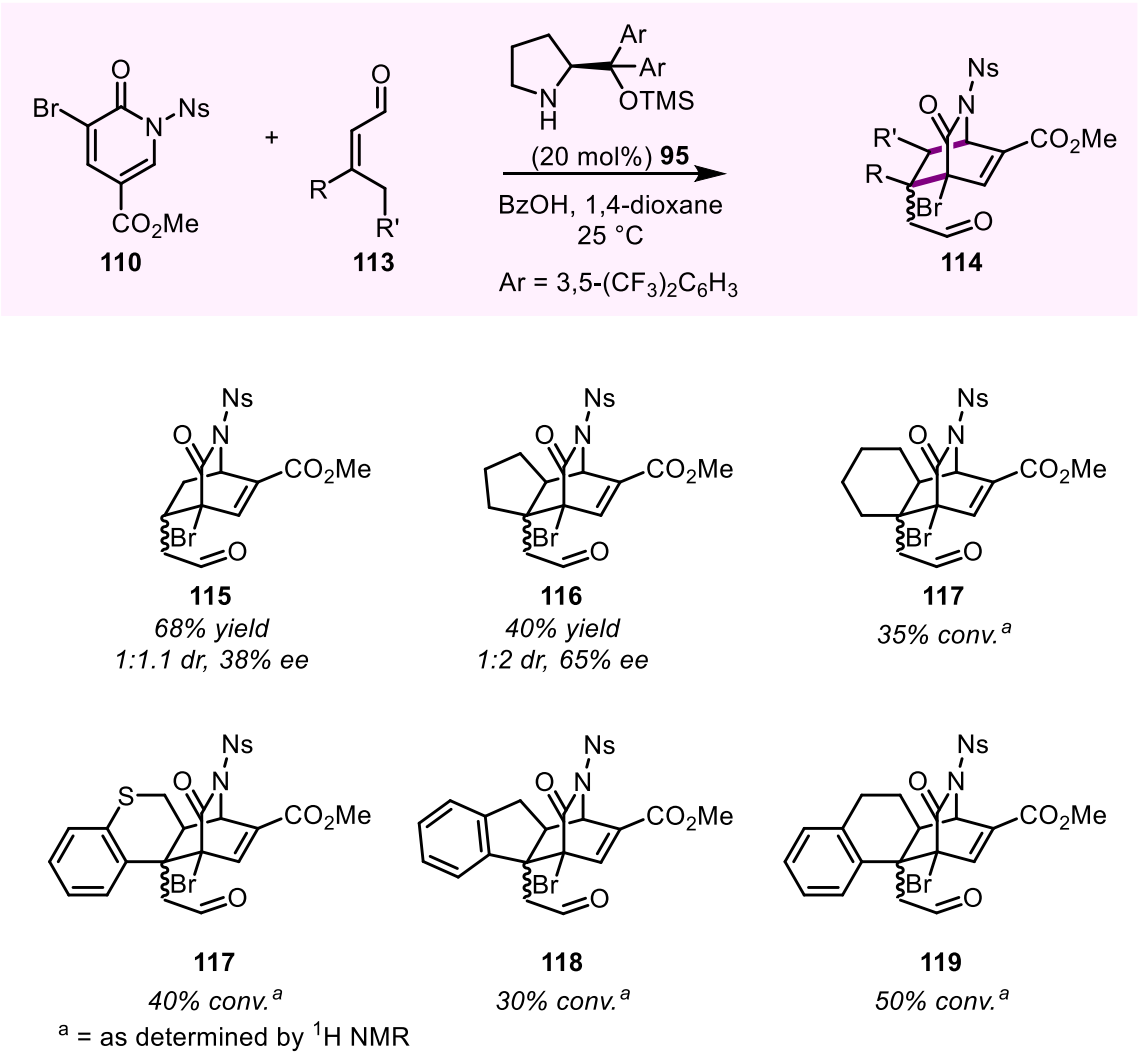

Scheme 2.18. Initial explorations of a novel inverse electron-demand pyridone Diels–Alder reaction.

Unfortunately, substrates that performed well in the pyrone variant of this reaction did not translate as smoothly here, despite much additional screening of conditions and catalytic systems with the general outcome being low conversion and enantioselectivity. Only the best-performing enal within the pyrone Diels–Alder method, leading to cycloadduct **XX**, converted, yet with dissatisfactory yield and a non-optimal *ee*. Despite further screening of reaction conditions and modes of catalysis we were unable to improve on these results. As such, we decided not to pursue development of this method and focused on elaborating cycloadduct **XX** toward the total synthesis of koumine (**1**).

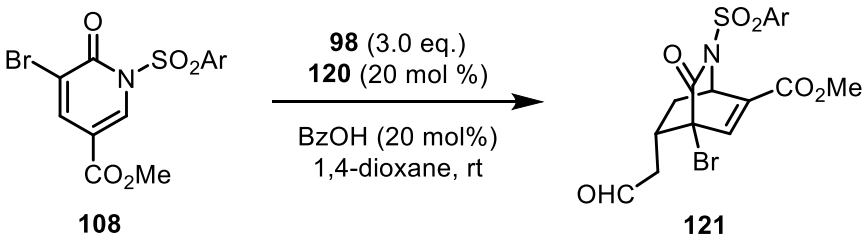

108 **121**

Entry	Substrate	Yield	d.r. (*exo*:*endo*)
1	**109**	*38*	*n.d.*
2	**110**	*60*	*1.1*:*1.*
3	**111**	*75*	*1.6*:1
4	**112**	*NR*	*N/A*

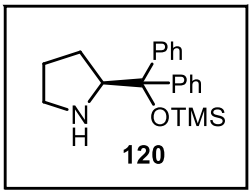

120

Scheme 2.19. Effect of sulfonamide protecting group on the pyridone Diels–Alder reaction.

Pressing forward with our synthetic studies toward koumine (**1**), we tested our remaining pyridones and found that besides the aforementioned *p*-Ns-pyridone **110**, both the *p*-Ts-pyridone **109** and the highly electron-deficient 2,4-DNs-pyridone **111** were competent in producing the desired cycloadduct. Interestingly, the *o*-Ns-pyridone did not show any desired product. Both due to the higher yield observed during the cycloaddition and the mild deprotection conditions, we decided to continue our investigation with the 2,4-DNs-protected cycloadduct **126** (Scheme 2.21). Typical deprotection of nitrosulfonamides proceeds via a S_NAr mechanism in which a sufficiently strong nucleophile attacks at the *ipso* carbon of the generic sulfonamide **122** (Scheme 2.20), which leads to the Meisenheimer complex **123** that ultimately expels SO_2 and releases the deprotected secondary amine.[41] For *p*-Ns-protected amines or amides a typical nucleophile used for deprotection is thiol in the presence of inorganic base. Unfortunately, in our cycloadducts, thiophenol, among other common thiol-based deprotection reagents, efficiently underwent a *thia*-Michael reaction with the enoate **115** in addition to performing the desired deprotection. To temporarily resolve this issue, a decision was made to use the 2,4-DNs-protected pyridone, as deprotection takes place by treatment with *n*$PrNH_2$, an even milder alternative.

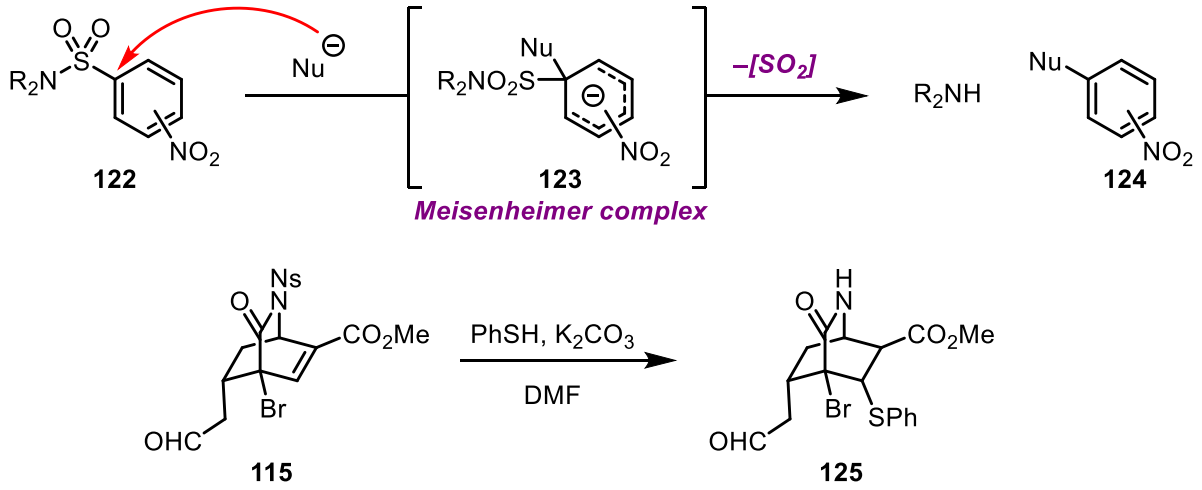

Scheme 2.20. Meisenheimer complex **123** in the S_NAr deprotection of *nitrobenzenesulfonamides.*

The next objective in our synthetic strategy was formation of the tricycle **91**, following the precedent set in our group's total synthesis of scholarisine A (**4**). For this, we needed to install a functional handle that would allow us to trigger a Giese reaction into the enoate within **126**. With sufficient quantities of cycloadduct **126** in hand, a number of olefination procedures were investigated. Widely used methods, such as Takai, Tebbe, Wittig, and Horner–Wadsworth–Emmons olefinations did not yield any desired vinyl halide product. It was discovered, however, that a Stork–Zhao olefination could provide vinyl iodide **128**, but only in low yields despite extensive screening of reaction conditions, including the use of a salt-free olefination.[42,43] Moderate to low yields are common for Stork–Zhao olefinations, but we hypothesize that the highly reactive sulfonamide protected, bridged lactam might contribute to the large amount of decomposition observed. In addition, the pendant aldehyde in **126**, once deprotonated at the a-position, is primed for a retro-vinylogous Michael reaction, with the resultant ring-opened intermediate being susceptible to a multitude of decomposition pathways. Subsequent deprotection of the 2,4-dinitrosulfonamide in **128** with *n*$PrNH_2$ and *N*-methylation proceeded in good yield to afford radical precursor **130**.[44] We envisioned forging this third ring via a radical-initiated 6-*exo*-

trig cyclization of a vinyl radical into the β-carbon of the α,β-unsaturated ester, trapping the resultant tertiary radical with *n*-Bu_3SnH. Based on previous work with scholarisine A (**4**), this process was hypothesized to give **91** as a single diastereomer, with hydride trapping from the *exo* face. Initial attempts gave either debromination, deiodination, sulfonamide cleavage, or uncontrolled decomposition of the material. A variety of other radical conditions were attempted; however, no desired product was ever obtained (Scheme 2.21).

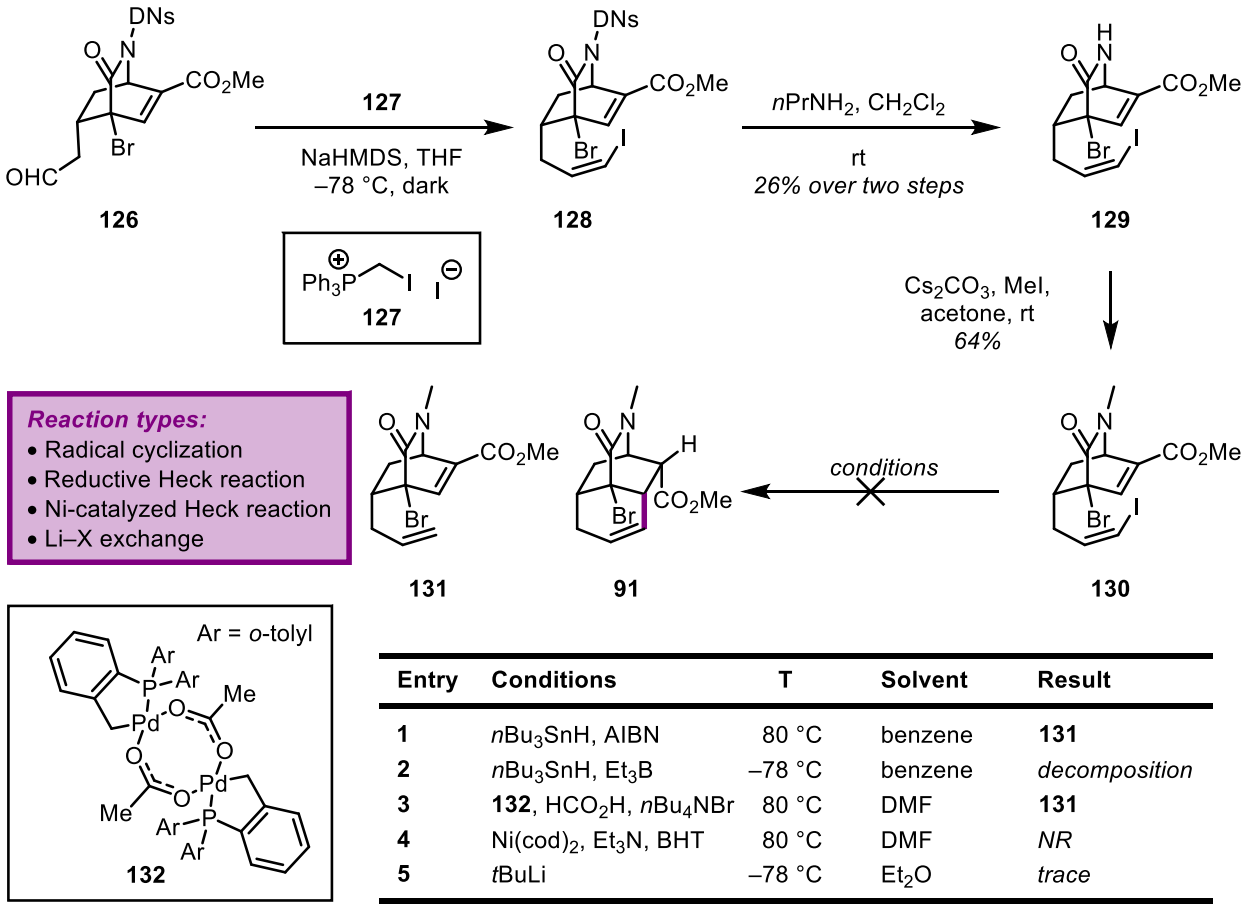

Entry	Conditions	T	Solvent	Result
1	*n*Bu_3SnH, AIBN	80 °C	benzene	**131**
2	*n*Bu_3SnH, Et_3B	–78 °C	benzene	*decomposition*
3	**132**, HCO_2H, *n*Bu_4NBr	80 °C	DMF	**131**
4	$Ni(cod)_2$, Et_3N, BHT	80 °C	DMF	*NR*
5	*t*BuLi	–78 °C	Et_2O	*trace*

Scheme 2.21. Attempts at forging tricyclic lactam **91** via several reaction types.

We then decided to turn to a reductive Heck-coupling approach. Using several Pd and Ni based procedures, including conditions reported by Baran *et al.*, we solely observed decomposition of our vinyl iodide starting material.[45] Treatment of **130** with *t*BuLi to trigger a Li–halogen

exchange, by which we hoped to create a transient vinyllithium species that could subsequently undergo an intramolecular 6-*exo*-trig conjugate addition, led to a trace amount of what we hypothesized to be the desired product, but mass recovery was minimal.

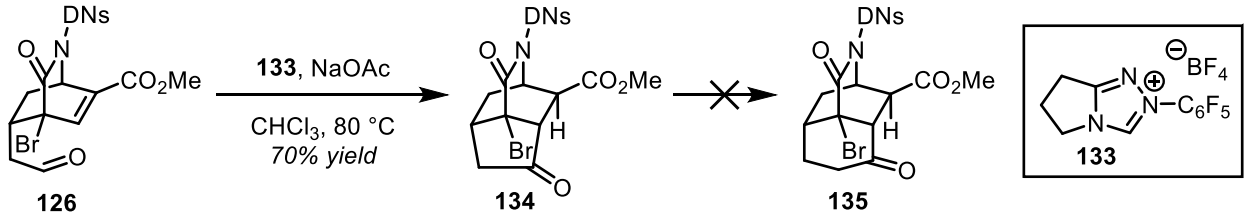

Scheme 2.22. Stetter reaction transforms **126** to tricyclic ketone **134**.

A final attempt in this initial route toward the total synthesis of koumine (**1**) was made using the cycloadduct **126** and performing an intramolecular Stetter reaction. Upon treatment with triazolium salt **133**, the aldehyde within **126** underwent an *Umpolung*-mediated nucleophilic addition into the enoate to furnish tricyclic ketone **134**.[31,46] From this stage, we attempted several ring expansion reaction conditions, but unfortunately remained unsuccessful. Despite promising initial results, the route had to be abandoned due to uneconomical material supply, especially through the latter stages of the synthesis and significant challenges elaborating the *aza*-bicycle.

*Section 2.4: Development of a Dearomative Au^{I}-catalyzed Spirocyclization Strategy Toward the Total Synthesis of Koumine (**1**)*

Moving on from our unsuccessful pyridone Diels–Alder reaction strategy, we set out to design a further route toward the total synthesis of koumine (**1**) that avoids the biomimetic quinuclidine rearrangement or general cyclization paradigm. We decided to forge the two quaternary centers early in the synthesis (Scheme 2.23), a contrasting design to previously published total syntheses by Magnus, Takayama, Zhang, and Kerr.

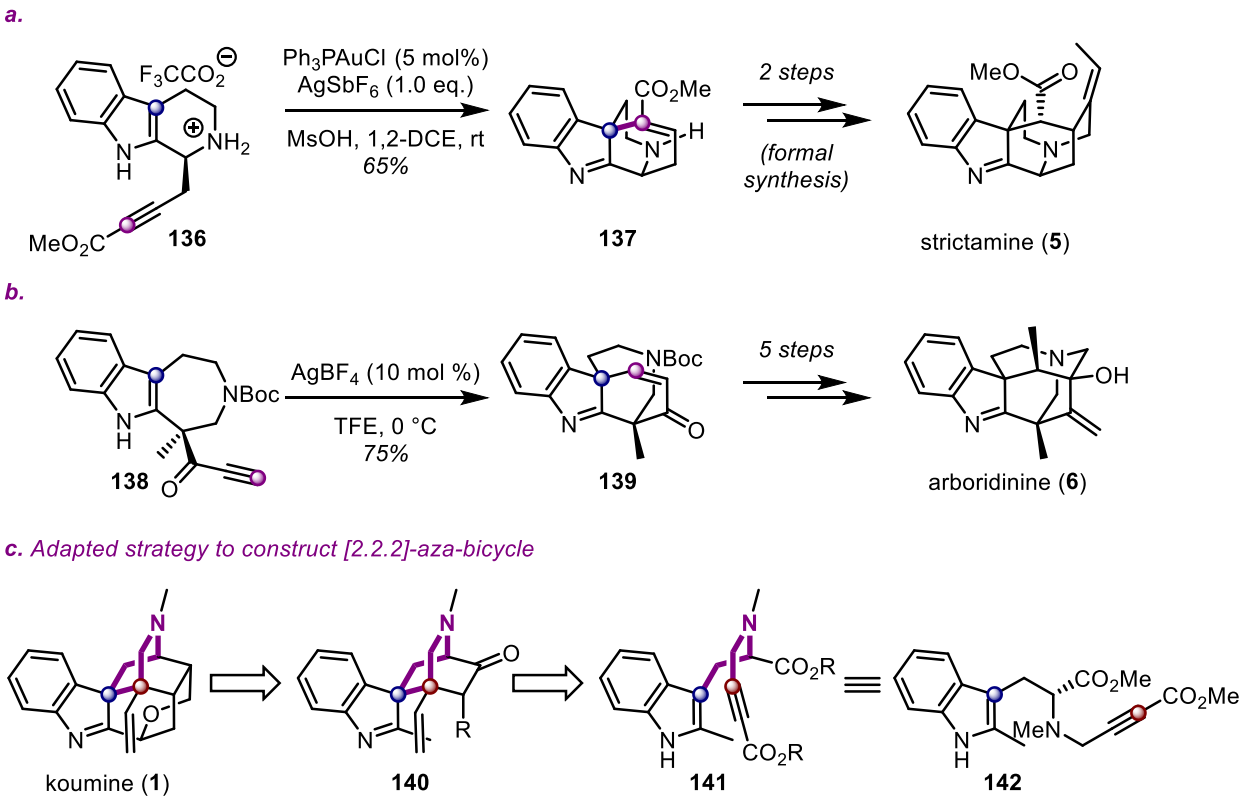

Scheme 2.23. *a.* Snyder synthesis of strictamine (**5**). *b.* Snyder synthesis of arboridinine (**6**). *c.* adapted strategy toward the total synthesis of koumine (**1**).

For this transformation we took inspiration from prior syntheses of monoterpenoid indole alkaloids in the Snyder group, such as strictamine (**5**) and arboridinine (**6**).[9,10] Both of these reports relied on the early-stage formation of the spiroindolenine moiety found within the natural products, which accelerated the completion of the carbocyclic framework in both cases (Scheme 2.23.a and 2.23.b). In the case of strictamine (**5**), a Au^{I}-catalyzed 6-*endo*-dig cyclization forges the desired tetracyclic spiroindolenine **137** (cf. Chapter 1 for more information on this synthesis). The total synthesis of arboridine (**6**) features a similar 6-*endo*-dig cyclization onto the ynone within **138**, in this case catalyzed by Ag^{I}, to afford the tetracyclic spiroindolenine **139**. Both total syntheses conclude in relatively short order, as **137** intercepts an advanced intermediate in the Zhu group's total synthesis of strictamine (**4**) and **139** is elaborated to arboridinine (**6**) in a five-step sequence

featuring the formation of the final ring via an elegantly designed Hosomi–Sakurai-type allylation reaction.[47]

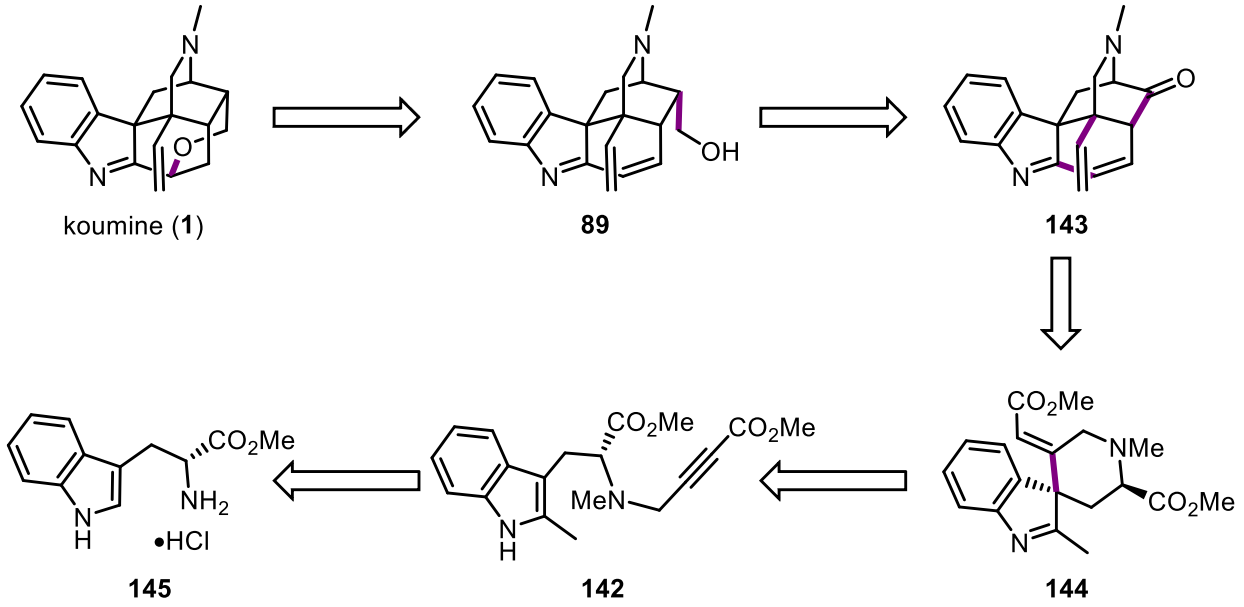

Scheme 2.24. Retrosynthetic analysis of a spirocyclization reaction approach toward the total synthesis of koumine (**1**).

It was our idea in designing this second-generation route to then form the piperidine ring found within koumine (**1**) at an early stage and construct the remaining three rings around a central spiroindolenine species. Our retrosynthetic analysis for this route somewhat follows the one devised for our pyridone Diels–Alder route (Scheme 2.14), as the key bond formation event similarly takes place early on (Scheme 2.24). As such, we envisioned that the pyran ring could be closed by an intramolecular etherifcation event with alcohol **89**, which, in turn, could be derived from a methylenation and hydroboration sequence of ketone **143**. Then, [2.2.2]-*aza*-bicycle **143** would be derived from a sequential Michael–Dieckmann–Stork enamine-type cascade from spirocycle **144**. We viewed this cascade as an intriguing point for reaction design, potentially forging not only the *aza*-bicycle, but also the cyclohexane moiety adjacent to the spiroindolenine

within koumine (**1**) in the same synthetic operation. Spirocycle **144** is envisioned to be formed via a metal-mediated dearomative 6-*exo*-dig spirocyclization of tryptophan derivative **142**.

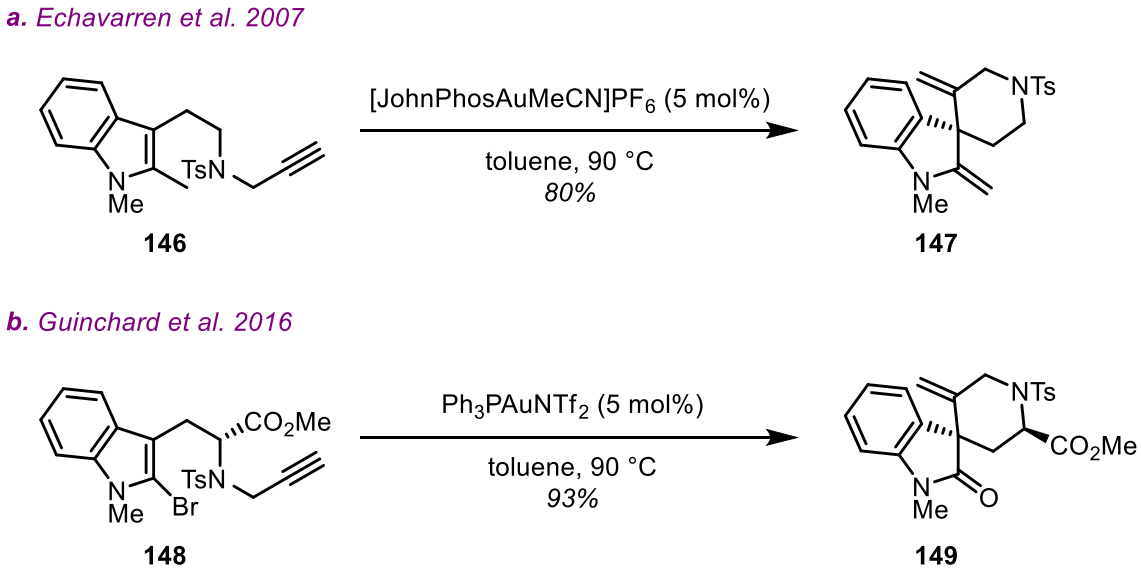

Scheme 2.25. Au^{I}-catalyzed spirocyclizations affording spiroindolenines (**147**) or spirooxindoles (**149**).

In our search for suitable conditions and substrates for our proposed synthesis of koumine (**1**), we first turned to literature methods for the preparation of spirocyclic tryptophan derivatives, examples of which have been reported by Echavarren and Guinchard.[48–51] These reactions mainly rely on 6-*exo*-dig cyclizations of tryptophan-tethered alkynes using Au^{I} catalysis to form spiroindolenines and spirooxindoles (Scheme 2.25). Such reactions follow the generally accepted pathways of Au^{I} catalysis as presented in Chapter 1, in which the gold complex acts as a strong π-acid (Scheme 2.26).[49,52] The cationic Au^{I} species first coordinates to the alkyne within **150**, thus activating it for nucleophilic attack from the indole. A 6-*exo*-dig cyclization forms the spirocycle, and subsequent protodeuaration provides the exocyclic alkene product. In our attempts to reach the spirocyclic ester **144** as identified in our retrosynthetic analysis, we undertook several approaches, mainly centered around installing an appropriate alkyne side chain.

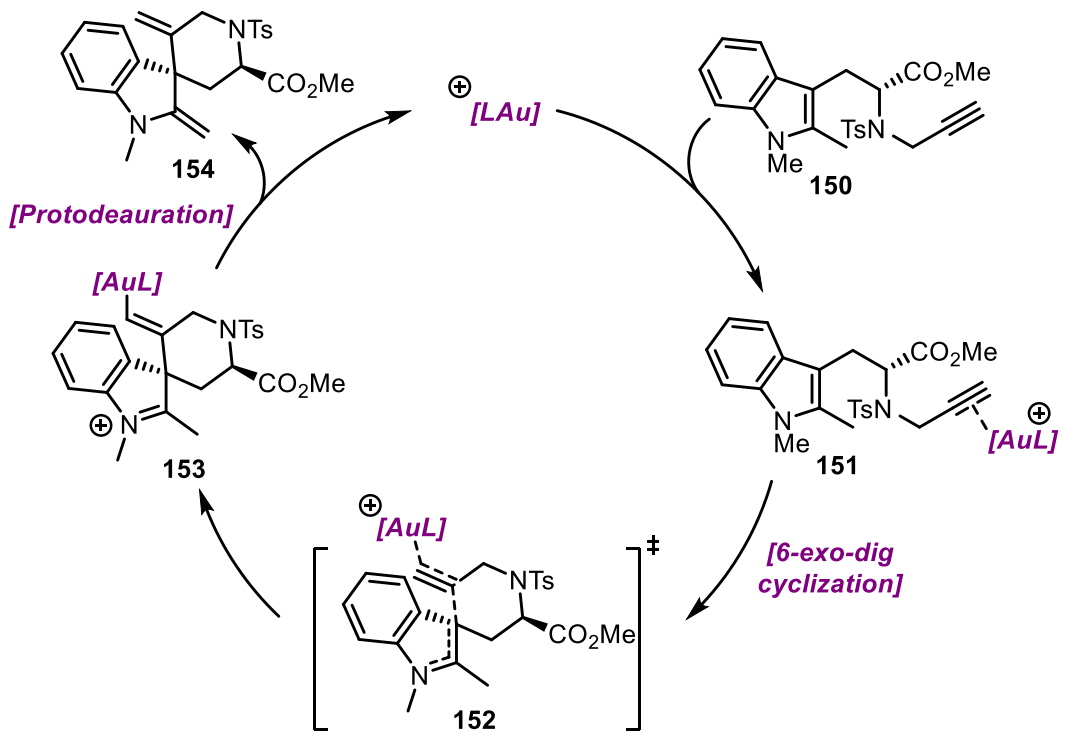

Scheme 2.26. Mechanism of Au^{I}-catalyzed spirocyclization on a substrate suitable to our studies toward the total synthesis of koumine (**1**).

In addition to the spirocyclization event used to introduce a key quaternary center, we sought to utilize the resulting exocyclic alkene as a functional handle to initiate a cascade to form the quinuclidine core. The cascade reaction that we proposed to form the [2.2.2]-*aza*-bicycle relies on a sequence of transformations including an initial conjugate addition at the β-carbon of spirocyclic α,β-unsaturated carbonyl species **157**, followed by a Dieckmann condensation with the pendant ester to form the bicycle **160** (Scheme 2.27). Such a cascade has been shown by Stetter *et al*. on a simpler system, in which the all-carbon [2.2.2]-bicycle **156** was formed by initial conjugate addition of cyanide and subsequent Dieckmann condensation.[53] If successful, this would forge the central *aza*-bicycle within koumine (**1**) in a novel fashion. Going even further, we speculated that given the cage-shaped nature of **1**, it may be possible to assemble the front ring in the same step via a Stork-enamine type addition into the remaining ester under reversible base conditions.

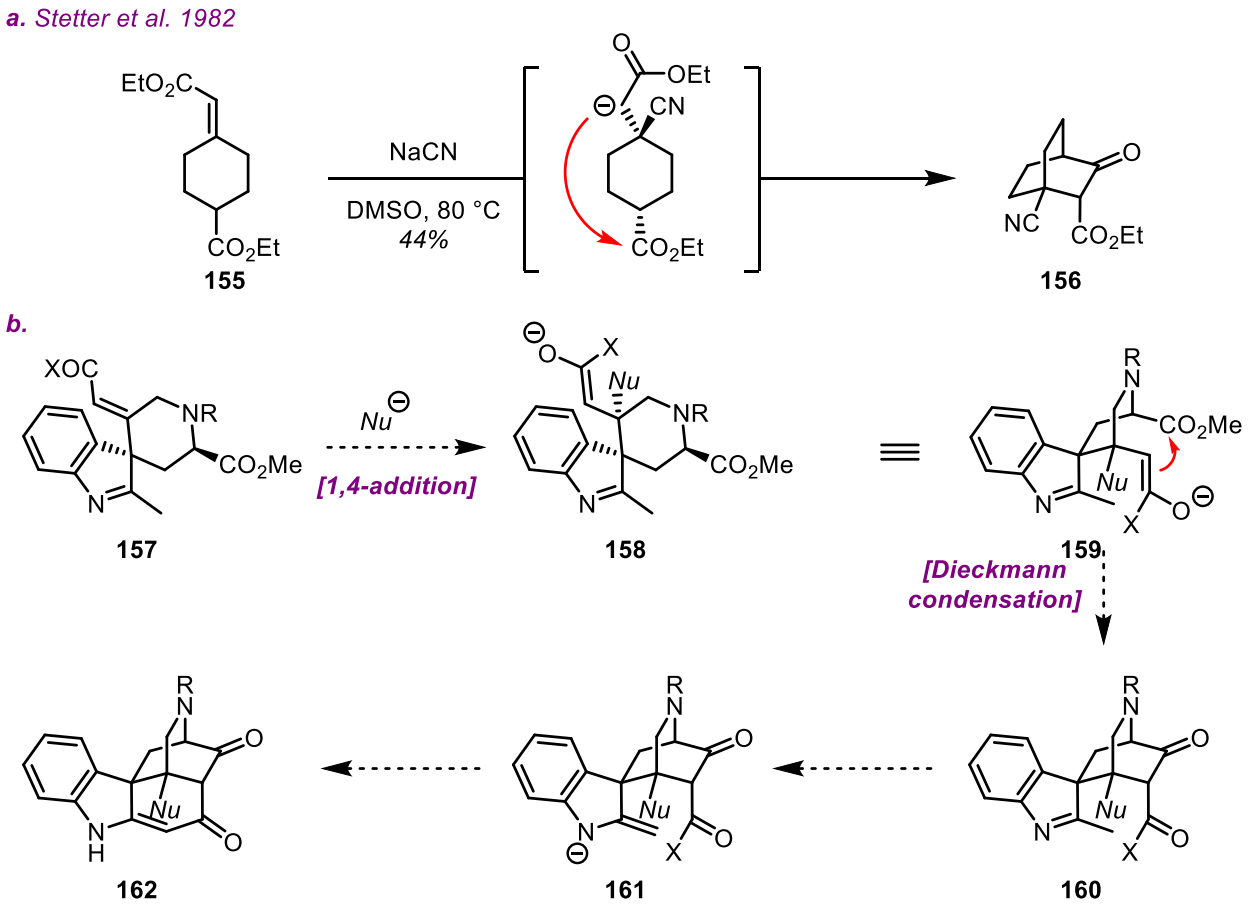

Scheme 2.27. *a.* Bicycle-forming cascade reported by Stetter *et al*. *b.* Proposed adaptation to the total synthesis of koumine (**1**).

Our second route toward the total synthesis of koumine (**1**) starts from commercial D-tryptophan methyl ester (**145**), which would eventually produce the unnatural enantiomer of koumine (**1**), however the material was more readily available to us at the time relative to the L-isomer. Initially, D-tryptophan methyl ester (**145**) was protected as its *p*-nitrobenzenesulfonamide and brominated to afford **164** (Scheme 2.28). A subsequent Stille coupling installed the C-2 methyl group on the indole in good yield.[54] Alkylation with propargyl bromide and subsequent Au^{I}-catalyzed 6-*exo*-dig cyclization using $Ph_3PAuNTf_2$ provided us with spirocycle **167** in excellent yield.

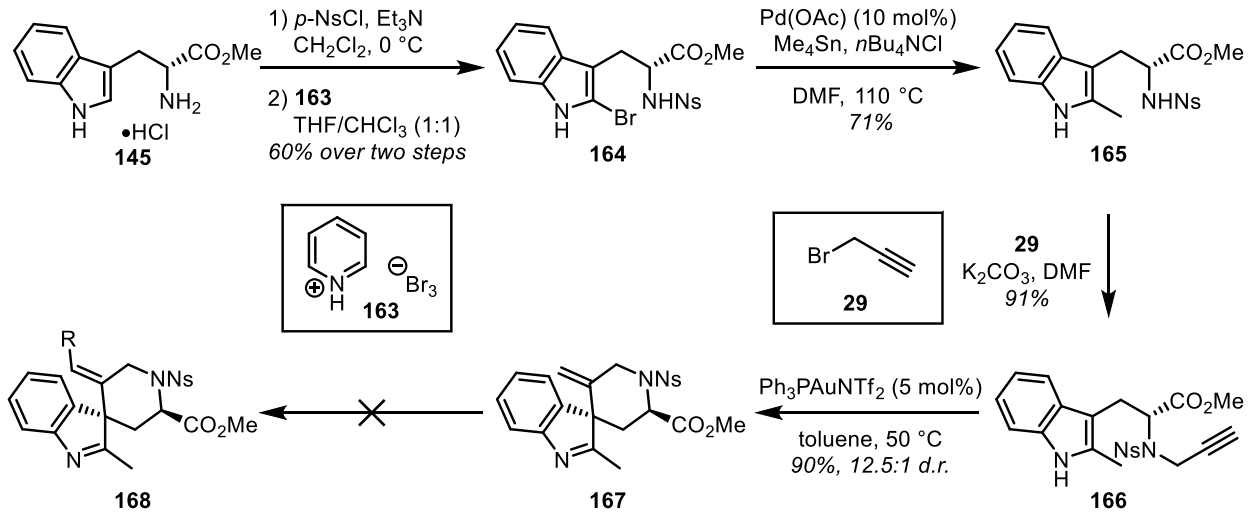

Scheme 2.28. Synthesis of spiroindolenine **167** and unsuccessful derivatization at 1,1-disubstituted olefin.

Unfortunately, we were unable to convert this terminal alkene species into the α,β-unsaturated carbonyl species necessary for our proposed *aza*-bicycle-forming cascade. Oxidative cleavage of the terminal alkene to the respective ketone was unsuccessful under ozonolysis or Lemieux–Johnson oxidation conditions.[55] Further attempts at functionalizing this olefin remained unsuccessful. As such, carbonylation of the terminal alkyne within **167** was investigated extensively. While the metal-mediated conditions previously reported in the synthesis of strictamine (**5**) were low-yielding, and deprotonation of the alkyne with LDA, followed by trapping of the carbanion with methyl chloroformate led to decomposition of starting material, a method developed by Tsuji, using $PdCl_2/CuCl_2$ under CO atmosphere proved successful to give the desired ynoate **169**.[56] In this reaction, $CuCl_2$ serves two roles, the first being as an oxidizing agent, helping to turn over the Pd^0 that is formed during reaction. In addition, resultant CuCl readily forms a Cu^I acetylide with the alkyne within **166**, which is then able to efficiently transmetalate with Pd^{II}. The subsequent Au^I-catalyzed cyclization of ynoate **169** utilizing the conditions that were successful with the terminal alkyne did not proceed, but using stoichiometric

$AgBF_4$ as a Lewis acid proved successful in mediating the desired spirocyclization to give spirocycle **170** as a single diastereomer (Scheme 2.29).

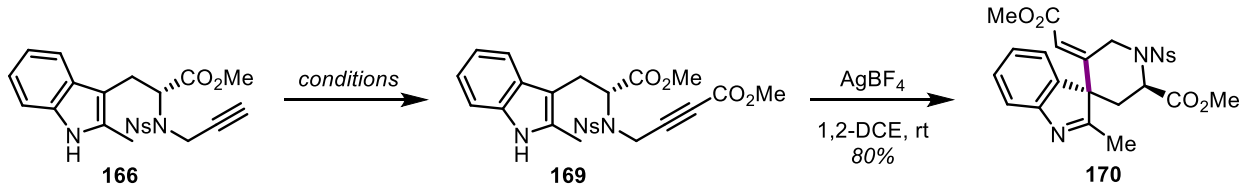

Entry	Conditions	Solvent	T	Yield
1	$Pd(OAc)_2$ (30 mol%), PPh_3, CO/O_2 (atm.)	DMF/MeOH (1:1)	rt	*11%*
2	$CuCl_2$ (10 mol%), NaOAc, CO (atm.)	MeOH	rt	*30%*
3	LDA; $ClCO_2Me$	THF	–78 °C	*decomposition*

Scheme 2.29. Carbonylation of the terminal alkyne within **166** and successful spirocyclization.

However, similar to our observations when attempting Ns deprotection with the pyridone Diels–Alder product, the α,β-unsaturated ester within **170** proved to be an obstacle, with conjugate addition of PhSH occurring faster than the S_NAr deprotection, leading to the β-thioether **171**. We sought to circumvent this issue by sulfonamide deprotection earlier in the sequence, followed by *N*-methylation and alkyne carbonylation. Deprotection of sulfonamide **166** was followed by a reductive amination, which had worked without issues in a similar system bearing a bromide at the C-2 position of the indole within **166**. Unfortunately, upon condensation of the secondary amine onto formaldehyde, reduction with $NaCNBH_3$ was not observed. Instead, an intramolecular interrupted Pictet-Spengler type reaction occurred to produce the spirocyclic by-product **175**.

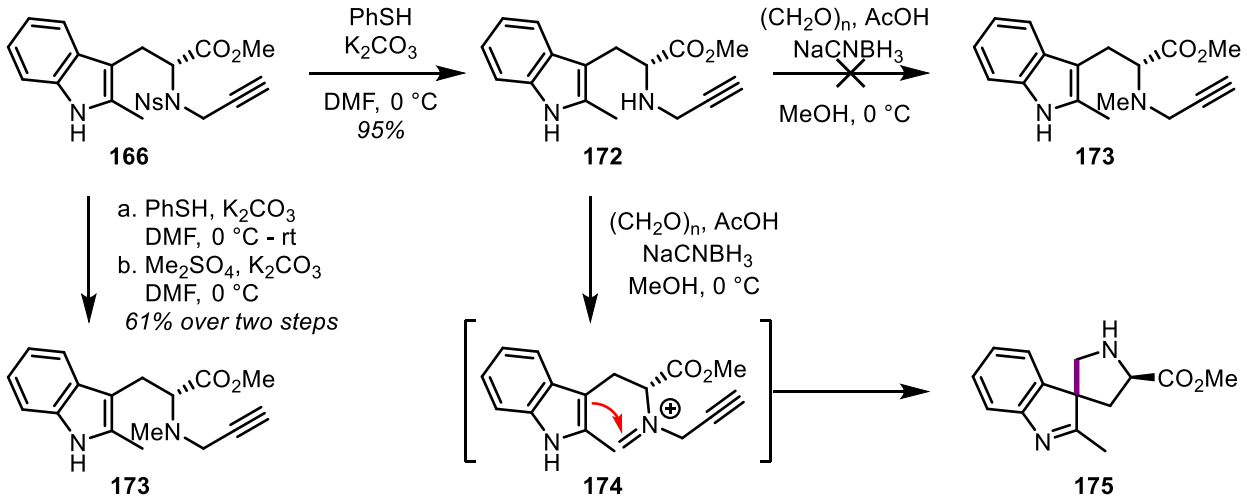

Scheme 2.30. Deprotection and *N*-methylation of **166.**

The desired *N*-methylation was alternatively achieved with Me_2SO_4 and the resulting tertiary amine **173** was subjected to carbonylation conditions. We found that under $PdCl_2/CuCl_2$ conditions, which despite a lower yield did not produce side products previously, in this case **173** underwent an intermolecular Glaser coupling to produce a dimeric product. In their seminal publication, the Tsuji group described such a product, especially in the presence of tertiary amines, placing our observations in line with those of previous works.[56–58] Other oxidants reported by Tsuji *et al.* such as benzoquinone and O_2 did not produce any desired ynoate product.

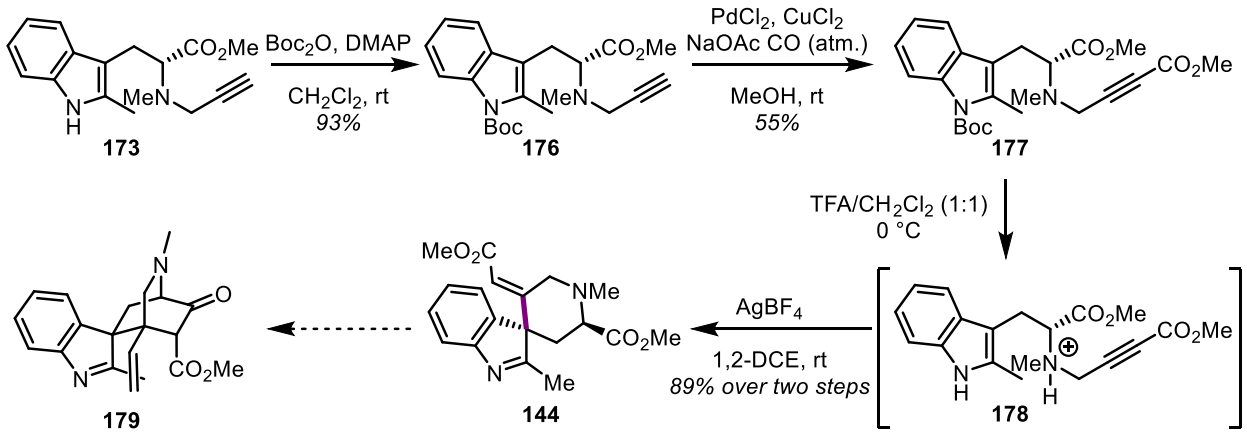

Scheme 2.31. Carbonylation of terminal alkyne **176** and successful spirocyclization reaction**.**

Eventually, we found that carbonylation did proceed with *N*-Boc protected indole **176** under Tsuji conditions in moderate yield without any observed side products. TFA deprotection and Ag^{I}-promoted cyclization readily produced spirocycle **144**. With this material in hand, we attempted various functionalization reactions at the β-position of the enoate within **144**, in order to effect our envisioned cascade reaction. To our dismay, despite extensive screening, none of the carbon-based nucleophiles that were tested underwent conjugate addition. When Nagata's reagent (Et_2AlCN), which is known to add to highly encumbered α,β-unsaturated carbonyls did not undergo the desired addition reaction, we were forced to reconsider our options with this route. Selective derivatization of the ester moiety within **144** failed as well.[59]

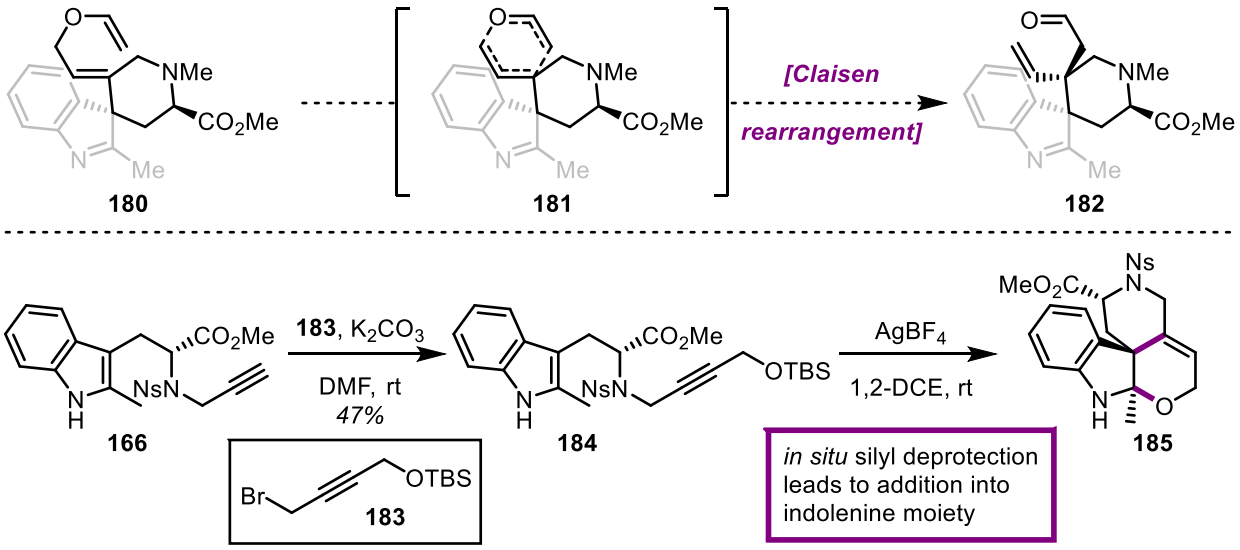

Scheme 2.32. Proposed Claisen rearrangement to introduce the vinyl group at C-20 within **182**.

A potentially promising approach was to deliver the carbon nucleophile to the sterically encumbered β-position intramolecularly. One of the most straightforward approaches, to us, was a Claisen rearrangement (Scheme 2.32). Though shown as the classic [3,3]-sigmatropic rearrangement of an allyl vinyl ether such as **180**, we were encouraged that availability of different

variants of this reaction would allow for strategic flexibility in achieving the synthesis of a rearrangement product like aldehyde **182**.[60]

In a preliminary set of experiments, we attempted to adapt the Au^{I}-catalyzed spirocyclization to the readily accessible propargylic silyl ether **184**. Propargyl bromide derivative **183** was accessed from 1,4-butynediol in two steps. While alkylation proceeded smoothly, upon treatment with Au^{I}, the desired product was not observed, but rather a compound in which the C-2 methyl protons are shifted upfield. We hypothesize that the desired 6-*exo*-trig cyclization is followed by *in situ* deprotection of the labile silyl ether. The free allylic alcohol could then act as a nucleophile to form a new ring via 1,2-addition into the indolenine to produce **185**. While we believe that this issue can be fixed by careful redesign of the cyclization substrate, this may need to be taken up at another time. Future explorations will focus on forming the desired spirocycle **192** in order to proceed with our proposed [2.2.2]-*aza*-bicycle formation toward the total synthesis of koumine (**1**).

SECTION 2.5: CONCLUSION

In conclusion, we have reported progress towards the total synthesis of koumine on two separate routes. Our initial approach showcases the synthetic potential of an inverse electron demand pyridone Diels–Alder reaction. Through this route we hoped to access the core azabicyclo[2.2.2]octane system in an asymmetric fashion. Despite obtaining the cycloadduct efficiently, achieving satisfactory enantiomeric excess and derivatizing this compound proved difficult and led to the abandonment of this route.

The second approach sought to install the all-carbon quaternary centers at an early stage of the synthesis, a departure from the previous reported total syntheses of koumine (**1**). Although the

desired spirocycle has been obtained with a variety of substitution patterns, none proved capable of undergoing the desired cascade to forge the *aza*-bicycle. The primary knowledge gained in this synthetic study toward the total synthesis of the monoterpene indole alkaloid koumine (**1**), is that while being a compelling strategy, installing the two all-carbon quaternary centers at an early stage can be as much of a strategic advantage as a major hurdle. If the proposed cascade proves to be workable in the future, the total synthesis of koumine (**1**) could be achieved in only a few additional transformations, with the overall strategy setting itself apart from all existing approaches in the literature and facing the challenge of early quaternary center installation head on.

SECTION 2.6: REFERENCES:

(1) Takayama, H.; Sakai, S.-I. *Synth. Org. Chem.* **1990**, *48*, 876–890.

(2) Jin, G.-L.; Su, Y.-P.; Liu, M.; Xu, Y.; Yang, J.; Liao, K.-J.; Yu, C.-X. *J. Ethnopharmacol.* **2014**, *152*, 33–52.

(3) Chou, T. Q.; Pak, C.; Hou, H. C.; Liu, J. C. *Chin. J. Physiol.* **1931**, *5*, 345–352.

(4) Liu, C.-T.; Wang, Q.-W.; Wang, C.-H. *J. Am. Chem. Soc.* **1981**, *103*, 4634–4635.

(5) Khuong-Huu, F.; Chiaroni, A.; Riche, C. *Tetrahedron Lett.* **1981**, *22*, 733–734.

(6) Takayama, H.; Kitajima, M.; Sakai, S.-I. *Heterocycles* **1990**, *30*, 325–327.

(7) Xu, Y.; Qiu, H.-Q.; Liu, H.; Liu, M.; Huang, Z.-Y.; Yang, J.; Su, Y.-P.; Yu, C.-X. *Pharmacol. Biochem. Behav.* **2012**, *101*, 504–514.

(8) Smith, M. W.; Snyder, S. A. *J. Am. Chem. Soc.* **2013**, *135*.

(9) Smith, M. W.; Zhou, Z.; Gao, A. X.; Shimbayashi, T.; Snyder, S. A. *Org. Lett.* **2017**, *19*, 1004–1007.

(10) Gan, P.; Pitzen, J.; Qu, P.; Snyder, S. A. **2018**, *140*.

(11) O'Connor, S. E.; Maresh, J. J. *Nat. Prod. Rep.* **2006**, *23*, 532–547.

(12) Medema, M. H.; Fischbach, M. A. *Nat. Chem. Biol.* **2015**, *11*, 639–648.

(13) Franke, J.; Kim, J.; Hamilton, J. P.; Zhao, D.; Pham, G. M.; Wiegert-Rininger, K.; Crisovan, E.; Newton, L.; Vaillancourt, B.; Tatsis, E.; Buell, C. R.; O'Connor, S. E. *ChemBioChem* **2019**, *20*, 83–87.

(14) Battersby, A. R.; Burnett, A. R.; Hall, E. S.; Parsons, P. G. *Chem. Commun.* **1968**, No. 24, 1582–1583.

(15) Hong, B.; Grzech, D.; Caputi, L.; Sonawane, P.; López, C. E. R.; Kamileen, M. O.; Hernández Lozada, N. J.; Grabe, V.; O'Connor, S. E. *Nature* **2022**, *607*, 617–622.

(16) Schmidt, D.; Stockigt, J. *Planta Med.* **1995**, *61*, 254–158.

(17) Dang, T. T. T.; Franke, J.; Carqueijeiro, I. S. T.; Langley, C.; Courdavault, V.; O'Connor, S. E. *Nat. Chem. Biol.* **2018**, *14*, 760–763.

(18) Pfitzner, A.; Stöckigt, J. *J. Chem. Soc. Chem. Commun.* **1983**, *0*, 459–460.

(19) Lounasmaa, M.; Koskinen, A. *Planta Med.* **1982**, *44*, 120–121.

(20) Ponglux, D.; Wongseripipatana, S.; Subhadhirasakul, S.; Takayama, H.; Yokota, M.; Ogata, K.; Phisalaphong, C.; Aimi, N.; Sakai, S.-I. *Tetrahedron* **1988**, *44*, 5075–5094.

(21) Chu-Tsin, L.; Qian-Sheng, Y. *Acta Chim. Sin. English Ed.* **1987**, *5*, 181–187.

(22) Magnus, P.; Mugrage, B.; DeLuca, M. R.; Cain, G. A. *J. Am. Chem. Soc.* **1990**, *112*, 5220–5230.

(23) Magnus, P.; Mugrage, B.; DeLuca, M.; Cain, G. A. *J. Am. Chem. Soc.* **1989**, *111*, 786–789.

(24) Kitajima, M.; Watanabe, K.; Maeda, H.; Kogure, N.; Takayama, H. *Org. Lett.* **2016**, *18*, 1912–1915.

(25) Kerkovius, J. K.; Kerr, M. A. *J. Am. Chem. Soc.* **2018**, *140*, 8415–8419.

(26) Yang, Z.; Tan, Q.; Jiang, Y.; Yang, J.; Su, X.; Qiao, Z.; Zhou, W.; He, L.; Qiu, H.; Zhang, M. *Angew. Chemie Int. Ed.* **2021**, *60*, 13105–13111.

(27) Chen, W.; Ma, Y.; He, W.; Wu, Y.; Huang, Y.; Zhang, Y.; Tian, H.; Wei, K.; Yang, X.; Zhang, H. *Nat. Commun. 2022 131* **2022**, *13*, 1–12.

(28) Michel, P.; Rassat, A. *J. Org. Chem.* **2000**, *65*, 2572–2573.

(29) Chen, G.-Z.; Hong, R. *Cell Reports Phys. Sci.* **2022**, 101097.

(30) Smith, M. W.; Snyder, S. A. *J. Am. Chem. Soc.* **2013**, *135*, 12964–12967.

(31) Cole, C. J. F.; Fuentes, L.; Snyder, S. A. *Chem. Sci.* **2020**, *11*, 2175–2180.

(32) Saktura, M.; Grzelak, P.; Dybowska, J.; Albrecht, L. *Org. Lett.* **2020**, *22*, 1813–1817.

(33) Bertelsen, S.; Jørgensen, K. A. *Chem. Soc. Rev.* **2009**, *38*, 2178–2189.

(34) Posner, G. H.; Vinader, V.; Afarinkia, K. *J. Org. Chem* **1992**, *57*, 4088–4097.

(35) Okamura, H.; Nagaike, H.; Iwagawa, T.; Nakatani, M. *Tetrahedron Lett.* **2000**, *41*, 8317–8321.

(36) Soh, J. Y.-T.; Tan, C.-H. *J. Am. Chem. Soc.* **2009**, *131*, 6904–6905.

(37) Posner, G. H.; Switzer, C. *J. Org. Chem.* **1987**, *52*, 1644–1646.

(38) Fukuyama, T.; Liu, G. *J. Am. Chem. Soc.* **1996**, *118*, 7426–7427.

(39) Newcombe, N. J.; Fang, Y.; Vijn, R. J.; Hiemstra, H.; Speckamp, W. N. *J. Chem. Soc., Chem. Commun.* **1994**, 767–768.

(40) Ishii, A.; Kawai, T.; Noji, M.; Nakayama, J. *Tetrahedron* **2005**, *61*, 6693–6699.

(41) Wuts, P. G. M. *Greene's Protective Groups in Organic Synthesis*, 5th ed.; John Wiley and Sons, 2014.

(42) Stork, G.; Zhao, K. *Tetrahedron Lett.* **1989**, *30*, 2173–2174.

(43) Byrne, P. A.; Gilheany, D. G. *J. Am. Chem. Soc* **2012**, *134*, 9225–9239.

(44) Deng, L.; Xu, T.; Li, H.; Dong, G. *J. Am. Chem. Soc.* **2015**, *138*, 369–374.

(45) Maimone, T. J.; Ishihara, Y.; Baran, P. S. *Tetrahedron* **2015**, *71*, 3652–3665.

(46) Li, J.-L.; Zhou, S.-L.; Chen, P.-Q.; Dong, L.; Liu, T.-Y.; Chen, Y.-C. *Chem. Sci.* **2012**, *3*, 1879–1882.

(47) Ren, W.; Wang, Q.; Zhu, J. *Angew. Chemie Int. Ed.* **2016**, *55*, 3500–3503.

(48) Ferrer, C.; Amijs, C. H. M.; Echavarren, A. M. *Chem. - A Eur. J.* **2007**, *13*, 1358–1373.

(49) Magné, V.; Blanchard, F.; Marinetti, A.; Voituriez, A.; Guinchard, X. *Adv. Synth. Catal.* **2016**, *358*, 3355–3361.

(50) Magné, V.; Marinetti, A.; Gandon, V.; Voituriez, A.; Guinchard, X. *Adv. Synth. Catal.* **2017**, *359*, 4036–4042.

(51) James, M. J.; O'Brien, P.; Taylor, R. J. K.; Unsworth, W. P. *Chem. - A Eur. J.* **2016**, *22*, 2856–2881.

(52) Dorel, R.; Echavarren, A. M. *Chem. Rev.* **2015**, *115*, 9028–9072.

(53) Stetter, H.; Marten, K. *Liebigs Ann. der Chemie* **1982**, 250–253.

(54) Somei, M.; Sayama, S.; Naka, K.; Shinmoto, K.; Yamada, F. *Heterocycles* **2007**, *73*, 537–554.

(55) Pappo, R.; Allen, D. S.; Lemieux, R. U.; Johnson, W. S. *J. Org. Chem.* **1955**, *21*, 478–479.

(56) Tsuji, J.; Takahashi, M.; Takahashi, T. *Tetrahedron Lett.* **1980**, *21*, 849–850.

(57) Beller, M. *Catalytic Carbonylation Reactions*; Beller, M., Ed.; Springer Berlin Heidelberg: Berlin, 2006; Vol. Catalytic.

(58) Brennführer, A.; Neumann, H.; Beller, M. *ChemCatChem* **2009**, *1*, 28–41.

(59) Nakai, T.; Tomooka, K.; Kanduluru, A. K. 1–10.

(60) Lutz, R. P. *Chem. Rev.* **1984**, *84*, 205–247.

SECTION 2.7: EXPERIMENTAL SECTION

General Procedures.

All reactions were carried out under an argon atmosphere with anhydrous solvents under anhydrous conditions, unless otherwise noted. Anhydrous THF, toluene, Et_2O, CH_2Cl_2, and MeCN were obtained by passing commercially available pre-dried, oxygen-free formulations through activated alumina columns. Yields refer to chromatographically and spectroscopically (^1H and ^{13}C NMR) homogeneous materials, unless otherwise stated. Reagents were purchased at the highest commercial quality and used without further purification, unless otherwise stated. Reactions were magnetically stirred and monitored by TLC carried out on 0.25 mm Merck silica gel plates (60F-254) using UV light as visualizing agent, and an aqueous solution of cerium ammonium molybdate, a solution of anisaldehyde in EtOH, or a solution of $KMnO_4$ in aqueous $NaHCO_3$ and heat as developing agents. SiliCycle silica gel (60, academic grade, particle size 0.040–0.063 mm) was used for flash column chromatography. Preparative TLC separations were carried out on 0.50 mm E. Merck silica gel plates (60F-254). NMR spectra were recorded on Bruker 400 and 500 MHz instruments and calibrated using residual undeuterated solvent as an internal reference. The following abbreviations were used to explain the multiplicities: s = singlet, d = doublet, t = triplet, q = quartet, br = broad, app = apparent, m = multiplet.

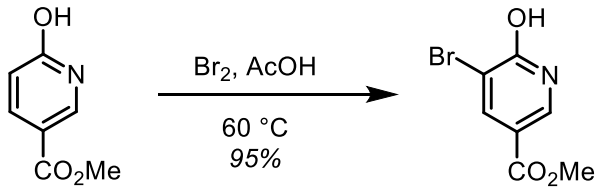

106 **107**

Hydroxypyridine 107. To a flame-dried 25 mL flask was added 6-hydroxynicotinic acid methyl ester (800 mg, 5.23 mmol, 1.0 equiv.) and AcOH (4 mL). Bromine (400 µL, 7.85 mmol, 1.5 equiv.) was then added dropwise and the mixture was heated to reflux for 18 hours. Upon completion of the reaction, the mixture is cooled to room temperature and the remaining bromine was quenched by the addition of aqueous $Na_2S_2O_3$, followed by slow addition of aqueous $NaHCO_3$ (3 mL). The pH was adjusted to 7 by addition of 1 N NaOH. The solids which precipitated were collected by filtration and dried under vacuum to give the desired **Hydroxypyridine 107** (1.15 g, 95% yield) as a pale yellow solid.

107:

^{1}H NMR (500 MHz, DMSO-d_6) δ 12.70 (s, 1H), 8.18 (d, J = 2.4 Hz, 1H), 8.10 (d, J = 2.4 Hz, 1H), 3.78 (s, 3H).

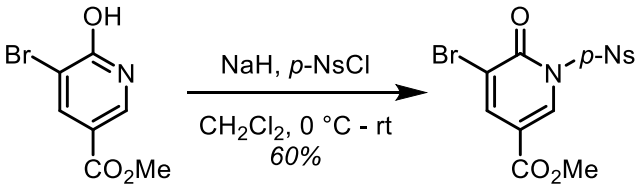

107 **110**

Pyridone 110. To a flame-dried 500 mL flask was added NaH (60% suspension in mineral oil, 880 mg, 22 mmol, 2.2 equiv.) and CH_2Cl_2 (200 mL) at 0 °C. The mixture is allowed to stir for

0.25 h, followed by portionwise addition of **107** (2.3 g, 10 mmol, 1.0 equiv.) as a solid. After another 0.25 h of stirring at 0 °C, *p*-NsCl (4.0 g, 18 mmol, 1.8 equiv.) was added portionwise. Upon completion of addition, the mixture was allowed to warm to 25 °C and stirred for 12 h. Once complete, the reaction was quenched by the slow, dropwise addition of H_2O (20 mL) and was then neutralized by addition of aqueous $NaHCO_3$ (100 mL) and the contents transferred to a separatory funnel. The layers were separated, and the aqueous layer was further extracted with CH_2Cl_2 (3 × 100 mL). The combined organic layers were dried over Na_2SO_4 and concentrated in vacuo. The resultant crude product was further purified by flash column chromatography (silica gel, Hexanes/EtOAc, 4:1) to give the desired **Pyridone 110** (2.52 g, 60% yield) as a white solid.

110:

^{1}H NMR (500 MHz, $CDCl_3$) δ 8.90 (d, *J* = 2.2 Hz, 1H), 8.43 (d, *J* = 9.0 Hz, 2H), 8.37 (d, *J* = 9.0 Hz, 2H), 8.29 (d, *J* = 2.2 Hz, 1H), 3.94 (s, 3H).

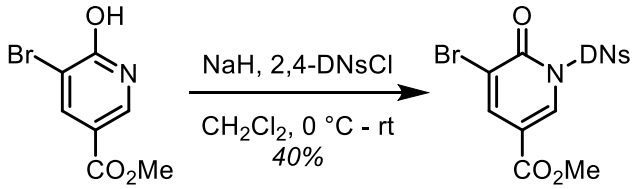

107 **111**

Pyridone 111. To a flame-dried 500 mL flask was added NaH (60% suspension in mineral oil, 1.24 g, 31 mmol, 1.8 equiv.) and CH_2Cl_2 (170 mL) at 0 °C. The mixture is allowed to stir for 0.25 h, followed by portionwise addition of **107** (4.0 g, 17.23 mmol, 1.0 equiv.) as a solid. After another 0.25 h of stirring at 0 °C, 2,4-DNsCl (9.19 g, 34.5 mmol, 2.2 equiv.) was added as a solution in CH_2Cl_2 (50 mL). Upon completion of addition, the mixture was allowed to warm to

25 °C and stirred for 12 h. Once complete, the reaction was quenched by the slow, dropwise addition of H_2O (20 mL) and was then neutralized by addition of aqueous $NaHCO_3$ (100 mL) and the contents transferred to a separatory funnel. The layers were separated, and the aqueous layer was further extracted with CH_2Cl_2 (3 × 100 mL). The combined organic layers were dried over Na_2SO_4 and concentrated in vacuo. The resultant crude product was further purified by flash column chromatography (silica gel, Hexanes/EtOAc, 6:1) to give the **Pyridone 111** (3.07 g, 38% yield) as a yellow solid.

111:

^{1}H NMR (500 MHz, $CDCl_3$) δ 8.94 (d, *J* = 8.6 Hz, 1H), 8.73 – 8.66 (m, 3H), 8.38 (d, *J* = 2.1 Hz, 1H), 3.96 (s, 3H).

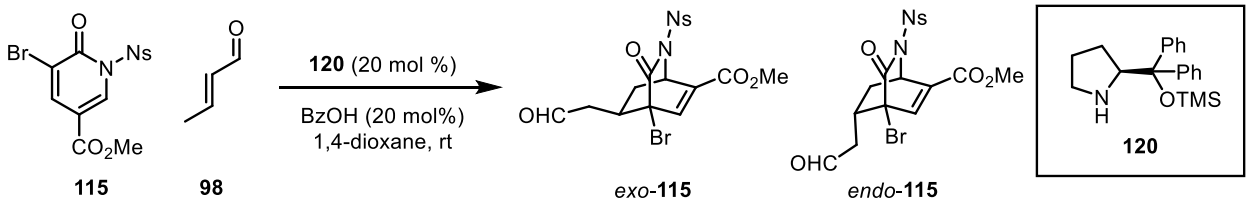

Cycloadduct 115. To a 1-dram vial was added **110** (83.4 mg, 0.2 mmol, 1.0 equiv.), **120** (13 mg, 0.04 mmol, 0.2 equiv.), BzOH (5.0 mg, 0.04 mmol, 0.2 equiv.), and 1,4-dioxane (1 mL) at 25 °C. Then, freshly distilled **98** (50 µL, 0.6 mmol, 3.0 equiv.) is added dropwise and the mixture is allowed to stir for 24 h at 25 °C. Once complete, the reaction was quenched with aqueous NH_4Cl (1 mL) diluted with EtOAc (3 mL) and the contents transferred to a separatory funnel and diluted with aqueous NH_4Cl (2 mL). The layers were separated, and the aqueous layer was further extracted with EtOAc (3 × 5 mL). The combined organic layers were dried over Na_2SO_4 and concentrated in vacuo. The resultant crude product was further purified by flash column

chromatography (silica gel, Hexanes/EtOAc, 3:1 → 1:2) to give the desired **cycloadducts** *exo*-**115** (30 mg), and *endo*-**115** (27 mg, 60% yield, 1.1:1 d.r.) as yellow foams.

exo-**115**:

^{1}H NMR (500 MHz, $CDCl_3$) δ 9.77 (s, 1H), 8.35 (d, *J* = 8.9 Hz, 2H), 8.17 (d, *J* = 8.9 Hz, 2H), 7.20 (d, *J* = 2.3 Hz, 1H), 5.92 – 5.80 (m, 1H), 3.84 (s, 3H), 3.22 (dd, *J* = 18.7, 2.6 Hz, 1H), 2.77 (dddd, *J* = 12.3, 10.3, 4.0, 2.5 Hz, 1H), 2.38 – 2.23 (m, 2H), 1.93 – 1.85 (m, 1H).

endo-**115**:

^{1}H NMR (500 MHz, $CDCl_3$) δ 9.76 (s, 1H), 8.43 – 8.34 (m, 2H), 8.27 – 8.13 (m, 2H), 7.08 (d, *J* = 1.9 Hz, 1H), 5.95 – 5.85 (m, 1H), 3.87 (s, 3H), 3.28 (dd, *J* = 18.4, 3.0 Hz, 1H), 2.81 (dq, *J* = 11.3, 4.5, 3.3 Hz, 1H), 2.78 – 2.72 (m, 1H), 2.37 (dd, *J* = 18.5, 11.0 Hz, 1H).

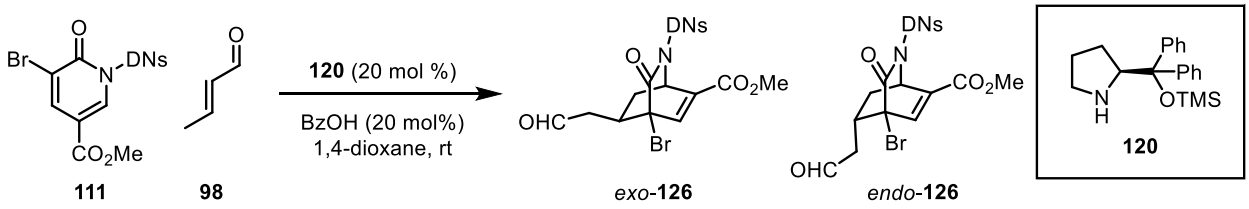

Cycloadduct 126. To a 50 mL flask was added **111** (1.16 g, 2.5 mmol, 1.0 equiv.), BzOH (61 mg, 0.5 mmol, 0.2 equiv.), and 1,4-dioxane (12.5 mL) at 25 °C. Then, freshly distilled **98** (520 µL, 7.5 mmol, 3.0 equiv.) is added dropwise. **120** (163 mg, 0.5 mmol, 0.2 equiv.) in 1,4-dioxane (3 mL) is added via syringe pump over 2 h and the mixture is allowed to stir for 24 h at 25 °C. Once complete, the reaction was quenched with aqueous NH_4Cl (5 mL) diluted with EtOAc (10 mL) and the contents transferred to a separatory funnel and diluted with aqueous NH_4Cl (20 mL) and EtOAc (50 mL). The layers were separated, and the aqueous layer was further extracted with

EtOAc (3 × 30 mL). The combined organic layers were dried over Na_2SO_4 and concentrated in vacuo. The resultant crude product was further purified by flash column chromatography (silica gel, Hexanes/EtOAc, 3:1 → 2:1) to give the desired **cycloadducts** *exo*-**126** (610.2 mg), and *endo*-**126** (382.5 mg, 75% yield, 1.6:1 d.r.) as orange foams.

exo-**126**:

^{1}H NMR (500 MHz, $CDCl_3$) δ 9.82 (s, 1H), 8.70 (d, *J* = 9.1 Hz, 1H), 8.60 – 8.54 (m, 2H), 5.80 (s, 1H), 3.90 (d, *J* = 2.2 Hz, 4H), 3.25 (d, *J* = 18.7 Hz, 1H), 2.84 (t, *J* = 11.1 Hz, 1H), 2.49 (dd, *J* = 18.7, 11.5 Hz, 1H), 2.40 (t, *J* = 11.8 Hz, 1H), 1.99 (d, *J* = 13.9 Hz, 1H).

endo-**126**:

^{1}H NMR (500 MHz, $CDCl_3$) δ 9.77 (s, 1H), 8.73 (d, *J* = 8.8 Hz, 1H), 8.61 – 8.53 (m, 2H), 7.10 (s, 1H), 5.79 (s, 1H), 3.93 – 3.86 (m, 3H), 3.28 (d, *J* = 18.3 Hz, 1H), 3.01 – 2.88 (m, 2H), 2.40 (dd, *J* = 18.4, 9.7 Hz, 1H).

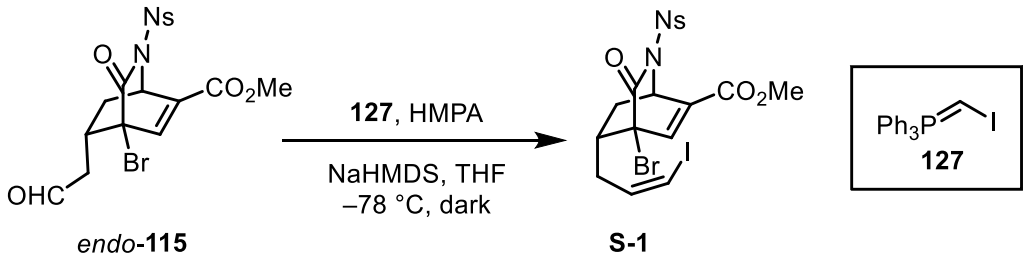

Vinyl iodide S-1. To a flame-dried 25 mL flask was added **127** (81 mg, 0.153 mmol, 3.0 equiv.) and THF (1.7 mL) at 25 °C. NaHMDS (1 M in THF, 140 µL, 0.14 mmol, 2.8 equiv.) was added dropwise and the mixture was allowed to stir for 0.25 h at 25 °C, followed by cooling the mixture to –78 °C. HMPA was added dropwise and the mixture is allowed to stir for 0.25 h.

endo-**115** (25 mg, 0.051 mmol, 1.0 equiv.) was added as a solution in THF (1.7 mL). After another 0.25 h of stirring at –78 °C, the reaction was complete. The mixture was quenched by dropwise addition of aqueous NH_4Cl (5 mL). The mixture was warmed to 25 °C and diluted with EtOAc (10 mL), the contents transferred to a separatory funnel. The layers were separated, and the aqueous layer was further extracted with EtOAc (3 × 10 mL). The combined organic layers were dried over Na_2SO_4 and concentrated in vacuo. The resultant crude product was further purified by flash column chromatography (silica gel, Hexanes/EtOAc, 4:1) to give the desired **Vinyl iodide S-1** (8.1 mg, 26% yield) as an orange-red oil.

S-1:

^{1}H NMR (500 MHz, $CDCl_3$) δ 8.35 (d, *J* = 8.8 Hz, 2H), 8.18 (d, *J* = 8.8 Hz, 2H), 7.08 (t, *J* = 1.4 Hz, 1H), 6.43 (d, *J* = 7.5 Hz, 1H), 6.09 (td, *J* = 7.9, 6.0 Hz, 1H), 5.91 – 5.83 (m, 1H), 3.86 (s, 3H), 2.81 (d, *J* = 14.0 Hz, 1H), 2.48 (dp, *J* = 10.3, 3.7 Hz, 1H), 2.41 (ddd, *J* = 12.9, 9.3, 3.7 Hz, 1H), 2.04 (ddd, *J* = 14.4, 10.6, 7.9 Hz, 1H), 1.65 – 1.62 (m, 1H).

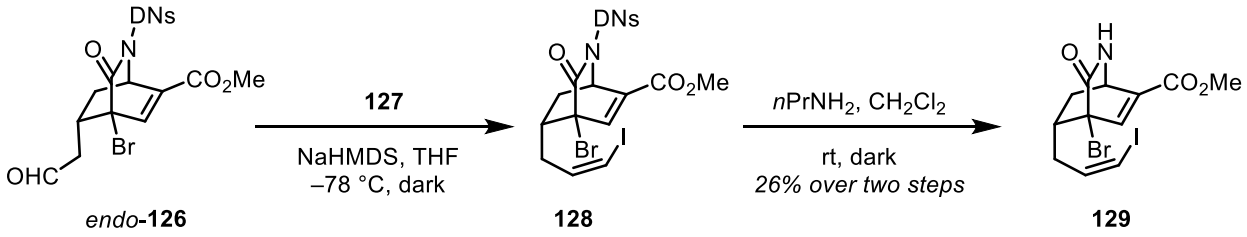

endo-**126** **128** **129**

Vinyl iodide 129. To a flame-dried 100 mL flask was added **127** (869 mg, 2.16 mmol, 3.0 equiv.) and THF (15 mL) at 25 °C. NaHMDS (1 M in THF, 2.02 mL, 2.02 mmol, 2.8 equiv.) was added dropwise and the mixture was allowed to stir for 0.25 h at 25 °C, followed by cooling the mixture to –78 °C. HMPA was added dropwise and the mixture is allowed to stir for 0.25 h.

endo-**126** (382 mg, 0.72 mmol, 1.0 equiv.) was added as a solution in THF (5 mL). After another 0.25 h of stirring at –78 °C, the reaction was complete. The mixture was quenched by dropwise addition of aqueous NH_4Cl (20 mL). The mixture was warmed to 25 °C and diluted with aqueous NH_4Cl (10 mL) and EtOAc (30 mL), the contents transferred to a separatory funnel. The layers were separated, and the aqueous layer was further extracted with EtOAc (3 × 30 mL). The combined organic layers were dried over Na_2SO_4 and concentrated in vacuo. The resultant crude vinyl iodide **128** was used in the next step without further purification. In a 25 mL flask, **128** (approximately 0.2 mmol) was taken up in CH_2Cl_2 (4 mL). *n*$PrNH_2$ (52 µL, 0.80 mmol, 4.0 equiv.) is added in 13 µL (1.0 equiv.) portions every 0.25 h and the mixture is stirred at 25 °C and closely monitored by TLC. Upon completion, the mixture is reduced in vacuo. The resultant crude product was further purified by flash column chromatography (silica gel, Hexanes/EtOAc, 3:1 → 1:2) to give the desired **vinyl iodide 129** (122 mg, 26% yield over two steps) as an orange-red oil.

129:

^{1}H NMR (500 MHz, $CDCl_3$) δ 7.39 (d, *J* = 2.5 Hz, 1H), 6.42 (d, *J* = 7.6 Hz, 1H), 6.26 – 6.17 (m, 1H), 4.80 (d, *J* = 5.9 Hz, 1H), 3.82 (s, 3H), 2.90 (d, *J* = 13.8 Hz, 1H), 2.42 – 2.31 (m, 1H), 2.14 – 2.08 (m, 1H), 1.91 (d, *J* = 5.2 Hz, 2H).

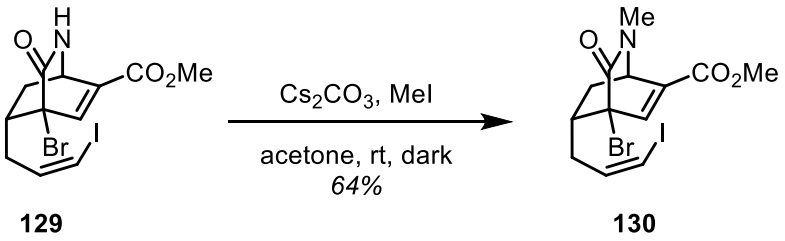

129 **130**

Vinyl iodide 130. To a flame-dried 25 mL flask was added **129** (30 mg, 0.07 mmol, 1.0 equiv.) and acetone (7 mL) at 25 °C. Cs_2CO_3 (160 mg, 0.49 mmol, 7.0 equiv.) and MeI (26 µL, 0.42 mmol, 6.0 equiv.) were added sequentially and the mixture was stirred in the dark for 24 h. Once complete, the reaction was quenched by the slow, dropwise addition of NH_4Cl (5 mL), the contents transferred to a separatory funnel and diluted with EtOAc (10 mL) and H_2O (10 mL). The layers were separated, and the aqueous layer was further extracted with EtOAc (3 × 10 mL). The combined organic layers were dried over Na_2SO_4 and concentrated in vacuo. The resultant crude product was further purified by flash column chromatography (silica gel, Hexanes/EtOAc, 1:1) to give the desired **vinyl iodide 130** (19.7 mg, 64% yield) as a yellow oil.

130:

^{1}H NMR (500 MHz, $CDCl_3$) δ 7.33 (d, *J* = 2.2 Hz, 1H), 6.38 (d, *J* = 7.5 Hz, 1H), 6.14 (td, *J* = 8.0, 6.0 Hz, 1H), 4.67 – 4.52 (m, 1H), 3.80 (d, *J* = 2.0 Hz, 3H), 3.03 (s, 3H), 2.88 – 2.79 (m, 1H), 2.37 – 2.25 (m, 1H), 2.00 (ddd, *J* = 14.0, 11.4, 8.3 Hz, 1H), 1.91 – 1.76 (m, 2H).

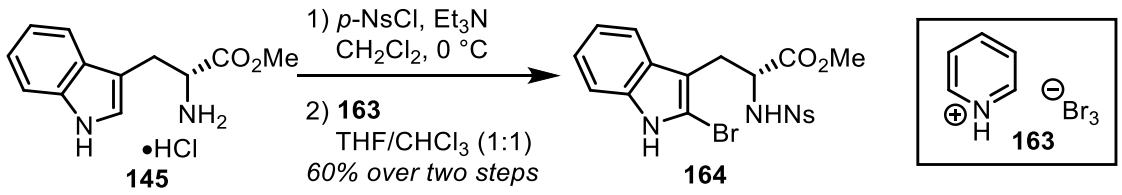

Bromoindole 164. To a flame-dried 100 mL flask was added **145** (2.54 g, 10 mmol, 1.0 equiv.) and CH_2Cl_2 (20 mL) at 25 °C. The suspension was cooled to 0 °C and Et_3N (3.05 mL, 22 mmol, 2.2 equiv.) was added, followed by *p*-NsCl (2.66 g, 12 mmol, 1.2 equiv.) in three portions over 0.25 h. The reaction mixture was stirred at 0 °C for 3 h. Once complete, the reaction was quenched by addition of H_2O (20 mL) and the contents were transferred to a separatory funnel. The layers were separated, and the organic layer was washed with aqueous $NaHCO_3$ (50 mL) and brine (30 mL). The organic layer was dried over Na_2SO_4 and concentrated in vacuo. The resultant orange foam was utilized in the next step without further purification. The crude product was taken up in THF/$CHCl_3$ (40 mL, 1:1) and cooled to 0 °C. **163** (3.52 g, 11 mmol, 1.1 equiv.) was added in portions over 0.5 h. Upon completion of addition, the mixture was stirred at 0 °C for 2 h. Once complete, the mixture was quenched by dropwise addition of aqueous $Na_2S_2O_3$ in order to quench remaining bromine, followed by addition of aqueous $NaHCO_3$ (30 mL), the contents were transferred to a separatory funnel and diluted with CH_2Cl_2 (30 mL). The layers were separated, and the aqueous layer was extracted with CH_2Cl_2 (3 × 50 mL). The combined organic layers were dried over Na_2SO_4 and concentrated in vacuo. The resultant crude product was further purified by trituration to give the desired **Bromoindole 164** (2.9 g, 60% yield over two steps) as a yellow solid.

164:

^{1}H NMR (500 MHz, $CDCl_3$) δ 8.57 (s, 1H), 8.29 (d, *J* = 8.3 Hz, 2H), 7.87 (d, *J* = 8.4 Hz, 2H), 7.38 (d, *J* = 8.0 Hz, 1H), 7.28 – 7.24 (m, 1H), 7.18 (t, *J* = 7.6 Hz, 1H), 7.12 (t, *J* = 7.5 Hz, 1H), 4.76 (dd, *J* = 9.4, 4.9 Hz, 1H), 3.83 (d, *J* = 1.1 Hz, 3H), 3.16 – 3.02 (m, 3H).

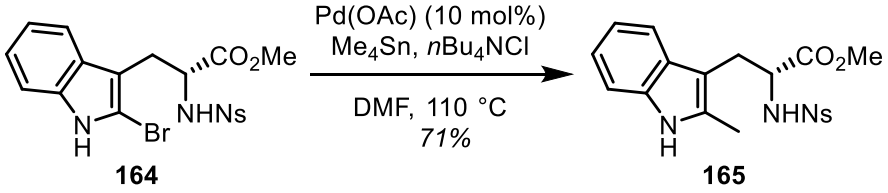

Methylindole 165. To a flame-dried 250 mL pressure flask was added **164** (7 g, 14.61 mmol, 1.0 equiv.) and DMF (65 mL) at 25 °C. Me_4Sn (3 mL, 21.92 mmol, 1.5 equiv.), $Pd(OAc)_2$ (330 mg, 1.46 mmol, 0.1 equiv.), and nBu$_4$Cl (9.33 g, 33.6 mmol, 2.3 equiv.) were added to this solution under argon. The pressure flask was sealed and the reaction mixture was heated at 110 °C for 3 h. Once complete, the mixture was diluted with EtOAc (100 mL) and the contents were transferred to a separatory funnel. The organic layerr was washed with H_2O (5 × 100 mL) and brine (50 mL). The organic layer was dried over Na_2SO_4 and concentrated in vacuo. The resultant crude product was further purified by flash column chromatography (silica gel, Hexanes/EtOAc, 2:1) to give the desired **Methylindole 165** (4.27 g, 71% yield) as a yellow foam.

165:

^{1}H NMR (500 MHz, $CDCl_3$) δ 7.97 (d, *J* = 8.8 Hz, 2H), 7.73 (s, 1H), 7.61 (d, *J* = 8.8 Hz, 2H), 7.26 (s, 1H), 7.14 – 7.10 (m, 1H), 7.06 (ddd, *J* = 8.0, 5.4, 1.2 Hz, 1H), 7.00 (td, *J* = 7.4, 7.0, 1.2 Hz, 1H), 5.21 (d, *J* = 9.4 Hz, 1H), 4.28 – 4.18 (m, 1H), 3.67 (s, 3H), 3.21 (dd, *J* = 14.8, 4.8 Hz, 1H), 3.00 (dd, *J* = 14.7, 8.3 Hz, 1H), 2.32 (s, 3H).

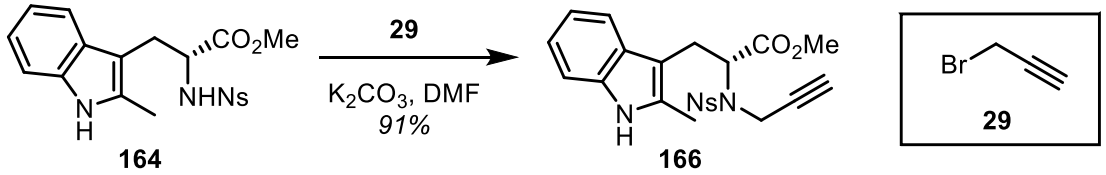

Sulfonamide 166. To a flame-dried 200 mL flask was added **165** (4.25 g, 10.18 mmol, 1.0 equiv.) and DMF (50 mL) at 25 °C. The mixture was cooled to 0 °C and K_2CO_3 (1.7 g, 12.2 mmol, 1.2 equiv.) was added. After 0.15 h, **29** (70% in toluene, 4.5 mL, 30.5 mmol, 3.0 equiv.) was added dropwise. Upon completion of addition, the mixture was allowed to warm to 25 °C over 2 h. After 15 h, the reaction was complete and the mixture was quenched with aqueous $NaHCO_3$ (100 mL) and diluted with EtOAc (100 mL), the contents were transferred to a separatory funnel. The layers were separated and the organic layer was washed with H_2O (5 × 100 mL) and brine (50 mL). The organic layer was dried over Na_2SO_4 and concentrated in vacuo. The resultant product was further purified by flash column chromatography (silica gel, Hexanes/EtOAc, 3:1) to give the desired **Sulfonamide 166** (4.3 g, 91% yield) as a yellow foam.

166:

^{1}H NMR (500 MHz, $CDCl_3$) δ 8.03 (d, *J* = 8.9 Hz, 2H), 7.80 (d, *J* = 8.8 Hz, 2H), 7.74 (s, 1H), 7.43 (d, *J* = 7.6 Hz, 1H), 7.19 (d, *J* = 7.8 Hz, 1H), 7.13 – 7.08 (m, 1H), 7.06 (td, *J* = 7.5, 1.2 Hz,

1H), 4.84 (t, *J* = 7.4 Hz, 1H), 4.41 (dd, *J* = 18.6, 2.5 Hz, 1H), 4.36 (dd, *J* = 18.5, 2.6 Hz, 1H), 3.89 (s, 1H), 3.56 (s, 3H), 3.44 (dd, *J* = 14.7, 7.6 Hz, 1H), 3.09 (dd, *J* = 14.7, 7.3 Hz, 1H), 2.35 (s, 3H).

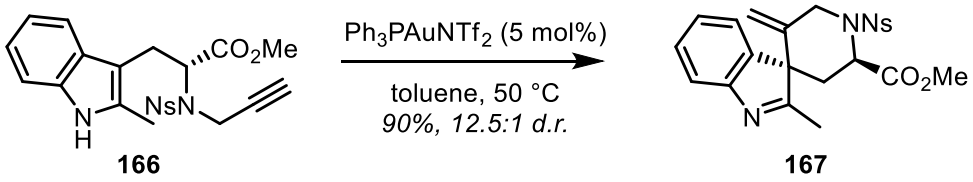

166 **167**

Spiroindolenine 167. To a flame-dried 50 mL flask was added **166** (180 mg, 0.395 mmol, 1.0 equiv.), toluene (10 mL), and $Ph_3PAuNTf_2$ (14.6 mg, 0.02 mmol, 0.05 equiv.) at 25 ° C. The mixture was heated at 50 °C for 20 h. Upon completion of addition, the mixture was allowed to cool to 25 °C and the reaction was quenched with aqueous $NaHCO_3$ (10 mL) and diluted with EtOAc (15 mL). The contents were transferred to a separatory funnel. The layers were separated and the aqueous layer was extracted with CH_2Cl_2 (3 × 20 mL). The combined organic layers were dried over Na_2SO_4 and concentrated in vacuo. The resultant product was further purified by flash column chromatography (silica gel, Hexanes/EtOAc, 1:1) to give the desired **Spiroindolenine 167** (162 mg, 90% yield, 12.5:1 d.r.) as a yellow foam.

major-**167**:

^{1}H NMR (500 MHz, $CDCl_3$) δ 8.41 (d, *J* = 8.9 Hz, 2H), 8.13 (d, *J* = 8.8 Hz, 2H), 7.55 (d, *J* = 7.7 Hz, 1H), 7.35 (td, *J* = 7.5, 1.5 Hz, 1H), 7.20 – 7.11 (m, 2H), 5.00 (s, 1H), 4.83 (dd, *J* = 11.4, 6.0 Hz, 1H), 4.48 (d, *J* = 15.3 Hz, 1H), 4.38 (d, *J* = 1.6 Hz, 1H), 4.23 – 4.17 (m, 1H), 3.64 (s, 3H), 2.40 (dd, *J* = 14.0, 11.4 Hz, 1H), 2.23 (s, 3H), 1.86 (dd, *J* = 14.0, 6.0 Hz, 1H).

minor-**167**:

^{1}H NMR (500 MHz, $CDCl_3$) δ 8.40 (d, *J* = 8.9 Hz, 2H), 8.09 (d, *J* = 8.9 Hz, 2H), 7.54 (d, *J* = 7.7 Hz, 1H), 7.30 (td, *J* = 7.5, 1.4 Hz, 1H), 7.14 – 7.04 (m, 2H), 5.00 (dd, *J* = 7.2, 3.8 Hz, 1H), 4.95 (d, *J* = 1.7 Hz, 1H), 4.51 – 4.44 (m, 2H), 4.32 – 4.27 (m, 1H), 3.55 (s, 3H), 2.44 (dd, *J* = 14.3, 7.3 Hz, 1H), 2.29 (s, 3H), 2.16 (dd, *J* = 14.3, 3.7 Hz, 1H).

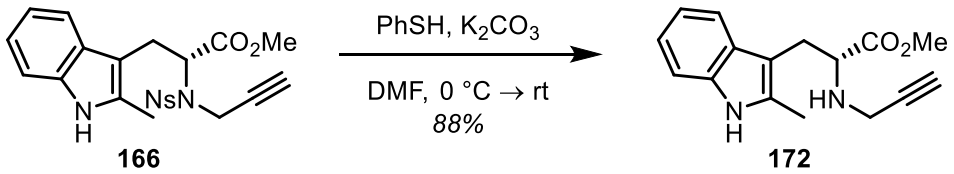

Amine 172. To a flame-dried 200 mL flask was added **166** (4.3 g, 9.44 mmol, 1.0 equiv.), and DMF (47 mL), and K_2CO_3 (5.2 g, 37.7 mmol, 4.0 equiv.) at 25 °C. After 0.25 h, PhSH (4.7 mL, 47.2 mmol, 5.0 equiv.) was added and the reaction mixture was stirred at 25 °C for 2 h. Once complete, the reaction was quenched by addition of H_2O (50 mL) and the contents were transferred to a separatory funnel and diluted with EtOAc (100 mL). The layers were separated and the organic layer was washed with H_2O (5 × 100 mL) and brine (50 mL). The organic layer was dried over Na_2SO_4 and concentrated in vacuo. The resultant product was further purified by flash column chromatography (silica gel, Hexanes/EtOAc, 3:2) to give the desired **Amine 172** (2.24 g, 88% yield) as an off-white solid.

172:

^{1}H NMR (500 MHz, $CDCl_3$) δ 7.81 (s, 1H), 7.53 (dd, *J* = 7.6, 1.4 Hz, 1H), 7.27 (d, *J* = 1.4 Hz, 1H), 7.11 (ddd, *J* = 7.9, 7.1, 1.4 Hz, 1H), 7.07 (td, *J* = 7.4, 1.3 Hz, 1H), 3.81 (dd, *J* = 7.6, 6.3 Hz,

1H), 3.65 (s, 3H), 3.42 (dd, *J* = 17.0, 2.5 Hz, 1H), 3.33 (dd, *J* = 17.1, 2.4 Hz, 1H), 3.16 (dd, *J* = 14.3, 6.3 Hz, 1H), 3.07 (dd, *J* = 14.4, 7.6 Hz, 1H), 2.39 (s, 3H), 2.11 (t, *J* = 2.4 Hz, 1H).

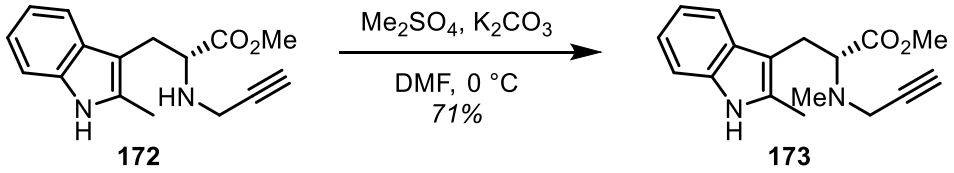

Amine 173. To a flame-dried 200 mL flask was added **172** (1.34 g, 4.96 mmol, 1.0 equiv.), DMF (50 mL), and K_2CO_3 (891 mg, 6.44 mmol, 1.3 equiv.) at 0 °C. After 0.25 h, Me_2SO_4 (570 µL, 5.95 mmol, 1.2 equiv.) was added and the reaction mixture was allowed to slowly warm to 25 °C over 2 h. Once complete, the reaction was quenched by addition of H_2O (50 mL) and the contents were transferred to a separatory funnel and diluted with EtOAc (100 mL). The layers were separated and the organic layer was washed with H_2O (5 × 100 mL) and brine (50 mL). The organic layer was dried over Na_2SO_4 and concentrated in vacuo. The resultant product was further purified by flash column chromatography (silica gel, Hexanes/EtOAc, 2:1) to give the desired **Amine 173** (1.0 g, 71% yield) as a white solid.

173:

^{1}H NMR (500 MHz, $CDCl_3$) δ 7.78 (s, 1H), 7.55 – 7.52 (m, 1H), 7.25 – 7.22 (m, 1H), 7.13 – 7.05 (m, 2H), 3.72 – 3.63 (m, 2H), 3.50 – 3.44 (m, 4H), 3.18 (dd, *J* = 13.7, 10.6 Hz, 1H), 3.10 (dd, *J* = 13.8, 4.8 Hz, 1H), 2.50 (s, 3H), 2.36 (s, 3H), 2.31 (t, *J* = 2.4 Hz, 1H).

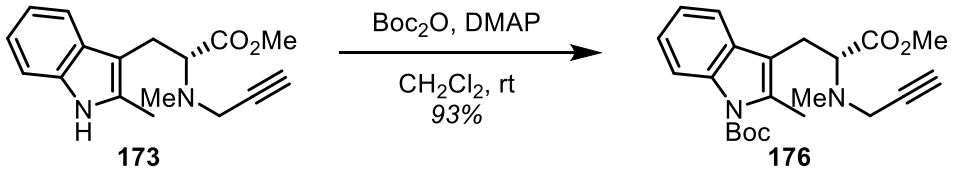

Amine 176. To a flame-dried 10 mL flask was added **173** (100 mg, 0.352 mmol, 1.0 equiv.), CH_2Cl_2 (3.5 mL), Boc_2O (100 mg, 0.457 mmol, 1.3 equiv.), and DMAP (2.2 mg, 0.018 mmol, 0.05 equiv.) at 25 °C and the mixture was allowed to stir for 2 h. Once complete, the reaction was quenched by addition of H_2O (5 mL) and the contents were transferred to a separatory funnel and diluted with CH_2Cl_2 (5 mL). The layers were separated and the aqueous layer was washed with CH_2Cl_2 (3 × 5 mL). The combined organic layers were dried over Na_2SO_4 and concentrated in vacuo. The resultant product was further purified by flash column chromatography (silica gel, Hexanes/EtOAc, 3:1) to give the desired **Amine 176** (125.9 mg, 93% yield) as a white solid.

176:

^{1}H NMR (500 MHz, $CDCl_3$) δ 8.07 (dd, *J* = 8.0, 1.4 Hz, 1H), 7.49 (dd, *J* = 7.4, 1.7 Hz, 1H), 7.24 – 7.18 (m, 2H), 3.74 – 3.62 (m, 2H), 3.56 – 3.44 (m, 4H), 3.17 (dd, *J* = 13.8, 10.5 Hz, 1H), 3.05 (dd, *J* = 13.8, 4.8 Hz, 1H), 2.53 (s, 3H), 2.50 (s, 3H), 2.30 (t, *J* = 2.4 Hz, 1H), 1.68 (d, *J* = 2.1 Hz, 9H).

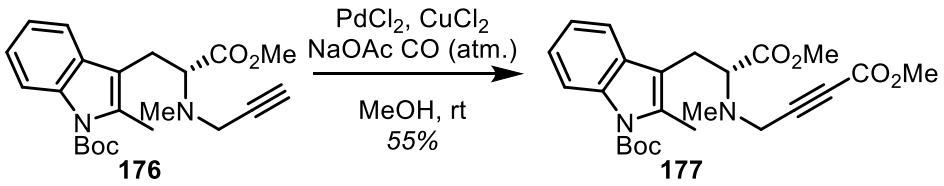

Ynoate 177. To a flame-dried 5 mL microwave tube was added MeOH (0.5 mL). The tube was fitted with a septum and the mixture was sparged with CO (atm.) for 0.25 h. Then, **176** (14 mg, 0.036 mmol, 1.0 equiv.), $CuCl_2$ (10 mg, 0.072 mmol, 2.0 equiv.), NaOAc (10 mg, 0.072 mmol, 2.0 equiv.), and $PdCl_2$ (0.6 mg, 0.0036 mmol, 0.1 equiv.) and the mixture was stirred under CO (atm.) at 25 °C for 2 h. Once complete, the reaction mixture was concentrated in vacuo. The resultant crude product was further purified by flash column chromatography (silica gel, Hexanes/EtOAc, 4:1) to give the desired **Ynoate 177** (8.7 mg, 55% yield) as a white solid.

177:

^{1}H NMR (500 MHz, $CDCl_3$) δ 8.08 (dd, *J* = 8.2, 1.5 Hz, 1H), 7.47 (dd, *J* = 7.4, 1.6 Hz, 1H), 7.25 – 7.18 (m, 2H), 3.78 (s, 3H), 3.67 – 3.59 (m, 2H), 3.54 (s, 3H), 3.18 (dd, *J* = 13.9, 10.1 Hz, 1H), 3.01 (dd, *J* = 13.9, 5.0 Hz, 1H), 2.53 (s, 3H), 2.51 (s, 3H), 1.67 (s, 9H).

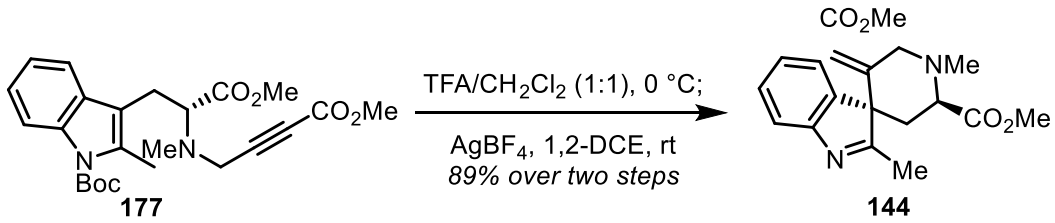

Spiroindolenine 144. To a flame-dried 25 mL flask was added **177** (72 mg, 0.162 mmol, 1.0 equiv.) and CH_2Cl_2 (2 mL) and the mixture is cooled to 0 °C. TFA (2 mL) is added dropwise and the mixture was stirred at 0 °C for 0.5 h. Once complete, the reaction mixture was neutralized

with $NaHCO_3$ (10 mL) and the contents were transferred to a separatory funnel and diluted with CH_2Cl_2 (5 mL). The layers were separated and the aqueous layer was washed with CH_2Cl_2 (5 × 5 mL). The combined organic layers were dried over Na_2SO_4 and concentrated in vacuo. The resultant crude product was taken up in 1,2-DCE (3 mL) and $AgBF_4$ (29 mg, 0.15 mmol, 0.9 equiv.) was add and the mixture was allowed to stir at 25 °C for 4 h. The mixture was directly submitted to flash column chromatography (silica gel, Hexanes/EtOAc, 2:1) to give the desired **Spiroindolenine 144** (49.4 mg, 89% yield over two steps, 10:1 d.r.) as an off-white solid.

144:

^{1}H NMR (500 MHz, $CDCl_3$) δ 7.60 (d, *J* = 7.7 Hz, 1H), 7.47 (d, *J* = 7.4 Hz, 1H), 7.36 (t, *J* = 7.6 Hz, 1H), 7.18 (t, *J* = 7.5 Hz, 1H), 5.82 (s, 1H), 3.90 (d, *J* = 15.1 Hz, 1H), 3.70 (s, 3H), 3.45 (dd, *J* = 12.0, 3.5 Hz, 1H), 3.36 (s, 3H), 2.52 (s, 3H), 2.43 – 2.33 (m, 2H), 2.21 (s, 3H).

^{13}C NMR (126 MHz, $CDCl_3$) δ 182.89, 172.67, 164.83, 154.96, 146.46, 142.31, 128.33, 125.03, 122.40, 120.68, 118.56, 77.30, 77.04, 76.79, 62.17, 60.63, 59.80, 52.22, 50.93, 42.85, 36.22, 16.46.

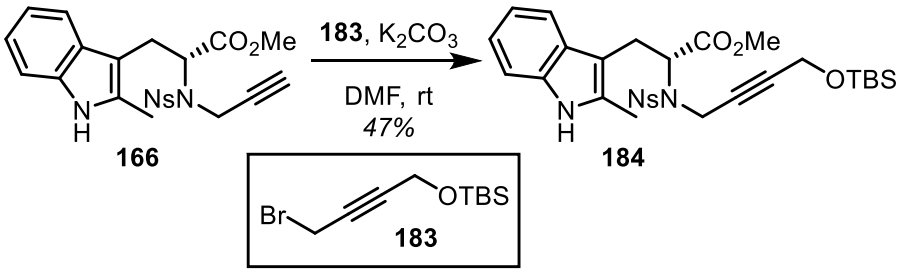

Sulfonamide 184. To a flame-dried 10 mL flask was added **166** (250 mg, 0.6 mmol, 1.0 equiv.) and DMF (3 mL) at 25 °C. The mixture was cooled to 0 °C and K_2CO_3 (99.5 mg, 0.72 mmol, 1.2 equiv.) was added. After 0.15 h, **183** (395 mg, 1.5 mmol, 2.5 equiv.) in DMF (1 mL) was added

dropwise. Upon completion of addition, the mixture was allowed to warm to 25 °C over 2 h. After 15 h, the reaction was complete and the mixture was quenched with aqueous $NaHCO_3$ (2 mL), the contents were transferred to a separatory funnel and diluted with EtOAc (10 mL). The layers were separated and the organic layer was washed with H_2O (5 × 10 mL) and brine (10 mL). The organic layer was dried over Na_2SO_4 and concentrated in vacuo. The resultant product was further purified by flash column chromatography (silica gel, Hexanes/EtOAc, 9:1) to give the desired **Sulfonamide 184** (170 mg, 47% yield) as a yellow foam.

184:

^{1}H NMR (500 MHz, $CDCl_3$) δ 8.05 – 7.99 (m, 2H), 7.79 (d, *J* = 8.8 Hz, 2H), 7.73 (s, 1H), 7.43 (d, *J* = 7.7 Hz, 1H), 7.21 – 7.17 (m, 1H), 7.12 – 7.08 (m, 1H), 7.05 (td, *J* = 7.4, 1.2 Hz, 1H), 4.83 (t, *J* = 7.4 Hz, 1H), 4.43 (dt, *J* = 18.3, 2.0 Hz, 1H), 4.37 (dt, *J* = 18.3, 1.9 Hz, 1H), 4.19 (t, *J* = 1.9 Hz, 2H), 3.56 (s, 3H), 3.43 (dd, *J* = 14.7, 7.4 Hz, 1H), 3.08 (dd, *J* = 14.7, 7.4 Hz, 1H), 2.34 (s, 3H), 0.89 (s, 9H), 0.09 (d, *J* = 1.0 Hz, 6H).

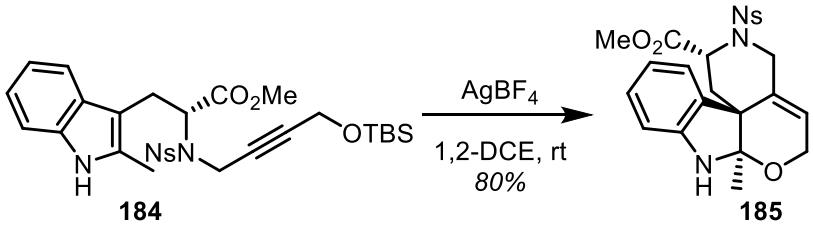

Indoline 185. To a flame-dried 1-dram vial was added **184** (10 mg, 0.0167 mmol, 1.0 equiv.) and 1,2-DCE (0.33 mL) and $AgBF_4$ (3.2 mg, 0.0167 mmol, 1.0 equiv.) was add and the mixture was allowed to stir at 25 °C for 4 h. The mixture was directly submitted to flash column

chromatography (silica gel, Hexanes/EtOAc, 4:1) to give the desired **Indolie 185** (6.5 mg, 80% yield) as an off-white solid.

185:

^{1}H NMR (500 MHz, $CDCl_3$) δ 8.40 (d, *J* = 8.9 Hz, 2H), 8.05 (d, *J* = 8.9 Hz, 2H), 7.20 (d, *J* = 7.4 Hz, 1H), 7.09 – 7.05 (m, 1H), 6.74 – 6.68 (m, 1H), 6.62 (d, *J* = 7.8 Hz, 1H), 5.72 (s, 1H), 4.68 (t, *J* = 6.2 Hz, 1H), 4.35 (d, *J* = 16.6 Hz, 1H), 4.21 (d, *J* = 12.6 Hz, 1H), 3.98 (d, *J* = 16.4 Hz, 1H), 3.78 (d, *J* = 12.6 Hz, 1H), 3.57 (s, 3H), 2.51 – 2.41 (m, 2H), 1.44 (s, 3H).

SECTION 2.8: ^{1}H AND ^{13}C NMR SPECTRA

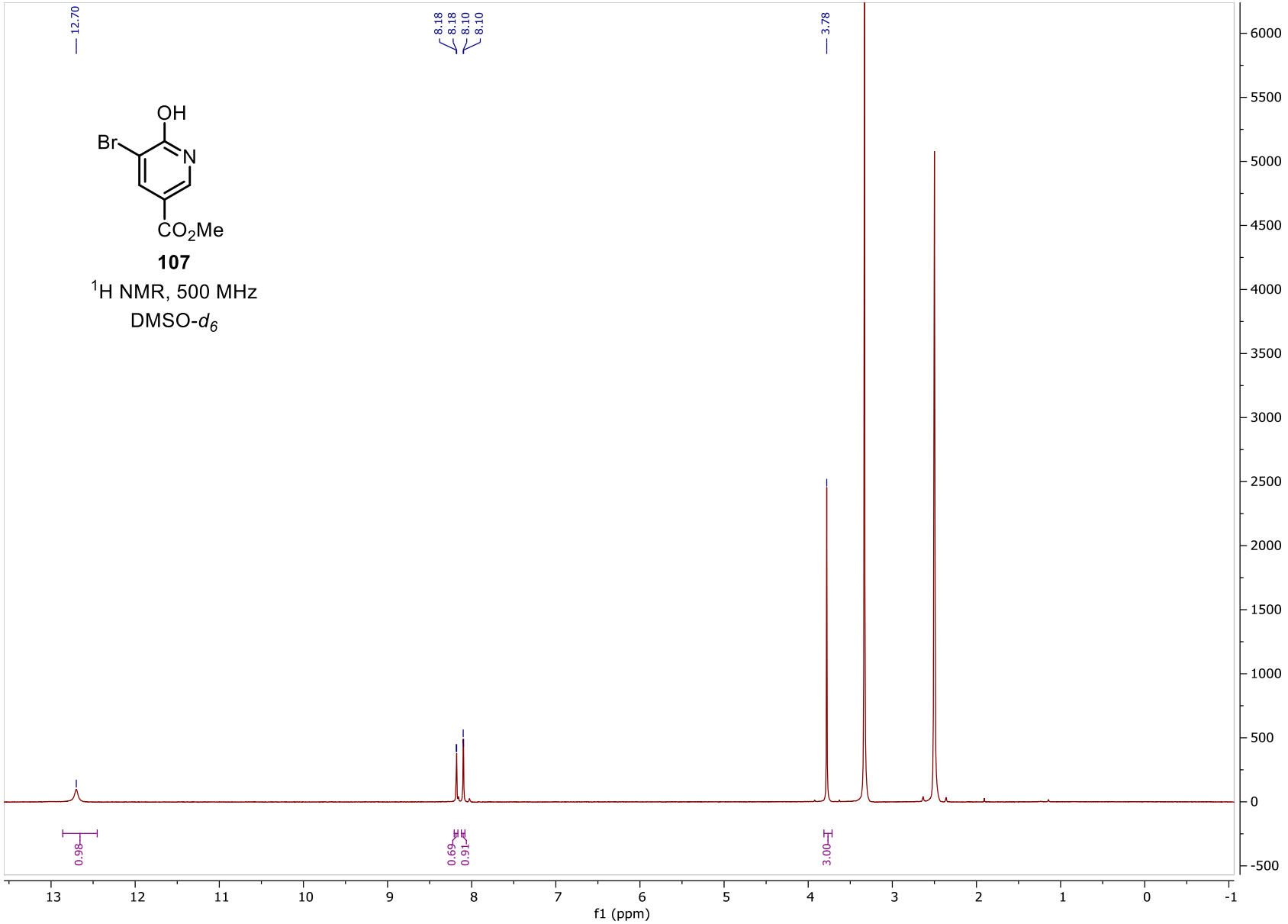
12.70
8.18
8.18
8.10
8.10
3.78
OH
Br
N
CO2Me
107
1H NMR, 500 MHz
DMSO-d6
0.98
0.69
0.91
3.00
f1 (ppm)

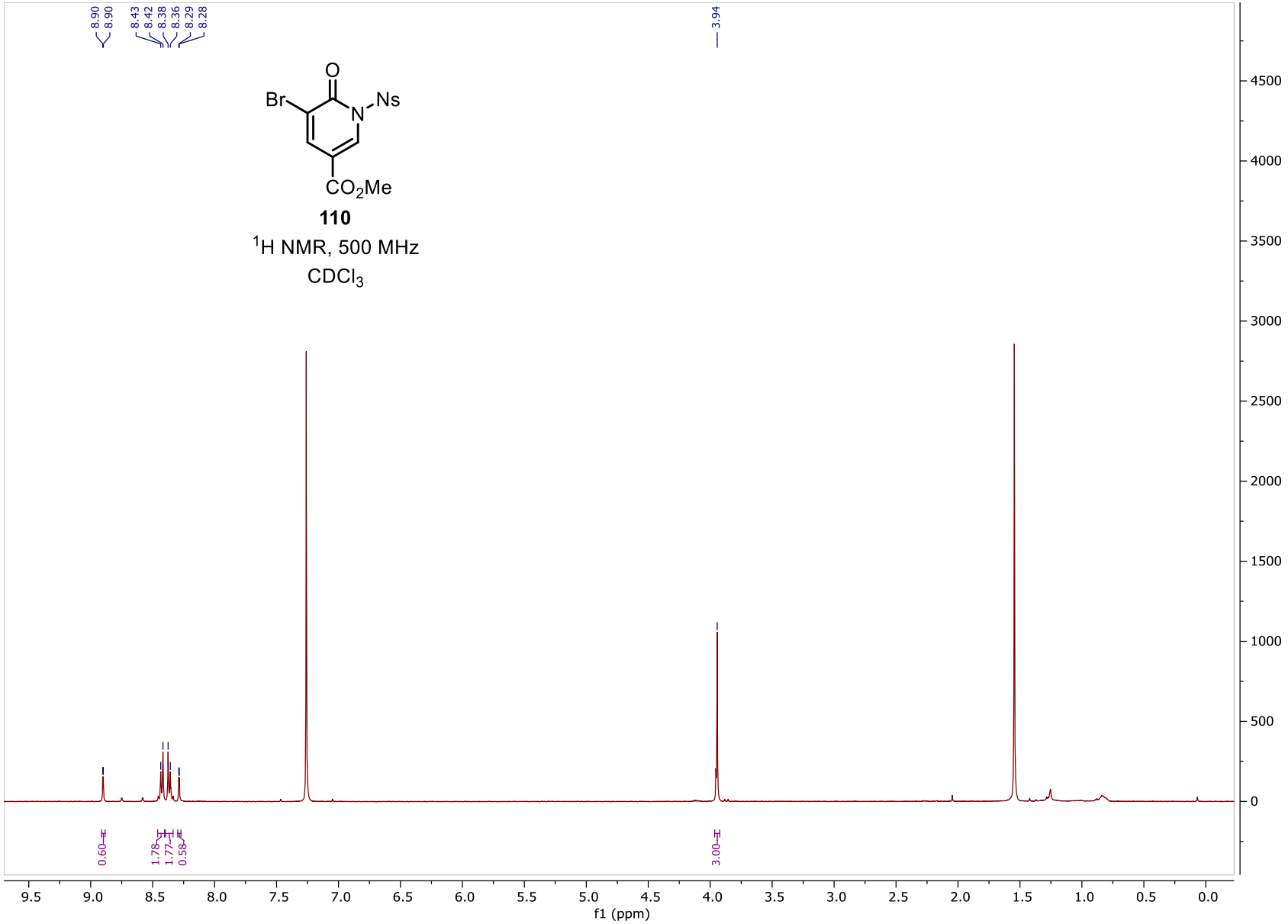
8.90
8.90
8.43
8.42
8.38
8.36
8.29
8.28
3.94
Br
O
N
Ns
CO2Me
110
1H NMR, 500 MHz
CDCl3
4500
4000
3500
3000
2500
2000
1500
1000
500
0
0.60
1.78
1.77
0.58
3.00
9.5
9.0
8.5
8.0
7.5
7.0
6.5
6.0
5.5
5.0
4.5
4.0
3.5
3.0
2.5
2.0
1.5
1.0
0.5
0.0
f1 (ppm)

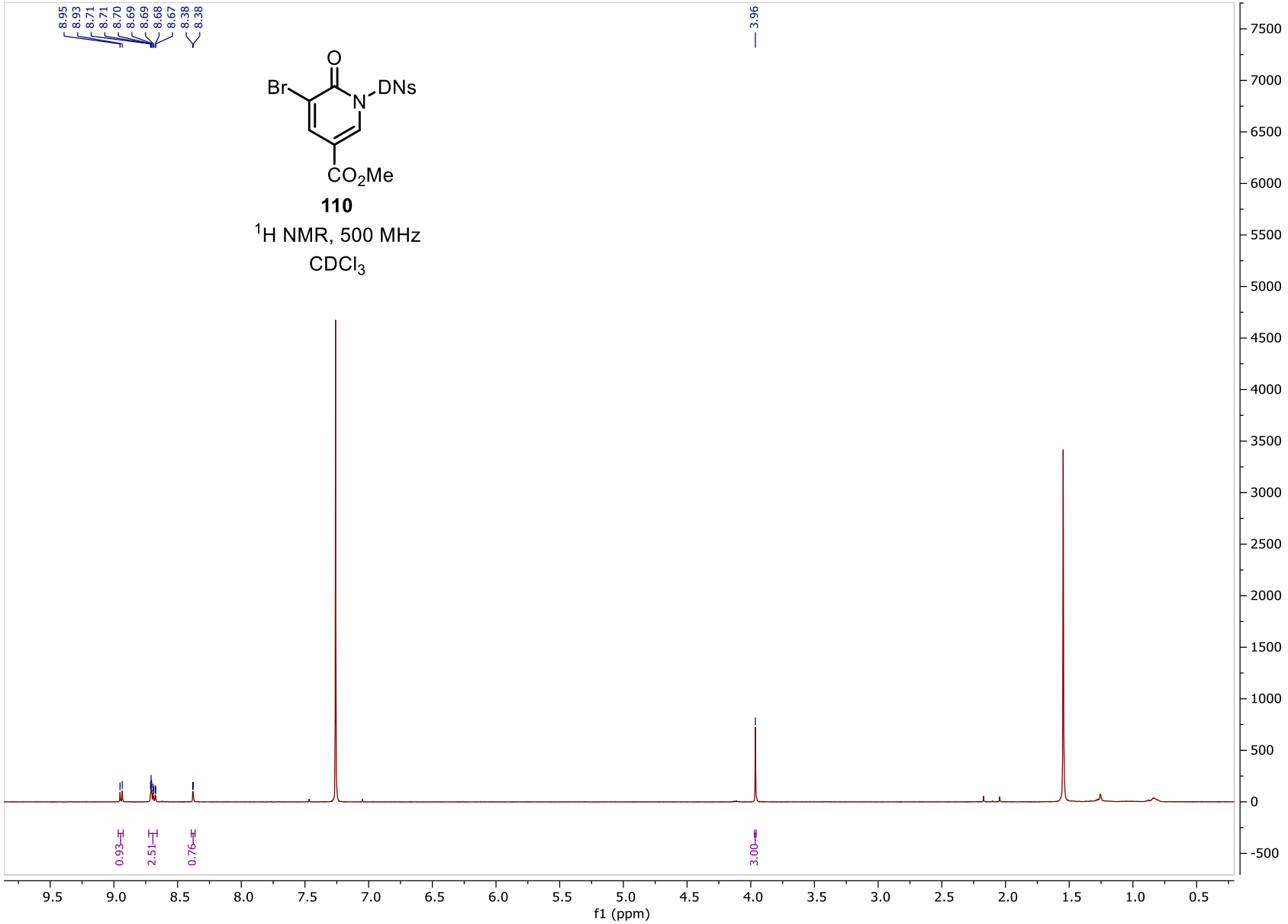
8.95
8.93
8.71
8.71
8.70
8.69
8.69
8.68
8.67
8.38
8.38
3.96
Br
O
N
DNs
CO2Me
110
1H NMR, 500 MHz
CDCl3
0.93
2.51
0.76
3.00
f1 (ppm)

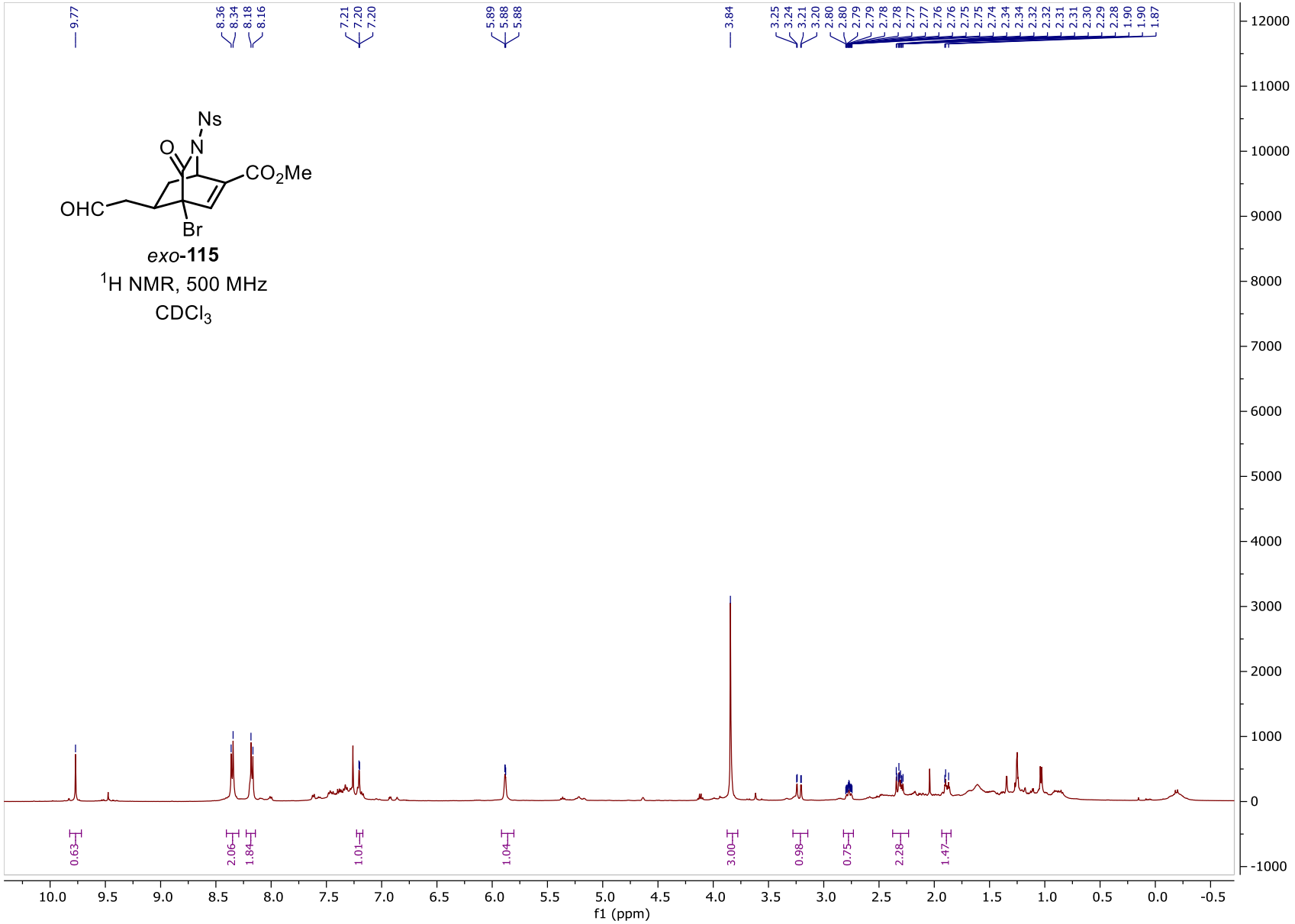
9.77
8.36
8.34
8.18
8.16
7.21
7.20
7.20
5.89
5.88
5.88
3.84
3.25
3.24
3.21
3.20
2.80
2.80
2.79
2.79
2.78
2.78
2.77
2.77
2.76
2.76
2.75
2.75
2.74
2.34
2.34
2.32
2.32
2.31
2.31
2.30
2.29
2.28
1.90
1.90
1.87
Ns
O
N
CO2Me
OHC
Br
exo-115
1H NMR, 500 MHz
CDCl3
0.63
2.06
1.84
1.01
1.04
3.00
0.98
0.75
2.28
1.47
f1 (ppm)

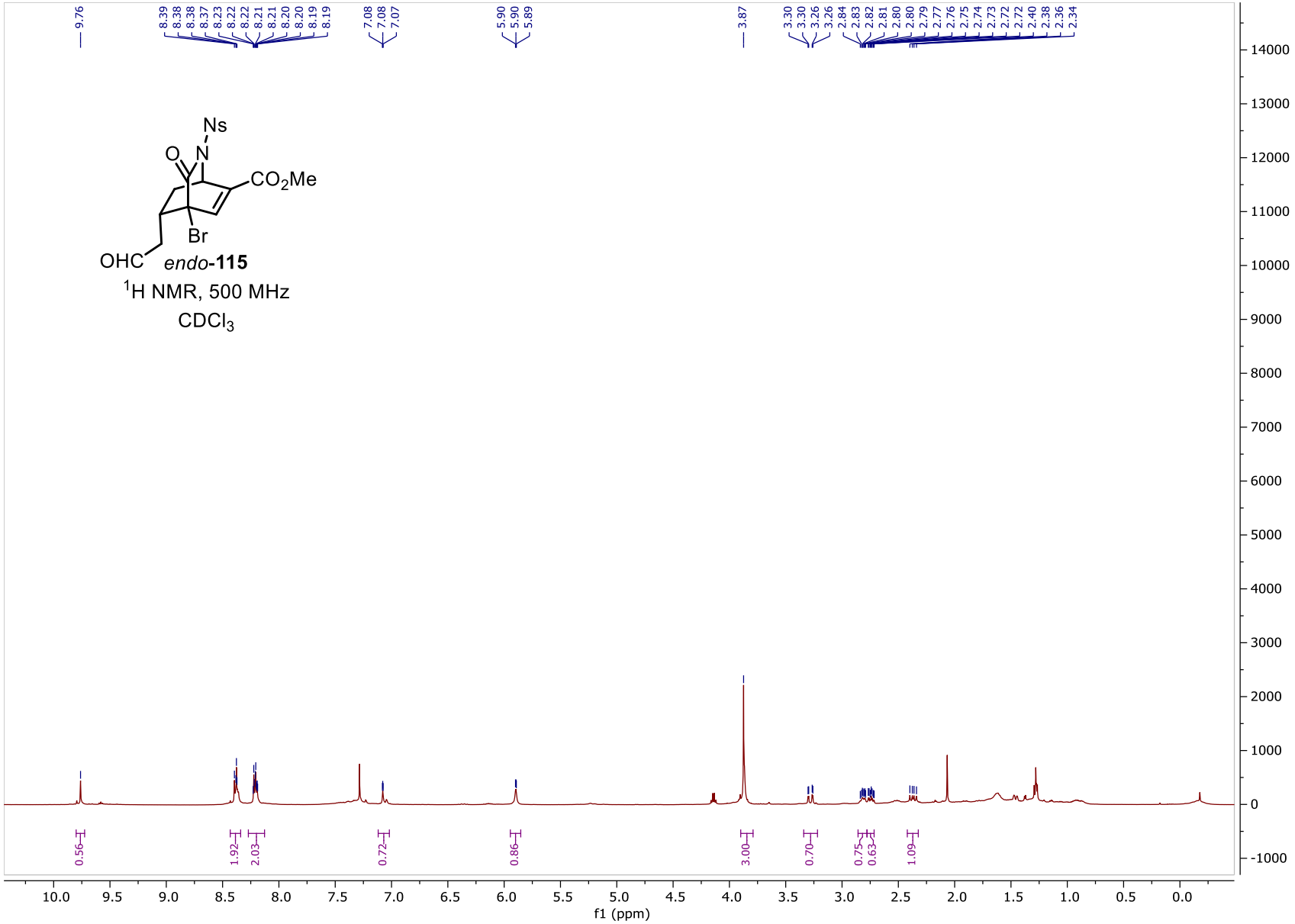
9.76
8.39
8.38
8.38
8.37
8.23
8.22
8.22
8.21
8.21
8.20
8.20
8.19
8.19
7.08
7.08
7.07
5.90
5.90
5.89
3.87
3.30
3.30
3.26
3.26
2.84
2.83
2.82
2.81
2.80
2.80
2.79
2.77
2.76
2.75
2.74
2.73
2.72
2.72
2.40
2.38
2.36
2.34
Ns
O
N
CO2Me
Br
OHC
endo-115
1H NMR, 500 MHz
CDCl3
0.56
1.92
2.03
0.72
0.86
3.00
0.70
0.75
0.63
1.09
f1 (ppm)

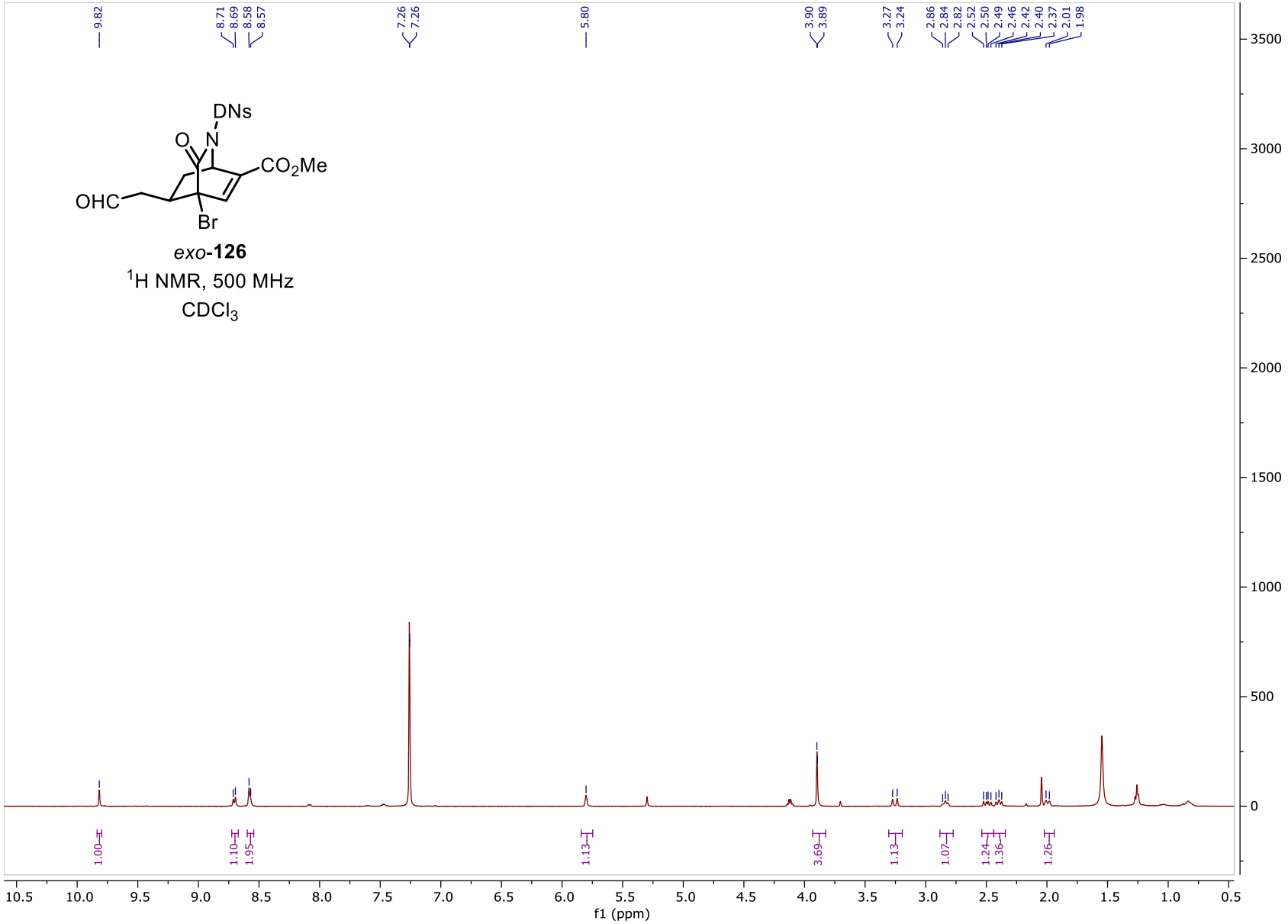
9.82
8.71
8.69
8.58
8.57
7.26
7.26
5.80
3.90
3.89
3.27
3.24
2.86
2.84
2.82
2.52
2.50
2.49
2.46
2.42
2.40
2.37
2.01
1.98
DNs
O
N
CO2Me
OHC
Br
exo-126
1H NMR, 500 MHz
CDCl3
1.00
1.10
1.95
1.13
3.69
1.13
1.07
1.24
1.36
1.26
3500
3000
2500
2000
1500
1000
500
0
10.5
10.0
9.5
9.0
8.5
8.0
7.5
7.0
6.5
6.0
5.5
5.0
4.5
4.0
3.5
3.0
2.5
2.0
1.5
1.0
0.5
f1 (ppm)

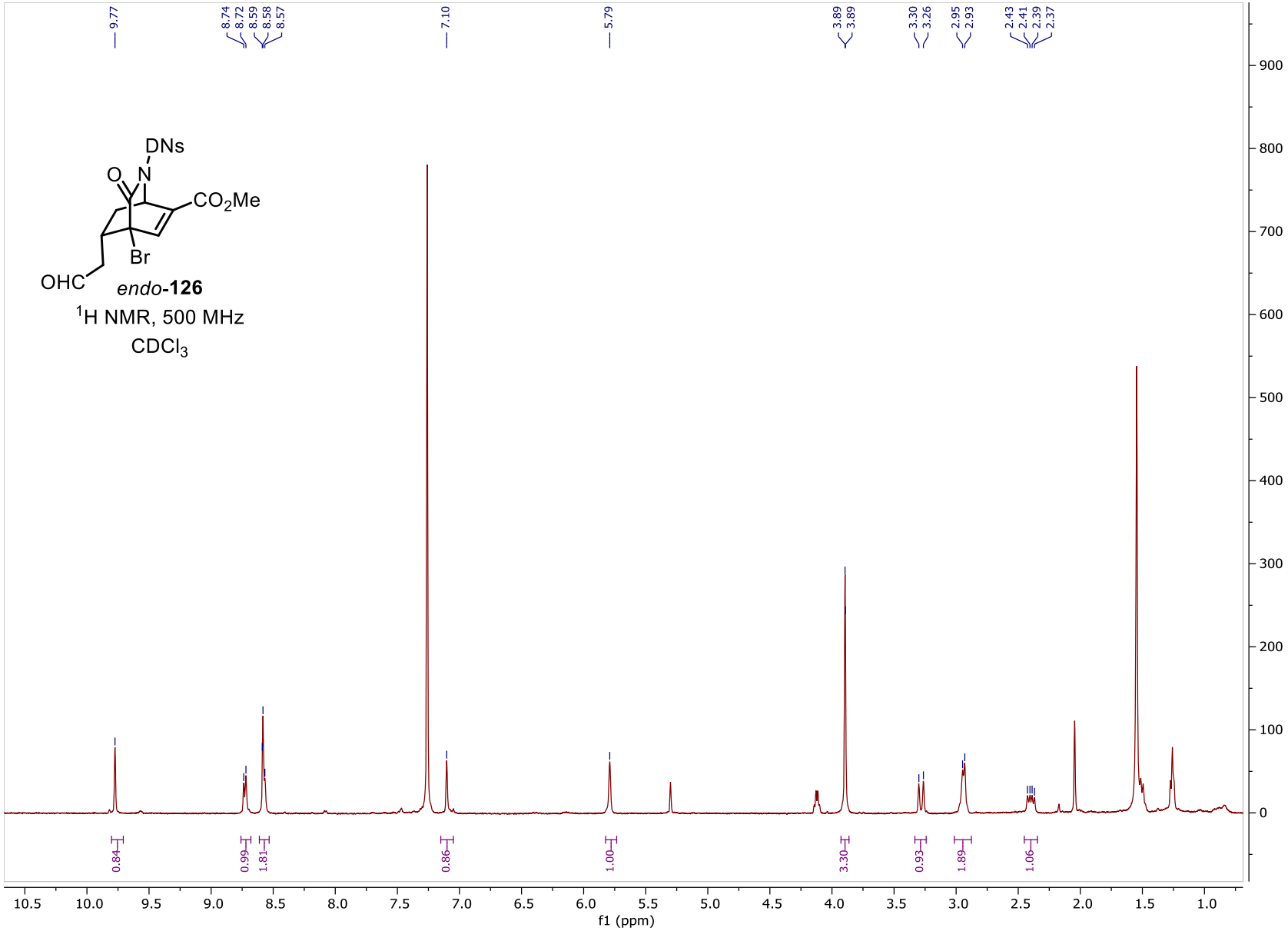
9.77
8.74
8.72
8.59
8.58
8.57
7.10
5.79
3.89
3.89
3.30
3.26
2.95
2.93
2.43
2.41
2.39
2.37
DNs
O
N
CO2Me
Br
OHC
endo-126
1H NMR, 500 MHz
CDCl3
0.84
0.99
1.81
0.86
1.00
3.30
0.93
1.89
1.06
f1 (ppm)

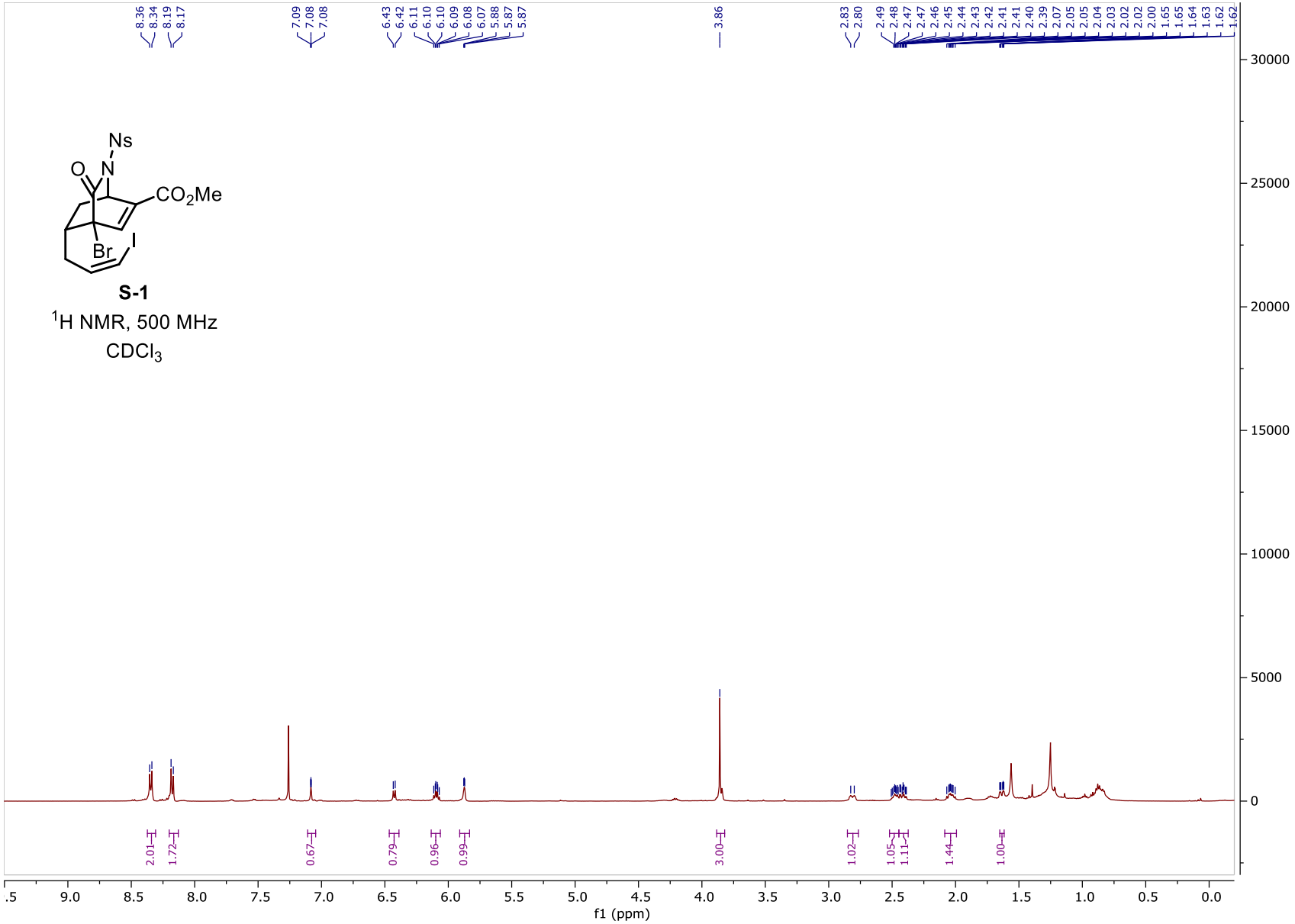
Ns
O
N
CO2Me
Br
I
S-1
1H NMR, 500 MHz
CDCl3
f1 (ppm)

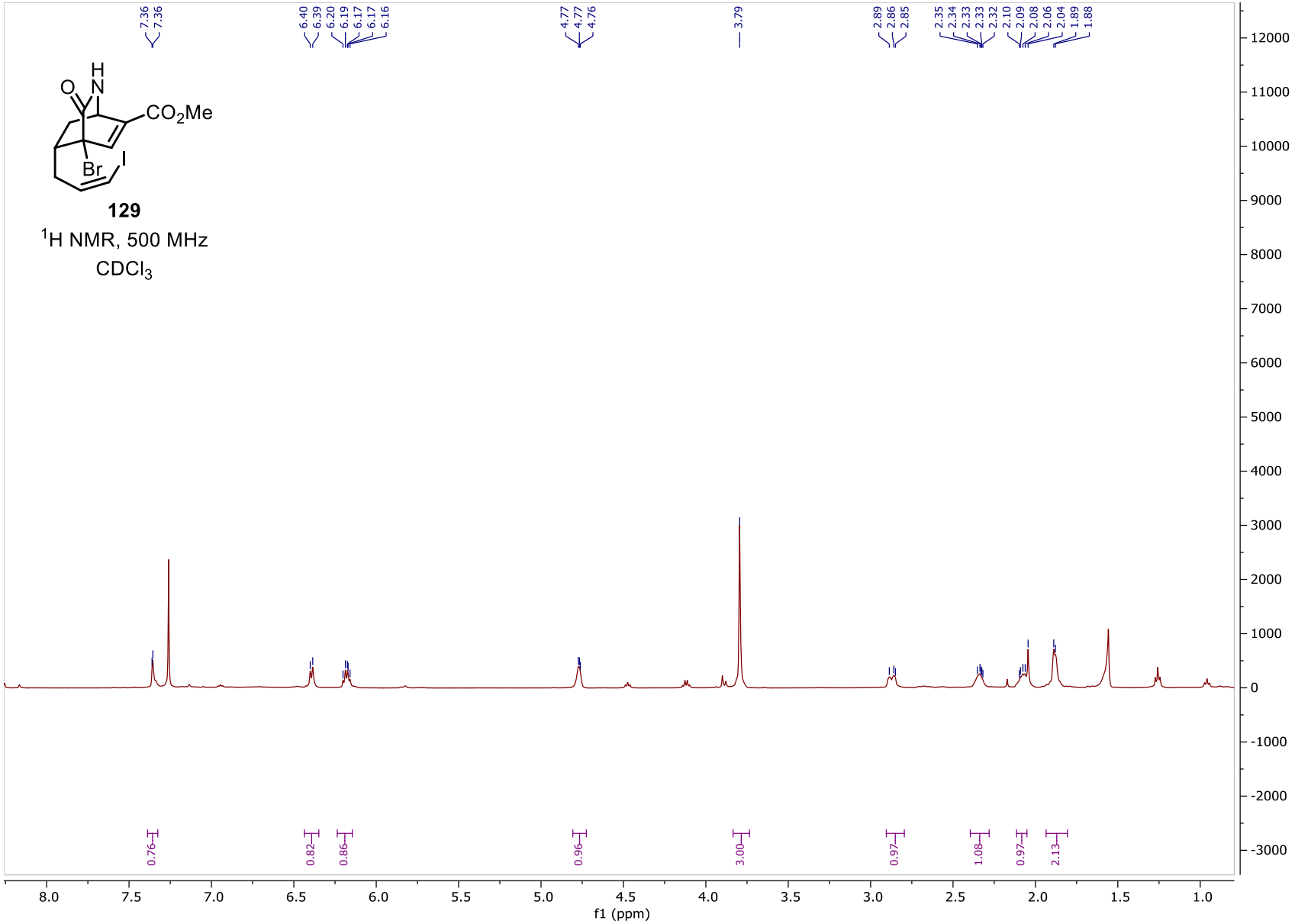
7.36
7.36
6.40
6.39
6.20
6.19
6.17
6.17
6.16
4.77
4.77
4.76
3.79
2.89
2.86
2.85
2.35
2.34
2.33
2.33
2.32
2.10
2.09
2.08
2.06
2.04
1.89
1.88
H
N
O
CO2Me
Br
I
129
1H NMR, 500 MHz
CDCl3
0.76
0.82
0.86
0.96
3.00
0.97
1.08
0.97
2.13
f1 (ppm)

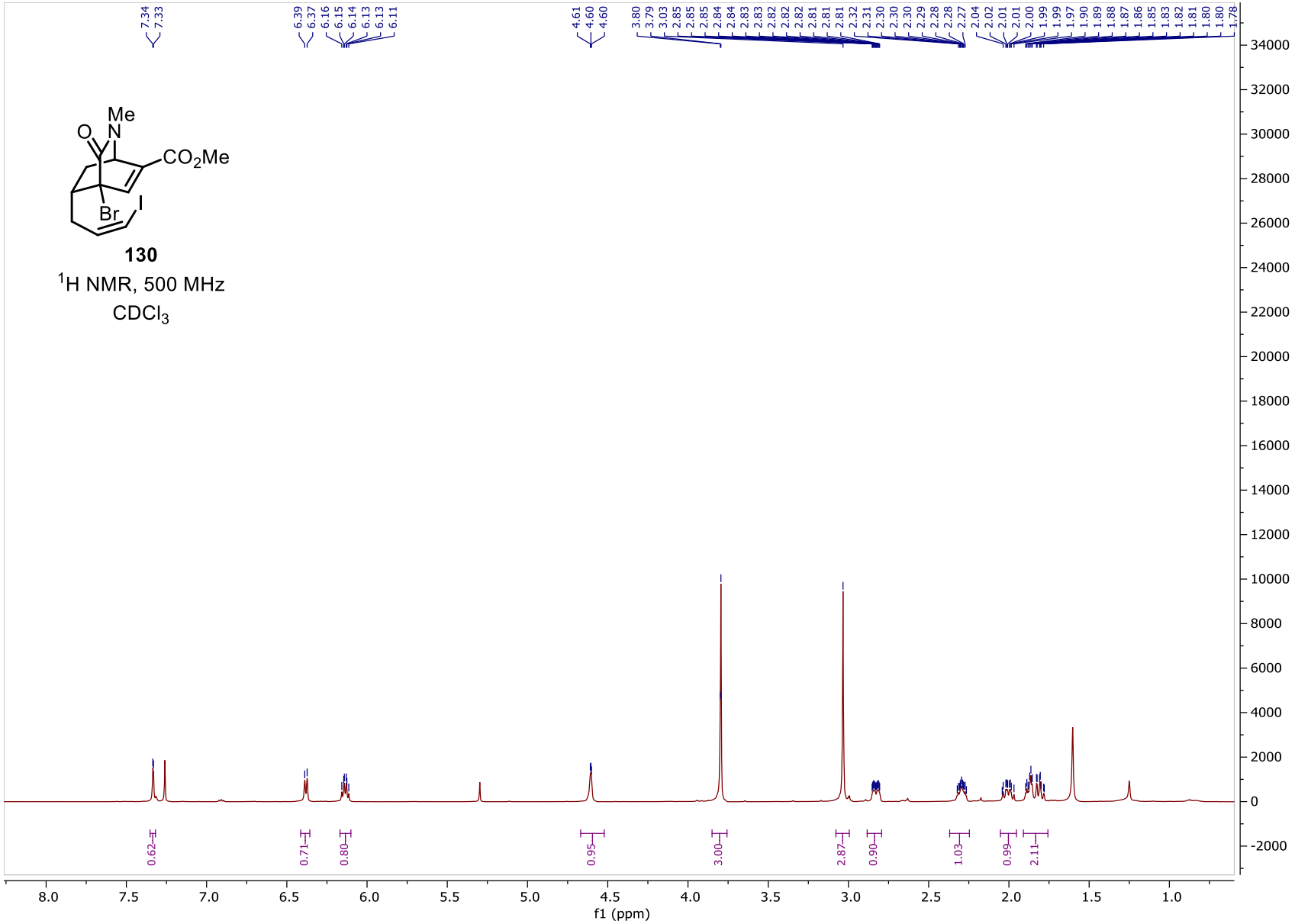
Me
O
N
CO2Me
Br
I
130
1H NMR, 500 MHz
CDCl3
f1 (ppm)

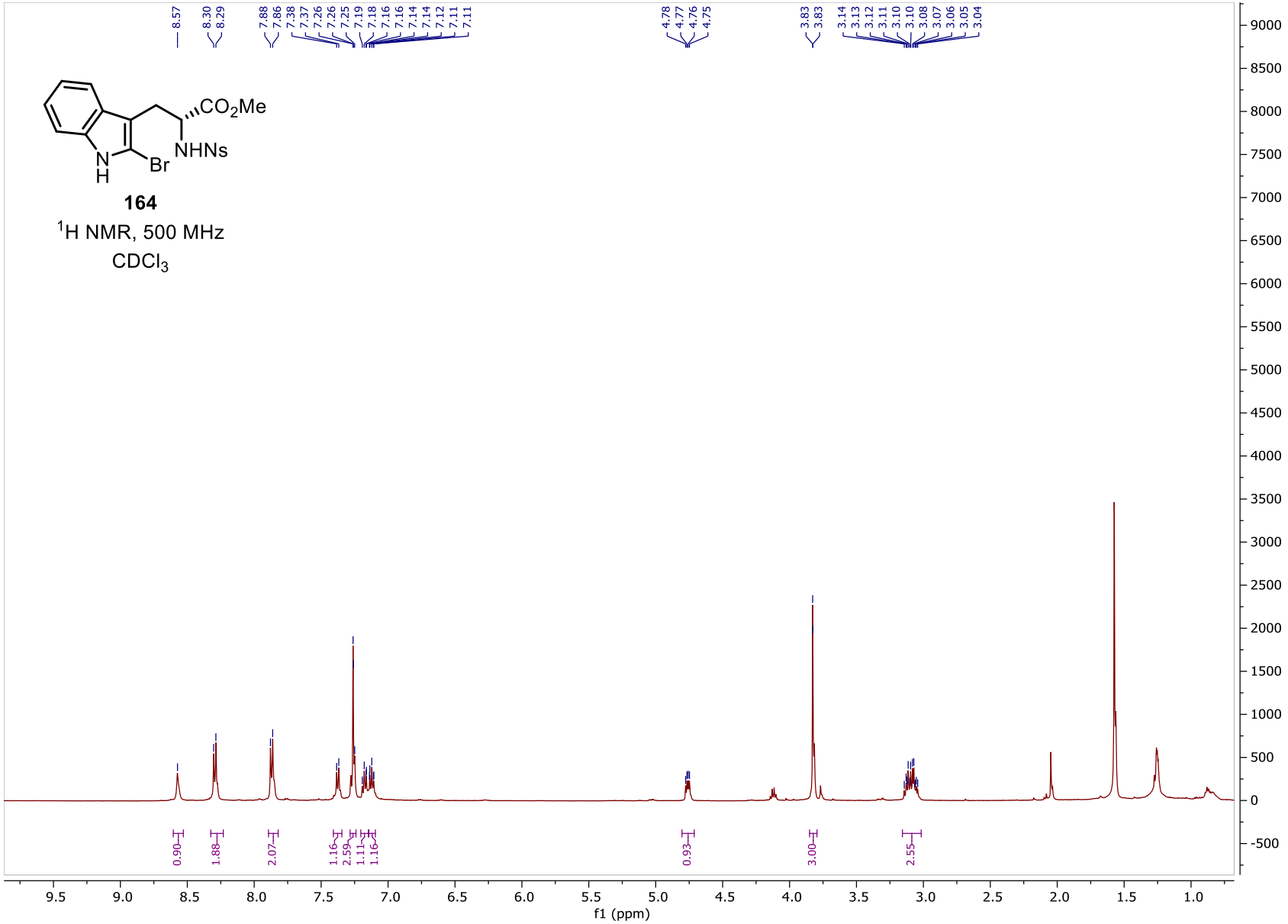
8.57
8.30
8.29
7.88
7.86
7.38
7.37
7.26
7.25
7.19
7.18
7.16
7.16
7.14
7.14
7.12
7.11
7.11
4.78
4.77
4.76
4.75
3.83
3.83
3.14
3.13
3.12
3.11
3.10
3.10
3.08
3.07
3.06
3.05
3.04
CO2Me
NHNs
N
H
Br
164
1H NMR, 500 MHz
CDCl3
0.90
1.88
2.07
1.16
2.59
1.11
1.16
0.93
3.00
2.55
f1 (ppm)

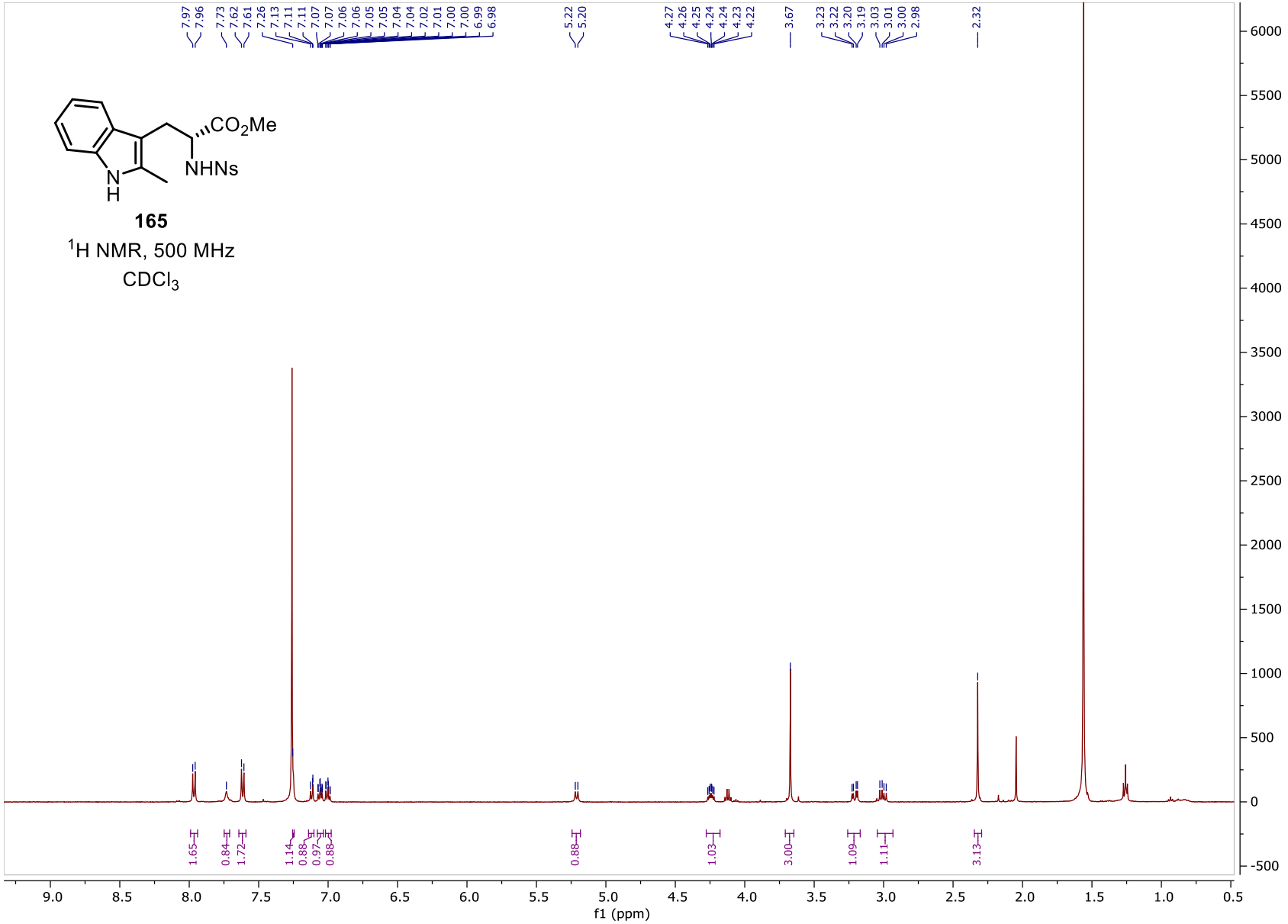
7.97
7.96
7.73
7.62
7.61
7.26
7.13
7.11
7.11
7.07
7.07
7.06
7.06
7.05
7.05
7.04
7.04
7.02
7.01
7.00
7.00
6.99
6.98
5.22
5.20
4.27
4.26
4.25
4.24
4.24
4.23
4.22
3.67
3.23
3.22
3.20
3.19
3.03
3.01
3.00
2.98
2.32
CO2Me
NHNs
N
H
165
1H NMR, 500 MHz
CDCl3
1.65
0.84
1.72
1.14
0.88
0.97
0.88
0.88
1.03
3.00
1.09
1.11
3.13
f1 (ppm)

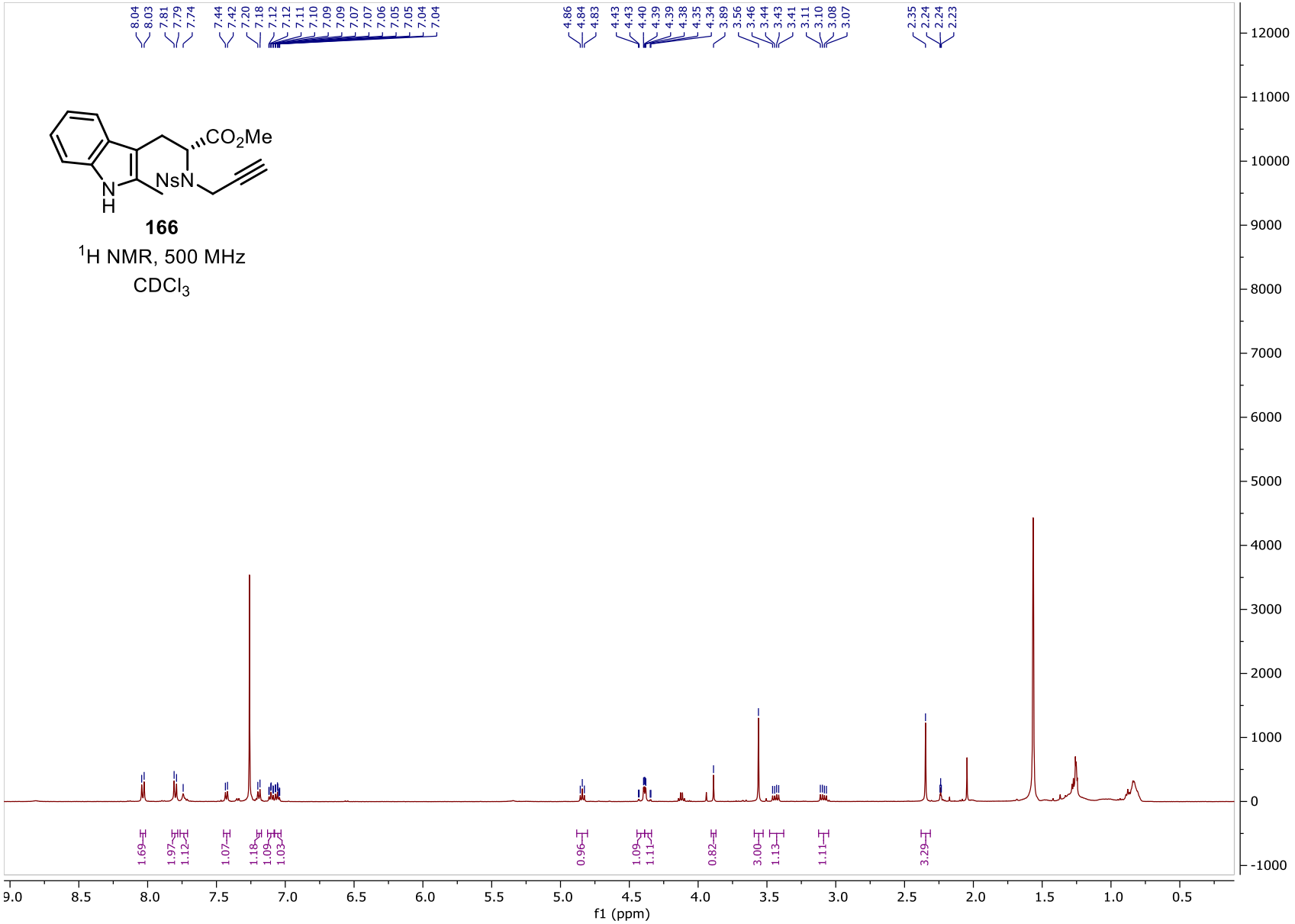
8.04
8.03
7.81
7.79
7.74
7.44
7.42
7.20
7.18
7.12
7.12
7.11
7.10
7.09
7.09
7.07
7.07
7.06
7.05
7.05
7.04
7.04
4.86
4.84
4.83
4.43
4.43
4.40
4.39
4.39
4.38
4.35
4.34
3.89
3.56
3.46
3.44
3.43
3.41
3.11
3.10
3.08
3.07
2.35
2.24
2.24
2.23
CO2Me
NsN
N
H
166
1H NMR, 500 MHz
CDCl3
1.69
1.97
1.12
1.07
1.18
1.09
1.03
0.96
1.09
1.11
0.82
3.00
1.13
1.11
3.29
12000
11000
10000
9000
8000
7000
6000
5000
4000
3000
2000
1000
0
-1000
9.0
8.5
8.0
7.5
7.0
6.5
6.0
5.5
5.0
4.5
4.0
3.5
3.0
2.5
2.0
1.5
1.0
0.5
f1 (ppm)

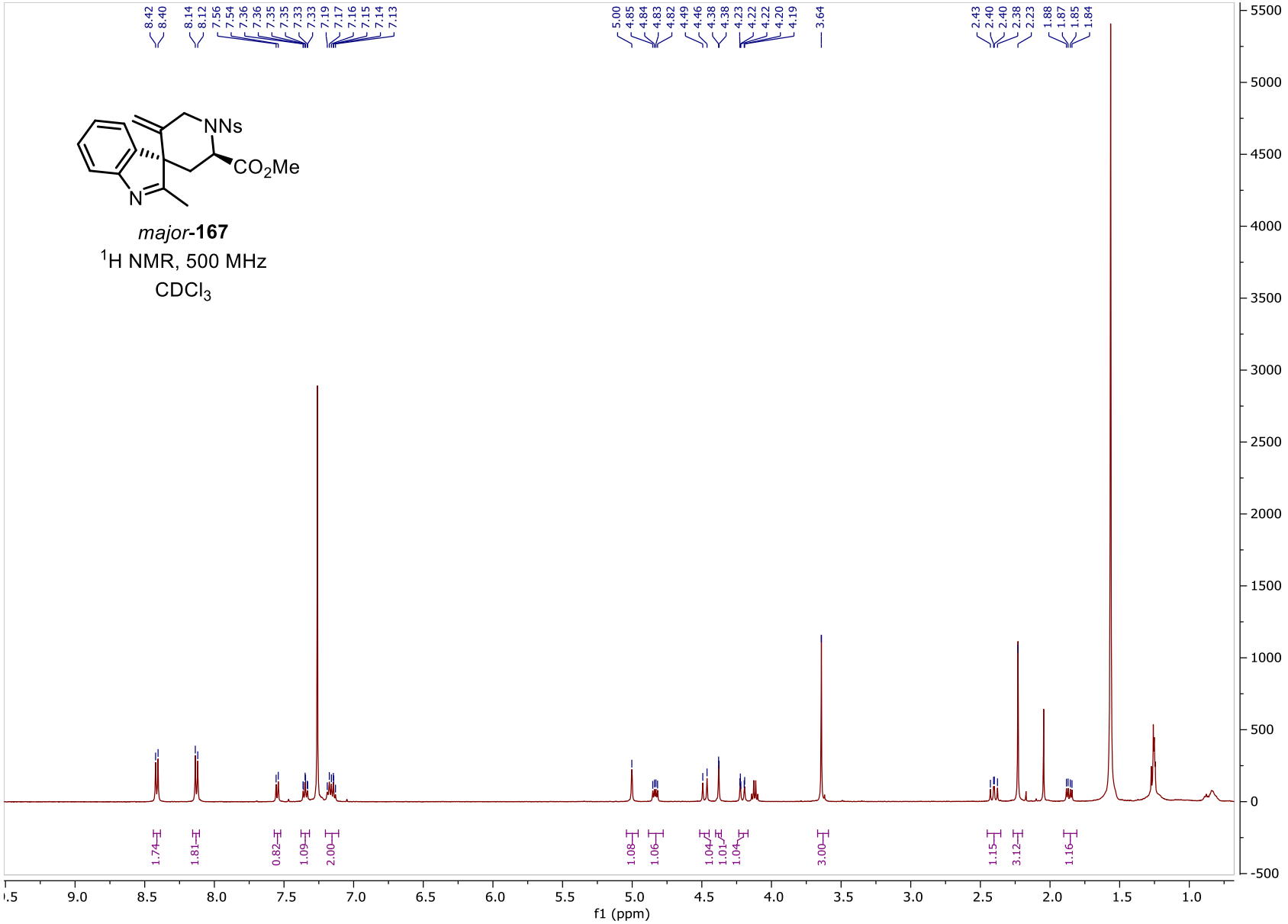
NNs
CO2Me
N
major-167
1H NMR, 500 MHz
CDCl3
f1 (ppm)

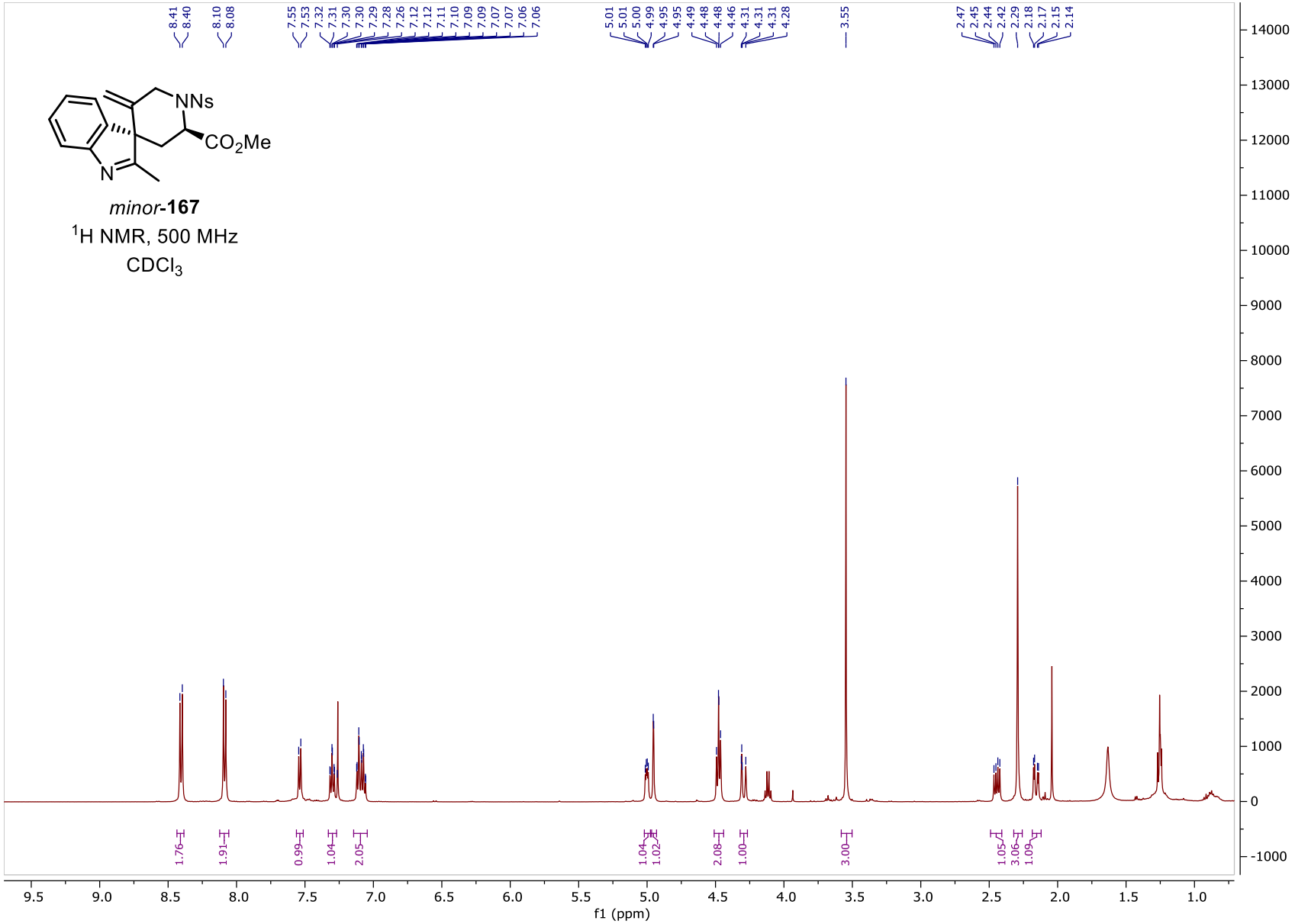
NNs
CO2Me
N
minor-167
1H NMR, 500 MHz
CDCl3
f1 (ppm)

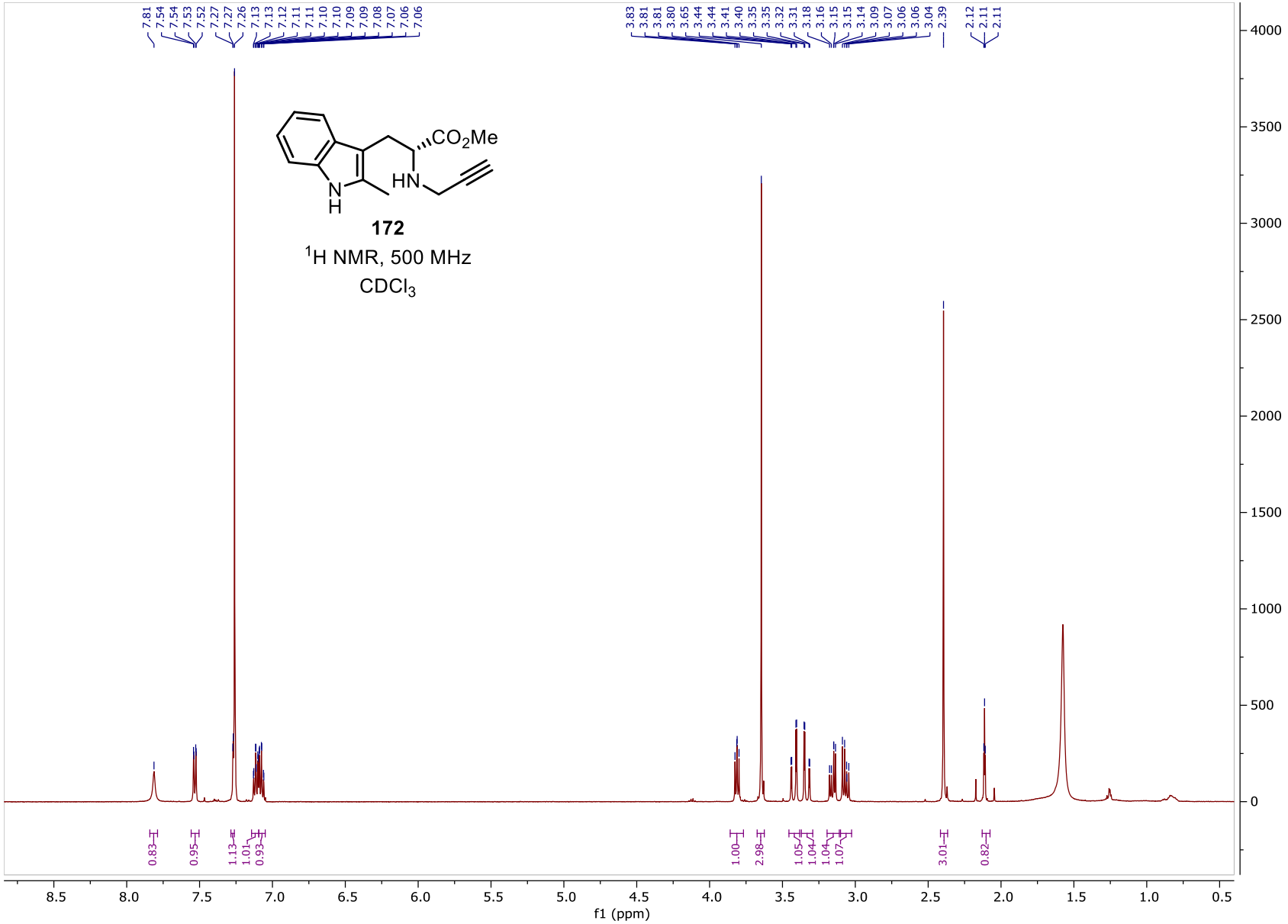
7.81 7.54 7.54 7.53 7.52 7.27 7.27 7.26 7.13 7.13 7.12 7.11 7.11 7.10 7.10 7.09 7.09 7.08 7.07 7.06 7.06
3.83 3.81 3.81 3.80 3.65 3.44 3.44 3.41 3.40 3.35 3.35 3.32 3.31 3.18 3.16 3.15 3.15 3.14 3.09 3.07 3.06 3.06 3.04 2.39
2.12 2.11 2.11
CO2Me
HN
N
H
172
1H NMR, 500 MHz
CDCl3
0.83 0.95 1.13 1.01 0.93 1.00 2.98 1.05 1.04 1.04 1.07 3.01 0.82
4000 3500 3000 2500 2000 1500 1000 500 0
8.5 8.0 7.5 7.0 6.5 6.0 5.5 5.0 4.5 4.0 3.5 3.0 2.5 2.0 1.5 1.0 0.5
f1 (ppm)

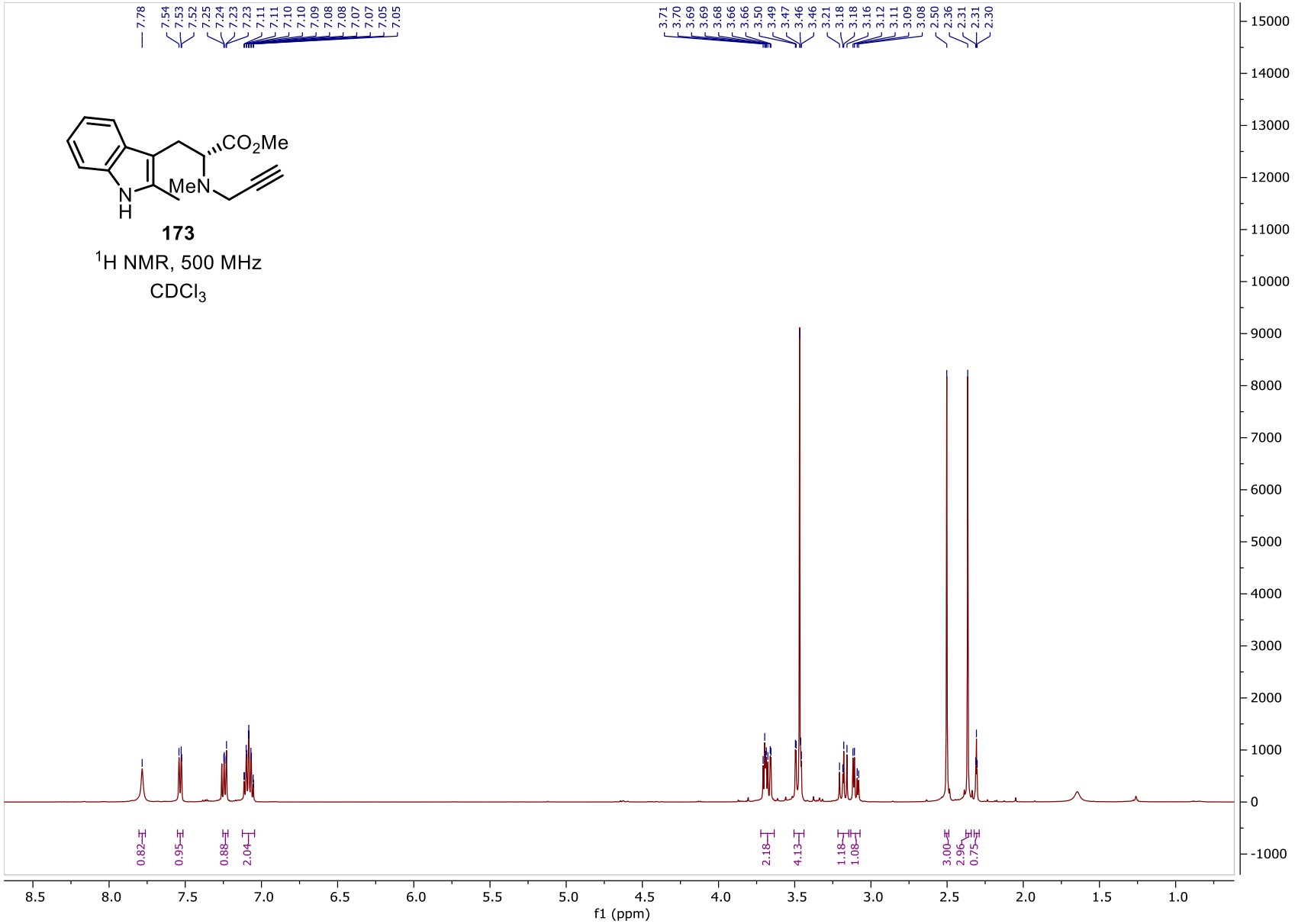
7.78
7.54
7.53
7.52
7.25
7.24
7.23
7.23
7.11
7.11
7.10
7.10
7.09
7.08
7.08
7.07
7.07
7.05
7.05
3.71
3.70
3.69
3.69
3.68
3.66
3.66
3.50
3.49
3.47
3.46
3.46
3.21
3.18
3.18
3.16
3.12
3.11
3.09
3.08
2.50
2.36
2.31
2.31
2.30
CO2Me
MeN
N
H
173
1H NMR, 500 MHz
CDCl3
0.82
0.95
0.88
2.04
2.18
4.13
1.18
1.08
3.00
2.96
0.75
f1 (ppm)

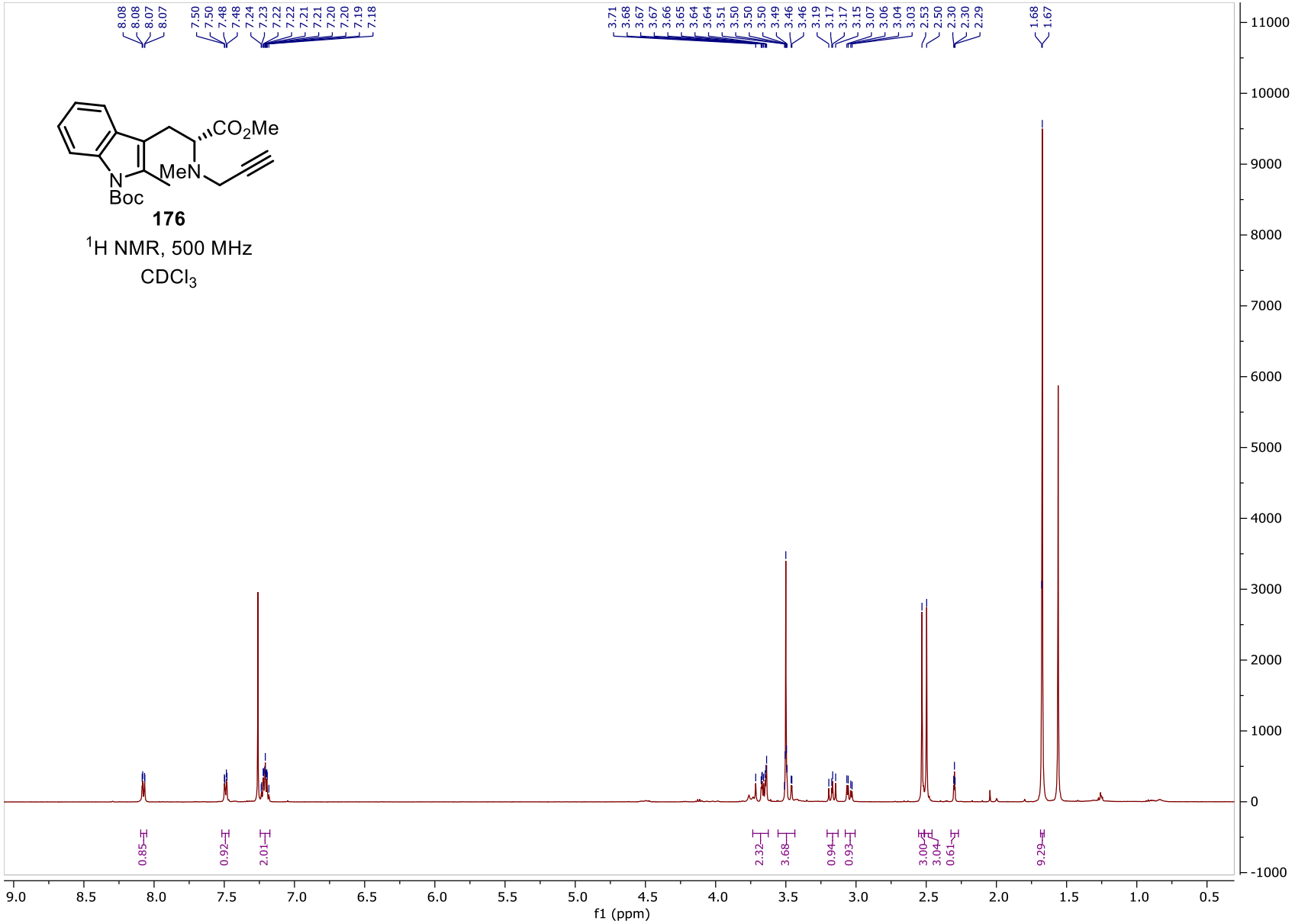
8.08
8.08
8.07
8.07
7.50
7.50
7.48
7.48
7.24
7.23
7.22
7.22
7.21
7.21
7.20
7.20
7.19
7.18
3.71
3.68
3.67
3.67
3.66
3.65
3.64
3.64
3.51
3.50
3.50
3.50
3.49
3.46
3.46
3.19
3.17
3.17
3.15
3.07
3.06
3.04
3.03
2.53
2.50
2.30
2.30
2.29
1.68
1.67
CO2Me
MeN
N
Boc
176
1H NMR, 500 MHz
CDCl3
0.85
0.92
2.01
2.32
3.68
0.94
0.93
3.00
3.04
0.61
9.29
f1 (ppm)

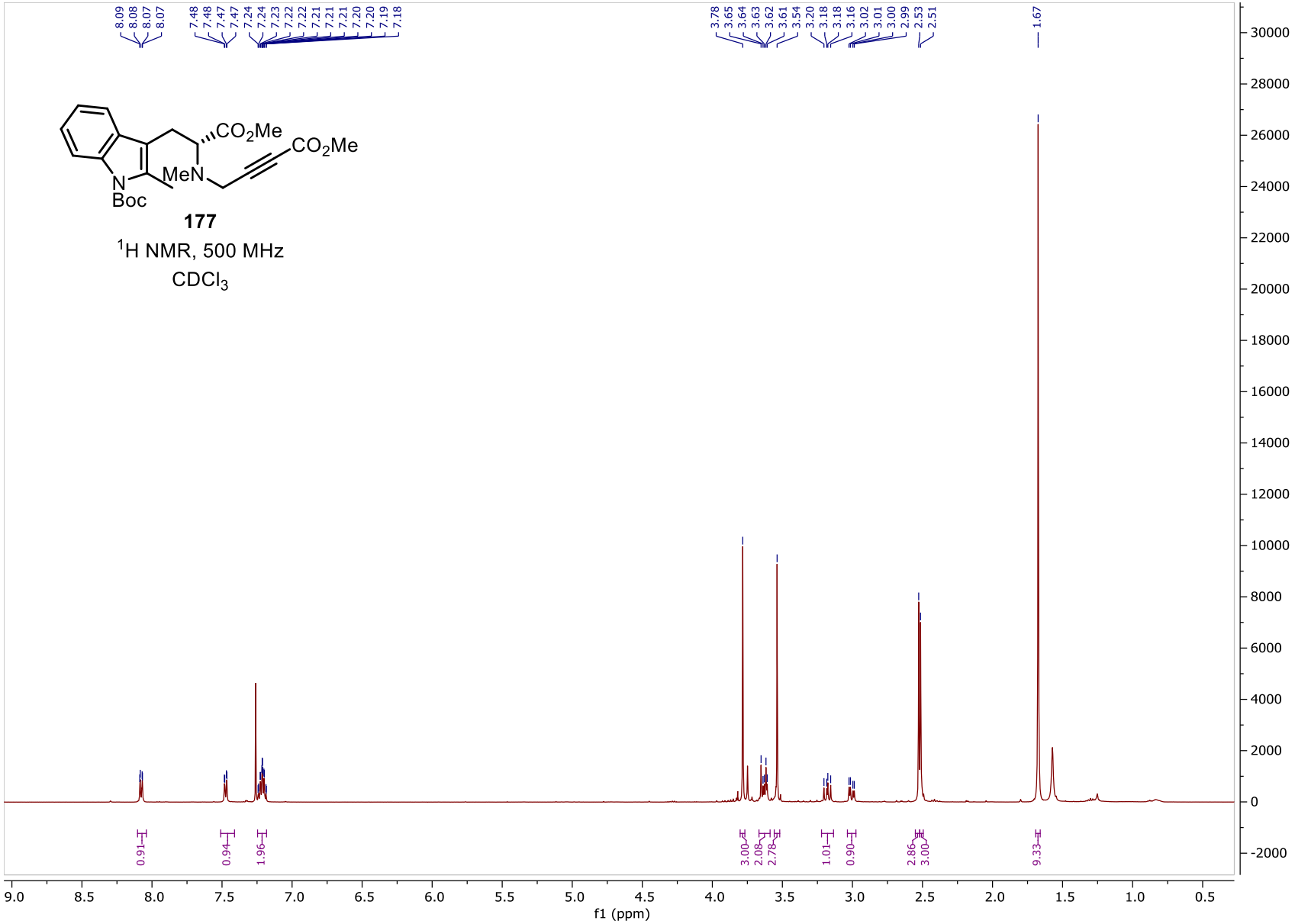
8.09
8.08
8.07
8.07
7.48
7.48
7.47
7.47
7.24
7.24
7.23
7.22
7.22
7.21
7.21
7.21
7.20
7.20
7.19
7.18
3.78
3.65
3.64
3.63
3.62
3.61
3.54
3.20
3.18
3.18
3.16
3.02
3.01
3.00
2.99
2.53
2.51
1.67
CO2Me
CO2Me
MeN
N
Boc
177
1H NMR, 500 MHz
CDCl3
0.91
0.94
1.96
3.00
2.08
2.78
1.01
0.90
2.86
3.00
9.33
f1 (ppm)

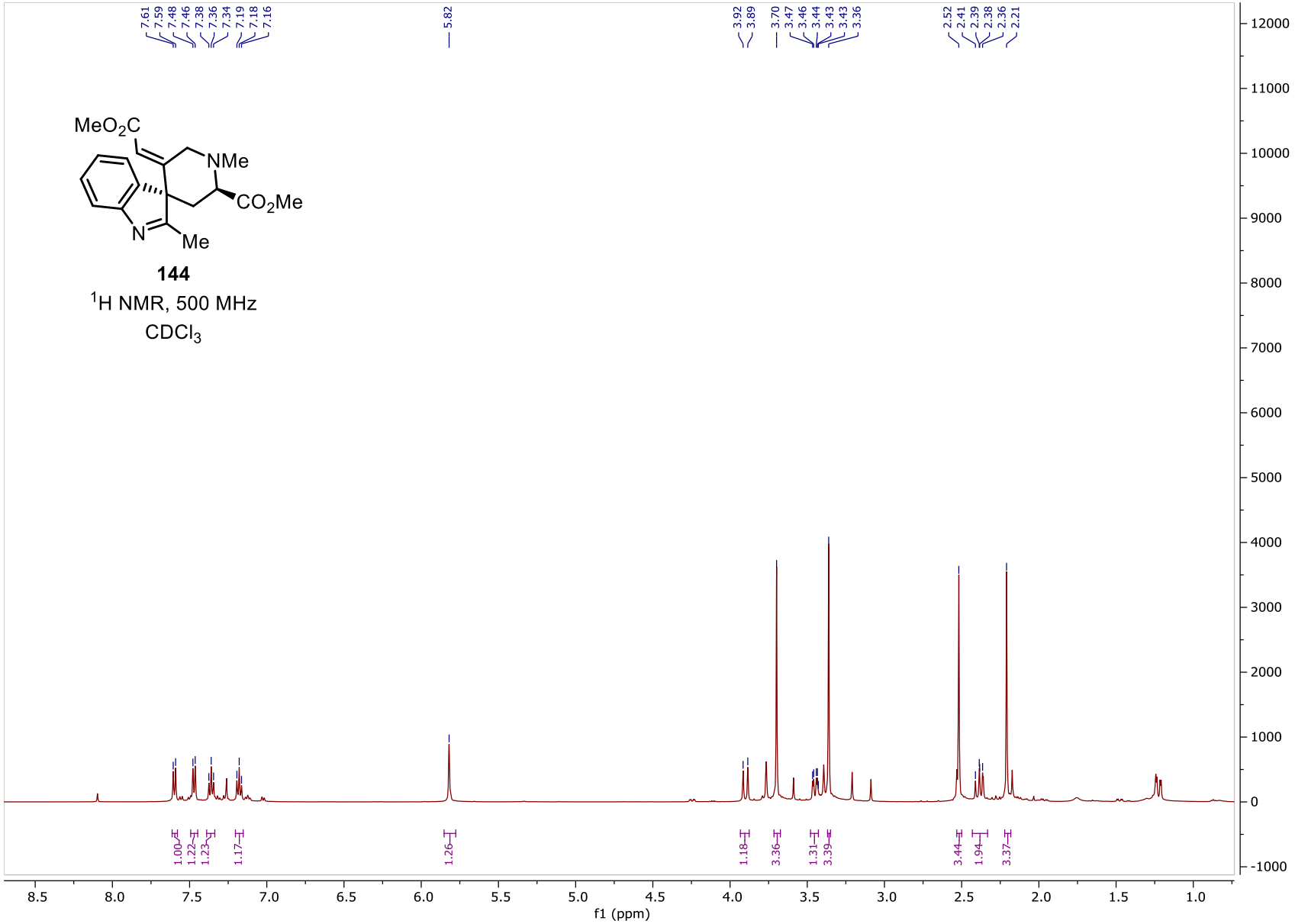
MeO2C
NMe
CO2Me
N
Me
144
1H NMR, 500 MHz
CDCl3
7.61
7.59
7.48
7.46
7.38
7.36
7.34
7.19
7.18
7.16
5.82
3.92
3.89
3.70
3.47
3.46
3.44
3.43
3.43
3.36
2.52
2.41
2.39
2.38
2.36
2.21
1.00
1.22
1.23
1.17
1.26
1.18
3.36
1.31
3.39
3.44
1.94
3.37
f1 (ppm)

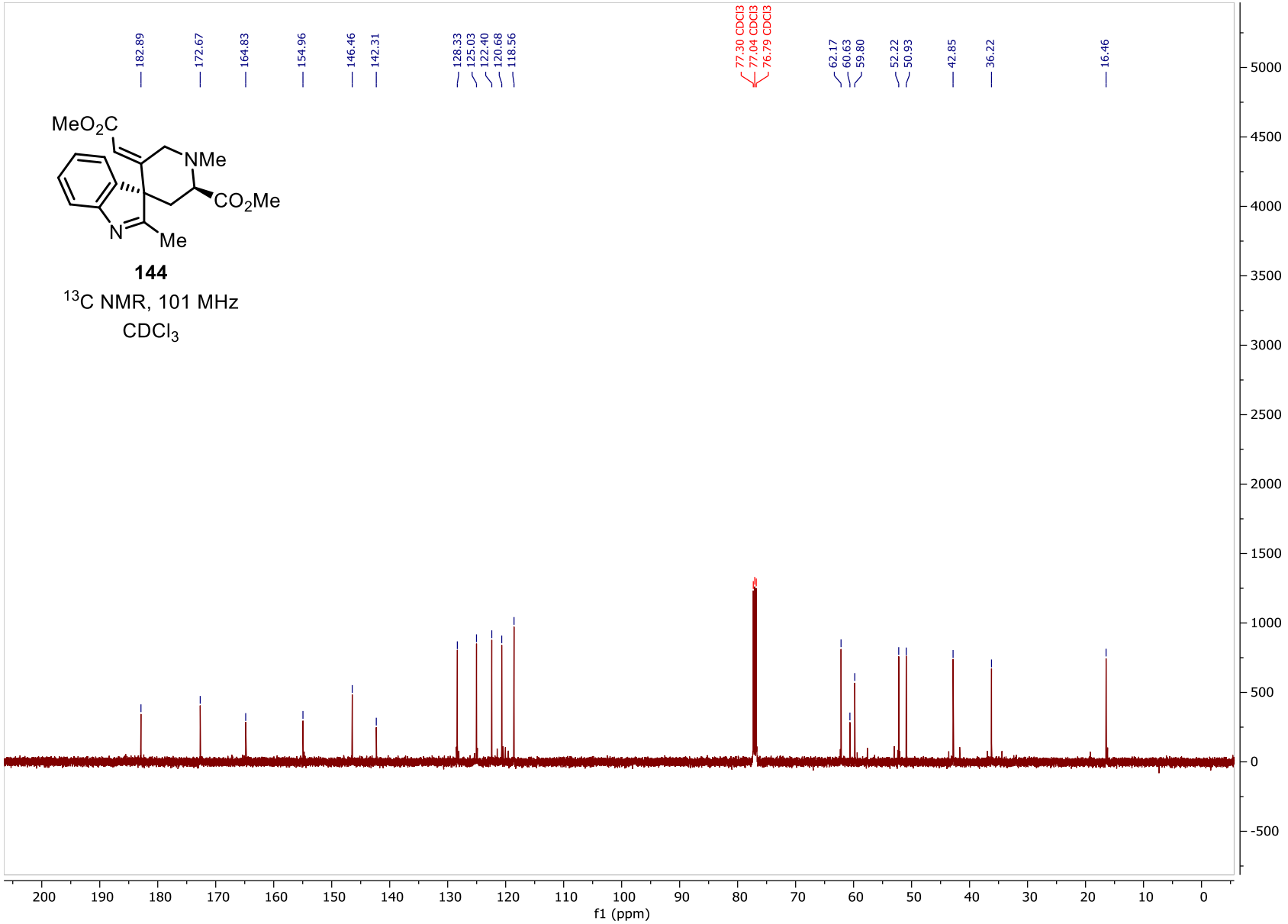
182.89
172.67
164.83
154.96
146.46
142.31
128.33
125.03
122.40
120.68
118.56
77.30 CDCl3
77.04 CDCl3
76.79 CDCl3
62.17
60.63
59.80
52.22
50.93
42.85
36.22
16.46
MeO2C
NMe
CO2Me
N
Me
144
13C NMR, 101 MHz
CDCl3
f1 (ppm)

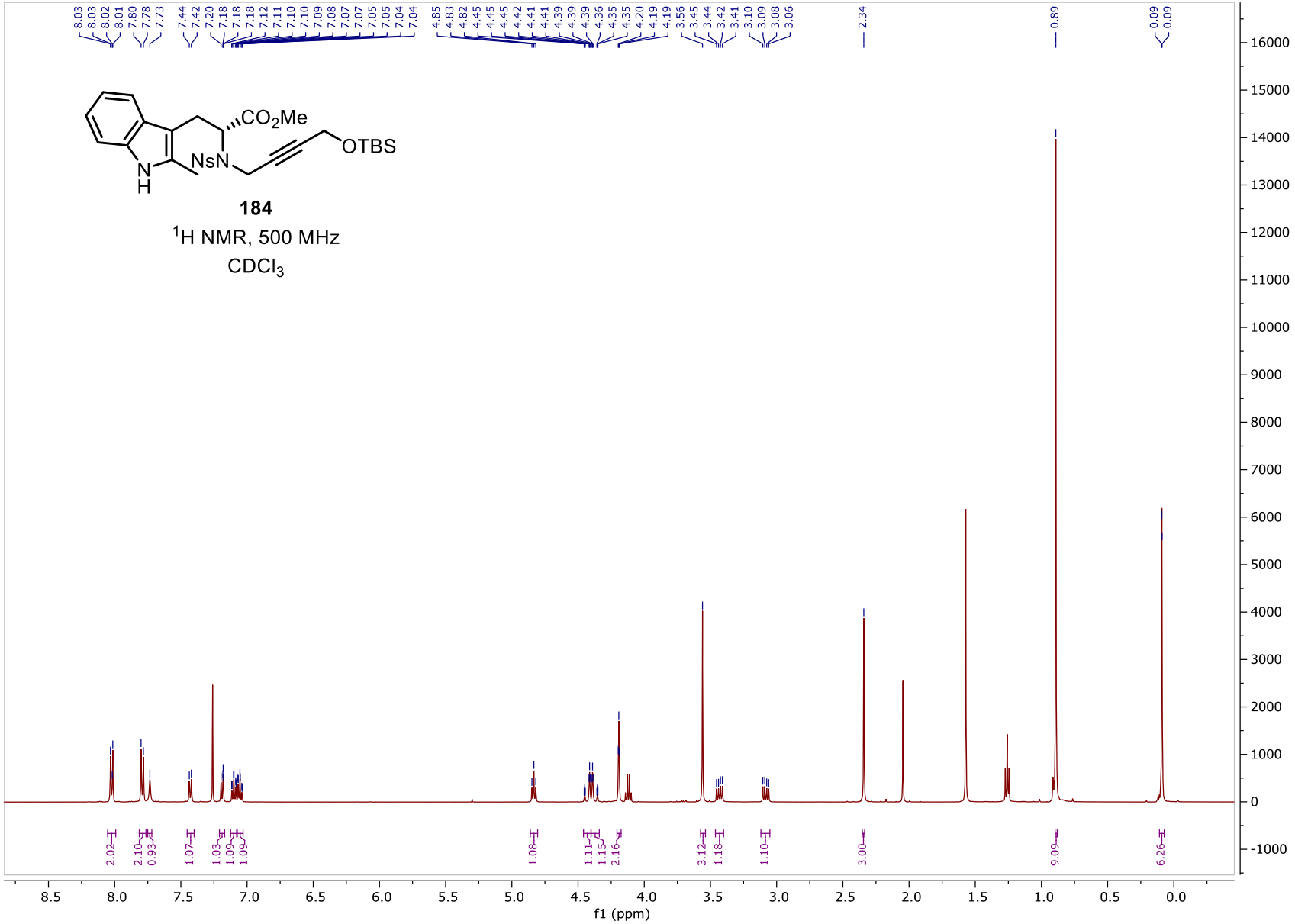
CO2Me
OTBS
NsN
N
H
184
1H NMR, 500 MHz
CDCl3
f1 (ppm)

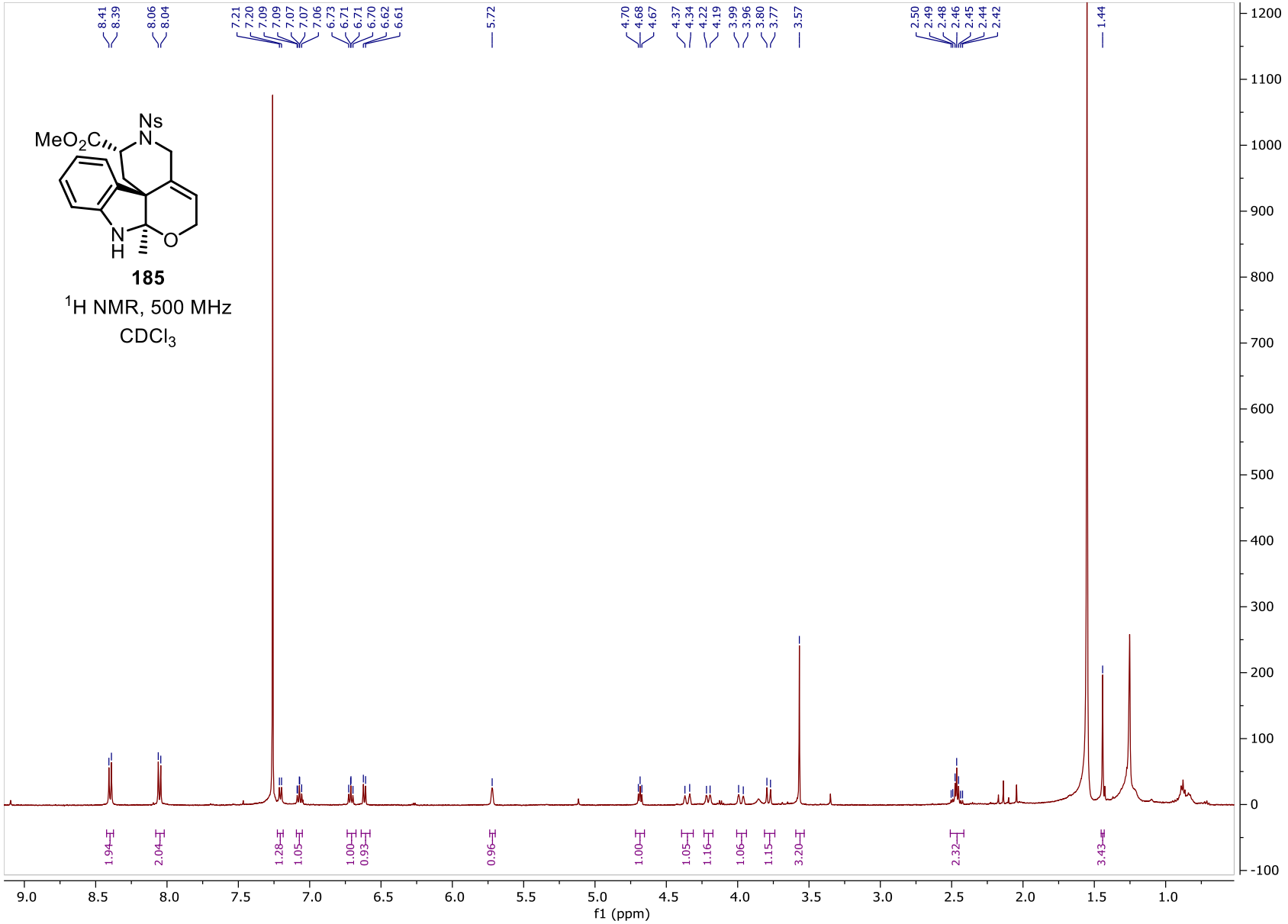
8.41
8.39
8.06
8.04
7.21
7.20
7.09
7.09
7.07
7.07
7.06
6.73
6.71
6.71
6.70
6.62
6.61
5.72
4.70
4.68
4.67
4.37
4.34
4.22
4.19
3.99
3.96
3.80
3.77
3.57
2.50
2.49
2.48
2.46
2.45
2.44
2.42
1.44
Ns
N
MeO2C
N
H
O
185
1H NMR, 500 MHz
CDCl3
1.94
2.04
1.28
1.05
1.00
0.93
0.96
1.00
1.05
1.16
1.06
1.15
3.20
2.32
3.43
f1 (ppm)

CHAPTER III:

THE DIVERGENT TOTAL SYNTHESIS OF HARZIANE DITERPENES VIA A Au^{I}-CATALYZED [2+2] CYCLIZATION REACTION

SECTION 3.1: INTRODUCTION

Research in the Snyder group has heavily focused on the construction of all-carbon quaternary centers as a means to significantly expedite the total synthesis of complex natural products. Through the synthesis of several sparsely functionalized natural products such as presilphiperfolan-8-ol (**1**), the conidiogenones (**2**-**4**), and spiroviolene (**5**) and spirograterpene A (**6**), the group has showcased how all-carbon quaternary centers both enable desired reaction pathways while also precluding undesired reactivity.[1–3] In addition, the Au^{I}/Ag^{I}-mediated dearomative formation of quaternary centers has been a hallmark of our synthetic arsenal in the pursuit of a variety of indole alkaloids, including the total syntheses of scholarisine A (**7**), strictamine (**8**), arboridinine (**9**), and arborisidine (**10**).[4–6] Finally, the syntheses of the scaparvins B-D (**11**-**13**) and waihoensene (**14**) take advantage of a key Conia-ene cyclization to establish the key quaternary centers.[7,8]

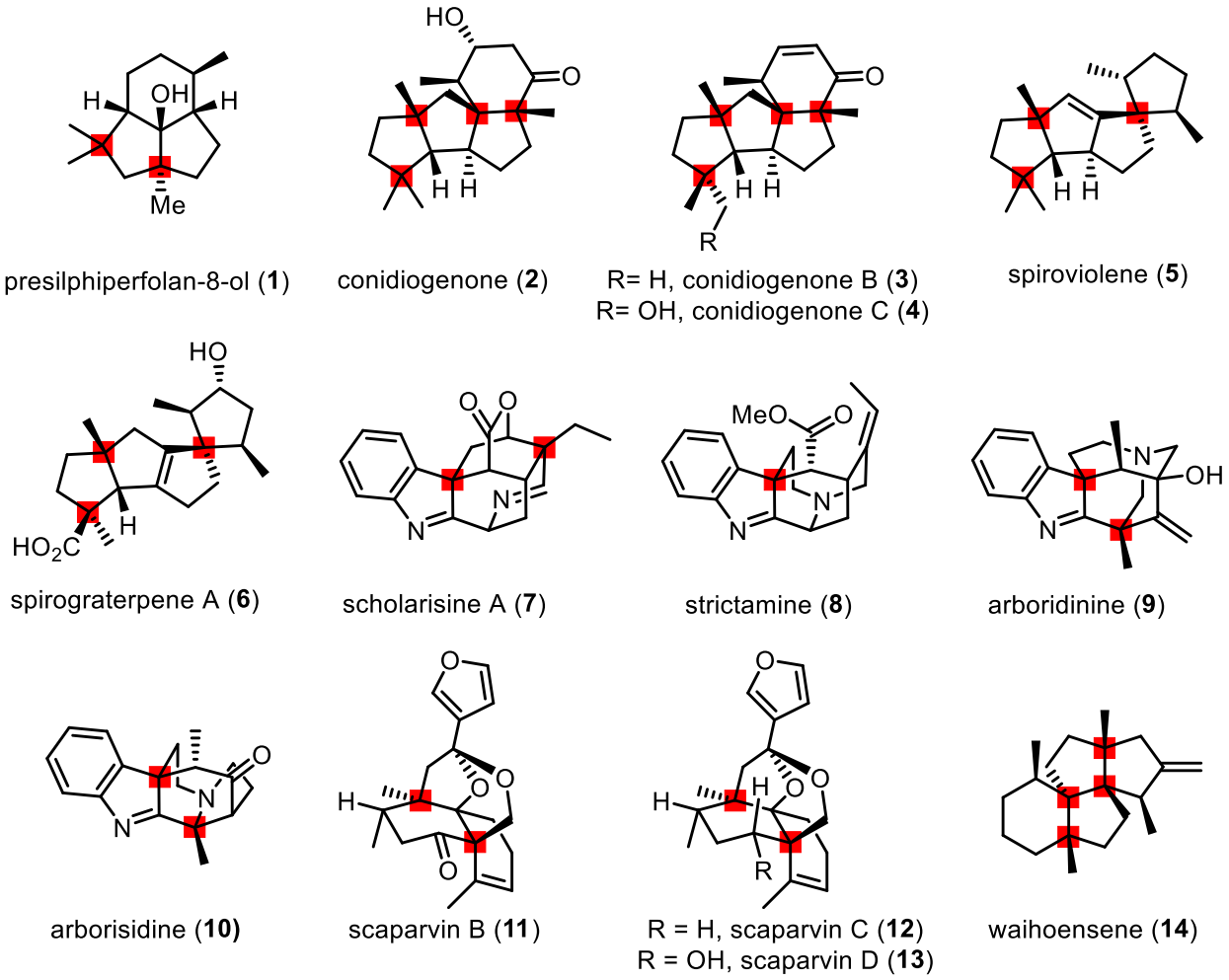

Figure 3.1. Natural product targets synthesized by the Snyder group, which showcase the challenges and strategic opportunities of all-carbon quaternary centers in total synthesis.

Our experience with Au^{I}/Ag^{I}-mediated cyclizations, both as a dearomative strategy for cage-shaped indole alkaloids, as well as in the construction of all-carbon quaternary centers *via* Conia-ene reactions, has motivated us to further explore the utility of such π-acid promoted transformations to rapidly deliver challenging, sterically congested quaternary centers in natural product targets.[9–11] In so doing, we envisioned targeting a family of diterpenoid natural products, with late-stage divergence being at the center of our approach. The harziane diterpenes met our requirements quite readily, with all members containing three all-carbon quaternary centers (highlighted in purple, Scheme 3.2) and four contiguous stereocenters and all members presenting

a structurally fascinating and sterically challenging 6/5/7/4 ring system. Our analysis of the structure of the harziane diterpene family (Figure 3.2) found that establishment of the ring fused-cyclobutyl moiety would be a central element to achieving a concise synthesis. Within the literature, a plethora of methods have been published to establish such moieties, including the use of photochemical, Lewis acid-catalyzed,[12] and transition metal-catalyzed [2+2] cycloadditions.[13–17] Drawing inspiration from the previously reported Au^{I}-catalyzed [2+2] cyclization of 1,8-enynes, we proposed a divergent total synthesis of the harziane diterpene family that centered around the construction of the fused 7/4 ring system and accounted for the wide range of oxidation states and substitution patterns found within this class of targets.[18]

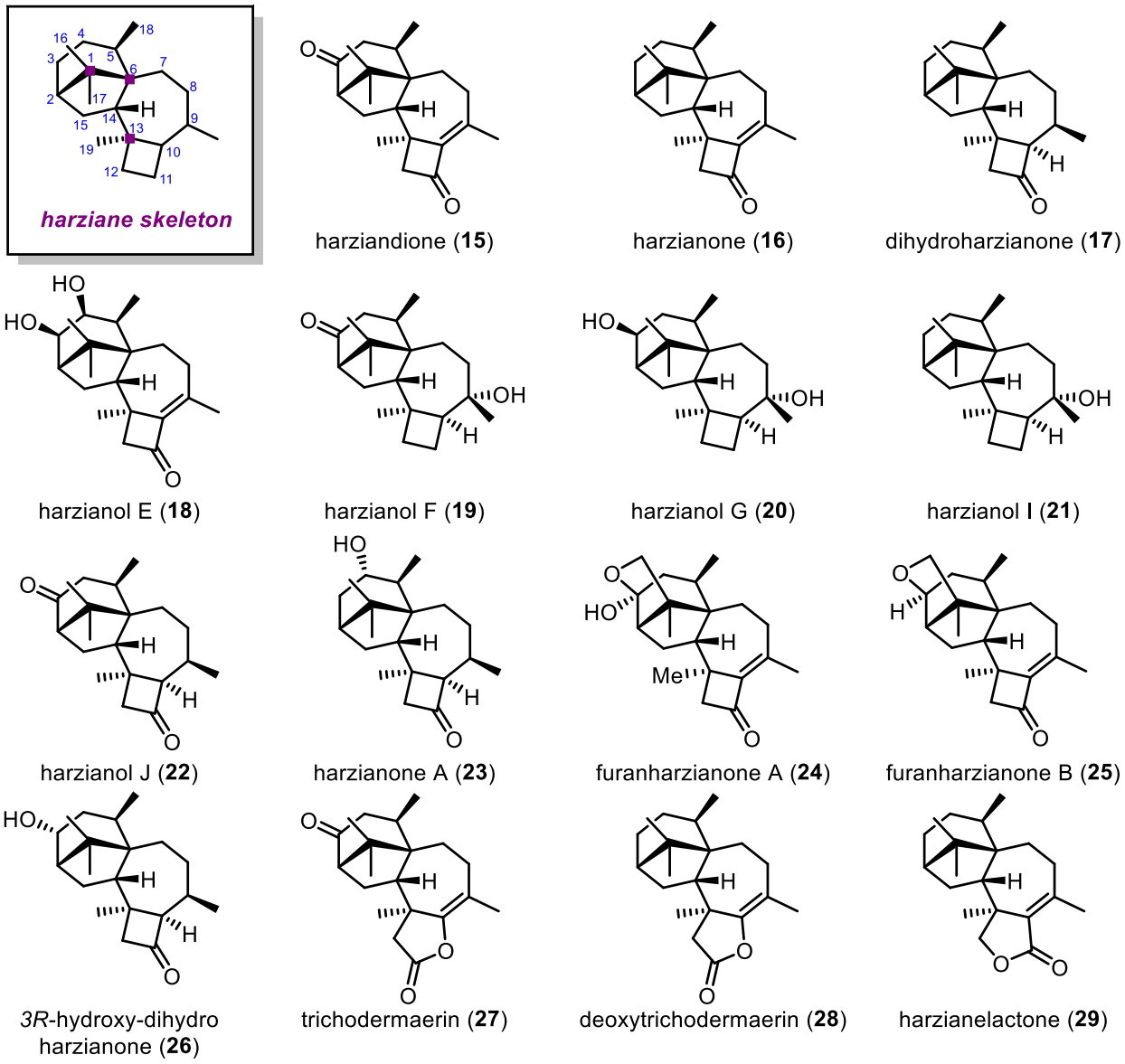

Figure 3.2: Harziane diterpene natural products displaying a unique 6/5/7/4 ring system.

The isolation of the first harziane diterpene, harzianedione (**15**) was reported in 1992,[19] followed by more recent reports of a large variety of congeners.[20–27] Isolated from the marine fungus *Trichoderma harzianum* and closely related species, some of the harziane diterpenes have shown strong antifungal activity against rivaling fungi.[28,29] *Trichoderma* extract is even sold as an antifungal agent used, for example, to protect grain seeds from mold.[30] The natural product within the family that is most responsible for this antifungal activity is harziandione (**15**), while congener

harzianone (**16**) is inactive, thereby implicating the ketone at C-3 as likely responsible for this observed activity.[31]

A biosynthetic study by Dickschat and co-workers has proposed the biosynthetic pathway of **15**, **16** and **21,** and points to the biosynthetic origins of several other harziane diterpene family members.[32] The harziane diterpenoid natural product family can be classified into four different subgroups of compounds:

(1) those containing a cyclobutenone moiety (**15**-**18**)

(2) those with a fully saturated cyclobutane ring (**19**-**21**)

(3) those containing a bridged tetrahydrofuran ring (**24**-**25**)

(4) those in which the cyclobutane moiety has been replaced by a γ-lactone (**27**-**29**), which may be envisioned to arise, biosynthetically, via reaction with a Baeyer-Villiger monooxygenase.

SECTION 3.1.1: BIOSYNTHESIS OF THE HARZIANE DITERPENOID NATURAL PRODUCTS

While the producing organisms, among them *Trichoderma harzianum*, yield varying amounts of the harziane diterpenoid natural products isolated and characterized to date, the exact biosynthetic pathway remained elusive until 2017, when the Dickschat *et al.* published their analysis of the cyclization mechanism.[32] As with previous work from the Dickschat group on the mechanism of the spiroviolene (**5**) terpene cyclase,[33,34] this work has provided us with both some insight on how nature elegantly folds up linear precursors into complex frameworks and informed parts of our synthetic strategy in the total synthesis of the harziane diterpenes.

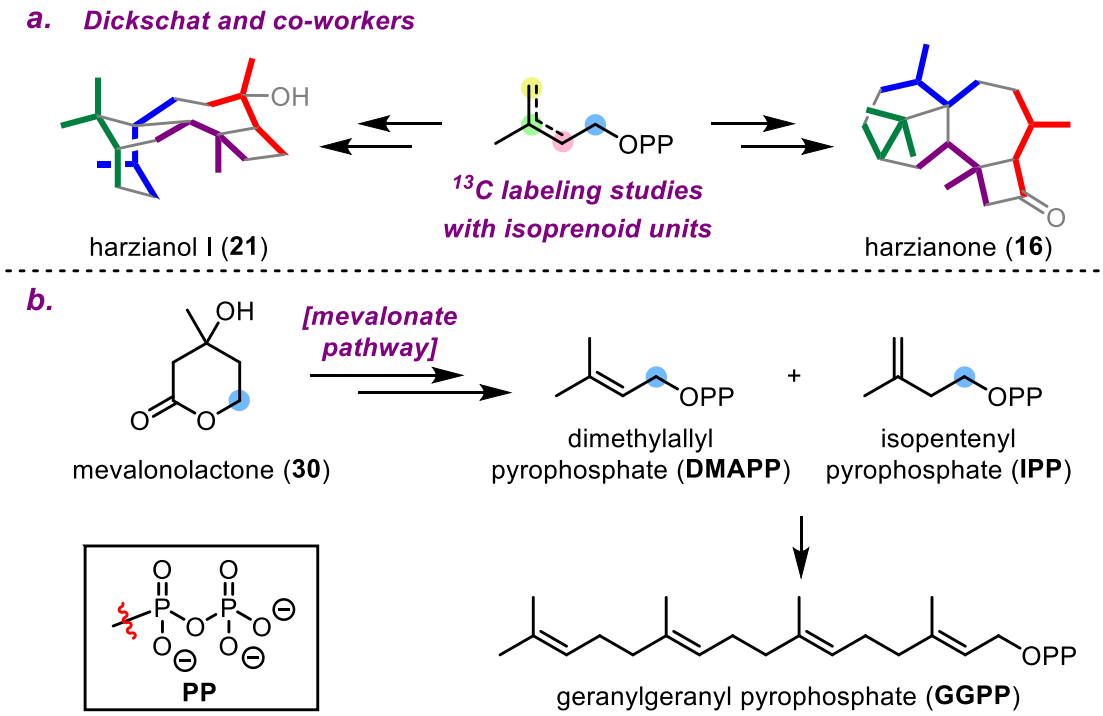

Scheme 3.1. *a.* Isotope labeling studies reveal building block arrangement in the biosynthesis of harziane diterpenoid natural products. *b.* Utilization of the mevalonate pathway as an entry to identify biosynthetic intermediates.

The first foray into elucidating the biosynthetic origin the harziane diterpene natural products were feeding studies to determine to which terpene building blocks each carbon in the harziane skeleton could be traced. With 20 carbons in the framework, it stands to reason that the harziane diterpenes may be made up of four isoprene units. A common pathway for terpene biosynthesis, the mevalonate pathway is a source of isoprenoid monomers and their oligomers. Initial feeding studies with fully labeled mevalonolactone (**30**) led to the production of harzianone (**16**) with high rates of ^{13}C incorporation at every carbon. As such, the Dickschat group concluded that the harziane diterpenes arise from a cyclization event of geranylgeranyl pyrophosphate (**GGPP**). Further feeding studies conducted by the Dickschat group shed light on the specific locations to which each isoprenoid unit of **DMAPP** and **IPP** can be assigned (cf. colored sections of **16** and **21** in Scheme 3.1).

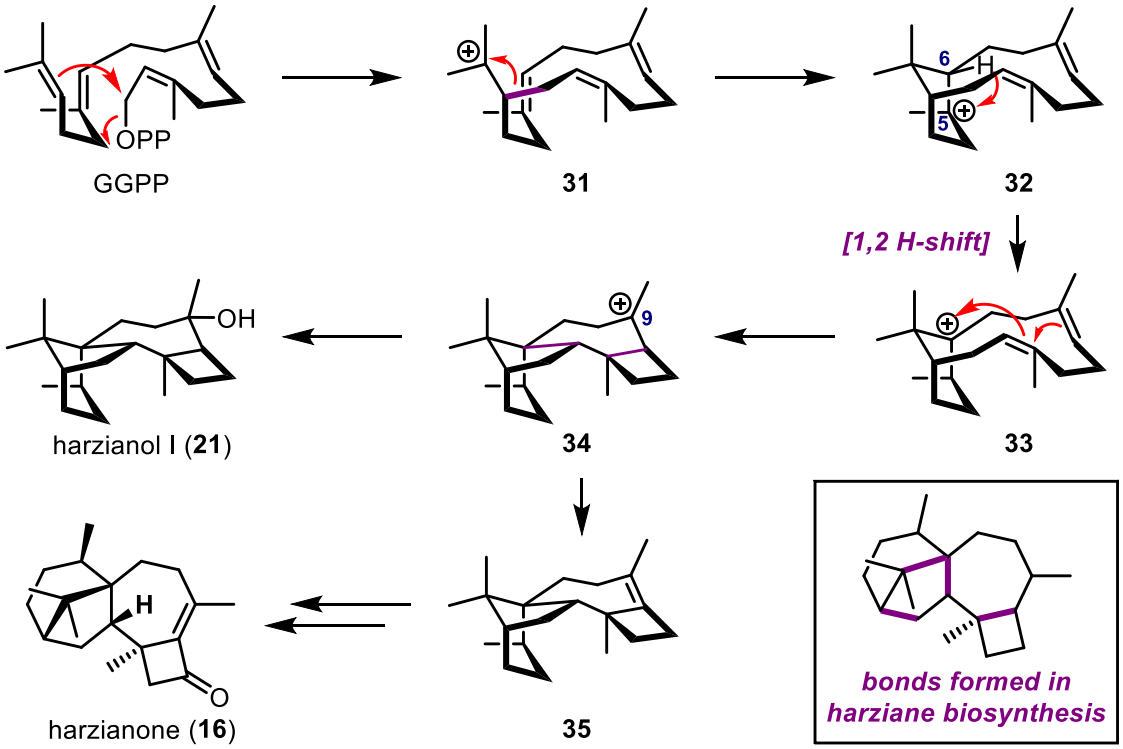

Scheme 3.2. Dickschat *et al*.'s proposed biosynthetic pathway of the harziane diterpenoid natural products.

With these results in hand, as well as mass spectrometry studies of the potential intermediates involved in this pathway, the authors were able to propose a plausible cyclization mechanism of **GGPP** to the harziane diterpenoid natural products **16** and **21**. Initial formation of macrocycle **31** is followed by six-membered ring formation and a subsequent 1,2-H shift from C-6 to C-5 to **33**, which was confirmed by deuterium labeling studies. A final double cyclization event then completes the ring system of the harziane diterpenes. At this point, the biosynthesis of the harziane diterpenoid natural products diverges. Capture of the tertiary carbocation at C-9 with water leads to harzianol I (**21**) and related natural products, while elimination to tetrasubstituted olefin **35** is an intermediate toward the biosynthesis of harzianone (**16**) following several latter oxidation state changes. In fact, this proposed late-stage divergence of the biosynthesis inspired us

to design a similarly divergent synthetic approach that would be able to access various harziane diterpenoid natural products from a common intermediate.

Section 3.1.2: Prior Synthetic Approaches to the Harziane Diterpenoid Natural Products

During our group's exploration of the total synthesis of the harziane diterpene family, the Carreira group published their own total synthesis of harzianol I (**21**) in 26 linear steps (Scheme 3.3-6).[35] Central to this first reported total synthesis of a harziane diterpenoid is an intramolecular Au^{I}-catalyzed cycloisomerization to establish a 5/6/4 tricyclic framework. The ring expansion to the seven-membered ring encountered in the natural product and the aldol condensation to furnish the bridged bicycle, followed by a range of redox transformations achieves the total synthesis of **21** in 26 steps. In addition, the synthesis of both diastereomers at C-9 revealed that the stereocenter had been wrongly assigned by the isolation team, a further highlight of the importance of the total synthesis of such targets in establishing proof of structure.

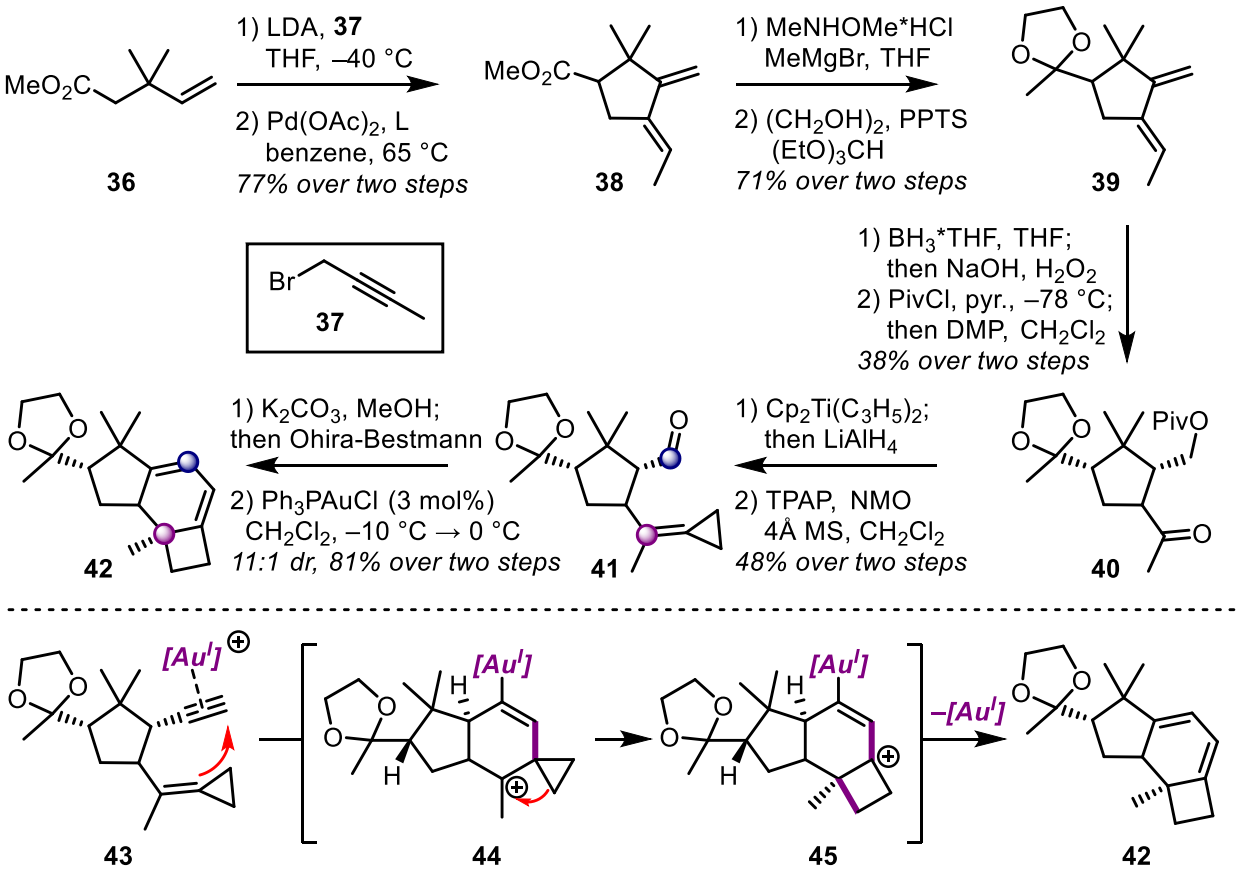

Scheme 3.3. Pd^{II}- and Au^{I}-catalyzed cycloisomerization reactions in the early stage of the Carreira group's synthesis of harzianol I (**21**).

The synthesis commenced with the alkylation of commercially available methyl ester **36**, with 1-bromobut-2-yne (**37**), followed by Pd^{II}-catalyzed cycloisomerization to furnish the 1,3-diene within **38**. In a one-pot procedure, the ester is then converted to a ketone via the Weinreb amide and then protected as the cyclic ketal. Resultant diene **39** then undergoes a double hydroboration/oxidation to afford the intermediate diol. In order to selectively oxidize the secondary alcohol arising from the vinylidene group within **39**, the primary alcohol is selectively protected *in situ* as its pivalate ester **40**. The Carreira group's next objective was to introduce the required functional group handles for their proposed Au^{I}-catalyzed cycloisomerization (cf. Ch. I, Scheme XX). Ti^{IV}-mediated olefination forms the cyclopropylidene group in **41**, while the alkyne is introduced via treatment of the pendant aldehyde with Ohira–Bestmann reagent. Subsequent

treatment with catalytic Ph_3PAuCl then effects the desired cycloisomerization to the tricyclic diene **42** in good yield and excellent d.r.

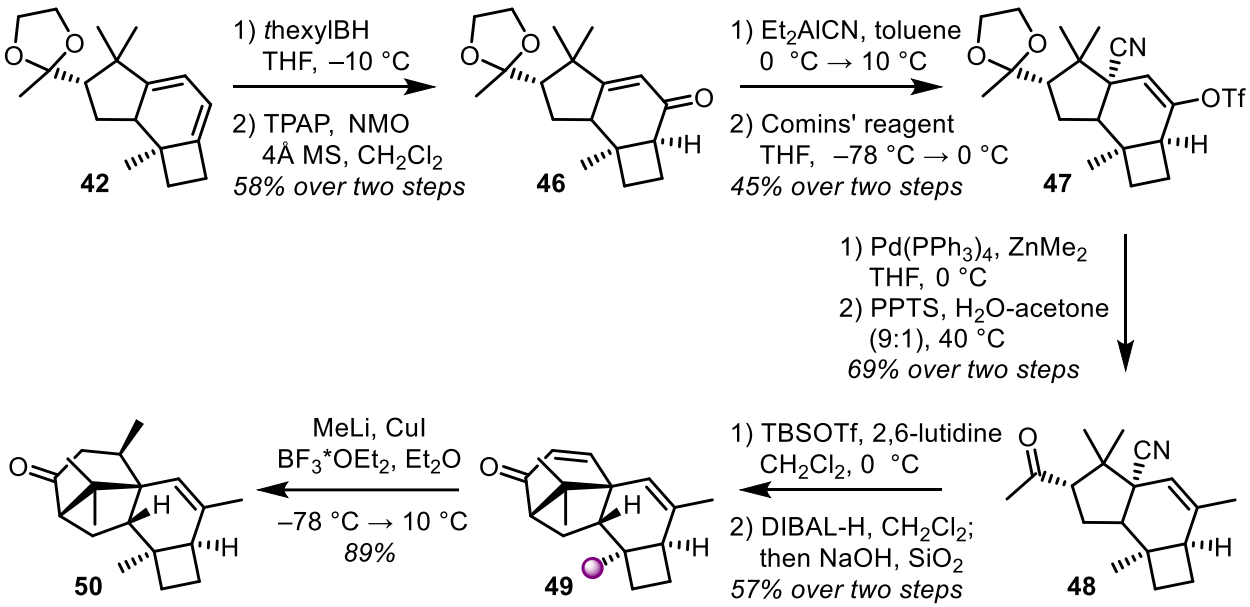

Scheme 3.4. [3.2.1]-bicycle formation via an intramolecular aldol condensation in the Carreira group's synthesis of harzianol I (**21**).

The next objective in the synthesis was the formation of the [3.2.1]-bicyclic system within harzianol I (**21**). Selective hydroboration and subsequent oxidation of the diene within **42** delivers enone **46**. Formation of the significantly less strained *cis*-6/4 ring system is favored despite steric encumbrance of the *re*-face by the adjacent methyl group in **42**. Treatment with Nagata's reagent (Et_2AlCN), with the resultant nitrile to serve as the electrophilic handle in the latter cyclization, is followed by formation of vinyl triflate **47**. The vinyl triflate is methylated and the ketal deprotected upon treatment with acid. With ketonitrile **48** in hand, the Carreira group set sights on the cyclization sequence. While the authors had tried a wide variety of strategies to establish the [3.2.1]-bicyclic system, it was ultimately an intramolecular Mukaiyama aldol condensation that delivered the tetracyclic enone **50**. After formation of a silyl enol ether at the methyl ketone, the nitrile is reduced to the intermediate imine species. In the same pot, addition of NaOH and silica

gel successfully triggered the desired imine hydrolysis and aldol condensation to enone **50**. The conjugate addition into **50** proceeds with facial selectivity as the *re*-face of the molecule is blocked by the highlighted methyl group. Hence, Carreira and co-workers have successfully established the tetracylic 6/5/6/4 ring system of harzianol I (**21**), leaving a ring expansion and several redox manipulations to the last stage of their total synthetic efforts.

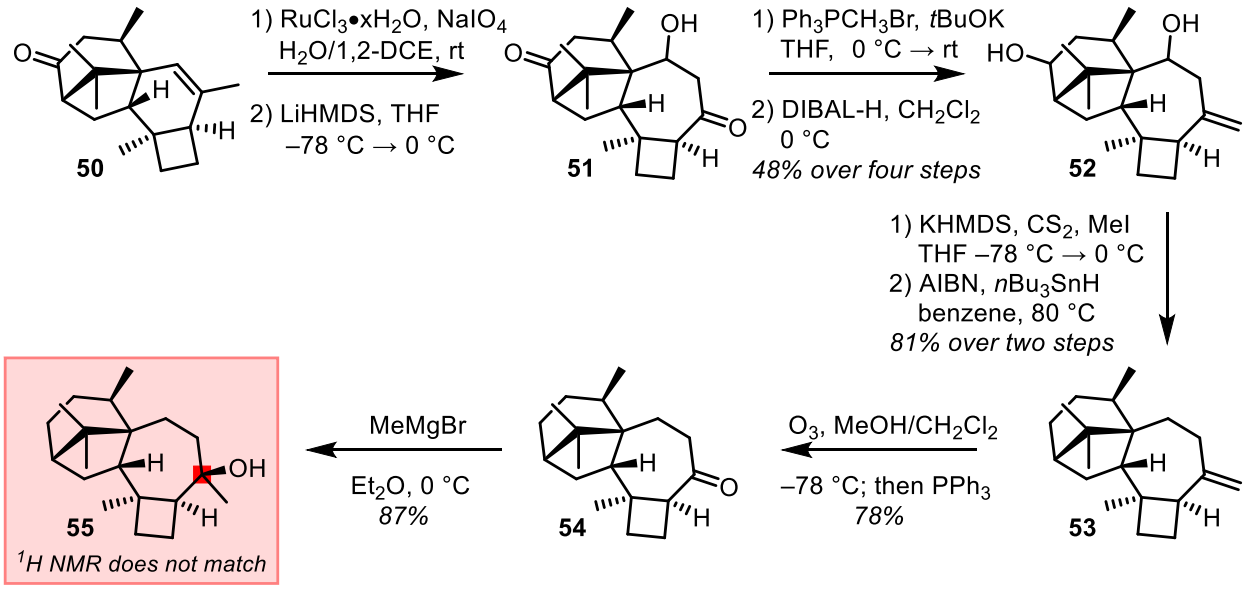

Scheme 3.5. Ring expansion and deoxygenation sequence and synthesis of the C-20 epimer of harzianol I (**21**) by Carreira and co-worker.

The ring expansion of the six-membered ring within **50** commences with a oxidative cleavage reaction, similar to the more commonly applied Lemieux–Johnson conditions. The resultant ketoaldehyde then undergoes an aldol reaction to ketoalcohol **51**. At this stage, a Wittig methylenation at the newly-formed seven-membered ring is followed by DIBAL-H reduction of the remaining ketone, after which the diol **52** is subjected to a double-Barton–McCombie deoxygenation to afford olefin **53**. Ozonolysis, followed by Grignard addition then delivered the tertiary alcohol **55** in good yield. Upon analysis of this compound, the authors noticed that the ^{1}H NMR spectrum did not match the one reported by the isolation team. Suspecting that the tertiary

alcohol stereocenter had been misassigned, the putative diastereomer was synthesized via a Mukaiyama hydration of **53**. This time, the resultant compound matched in all regards to the data obtained by the isolation team, thereby completing the first total synthesis of harzianol I (**21**) in a total of 26 steps and a key stereocenter within the target correctly reassigned. The Carreira group hypothesized that *si*-face approach of the oxygen nucleophile to the olefin was favored due to steric encumbrance of the *re*-face, caused mainly by the position of the four-membered ring.

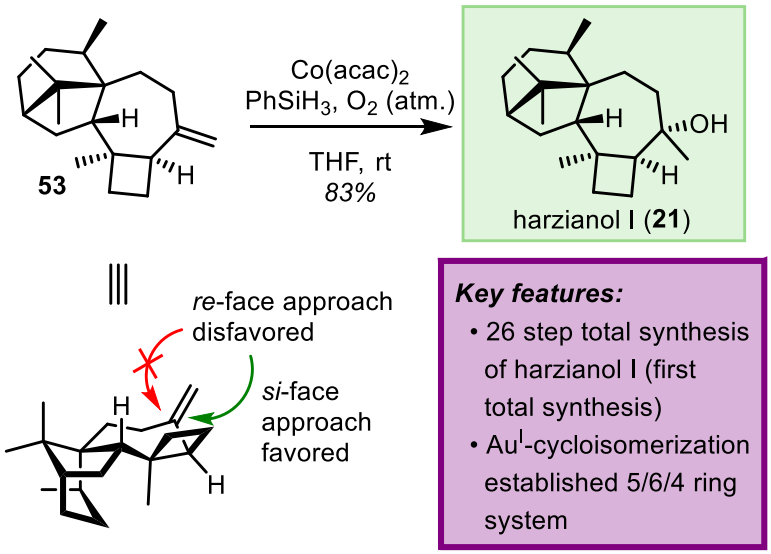

Scheme 3.6. Completion of the total synthesis of harzianol I (**21**) by Carreira and co-worker via a final Mukaiyama hydration.

The Carreira synthesis of harzianol I (**21**) sets a high standard for further synthetic approaches toward the harziane diterpene natural product family. It solved a variety of problems in accessing the congested carbocyclic framework and utilized elegant cycloisomerization strategies to rapidly introduce complexity, making it a classic example of modern natural product total synthesis. In particulat, the structural reassignment reaffirms the utility of these synthetic endeavors.[36] At the same time, the central challenge of providing a unified, asymmetric, and step-economic synthesis for the entire family of harziane diterpenes remains. The mode in which the structurally intriguing 7/4-fused ring system was established by the Carreira group does not include

a direct strategy to accessing the more highly oxidized family members such as harziandione (**15**). Identifying and strategically executing such an approach would grant access to several harziane diterpenes, ranging from the sparsely functionalized harzianol I (**21**) to the more oxidized and complex furanharzianone B (**25**).

Another contemporary approach to the total synthesis of the harziane diterpenes was disclosed by the Yang group in 2021.[37] Their strategy toward the synthesis of the harziane diterpene framework places construction of each ring in a different order to that reported by Carreira and co-workers. Here the central [3.2.1]-bicycle is formed at an early stage of the route via an oxidative radical cyclization, while a much later Au^{I}-catalyzed cycloisomerization furnishes the 7/4-ring system.[18] While this synthesis, as described below, significantly shortens the number of synthetic transformations required to complete the carbon skeleton of the harziane diterpenes, it does not ultimately achieve the total synthesis of any of the natural products, in part due to the highly congested nature of their advanced intermediates

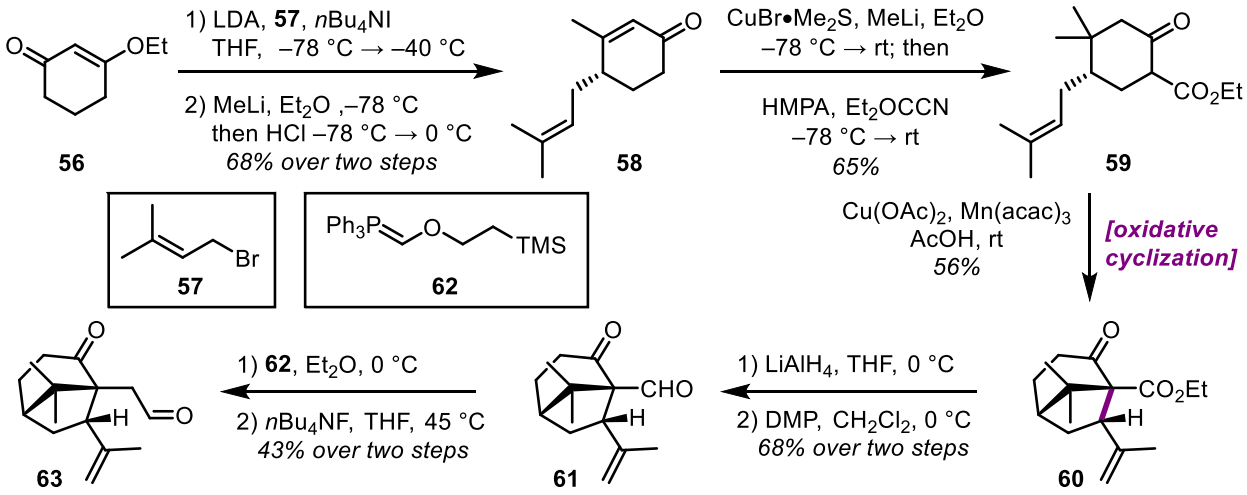

Scheme 3.7. [3.2.1]-bicycle formation via oxidative radical cyclization in the synthetic studies toward the harziane diterpenes by Yang *et al.*

The Yang group's synthetic efforts start with the synthesis of their oxidative cyclization precursor **59**. The prenyl side chain is introduced by alkylation of vinylogous ester of 1,3-cyclohexanedione (**56**), followed by sequential installation of the *gem*-dimethyl group. Treatment of β-ketoester **59** with conditions popularized by Snider, effects the desired oxidative radical cyclization to furnish [3.2.1]-bicyclic ketoester **60**. The bridgehead ethyl ester is then used as a handle to install the enyne side chain needed for the subsequent Au^{I}-catalyzed cycloisomerization. A four-step Wittig-type homologation sequence yielded aldehyde **63**, which then was treated with phosphonate **64** to form enoate via a Still–Gennari olefination. Another reduction-oxidation sequence gave rise to enal **66**, which was transformed to the homologated enyne **67** in a Colvin-type rearrangement.[38]

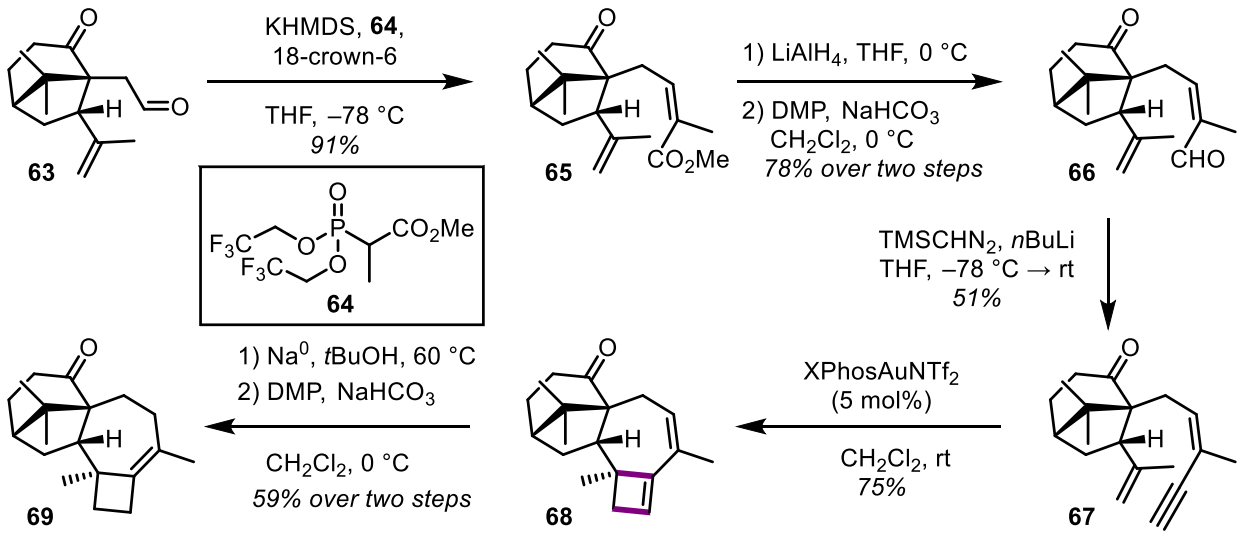

Scheme 3.8. Au^{I}-catalyzed cycloisomerization completes the carbocyclic framework of the harziane diterpenes by Yang *et al*.

With cycloisomerization precursor **67** in hand, treatment with $XPhosAuNTf_2$ efficiently furnished the 7/4 ring system, thus completing the carbocyclic framework of the harziane diterpene natural products. Reduction of diene **68** and subsequent alcohol oxidation led to tetrasubstituted olefin **69**, which was then investigated for further oxidative transformations. The Yang group

describes one specific allylic oxidation condition in their report. An attempted Riley oxidation with SeO_2 failed to deliver the desired selective oxidation at the cyclobutene position, instead favoring oxidation at the allylic methyl position in **69**.

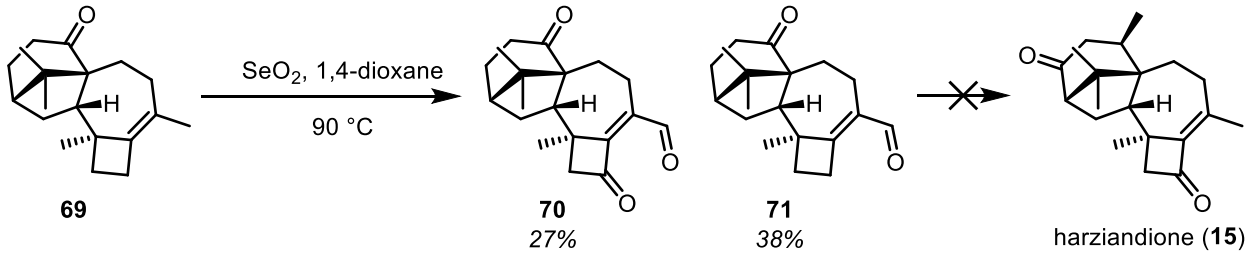

Scheme 3.9. Riley oxidation does not afford the desired oxidation pattern to access harziandione (**15**)

Yang and co-workers conclude their synthetic efforts toward the harziane diterpene natural products unable to achieve their desired oxidation. While further redox-chemistry was explored on the right side of the molecule, no modifications of the bicyclic system on the left-hand side were disclosed. It is possible that such efforts were largely fruitless due to the extreme steric encumbrance of the ketone in **69**, owing to the vicinal quaternary center and the fact that it is flanked by methyl groups, both from the top and bottom faces. While the Yang group was able to furnish the congested 6/5/7/4-ring system in a concise manner, the choice to introduce much of the structural complexity so early in the route may have in fact hindered critical late-stage transformations.

Section 3.1.3: Late-Stage Divergent Synthetic Strategy Toward the Harziane Diterpenoid Natural Products

In the previous synthetic studies of the harziane diterpenoids, the strategies significantly differed, with a variety of bond disconnections performed, in particular, the Carreira and Yang groups sought to construct the [3.2.1]-bicyclooctane ring in different fashions. On one hand, the Carreira group focused on building the five-membered ring first, followed by establishing a

tricyclic precursor to the 5/7/4 ring system within the natural products, with the formation of the bridged bicycle appearing towards the end of the route. On the other hand, Yang *et al*. began their synthesis with the six-membered ring, utilizing an oxidative radical cyclization to furnish the bridged bicycle and concluding their synthetic endeavors with construction of the 7/4-fused ring system. Of note, both of these approaches contrast the proposed biosynthesis of the harziane diterpenes, which undergoes a series of transannular cyclizations after initial macrocyclization.

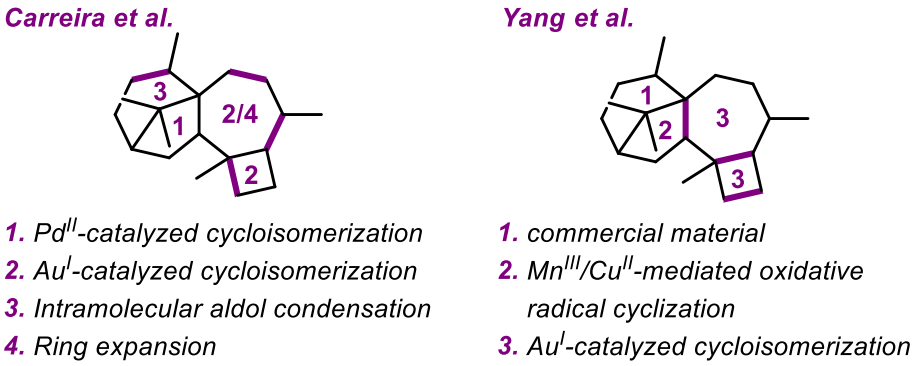

Figure 3.3. Summary of the synthetic strategy applied by Carreira and Yang in constructing the carbocyclic core of the harziane diterpenes.

In our retrosynthetic analysis, we were particularly intrigued by the 7/4-fused ring system, which directly mapped onto a Au^{I}-catalyzed, formal [2+2] cycloisomerization reaction of 1,8-enynes as developed by the Gagosz group.[18] This approach to the right side of the molecule would allow for rapid construction of the ring system and is similar to that of the Yang group's contemporary studies. With our eyes set on this key disconnection, we then turned our attention to the formation of the bridged [3.2.1] bicycle on the left side of the molecule. While somewhat more common in natural product total synthesis, this fragment still posed a daunting challenge with its vicinal all-carbon quaternary centers and the resultant steric congestion. Nonetheless, we were hopeful to shorten our synthetic route by using the presence of these quaternary centers to preclude undesired reactivity by blocking adjacent functional groups. As discussed above, this logic has

been applied in several successful terpene and alkaloid syntheses in the Snyder group, viewing quaternary centers as strategic advantages as opposed to synthetic hurdles.

Ultimately, we decided to pursue the same disconnection Carreira had employed in the total synthesis of harzianol I (**21**), planning to forge the six-membered ring of the bridged bicycle, last. As such, our approach was reduced to identifying a suitable ring system, which (1) allowed for facile Au^{I}-catalyzed cycloisomerization of a tethered enyne and (2) put the requisite functional groups in place to set up the formation of the bridged bicycle. Our principal concern was that any rigidity imposed by a decorated cyclic system could impede the cycloisomerization reaction by imposing insurmountable geometric constraints.

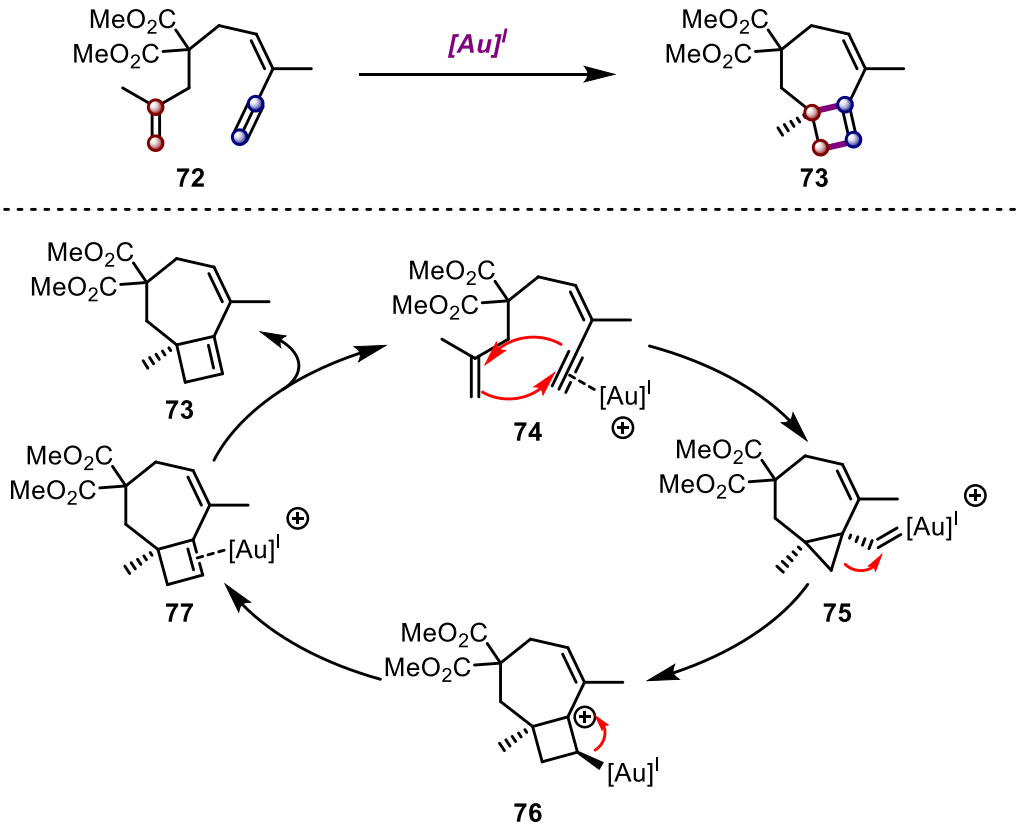

Scheme 3.10. Mechanism of the Au^{I}-catalyzed cycloisomerization of 1,8-enynes by Gagosz *et al.* to access cyclobutene derivatives.

The Au^I-catalyzed cycloisomerization reaction reported by Gagosz and co-workers is described as a formal [2+2] cycloaddition. The proposed mechanism is quite similar to that described for the cycloisomerization reactions of enynes in Chapter I: initial electrophilic cyclopropanation of the olefin by the activated alkyne leads to formation of the Au^I-carbene **75**. Ring opening of the cyclopropane and subsequent dissociation is then postulated to lead to the cyclobutene moiety, followed by dissociation of the Au^I catalyst to release the title diene **73**. This product has been previously described as an intermediate in similar transformations, as further reaction with Au^I can lead to a retro-4π-electrocyclization to open the cyclobutene to triene **80** (Scheme 3.11).[9,18] The Gagosz group found that this undesired reaction predominates when using relatively small ligands such as PPh_3. By exploiting the steric constraints put onto the catalytic system by the bulkier XPhos (**82**), they can promote the dissociation step of the catalytic cycle and prevent further rearrangements after formation of cyclobutene **79**. As would be expected, the Gagosz group noted that elevated reaction temperatures and prolonged reaction times both increased the prevalence of the retro-4π-electrocyclization pathway.

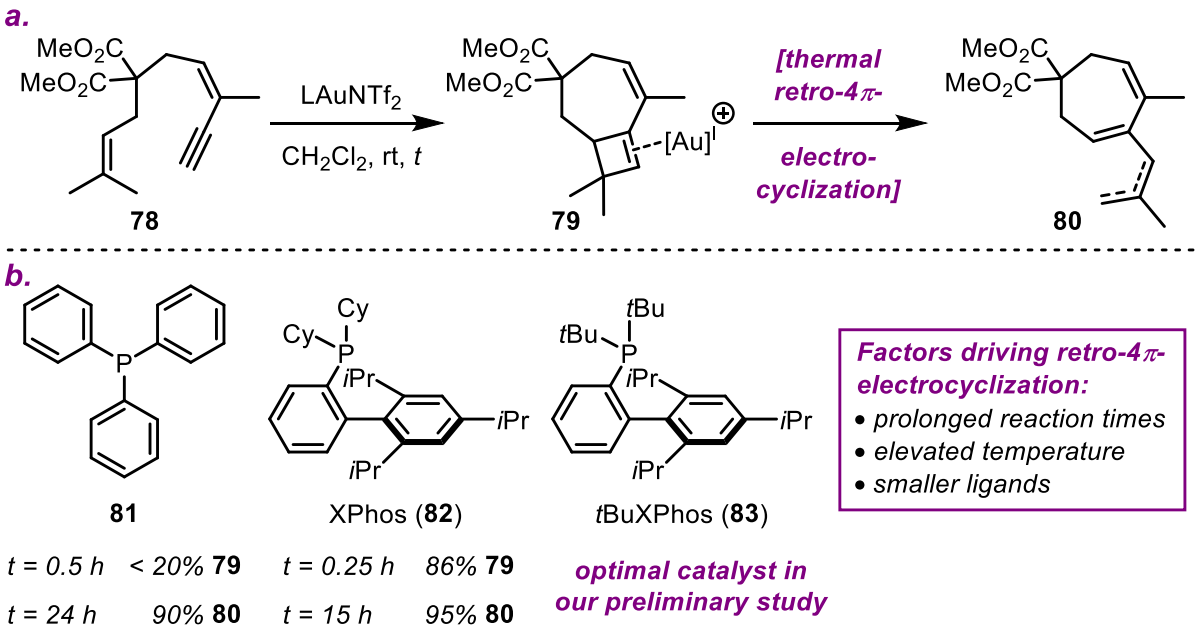

Scheme 3.11. *a*. Undesired thermal retro-4π-electrocyclization. *b*. Effect of ligand properties on product distribution and rate of retro-4π-electrocyclization.

In our preliminary study to identify a ring system suitable for the synthetic approach discussed above, we also attempted to find a phosphine ligand that would efficiently catalyze the desired cycloisomerization and preclude formation of the triene side product (Scheme 3.12). Initially, we hoped to base our synthetic strategy on decorating a five-membered ring species, akin to Carreira's approach, but found that model compound **84** did not efficiently convert to the desired tricyclic diene **85**. This outcome is likely due to the heightened ring strain imposed by the saturated five-membered ring. Unfortunately, subjecting such systems to prolonged reaction times or elevated temperatures have only led to a higher degree of retro-4π-electrocyclization product.

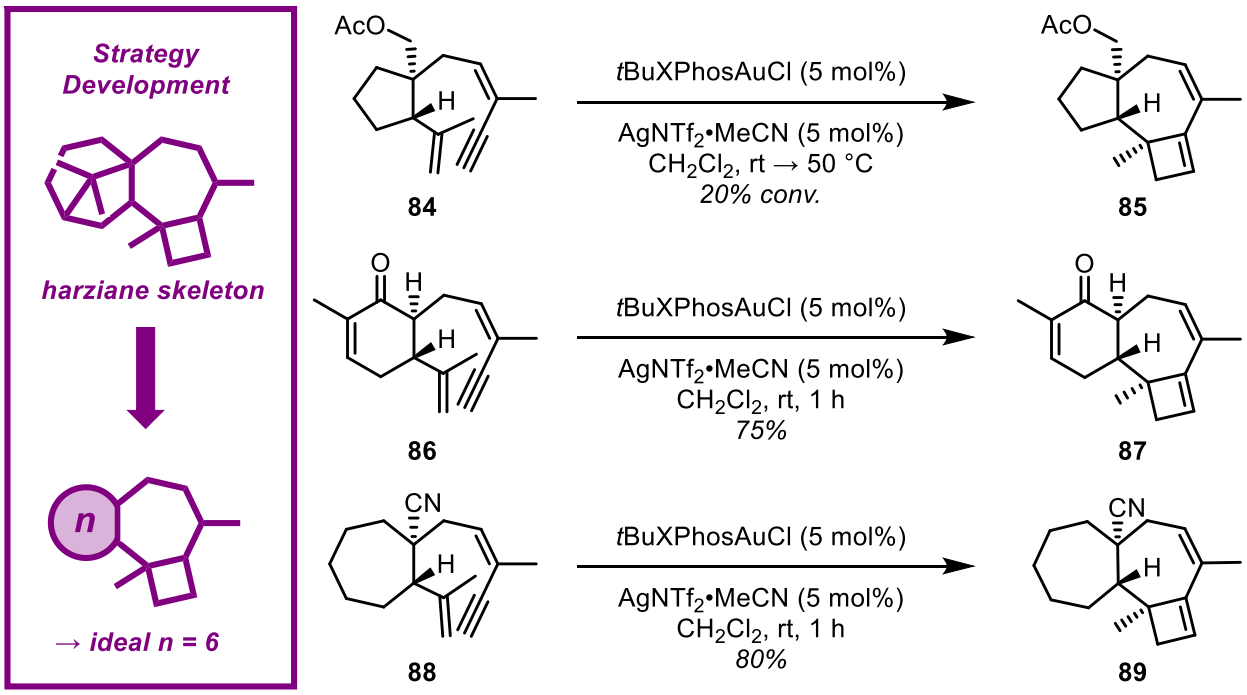

Scheme 3.12. Preliminary experiments to determine optimal ring system for the Au^{I}-catalyzed cycloisomerization reaction within our synthetic strategy development.

With this result in hand, we had to consider altering the size of ring system in the starting material, keeping in mind that we may need to modify ring size after formation of the *n*/7/4-fused tricyclic system. Au^{I}-catalyzed [2+2] cyclization of both the carvone-derived enyne **86** and the cycloheptanone-derived enyne **88** efficiently furnished the 6/7/4 and 7/7/4 ring systems respectively. Given the wide array of synthetic transformations available for the preparation and derivatization of six-membered ring systems in organic synthesis, we decided to pursue targets such as **87**, in the hope that we could concisely fashion our desired cycloisomerization precursor.

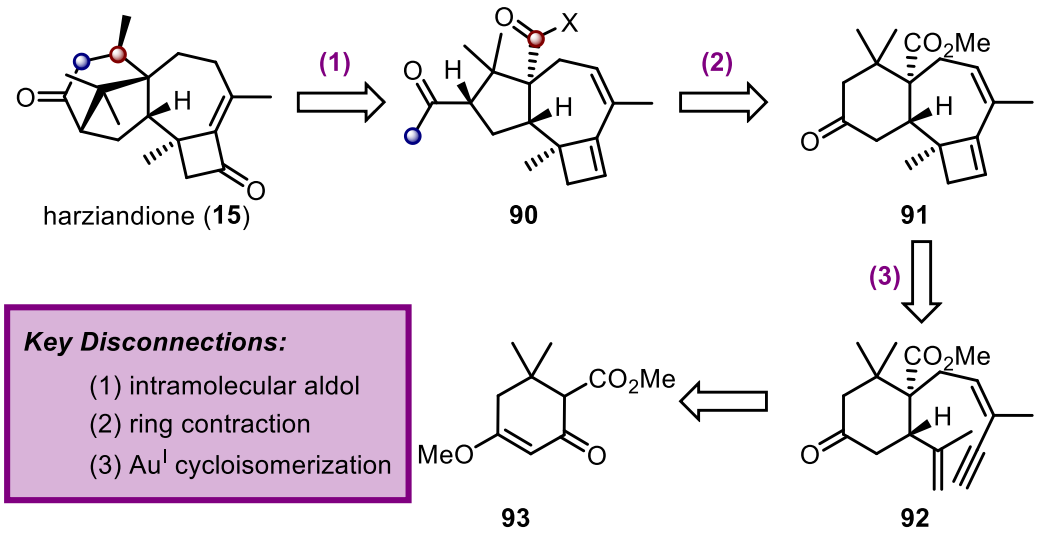

Scheme 3.13. Retrosynthetic analysis of harziandione (**15**), as a representative example in our studies toward the divergent total synthesis of the harziane diterpenoid natural products

Following this preliminary study, our retrosynthetic analysis of the representative natural product harziandione (**15**) had begun to take shape. As discussed above, we envisioned forming the bridged bicycle via an intramolecular aldol-type reaction from the tricyclic dicarbonyl species **90** which, in turn, is derived from the ring contraction reaction of 6/7/4 tricycle **91**. Appropriate strategies for such a ring contraction are discussed below (Scheme 3.14). **91** can be traced back to **92** via the Au^{I}-catalyzed cycloisomerization, which we have identified as a key enabling reaction to rapidly furnish the tricyclic ring system. The appropriate functional group handles to form the requisite enyne could then be introduced via the dimedone-derived β-ketoester **93**.

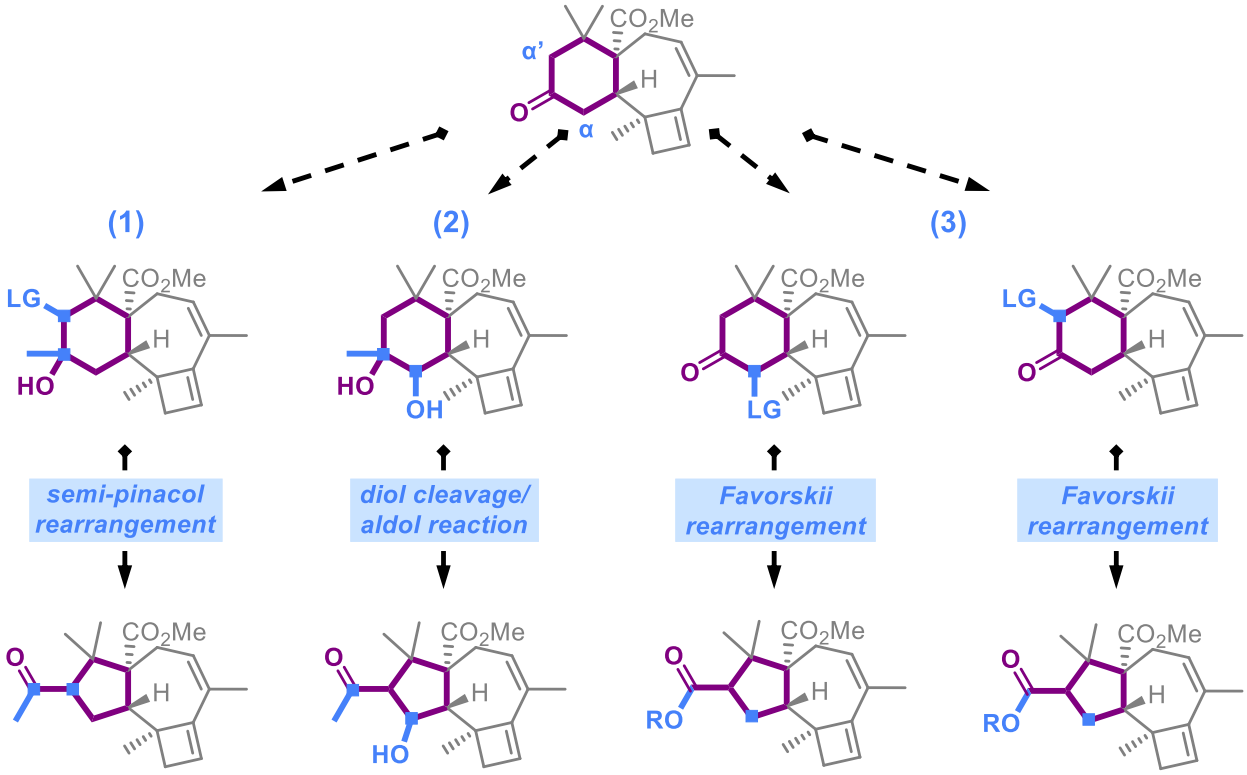

Scheme 3.14. Analysis of envisioned ring contraction strategies in our proposed total synthesis of the harziane diterpenoid natural products.

With **91** identified as the target intermediate *en route* to the δ-dicarbonyl species **90**, we weighed a variety of strategies to effect a ring contraction of the six-membered ring within the 6/7/4-fused ring system to access the necessary 5/7/4 system. Each of the strategies require placing a functional handle at one of the α-carbons to enable the ring contraction. In addition, the first two options described below, rely on a 1,2-addition into the starting ketone, to afford the tertiary alcohol required for the subsequent rearrangement.[39]

(1) The semi-pinacol rearrangement upon initial analysis is promising, as it has been widely applied in natural product synthesis and thus is tolerant even of complex molecular frameworks.[40] A possible challenge of this approach may be selective introduction of a leaving group at the more sterically encumbered α' position of the ketone.

(2) Oxidative cleavage of a 1,2-diol, followed by an intramolecular aldol reaction has likewise been used in complex molecule synthesis, such as Woodward's classic steroid synthesis.[41] While this approach has been applied in a number of systems, here it will require further reductive transformations to remove the resultant β-hydroxyl group and selective α-oxygenation would be needed.

(3) The last two approaches rely on a Favorskii rearrangement, which due to the intermediate cyclopropanone, could be triggered by leaving groups placed at either of the two α-carbons. The precursor could be accessed in short order, thus making this a promising strategy. The downside of this approach is that regioselectivity of carbon migration is specific to the cyclopropanone intermediate based on individual steric and electronic effects/demands, potentially leading to a structural preference for the undesired regioisomer.[42] Furthermore, the resultant ester would need to be converted to a functional group more amenable to the desired bicycle formation.

We had also considered a Wolff-rearrangement as an alternative option for ring contraction. However, we decided not to investigate it, as we worried that, under the requisite photochemical conditions, the cyclobutene moiety could undergo a disrotatory retro-4π-electrocyclization.

Work in this chapter was performed with Dr. Zhiyao Zhou, who initiated and led this project in its initial stages (Sections, 3.2.1-2)[43] and Sohee Kim, who contributed most to the route redesign and completion of harziandione (**15**).

SECTION 3.2.1: OXIDATIVE FAVORSKII REARRANGEMENT APPROACH

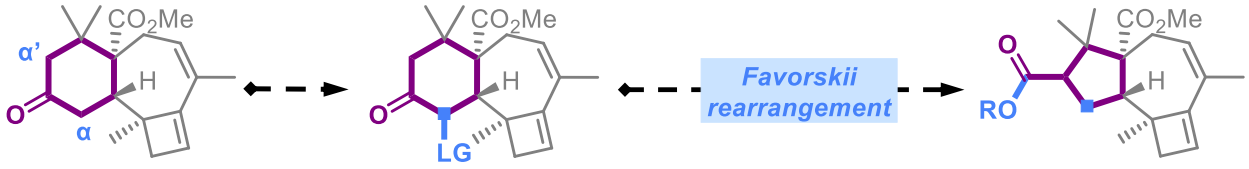

Scheme 3.15. Oxidative Favorskii rearrangement strategy toward 5/7/4 ring system.

The first ring contraction we sought to test was a hypervalent iodine-initiated Favorskii rearrangement, as reported by Moriarty *et al*.[42] This transformation allows for *in situ* installation of the required leaving group, and could thereby accelerate our synthetic efforts. Our first approach to the desired 5/7/4-fused tricyclic ring system commenced with the synthesis of decorated cyclohexanone **92**. Vinylogous ester **94** was prepared in one step from dimedone and subsequently transformed into β-ketoester **93** by addition of Mander's reagent (Scheme 3.16).[44] Alkylation with known allylic bromide **95**,[45] prepared from 2-butyn-1-ol in three steps, and selective reduction of the vinylogous ester then furnished enone **97**. Solvent choice proved crucial in this case, as using THF, a coordinating ethereal solvent, avoided reduction of the sterically hindered methyl ester within **96**, while a solution of DIBAL-H in CH_2Cl_2 led to a complex mixture of ester reduction products.

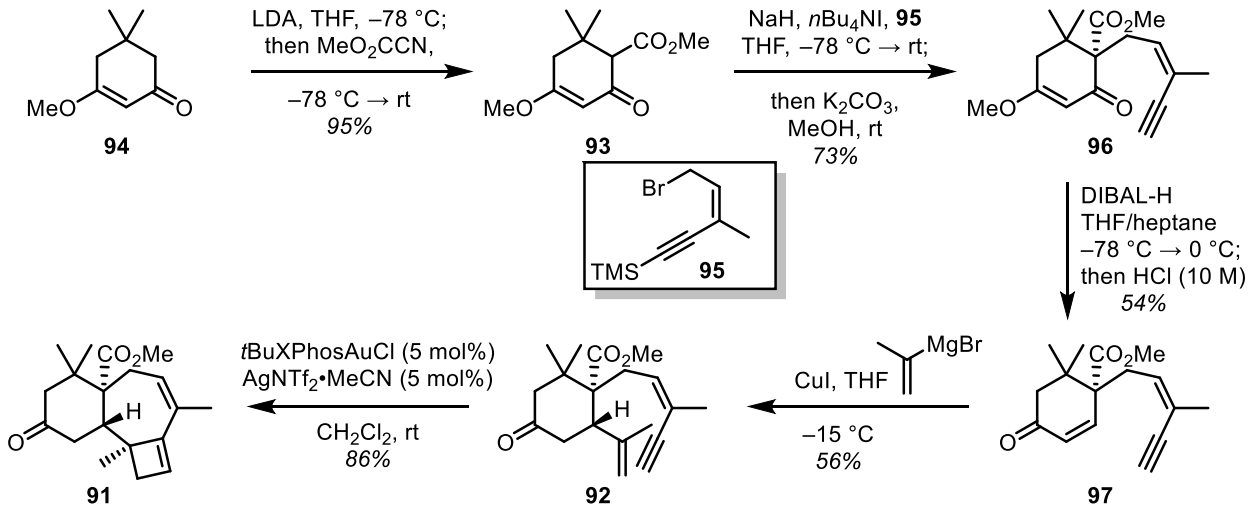

Scheme 3.16. Synthesis of the 6/7/4 tricyclic ketone **91**

Curiously, hydrolysis of the intermediate allylic alcohol in the reduction of the vinylogous ester required excess concentrated acid and a homogenous solution, complicating our initial synthesis. We hypothesize that this outcome is due to a stabilizing chelation of the aluminates between the allylic alcohol and the neopentyl ester. The formation of enone **97** was then followed by a cuprate-mediated conjugate addition to install the isopropenyl group, the other partner in our key [2+2] cyclization. Treatment with catalytic *t*BuXPhosAuCl and $AgNTf_2$•MeCN gave the desired 6/7/4-tricyclic ketone **91** in high yield.

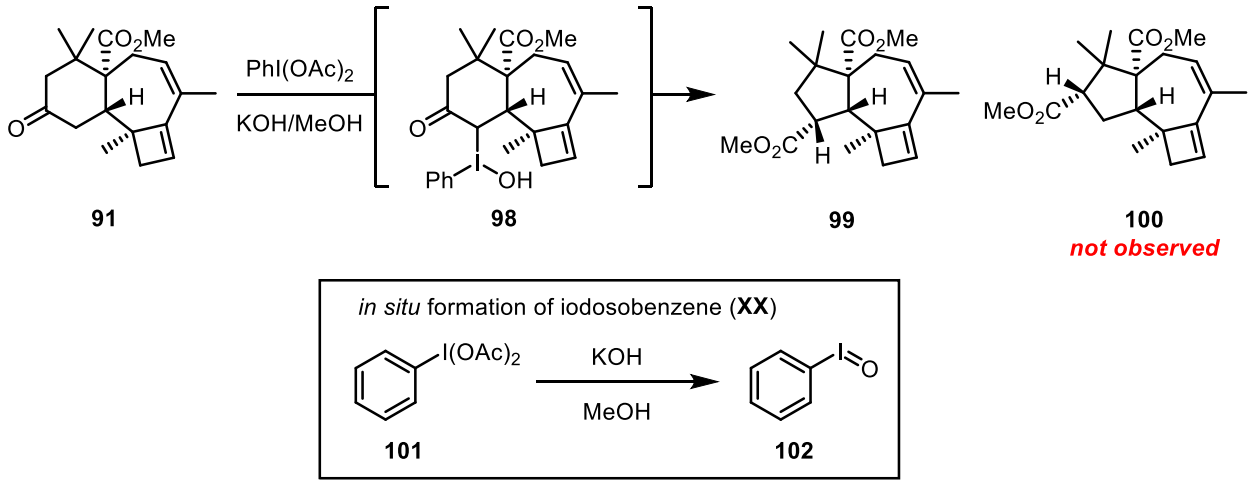

Scheme 3.17. Attempted oxidative Favorskii rearrangement of tricyclic ketone **91**

Ketone **91** then allowed us to test our first ring contraction strategy, the oxidative Favorskii rearrangement. In this one-pot procedure, exposure of $PhI(OAc)_2$ (**102**) to a strong base leads to an *in situ* formation of iodosobenzene (**102**). This highly electrophilic species reacts with the cyclohexanone enolate in a 1,2-fashion, thus installing a transient trivalent iodine leaving group at the a-position of the ketone. In the strongly basic conditions, a Favorskii rearrangement of intermediate **98** takes place rapidly via the cyclopropenone intermediate (not shown) and leads to the ring contracted methyl ester **99**. Upon analysis of this compound, we found that unfortunately the undesired regioisomer had formed. The reaction mechanism and the observed result will be discussed in depth in Section 3.2.3.

SECTION 3.2.2: OXIDATIVE CLEAVAGE/ALDOL REACTION APPROACH

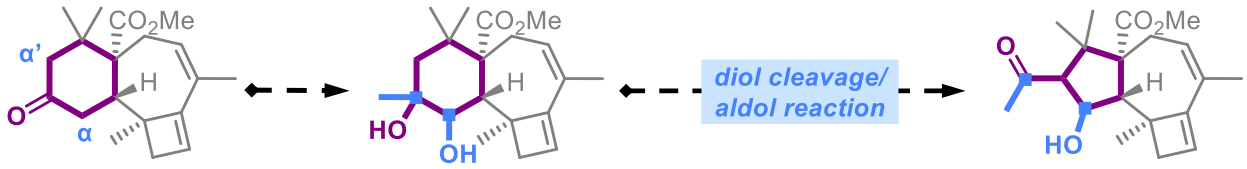

Scheme 3.18. Oxidative cleavage/aldol reaction strategy toward 5/7/4 ring system.

We then turned to the oxidative cleavage/aldol reaction sequence, in order to achieve the desired ring contraction product. Selective α-oxygenation with Davis oxaziridine (**103**) was inefficient, likely due to the extreme steric encumbrance and rigidity of the tricyclic system. Subsequent 1,2-addition with MeMgBr set up the potential ring contraction precursor, vicinal diol **105**. $PhI(OAc)_2$-mediated oxidative cleavage formed the desired ketoaldehyde **106**. This initial result was heartening, yet low yields in previous steps led us to devise a more reliable synthesis of diol **105**.

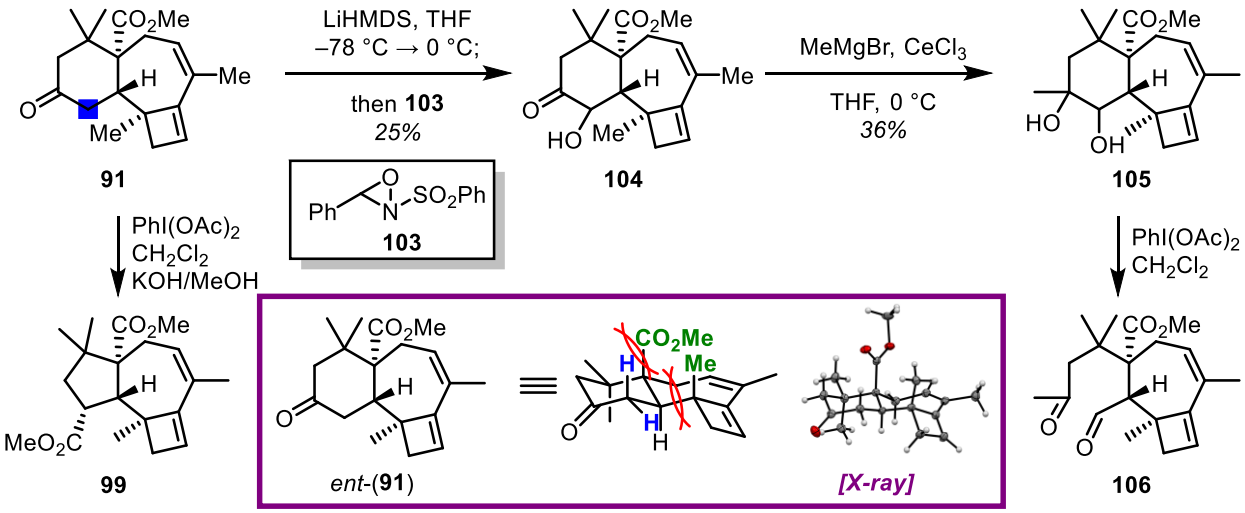

Scheme 3.19. Early exploration of α-oxygenation of ketone **91**.

Cuprate-mediated conjugate addition of the isopropenyl group to enone **97**, was followed by trapping of the metal enolate with TMSCl to furnish silyl enol ether **107**. Subsequent Rubottom oxidation and deprotection of the 2° silyl ether revealed α-hydroxyketone **108**.[46] Grignard addition gave us ring contraction precursor **109**. Au^{I}-catalyzed cycloisomerization of unprotected diol **109** unfortunately did not proceed, presumably due to coordination of the cationic Au^{I} species, but protection as carbonate **111** or alternatively as cyclic boronate allowed for formation of cyclobutene **112** in high yield.

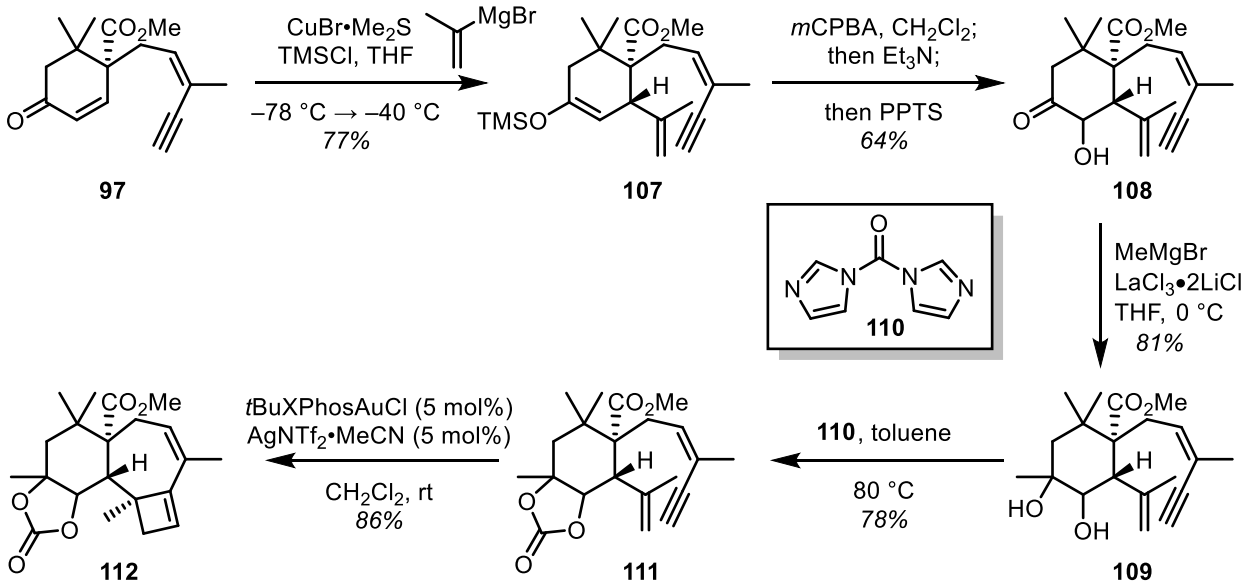

Scheme 3.20. Rubottom oxidation sequence toward carbonate **112**, an oxidative ring contraction precursor

Subsequent deprotection of the carbonate in **112** then concluded a more efficient synthesis of 1,2-diol **105**. In addition, we found that this protocol also efficiently removed any remaining traces of the Au^{I} catalyst, thus precluding any undesired retro-4π-electrocyclization upon storage. Oxidative cleavage of diol **105** proceeded smoothly and was followed by an intramolecular aldol reaction in the same pot to provide methyl ketone **113**. In order to achieve the desired oxidation state required for the next stage of our synthesis, the bridged bicycle formation, we needed to develop an efficient deoxygenation protocol for **113**.

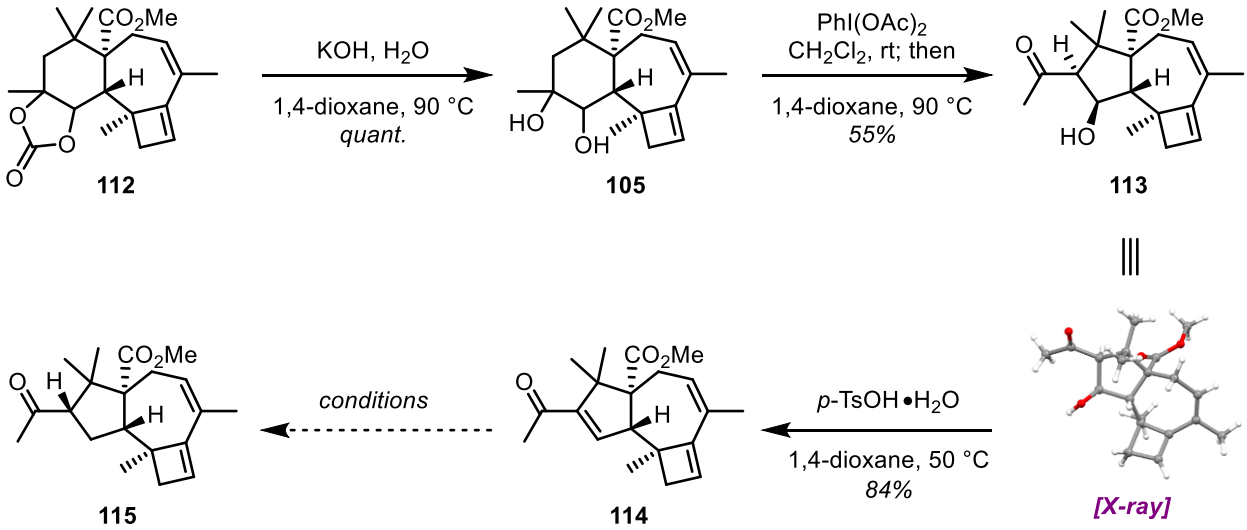

Scheme 3.21. Oxidative cleavage and subsequent aldol reaction of diol **105**, effects ring contraction

Despite repeated efforts, a classic Barton–McCombie deoxygenation did not produce the desired ketoester **115** or its α-epimer in high yield, potentially due to a competing retro-aldol reaction in the formation of the requisite xanthate. X-ray analysis of **113** revealed a *trans* relationship between the ketone and the ester, thereby complicating the formation of the bridged bicycle via condensation chemistry, as it would require a successful epimerization event prior to the desired cyclization. As such, we sought to eliminate the secondary alcohol and perform a conjugate reduction of the resulting enone. After treating ketoalcohol **113** with *p*-TsOH•H_2O under moderate heating, we recovered the desired enone **114** in good yield.

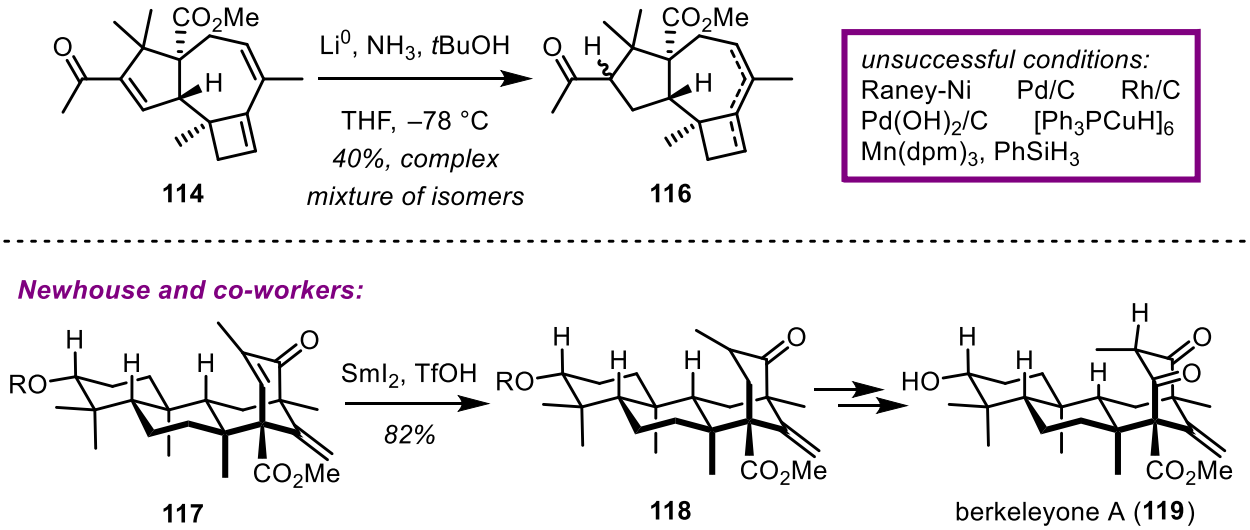

Scheme 3.22. Attempts to reduce tricyclic enone **114** and literature precedent for Sm^{II}-mediated reduction in total synthesis

Our initial attempt to reduce enone **114** under dissolving metal conditions did lead to the desired ketone in moderate yield, however, we also observed a significant amount of diene reduction and isomerization products that were difficult to separate from the desired product. Any additional conditions we attempted either offered no reaction, such as Stryker's reagent ($[Ph_3PCuH]_6$),[47] or proceeded to afford the fully saturated framework. With these disappointing results in hand, we were inspired by Newhouse and co-workers' impressive total synthesis of berkeleyone A (**119**), in which enone **117** was selectively reduced to ketone **118** by SmI_2 after a similarly exhaustive effort.[48] To our delight, this method, generating TfOH *in situ* from TESOTf and H_2O, allowed for selective enone reduction in moderate yield and favorable d.r.

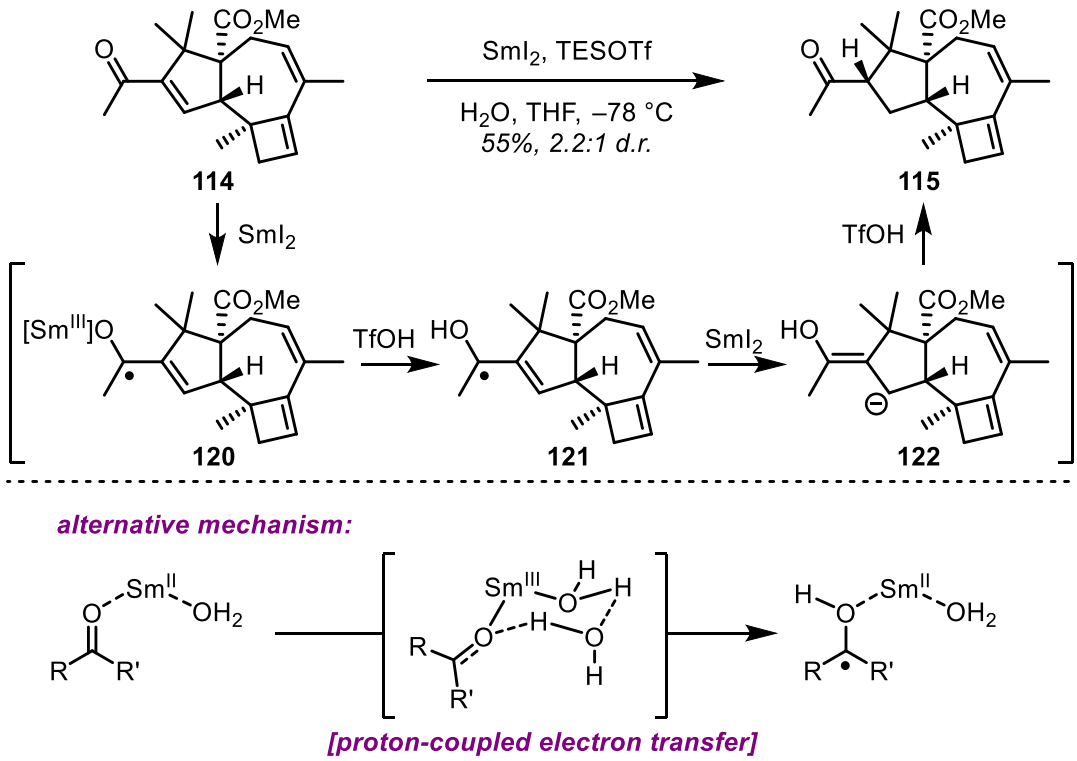

Scheme 3.23. Sm^{II}-mediated reduction of enone **114** furnishes ketoester **115** and the role of a strong proton donor in the reduction mechanism.

This selectivity for the enone olefin can be explained by the mechanism of typical Sm^{II}-mediated carbonyl reductions, shown for our system in Scheme 3.23.[49–51] Initial single-electron transfer to the carbonyl forms ketyl radical **120**. In other systems, this radical can undergo a variety of intramolecular coupling reactions, contributing to its wide use. In the presence of a strong proton donor, such as TfOH, the organosamarium species undergoes protonolysis, followed by additional single-electron transfer to allyl anion **122**.[51] Protonation at the β-position and tautomerization of the resultant enol **122** delivers the desired ketone **115**. Recently, an alternative mechanism for this reaction has been proposed, involving an initial proton-coupled electron transfer.[52] While either mechanism is plausible, in our system, the low concentration of H_2O suggests that the step-wise mechanism predominates.

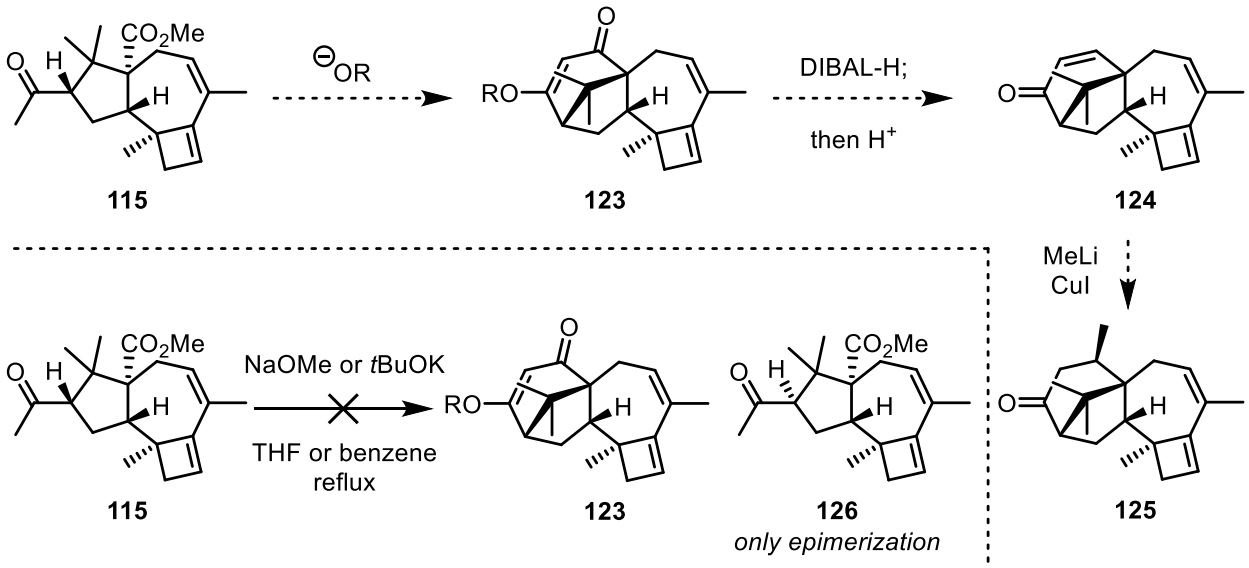

Scheme 3.24. Outline of our strategy toward the formation of the tetracyclic ketone **125** and unsuccessful Dieckmann condensation

With the desired tricyclic *cis*-ketoster **115** in hand, we planned to move on to the next stage of our synthesis, completing the last ring remaining in the harziane diterpenoid natural products. Our strategy was to trigger a base mediated Dieckmann condensation, followed by formation of vinylogous ester **123**. This would provide access to tetracyclic enone **124** via DIBAL-H reduction. Initial attempts to effect our desired Dieckmann condensation proved fruitless, as the *cis*-ketoester simply isomerized to the undesired *trans*-ketoster, making this approach unfeasible. Despite this setback, we continued to screen alternative conditions, among them reversible acidic conditions and irreversible base conditions, none of which provided the tetracyclic material. We presume that the thermodynamic favorability of the *trans*-isomer, alongside the steric congestion and reduced electrophilicity of the neo-pentylic ester impeded this transformation. As such, we decided to explore the synthesis of the more reactive ketoaldehyde counterpart, which might allow for a successful aldol condensation. At the same time, we redesigned our synthetic route to ketoester **115**, since material throughput proved to be a bottleneck in our synthetic investigations.

SECTION 3.2.3: ROUTE REDESIGN: RELIABLE SEMI-PINACOL REARRANGEMENT AND COMPLETION OF THE CARBON FRAMEWORK

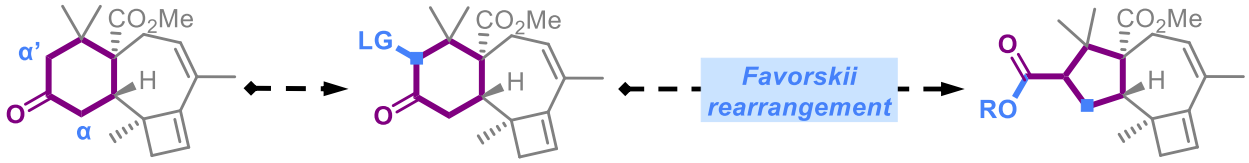

Scheme 3.25. Favorskii rearrangement strategy toward 5/7/4 ring system with α'-substituted ketone.

While our previous route toward ketoester **115** successfully achieved its objective of concise ring contraction, via an oxidative cleavage of 1,2-diol **105** and subsequent aldol reaction, this route was laden with inefficient transformations and several functional group interconversions, which hurt step economy. We returned to the drawing board and proposed an alternative route which, if successful, could provide more efficient access to ketoester **115**, thus enabling reaction investigation in the latter part of the route. In our discussion of ring contraction strategies (Scheme 3.14), we proposed that installation of a leaving group at the more sterically encumbered α'-position may allow us to access a substrate that could undergo a semi-pinacol rearrangement to the desired 5/7/4-ring system. In this capacity we also decided to revisit the Favorskii-rearrangement discussed in Section 3.2.2.

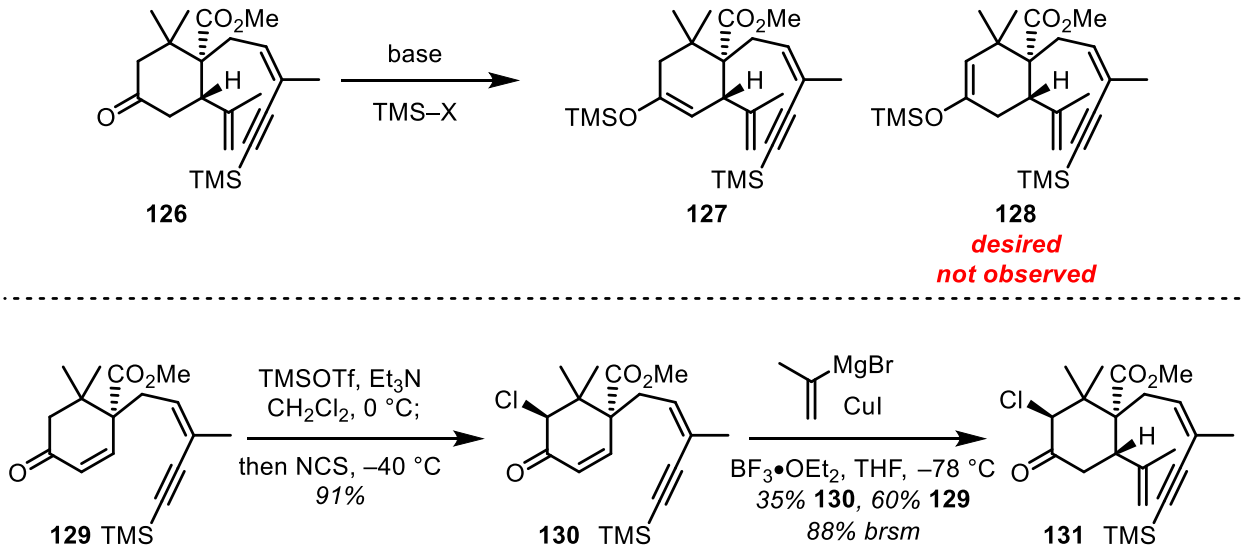

Scheme 3.26. Synthesis of α'-substituted ketone **131** has to be done via chloroenone **130** and a challenging conjugate addition with isopropenyl cuprate with concomitant dehalogenation

Our concerns that functionalization at the α'-carbon of ketone **126** would be challenging were confirmed, as silyl enol ether formation utilizing either kinetic or thermodynamic control exclusively produced **127**. As such, we decided to attempt α'-functionalization of enone **129**. To our delight, electrophilic chlorination proceeded smoothly to form chloroenone **130** in high yield and as a single diastereomer. Efforts to synthesize analogs of **130** with alternative leaving groups utilized in semi-pinacol rearrangements such as bromide, halide, sulfide, or selenide did not succeed.

One main caveat of this approach is that cuprate-mediated conjugate addition was expected to lead to a considerable amount of undesired dehalogenation.[53,54] To the best of our knowledge, no such conjugate addition with an α'-halogenated enone has been reported in the literature, so we were relieved that chloroketone **131** was formed in acceptable yield, despite significant amounts of dehalogenation. Furthermore, dehalogenation prior to cuprate addition was

the only side reaction we observed, such that we were able to recycle starting enone **129**. This route could be reliably carried out on multi-gram scale.

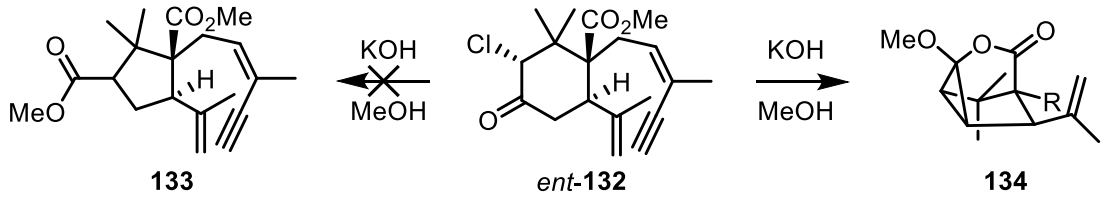

133 *ent*-**132** **134**

Scheme 3.27. Interrupted Favorskii rearrangement of α'-chloroketone **132**

At this point, we decided to once again attempt a Favorskii rearrangement, now with a pre-installed leaving group at the α'-position. We sought to test whether the regioselectivity of the iodosobenzene-mediated oxidative Favorskii rearrangement holds for a more classical approach using our haloketone **132**. Favorskii rearrangement was tried with both the tricyclic ketone **142** (Scheme 3.29) and monocyclic chloroketone **132** (Scheme 3.27). The more flexible **132** underwent rapid reaction to an unexpected product. After intensive analysis of the ^{1}H NMR spectrum and studying the mechanism and relevant intermediates of this reaction, we concluded that the Favorskii rearrangement was interrupted by a competing intramolecular transesterification to putative lactone/ketal **134** (Scheme 3.28).

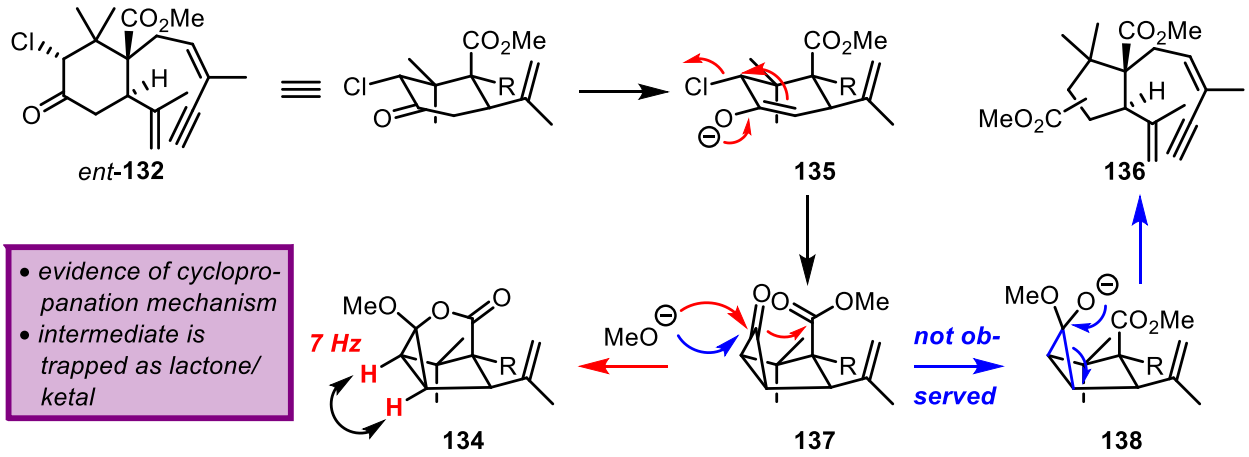

ent-**132** **135** **136** **134** **137** **138**

Scheme 3.28. Interrupted Favorskii rearrangement shows evidence for cyclopropanone intermediate

In order to best illustrate the proposed pathway, we have decided to show the enantiomer of our haloketone, *ent*-**132**. The expected enolate formation and intramolecular S_N2 reaction leads to cyclopropane intermediate **137**. In the classic Favorskii rearrangement, nucleophilic addition of an alkoxide would lead to intermediate **138** (blue path), followed by ring-strain promoted cleavage of one of the adjacent bonds of the three-membered ring. Instead, the neopentyl ester is positioned such that lactonization with the transient hemiketal is facile. Products of this type are known in the literature and serve as a confirmation of the cyclopropane mechanism.[55,56] Unfortunately, further derivatization of **134**, such as driving the Favorskii rearrangement to completion or Au^I-catalyzed cycloisomerization of the tethered enyne were unsuccessful.

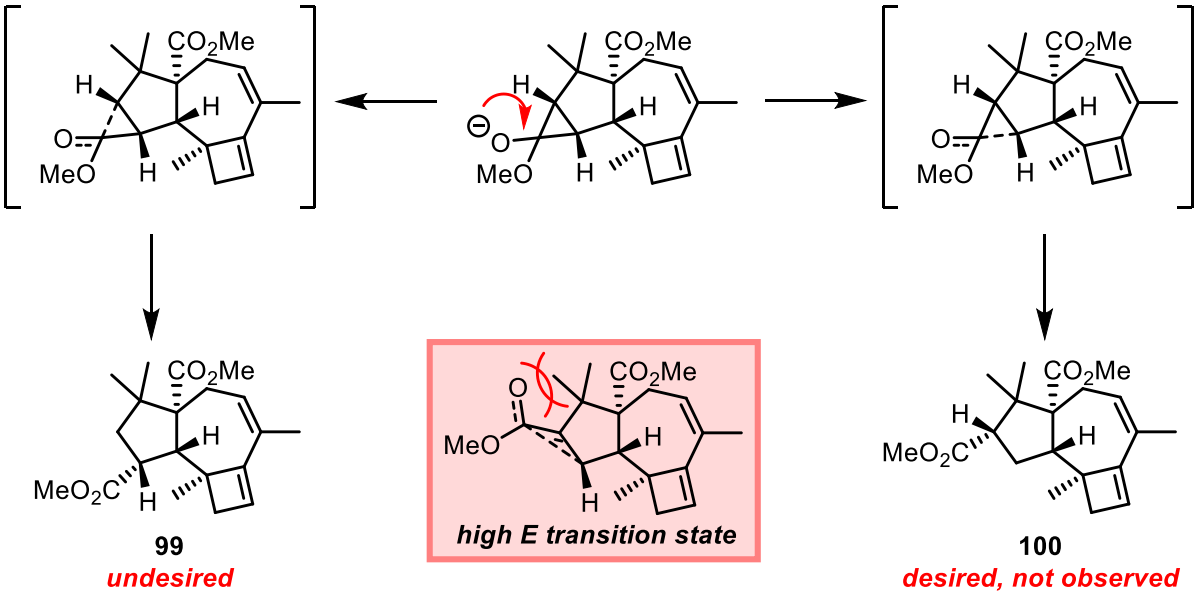

Scheme 3.29. Rationale for formation of the undesired diester **99** from a Favorskii rearrangement of tricyclic chloroketone **100**.

After Au^I-catalyzed cycloisomerization of **132**, we subjected the more rigid tricyclic haloketone **142** to the classic Favorskii rearrangement conditions. The ring contraction was observed; however, the spectral properties of the obtained product matched the undesired regioisomer **99** that we obtained in our earlier studies (Scheme 3.29). This result led us to the

conclusion that further pursuit of the Favorksii rearrangement strategy was not feasible. Upon collapse of the hemiketal, one of the two bonds of the three-membered ring intermediate would be cleaved and, following protonation of the resultant carbanion, would form either **99** or **100**. We hypothesized that the undesired regioisomer predominates due to the steric congestion, and likely higher transition state energy, required for formation of diester **100**.

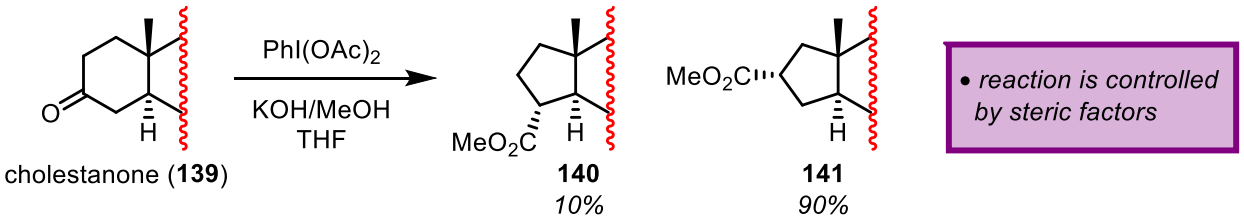

Scheme 3.30. Literature precedent for sterically controlled Favorskii rearrangement in cholestanone (**139**) reported by Moriarty *et al*.

Within the literature, we found a similar example of steric control, providing further evidence supporting our hypothesis. Moriarty and co-workers, who reported the oxidative Favorskii rearrangement utilizing $PhI(OAc)_2$, observed that ring contraction of cholestanone (**139**) largely afforded the less sterically encumbered product, noting that in their case the influencing quaternary center is even more distal to the reactive site than in **138**.[42]

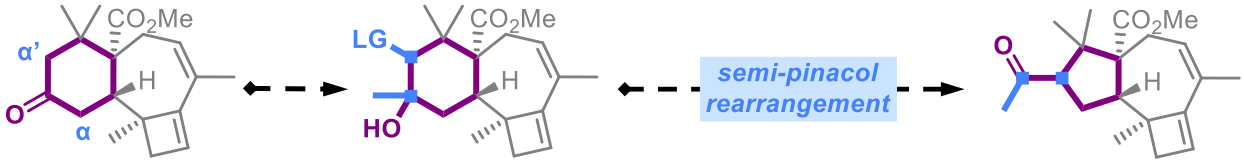

Scheme 3.31. Semi-pinacol rearrangement strategy toward 5/7/4 ring system with α'-substituted ketone.

As such, we focused our attention on the remaining ring contraction strategy, the semi-pinacol rearrangement. Au^I-catalyzed cycloisomerization of chloroketone **131**, followed by 1,2-addition of MeMgBr in the same pot forms the desired ring contraction precursor chlorohydrin **143**. Initial attempts at effecting the desired ring contraction by sequestering the chloride leaving

group with Ag^I-salts failed even at elevated temperatures.[57] Interestingly, we found that treatment with an excess of *t*BuOK in THF efficiently triggered the desired reaction to deliver a mixture of *trans*- and *cis*-ketoesters **126** and **115** in excellent yield and a 2.2:1 diastereomeric ratio.

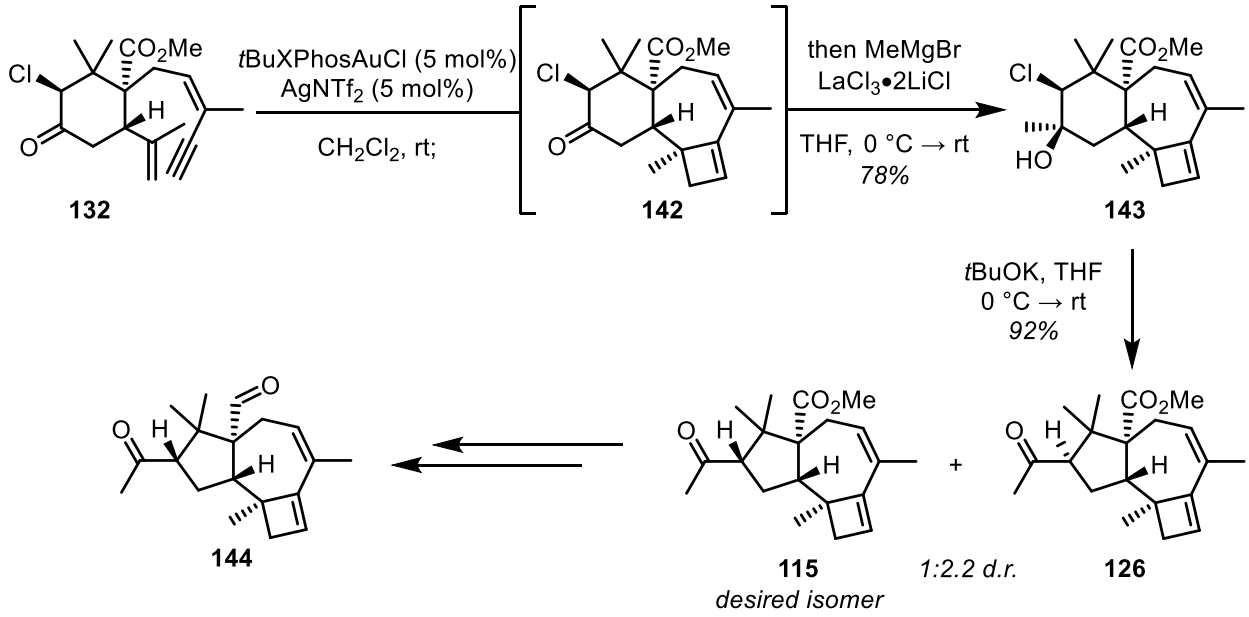

Scheme 3.32. Au^I-catalyzed cycloisomerization of chloroketone **131** and semi-pinacol rearrangement to desired ketoester **115**

The success of this reaction relied on the relative stereochemistry of our decorated cyclohexane **131**. First, the *cis* relationship between the tertiary alcohol and the chloride leaving group precludes an intramolecular S_N2 reaction to furnish an undesired epoxide, often observed in *trans*-diaxial systems. Second, within the rigid tricyclic ring system, the migrating σ-bond is oriented anti-periplanar to the C–Cl σ* orbital (Scheme 3.33). It is notable that in addition to the *trans*-ketoester **126**, predicted to be the product by our conformational analysis, *cis*-ketoester **115** was isolated as the minor product. A plausible explanation is that in these reversible base conditions, epimerization can take place. However, attempting to shift this ratio by prolonging the reaction time leads to formation of an unidentified decomposition product. These results are in line with observations made during our attempts to construct the bridged bicycle via a Dieckmann

condsensation (*vide supra*). Given that the *trans* isomer is slightly favored under such reversible conditions and that, when subjected to similar conditions, reaction mixtures favoring the *cis*-isomer undergo epimerization (Scheme 3.24), one could presume that the *trans*-species is thermodynamically favored.

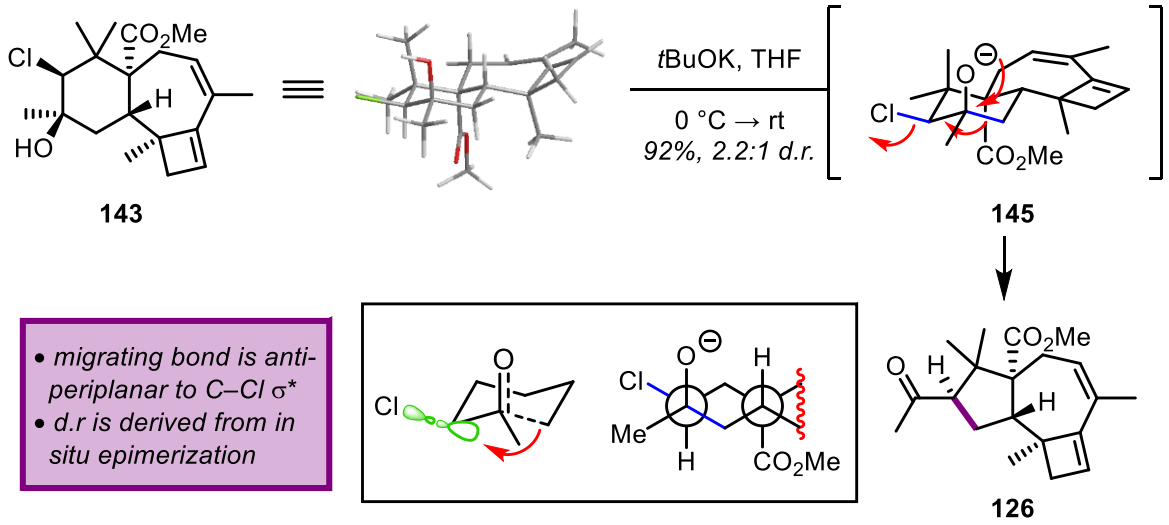

Scheme 3.33. Favorable orbital alignment explains efficiency and diastereoselectivity of the semi-pinacol rearrangement to the ring contraction product ketoester **126**.

Separation of the two ketoester epimers proved to be facile, allowing for further exploration of [3.2.1]-bicyclooctane formation. The undesired *trans*-diastereomer **126**, obtained as the major product, was used as a model compound to test various functionalization reactions of the diene in the 7/4-ring system, discussed later in this chapter. In addition, we invested time in identifying suitable epimerization conditions to the desired *cis*-ketoester **115**, in order to improve material throughput. Since reversible conditions appeared to favor the undesired *trans*-isomer, as discussed above, we looked to achieve the desired stereochemistry via kinetic control. As inspiration, we considered the samarium-mediated conjugate reduction chemistry as discussed in *Section 3.2.2*. In that case, following ketyl radical formation and subsequent oxidation, the resulting allylic carbanion could isomerize to the tetra substituted enol, which, upon quench in protic solvent

affords, a mixture favoring the *cis*-epimer. We postulated that formation and subsequent hydrolysis of the thermodynamic silyl enol ether in this case could similarly favor the desired *cis*-epimer.

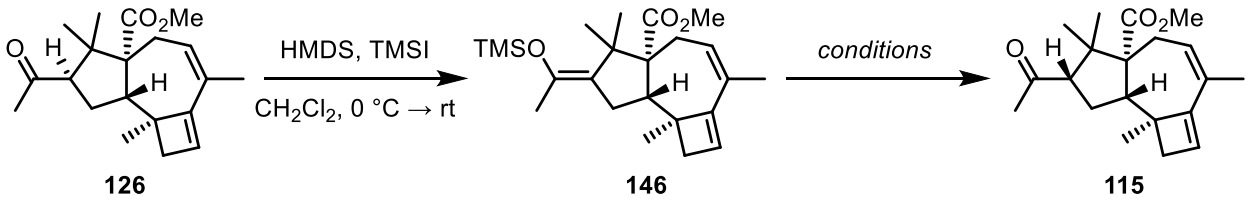

126 **146** **115**

Entry	*Acid*	*Solvent*	*T*	**126** *:* **115**
1	*p*TsOH•H_2O	MeOH/THF = 1/10	rt	*1 : 0.4*
2	TFA	MeOH/THF = 1/10	rt	*1 : 0.9*
3	(±)-CSA	MeOH/THF = 1/10	rt	*1 : 1.1*
4	(±)-CSA	HFIP/THF = 1/10	rt	*1 : 1.2*
5	(±)-BINOL + $SnCl_4$	toluene	–78 °C	*1 : 0.4*
6	(±)-BINOL + BF_3•OEt_2	toluene	–78 °C	*1 : 3.5*[a]

[a] *small scale reaction (0.03 mmol), scale-up unsuccessful*

Table 3.1. Investigation of the epimerization of *trans*-ketoester **126** to the desired *cis*-ketoester **115**

Treatment of **126** with TMSI/HMDS selectively provided the tetrasubstituted silyl enol ether.[58] Notably, *cis*-ketoester **115** only exhibits minimal conversion under these conditions. From there, we decided to screen a variety of hydrolysis conditions. It was our hypothesis that protonation from the more accessible top face may further predominate when using sterically encumbered proton sources. We found that hydrolysis was effective with a variety proton sources, with the best result, combining diastereomeric ratio and yield, being entry 4 (Table 3.1). Lewis acid-mediated conditions developed by Yamamoto (entry 6) produced an excellent ratio in favor of our desired ketoester **115**; however this result was not reproducible on larger scale.[59]

With a reliable supply of *cis*-ketoester **116** in hand, we proceeded to work toward completing the carbon skeleton of the harziane diterpenoid natural products. As prior attempts at Dieckmann condensation were fruitless, we targeted ketoaldehyde **144** as a promising cyclization precursor to tetracyclic enone **124**, given the success of this reaction in the Carreira approach. Full

reduction of **115** to diol **149** proved to be challenging due to the extreme steric encumbrance of the neopentyl ester. While $LiAlH_4$ in refluxing THF only reduced the ketone, heating with DIBAL-H in CH_2Cl_2 at 90 °C in a sealed tube successfully produced a diastereomeric mixture at the secondary alcohol within the resultant diol **149**.

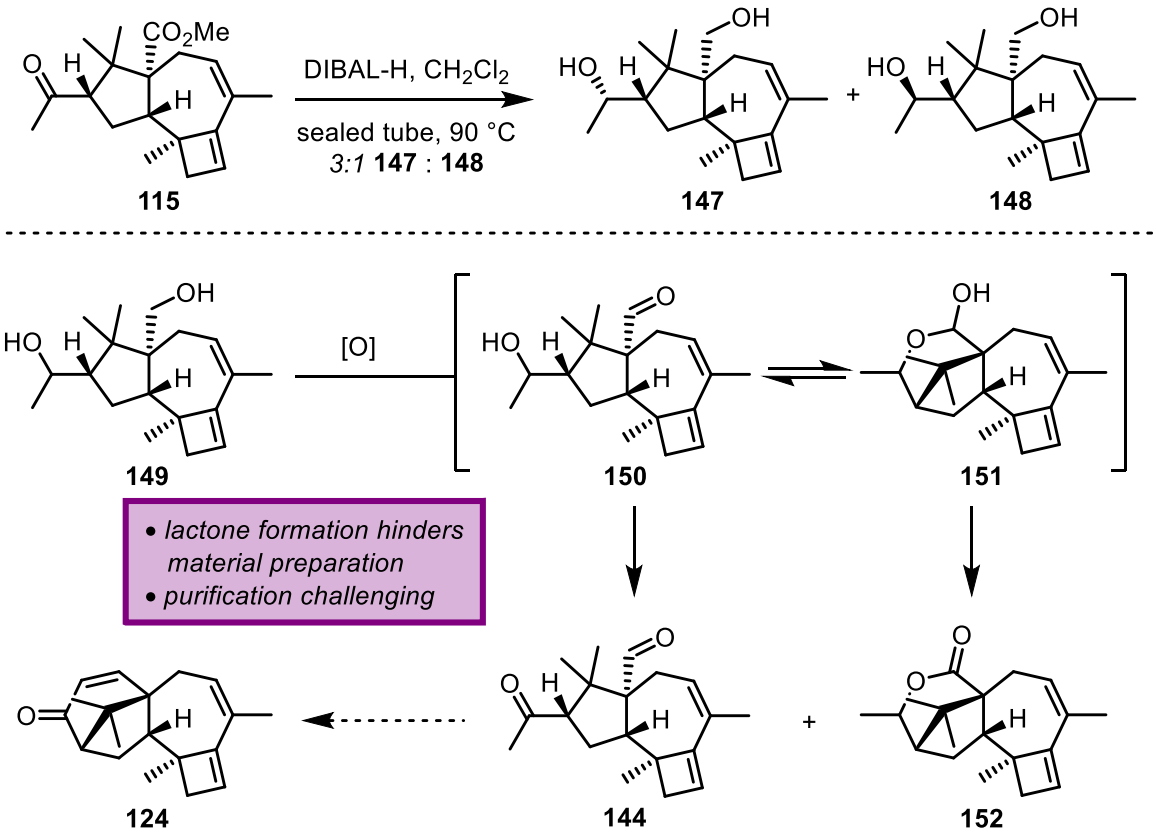

Scheme 3.34. Reduction of ketoester **115** and a challenging side reaction in the subsequent oxidation to ketoaldehyde **144**

Initially, we did not take issue with the presence of the two diastereomers, as oxidation to ketoaldehyde **144** in the subsequent step would remove this particular stereocenter. During our screen of oxidation conditions, we were surprised to find that a persistent side product was lactone **152**, arising from oxidation of lactol **151**, which in turn is reversibly formed following the

oxidation of the primary alcohol to the aldehyde within **150**.[60] This result complicated preparation of ketoaldehyde **144**, lowering yield and significantly impeding purification. Purification of the diol diastereomers revealed that the minor diol diastereomer had a higher propensity for lactol formation as opposed to the major diastereomer. This difference in reactivity is likely a result of clashing between the methyl group of the secondary alcohol and the *gem*-dimethyl group during lactol formation in the major diastereomer. Upon screening of different oxidation manifolds, Ley oxidation proved to be the most efficient at producing the desired oxidation product, with lactone formation being a minor byproduct.[61] It was thought that Swern oxidation could preclude formation of lactol **151**, as oxidation only happens upon quenching the reaction, but unfortunately other unidentified side products were formed in the course of the reaction.

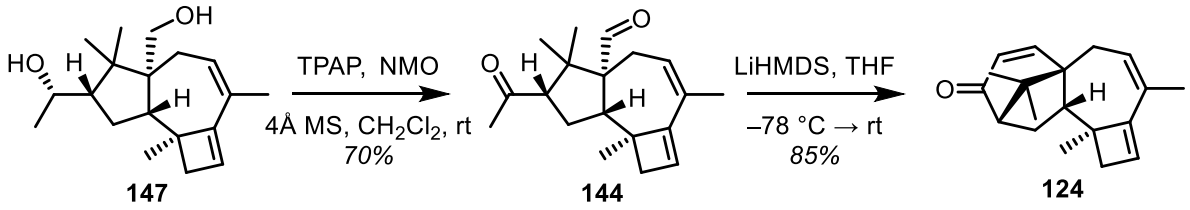

Entry	*Reagent*	*Solvent*	*T*	*Result*
1	NaOMe	MeOH/THF (1:1)	70 °C	*epimerization*
2	*t*BuOK	THF	70 °C	*decomposition*
3	**153**	benzene	80 °C	*no reaction*
4	**153**	THF	70 °C	*no reaction*
5	**154**	benzene	80 °C	*no reaction*
6	**155**	benzene	80 °C	*no reaction*
7	*p*TsOH•H_2O	toluene	90 °C	*epimerization*

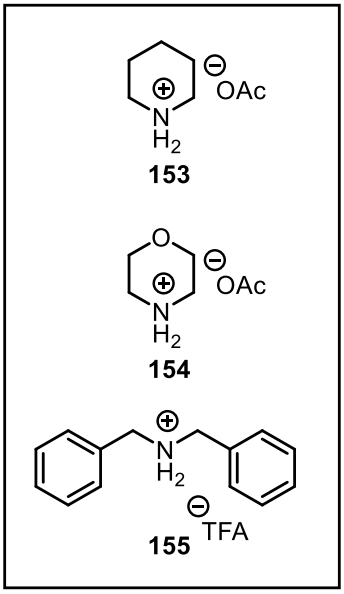

Scheme 3.35. Synthesis of tetracyclic enone **124** from ketoaldehyde **144** via intramolecular aldol condensation

To our delight, completion of the tetracyclic core of the harziane diterpenoid natural products was finally achieved via an intramolecular aldol condensation of ketoaldehyde **144** to afford enone **124**. Our approach of careful deprotonation at the methyl ketone with LiHMDS and subsequent cyclization upon slow warming was not, however, among the first cyclization conditions attempted. Following the more canonical approach of reversible base conditions (Scheme 3.35, entries 1 & 2) proved just as fruitless as treatment with ammonium salts (entries 3-6), which have widely been shown to be competent at effecting aldol condensation reactions.[62] In addition to heating with a small, reversible base (entry 1), strong acid (entry 7) also caused epimerization to the unreactive *trans*-ketoaldehyde epimer.

Following this breakthrough, we were hopeful to complete the total synthesis of a variety of harziane diterpene natural products from this key intermediate. The two major challenges we foresaw were addition of the remaining methyl group to the tetracyclic enone **124** in a stereoselective manner, and selective functionalization of the diene moiety. As discussed earlier in this chapter, one aspect of our route design was the potential to achieve a synthesis that allowed for late-stage divergence to access the various oxidation states found within the natural product family.

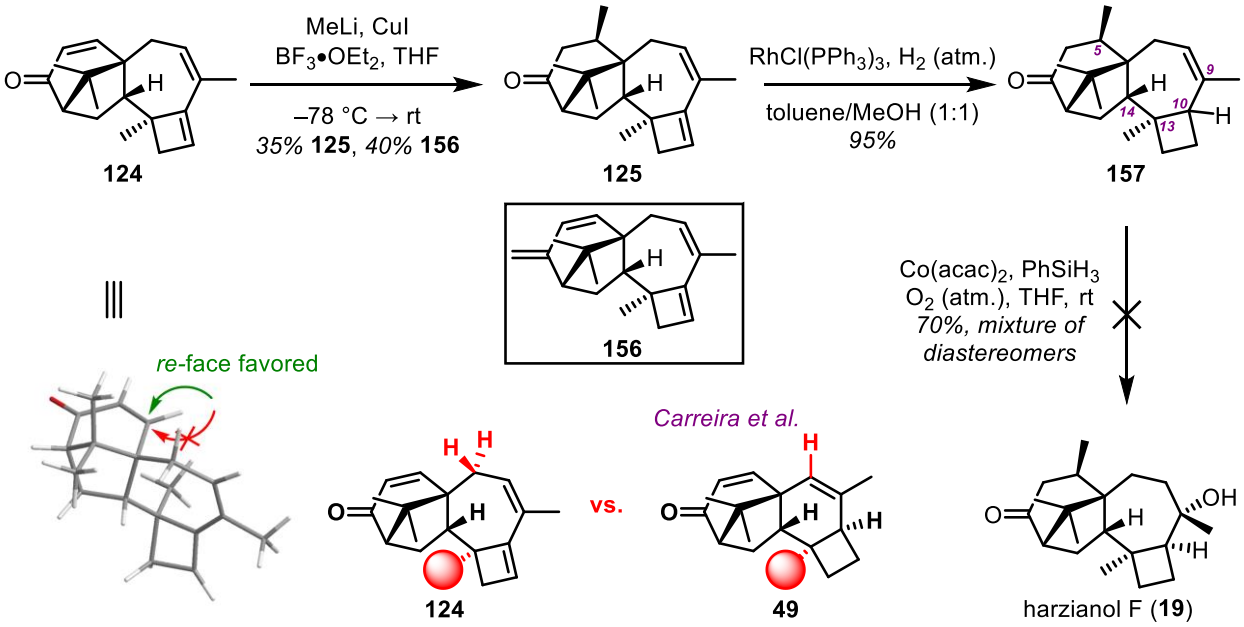

Scheme 3.36. Transformation of tetracyclic enone **124** to ketone **125** and analysis of *re*-face addition and unsuccessful attempt to complete the total synthesis of harzianol F (**19**)

Our plan for conjugate addition to enone **124** initially resembled that of Carreira's synthesis of harzianol I (**21**).[63] There, methyl cuprate added in a facially selective manner, as the bottom face of the β-carbon within enone **49** is blocked. Analysis of a 3D model reveals the potential for a similar sterically-induced bias in our system, however, a higher degree of saturation around the adjacent all-carbon quaternary center could obstruct approach to the β-carbon. Despite screening a variety of conditions for conjugate methyl cuprate addition, we were unable to identify an optimal set of conditions to furnish ketone **125**, as competing 1,2-addition and elimination to tetraene **156** predominated. In order to access the natural products containing a saturated cyclobutane ring, we hydrogenated the more strained cyclobutene in excellent yield and chemoselectivity to obtain **157**. Closely following the analogous conditions reported by Carreira *et al*., we hoped that a Mukaiyama hydration would lead to the total synthesis of harzianol F (**19**). While the reaction proceeded smoothly, we ended up isolating more than one diastereomer, neither of which matched the reported ^{1}H NMR spectrum of natural harzianol F (**19**).[24]

In light of this unexpected result, we were concerned that one of our stereocenters within the starting material, tetracyclic olefin **157**, was incorrect. As we isolated what were presumably the two diastereomers at C-9 from the Mukaiyama hydration, we ruled this stereocenter out as our potential culprit. In addition, C-13 and C-14 were unlikely to have epimerized since our last definite structural confirmation of chlorohydrin **143**. Facial approach of the cuprate nucleophile to enone **124** has been discussed above and was likewise excluded as a possibility. The last option, inverse stereochemistry at C-10 would mean that the 7/4-ring system had an undesired *trans* fusion. This seemed implausible to us as ring strain would seem to be enormous, upon analysis of a 3D model.

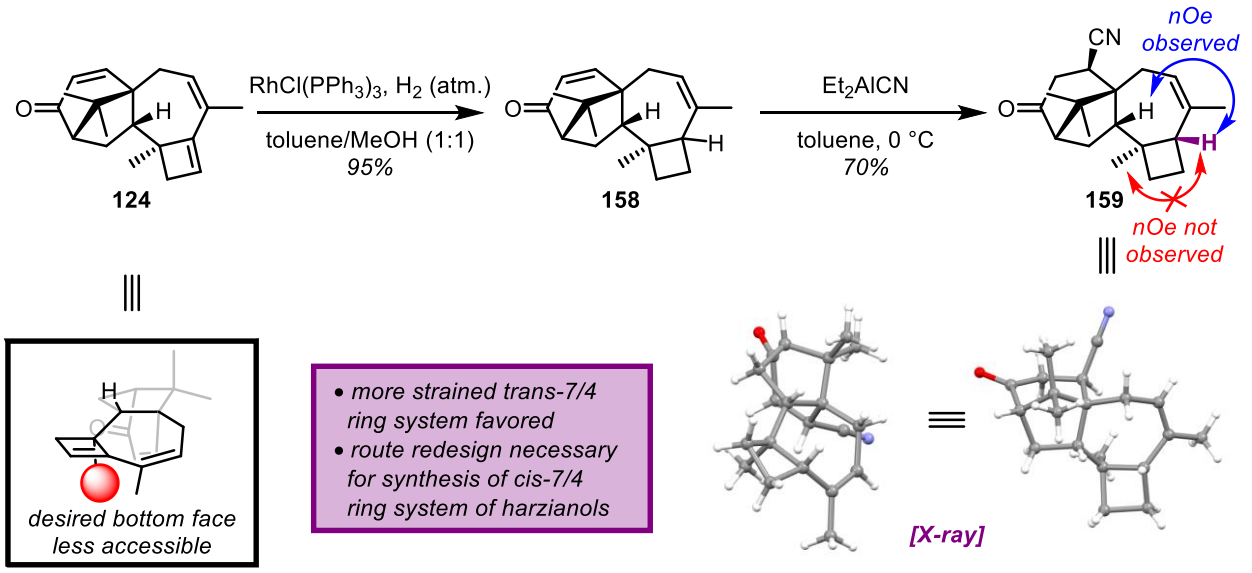

Scheme 3.37. ^{1}H NMR experiments and X-ray crystal structure analysis of nitrile **159** reveal unusual and undesired *trans*-7/4 ring system arising from a hydrogenation reaction

In order to obtain more conclusive evidence, we decided to derivatize enone **124**. Wilkinson's catalyst-mediated hydrogenation was followed by treatment with Nagata's reagent (Et_2AlCN) to furnish nitrile **159** in good overall yield as a single diastereomer.[64] Upon analysis of **159**, we observed a nuclear Overhauser effect (nOe) between the two indicated protons at C10 and

C14. The expected nOe between the proton at C10 and the methyl group at the 7/4 ring junction was not observed. The presence and absence, respectively, of the expected nOe signals was good evidence alone that we formed the undesired *trans* 7/4 ring system during the hydrogenation step. Conclusive evidence was provided by single crystal X-ray diffraction analysis, confirming the existence of this unusual ring junction.

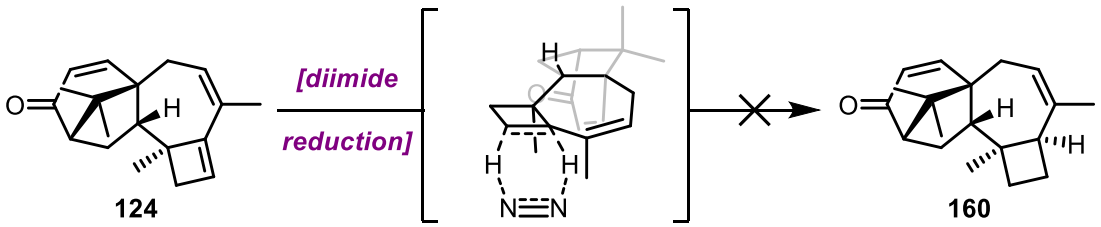

Scheme 3.38. Diimide reduction as an attempt to effect *re*-face approach during hydrogenation

Steric control at the *re*-face of the four-membered ring explains this selectivity and significantly hindered our progress. In an attempt to salvage our planned route, we sought to utilize a variety of other hydrogenation conditions for the selective functionalization of the diene moiety within enone **124**. Heterogenous and homogenous transition metal catalysts were unsuccessful at furnishing the desired *cis* 7/4-fused ring system and in most cases lacked chemoselectivity for the cyclobutene over the cycloheptene. Hydrogen atom transfer (HAT) conditions such as those developed by Shenvi *et al*. led to complex mixtures of unidentified products.[65] To us, reduction with *in situ* diimide were most promising, owing to the small size of the hydrogen source.[66] With it, we hoped access to the *re*-face would be possible, furnishing the less strained *cis*-fused ring system, yet none of the reported protocols worked in our hands. With our options of direct access to the *cis*-fused ring system within enone **124** frustrated, we bifurcated our investigation, to develop alternative approaches to harzianol F (**19**), while at the same time pursuing the synthesis of harziandione (**15**).

The rigid structure and steric congestion of our intermediates have at times enabled and at times impeded desired reactivity. This ambivalent nature of complex molecular systems is a key characteristic in the field of total synthesis and identifying the moments of opportunity to solve problems creatively is a key skill we learned in the course of this project. Of the two approaches covered in the following section, one seeks to exploit the existing arrangement of functional groups to trigger selective reactions intramolecularly, whereas the other makes the best of the proverbial hand we were dealt.

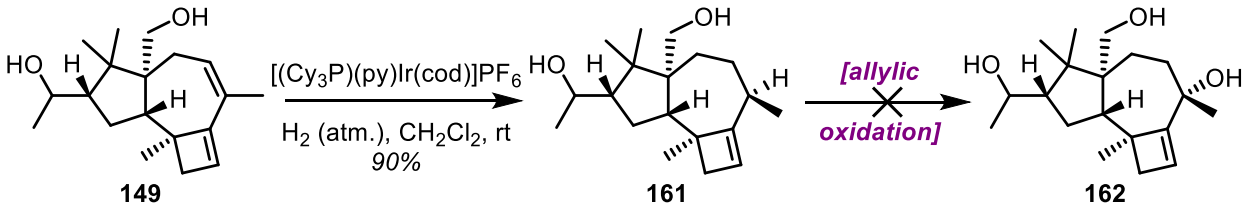

Scheme 3.39. Crabtree catalyst allows for hydroxyl-directed chemoselective hydrogenation of the cycloheptene

We hypothesized that we could use the directing effect of the primary alcohol within diol **149**, to selectively hydrogenate the less strained olefin, a reactivity that is orthogonal to that observed with Wilkinson's catalyst as discussed above. To our delight, Crabtree's catalyst, a cationic Ir^{I} species, proved to be competent in catalyzing this directed hydrogenation in a chemo- and stereoselective fashion under mild conditions.[67] At this stage, we attempted to introduce the desired tertiary alcohol via allylic oxidation, such that we could successfully hydrogenate the remaining olefin within **161** in a similarly directed manner to furnish the *cis*-7/4 ring system, however our efforts remained fruitless. This result, nonetheless, was an encouraging entry point, as it was a proof of concept for intramolecular functionalization reactions.

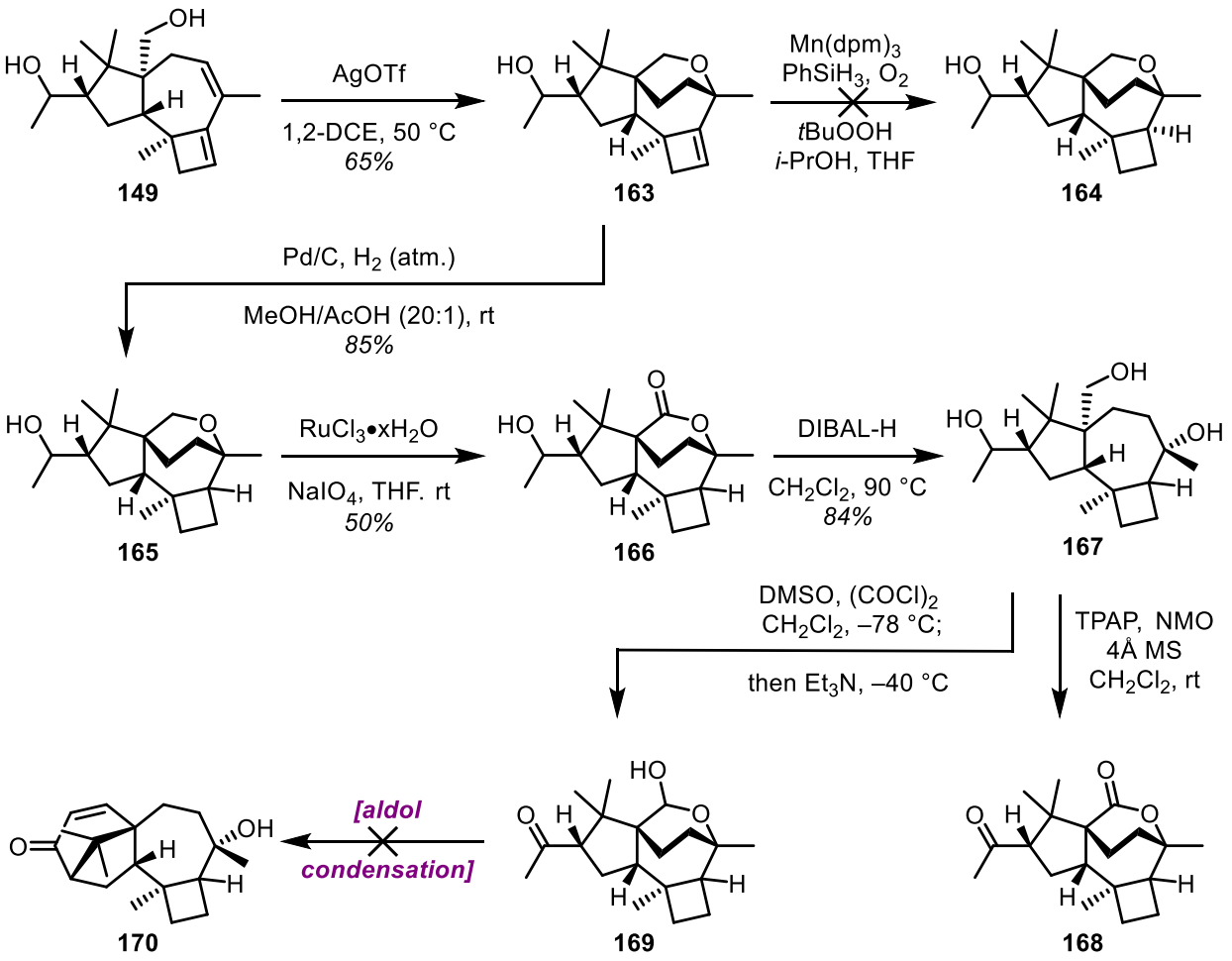

Scheme 3.40. Selective intramolecular hydroalkoxylation of diol **149** and subsequent derivatization reactions

In an effort to install the desired alcohol functional group at C-10 in pursuit of tetracyclic enone **170**, we decided to attempt an intramolecular hydroalkoxylation reaction. Such a reaction has previously been reported by He and others.[68,69] Utilizing He's conditions with catalytic AgOTf, hydroalkoxylation delivered ether **163** in good yield. This reaction is presumably catalyzed by trace amounts of TfOH, combined with the cationic Ag^{I} aiding in activation of the conjugated π-system.[70] This hypothesis was confirmed by low conversion when treating **149** with $AgPF_6$ and by He and co-workers' observation that Lewis acids such as $Zn(OTf)_2$ did not catalyze similar reactions. With ether **163** in hand, we hoped to trigger an efficient cleavage of the cyclic ether to

triol **167**, however, any such attempts with classical ether bond cleaving reagents such as BBr_3 led to decomposition.

As further strategies, such as oxidation at the α-carbon of the ether within **163**, proceeded under conditions incompatible with the presence of olefins, we moved to attempt hydrogenation with the hope that the [3.2.2]-bicycle would impede catalyst approach from the top face to form the *cis*-fused ring system. HAT mediated hydrogenation only led to decomposition, but heterogenous Pd/C in the presence of MeOH and AcOH under a hydrogen atmosphere gave cyclobutane **165**. Unfortunately, we were unable to conclusively confirm whether the desired *cis*-7/4 ring system had formed. The ether was subsequently oxidized to lactone **166** and fully reduced to tricyclic triol **167**.[71] To our surprise, the conformation of the seven-membered ring in **167** is such that upon oxidation of the triol under Ley oxidation conditions, the lactone **168** is obtained, presumably via the intermediate lactol. The analogous lactol **169** was formed selectively during Swern oxidation and exists in equilibrium with the desired ketoaldehyde. We hoped that our previously successful aldol condensation conditions, when applied to the afore mentioned lactol/ketoaldehyde mixture, would provide us with tetracyclic enone **170**. Yet treating lactol **169** with LiHMDS led to prompt decomposition. Unfortunately, efforts to selectively protect the tertiary alcohol within the ring opened species failed, but we have plans to revisit this part of our investigation in the future.

Given the challenges associated with reduction of the cyclobutene olefin, we pivoted our focus to pursuing the total synthesis of harziandione (**15**) from tetracyclic enone **124**. To do so, we needed to selectively convert the 1,3-diene to an enone. We will first touch on the efforts we have undertaken to selectively transform the diene moiety on a variety of model compounds and then detail the successful strategy that led to the completion of the total synthesis of harziandione (**15**).

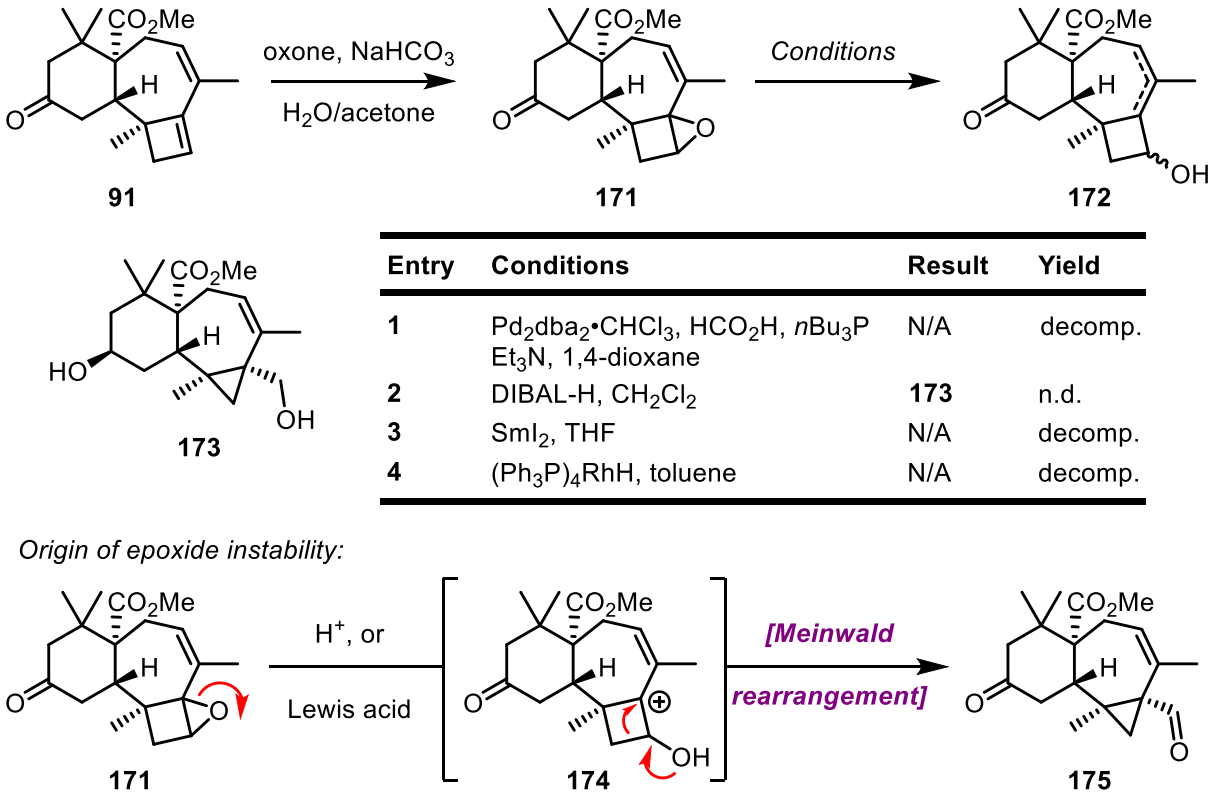

Entry	Conditions	Result	Yield
1	Pd_2dba_2•$CHCl_3$, HCO_2H, nBu_3P Et_3N, 1,4-dioxane	N/A	decomp.
2	DIBAL-H, CH_2Cl_2	**173**	n.d.
3	SmI_2, THF	N/A	decomp.
4	$(Ph_3P)_4RhH$, toluene	N/A	decomp.

Origin of epoxide instability:

Scheme 3.41. Epoxidation of cyclobutene in tricyclic ketone **91** and instability of vinyl epoxide **171** due to facile Meinwald rearrangement

At the time of our early studies on the ring contraction of tricyclic ketone **91**, we worked to identify oxidative transformations that would furnish the enone found in harziandione (**15**), and other harziane diterpenoid natural products, from the ring fused cyclobutene. Epoxidation of the 1,3-diene within **91** was unsuccessful with *m*-CPBA, but we found that *in situ* prepared DMDO produced a discernible vinyl epoxide **171**, which proved unstable upon storage. Attempts at ring-opening of the epoxide, such as reductive Tsuji-Trost conditions,[72]oshimao envisioned to form allyl alcohol **172**, or single electron epoxide opening mediated by SmI_2, only led to decomposition of the starting material.[73]

As DIBAL-H has been shown to open epoxides *via* a hydride transfer in a S_N2' fashion, we hoped that addition of hydride at the olefin was a possible solution in this case. However, when

applied here, hydride transfer did not occur. Instead, DIBAL-H acted as a Lewis acid, triggering a Meinwald rearrangement leading to ring contraction of the cyclobutanol to form the corresponding cyclopropane and reducing the resultant neopentyl aldehyde **175**. Dess-Martin periodinane-mediated oxidation of alcohol **173** back to the neopentyl aldehyde confirmed this proposed reactivity. It should be noted that such a ring contraction has been reported in the literature by Echavarren and co-workers on aryl-substituted cyclobutenes.[14]

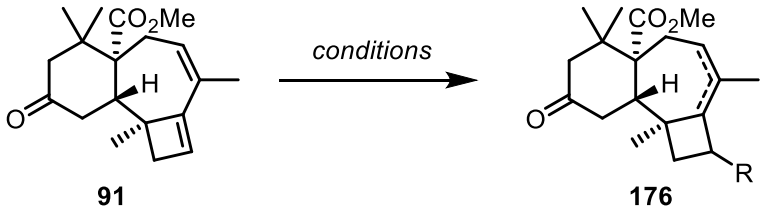

91 **176**

Entry	Conditions	R	Yield
1	Pd/C, EtOH, H_2	H	n.d.
2	Rh/C, EtOAc/toluene (2:1), H_2	H	n.d.
3	Raney Ni, EtOH, H_2	H	n.d.
4	$RhCl(PPh_3)_3$, toluene/MeOH (1:1)	H	86%
5	Li, $NH_{3(l)}$, THF, *t*BuOH	H	52%
6	$RhCl(PPh_3)_3$, THF, HBcat	Bcat	N.R
7	Karstedt cat., $PhMe_2SiH$, CH_2Cl_2	$SiMe_2Ph$	N.R.
8	NBS, THF/H_2O (9:1)	Br	decomp.
9	BDSB, CH_2Cl_2	Br	decomp.

Table 3.2. Investigation of selective diene functionalization within tricyclic ketone **91**

After ruling out epoxidation, we instead focused on a variety of other olefin functionalization reactions, of which a selection is presented in Table 3.2. Utilizing **91** as a model substrate again, we attempted a range of hydrogenation conditions. Entries 1-3 did not lead to the selective cyclobutene hydrogenation, or 1,4-hydrogenation to a tetrasubstituted olefin, instead producing complex mixtures of partially and fully saturated products. As presented on more

complex systems, Wilkinson's catalyst selectively reduced the cyclobutene, while dissolving metal reduction a mixture of tri- and tetrasubstituted olefin products and proved difficult to reproduce.

Hydroboration of the cyclobutene using catecholborane and other borane derivatives, as well as Cu(I)-catalyzed hydroboration, has thus far been unsuccessful.[74,75] Similarly, a sequence of hydrosilylation of the cyclobutene with Karstedt's catalyst,[76] followed by a proposed Fleming-Tamao oxidation, did not proceed. In addition, our attempts at electrophilic halogenations with NBS and BDSB, the latter of which was developed by our group, did not yield the desired cyclobutyl halides, and solely decomposition of the starting material was observed.[77]

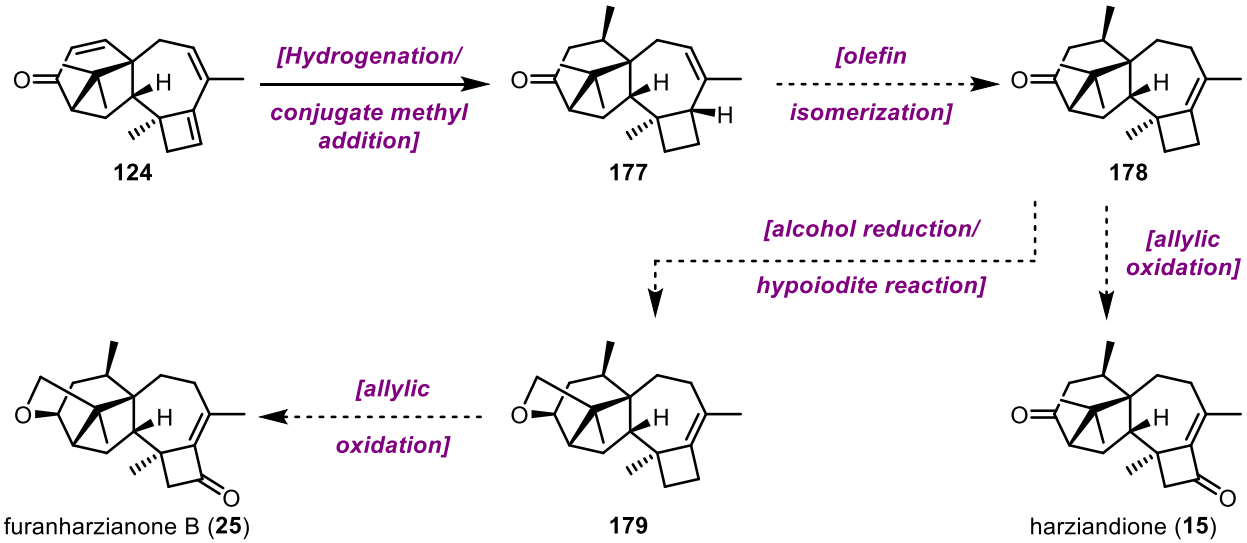

Scheme 3.42. Proposed end game strategy toward the total synthesis of **15** and **25** via olefin isomerization

As the selective functionalization of the diene moiety proved to be surprisingly challenging, we took inspiration from nature. In the biosynthetic pathway of the harziane diterpenes proposed by Dickschat and co-workers (discussed in Section 3.1.1), harziandione (**15**) is proposed to arise from an allylic oxidation of the tetrasubstituted olefin within **35**. While our synthetic approach is unable to replicate the skillful folding of the macrocyclic intermediate, as found in the biosynthesis, we believed that we could emulate the oxidative modification of the

harziane skeleton employing some of the many tools in the organic chemist's arsenal. To test a variety of olefin isomerization and allylic oxidation conditions, we decided to utilize the tricyclic ketoester **126** as a model system. Successful oxidation would not only provide access to harziandione (**15**) but also to the natural product furanharzianone B (**25**), which could be accessed via a hypoiodite-mediated annulation to introduce the bridged THF ring.[78]

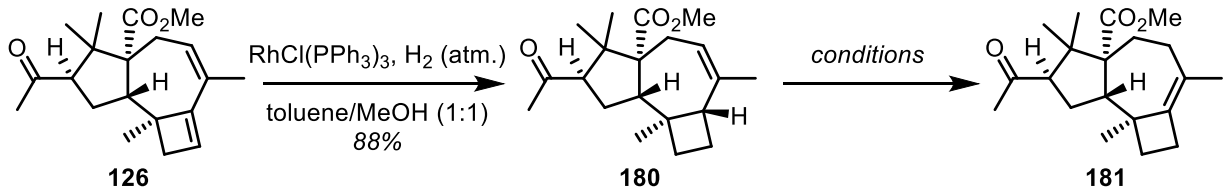

Entry	*Reagent*	*Solvent*	*T*	*Result*
1	HCl/1,4-dioxane	1,4-dioxane	80 °C	**181** + **182**, *low yield*
2	TFA	THF	70 °C	*no reaction*
3	(±)-CSA	1,4-dioxane	110 °C	*no reaction*
4	*p*-TsOH	benzene	80 °C	*decomposition*
5	*p*-TsOH	1,4-dioxane	110 °C	*50%* **181**
6	$[Pd(MeCN)_4](BF_4)_2$	MeCN	rt	*70%* **181**

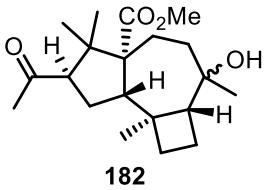

Table 3.3. Olefin isomerization of trisubstituted olefin within **180** to **181**

Following hydrogenation of ketoester **126** with Wilkinson's catalyst, we decided to screen a number of previously reported alkene isomerization conditions in order to gain access to tetrasubstituted olefin **180**. Acid-mediated isomerization reactions have previously been utilized to form the more substituted and thus thermodynamically favored olefin isomers, including in the total synthesis of spirograterpene A (**6**) as published by the Snyder group.[3] In the case of **6**, the conditions in entry 1 (Table 3.3) were the only ones that lead to the desired isomerization product. Upon treatment of ketoester **126** with these conditions, we found both isomerization and hydration products in low yield overall. Organic acids such as TFA and CSA did not provide any conversion, as they presumably are not sufficiently acidic. The more acidic *p*-TsOH (entries 4 and 5)

successfully delivered desired tetrasubstituted olefin **181** in moderate yield when run in 1,4-dioxane. Ultimately, the most efficient isomerization was observed under transition metal-mediated conditions, using the cationic Pd^{II} catalyst, $[Pd(MeCN)_4](BF_4)_2$ at ambient temperature (entry 7).[79]

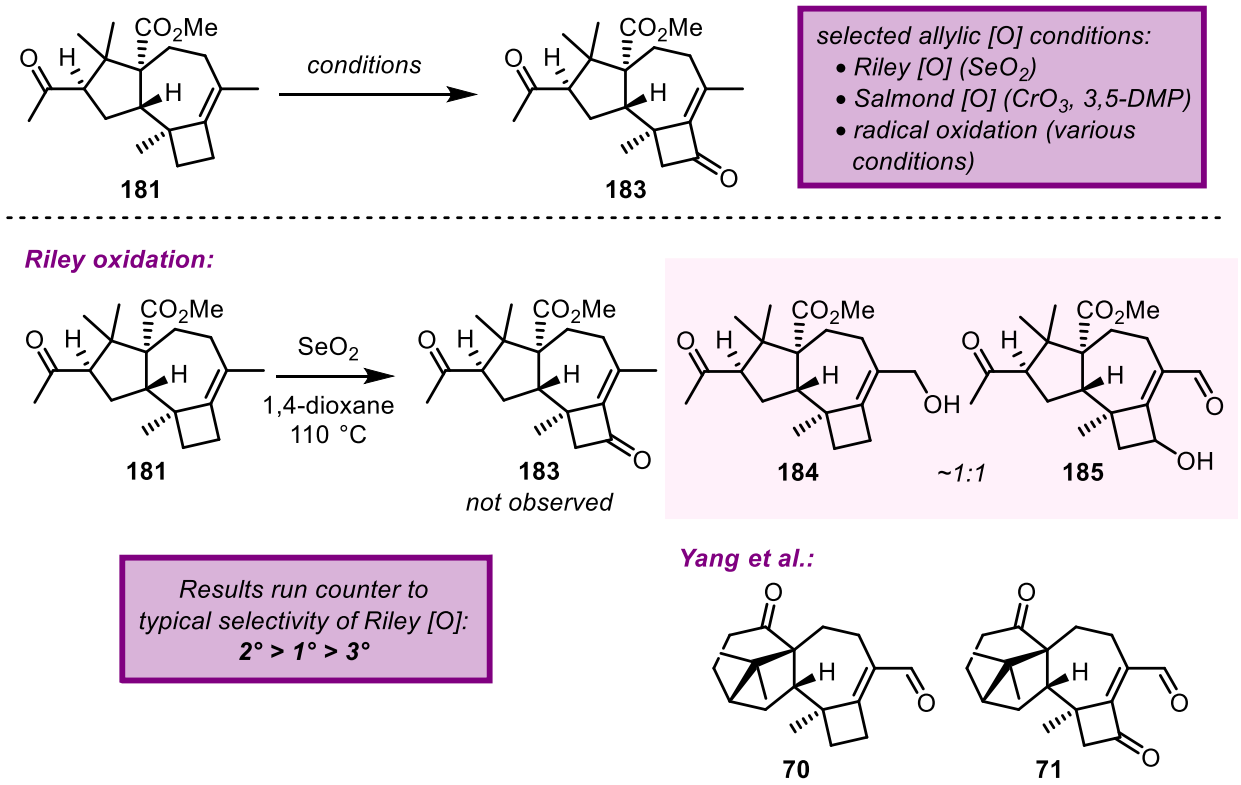

Scheme 3.43. Riley oxidation of tetrasubstituted olefin **181**, a model substrate for late-stage allylic oxidation toward the total synthesis of harziandione (**15**).

With ketoester **181** in hand, we selected three common types of allylic oxidation reactions found in the literature: Riley oxidation via an ene-type mechanism between SeO_2 and an olefin, Salmond oxidation with Cr^{VI} or Cr^{V} species serving as the oxidants, and radical-mediated oxidations involving generation of allylic radical intermediates.[80–83] Yang *et* al. demonstrated in their synthetic studies toward the harziane diterpenoid natural products that SeO_2 preferentially oxidized the methyl position to produce **70** and **71**. Upon treatment of ketoester **181** with SeO_2,

we observed a similar outcome, which was striking considering the typical selectivity of the Riley oxidation, which favors oxidation at secondary carbons over primary carbons, as well as a preference for endocyclic carbon atoms. It is conceivable that the steric congestion of our system may trump this canonical reactivity, something that is also observed in the Riley oxidation of α-pinene.[84]

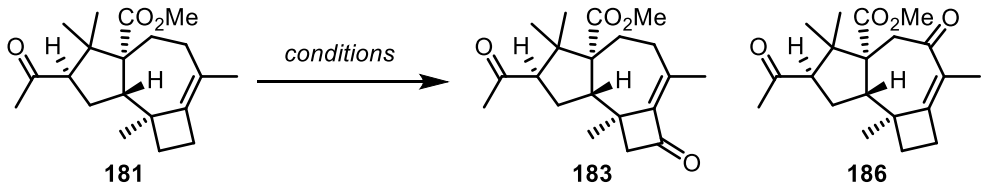

181 **183** **186**

Entry	*Reagent*	*Solvent*	*T*	*Result*
1	CrO_3, 3,5-DMP	CH_2Cl_2	–20 °C → rt	*decomposition*
2	PCC	CH_2Cl_2	40 °C	*no reaction*
3	PDC	benzene	80 °C	*no reaction*
4	**187**, MnO_2, 15-C-5	$PhCF_3$	80 °C	*no reaction*

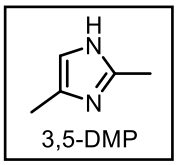

3,5-DMP

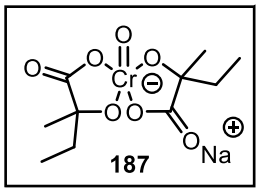

187

Table 3.4. Unsuccessful Cr^{VI}- and Cr^{V}-mediated allylic oxidation of tetrasubstituted olefin **181**

Another promising approach was the Salmond oxidation conditions, where a complex of CrO_3 and 3,5-dimethylpyrazole (3,5-DMP) leads to allylic oxidation of olefins to enones or enals. These conditions, as well as utilizing other Cr^{VI} oxidants were unsuccessful in oxidizing olefin **181**. Though reported by Baran and co-workers to effect desired allylic oxidation in a taxane framework where Cr^{VI} oxidants proved incompatible, treatment of our model ketoester **181** with the Cr^{V} complex **187** did not lead to the desired enone product.

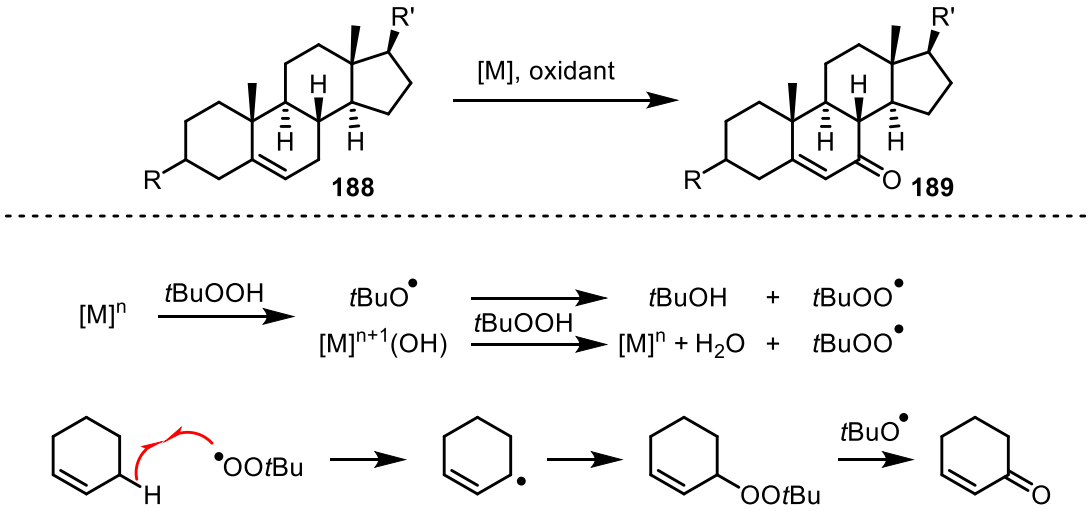

Scheme 3.44. Literature-precedented radical allylic oxidation of steroid frameworks and typical mechanism of radical allylic oxidations with *t*BuOOH as a terminal oxidant

With these results, we turned our attention to screen a variety of radical mediated allylic oxidation conditions. Mechanistically, such transformations undergo an initial hydrogen atom abstraction event to afford an allylic radical that is further oxidized by a terminal oxidant.[85–88] A common substrate for allylic oxidation methods of this kind are steroid frameworks such as **188**. A typical mechanism for a transition metal-mediated allylic oxidation is shown in Scheme 3.44. The metal complex undergoes a series of oxidation events with *t*BuOOH, leading to the active peroxy-radical species that abstracts a hydrogen atom from the reaction substrate. Combination with another peroxy-radical and subsequent oxidation furnishes the desired enone products.

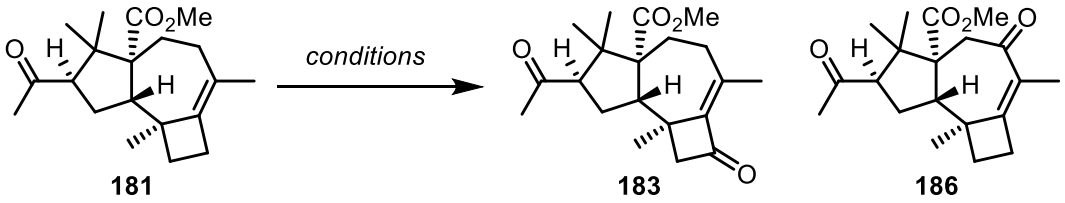

181 **183** **186**

Entry	*M*	*Oxidant*	*Solvent*	*T*	*Products*	*Yield/conv.*
1	$Fe(acac)_3$ (10 mol%)	*t*BuOOH (5 eq.)	CH_2Cl_2	70 °C	**186**	*~20% yield*
2	CuI (10 mol%)	*t*BuOOH (5 eq.)	MeCN	50 °C	**183** + **186** (~1:1)	*low yield*
3	CuI (10 mol%)	*t*BuOOH (5 eq.)	MeCN	70 °C	**186**	*40% yield*
4	CuI (10 mol%)	*t*BuOOH (5 eq.)	MeCN	rt	**183**	*low yield*
5	CuI (10 mol%), bpy	*t*BuOOH (5 eq.)	MeCN	rt	**183**	*35%*
6	$K_2Cr_2O_7$ (3 eq.)	NHPI (2 eq.)	acetone	rt	**183**	*55% yield*
7	$Rh_2(cap)_4$ (10 mol%)	*t*BuOOH (10 eq.)	1,2-DCE	rt	**183**	*20% conv.*
8	$Rh_2(esp)_2$ (10 mol%)	*t*BuOOH (10 eq.)	heptane	40 °C	**183** + **186**	*20% conv.*

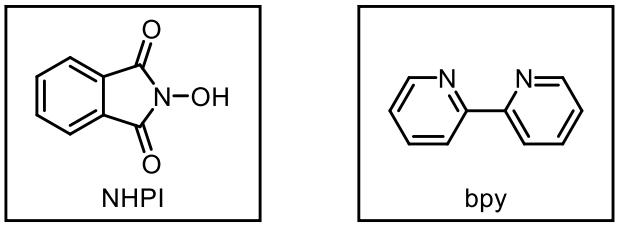

Table 3.5. Screening of radical allylic oxidation conditions on the tricyclic model compound **181**

With this background, we decided to screen a number of catalytic systems previously reported to effect the desired allylic oxidation in steroidal frameworks. We found that both secondary allylic positions were reactive under these conditions and as such hoped to identify conditions that would afford regioselective hydrogen atom abstraction at the four-membered ring allylic carbon to generate the desired enone **183**. At elevated temperatures, we observed formation of the undesired enone **186** (entries 1-3),[89,90] with higher reaction temperatures leading to exclusive formation of this product. As such, we lowered the temperature of the reaction, which led to slower conversion, but regioselective oxidation to **183**, albeit in relatively low yield (entry 4). Stabilization of the Cu^I catalyst with bpy as the ligand (entry 5) increased the yield of the reaction and decreased the predominance of side reactions. Through screening of reaction conditions, we

found that using NHPI as the terminal oxidant, in concert with $K_2Cr_2O_7$, was the optimal system for allylic oxidation on this model compound, producing the desired enone **183** in moderate yield (entry 6).[91] Dirhodium catalysts, while leading to a cleaner reaction profile, stalled at relatively low conversion (entries 7 and 8).[86,92] Other combinations of metal complexes and terminal oxidant did not furnish any allylic oxidation products.

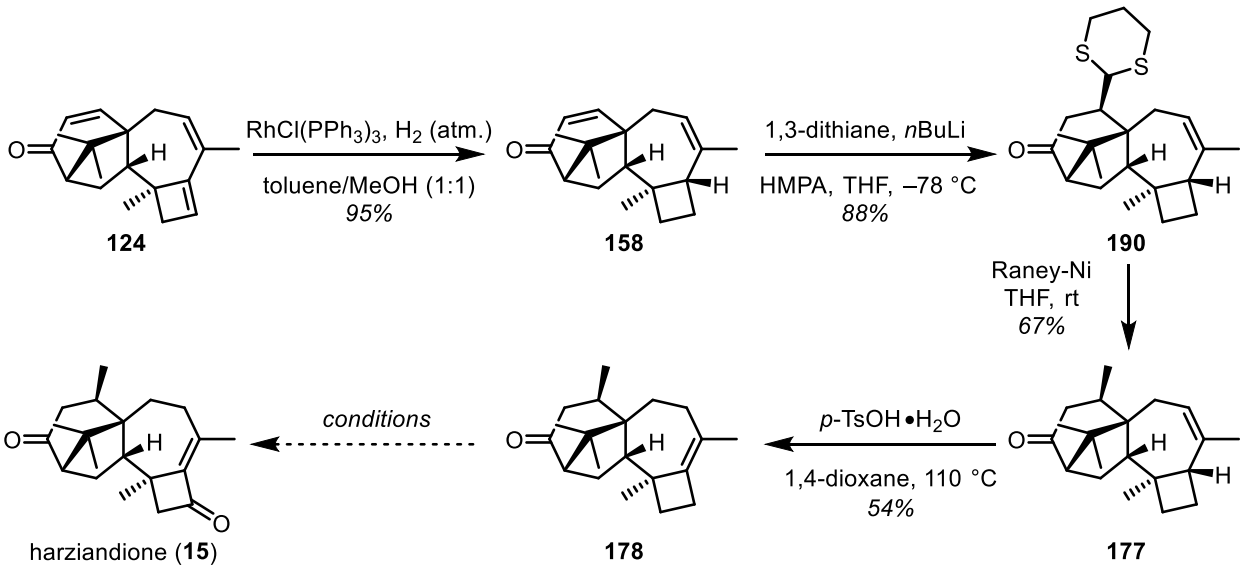

Scheme 3.45. Improved synthesis of ketone **190** via 1,3-dithiane addition to enone **124** and synthesis of the allylic oxidation precursor **178**

Though we had previously described a suitable reaction sequence to access **125** via methyl cuprate addition, selectivity and yield were dissatisfactory (Scheme 3.36). As such, we developed a two-step sequence to access ketone **177** in a more reliable manner. Selective conjugate addition of lithiated 1,3-dithiane to enone **158** effectively furnished ketone **190**.[93] This established reaction is selective for 1,4-addition due to the stabilization of the carbanion by the adjacent sulfur atoms, as well as the presence of HMPA, which prevents complexation of the alkyl lithium species with the ketone within **158**. Such counterion-established proximity of the nucleophile is cited as the driving factor of 1,2-addition in other systems. Desulfurization of **190** with Raney-Ni at ambient

temperature successfully formed **177**.[94] Unfortunately, treatment with $[Pd(MeCN)_4](BF_4)_2$ did not convert **177** to the desired tetrasubstituted olefin product **178**. We hypothesize that increased steric encumbrance brought by the adjacent bicyclic ring system prevented approach of the catalyst. Pleasingly, the alternative acid catalyzed isomerization conditions involving *p*-TsOH•H_2O did lead to successful isomerization, setting the stage for the final allylic oxidation event to complete the total synthesis of harziandione (**15**).

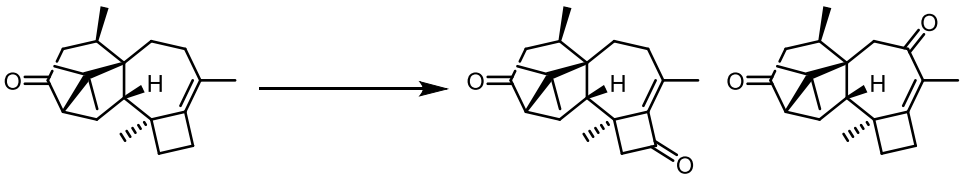

178 harziandione (**15**) **191**

Entry	*M*	*Oxidant*	*Solvent*	*T*	*Products*	*Yield/conv.*
1	$K_2Cr_2O_7$ (3 eq.)	NHPI (2 eq.)	acetone	rt	*N/A*	*no reaction*
2	CuI (10 mol%)	*t*BuOOH (5 eq.)	MeCN	50 °C	**15** + **191** (~1:1)	*low yield*
3	CuI (10 mol%)	*t*BuOOH (5 eq.)	MeCN	70 °C	**191**	*30% yield*
4	CuI (10 mol%)	*t*BuOOH (5 eq.)	MeCN	rt	**15**	*low yield*
5	CuI (10 mol%), bpy	*t*BuOOH (5 eq.)	MeCN	rt	**15**	*low yield*
6	$Rh_2(cap)_4$ (10 mol%)	*t*BuOOH (10 eq.)	1,2-DCE	rt	**15**	*10% conv.*
7	$Rh_2(esp)_2$ (1 mol%)	*t*BuOOH (10 eq.)	heptane	40 °C	**15** + **191**	*10% conv.*

Table 3.6. Screening of radical allylic oxidation conditions on the tetrasubstituted olefin within tetracyclic ketone **178** to complete the total synthesis of harziandione (**15**)

To our dismay, the optimal allylic oxidation conditions identified for our model compound, *trans*-ketoester **181**, failed to deliver harziandione (**15**). This result was perplexing, as we expected this reaction to translate well between the tri- and tetracyclic substrates. As with olefin isomerization, subtle changes in the steric environment may drastically impact reactivity. Undeterred, we tested the remaining conditions that successfully oxidized the model compound. CuI/*t*BuOOH acted analogously on **178** as it had on the tricyclic system, forming the undesired enone **191** at elevated temperatures.

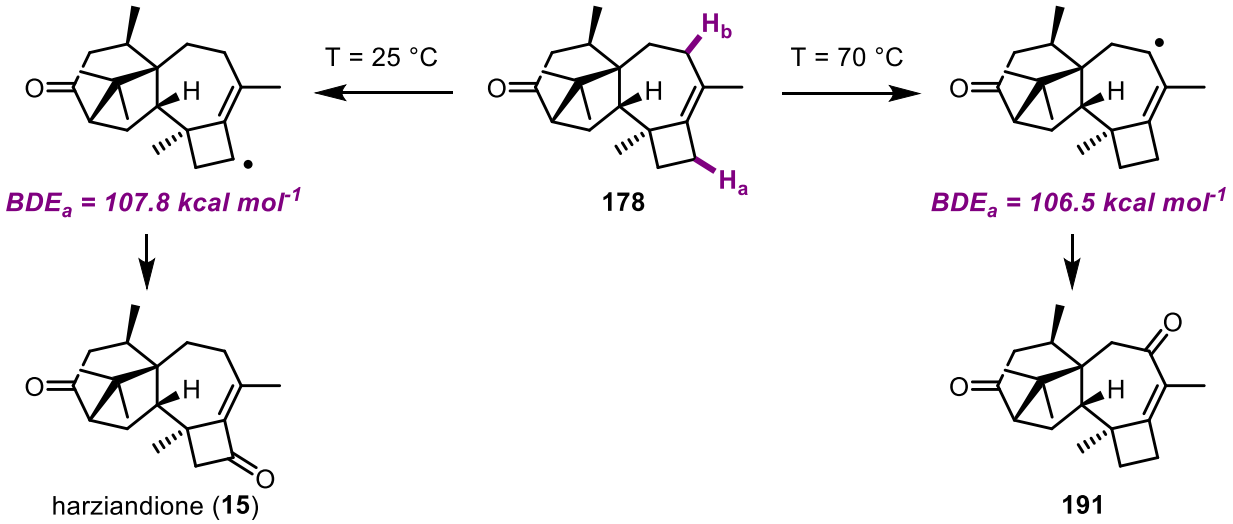

Scheme 3.46. Explanation for divergent outcomes of radical allylic oxidation at high and low temperature using the computationally derived BDE of allylic hydrogen atoms

At ambient temperature (entries 4 and 5) we were able to isolate harziandione (**15**) from the reaction mixture, albeit in a disappointingly low yield. Careful analysis of the ^{1}H NMR spectrum of synthetic **15** confirmed a match to that reported by several isolation teams. With the use of computationally generated C–H bond dissociation energies (BDE) of the allylic hydrogen atoms at the two secondary carbon positions, we generated a hypothesis to explain this divergent reactivity. With the lower BDE (ΔE = 1.3 kcal mol^{-1}), the C–H abstraction at the seven-membered ring (H_b) is thermodynamically favored. We believe that at ambient temperature the higher steric encumbrance at this position may overcome this thermodynamic bias, leading to predominance of kinetically favored C–H abstraction at the more accessible four-membered ring (H_a). Despite this initial observation, further experiments may be necessary to confirm our hypothesis.

With the desired allylic oxidation proceeding at room temperature, we were delighted to have achieved the first total synthesis of harziandione (**15**) in a total of 17 steps from commercial materials. Despite this success, we acknowledge that improvement in yield and production of larger quantities of **15** is needed for final confirmation of our feat, allowing us to obtain a clear ^{13}C

NMR spectrum and perhaps an X-ray crystal structure. To this end, investigations are currently ongoing.

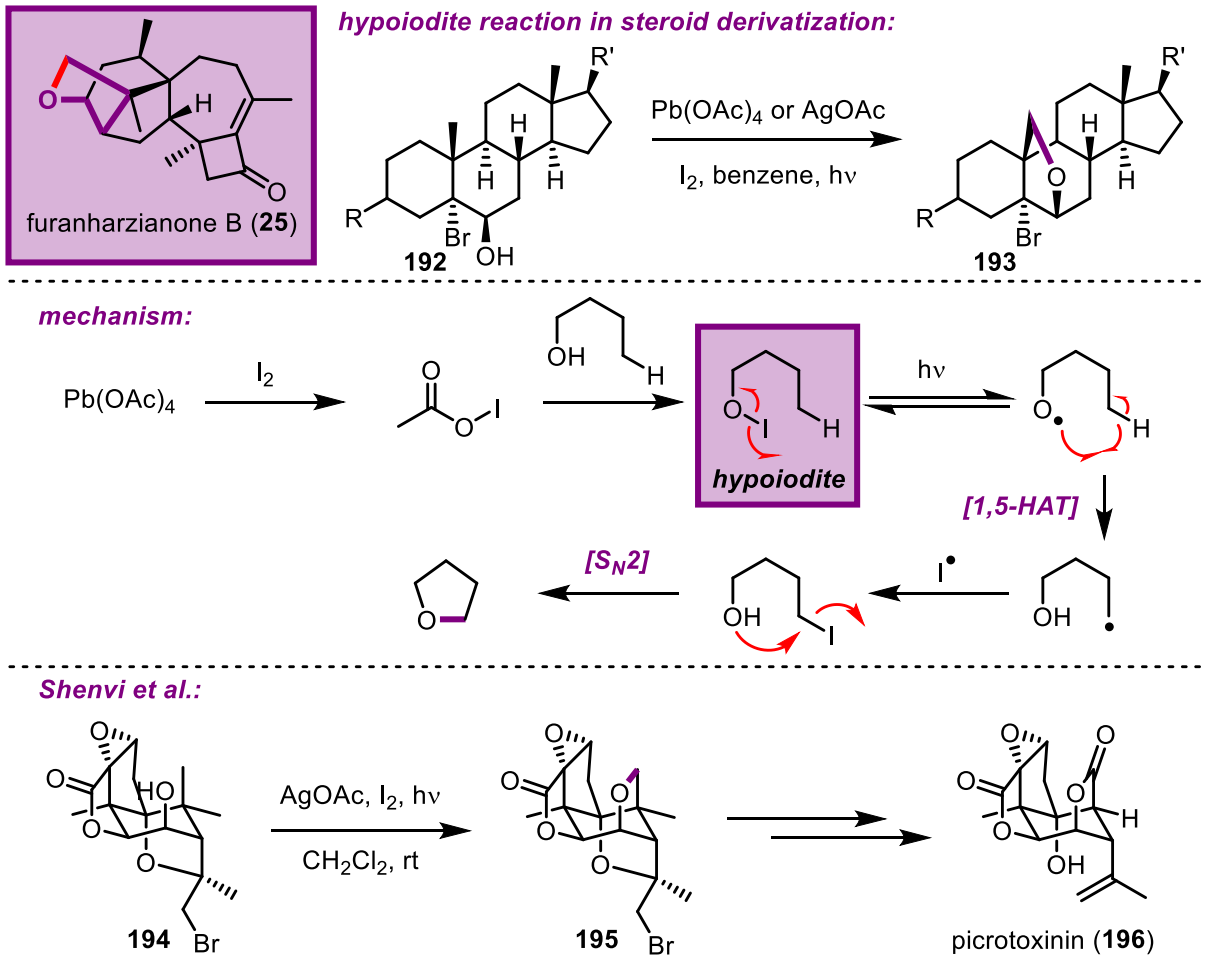

Scheme 3.47. Literature precedent for Suárez oxidation of a steroid framework, schematic mechanism of the hypoiodite reaction and recent application in the total synthesis of picrotoxinin (**196**) by Shenvi *et al.*

An immediate goal of ours is the total synthesis of furanharzianone B (**25**), a natural product that contains an additional tetrahydrofuran ring. This added ring could be forged via a hypoiodite reaction, one that is particularly common in steroid derivatization and was recently used in an acutely elegant way in the total synthesis of the natural product picrotoxinin (**196**) by Shenvi and co-workers.[95] It is notable that in each case, C–H functionalization of remote, typically unreactive methyl groups is achieved. While a variety of protocols for this reaction with different

initiating oxidants exist, the key reactive intermediate is iodine monoacetate. It is generated *in situ* from I_2 and a strong oxidant, typically $Pb(OAc)_4$.[78,96,97] Reaction with a nucleophilic hydroxyl group forms a hypoiodite intermediate that, upon irradiation with visible light, undergoes reversible homolytic O–I bond cleavage to form the oxygen-centered radical. 1,5-HAT then leads to the corresponding primary alkyl radical, which may recombine with the iodine radical produced in the homolytic hypoiodite cleavage to generate an alkyl iodide species. A relatively facile intramolecular S_N2 reaction then furnishes the tetrahydrofuran ring.

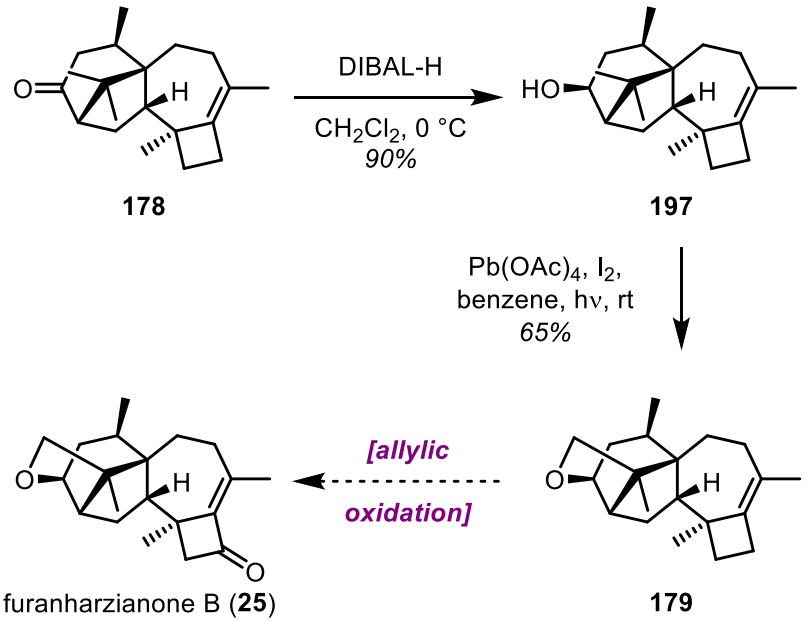

Scheme 3.48. Successful Suárez oxidation of alcohol **197** *en route* to the total synthesis of furanharzianone B (**25**)

The close spatial proximity of the alcohol to the targeted methyl group is a driving force of this reaction, as evidenced by the rapid conversion of alcohol **194** to cyclized **195** in the total synthesis of picrotoxinin (**196**). This is why we were not entirely surprised to find that following reduction of the ketone within **178**, the resultant alcohol rapidly cyclized to pentacyclic ether **179** upon exposure to classic Suárez oxidation conditions. With all necessary aspects of the framework

established, completion of the total synthesis furanharzianone B (**25**) in a projected 19 steps would require a final allylic oxidation event as detailed in Scheme 3.48.

As detailed above a remaining target of our investigation is the successful total synthesis of the natural product harzianol F (**19**). In our initial attempts at producing this molecule, we found preparation of the *cis*-7/4-ring system to be particularly challenging. Though we had attempted formation of **19** via a number of approaches, the molecule has thus far proved elusive. Our current effort to complete this molecule exploits the undesired enone product **191** from thermodynamically controlled allylic oxidation at the seven-membered ring.

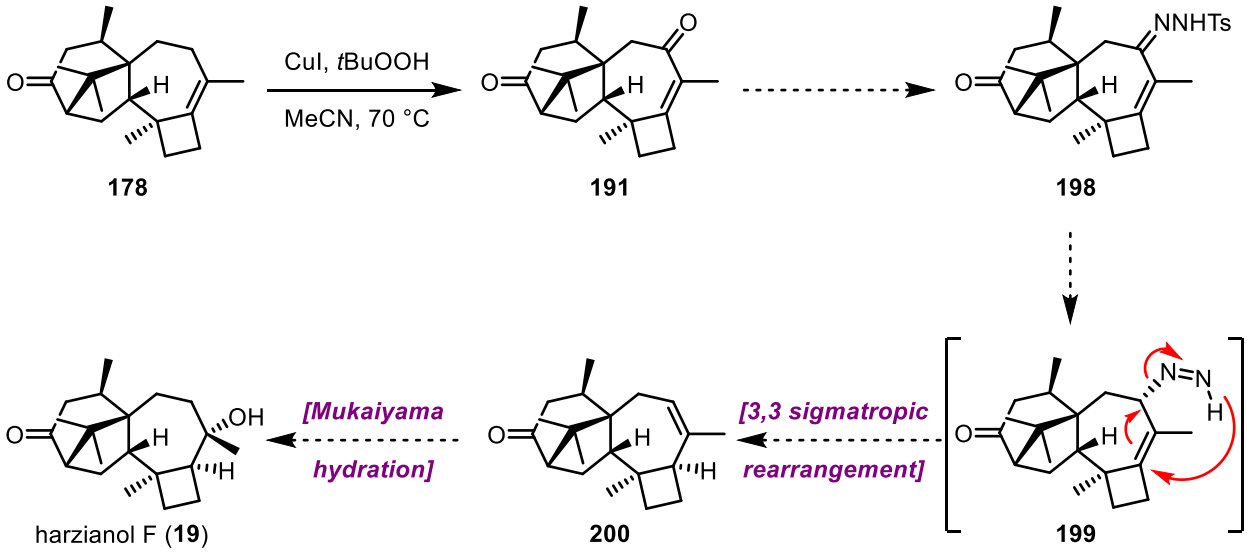

Scheme 3.49. Proposed use of the undesired thermodynamic allylic oxidation product enone **191** to allow access to the *cis*-fused 7/4 ring system via a reductive azo-rearrangement

In this design, we stayed true to our hypothesis that intramolecular reactions governed by existing relative stereochemistry of the functional groups involved (cf. the directed hydrogenation proposed in Scheme 3.39) may successfully form the desired *cis*-fused ring system. Formation of the hydrazone analog of enone **191**, could allow for the reductive allylic [3,3] azo-rearrangement to afford a facially selective delivery of hydride from the bottom face of the molecule. Subsequent Mukaiyama hydration of ketone **200** should then lead to the same stereochemical outcome as that

described in the Carreira synthesis of harzianol I (**21**).[63]m We acknowledge that this route toward the total synthesis of harzianol F (**19**) is by no means step economic and requires a suboptimal sequence of redox manipulations. However, if successful, it would further galvanize our divergent approach to this natural product family.

*Section 3.2.4: The Total Synthesis of Harziandione (**15**) and Studies Towards Other Harziane Diterpenoid Natural Products Through a Unified Route*

The successful total synthesis of the harziane diterpenoid natural product, harziandione (**15**) was a journey that included several disheartening setbacks, in which a number of centrally envisioned transformations did not deliver the desired results. Nonetheless, these setbacks and the many successful adjustments that we have made, have revealed to us the intricate nature and reactivity of the harziane diterpenoid framework.

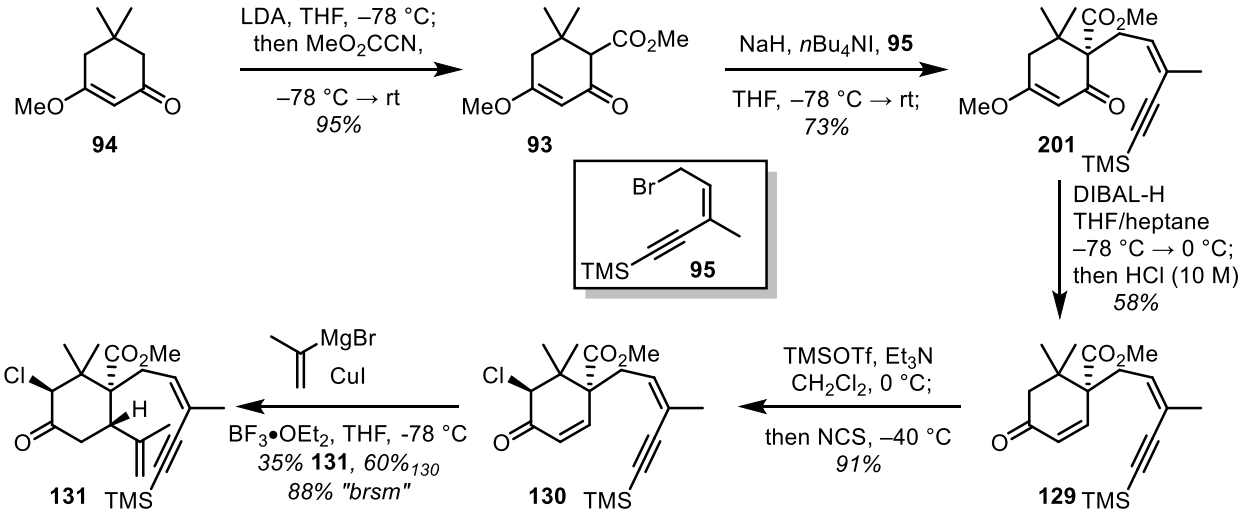

Scheme 3.50. Synthesis of the decorated cyclohexanone **131** to set up the key cyclization event

In this section, we will briefly summarize the current total synthetic route of harziandione (**15**) and review the insights we have gained in the process. An initial strategic decision to introduce the components required to furnish the carbocyclic framework to a six-membered ring that is to be

contracted later, and forging the remaining rings around it, significantly contributed to our concise route. The formation of the unusual 7/4-fused ring found in the harziane diterpenoid natural product family via a Au^{I}-catalyzed cycloisomerization offered a number of synthetic handles through which we could probe reactivity and functionalize the framework in a selective manner.

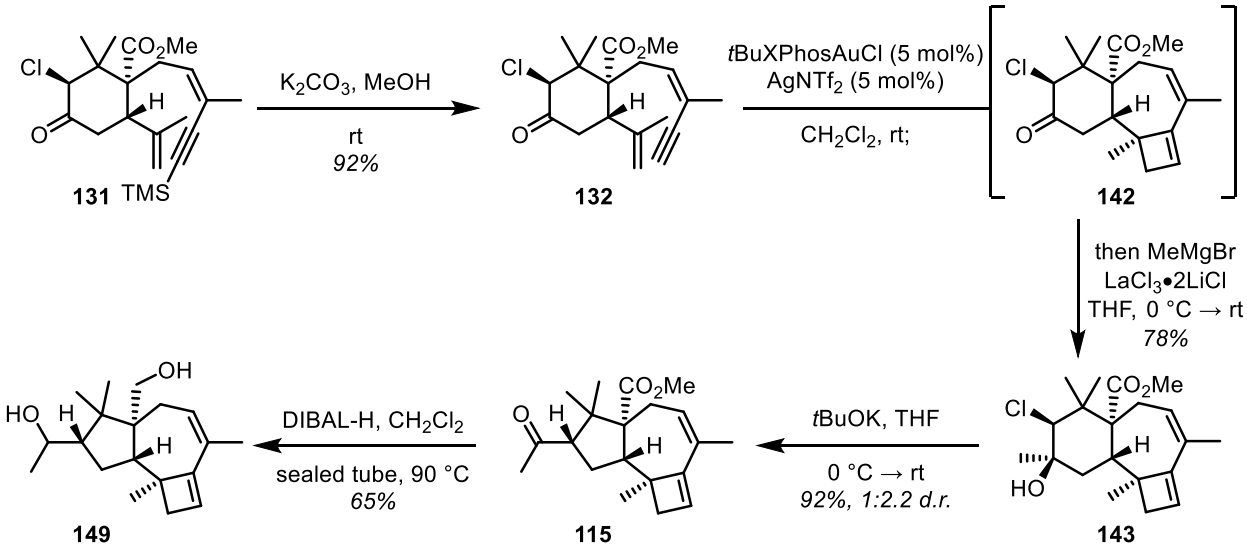

Scheme 3.51. Au^{I}-catalyzed cycloisomerization and semi-pinacol rearrangement afford tricyclic ketoester **115**

Vinylogous ester **94**, formed in one step from commercially available dimedone, was sequentially alkylated by Mander's reagent and literature-known allylic bromide (**95**) to generate the vicinal all-carbon quaternary center within **201**. The resultant compound was then reduced to the enone analog **129**. At this stage, we selectively installed the α'-chloride as a leaving group handle to set up our desired ring contraction. The challenging, and to our knowledge unprecedented, conjugate addition of isopropenyl cuprate to chloroenone **130** led to formation of the desired ketone **131** and recovery of dehalogenated enone **129**.

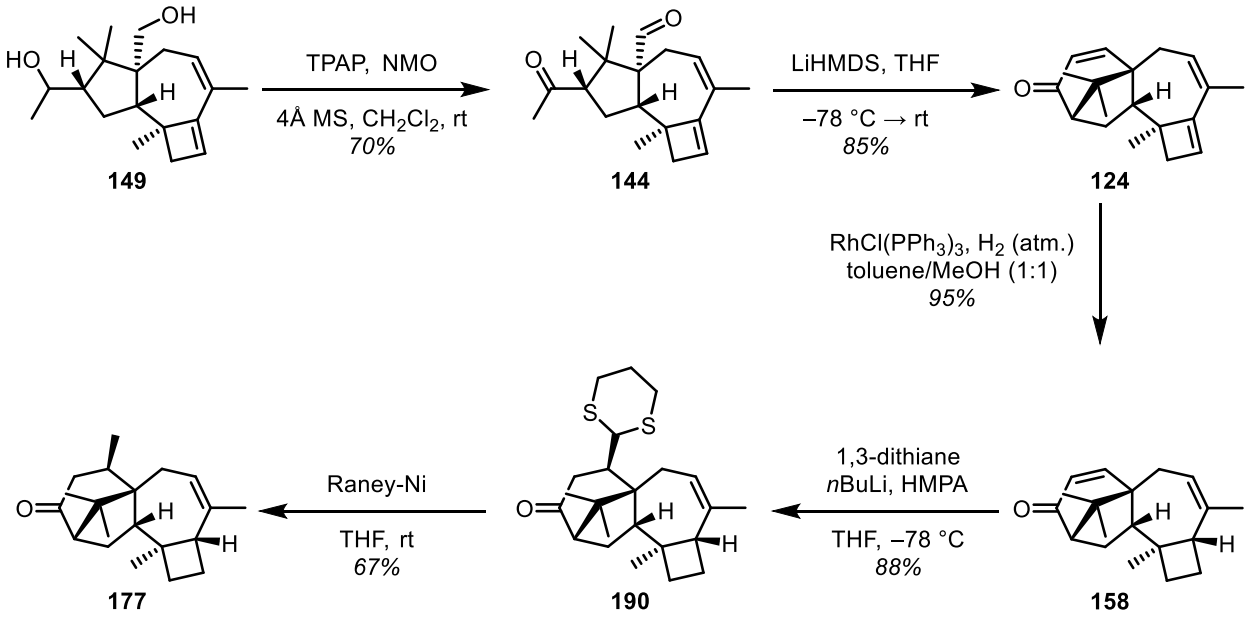

Scheme 3.52. Intramolecular aldol condensation completes the carbocyclic framework of the harziane diterpenes

With chloroketone **131** in hand, we deprotected the enyne side chain and then triggered our key Au^{I}-catalyzed cycloisomerization reaction and subsequent Grignard addition to efficiently afford tricyclic chlorohydrin **143**. This compound set the stage for a base-mediated ring contraction via a semi-pinacol rearrangement to ketoesters **115** and **126**. We moved forward with desired *cis*-ketoster **115** through a reduction and oxidation sequence to furnish ketoaldehyde **144**. This compound served as a precursor for an intramolecular aldol condensation to form enone **124**, which completed the 6/5/7/4-ring system found within the harziane diterpenoid natural product family.

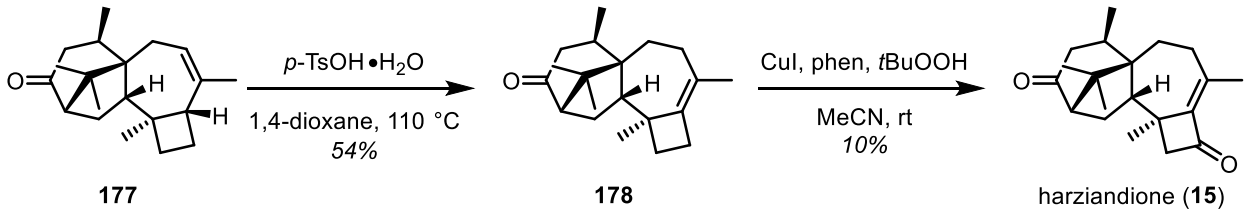

Scheme 3.53. Completion of the total synthesis of harziandione (**15**) in 17 steps

Although hydrogenation of the diene within **124** by treatment with Wilkinsons' catalyst did not proceed with the same desired facial selectivity, we were still able to utilize this undesired product in our synthetic efforts. The final stage of the total synthesis was continued with introduction of the last remaining carbon atom via facially selective conjugate addition of lithiated 1,3-dithiane to enone **158** and subsequent desulfurization. Isomerization to the tetrasubstituted olefin-containing **178** is followed by the selective allylic oxidation at the cyclobutane ring to complete the first total synthesis of harziandione (**15**) in 17 steps from commercial materials.

SECTION 3.3: CONCLUSION

In this chapter, we have outlined our contribution to the synthetic approaches toward the harziane diterpenoid natural products. This effort presents an alternative and concise strategy to this highly congested framework. While we share bond disconnections and methods to forge several of the rings with contemporary works, we have at the same time solved key challenges, unique to our approach and gained further insight into the capabilities of organic reactions to modify the carbocyclic framework of these natural products.

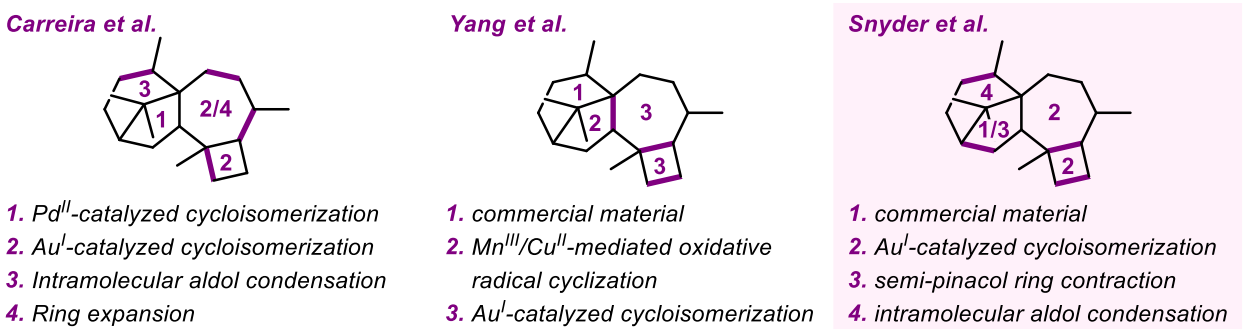

Figure 3.4. Comparison of the synthetic strategies applied by Carreira and Yang in constructing the carbocyclic core of the harziane diterpenes with the approach outlined in this chapter

Despite the volume of work achieved thus far, there still are some significant challenges that remain in the preparation of further harziane diterpene natural products and other non-natural compounds sharing this carbocyclic framework, yet with unusual oxidation patterns. Access to such compounds may further illuminate chemical space in the pursuit of ever more efficient synthetic approaches and generate novel bioactive molecules that may become the transformative drugs of the future.

SECTION 3.4: REFERENCES

(1) Hu, P.; Snyder, S. A. *J. Am. Chem. Soc.* **2017**, *139*, 5007–5010.

(2) Hu, P.; Chi, H. M.; DeBacker, K. C.; Gong, X.; Keim, J. H.; Hsu, I. T.; Snyder, S. A. *Nature* **2019**, *569*, 703–707.

(3) Chi, H. M.; Cole, C. J. F.; Hu, P.; Taylor, C. A.; Snyder, S. A. *Chem. Sci.* **2020**, *11*, 10939–10944.

(4) Smith, M. W.; Zhou, Z.; Gao, A. X.; Shimbayashi, T.; Snyder, S. A. *Org. Lett.* **2017**, *19*, 1004–1007.

(5) Gan, P.; Pitzen, J.; Qu, P.; Snyder, S. A. **2018**, *140*.

(6) Zhou, Z.; Gao, A. X.; Snyder, S. A. *J. Am. Chem. Soc.* **2019**, *141*, 7715–7720.

(7) Ye, Q.; Qu, P.; Snyder, S. A. *J. Am. Chem. Soc.* **2017**, *139*, 18428–18431.

(8) Peng, C.; Arya, P.; Zhou, Z.; Snyder, S. A. *Angew. Chemie Int. Ed.* **2020**.

(9) Mato, M.; Franchino, A.; García-Morales, C.; Echavarren, A. M. *Chem. Rev.* **2021**, *121*, 8613–8684.

(10) Obradors, C.; Echavarren, A. M. *Acc. Chem. Res.* **2014**, *47*, 902–912.

(11) Dorel, R.; Echavarren, A. M. *Chem. Rev.* **2015**, *115*, 9028–9072.

(12) Xu, Y.; Conner, M. L.; Brown, M. K. *Angew. Chemie Int. Ed.* **2015**, *54*, 11918–11928.

(13) Fürstner, A.; Aïssa, C. *J. Am. Chem. Soc.* **2006**, *128*, 6306–6307.

(14) Elena de Orbe, M.; Echavarren, A. M. *European J. Org. Chem.* **2018**, *2018*, 2740–2752.

(15) Luzung, M. R.; Mauleón, P.; Toste, F. D. *J. Am. Chem. Soc.* **2007**, *129*, 12402–12403.

(16) Nieto-Oberhuber, C.; López, S.; Jiménez-Núñez, E.; Echavarren, A. M. *Chem. - A Eur. J.* **2006**, *12*, 5916–5923.

(17) Jiménez-Núñez, E.; Claverie, C. K.; Nieto-Oberhuber, C.; Echavarren, A. M. *Angew. Chemie Int. Ed.* **2006**, *45*, 5452–5455.

(18) Odabachian, Y.; Gagosz, F. *Adv. Synth. Catal.* **2009**, *351*, 379–386.

(19) Ghisalberti, E. L.; Hockless, D. C. R.; Rowland, C.; White, A. H. *J. Nat. Prod.* **1992**, *55*, 1690–1694.

(20) Adelin, E.; Servy, C.; Martin, M. T.; Arcile, G.; Iorga, B. I.; Retailleau, P.; Bonfill, M.;

Ouazzani, J. *Phytochemistry* **2014**, *97*, 55–61.

(21) Zhang, M.; Liu, J. M.; Zhao, J. L.; Li, N.; Chen, R. D.; Xie, K. B.; Zhang, W. J.; Feng, K. P.; Yan, Z.; Wang, N.; Dai, J. G. *Chinese Chem. Lett.* **2016**, *27*, 957–960.

(22) Zhang, M.; Liu, J.; Chen, R.; Zhao, J.; Xie, K.; Chen, D.; Feng, K.; Dai, J. *Org. Lett.* **2017**, *19*, 1168–1171.

(23) Song, Y. P.; Miao, F. P.; Liang, X. R.; Yin, X. L.; Ji, N. Y. *Phytochem. Lett.* **2019**, *32*, 38–41.

(24) Li, W. Y.; Liu, Y.; Lin, Y. T.; Liu, Y. C.; Guo, K.; Li, X. N.; Luo, S. H.; Li, S. H. *Phytochemistry* **2020**, *170*, 112198.

(25) Miao, F. P.; Liang, X. R.; Yin, X. L.; Wang, G.; Ji, N. Y. *Org. Lett.* **2012**, *14*, 3815–3817.

(26) Song, Y. P.; Fang, S. T.; Miao, F. P.; Yin, X. L.; Ji, N. Y. *J. Nat. Prod.* **2018**, *81*, 2553–2559.

(27) Zou, J.-X.; Song, Y.-P.; Ji, N.-Y. *Nat. Prod. Res.* **2019**, *35*, 216–221.

(28) Ghisalberti, E. L.; Sivasithamparam, K. *Soil Biol. Biochem.* **1991**, *23*, 1011–1020.

(29) Papazivas, G. C. *Ann. Rev. Phytopathol.* **1985**, *23*, 23–54.

(30) Harman, G. E.; Howell, C. R.; Viterbo, A.; Chet, I.; Lorito, M. *Nat. Rev. Microbiol.* **2004**, *2*, 43–56.

(31) Mannina, L.; Segre, A. L.; Ritieni, A.; Fogliano, V.; Vinale, F.; Randazzo, G.; Maddau, L.; Bottalico, A. *Tetrahedron* **1997**, *53*, 3135–3144.

(32) Barra, L.; Dickschat, J. S. *ChemBioChem* **2017**, *18*, 2358–2365.

(33) Rabe, P.; Rinkel, J.; Dolja, E.; Schmitz, T.; Nubbemeyer, B.; Luu, T. H.; Dickschat, J. S. *Angew. Chemie Int. Ed.* **2017**, *56*, 2776–2779.

(34) Xu, H.; Dickschat, J. S. *ChemBioChem* **2021**, *22*, 850–854.

(35) Hönig, M.; Carreira, E. M. *Angew. Chemie* **2020**, *132*, 1208–1212.

(36) Nicolaou, K. C.; Snyder, S. A. *Angew. Chemie Int. Ed.* **2005**, *44*, 1012–1044.

(37) Tu, Q.; Wang, Z.; Zhang, Z.; Huang, J.; Yang, Z. *Org. Lett.* **2021**, *23*, 4088–4093.

(38) Miwa, K.; Aoyama, T.; Shioiri, T. *Synlett* **1994**, *1994*, 107–108.

(39) Chunngai Hui; Luke Craggs; P. Antonchick, A. *Chem. Soc. Rev.* **2022**.

(40) Song, Z. L.; Fan, C. A.; Tu, Y. Q. *Chem. Rev.* **2011**, *111*, 7523–7556.

(41) Woodward, R. B.; Sondheimer, F.; Taub, D.; Heusler, K.; McLamore, W. M. *J. Am. Chem. Soc.* **1952**, *74*, 4223–4251.

(42) Moriarty, R. M. *Tetrahedron Lett.* **1984**, *25*, 5867–5870.

(43) Zhou, Z. The University of Chicago, Chicago, 2020.

(44) Shapiro, B. L.; Johnston, M. D.; Proulx, T. W. *J. Am. Chem. Soc.* **1973**, *95*, 520–526.

(45) Odedra, A.; Wu, C.-J.; Madhushaw, R. J.; Wang, S.-L.; Liu, R.-S. *J. Am. Chem. Soc.* **2003**, *125*, 9610–9611.

(46) Brook, A. G.; Macrae, D. M. *J. Organomet. Chem.* **1974**, *77*, 19–21.

(47) Mahoney, W. S.; Brestensky, D. M.; Stryker, J. M. *J. Am. Chem. Soc.* **1988**, *110*, 291–293.

(48) Elkin, M.; Szewczyk, S. M.; Scruse, A. C.; Newhouse, T. R. *J. Am. Chem. Soc.* **2017**, *139*, 1790–1793.

(49) Molander, G. A. *Org. React.* **1994**, 211–367.

(50) Cabrera, A.; Alper, H. *Tetrahedron Lett.* **1992**, *33*, 5007–5008.

(51) Kolmar, S. S.; Mayer, J. M. *J. Am. Chem. Soc.* **2017**, *139*, 10687–10692.

(52) Chciuk, T. V.; Anderson, W. R.; Flowers, R. A. *J. Am. Chem. Soc.* **2016**, *138*, 8738–8741.

(53) Lipshutz, B. H.; Sengupta, S. *Org. React.* **1992**, 135–631.

(54) Posner, G. H. *Org. React.* **2011**, 1–114.

(55) Barbee, T. R.; Guy, H.; Heeg, M. J.; Albizati, K. F. *J. Org. Chem.* **1991**, *56*, 6773–6781.

(56) Tsuchida, N.; Yamazaki, S.; Yamabe, S. *Org. Biomol. Chem.* **2008**, *6*, 3109–3117.

(57) Harding, K. E.; Strickland, J. B.; Pommerville, J. *J. Org. Chem.* **1988**, *53*, 4877–4883.

(58) Miller, R. D.; McKean, D. R. *Synth.* **1979**, *1979*, 730–732.

(59) Ishihara, K.; Kaneeda, M.; Yamamoto, H. *J. Am. Chem. Soc.* **1994**, *116*, 11179–11180.

(60) Xie, X.; Stahl, S. S. *J. Am. Chem. Soc.* **2015**, *137*, 3767–3770.

(61) Ley, S. V.; Norman, J.; Griffith, W. P.; Marsden, S. P. *Synthesis*. Georg Thieme Verlag 1994, pp 639–666.

(62) Zumbansen, K.; Döhring, A.; List, B. *Adv. Synth. Catal.* **2010**, *352*, 1135–1138.

(63) Hönig, M.; Carreira, E. M. *Angew. Chemie Int. Ed.* **2020**, *59*, 1192–1196.

(64) Nakai, T.; Tomooka, K.; Kanduluru, A. K. 1–10.

(65) Iwasaki, K.; Wan, K. W.; Oppedisano, A.; Crossley, S. W. M.; Shenvi, R. A. *J. Am. Chem. Soc.* **2014**, *136*, 1300–1303.

(66) Pasto, D. J.; Taylor, R. T. *Org. React.* **1991**, 91–155.

(67) Crabtree, R. H.; Davis, M. W. *Organometallics* **1983**, *2*, 681–682.

(68) Yang, C. G.; Reich, N. W.; Shi, Z.; He, C. *Org. Lett.* **2005**, *7*, 4553–4556.

(69) Kennemur, J. L.; Maji, R.; Scharf, M. J.; List, B. *Chem. Rev.* **2021**, *121*, 14649–14681.

(70) Rosenfeld, D. C.; Shekhar, S.; Takemiya, A.; Utsunomiya, M.; Hartwig, J. F. *Org. Lett.* **2006**, *8*, 4179–4182.

(71) Gao, R.; Fan, R.; Canney, D. J. *Synlett* **2015**, *26*, 661–665.

(72) Oshima, M.; Yamazaki, H.; Shimizu, I.; Nisar, M.; Tsuji, J. *J. Am. Chem. Soc.* **1989**, *111*, 6280–6287.

(73) He, J.; Ling, J.; Chiu, P. *Chem. Rev.* **2014**, *114*, 8037–8128.

(74) Evans, D. A.; Fu, G. C. *J. Am. Chem. Soc.* **1991**, *113*, 4042–4043.

(75) Guisán-Ceinos, M.; Parra, A.; Martín-Heras, V.; Tortosa, M. *Angew. Chemie Int. Ed.* **2016**, *55*, 6969–6972.

(76) Karstedt, B. D. 3,775,452, 1973.

(77) Snyder, S. A.; Treitler, D. S. *Angew. Chemie - Int. Ed.* **2009**, *48*, 7899–7903.

(78) Giri, R.; Yu, J.-Q. In *Encyclopedia of Reagents for Organic Synthesis*; 2008.

(79) Sen, A.; Lai, T. W. *Inorg. Chem.* **1984**, *23*, 3257–3258.

(80) Wilde, N. C.; Isomura, M.; Mendoza, A.; Baran, P. S. *J. Am. Chem. Soc.* **2014**, *136*, 4909–4912.

(81) Salmond, W. G.; Barta, M. A.; Havens, J. L. *J. Org. Chem.* **1978**, *43*, 2057–2059.

(82) Parish, E. J.; Wei, T. Y. *Synth. Commun.* **1987**, *17*, 1227–1233.

(83) Krumpolc, M.; Roček, J. *J. Am. Chem. Soc.* **1979**, *101*, 3206–3209.

(84) Hoekstra, W. J.; Fairlamb, I. J. S.; Giroux, S.; Chen, Y. *Encycl. Reagents Org. Synth.* **2017**, 1–12.

(85) Weidmann, V.; Maison, W. *Synthesis (Stuttg).* **2013**, *45*, 2201–2221.

(86) Choi, H.; Doyle, M. P. *Org. Lett.* **2007**, *9*, 5349–5352.

(87) McLaughlin, E. C.; Choi, H.; Wang, K.; Chiou, G.; Doyle, M. P. *J. Org. Chem.* **2009**, *74*, 730–738.

(88) Catino, A. J.; Forslund, R. E.; Doyle, M. P. *J. Am. Chem. Soc.* **2004**, *126*, 13622–13623.

(89) Arsenou, E. S.; Koutsourea, A. I.; Fousteris, M. A.; Nikolaropoulos, S. S. *Steroids* **2003**, *68*, 407–414.

(90) Kimura, M.; Muto, T. *Chem. Pharm. Bull.* **1979**, *27*, 109–112.

(91) Marwah, P.; Lardy, H. A. US6384251B1, March 17, 1999.

(92) Wang, Y.; Wang, Y.; Kuang, Y. *Chem. Commun.* **2015**, *51*, 5852–5855.

(93) Bulman Page, P. C.; van Niel, M. B.; Prodger, J. C. *Tetrahedron* **1989**, *45*, 7643–7677.

(94) Snyder, S. A.; Corey, E. J. *J. Am. Chem. Soc.* **2006**, *128*, 740–742.

(95) Crossley, S. W. M.; Tong, G.; Lambrecht, M. J.; Burdge, H. E.; Shenvi, R. A. *J. Am. Chem. Soc.* **2020**, *142*, 11376–11381.

(96) Hauser, D.; Heusler, K.; Kalvoda, J.; Schaffner, K.; Jeger, O. *Helv. Chim. Acta* **1964**, *47*, 1961–1979.

(97) Kalvoda, J.; Heusler, K. *Synthesis (Stuttg).* **1971**, *10*, 501–526.

(98) Odedra, A.; Wu, C. J.; Madhushaw, R. J.; Wang, S. L.; Liu, R. S. *J. Am. Chem. Soc.* **2003**, *125*, 9610–9611.

(99) Choi, S.; Breugst, M.; Houk, K. N.; Poulter, C. D. *J. Org. Chem.* **2014**, *79*, 3572–3580.

(100) Girard, P.; Namy, J. L.; Kagan, B. *J. Am. Chem. Soc.* **1980**, *102*, 2693–2698.

SECTION 3.5: EXPERIMENTAL SECTION

General Procedures.

All reactions were carried out under an argon atmosphere with anhydrous solvents under anhydrous conditions, unless otherwise noted. Anhydrous THF, toluene, Et_2O, CH_2Cl_2, and MeCN were obtained by passing commercially available pre-dried, oxygen-free formulations through activated alumina columns. Yields refer to chromatographically and spectroscopically (^1H and ^{13}C NMR) homogeneous materials, unless otherwise stated. Reagents were purchased at the highest commercial quality and used without further purification, unless otherwise stated. Reactions were magnetically stirred and monitored by TLC carried out on 0.25 mm Merck silica gel plates (60F-254) using UV light as visualizing agent, and an aqueous solution of cerium ammonium molybdate, a solution of anisaldehyde in EtOH, or a solution of $KMnO_4$ in aqueous $NaHCO_3$ and heat as developing agents. SiliCycle silica gel (60, academic grade, particle size 0.040–0.063 mm) was used for flash column chromatography. Preparative TLC separations were carried out on 0.50 mm E. Merck silica gel plates (60F-254). NMR spectra were recorded on Bruker 400 and 500 MHz instruments and calibrated using residual undeuterated solvent as an internal reference. The following abbreviations were used to explain the multiplicities: s = singlet, d = doublet, t = triplet, q = quartet, br = broad, app = apparent, m = multiplet.

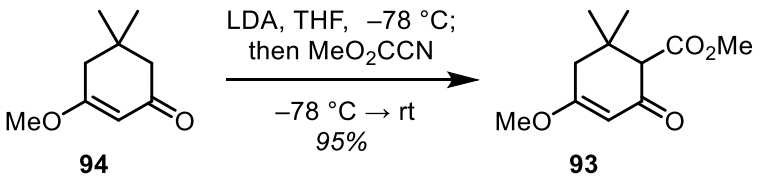

Vinylogous ester 93. To a flame-dried 500 mL flask was added *i*Pr$_2$NH (17.5 mL, 125 mmol, 1.25 equiv.) and THF (150 mL). The mixture was cooled to –78 °C and *n*BuLi (2.5 M in hexanes, 48 mL, 120 mmol, 1.2 equiv.) was then added dropwise. Upon completion of addition, the mixture is warmed to 0 °C and stirred for 1 h. The mixture was cooled to –78 °C. **94**[44] (15.42 g, 100 mmol, 1.0 equiv.) as a solution in THF (50 mL), was then added dropwise to this mixture and the mixture was stirred for 1 h at –78 °C. Then methyl cyanoformate (8.7 mL, 110 mmol, 1.1 equiv.) allowed to slowly warm to 0 °C over 2 h. Once complete, the reaction was quenched by the addition of aqueous $NaHCO_3$ (100 mL) and the contents transferred to a separatory funnel, diluting with EtOAc (100 mL). The layers were separated, and the aqueous layer was further extracted with EtOAc (3 × 100 mL). The combined organic layers were dried over Na_2SO_4 and concentrated in vacuo. The resultant crude product was further purified by flash column chromatography (silica gel, Hexanes/EtOAc, 4:1) to give the desired **Vinylogous ester 93** (20.16 g, 95% yield) as a yellow oil.

93:

^{1}H NMR (400 MHz, $CDCl_3$) δ 5.39 (d, *J* = 1.0 Hz, 1H), 3.72 (s, 3H), 3.70 (s, 3H), 3.15 (d, *J* = 0.6 Hz, 1H), 2.70 (dd, *J* = 17.4, 1.0 Hz, 1H), 2.15 (d, *J* = 17.4 Hz, 1H), 1.13 (s, 3H), 1.10 (s, 3H).

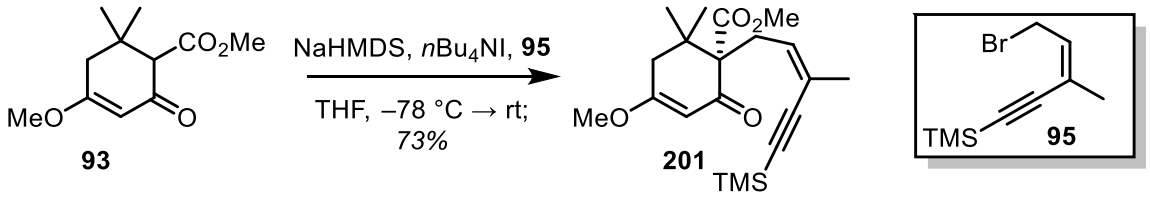

Vinylogous ester 201. To a flame-dried 1 L flask was added **93** (15 g, 70.75 mmol, 1.0 equiv.) and freshly distilled THF (200 mL). The mixture was cooled to –78 °C and NaHMDS (2.0 M in THF, 46 mL, 92 mmol, 1.3 equiv.) was then added dropwise. Upon completion of addition, the mixture was stirred for 1 h. Then freshly prepared **95**[98,99] (19.6 g, 85 mmol, 1.2 equiv.) as a dry solution in THF (30 mL) was added dropwise to this mixture, followed by *n*Bu$_4$NI (7.7 g, 21 mmol, 0.3 equiv.) and the mixture was allowed to slowly warm to 25 °C. After 18 h, the reaction was quenched by the addition of aqueous $NaHCO_3$ (100 mL) and the contents transferred to a separatory funnel, diluting with EtOAc (100 mL). The layers were separated, and the aqueous layer was further extracted with EtOAc (3 × 100 mL). The combined organic layers were dried over Na_2SO_4 and concentrated in vacuo. The resultant crude product was further purified by flash column chromatography (silica gel, Hexanes/EtOAc, 9:1 → 4:1) to give the desired **Vinylogous ester 201** (18.7 g, 73% yield) as a off-white solid.

201:

^{1}H NMR (500 MHz, $CDCl_3$) δ 5.80 (ddd, *J* = 8.8, 6.7, 1.6 Hz, 1H), 5.37 (s, 1H), 3.69 (s, 3H), 3.68 (s, 3H), 2.92 (ddq, *J* = 15.0, 7.2, 1.2 Hz, 1H), 2.85 (ddq, *J* = 14.8, 7.4, 1.2 Hz, 1H), 2.45 (d, *J* = 17.8 Hz, 1H), 2.34 (d, *J* = 17.8 Hz, 1H), 1.78 (d, *J* = 1.4 Hz, 3H), 1.21 (s, 3H), 1.07 (s, 3H), 0.17 (s, 9H).

^{13}C NMR (101 MHz, $CDCl_3$) δ 196.14, 174.74, 171.22, 135.93, 119.18, 104.59, 100.97, 97.68, 64.09, 55.62, 51.69, 42.34, 37.80, 32.00, 26.32, 24.94, 22.72, 0.00.

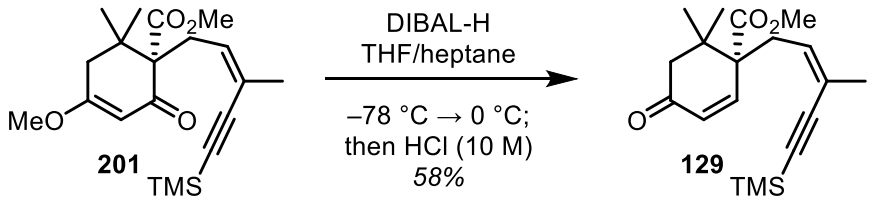

Enone 129. To a flame-dried 500 mL flask was added **201** (8.5 g, 23.4 mmol, 1.0 equiv.) and THF (100 mL). The mixture was cooled to –78 °C and DIBAL-H (1.0 M in heptane, 51.6 mL, 51.6 mmol, 2.2 equiv.) was then added dropwise. Upon completion of addition, the mixture was stirred for 0.5 h. The mixture was allowed to slowly warm to –40 °C. After 0.25 h, the reaction was quenched by the addition of concentrated aqueous HCl (14 mL, 140 mmol, 6.0 equiv.). After stirring for 0.25 h, the contents were transferred to a separatory funnel, diluting with EtOAc (100 mL). The layers were separated, and the aqueous layer was further extracted with EtOAc (3 × 100 mL). The combined organic layers were dried over Na_2SO_4 and concentrated in vacuo. The resultant crude product was further purified by flash column chromatography (silica gel, Hexanes/EtOAc, 9:1) to give the desired **Enone 129** (4.52 g, 58% yield) as a pale-yellow oil.

129:

^{1}H NMR (500 MHz, $CDCl_3$) δ 6.89 (d, *J* = 10.4 Hz, 1H), 6.04 (dd, *J* = 10.4, 0.7 Hz, 1H), 5.59 (ddq, *J* = 9.0, 6.0, 1.5 Hz, 1H), 3.74 (s, 3H), 2.89 (ddq, *J* = 13.5, 5.8, 1.2 Hz, 1H), 2.82 (dd, *J* = 13.5, 9.4 Hz, 1H), 2.49 (d, *J* = 16.7 Hz, 1H), 2.24 (d, *J* = 16.7 Hz, 1H), 1.82 (d, *J* = 0.6 Hz, 3H), 1.19 (s, 3H), 0.95 (s, 3H), 0.14 (s, 9H).

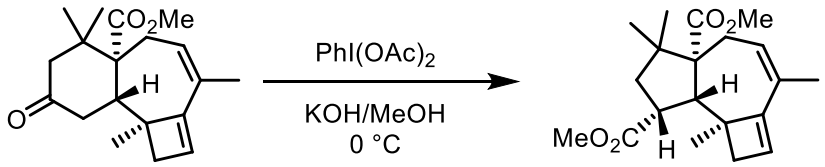

91 **99**

diester 99. To a flame-dried 5 mL microwave vial was added **91** (7 mg, 0.023 mmol, 1.0 equiv.) and dry MeOH (0.3 mL). The mixture was cooled to 0 °C and KOH (38.7 mg, 0.69 mmol, 30 equiv.) was then added, followed by $PhI(OAc)_2$ (8.4 mg, 0.026 mmol, 1.1 equiv.). The reaction mixture is stirred at 0 °C. Upon completion of the reaction, the mixture was diluted with EtOAc (2 mL) and quenched by slow addition of a saturated aqueous solution of $Na_2S_2O_3$ (1 mL) and the contents transferred to a separatory funnel, diluting with H_2O (5 mL). The layers were separated, and the aqueous layer was further extracted with EtOAc (3 × 5 mL). The combined organic layers were dried over Na_2SO_4 and concentrated in vacuo. The resultant crude product was further purified by flash column chromatography (silica gel, Hexanes/EtOAc, 9:1 → 4:1) to give the **diester 99** (3 mg, 39% yield) as a colorless oil.

99:

^{1}H NMR (500 MHz, $CDCl_3$) δ 5.73 (s, 1H), 5.63 (d, *J* = 8.2 Hz, 1H), 3.67 (s, 3H), 3.61 (s, 3H), 3.36 (ddd, *J* = 11.9, 8.6, 4.3 Hz, 1H), 2.77 (d, *J* = 11.4 Hz, 1H), 2.34 (dd, *J* = 14.4, 8.6 Hz, 1H), 2.17 (t, *J* = 12.5 Hz, 1H), 2.09 (d, *J* = 13.4 Hz, 1H), 1.97 (d, *J* = 13.4 Hz, 1H), 1.91 (d, *J* = 14.3 Hz, 1H), 1.77 – 1.73 (m, 3H), 1.71 (dd, *J* = 13.4, 4.7 Hz, 1H), 1.09 (s, 3H), 1.06 (s, 3H), 0.82 (s, 3H).

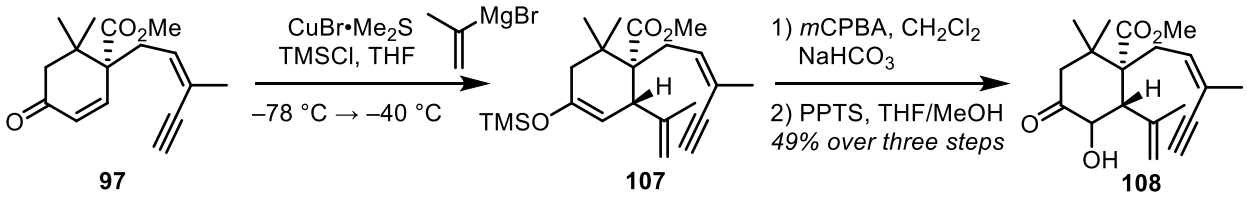

Ketone 108. To a flame-dried 500 mL flask was added CuBr•Me_2S (4.2 g, 16.12 mmol, 1.0 equiv.) and THF (160 mL). The mixture was cooled to –78 °C and isopropenylmagnesium bromide (0.5 M in THF, 80.6 mL, 40.3 mmol, 2.5 equiv.) was then added dropwise. Upon completion of addition, the mixture was stirred for 0.5 h at –78 °C. TMSCl (3.46 mL, 27.4 mmol, 1.7 equiv.), followed by **97** (4.2 g, 16.12 mmol, 1.0 equiv.) were added dropwise. The mixture was allowed to slowly warm to –40 °C. After 3 h, the reaction was quenched by the addition of Et_3N (20 mL) and a mixture of aqueous NH_4OH (6.0 N) and concentrated aqueous NH_4Cl (1:4, 100 mL). The contents were transferred to a separatory funnel, diluting with EtOAc (100 mL). The layers were separated, and the aqueous layer was further extracted with EtOAc (3 × 100 mL). The combined organic layers were dried over Na_2SO_4 and concentrated in vacuo. The resultant crude product was used without further purification and taken up in CH_2Cl_2 (100 mL) in a 500 mL flask. Freshly washed (aqueous $NaHCO_3$, 3 × 100 mL) *m*-CPBA (3.8 g, 16.8 mmol, 1.2 equiv.) in CH_2Cl_2 (100 mL) was added at 0 °C and the mixture was stirred for 1 h. Upon completion of the reaction, the reaction was quenched by the addition of aqueous $Na_2S_2O_3$ (100 mL), the contents transferred to a separatory funnel. The layers were separated, and the aqueous layer was further extracted with CH_2Cl_2 (3 × 50 mL). The combined organic layers were dried over Na_2SO_4 and concentrated in vacuo. The resultant crude product was used without further purification and taken up in THF (70 mL) and MeOH (70 mL). PPTS (3.87 g, 15.4 mmol, 1.1 equiv.) was added and the mixture was stirred at 25 °C for 2 h. Upon completion of the reaction, the reaction was quenched by the addition of aqueous $NaHCO_3$ (50 mL), the contents

transferred to a separatory funnel, diluting with EtOAc (100 mL) and aqueous $NaHCO_3$ (100 mL). The layers were separated, and the aqueous layer was further extracted with EtOAc (3 × 75 mL). The combined organic layers were dried over Na_2SO_4 and concentrated in vacuo. The crude residue was further purified by flash column chromatography (silica gel, Hexanes/EtOAc, 9:1 → 4:1) to give the desired **Ketone 108** (2.52 g, 49% yield) as an off-white solid.

108:

^{1}H NMR (500 MHz, $CDCl_3$) δ 6.07 (dt, *J* = 6.1, 3.2 Hz, 1H), 5.07 (s, 1H), 4.90 (s, 1H), 4.84 (dd, *J* = 11.7, 3.4 Hz, 1H), 3.79 (s, 3H), 3.54 (d, *J* = 3.5 Hz, 1H), 3.41 (d, *J* = 13.5 Hz, 1H), 2.77 (ddd, *J* = 15.7, 5.0, 2.5 Hz, 1H), 2.54 (dd, *J* = 15.9, 9.4 Hz, 1H), 2.44 (d, *J* = 11.7 Hz, 1H), 2.07 (d, *J* = 13.5 Hz, 1H), 1.85 (t, *J* = 1.8 Hz, 3H), 1.73 (s, 3H), 1.04 (s, 3H), 0.99 (s, 3H).

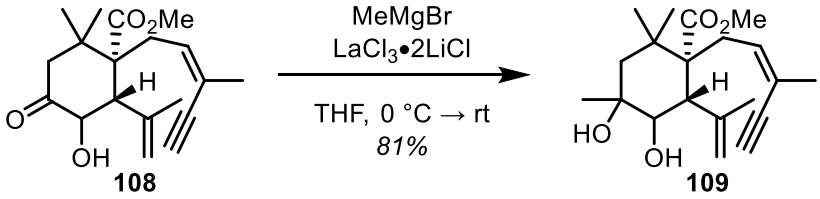

Diol 109. To a flame-dried 100 mL flask was added **108** (1.2 g, 3.77 mmol, 1.0 equiv.) and THF (38 mL) and the mixture is cooled to 0 °C. $LaCl_3$•2LiCl (0.6 M in THF, 12.6 mL, 7.54 mmol, 2.0 equiv.) is added dropwise and the mixture is stirred for 0.25 h. Then, MeMgBr (3.0 M in Et_2O, 3.77 mL, 11.31 mmol, 3.0 equiv.) was added dropwise. Upon completion of addition, the mixture was warmed to 25 °C and stirred for 16 h. The reaction was quenched by the addition of aqueous $NaHCO_3$ (30 mL) and aqueous Rochelle salt (10 mL) and stirred for 0.5 h. The contents were transferred to a separatory funnel, diluting with EtOAc (50 mL). The layers were separated, and the aqueous layer was further extracted with EtOAc (3 × 50 mL). The combined organic

layers were dried over Na_2SO_4 and concentrated in vacuo. The resultant crude product was further purified by flash column chromatography (silica gel, Hexanes/EtOAc, 3:1) to give the desired **diol 108** (1.02 g, 81% yield) as a white solid.

108:

^{1}H NMR (500 MHz, $CDCl_3$) δ 6.11 (t, *J* = 7.2 Hz, 1H), 5.07 – 4.98 (m, 1H), 4.93 (s, 1H), 4.15 – 4.09 (m, 2H), 3.69 (s, 3H), 3.14 (s, 1H), 2.63 – 2.51 (m, 3H), 2.09 (d, *J* = 9.2 Hz, 1H), 2.05 (s, 1H), 1.83 (d, *J* = 1.8 Hz, 4H), 1.44 (d, *J* = 14.9 Hz, 1H), 1.29 (s, 3H), 1.23 (s, 3H), 0.79 (s, 3H).

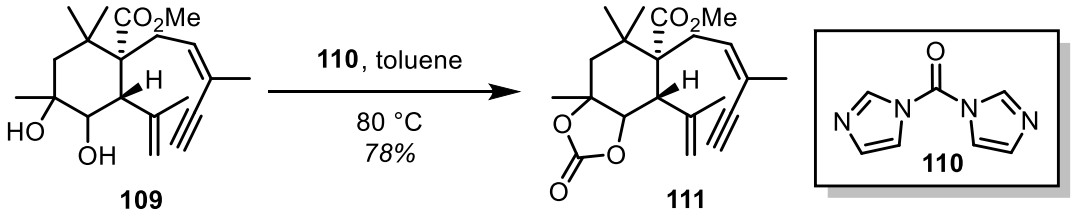

Carbonate 111. To a flame-dried 100 mL flask was added **109** (1.17 g, 3.5 mmol, 1.0 equiv.) and toluene (35 mL). CDI (**110**, 2.83 g, 17.5 mmol, 5.0 equiv.) is added in one portion and the mixture is heated to 80 °C. Upon completion, the reaction was cooled to 25 °C and carefully quenched by the addition of aqueous $NaHCO_3$ (30 mL). The contents were transferred to a separatory funnel, diluting with EtOAc (50 mL). The layers were separated, and the aqueous layer was further extracted with EtOAc (3 × 50 mL). The combined organic layers were dried over Na_2SO_4 and concentrated in vacuo. The resultant crude product was further purified by flash column chromatography (silica gel, Hexanes/EtOAc, 9:1) to give the desired **carbonate 111** (980 mg, 78% yield) as a white solid.

111:

^{1}H NMR (400 MHz, $CDCl_3$) δ 6.05 – 5.97 (m, 1H), 5.01 (t, *J* = 1.5 Hz, 1H), 4.91 (s, 1H), 4.71 (d, *J* = 10.0 Hz, 1H), 3.72 (s, 3H), 3.17 (s, 1H), 2.68 (ddd, *J* = 16.1, 6.4, 1.8 Hz, 1H), 2.56 (ddd, *J* = 16.0, 8.0, 1.4 Hz, 1H), 2.47 (d, *J* = 10.0 Hz, 1H), 1.94 (d, *J* = 16.2 Hz, 1H), 1.88 (s, 1H), 1.83 (q, *J* = 1.4 Hz, 3H), 1.69 (d, *J* = 0.7 Hz, 3H), 1.48 (s, 3H), 1.19 (s, 3H), 0.88 (s, 3H).

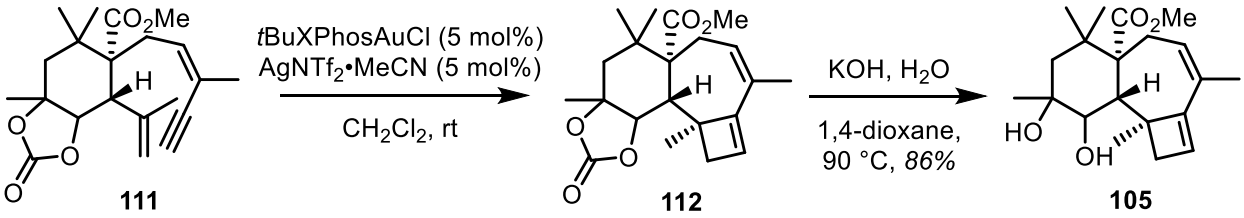

Diol 105. To a flame-dried 100 mL flask was added *t*BuXPhosAuCl (85.4 mg, 0.13 mmol, 0.05 equiv.), $AgNTf_2$•MeCN (55 mg, 0.13 mmol, 0.05 equiv.), and CH_2Cl_2 (52 mL). The mixture was stirred at 25 °C for 0.25 h. **111** (940 mg, 2.61 mmol, 1.0 equiv.) in CH_2Cl_2 (5 mL) was added and the mixture is stirred at 25 °C for 1 h. Upon completion, the reaction was quenched by the addition Et_3N (5 drops) and concentrated in vacuo. The resultant crude product was taken up in 1,4-dioxane (25 mL) and KOH (2.0 g, 37 mmol, 15.0 equiv.) and heated at 90 °C for 1 h. Upon completion, the reaction was cooled to 25 °C and neutralized with aqueous HCl (1.0 M), the contents transferred to a separatory funnel, diluting with EtOAc (20 mL). The layers were separated, and the aqueous layer was further extracted with EtOAc (5 × 25 mL). The combined organic layers were dried over Na_2SO_4 and concentrated in vacuo. The resultant crude product was further purified by flash column chromatography (silica gel, Hexanes/EtOAc, 4:1) to give the desired **diol 105** (750 mg, 86% yield) as an off-white solid.

105:

^{1}H NMR (400 MHz, $CDCl_3$) δ 5.78 (d, *J* = 1.2 Hz, 1H), 5.65 (ddd, *J* = 8.5, 3.8, 1.7 Hz, 1H), 4.54 (dd, *J* = 11.1, 7.4 Hz, 1H), 3.61 (s, 3H), 2.64 (d, *J* = 13.7 Hz, 1H), 2.36 – 2.28 (m, 2H), 2.24 (dd, *J* = 13.7, 1.1 Hz, 1H), 1.95 (ddd, *J* = 14.1, 4.0, 2.0 Hz, 1H), 1.75 (t, *J* = 1.7 Hz, 3H), 1.67 (d, *J* = 7.3 Hz, 1H), 1.44 (d, *J* = 14.7 Hz, 1H), 1.27 (s, 3H), 1.16 (s, 3H), 1.09 (d, *J* = 0.8 Hz, 3H), 0.73 (s, 3H).

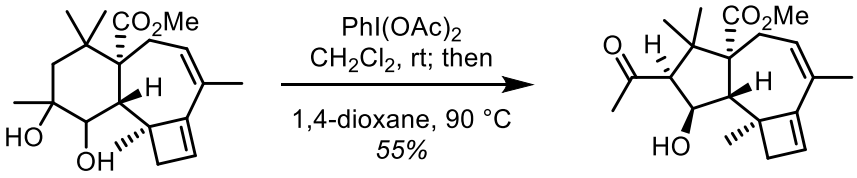

105 113

Ketoaldehyde 113. To a flame-dried 100 mL flask was added **105** (650 mg, 1.95 mmol, 1.0 equiv.), CH_2Cl_2 (20 mL), and DBU (750 µL, 4.88 mmol, 2.5 equiv.). $PhI(OAc)_2$ (690 mg, 2.41 mmol, 1.1 equiv.) in CH_2Cl_2 (5 mL) was added and the mixture is stirred at 25 °C for 0.25 h. Upon completion, the reaction was quenched by the addition of ethylene glycol (2 drops) and concentrated in vacuo. The resultant crude product was taken up in 1,4-dioxane (20 mL) and heated at 90 °C for 1 h. Upon completion, the reaction was cooled to 25 °C and quenched by addition of aqueous NH_4Cl (20 mL), the contents transferred to a separatory funnel, diluting with EtOAc (20 mL). The layers were separated, and the aqueous layer was further extracted with EtOAc (5 × 25 mL). The combined organic layers were dried over Na_2SO_4 and concentrated in vacuo. The resultant crude product was further purified by flash column chromatography (silica

gel, Hexanes/EtOAc, 6:1) to give the desired **ketoaldehyde 105** (355 mg, 55% yield) as an off-white solid.

113:

^{1}H NMR (500 MHz, $CDCl_3$) δ 5.79 (s, 1H), 5.60 (ddd, *J* = 8.3, 3.2, 1.6 Hz, 1H), 4.78 (q, *J* = 8.7 Hz, 1H), 3.94 (d, *J* = 8.5 Hz, 1H), 3.64 (s, 3H), 3.58 (d, *J* = 8.7 Hz, 1H), 2.68 (d, *J* = 13.9 Hz, 1H), 2.37 – 2.27 (m, 3H), 2.24 (s, 3H), 2.20 – 2.16 (m, 1H), 1.77 (s, 3H), 1.05 (s, 3H), 1.03 (s, 3H), 0.96 (s, 3H).

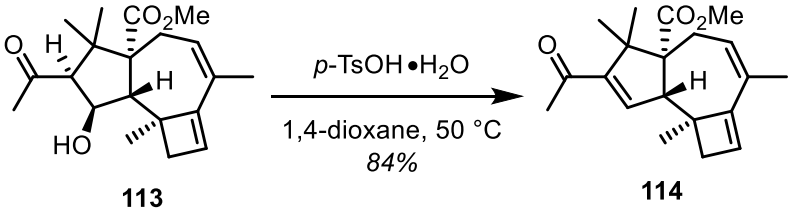

113 **114**

Enone 114. To a flame-dried 25 mL flask was added **113** (175 mg, 0.52 mmol, 1.0 equiv.), 1,4-dioxane (5 mL), and *p*-TsOH•H_2O (120 mg, 0.63 mmol, 1.2 equiv.). The mixture is heated at 50 °C for 24 h. Upon completion, the reaction was quenched by the addition of $NaHCO_3$ (10 mL), the contents transferred to a separatory funnel, diluting with EtOAc (20 mL) and aqueous $NaHCO_3$ (10 mL). The layers were separated, and the aqueous layer was further extracted with EtOAc (5 × 10 mL). The combined organic layers were dried over Na_2SO_4 and concentrated in vacuo. The resultant crude product was further purified by flash column chromatography (silica gel, Hexanes/EtOAc, 9:1) to give the desired **enone 114** (140 mg, 84% yield) as a colorless oil.

114:

^{1}H NMR (500 MHz, $CDCl_3$) δ 6.74 (d, *J* = 2.2 Hz, 1H), 5.80 (s, 1H), 5.69 (d, *J* = 8.5 Hz, 1H), 3.51 (s, 3H), 2.40 (dd, *J* = 14.7, 8.5 Hz, 1H), 2.31 (s, 3H), 2.28 (d, *J* = 3.2 Hz, 2H), 2.04 (dt, *J* = 14.2, 2.7 Hz, 1H), 1.78 (d, *J* = 1.9 Hz, 3H), 1.09 (s, 3H), 1.08 (s, 3H), 1.06 (s, 2H).

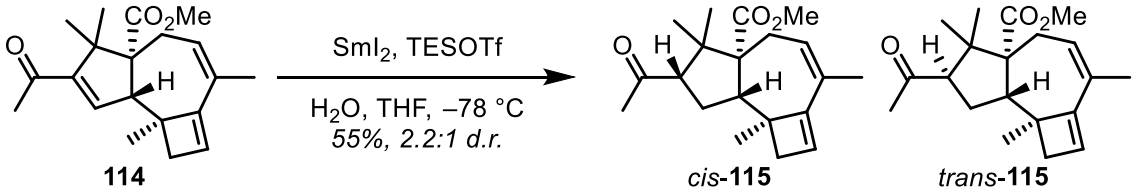

114 *cis*-**115** *trans*-**115**

Ketoester 115. To a flame-dried 100 mL flask was added a freshly prepared solution of SmI_2,[100] 0.05 M in THF (22.4 mL, 1.12 mmol, 14.0 equiv.) and cooled to –78 °C. **114** (27 mg, 0.085 mmol, 1.0 equiv.) and H_2O (7.2 µL, 0.4 mmol, 4.7 equiv.) were added as a solution in degassed THF (8.5 mL). Then, TESOTf (120 µL, 0.53 mmol, 6.2 equiv.) was added dropwise. Upon completion of addition, the mixture was stirred at –78 °C for 0.25 h. The mixture was then quenched by pouring it quickly into a separatory funnel containing Et_2O (100 mL) and $NaHCO_3$ (100 mL). The layers were separated, and the aqueous layer was further extracted with EtOAc (3 × 50 mL). The combined organic layers were dried over Na_2SO_4 and concentrated in vacuo. The resultant crude product was further purified by flash column chromatography (silica gel, Hexanes/Et_2O, 12:1 → 4:1) to give the desired **ketoester** *cis*-**115** (10.3 mg) and **ketoester** *trans*-**115** (4.7 mg, 2.2:1 d.r., 55% yield) as colorless oils. Both compounds solidified upon storage at –20 °C

trans-**115**:

^{1}H NMR (500 MHz, $CDCl_3$) δ 5.76 (d, *J* = 1.1 Hz, 1H), 5.62 (ddd, *J* = 8.6, 3.2, 1.7 Hz, 1H), 3.64 (s, 3H), 3.33 (dd, *J* = 10.9, 5.4 Hz, 1H), 2.41 (dd, *J* = 11.8, 9.7 Hz, 1H), 2.32 – 2.17 (m, 4H),

2.16 (s, 3H), 1.86 – 1.77 (m, 2H), 1.76 (dd, *J* = 2.2, 1.5 Hz, 3H), 1.07 (s, 3H), 0.99 – 0.97 (m, 3H), 0.79 (s, 3H).

cis-**115**:

^{1}H NMR (500 MHz, $CDCl_3$) δ 5.78 (d, *J* = 1.1 Hz, 1H), 5.65 (ddd, *J* = 8.5, 3.0, 1.5 Hz, 1H), 3.57 (s, 3H), 2.83 (ddd, *J* = 13.6, 12.1, 9.7 Hz, 1H), 2.74 – 2.66 (m, 1H), 2.39 – 2.19 (m, 4H), 2.18 (s, 3H), 1.87 (dt, *J* = 14.2, 2.6 Hz, 1H), 1.76 (dd, *J* = 2.3, 1.6 Hz, 3H), 1.71 (ddd, *J* = 12.1, 8.5, 6.7 Hz, 1H), 1.16 (s, 3H), 1.05 – 1.04 (m, 3H), 0.86 (s, 3H).

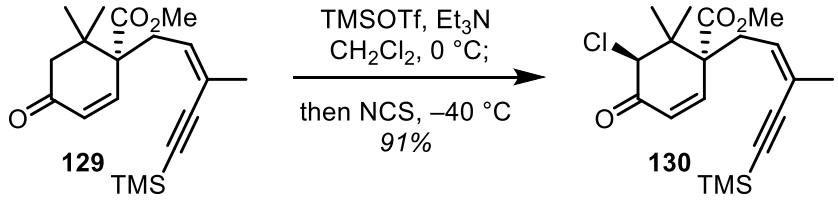

Chloroenone 130. To a flame-dried 250 mL flask was added **129** (4.1 g, 12.31 mmol, 1.0 equiv.) and CH_2Cl_2 (82 mL). The mixture was cooled to 0 °C and Et_3N (6.8 mL, 49.2 mmol, 4.0 equiv.) was then added, followed by dropwise addition of TMSOTf (2.7 mL, 14.8 mmol, 1.2 equiv.). Upon completion of addition, the mixture stirred for 1.5 h at 0 °C. The mixture was cooled to –40 °C. NCS (3.3 g, 24.6 mmol, 2.0 equiv.) was then added in two portions to this mixture and the mixture was stirred for 1 h at –40 °C. Once complete, the reaction was quenched at –40 °C by the addition of aqueous NH_4Cl (50 mL) and the mixture was allowed to warm to 25 °C. The contents were transferred to a separatory funnel, diluting with CH_2Cl_2 (50 mL). The layers were separated, and the aqueous layer was further extracted with CH_2Cl_2 (3 × 50 mL). The combined organic layers were washed with diluted aqueous HCl (0.1 M, 2 × 100 mL), dried over Na_2SO_4 and concentrated in vacuo. The resultant crude product was further purified by recrystallization

in EtOAc at –40 °C to give the desired **chloroenone 130** (4.11 g, 91% yield) as a white crystalline solid.

130:

^{1}H NMR (500 MHz, $CDCl_3$) δ 6.69 (d, *J* = 10.4 Hz, 1H), 6.20 (d, *J* = 10.4 Hz, 1H), 5.69 (ddt, *J* = 9.3, 4.7, 1.4 Hz, 1H), 4.82 (s, 1H), 3.76 (s, 3H), 2.94 – 2.86 (m, 1H), 2.83 – 2.76 (m, 1H), 1.87 (t, *J* = 1.5 Hz, 3H), 1.15 (s, 3H), 1.13 (s, 3H), 0.14 (s, 9H).

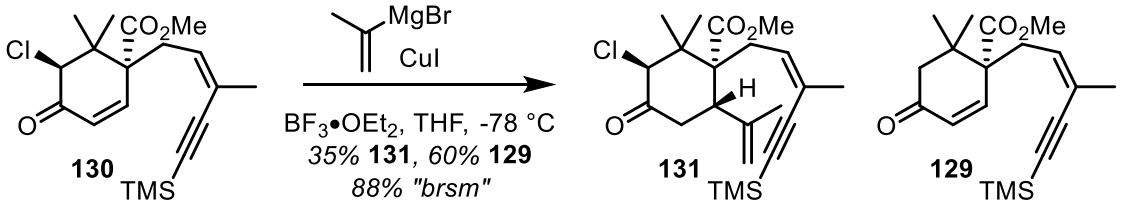

Chloroketone 131. To a flame-dried 500 mL flask was added CuI (6.57 g, 34.5 mmol, 2.3 equiv.) and evacuated and back-filled with argon three times. Then THF (75 mL) is added and the mixture was cooled to –78 °C. Isopropenylmagnesium bromide (0.5 M in THF, 138 mL, 69 mmol, 4.6 equiv.) was added dropwise and the yellow solution was stirred for 0.5 h at –78 °C. **130** (5.5 g, 15 mmol, 1.0 equiv.) in THF (25 mL) and BF_3•OEt_2 (48% in Et_2O, 32.4 mL, 105 mmol, 7.0 equiv.) were then separately and simultaneously added dropwise via syringe pump over 0.33 h. Upon completion of addition, the mixture was stirred for 2 h at –78 °C. Then, the reaction was quenched by the addition of a mixture of aqueous NH_4OH (6.0 N) and concentrated aqueous NH_4Cl (1:4, 150 mL) and the contents transferred to a separatory funnel, diluting with EtOAc (100 mL). The layers were separated, and the aqueous layer was further extracted with EtOAc (3 × 100 mL). The combined organic layers were washed with a mixture of aqueous NH_4OH (6.0 N) and concentrated aqueous NH_4Cl (1:4, 2 × 100 mL), dried over Na_2SO_4 and

concentrated in vacuo. The resultant crude product was further purified by flash column chromatography (silica gel, Hexanes/EtOAc, 19:1 → 9:1) to give the desired **chloroketone 131** (2.15 g, 39% yield) as a white solid and **enone 129** (3.00 g, 60 % yield).

131:

^{1}H NMR (500 MHz, $CDCl_3$) δ 6.04 – 5.96 (m, 1H), 5.63 (s, 1H), 4.90 (d, *J* = 1.5 Hz, 1H), 4.77 (s, 1H), 3.79 (s, 3H), 3.31 (ddd, *J* = 14.4, 13.5, 1.0 Hz, 1H), 2.82 (ddd, *J* = 15.7, 5.1, 2.2 Hz, 1H), 2.39 (dd, *J* = 13.5, 4.3 Hz, 1H), 1.82 (t, *J* = 1.5 Hz, 3H), 1.61 (dd, *J* = 1.5, 0.8 Hz, 3H), 1.14 (s, 3H), 1.06 (s, 3H), 0.17 (s, 9H).

^{13}C NMR (101 MHz, $CDCl_3$) δ 201.81, 174.40, 143.29, 137.24, 118.61, 115.77, 104.49, 98.89, 73.09, 56.83, 51.93, 50.85, 48.51, 44.09, 37.42, 24.26, 22.73, 20.82, 16.89, 0.28, 0.00.

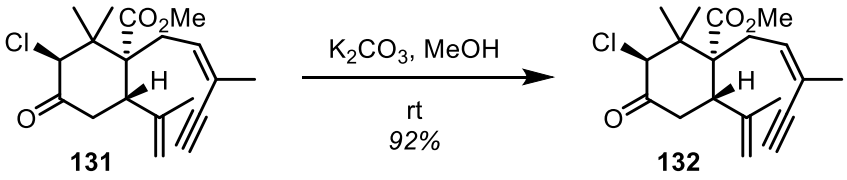

Chloroketone 132. To a 50 mL flask was added **131** (2.38 g, 5.82 mmol, 1.0 equiv.) and MeOH (25 mL) and THF (5 mL). K_2CO_3 (165 mg, 1.2 mmol, 0.2 equiv.) was then added in one portion. The mixture was stirred at 25 °C for 1 h. The reaction was quenched by the addition of aqueous $NaHCO_3$ (50 mL) and the contents transferred to a separatory funnel, diluting with EtOAc (30 mL). The layers were separated, and the aqueous layer was further extracted with EtOAc (5 × 30 mL). The combined organic layers were dried over Na_2SO_4 and concentrated in vacuo. The resultant crude product was further purified by flash column chromatography (silica gel, Hexanes/EtOAc, 9:1) to give the desired **chloroketone 132** (1.8 g, 92% yield) as a white solid.

132:

^{1}H NMR (500 MHz, $CDCl_3$) δ 6.04 (ddt, *J* = 7.6, 3.8, 1.2 Hz, 1H), 5.62 (s, 1H), 4.90 (s, 1H), 4.81 (s, 1H), 3.80 (s, 3H), 3.35 – 3.23 (m, 1H), 3.15 (s, 1H), 2.83 (ddd, *J* = 15.9, 5.2, 2.2 Hz, 1H), 2.74 (dd, *J* = 14.2, 4.4 Hz, 1H), 2.63 (dd, *J* = 16.1, 9.3 Hz, 1H), 2.38 (dd, *J* = 13.5, 4.4 Hz, 1H), 1.84 (d, *J* = 1.9 Hz, 3H), 1.63 – 1.61 (m, 3H), 1.14 (s, 3H), 1.05 (s, 3H).

^{13}C NMR (101 MHz, $CDCl_3$) δ 201.68, 174.36, 143.34, 137.37, 117.50, 115.94, 82.75, 81.98, 73.04, 56.78, 51.98, 50.55, 48.57, 44.17, 37.07, 24.30, 23.08, 20.94, 16.94.

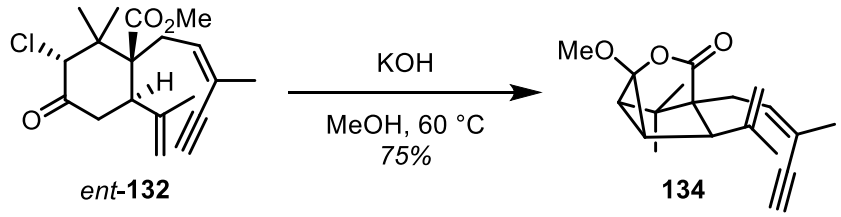

ent-**132** **134**

Lactone 134. To a 50 mL flask was added **132** (2.38 g, 5.82 mmol, 1.0 equiv.) and MeOH (25 mL) and THF (5 mL). K_2CO_3 (165 mg, 1.2 mmol, 0.2 equiv.) was then added in one portion. The mixture was stirred at 25 °C for 1 h. The reaction was quenched by the addition of aqueous $NaHCO_3$ (50 mL) and the contents transferred to a separatory funnel, diluting with EtOAc (30 mL). The layers were separated, and the aqueous layer was further extracted with EtOAc (5 × 30 mL). The combined organic layers were dried over Na_2SO_4 and concentrated in vacuo. The resultant crude product was further purified by flash column chromatography (silica gel, Hexanes/EtOAc, 9:1) to give **lactone 134** (1.8 g, 92% yield) as a colorless oil.

134:

^{1}H NMR (400 MHz, $CDCl_3$) δ 6.14 – 6.05 (m, 1H), 4.97 (p, *J* = 1.5 Hz, 1H), 4.96 – 4.95 (m, 1H), 3.56 (s, 3H), 3.15 (s, 1H), 2.90 (d, *J* = 2.9 Hz, 1H), 2.66 (ddd, *J* = 15.3, 5.0, 2.3 Hz, 1H), 2.53 (dd, *J* = 15.3, 9.7 Hz, 1H), 1.84 (t, *J* = 1.7 Hz, 3H), 1.81 (dd, *J* = 7.0, 2.9 Hz, 1H), 1.79 – 1.77 (m, 3H), 1.56 (d, *J* = 7.0 Hz, 1H), 1.12 (s, 3H), 1.02 (s, 3H).

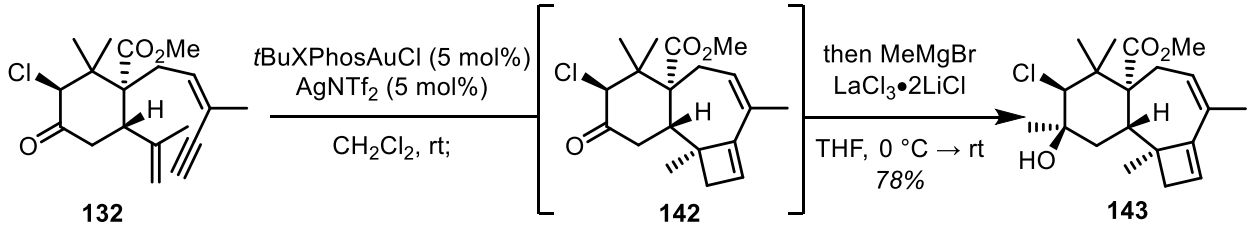

Chlorohydrin 143. To a flame-dried 250 mL flask was added **132** (1.8 g, 5.34 mmol, 1.0 equiv.) and CH_2Cl_2 (80 mL). A freshly prepared solution of *t*BuXPhosAuCl (177.4 mg, 0.27 mmol, 0.05 equiv.) and $AgNTf_2$•MeCN (118.3 mg, 0.27 mmol, 0.05 equiv.) in CH_2Cl_2 (26 mL) was then added by careful vacuum filtration through a pad of celite. The mixture was stirred at 25 °C for 1 h. The reaction was quenched by the addition of Et_3N (5 drops) and the mixture was concentrated in vacuo and in the same flask, the residue was taken up in THF (50 mL) and cooled to 0 °C. $LaCl_3$•2LiCl (0.6 M in THF, 13 mL, 7.8 mmol, 1.5 equiv.) is added dropwise and the mixture is stirred for 0.25 h. Then, MeMgBr (3.0 M in Et_2O, 5.2 mL, 15.6 mmol, 3.0 equiv.) was added dropwise. Upon completion of addition, the mixture was warmed to 25 °C and stirred for 16 h. The reaction was quenched by the addition of aqueous $NaHCO_3$ (50 mL) and aqueous Rochelle salt (50 mL) and stirred for 0.5 h. The contents were transferred to a separatory funnel, diluting with EtOAc (50 mL). The layers were separated, and the aqueous layer was further extracted with EtOAc (5 × 50 mL). The combined organic layers were dried over Na_2SO_4 and

concentrated in vacuo. The resultant crude product was further purified by flash column chromatography (silica gel, Hexanes/EtOAc, 19:1) to give the desired **chlorohydrin 143** (1.46 g, 78% yield) as a white solid.

143:

^{1}H NMR (500 MHz, $CDCl_3$) δ 5.81 (s, 1H), 5.71 – 5.65 (m, 1H), 4.51 (s, 1H), 3.66 (s, 3H), 2.50 – 2.33 (m, 3H), 2.28 (d, *J* = 13.3 Hz, 1H), 2.09 (dd, *J* = 13.2, 5.3 Hz, 2H), 1.87 (d, *J* = 2.3 Hz, 1H), 1.77 (t, *J* = 1.8 Hz, 3H), 1.67 (dd, *J* = 13.8, 3.3 Hz, 1H), 1.38 (s, 3H), 1.19 (s, 3H), 0.95 (s, 3H), 0.93 (s, 3H).

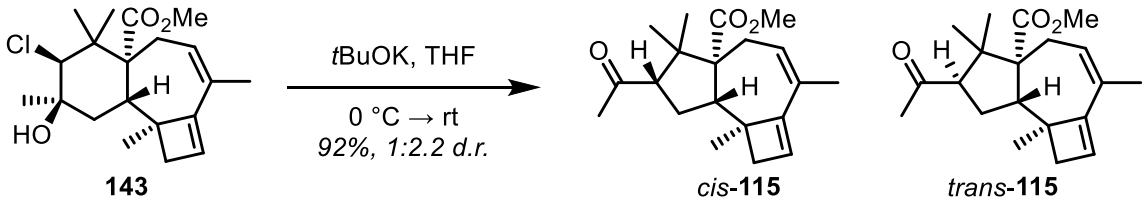

Ketoester 115. To a flame-dried 200 mL flask was added **143** (1.65 g, 4.69 mmol, 1.0 equiv.) and THF (47 mL) and the mixture was cooled to 0 °C. *t*BuOK (1.0 M in THF, 9.4 mL, 9.40 mmol, 2.0 equiv.) was then added dropwise. The mixture was warmed to 25 °C and closely monitored by TLC. Upon completion, typically after 0.33 h, the reaction was quenched by the addition of aqueous $NaHCO_3$ (50 mL) and the contents transferred to a separatory funnel, diluting with EtOAc (30 mL). The layers were separated, and the aqueous layer was further extracted with EtOAc (5 × 30 mL). The combined organic layers were dried over Na_2SO_4 and concentrated in vacuo. The resultant crude product was further purified by flash column chromatography (silica gel, Hexanes/Et_2O, 11:1 → 5:1) to give the desired **ketoester** ***cis*-115**

(405 mg) and **ketoester** *trans*-**115** (1.0 g, 1.0:2.2 d.r., 92% yield) as colorless oils. Both compounds solidified upon storage at –20 °C.

trans-**115**:

^{1}H NMR (500 MHz, $CDCl_3$) δ 5.76 (d, *J* = 1.1 Hz, 1H), 5.62 (ddd, *J* = 8.6, 3.2, 1.7 Hz, 1H), 3.64 (s, 3H), 3.33 (dd, *J* = 10.9, 5.4 Hz, 1H), 2.41 (dd, *J* = 11.8, 9.7 Hz, 1H), 2.32 – 2.17 (m, 4H), 2.16 (s, 3H), 1.86 – 1.77 (m, 2H), 1.76 (dd, *J* = 2.2, 1.5 Hz, 3H), 1.07 (s, 3H), 0.99 – 0.97 (m, 3H), 0.79 (s, 3H).

cis-**115**:

^{1}H NMR (500 MHz, $CDCl_3$) δ 5.78 (d, *J* = 1.1 Hz, 1H), 5.65 (ddd, *J* = 8.5, 3.0, 1.5 Hz, 1H), 3.57 (s, 3H), 2.83 (ddd, *J* = 13.6, 12.1, 9.7 Hz, 1H), 2.74 – 2.66 (m, 1H), 2.39 – 2.19 (m, 4H), 2.18 (s, 3H), 1.87 (dt, *J* = 14.2, 2.6 Hz, 1H), 1.76 (dd, *J* = 2.3, 1.6 Hz, 3H), 1.71 (ddd, *J* = 12.1, 8.5, 6.7 Hz, 1H), 1.16 (s, 3H), 1.05 – 1.04 (m, 3H), 0.86 (s, 3H).

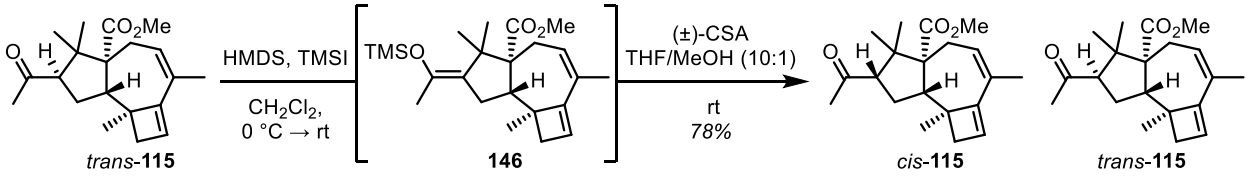

Ketoester 115. To a flame-dried 200 mL flask was added *cis*-**115** (1.79 g, 5.62 mmol, 1.0 equiv.) and CH_2Cl_2 (56 mL) and the mixture was cooled to 0 °C. HMDS (2.95 mL, 14.05 mmol, 2.5 equiv.) was then added dropwise, followed by dropwise addition of TMSI (965 µL, 6.74 mmol, 1.2 equiv.). Upon completion of addition, the mixture was warmed to 25 °C and and stirred for 1 h. The reaction was quenched by the addition of aqueous $NaHCO_3$ (30 mL) and aqueous $Na_2S_2O_3$ (10 mL) and the contents transferred to a separatory funnel, diluting with

CH_2Cl_2 (20 mL). The layers were separated, and the aqueous layer was further extracted with CH_2Cl_2 (3 × 30 mL). The combined organic layers were dried over Na_2SO_4 and concentrated in vacuo. The residue was taken up in THF (50 mL) and MeOH (5 mL). (±)-CSA was added in one portion and the mixture is stirred for 1 h at 25 °C. The reaction was quenched by the addition of aqueous $NaHCO_3$ (50 mL) and the contents transferred to a separatory funnel, diluting with EtOAc (30 mL). The layers were separated, and the aqueous layer was further extracted with EtOAc (5 × 30 mL). The combined organic layers were dried over Na_2SO_4 and concentrated in vacuo. The resultant crude product was further purified by flash column chromatography (silica gel, Hexanes/Et_2O, 11:1 → 5:1) to give the desired **ketoester** *cis*-**115** (840 mg) and **ketoester** *trans*-**115** (765 mg, 1.2:1.0 d.r., 90% yield) as colorless oils. Both compounds solidified upon storage at –20 °C.

146:

^{1}H NMR (500 MHz, $CDCl_3$) δ 5.75 (s, 1H), 5.69 (d, *J* = 8.2 Hz, 1H), 3.54 (s, 3H), 2.70 (t, *J* = 13.7 Hz, 1H), 2.35 – 2.26 (m, 2H), 2.19 (d, *J* = 13.1 Hz, 1H), 2.16 (ddd, *J* = 14.7, 8.4, 0.8 Hz, 1H), 2.06 (d, *J* = 13.3 Hz, 1H), 1.88 – 1.82 (m, 1H), 1.79 (d, *J* = 1.1 Hz, 3H), 1.77 – 1.75 (m, 3H), 1.06 (s, 3H), 1.02 (s, 3H), 0.99 (s, 3H), 0.19 (s, 9H).

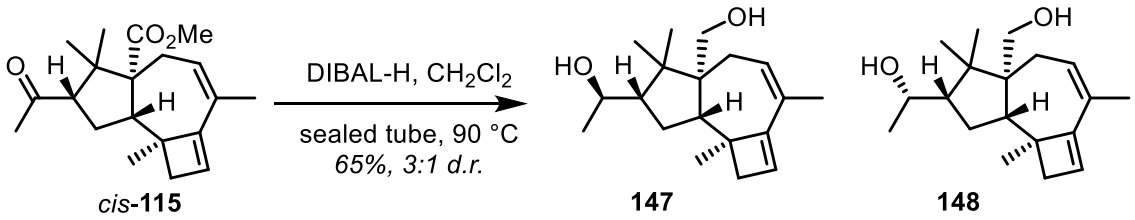

cis-**115** **147** **148**

Diol 149. To a flame-dried 20 mL microwave tube was added *cis*-**115** (730 mg, 2.29 mmol, 1.0 equiv.) and CH_2Cl_2 (3.5 mL). Open to air and at 25 °C, DIBAL-H (1.0 M in CH_2Cl_2, 11.5 mL, 11.46 mmol, 5.0 equiv.) was then added dropwise. The microwave tube was sealed and lowered into a pre-heated oil bath and heated at 90 °C for 0.75 h. Upon completion, the mixture was cooled to 25 °C and remaining DIBAL-H was quenched by careful dropwise addition of acetone (2 mL). The mixture was poured into a 250 mL flask with EtOAc (50 mL) and aqueous Rochelle salt (100 mL) and the mixture was stirred for 12 h. The contents were transferred to a separatory funnel. The layers were separated, and the aqueous layer was further extracted with EtOAc (5 × 30 mL). The combined organic layers were dried over Na_2SO_4 and concentrated in vacuo. The resultant crude product was further purified by flash column chromatography (silica gel, Hexanes/acetone, 5:1 → 4:1) to give the desired **diol 147** (322 mg) and **diol 148** (107 mg, 3:1 d.r., 65% yield), both as white solids.

147:

^{1}H NMR (500 MHz, $CDCl_3$) δ 5.82 (s, 1H), 5.34 (ddd, *J* = 8.7, 3.5, 1.7 Hz, 1H), 4.15 (qd, *J* = 6.4, 1.7 Hz, 1H), 4.08 (d, *J* = 12.0 Hz, 1H), 3.51 (d, *J* = 12.0 Hz, 1H), 2.20 (d, *J* = 13.1 Hz, 1H), 2.12 – 2.06 (m, 3H), 1.92 (dt, *J* = 14.6, 3.0 Hz, 1H), 1.80 (dd, *J* = 2.4, 1.6 Hz, 3H), 1.71 – 1.65 (m, 2H), 1.59 – 1.52 (m, 1H), 1.36 (s, 3H), 1.15 (d, *J* = 6.4 Hz, 3H), 1.13 (s, 3H), 0.90 (s, 3H).

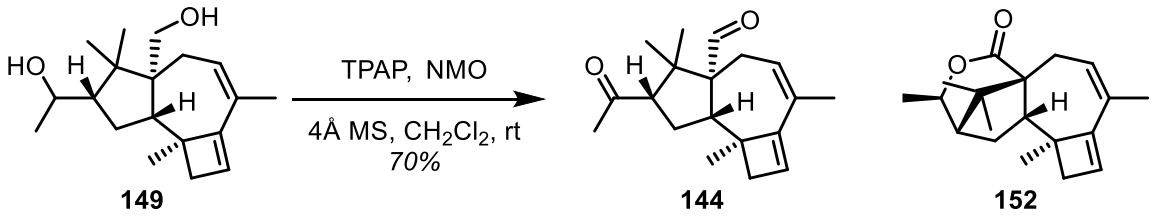

Ketoaldehyde 144. To a flame-dried 25 mL flask with 4Å MS was added **149** (254 mg, 0.875 mmol, 1.0 equiv.), CH_2Cl_2 (6 mL), and NMO (310 mg, 2.63 mmol, 3.0 equiv.). Then, TPAP (31 mg, 0.088 mmol, 0.1 equiv.) was added and the mixture was stirred at 25 °C for 24 h. Upon completion, the contents of the flask were filtered through a pad of silica and transferred to a separatory funnel, diluting with EtOAc (20 mL). The layers were separated, and the aqueous layer was further extracted with EtOAc (3 × 20 mL). The combined organic layers were dried over Na_2SO_4 and concentrated in vacuo. The resultant crude product was further purified by flash column chromatography (silica gel, Hexanes/acetone, 15:1 → 9:1) to give the desired **ketoaldehyde 144** (175 mg, 70% yield), as a clear oil.

144:

^{1}H NMR (500 MHz, $CDCl_3$) δ 9.77 (s, 1H), 5.77 (s, 1H), 5.68 – 5.61 (m, 1H), 3.05 (t, *J* = 8.9 Hz, 1H), 2.55 (td, *J* = 13.6, 8.9 Hz, 1H), 2.39 (dd, *J* = 13.9, 7.0 Hz, 1H), 2.24 – 2.16 (m, 5H), 2.10 (d, *J* = 13.3 Hz, 1H), 1.88 (ddd, *J* = 13.3, 8.8, 6.9 Hz, 1H), 1.77 – 1.71 (m, 4H), 1.16 (s, 3H), 1.07 (s, 3H), 0.77 (s, 3H).

^{13}C NMR (126 MHz, $CDCl_3$) δ 210.59, 205.55, 157.59, 131.76, 125.49, 123.54, 65.71, 59.81, 55.43, 47.67, 46.81, 43.58, 33.31, 31.12, 29.71, 29.65, 27.84, 22.32, 21.77, 19.86.

152:

^{1}H NMR (400 MHz, $CDCl_3$) δ 5.76 (s, 1H), 5.68 (dt, *J* = 8.0, 2.1 Hz, 1H), 4.61 (qd, *J* = 6.5, 2.5 Hz, 1H), 2.54 (dd, *J* = 10.8, 8.2 Hz, 1H), 2.34 (dd, *J* = 15.5, 8.2 Hz, 1H), 2.16 (d, *J* = 13.4 Hz, 1H), 2.08 (dd, *J* = 13.3, 0.9 Hz, 1H), 1.99 – 1.92 (m, 1H), 1.93 – 1.87 (m, 2H), 1.80 (dd, *J* = 2.5, 1.5 Hz, 3H), 1.67 (dt, *J* = 6.7, 2.2 Hz, 1H), 1.33 (d, *J* = 6.5 Hz, 3H), 1.18 (s, 3H), 1.06 (s, 3H), 1.05 (s, 3H).

^{13}C NMR (101 MHz, $CDCl_3$) δ 176.26, 158.27, 130.26, 125.65, 122.45, 77.34, 77.02, 76.70, 58.62, 54.55, 48.01, 47.34, 46.32, 43.54, 29.96, 22.93, 22.21, 21.70, 20.42, 18.34, 17.82.

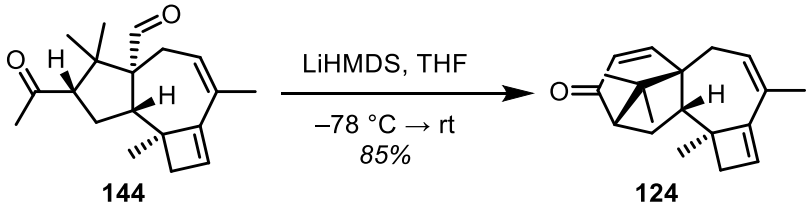

144 124

Enone 124. To a flame-dried 50 mL flask was added **144** (94 mg, 0.33 mmol, 1.0 equiv.) and THF (11 mL) and the mixture was cooled to –78 °C. LiHMDS (1 M in THF, 0.66 mL, 0.66 mmol, 2.0 equiv.) was added and the mixture was stirred at –78 °C for 1 hour and then slowly allowed to warm to 25 °C over 12 h. Upon completion, the reaction was quenched by the addition of aqueous $NaHCO_3$ (10 mL) and the contents transferred to a separatory funnel, diluting with EtOAc (10 mL). The layers were separated, and the aqueous layer was further extracted with EtOAc (3 × 10 mL). The combined organic layers were dried over Na_2SO_4 and concentrated in vacuo. The resultant crude product was further purified by flash column chromatography (silica gel, Hexanes/EtOAc, 9:1) to give the desired **enone 124** (75 mg, 85% yield), as a colorless oil.

124:

^{1}H NMR (400 MHz, $CDCl_3$) δ 6.97 (d, *J* = 9.8 Hz, 1H), 5.97 (dd, *J* = 9.8, 1.8 Hz, 1H), 5.83 (d, *J* = 1.4 Hz, 1H), 5.51 (ddd, *J* = 7.8, 3.8, 1.7 Hz, 1H), 2.69 (dd, *J* = 9.4, 7.5 Hz, 1H), 2.38 (dd, *J* = 7.9, 1.9 Hz, 1H), 2.24 (ddd, *J* = 14.4, 9.4, 7.9 Hz, 1H), 2.19 – 2.10 (m, 3H), 2.04 (d, *J* = 13.4 Hz, 1H), 1.85 (t, *J* = 1.9 Hz, 3H), 1.36 (dd, *J* = 14.4, 7.5 Hz, 1H), 0.99 (s, 3H), 0.98 (s, 3H), 0.91 (s, 3H).

^{13}C NMR (101 MHz, $CDCl_3$) δ 203.92, 157.51, 156.55, 135.91, 128.31, 124.21, 122.79, 59.96, 56.36, 54.35, 52.56, 47.54, 44.60, 30.87, 25.65, 23.62, 22.86, 22.48, 19.17.

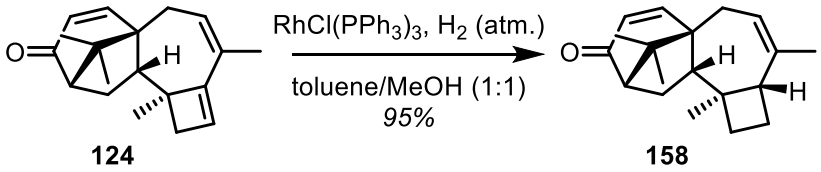

124 **158**

Enone 158. To a 5 mL microwave tube was added **124** (25.2 mg, 0.094 mmol, 1.0 equiv.), toluene (0.5 mL) and MeOH (0.5 mL). $RhCl(PPh_3)_3$ (26.1 mg, 0.0282 mmol, 0.3 equiv.) was then added in one portion. The microwave tube was fitted with a septum and H_2 was bubbled through the mixture for 0.25 h. The mixture was stirred under a H_2 atmosphere for 16 h. Upon completion, the mixture was sparged with argon and concentrated in vacuo. The resultant crude product was further purified by flash column chromatography (silica gel, Hexanes/EtOAc, 12:1) to give the desired **enone 158** (24 mg, 95% yield) as a colorless oil.

158:

^{1}H NMR (500 MHz, $CDCl_3$) δ 6.83 (d, *J* = 9.9 Hz, 1H), 5.91 (d, *J* = 10.0 Hz, 1H), 5.48 (s, 1H), 2.98 – 2.86 (m, 1H), 2.74 (t, *J* = 8.9 Hz, 1H), 2.34 (d, *J* = 7.9 Hz, 1H), 2.23 (d, *J* = 15.3 Hz, 1H), 2.18 (d, *J* = 13.0 Hz, 1H), 2.16 – 2.12 (m, 1H), 2.08 (dd, *J* = 14.4, 8.4 Hz, 1H), 1.95 – 1.86 (m, 1H), 1.76 (s, 3H), 1.71 (q, *J* = 9.4, 9.0 Hz, 1H), 1.53 – 1.49 (m, 1H), 1.18 (dd, *J* = 14.4, 8.7 Hz, 1H), 1.03 (s, 3H), 0.94 (s, 3H), 0.77 (s, 3H).

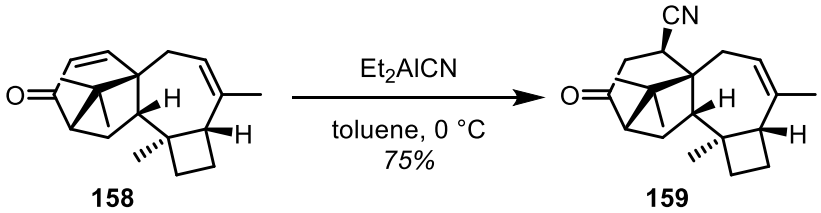

Nitrile 159. To a 5 mL microwave tube was added **158** (11 mg, 0.04 mmol, 1.0 equiv.) in toluene (0.5 mL) and the mixture was cooled to 0 °C. Et_2AlCN (1.0 M in toluene, 160 µL, 0.16 mmol, 4.0 equiv.) was then added dropwise. The mixture was stirred at 0 °C for 4 h. Upon completion, the reaction was quenched by addition of aqueous Rochelle salt and stirred at 25 °C for 1 h. The contents were transferred to a separatory funnel, diluting with EtOAc (5 mL). The layers were separated, and the aqueous layer was further extracted with EtOAc (3 × 5 mL). The combined organic layers were dried over Na_2SO_4 and concentrated in vacuo. The resultant crude product was further purified by flash column chromatography (silica gel, Hexanes/EtOAc, 9:1) to give the desired **nitrile 159** (8.9 mg, 75% yield) as a white solid.

159:

^{1}H NMR (500 MHz, $CDCl_3$) δ 5.60 (ddt, *J* = 8.3, 5.3, 1.8 Hz, 1H), 3.68 (dd, *J* = 11.5, 1.2 Hz, 1H), 3.05 – 2.96 (m, 1H), 2.81 – 2.72 (m, 2H), 2.55 – 2.49 (m, 1H), 2.49 – 2.44 (m, 1H), 2.39 – 2.32 (m, 2H), 2.23 (dtd, *J* = 12.1, 10.1, 7.3 Hz, 1H), 2.05 – 1.90 (m, 3H), 1.80 (q, *J* = 1.5 Hz, 3H), 1.74 – 1.67 (m, 1H), 1.30 (dd, *J* = 10.3, 1.2 Hz, 1H), 1.19 (d, *J* = 0.9 Hz, 3H), 1.18 (s, 3H), 1.11 (s, 3H).

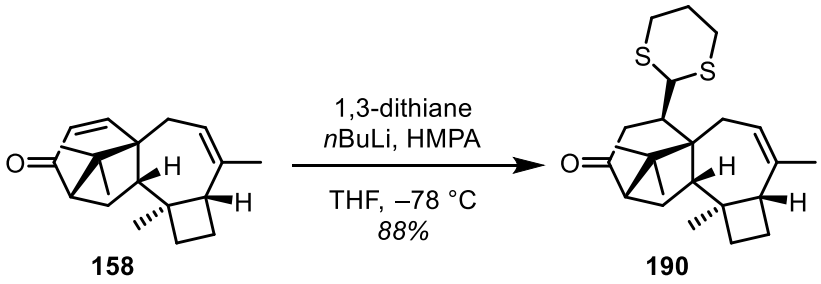

Ketone 190. To a flame-dried 10 mL flask was added 1,3-dithiane (43 mg, 0.356 mmol, 4.0 equiv.) and THF (1.8 mL) and the mixture was cooled to –78 °C. *n*BuLi (1.6 M in hexanes, 222 µL, 0.356 mmol, 4.0 equiv.) was added dropwise and the mixture was warmed to –35 °C and stirred for 1 hour. Then the mixture was cooled to –78 °C. HMPA (185 µL, 1.07 mmol, 12.0 equiv.) was added dropwise and the mixture was stirred for 1 h. **158** (24 mg, 0.089 mmol, 1.0 equiv.) in THF (1 mL) was added dropwise at –78 °C and continued to stir at that temperature. Upon completion, the reaction was quenched by the addition of aqueous NH_4Cl (2 mL) and the contents transferred to a separatory funnel, diluting with EtOAc (5 mL). The layers were separated, and the aqueous layer was further extracted with EtOAc (3 × 5 mL). The combined organic layers were dried over Na_2SO_4 and concentrated in vacuo. The resultant crude product was further purified by flash column chromatography (silica gel, Hexanes/EtOAc, 12:1) to give the desired **ketone 158** (30.8 mg, 88% yield), as a white solid.

158:

^{1}H NMR (400 MHz, $CDCl_3$) δ 5.53 (ddt, *J* = 8.4, 4.4, 2.1 Hz, 1H), 4.66 (d, *J* = 3.0 Hz, 1H), 3.00 (ddd, *J* = 14.2, 12.4, 2.6 Hz, 1H), 2.95 – 2.79 (m, 5H), 2.73 (dd, *J* = 11.1, 6.3 Hz, 1H), 2.67 (d, *J* = 7.0 Hz, 1H), 2.63 – 2.54 (m, 2H), 2.51 (dd, *J* = 11.4, 9.5 Hz, 1H), 2.25 – 2.14 (m, 3H), 2.08 – 1.98 (m, 2H), 1.94 – 1.84 (m, 2H), 1.74 (q, *J* = 1.6 Hz, 3H), 1.64 (td, *J* = 9.8, 7.0 Hz, 1H), 1.53 (ddd, *J* = 9.9, 7.4, 1.1 Hz, 1H), 1.16 (s, 3H), 1.09 (s, 3H), 1.04 (s, 3H).

^{13}C NMR (101 MHz, $CDCl_3$) δ 212.47, 141.33, 120.64, 61.89, 58.76, 52.34, 51.19, 50.42, 46.27, 43.55, 39.71, 37.54, 35.35, 32.85, 31.39, 29.50, 26.69, 25.48, 23.92, 23.79, 22.13, 20.98, 15.10.

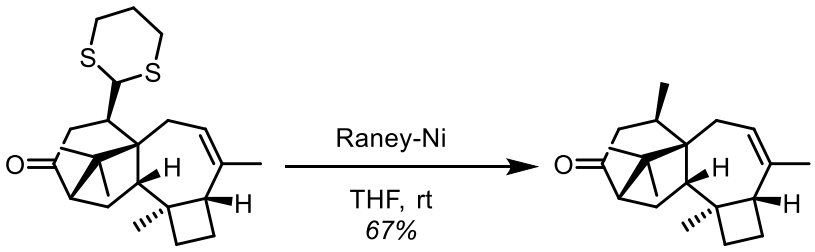

190 **177**

Ketone 177. To a 25 mL flask was added **158** (30.8 g, 0.079 mmol, 1.0 equiv.) and THF (1.6 mL). Raney-Ni W-2, washed sequentially with H_2O (3 × 5 mL), EtOH (3 × 5 mL), and THF (3 × 5 mL), as a suspension in THF (3 mL) was then added in one portion. The suspension was stirred at 25 °C for 0.5 h (*Note*: more Raney-Ni was added, as needed). Upon completion of the reaction, the suspension was filtered through a pad of celite. The filter cake was washed with EtOAc (3 × 10 mL) and the filtrate was concentrated in vacuo. The resultant crude product was further purified by flash column chromatography (silica gel, Hexanes/EtOAc, 12:1) to give the desired **ketone 177** (15.1 mg, 67% yield) as a colorless oil.

177:

^{1}H NMR (500 MHz, $CDCl_3$) δ 5.45 – 5.39 (m, 1H), 3.04 – 2.98 (m, 1H), 2.81 (dd, *J* = 17.9, 11.2 Hz, 1H), 2.68 (d, *J* = 10.8 Hz, 1H), 2.64 (d, *J* = 9.0 Hz, 1H), 2.26 – 2.14 (m, 4H), 1.98 – 1.86 (m, 4H), 1.76 (d, *J* = 1.2 Hz, 3H), 1.65 (dd, *J* = 9.9, 7.0 Hz, 1H), 1.31 (d, *J* = 2.5 Hz, 1H), 1.23 (d, *J* = 0.9 Hz, 3H), 1.07 (d, *J* = 7.5 Hz, 3H), 1.05 (s, 3H), 1.00 (s, 3H).

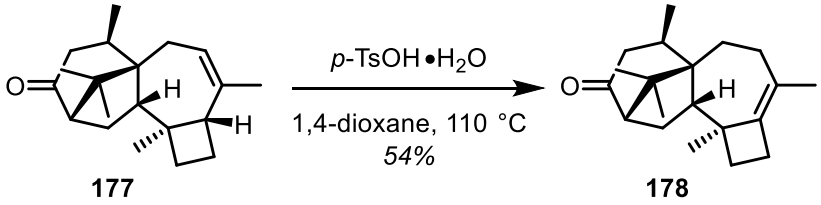

177 **178**

Ketone 178. To a flame-dried 1-dram vial was added **177** (22 mg, 0.077 mmol, 1.0 equiv.), 1,4-dioxane (1.5 mL) and *p*-TsOH•H_2O (14.5 mg, 0.077 mmol, 1.0 equiv.). The vial was sealed and the mixture was heated at 110 °C for 24 h. The reaction was quenched by the addition of aqueous NH_4Cl (2 mL) and the contents transferred to a separatory funnel, diluting with Et_2O (5 mL). The layers were separated, and the aqueous layer was further extracted with Et_2O (3 × 5 mL). The combined organic layers were washed with brine (10 mL), then dried over Na_2SO_4 and concentrated in vacuo. The resultant crude product was further purified by flash column chromatography (silica gel, Hexanes/EtOAc, 19:1) to give the desired **ketone 177** (11.9 mg, 54% yield) as a colorless oil.

178:

^{1}H NMR (500 MHz, $CDCl_3$) δ 2.90 – 2.79 (m, 1H), 2.78 – 2.61 (m, 2H), 2.59 – 2.48 (m, 1H), 2.44 (dd, *J* = 11.5, 9.3 Hz, 2H), 2.33 – 2.22 (m, 2H), 2.20 (d, *J* = 7.8 Hz, 1H), 2.01 (s, 1H), 1.98 – 1.93 (m, 1H), 1.94 – 1.86 (m, 2H), 1.83 – 1.75 (m, 2H), 1.74 – 1.69 (m, 1H), 1.57 (d, *J* = 1.6 Hz, 3H), 1.40 (s, 2H), 1.07 (d, *J* = 7.3 Hz, 3H), 0.95 (d, *J* = 1.9 Hz, 6H).

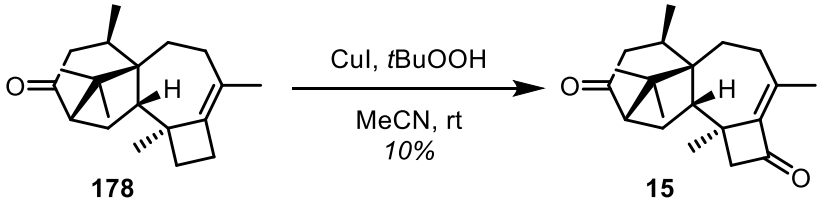

178 **15**

Harziandione (15). To a flame-dried 5 mL microwave tube was added **178** (2 mg, 0.007 mmol, 1.0 equiv.), MeCN (0.3 mL) and CuI (270 µg, 0.014 mmol, 0.2 equiv.). *t*BuOOH (14 µL, 0.07 mmol, 10.0 equiv.) was added and the reaction was stirred at room temperature for 16 h. Once complete, the mixture was diluted with Et_2O (2 mL) and the reaction was quenched by the addition of aqueous $NaHSO_3$ (1 mL) and the contents transferred to a separatory funnel, diluting with Et_2O (2 mL) and H_2O. The layers were separated, and the aqueous layer was further extracted with Et_2O (3 × 2 mL). The combined organic layers were washed with brine (5 mL), then dried over Na_2SO_4 and concentrated in vacuo. The resultant crude product was further purified by flash column chromatography (silica gel, pentane → pentane/EtOAc, 2:1) to give the desired **harziandione (15)** (0.2 mg, 10% yield) as a colorless oil.

Harziandione (15):

^{1}H NMR (500 MHz, $CDCl_3$) δ 2.97 – 2.86 (m, 2H), 2.57 (d, *J* = 16.3 Hz, 1H), 2.49 – 2.40 (m, 3H), 2.27 (d, *J* = 7.9 Hz, 1H), 2.22 (t, *J* = 7.6 Hz, 1H), 2.13 (s, 3H), 2.11 – 1.96 (m, 4H), 1.91 (dd, *J* = 13.6, 6.4 Hz, 1H), 1.52 (s, 3H), 1.12 (d, *J* = 7.1 Hz, 3H), 1.00 (s, 3H), 0.98 (s, 3H).

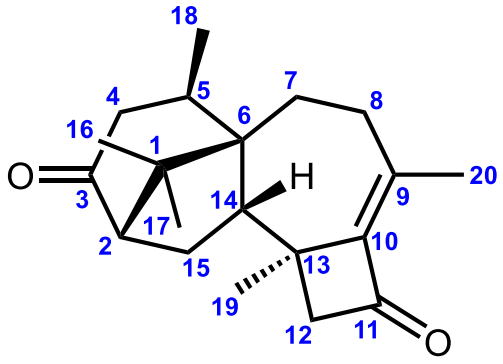

harziandione (**15**)

C#	lit.	lit. Multipl. (Hz)	Synthetic **15**	Synthetic **15** Multip. (Hz), if measurable	Difference ($ppm_{lit.}$ – $ppm_{synth.}$)
1	-				
2	2.30	ddd (8, 1, 1)	2.28	br d (7.9)	0.02
3	-				
4α	2.05	ddd (18, 1, 1)	2.06	unclear	-0.01
4					
4β	2.90	dd (18, 11)	2.90	unclear	0
5	2.95	ddq (1, 11, 7.2)	2.93	unclear	0.02
6	-				
7α	1.90	ddd (14, 6.5, 1)	1.91	dd (13.9, 6.2)	-0.01
7					
7β	1.44	m	1.43	unclear	0.01
8α	2.45	ddd (14, 12, 1)	2.43	unclear	0.02
8					
8β	2.00	m	2.00	m	0
9	-				
10	-				
11	-				
12α	2.45	dq (16, 1)	2.44	d (16.4)	0.01
12					
12β	2.58	dq (16, 1)	2.57	d (16.3)	0.01
13	-				
14	2.50	dd (13, 10)	2.48	dd (11.1, 9.5)	0.02
15α	1.55	ddd (13, 10, 1)	(H_2O)	-	
15					
15β	2.03	ddd (13, 13, 8)	2.03	unclear	0
16	1.00	br s	1.00	s	0
17	0.99	br s	0.98	s	0.01
18	1.12	d (7.2)	1.12	d (7.0)	0
19	1.52	br s	1.52	s	0
20	2.12	br s	2.13	br s	-0.01

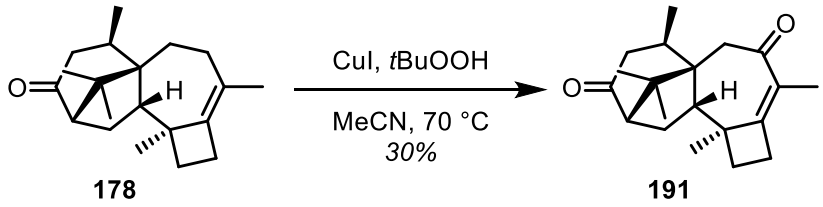

178 191

Enone 191. To a flame-dried 5 mL microwave tube was added **178** (6 mg, 0.021 mmol, 1.0 equiv.), MeCN (0.3 mL) and CuI (270 µg, 0.014 mmol, 0.2 equiv.). *t*BuOOH (14 µL, 0.07 mmol, 10.0 equiv.) was added and the reaction was heated at 70 °C for 16 h. Once complete, the mixture was diluted with Et_2O (2 mL) and the reaction was quenched by the addition of aqueous $NaHSO_3$ (1 mL) and the contents transferred to a separatory funnel, diluting with Et_2O (2 mL) and H_2O. The layers were separated, and the aqueous layer was further extracted with Et_2O (3 × 2 mL). The combined organic layers were washed with brine (5 mL), then dried over Na_2SO_4 and concentrated in vacuo. The resultant crude product was further purified by flash column chromatography (silica gel, pentane → pentane/EtOAc, 2:1) to give the desired **enone 191** (1.9 mg, 30% yield) as a colorless oil.

191:

^{1}H NMR (500 MHz, $CDCl_3$) δ 3.07 – 2.97 (m, 1H), 2.89 (dd, *J* = 18.6, 11.6 Hz, 1H), 2.76 (dt, *J* = 14.4, 3.3 Hz, 1H), 2.34 (s, 1H), 2.33 (d, *J* = 7.9 Hz, 1H), 2.28 – 2.18 (m, 2H), 2.12 (d, *J* = 11.3 Hz, 1H), 2.10 – 2.02 (m, 2H), 2.01 – 1.87 (m, 2H), 1.72 (d, *J* = 1.3 Hz, 3H), 1.35 (s, 3H), 1.19 (d, *J* = 7.5 Hz, 3H), 1.02 (s, 3H), 0.96 (s, 3H).

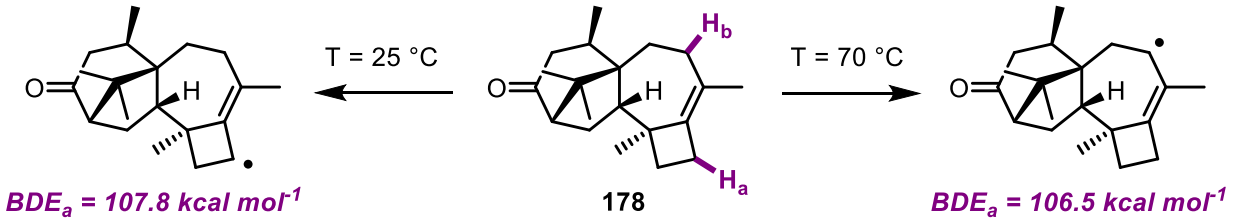

Opt energies:
Ground State molecule: -536629.7532 kJ/mol
4 membered abstraction: -536230.7403 kJ/mol
7 membered abstraction: -536236.1454 kJ/mol
Methyl Abstraction: -536231.8733 kJ/mol
BDEs:
4 membered ring: 451.0129179 kJ/mol
7 membered ring: 445.6077584 kJ/mol
Methyl: 449.8798983 kJ/mol

DFT optimizations were performed by Julia Noel through Gaussian 16 on the Midway2 Cluster at the University of Chicago's Research Computing Center. Ground state geometry optimizations were determined using the B3LYP/cc-pVDZ level of theory in the gas phase at 298K. In some instances, final free energies (kcal/mol) were determined through a single point calculation using the B3LYP/cc-pVTZ level of theory in the gas phase at 298K and are denoted as such. All ground state structures display no imaginary frequencies, and the free energies are zero-point energy corrected.

<u>4 membered ring abstracted</u>

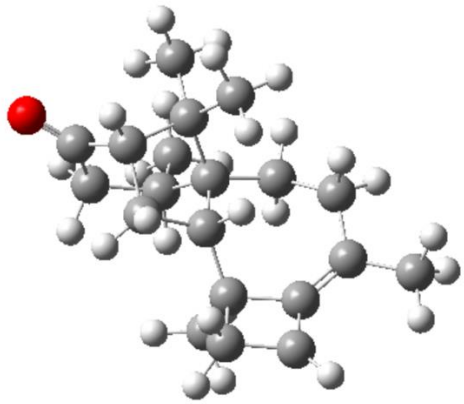

Zero-point correction= 0.442848 (Hartree/Particle)
Thermal correction to Energy= 0.463386
Thermal correction to Enthalpy= 0.464330
Thermal correction to Gibbs Free Energy= 0.396402

Sum of electronic and zero-point Energies= -854.294723
Sum of electronic and thermal Energies= -854.274185
Sum of electronic and thermal Enthalpies= -854.273241
Sum of electronic and thermal Free Energies= -854.341169

0 2

C	2.60900000	-0.99500000	1.52100000
C	1.67800000	-0.10900000	0.75400000
C	4.05600000	-1.08400000	1.05600000
C	4.03800000	-1.33500000	-0.48400000
C	2.34500000	1.24400000	0.44700000
H	0.66700000	-0.01900000	1.20800000
H	1.50900000	-0.60800000	-0.22000000
C	3.91400000	1.10800000	0.07300000
C	4.16700000	0.09000000	-1.08700000
H	3.15000000	-1.91800000	-0.80700000
H	4.92000000	-1.93800000	-0.80000000
C	3.76000000	0.45500000	-2.54500000
H	5.25700000	0.10100000	-1.21300000
C	4.38300000	2.54400000	-0.35300000
C	4.81400000	1.28400000	-3.18500000
C	5.62300000	2.78100000	-1.24200000
H	3.57100000	3.01000000	-0.95000000
H	4.49100000	3.15400000	0.56800000
C	5.65200000	2.23500000	-2.67800000
H	5.68600000	3.88700000	-1.33800000
H	6.54600000	2.45700000	-0.72400000
C	4.15400000	-0.57300000	-3.65300000
C	4.95600000	0.51200000	-4.43500000
H	4.89400000	-1.29500000	-3.23400000
H	3.35200000	-1.10700000	-4.20700000
H	4.36900000	1.02000000	-5.23000000
C	4.70600000	0.32700000	1.23400000
C	4.55000000	0.85800000	2.68800000
H	3.54300000	0.74000000	3.10700000
H	4.88200000	1.91500000	2.76100000
H	5.16000000	0.25400000	3.39500000
C	6.26600000	0.24300000	1.06500000
H	6.66800000	-0.24000000	0.15800000
H	6.70100000	-0.37900000	1.87700000
H	6.71800000	1.25100000	1.15600000
C	2.34700000	0.98800000	-2.84400000
H	2.19300000	1.99800000	-2.42600000

H	1.58100000	0.27600000	-2.47400000
H	2.18600000	1.11600000	-3.93700000
C	1.95000000	2.32800000	1.48700000
H	2.28300000	2.19200000	2.51900000
H	0.84100000	2.38700000	1.54500000
H	2.28900000	3.33200000	1.16100000
H	1.78900000	1.62700000	-0.41800000
O	2.21800000	-1.62200000	2.49300000
H	4.55500000	-1.88700000	1.64300000
C	6.78800000	2.76000000	-3.52700000
H	6.69800000	3.86300000	-3.61900000
H	6.80300000	2.34300000	-4.55400000
H	7.75600000	2.51800000	-3.04100000

Starting Opt.

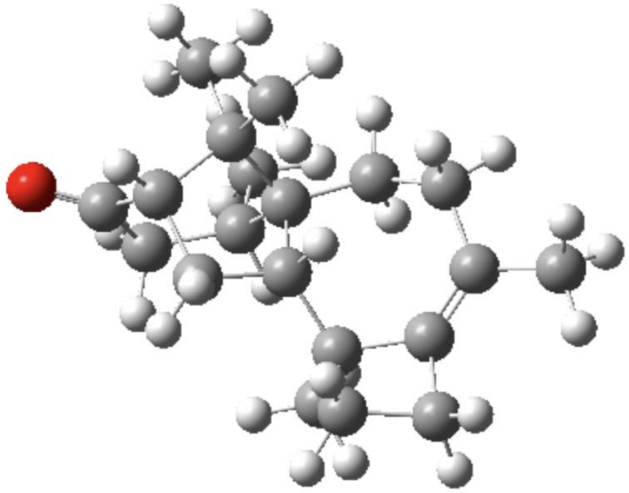

Zero-point correction= 0.456924 (Hartree/Particle)

Thermal correction to Energy= 0.477314

Thermal correction to Enthalpy= 0.478258

Thermal correction to Gibbs Free Energy= 0.411476

Sum of electronic and zero-point Energies= -854.928434

Sum of electronic and thermal Energies= -854.908044

Sum of electronic and thermal Enthalpies= -854.907100

Sum of electronic and thermal Free Energies= -854.973883

0 1

C	2.60900000	-0.99500000	1.52100000
C	1.67800000	-0.10900000	0.75400000
C	4.05600000	-1.08400000	1.05600000
C	4.03800000	-1.33500000	-0.48400000
C	2.34500000	1.24400000	0.44700000
H	0.66700000	-0.01900000	1.20800000
H	1.50900000	-0.60800000	-0.22000000
C	3.91400000	1.10800000	0.07300000
C	4.16700000	0.09000000	-1.08700000
H	3.15000000	-1.91800000	-0.80700000
H	4.92000000	-1.93800000	-0.80000000
C	3.76000000	0.45500000	-2.54500000
H	5.25700000	0.10100000	-1.21300000
C	4.38300000	2.54400000	-0.35300000
C	4.81400000	1.28400000	-3.18500000
C	5.62300000	2.78100000	-1.24200000
H	3.57100000	3.01000000	-0.95000000
H	4.49100000	3.15400000	0.56800000
C	5.65200000	2.23500000	-2.67800000
H	5.68600000	3.88700000	-1.33800000
H	6.54600000	2.45700000	-0.72400000
C	4.15400000	-0.57300000	-3.65300000

C	4.95600000	0.51200000	-4.43500000
H	4.89400000	-1.29500000	-3.23400000
H	3.35200000	-1.10700000	-4.20700000
H	5.96700000	0.13900000	-4.70800000
H	4.36900000	1.02000000	-5.23000000
C	4.70600000	0.32700000	1.23400000
C	4.55000000	0.85800000	2.68800000
H	3.54300000	0.74000000	3.10700000
H	4.88200000	1.91500000	2.76100000
H	5.16000000	0.25400000	3.39500000
C	6.26600000	0.24300000	1.06500000
H	6.66800000	-0.24000000	0.15800000
H	6.70100000	-0.37900000	1.87700000
H	6.71800000	1.25100000	1.15600000
C	2.34700000	0.98800000	-2.84400000
H	2.19300000	1.99800000	-2.42600000
H	1.58100000	0.27600000	-2.47400000
H	2.18600000	1.11600000	-3.93700000
C	1.95000000	2.32800000	1.48700000
H	2.28300000	2.19200000	2.51900000
H	0.84100000	2.38700000	1.54500000
H	2.28900000	3.33200000	1.16100000
H	1.78900000	1.62700000	-0.41800000
O	2.21800000	-1.62200000	2.49300000
H	4.55500000	-1.88700000	1.64300000
C	6.78800000	2.76000000	-3.52700000
H	6.69800000	3.86300000	-3.61900000
H	6.80300000	2.34300000	-4.55400000

H	7.75600000	2.51800000	-3.04100000

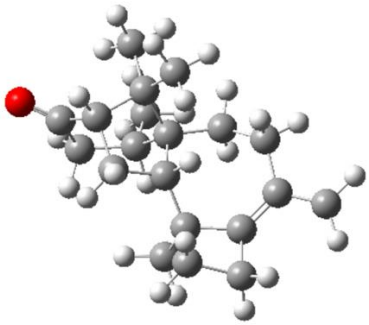

Methyl abstraction:

Zero-point correction= 0.444003 (Hartree/Particle)
Thermal correction to Energy= 0.464039
Thermal correction to Enthalpy= 0.464983
Thermal correction to Gibbs Free Energy= 0.398263
Sum of electronic and zero-point Energies= -854.296626
Sum of electronic and thermal Energies= -854.276590
Sum of electronic and thermal Enthalpies= -854.275646
Sum of electronic and thermal Free Energies= -854.342366

0 2

C	2.40100000	-0.94100000	2.47500000
C	1.49800000	0.07800000	1.85400000
C	3.76900000	-1.16400000	1.84500000
C	3.55500000	-1.33400000	0.30900000
C	2.27700000	1.36400000	1.52500000
H	0.56000000	0.25400000	2.42300000
H	1.16800000	-0.35100000	0.88800000
C	3.77000000	1.07700000	0.96800000
C	3.77700000	0.09800000	-0.25100000
H	2.57700000	-1.80000000	0.06800000
H	4.32400000	-2.01200000	-0.12800000
C	3.25500000	0.57200000	-1.63900000
H	4.84100000	-0.00200000	-0.50100000
C	4.35100000	2.47400000	0.54800000
C	4.31300000	1.32800000	-2.35700000

C	5.50700000	2.61900000	-0.46600000
H	3.53700000	3.05500000	0.06500000
H	4.62700000	3.02100000	1.47400000
C	5.30300000	2.14600000	-1.91100000
H	5.68900000	3.71400000	-0.52900000
C	3.42700000	-0.42900000	-2.82500000
C	4.24400000	0.61700000	-3.64600000
H	4.13400000	-1.23800000	-2.52200000
H	2.52200000	-0.85700000	-3.30800000
H	5.18500000	0.18000000	-4.04500000
C	4.59100000	0.15800000	2.00100000
C	4.65600000	0.62800000	3.48200000
H	3.69400000	0.59900000	4.00900000
H	5.11200000	1.63800000	3.55700000
H	5.26700000	-0.07300000	4.09100000
C	6.10300000	-0.08700000	1.65200000
H	6.34500000	-0.56400000	0.68700000
H	6.55000000	-0.79300000	2.38400000
H	6.67400000	0.86000000	1.72900000
C	1.88000000	1.25500000	-1.75600000
H	1.87900000	2.25300000	-1.28500000
H	1.09000000	0.60400000	-1.33000000
H	1.61600000	1.45200000	-2.81800000
C	2.12400000	2.43100000	2.64300000
H	2.54900000	2.20700000	3.62400000
H	1.04200000	2.60600000	2.83000000
H	2.53700000	3.40700000	2.31900000
H	1.67700000	1.84900000	0.74400000
O	2.05000000	-1.57100000	3.46100000
H	4.23500000	-2.04400000	2.34100000
C	6.36700000	2.54600000	-2.89000000
H	6.40500000	3.65100000	-2.98300000
H	7.35500000	2.16200000	-2.55900000
H	6.43700000	2.16600000	-0.07400000
H	3.62500000	1.21800000	-4.34700000

7 Membered ring

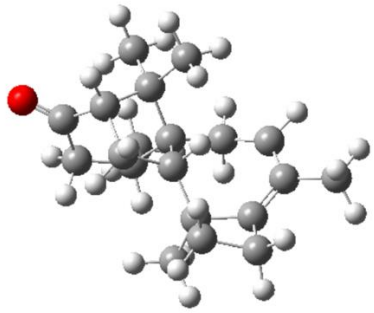

Zero-point correction= 0.443182 (Hartree/Particle)

Thermal correction to Energy= 0.463758

Thermal correction to Enthalpy= 0.464702

Thermal correction to Gibbs Free Energy= 0.396579

Sum of electronic and zero-point Energies= -854.303312

Sum of electronic and thermal Energies= -854.282737

Sum of electronic and thermal Enthalpies= -854.281793

Sum of electronic and thermal Free Energies= -854.349916

0 2

C	2.04700000	-1.18500000	2.58000000
C	1.32000000	-0.01800000	1.98900000
C	3.38600000	-1.57700000	1.97200000
C	3.19700000	-1.64600000	0.42500000
C	2.28600000	1.15500000	1.74100000
H	0.40100000	0.26800000	2.54500000
H	0.96000000	-0.35100000	0.99700000
C	3.73600000	0.67800000	1.20500000
C	3.64200000	-0.24100000	-0.06100000
H	2.16800000	-1.95300000	0.13900000
H	3.87100000	-2.41000000	-0.02600000

C	3.23400000	0.36200000	-1.43700000
H	4.68600000	-0.48200000	-0.29600000
C	4.52600000	1.99100000	0.86500000
C	4.39700000	1.00500000	-2.10200000
C	5.70900000	1.96200000	-0.11500000
H	3.83500000	2.71000000	0.38100000
H	4.86300000	2.46300000	1.81100000
C	5.48000000	1.66200000	-1.59700000
H	6.57500000	1.38900000	0.26700000
C	3.29100000	-0.58800000	-2.67400000
C	4.24000000	0.39200000	-3.43500000
H	3.89000000	-1.49200000	-2.40700000
H	2.34600000	-0.88100000	-3.17900000
H	5.10700000	-0.15100000	-3.86900000
H	3.70700000	1.11000000	-4.09400000
C	4.38400000	-0.39700000	2.21000000
C	4.47300000	-0.00800000	3.71400000
H	3.50200000	0.07900000	4.21700000
H	5.06700000	0.92100000	3.84800000
H	4.95900000	-0.81700000	4.30200000
C	5.85500000	-0.84400000	1.88500000
H	6.05500000	-1.30600000	0.90400000
H	6.17300000	-1.64100000	2.59200000
H	6.55500000	0.00500000	2.02400000
C	1.96800000	1.23300000	-1.54300000
H	2.09500000	2.20100000	-1.02800000
H	1.08600000	0.68100000	-1.16000000
H	1.75300000	1.51300000	-2.59700000

C	2.25800000	2.18100000	2.90600000
H	2.61700000	1.85400000	3.88400000
H	1.20800000	2.50600000	3.07700000
H	2.82000000	3.09900000	2.63800000
H	1.78600000	1.75800000	0.97200000
O	1.57900000	-1.80000000	3.52600000
H	3.70500000	-2.53700000	2.43500000
C	6.62200000	2.05300000	-2.50000000
H	6.78400000	3.14900000	-2.42900000
H	6.44100000	1.80900000	-3.56600000
H	7.54700000	1.53200000	-2.17600000

SECTION 3.6: X-RAY CRYSTALLOGRAPHIC DATA

General information: The diffraction data were measured at 100 K on a Bruker D8 VENTURE diffractometer equipped with a microfocus Mo-target X-ray tube (λ = 0.71073 Å) and PHOTON 100 CMOS detector. Data were collected using ω scans to survey a sphere of reciprocal space. Data reduction and integration were performed with the Bruker APEX3 software package (Bruker AXS, version 2017.3-0, 2018). Data were scaled and corrected for absorption effects using the multi-scan procedure as implemented in SADABS (Bruker AXS, version 2014/5, Krause, Herbst-Irmer, Sheldrick & Stalke, *J. Appl. Cryst.* **2015**, *48*, 3-10). The structure was solved by SHELXT (Version 2018/2: Sheldrick, G. M. *Acta Crystallogr*. **2015**, ***A71***, 3-8) and refined by a full-matrix least-squares procedure using OLEX2 (O. V. Dolomanov, L. J. Bourhis, R. J. Gildea, J. A. K. Howard and H. Puschmann. J. Appl. Crystallogr. **2009**, *42*, 339-341) (XL refinement program version 2018/3, Sheldrick, G. M. Acta Crystallogr. **2015**, *C71*, 3-8). Crystallographic data and details of the data collection and structure refinement are listed in Table 1.

Specific details for structure refinement: All atoms were refined with anisotropic thermal parameters. All hydrogen atoms were included in idealized positions for structure factor calculations except the hydrogen atom of the OH group which was found in the difference Fourier map. All structures are drawn with thermal ellipsoids at 50% probability.

Figure 3.5. ORTEP representation of **113**

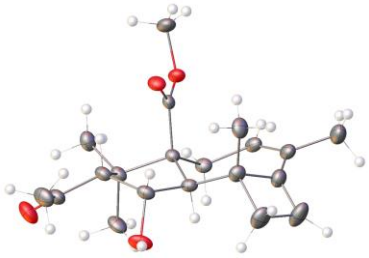

Crystal data and structure refinement for 0975_PG_Snyder_1.

Identification code	0975_PG_Snyder_1
Empirical formula	$C_{20}H_{28}O_4$
Formula weight	332.42
Temperature/K	100(2)
Crystal system	monoclinic
Space group	$P2_1/n$
a/Å	6.5954(4)
b/Å	30.3172(17)
c/Å	9.6045(5)
α/°	90
β/°	108.892(2)
γ/°	90
Volume/Å^3	1817.00(18)
Z	4
ρ_{calc}g/cm^3	1.215
μ/mm^{-1}	0.083
F(000)	720.0
Crystal size/mm^3	0.41 × 0.28 × 0.25
Radiation	MoKα (λ = 0.71073)
2Θ range for data collection/°	4.68 to 59.876
Index ranges	$-9 \le h \le 9$, $-37 \le k \le 38$, $-13 \le l \le 12$
Reflections collected	28131
Independent reflections	4533 [R_{int} = 0.0424, R_{sigma} = 0.0412]
Data/restraints/parameters	4533/0/227
Goodness-of-fit on F^2	1.019
Final R indexes [I>=2σ (I)]	R_1 = 0.0519, wR_2 = 0.1132
Final R indexes [all data]	R_1 = 0.0799, wR_2 = 0.1243
Largest diff. peak/hole / e Å^{-3}	0.55/-0.18

$R_{int} = \Sigma \mid F_o^2 - \langle F_o^2 \rangle \mid / \Sigma \mid F_o^2 \mid$

$R1 = \Sigma \mid \mid F_o \mid - \mid F_c \mid \mid / \Sigma \mid F_o \mid$

$wR2 = [\Sigma [w (F_o^2 - F_c^2)^2] / \Sigma [w (F_o^2)^2]]^{1/2}$

$\text{Goodness-of-fit} = [\Sigma [w (F_o^2 - F_c^2)^2] / (n-p)]^{1/2}$

n: number of independent reflections; p: number of refined parameters

Figure 3.6. ORTEP representation of **130**

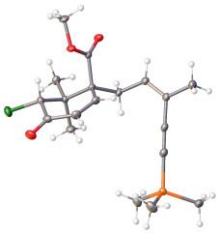

Crystal data and structure refinement for 1065_PG_Snyder2.

Identification code	1065_PG_Snyder2
Empirical formula	$C_{19}H_{27}ClO_3Si$
Formula weight	366.94
Temperature/K	100(2)
Crystal system	triclinic
Space group	P-1
a/Å	9.2270(9)
b/Å	10.4312(10)
c/Å	11.3965(11)
α/°	98.633(2)
β/°	111.403(2)
γ/°	93.143(2)
Volume/Å^3	1002.50(17)
Z	2
ρ_{calc}g/cm^3	1.216
μ/mm^{-1}	0.264
F(000)	392.0
Crystal size/mm^3	0.319 × 0.29 × 0.198
Radiation	MoKα (λ = 0.71073)
2Θ range for data collection/°	4.776 to 60.23
Index ranges	-13 ≤ h ≤ 13, -14 ≤ k ≤ 14, -16 ≤ l ≤ 16
Reflections collected	42750
Independent reflections	5883 [R_{int} = 0.0241, R_{sigma} = 0.0132]
Data/restraints/parameters	5883/0/224
Goodness-of-fit on F^2	1.029
Final R indexes [I>=2σ (I)]	R_1 = 0.0293, wR_2 = 0.0778
Final R indexes [all data]	R_1 = 0.0329, wR_2 = 0.0803
Largest diff. peak/hole / e Å^{-3}	0.46/-0.20

$R_{int} = \Sigma \mid F_o^2 - \langle F_o^2 \rangle \mid / \Sigma \mid F_o^2 \mid$

$R1 = \Sigma \mid \mid F_o \mid - \mid F_c \mid \mid / \Sigma \mid F_o \mid$

$wR2 = [\Sigma [w (F_o^2 - F_c^2)^2] / \Sigma [w (F_o^2)^2]]^{1/2}$

Goodness-of-fit = $[\Sigma [w (F_o^2 - F_c^2)^2] / (n-p)]^{1/2}$

n: number of independent reflections; p: number of refined parameters

SECTION 3.7: ^{1}H AND ^{13}C NMR SPECTRA

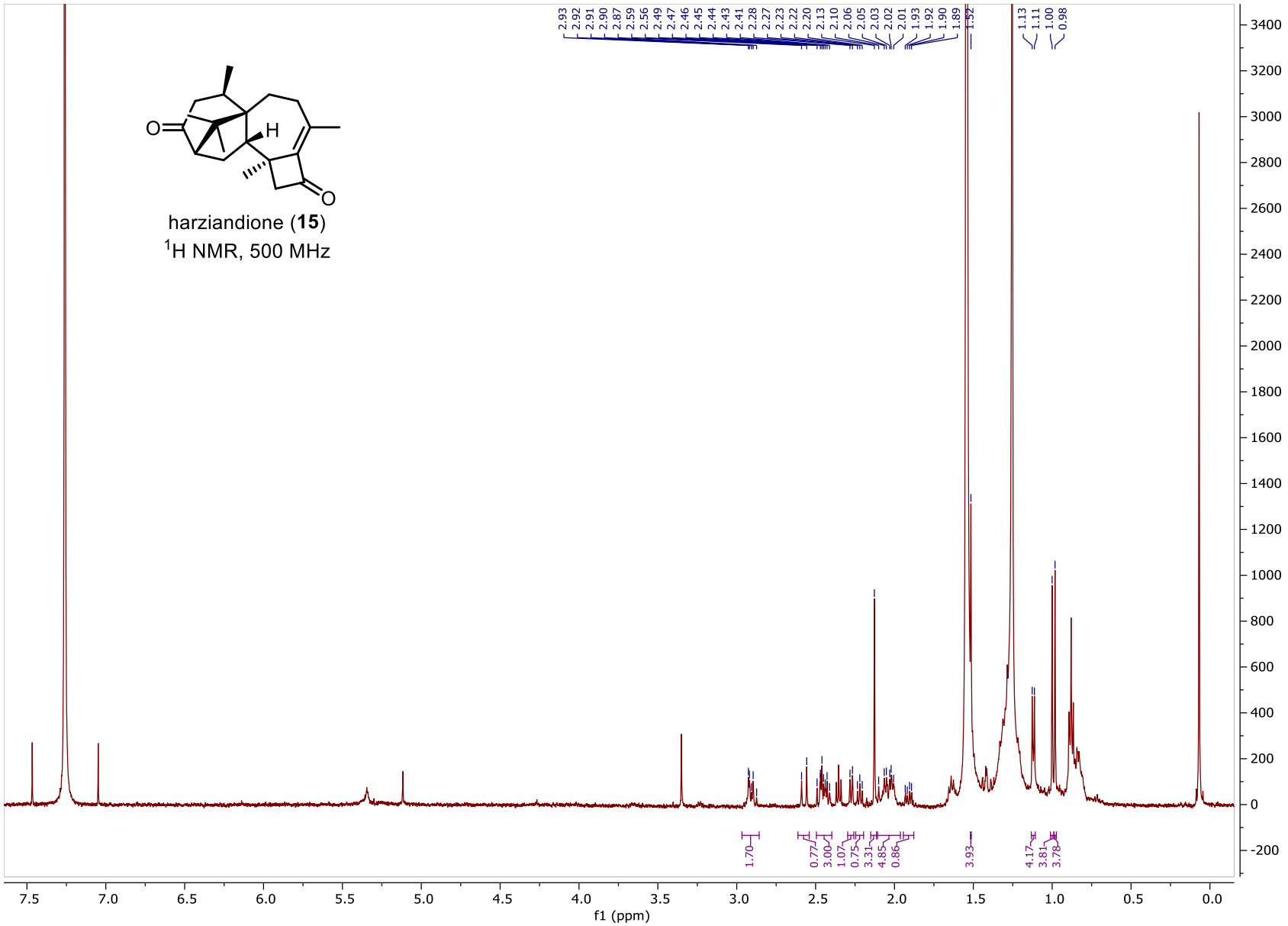
harziandione (15)
1H NMR, 500 MHz
f1 (ppm)

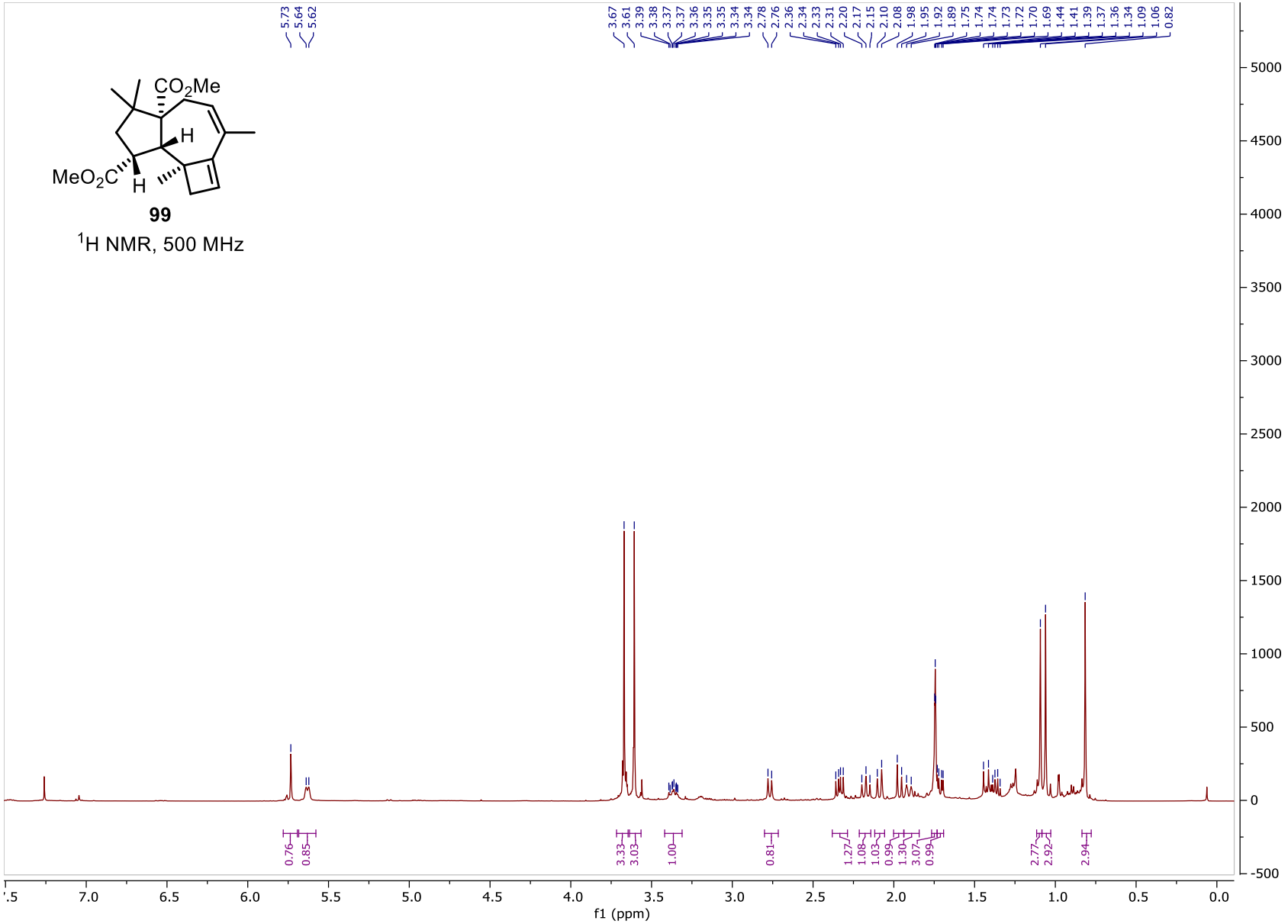
CO2Me
H
MeO2C
H
99
1H NMR, 500 MHz
f1 (ppm)

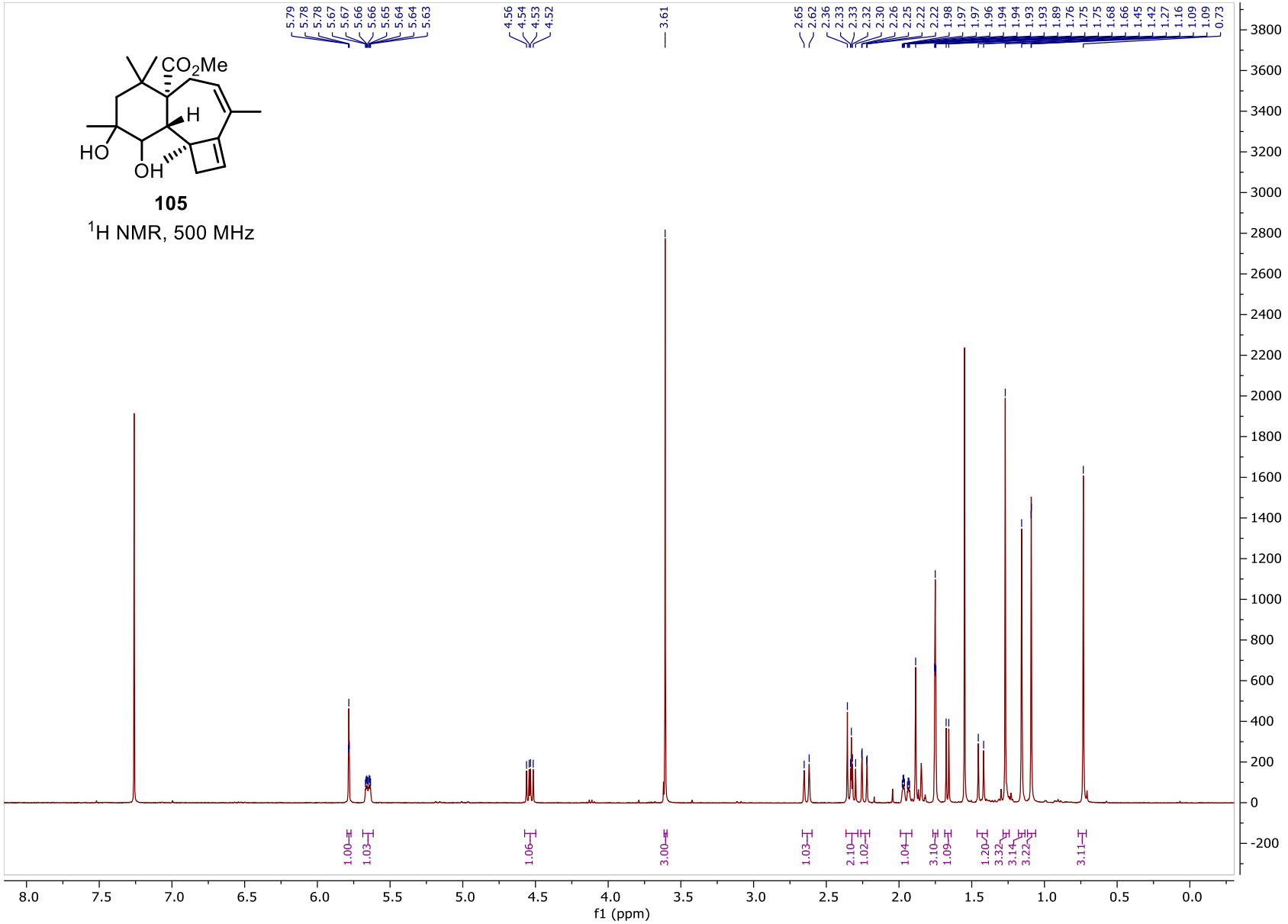
CO2Me
H
HO
OH
105
1H NMR, 500 MHz
f1 (ppm)

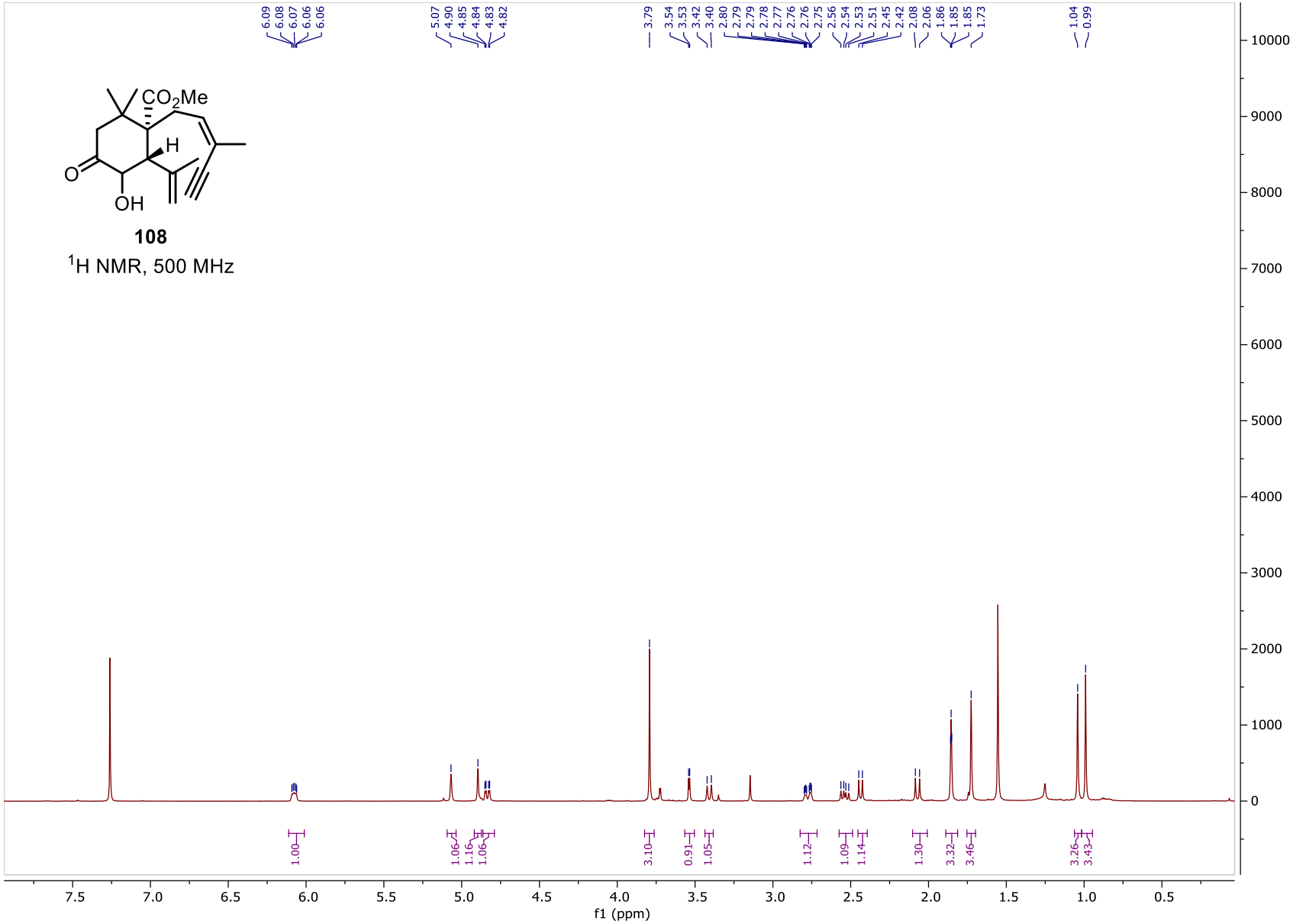
CO2Me
H
O
OH
108
1H NMR, 500 MHz
6.09
6.08
6.07
6.06
6.06
5.07
4.90
4.85
4.84
4.83
4.82
3.79
3.54
3.53
3.42
3.40
2.80
2.79
2.79
2.78
2.77
2.76
2.76
2.75
2.56
2.54
2.53
2.51
2.45
2.42
2.08
2.06
1.86
1.85
1.85
1.73
1.04
0.99
1.00
1.06
1.16
1.06
3.10
0.91
1.05
1.12
1.09
1.14
1.30
3.32
3.46
3.26
3.43
f1 (ppm)

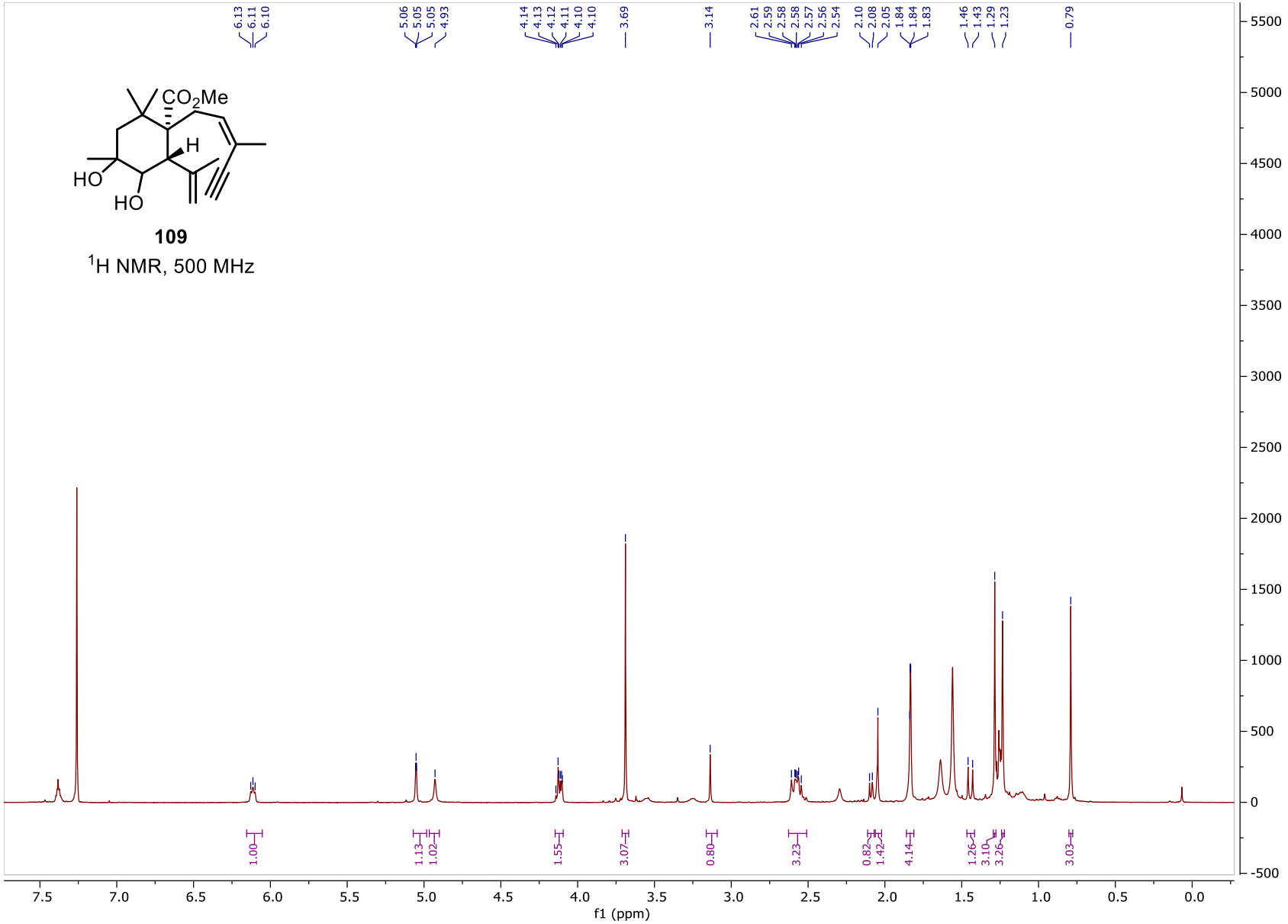
CO2Me
H
HO
HO
109
1H NMR, 500 MHz
f1 (ppm)

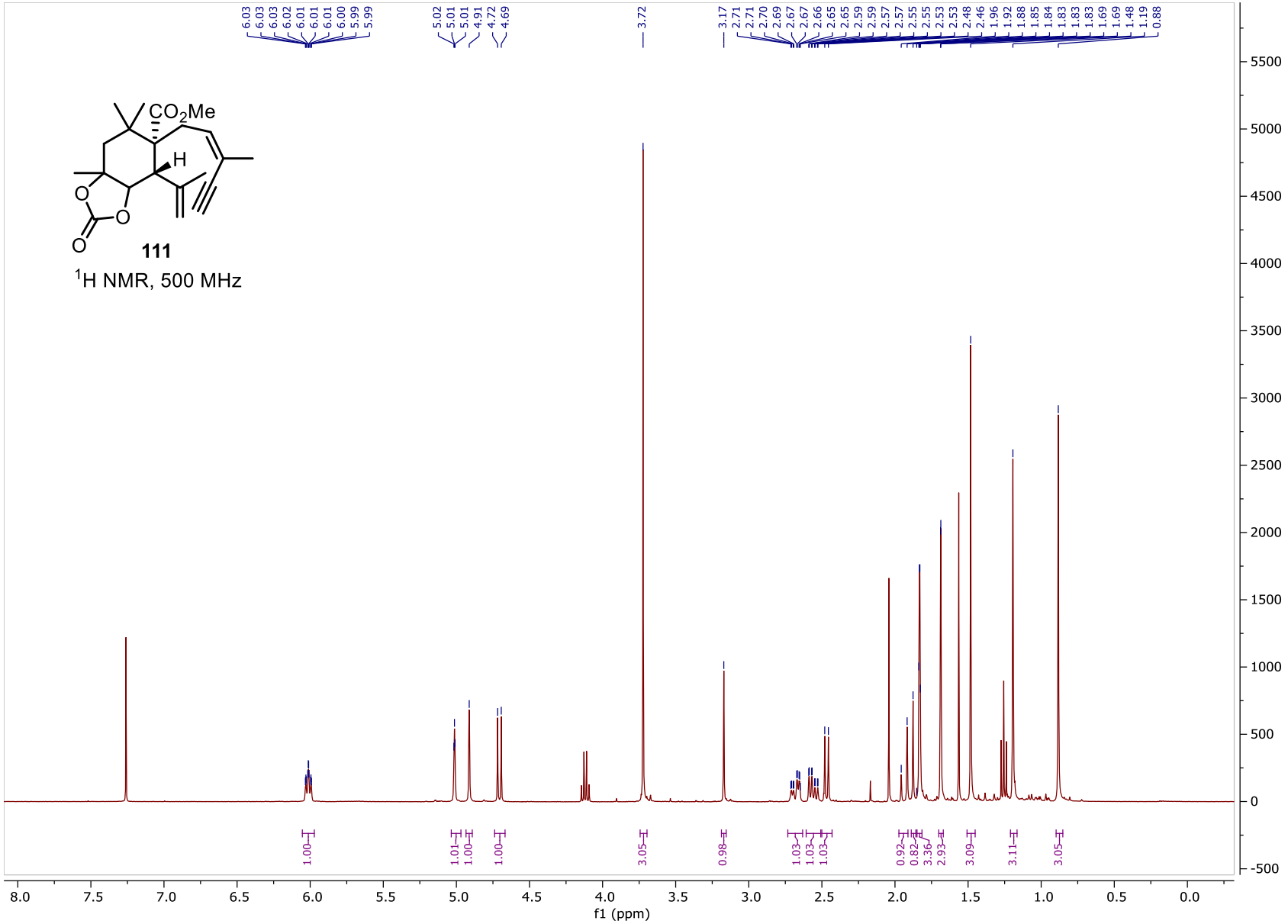
CO2Me
H
O
O
O
111
1H NMR, 500 MHz
f1 (ppm)

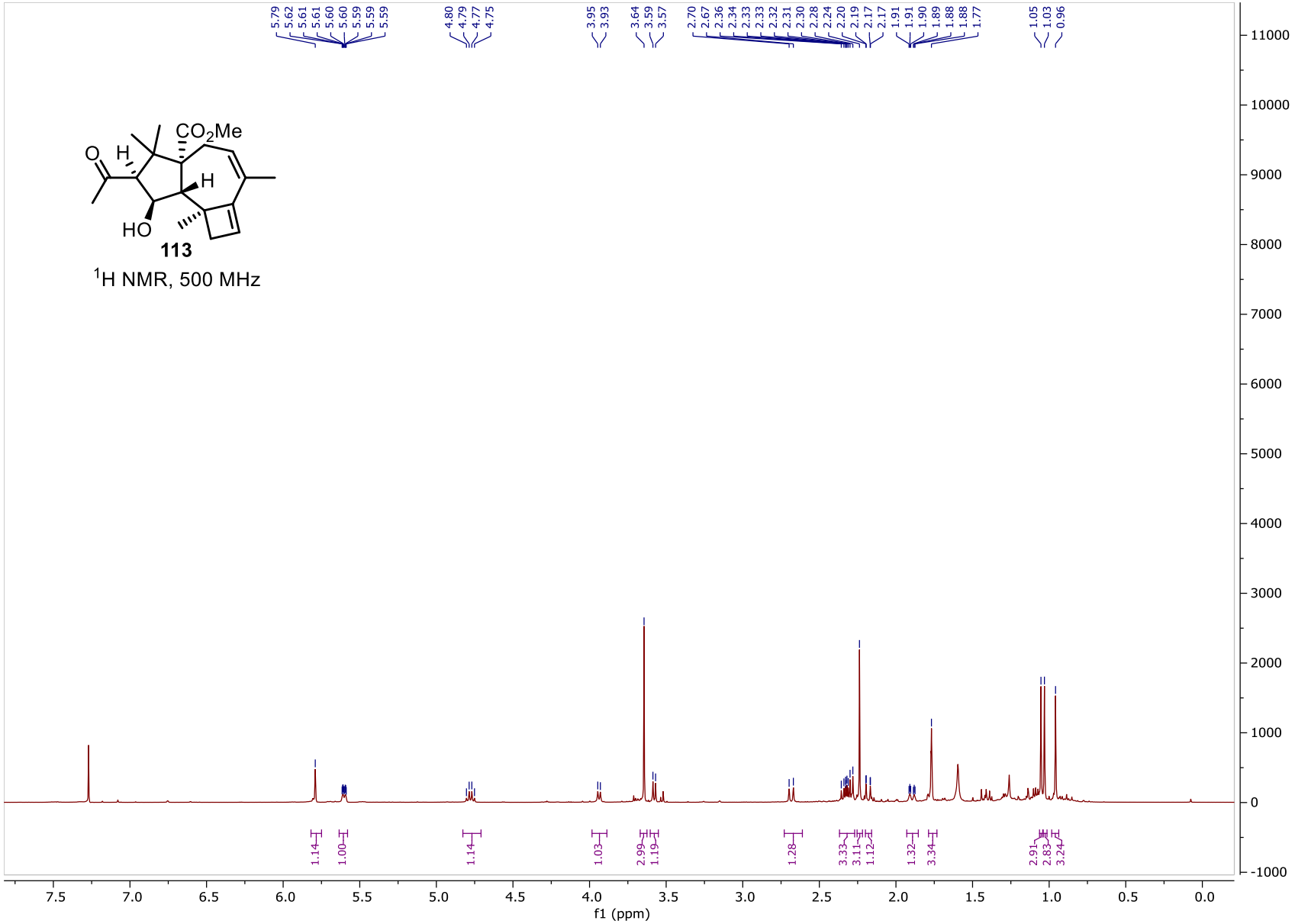
5.79
5.62
5.61
5.61
5.60
5.60
5.59
5.59
5.59
4.80
4.79
4.77
4.75
3.95
3.93
3.64
3.59
3.57
2.70
2.67
2.36
2.34
2.33
2.33
2.32
2.31
2.30
2.28
2.24
2.20
2.19
2.17
2.17
1.91
1.91
1.90
1.89
1.88
1.88
1.77
1.05
1.03
0.96
CO2Me
O
H
H
HO
113
1H NMR, 500 MHz
1.14
1.00
1.14
1.03
2.99
1.19
1.28
3.33
3.11
1.12
1.32
3.34
2.91
2.83
3.24
11000
10000
9000
8000
7000
6000
5000
4000
3000
2000
1000
0
-1000
7.5
7.0
6.5
6.0
5.5
5.0
4.5
4.0
3.5
3.0
2.5
2.0
1.5
1.0
0.5
0.0
f1 (ppm)

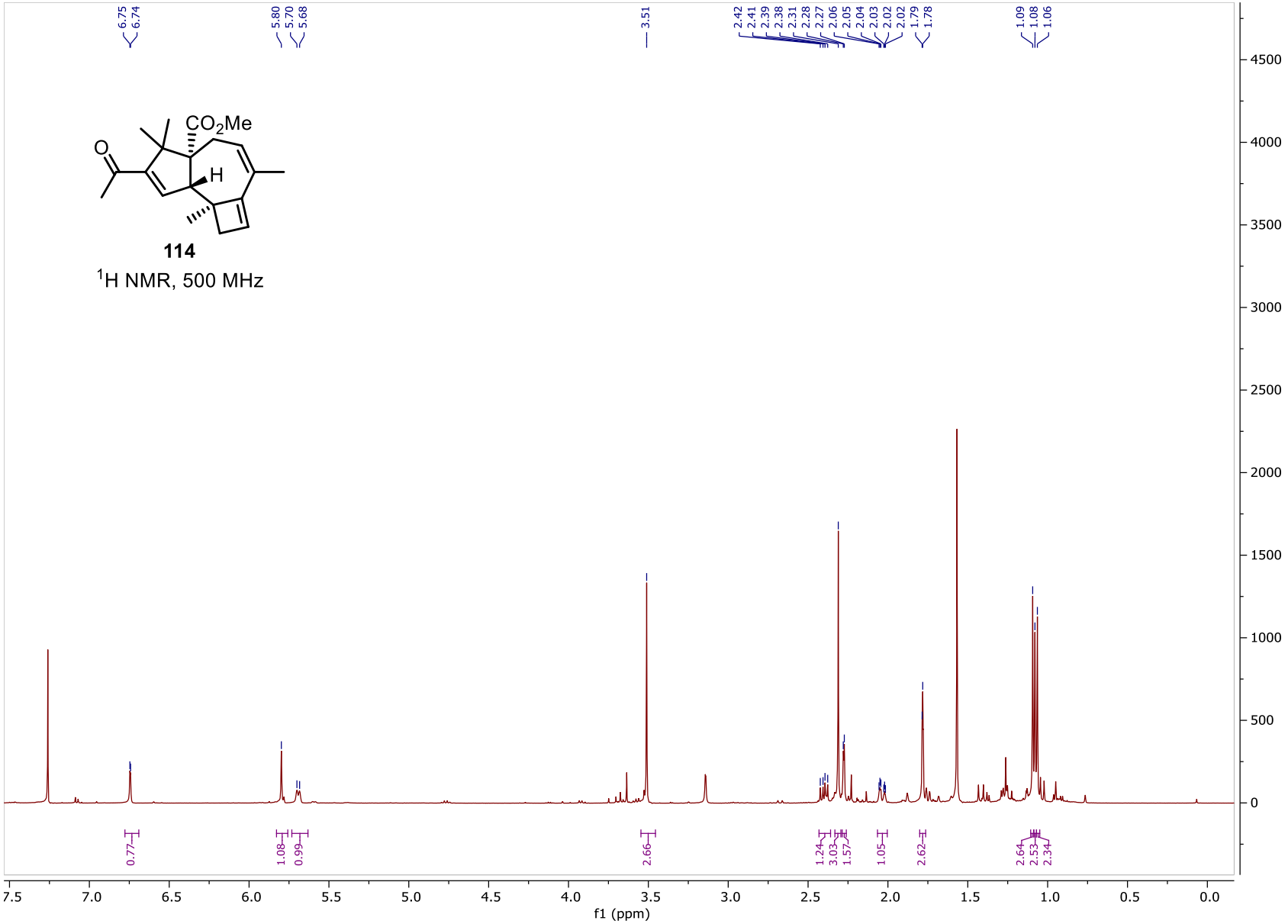
6.75
6.74
5.80
5.70
5.68
3.51
2.42
2.41
2.39
2.38
2.31
2.28
2.27
2.06
2.05
2.04
2.03
2.02
2.02
1.79
1.78
1.09
1.08
1.06
CO2Me
O
H
114
1H NMR, 500 MHz
0.77
1.08
0.99
2.66
1.24
3.03
1.57
1.05
2.62
2.64
2.53
2.34
f1 (ppm)

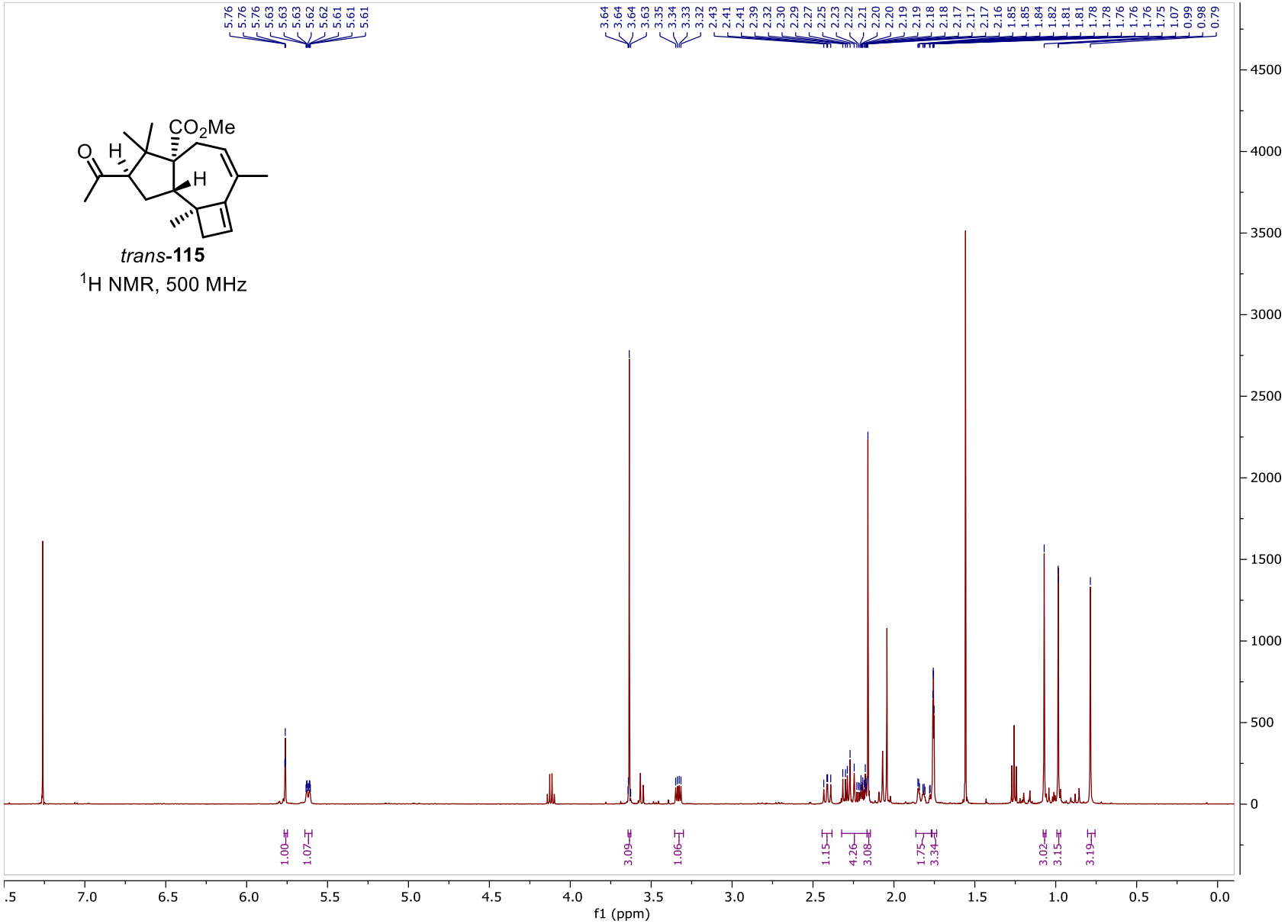
CO2Me
O
H
H
trans-115
1H NMR, 500 MHz
f1 (ppm)

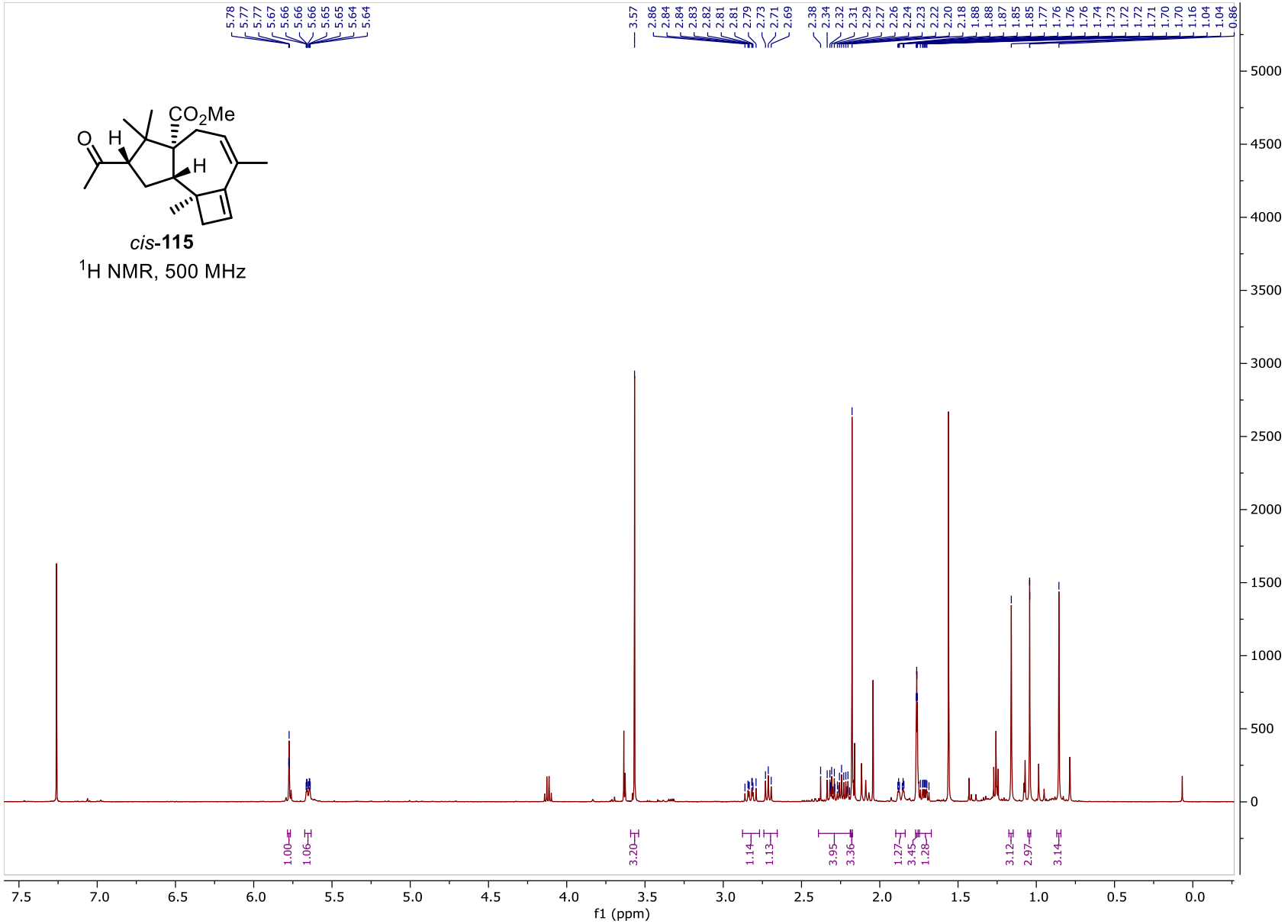
CO2Me
O
H
H
cis-115
1H NMR, 500 MHz
f1 (ppm)

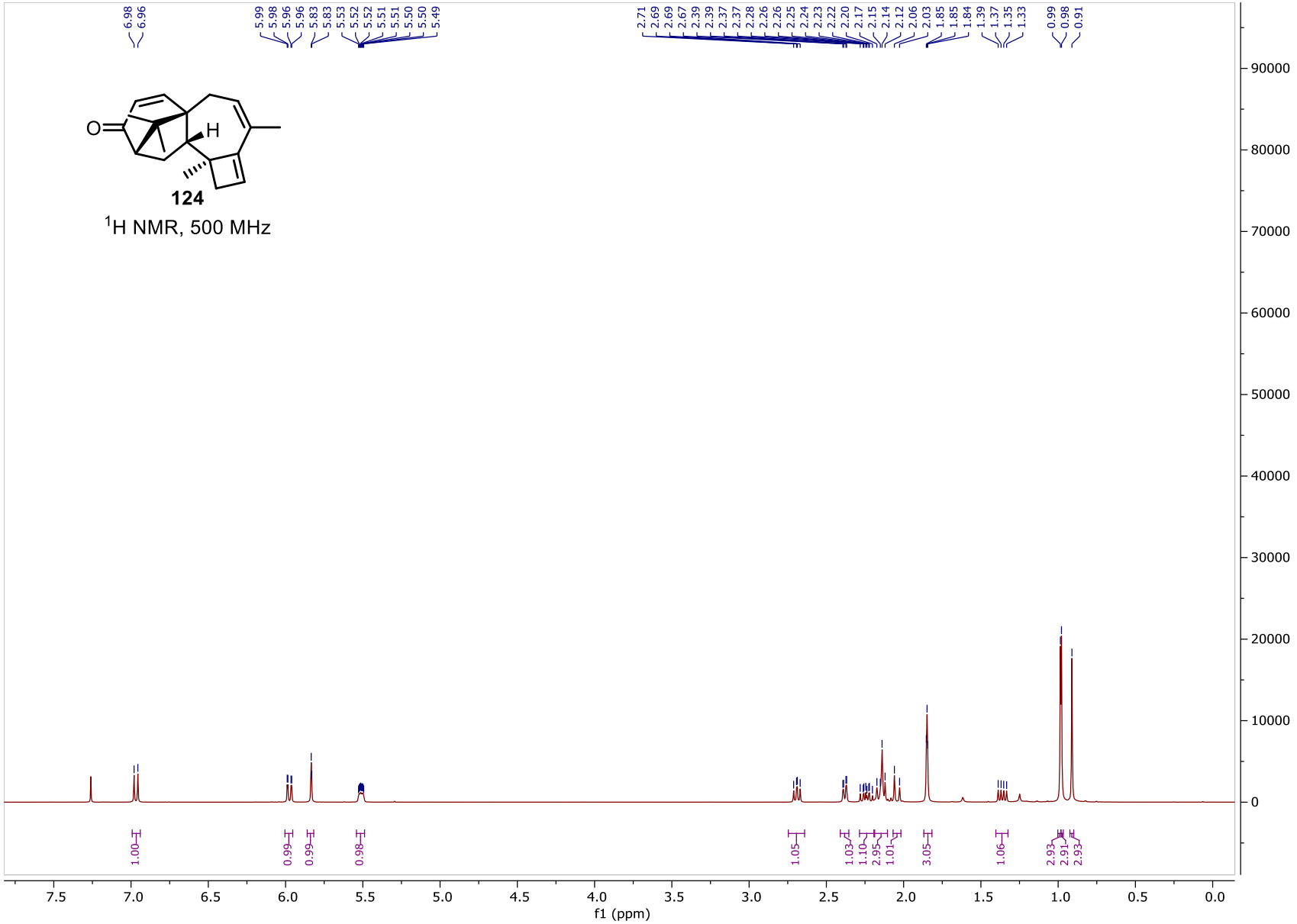
6.98
6.96
5.99
5.98
5.96
5.96
5.83
5.83
5.53
5.52
5.52
5.51
5.51
5.50
5.50
5.49
2.71
2.69
2.69
2.67
2.39
2.39
2.37
2.37
2.28
2.26
2.26
2.25
2.24
2.23
2.22
2.20
2.17
2.15
2.14
2.12
2.06
2.03
1.85
1.85
1.84
1.39
1.37
1.35
1.33
0.99
0.98
0.91
O
H
124
1H NMR, 500 MHz
90000
80000
70000
60000
50000
40000
30000
20000
10000
0
1.00
0.99
0.99
0.98
1.05
1.03
1.10
2.95
1.01
3.05
1.06
2.93
2.91
2.93
7.5
7.0
6.5
6.0
5.5
5.0
4.5
4.0
3.5
3.0
2.5
2.0
1.5
1.0
0.5
0.0
f1 (ppm)

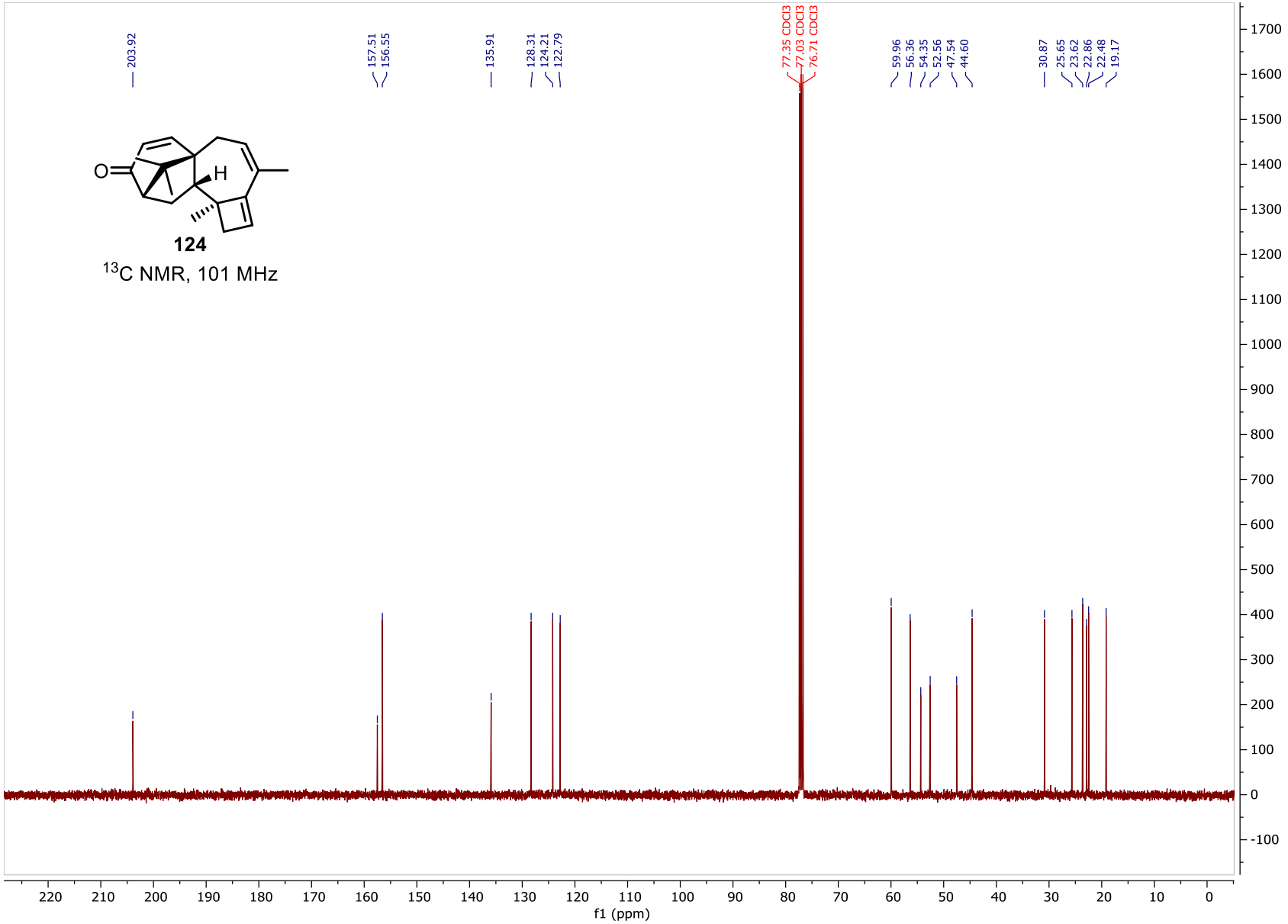
203.92
157.51
156.55
135.91
128.31
124.21
122.79
77.35 CDCl3
77.03 CDCl3
76.71 CDCl3
59.96
56.36
54.35
52.56
47.54
44.60
30.87
25.65
23.62
22.86
22.48
19.17
O
H
124
13C NMR, 101 MHz
f1 (ppm)

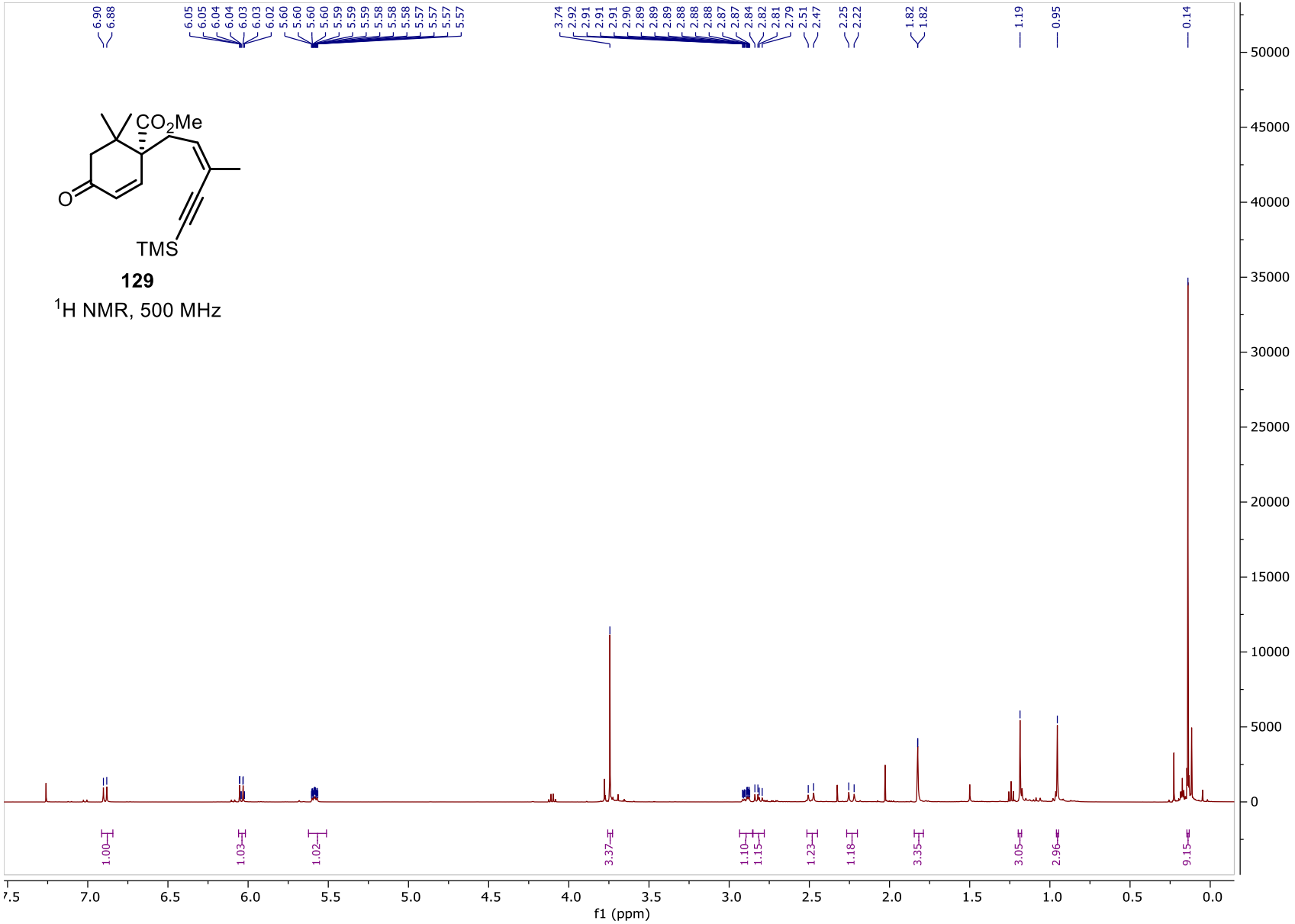
CO2Me
O
TMS
129
1H NMR, 500 MHz
f1 (ppm)

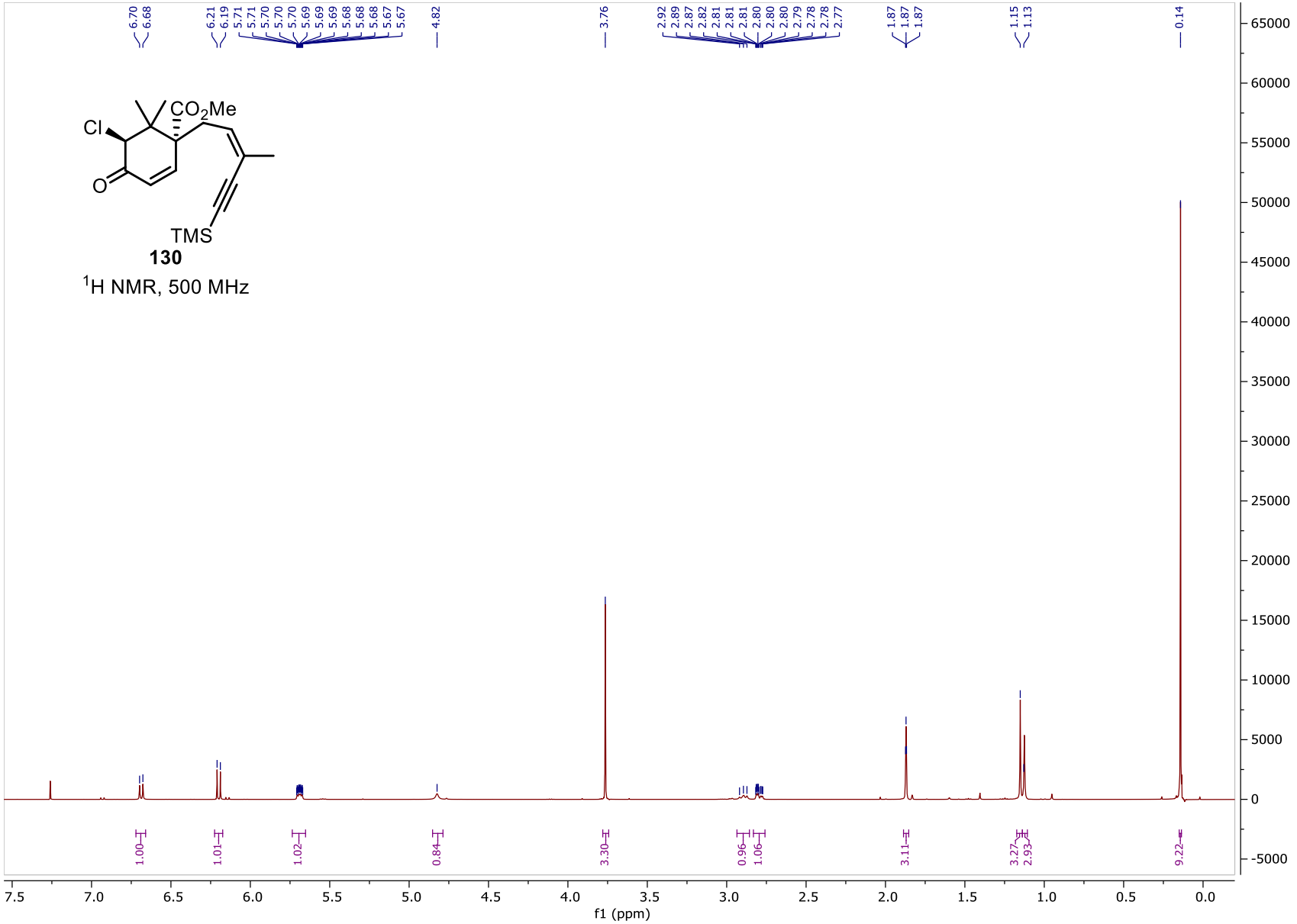
Cl
CO2Me
O
TMS
130
1H NMR, 500 MHz
f1 (ppm)

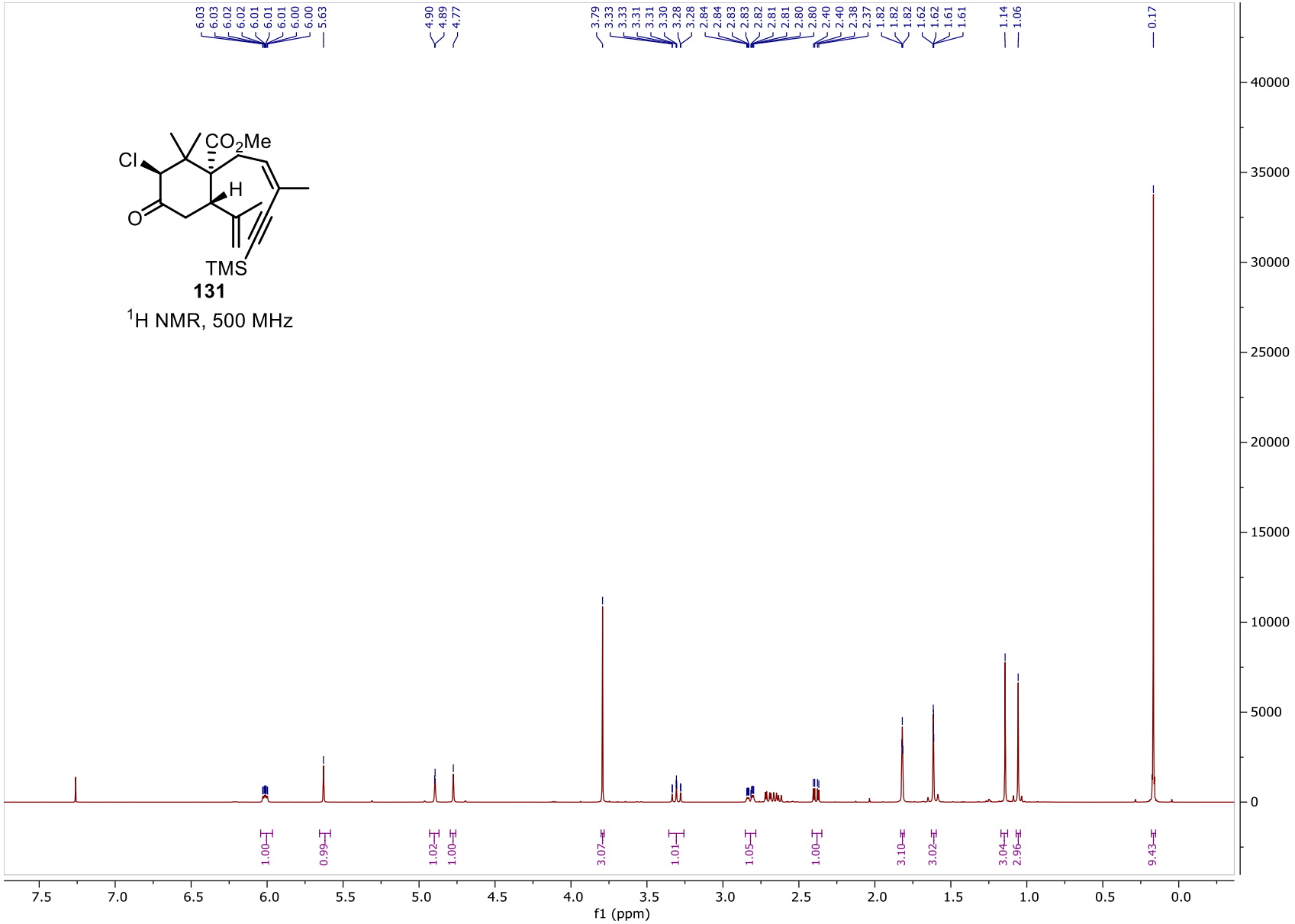
Cl
CO2Me
H
O
TMS
131
1H NMR, 500 MHz
f1 (ppm)

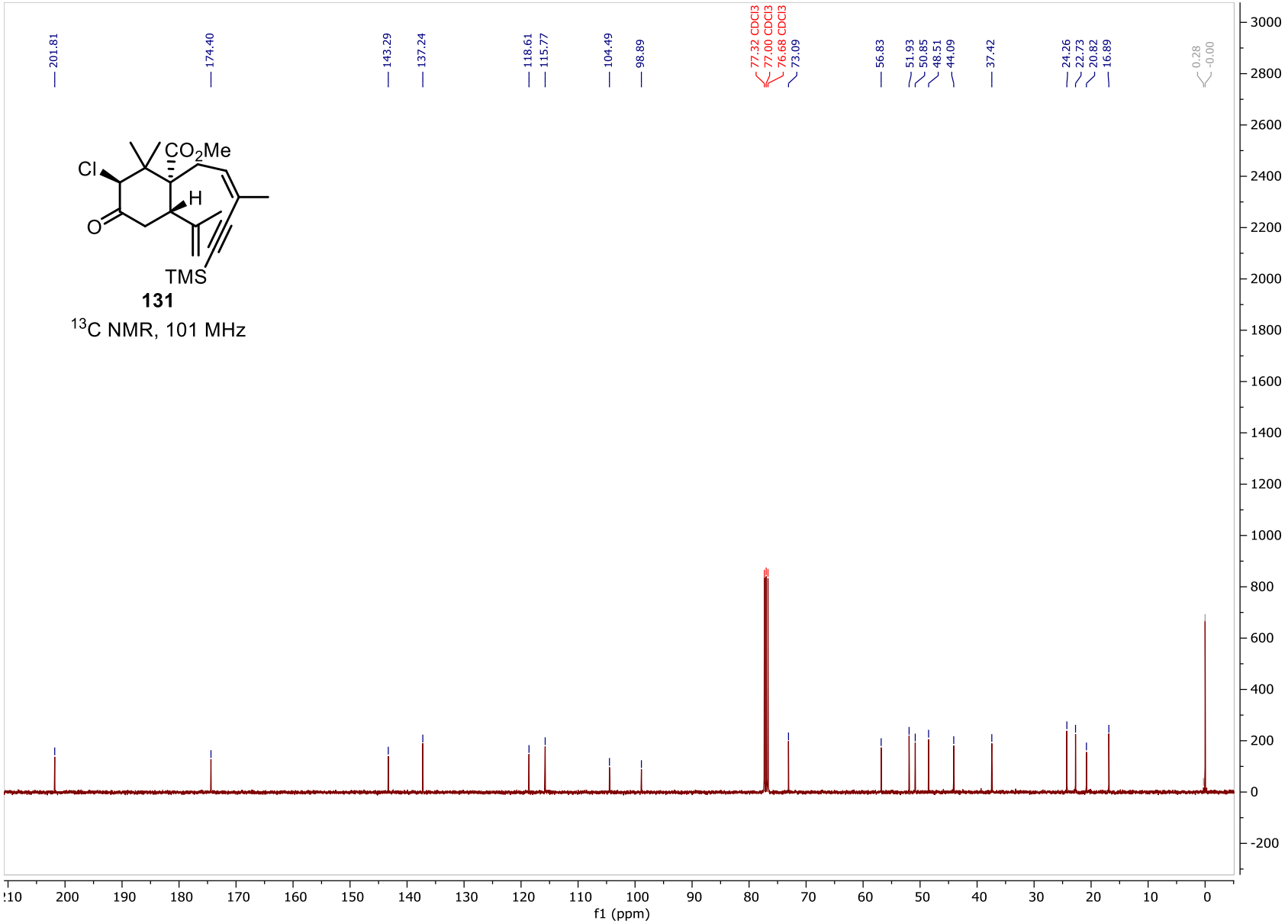
201.81
174.40
143.29
137.24
118.61
115.77
104.49
98.89
77.32 CDCl3
77.00 CDCl3
76.68 CDCl3
73.09
56.83
51.93
50.85
48.51
44.09
37.42
24.26
22.73
20.82
16.89
0.28
-0.00
Cl
CO2Me
H
O
TMS
131
13C NMR, 101 MHz
f1 (ppm)

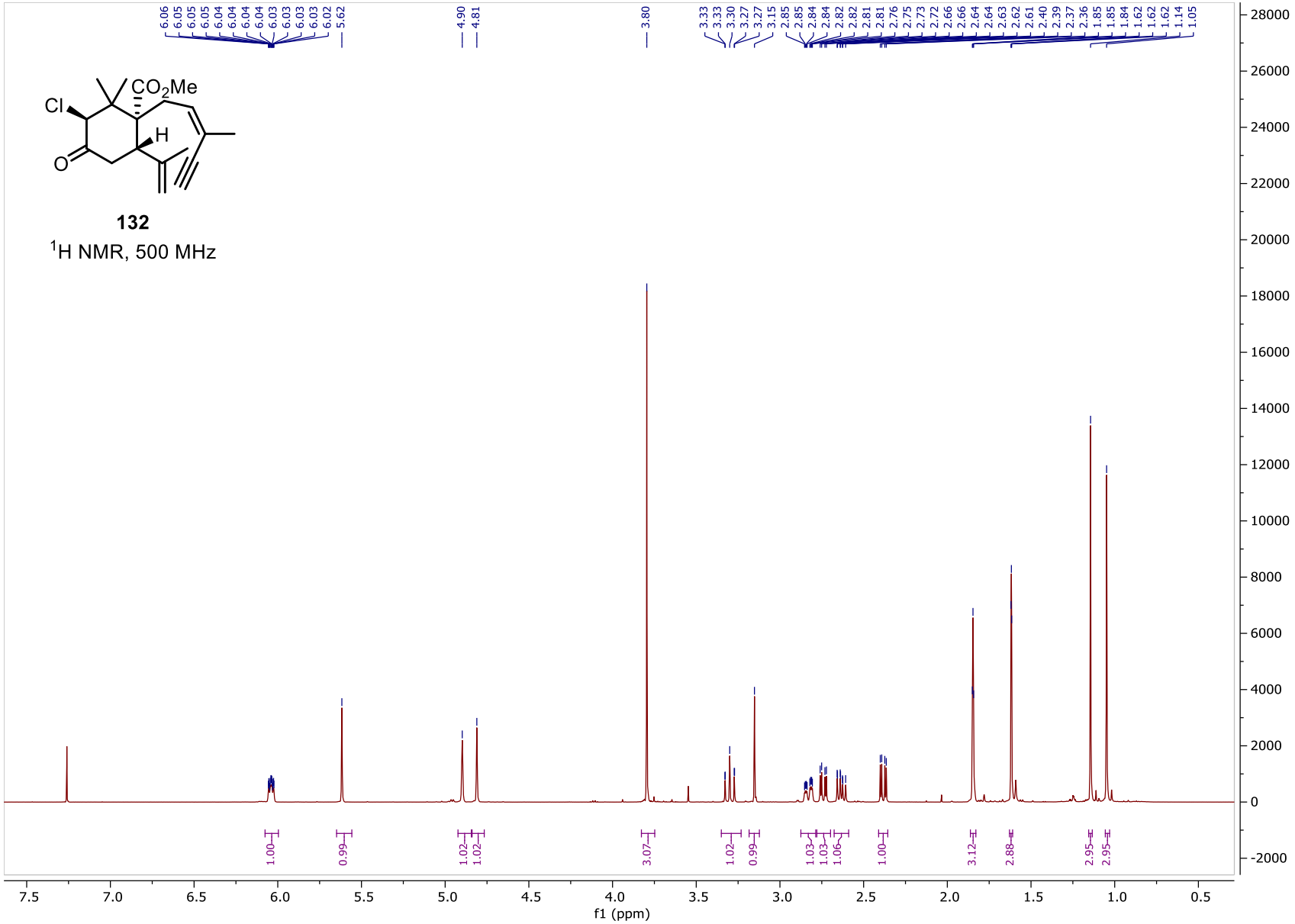
Cl
CO2Me
H
O
132
1H NMR, 500 MHz
f1 (ppm)

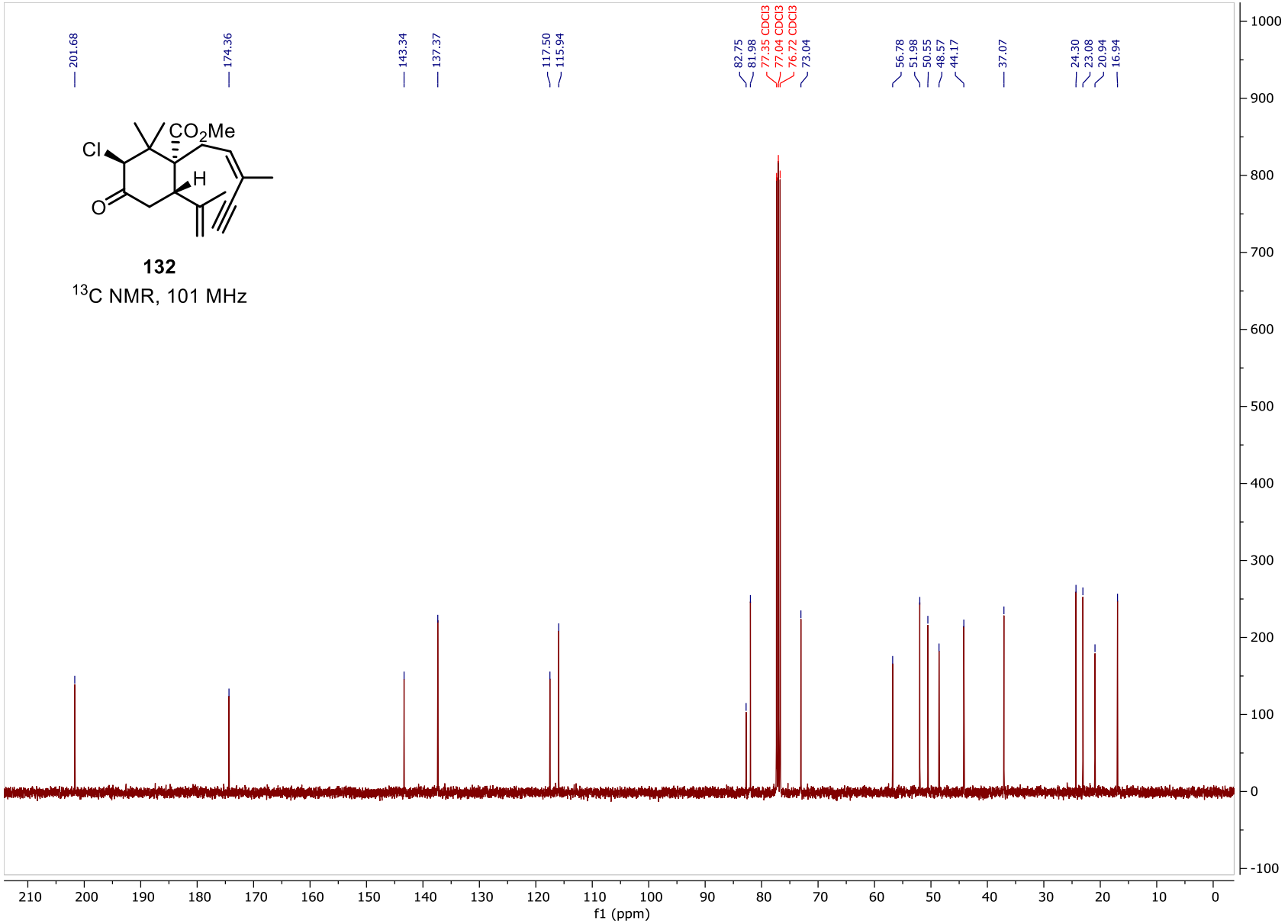
201.68
174.36
143.34
137.37
117.50
115.94
82.75
81.98
77.35 CDCl3
77.04 CDCl3
76.72 CDCl3
73.04
56.78
51.98
50.55
48.57
44.17
37.07
24.30
23.08
20.94
16.94
CO2Me
Cl
H
O
132
13C NMR, 101 MHz
f1 (ppm)

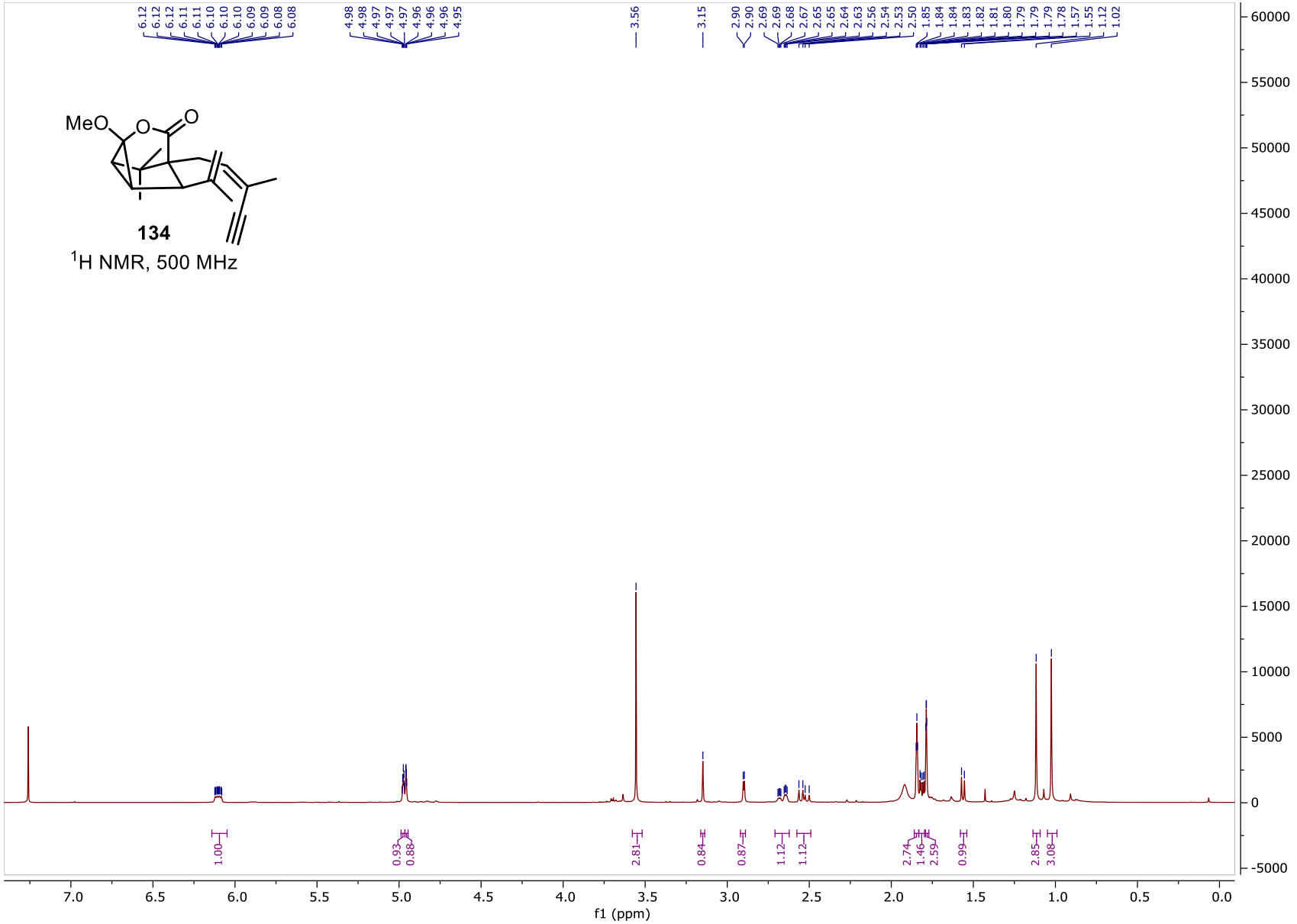
MeO
O
O
134
1H NMR, 500 MHz
f1 (ppm)

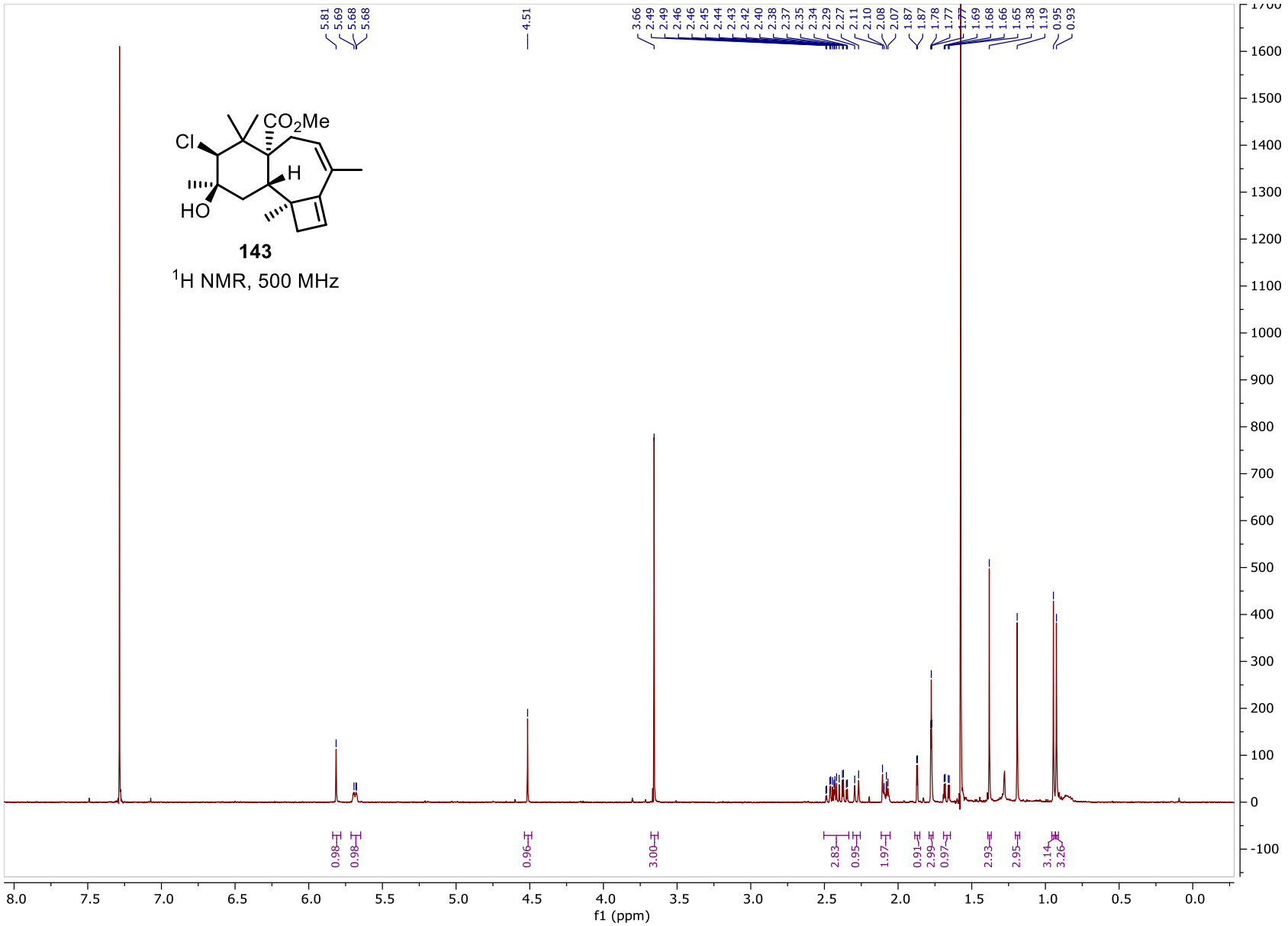
Cl
CO2Me
H
HO
143
1H NMR, 500 MHz
f1 (ppm)

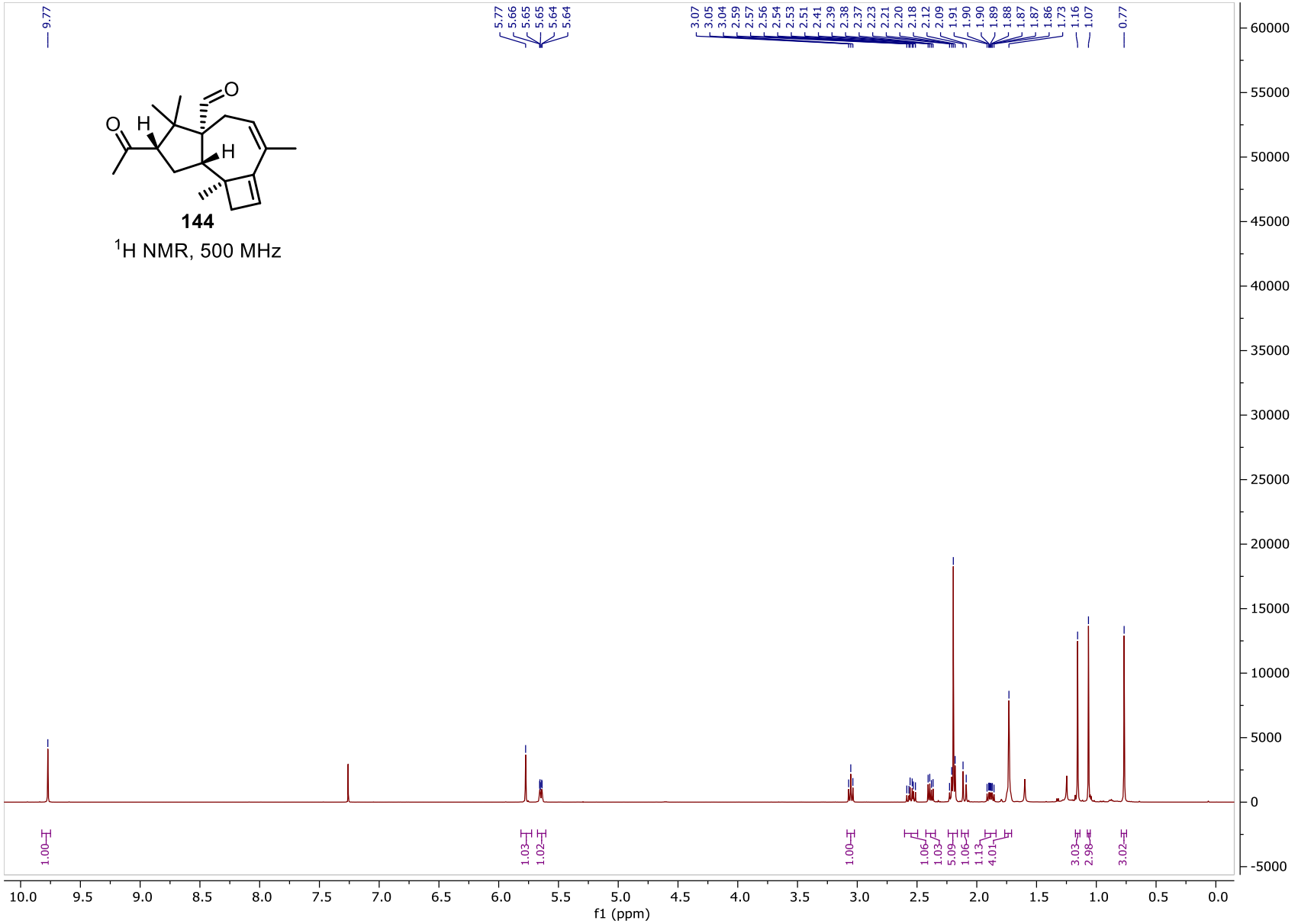
9.77
5.77
5.66
5.65
5.65
5.64
5.64
3.07
3.05
3.04
2.59
2.57
2.56
2.54
2.53
2.51
2.41
2.39
2.38
2.37
2.23
2.21
2.20
2.18
2.12
2.09
1.91
1.90
1.90
1.89
1.88
1.87
1.87
1.86
1.73
1.16
1.07
0.77
O
O
H
H
144
1H NMR, 500 MHz
1.00
1.03
1.02
1.00
1.06
1.03
5.09
1.06
1.13
4.01
3.03
2.98
3.02
f1 (ppm)

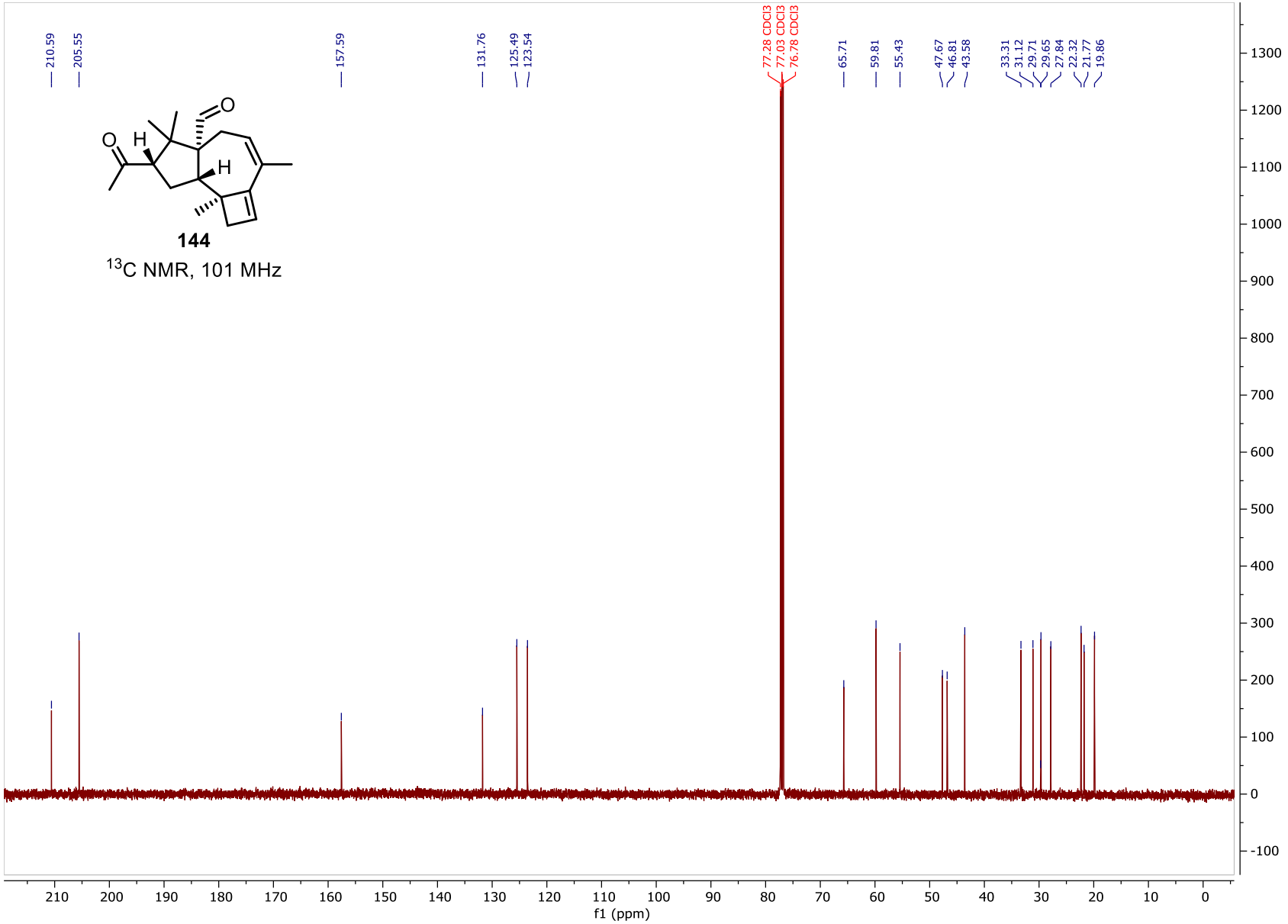
210.59
205.55
157.59
131.76
125.49
123.54
77.28 CDCl3
77.03 CDCl3
76.78 CDCl3
65.71
59.81
55.43
47.67
46.81
43.58
33.31
31.12
29.71
29.65
27.84
22.32
21.77
19.86
O
H
O
H
144
13C NMR, 101 MHz
f1 (ppm)

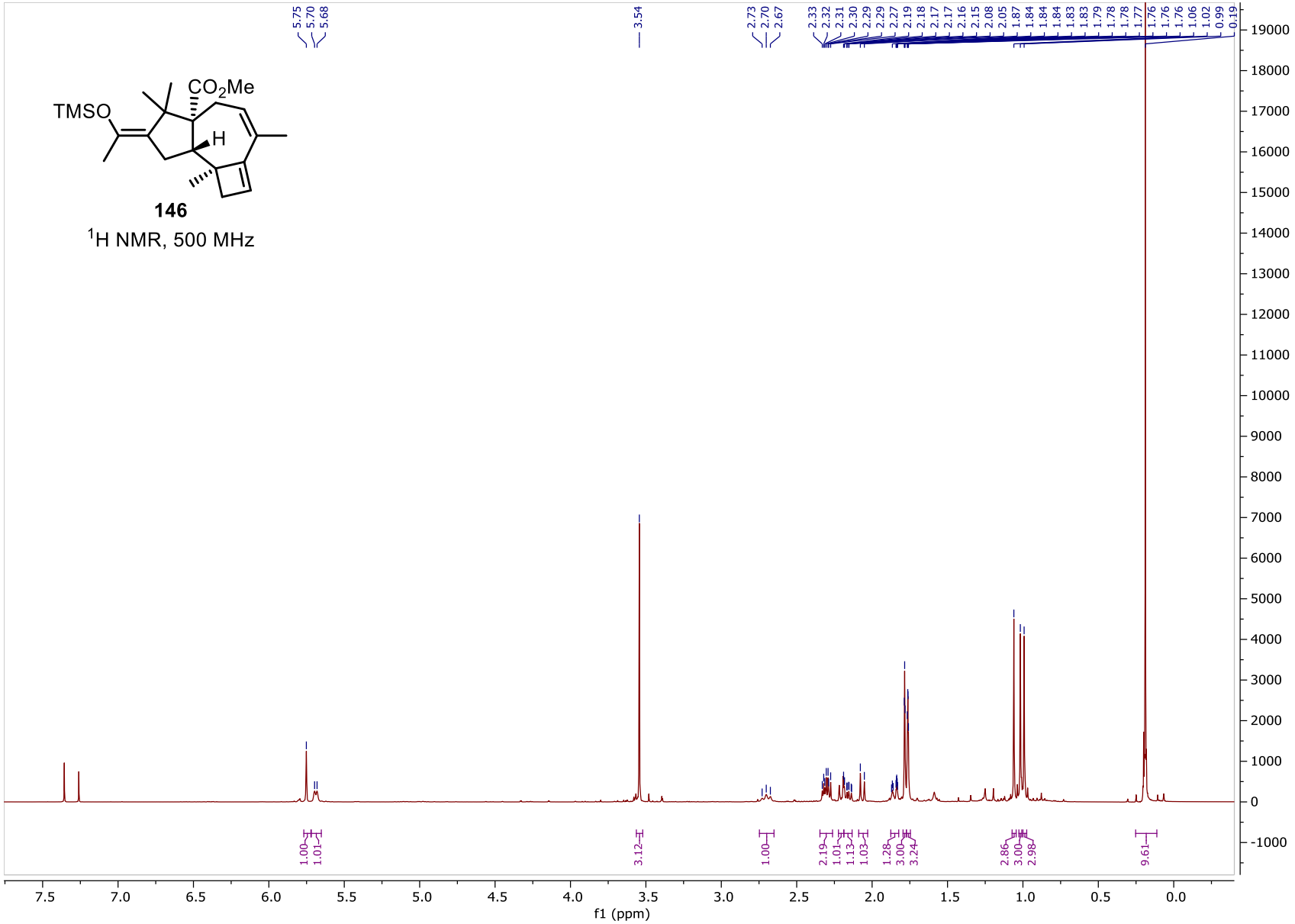
TMSO
CO2Me
H
146
1H NMR, 500 MHz
f1 (ppm)

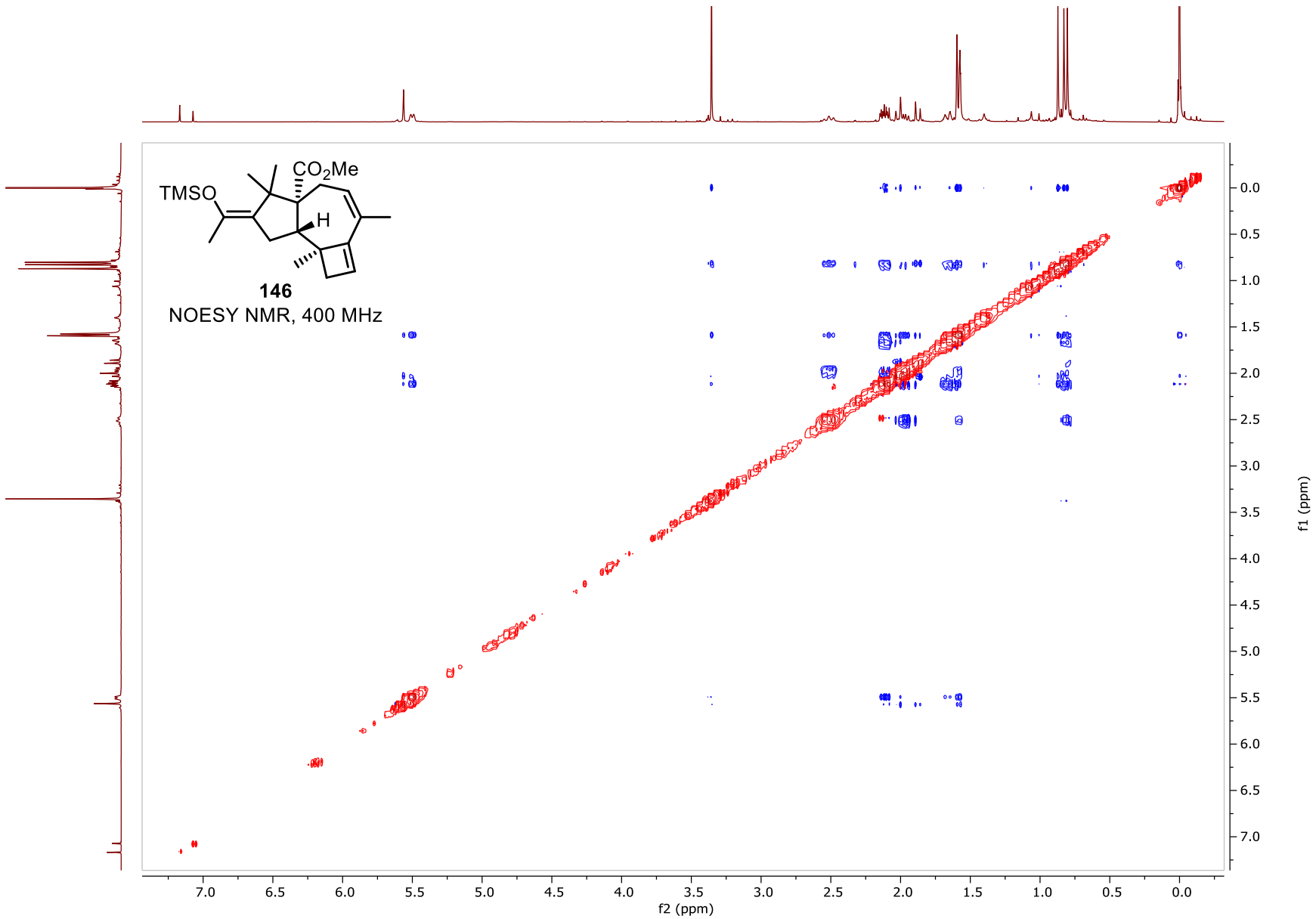
TMSO
CO2Me
H
146
NOESY NMR, 400 MHz
f2 (ppm)
f1 (ppm)

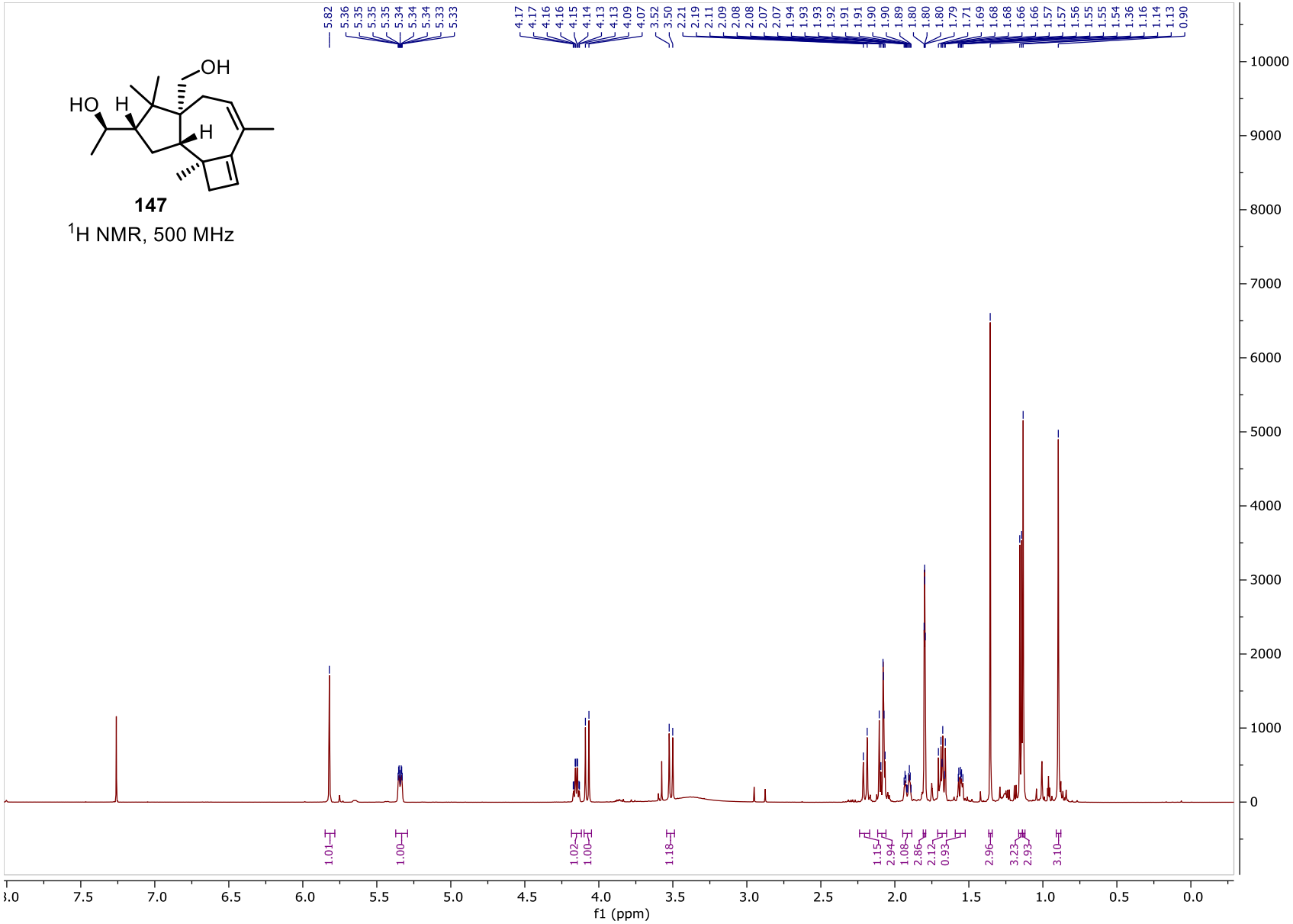
OH
HO
H
H
147
1H NMR, 500 MHz
f1 (ppm)

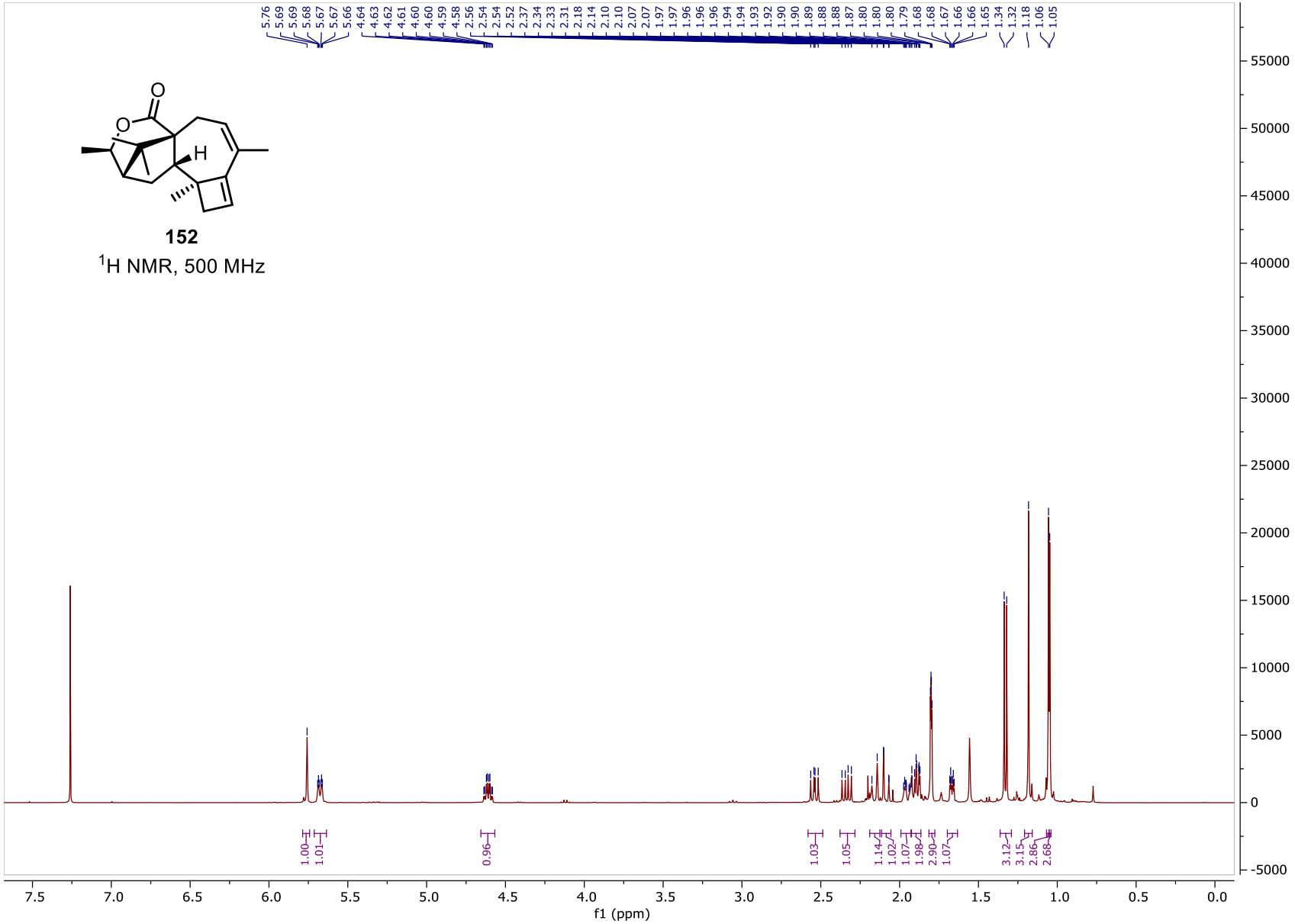
152
1H NMR, 500 MHz
f1 (ppm)

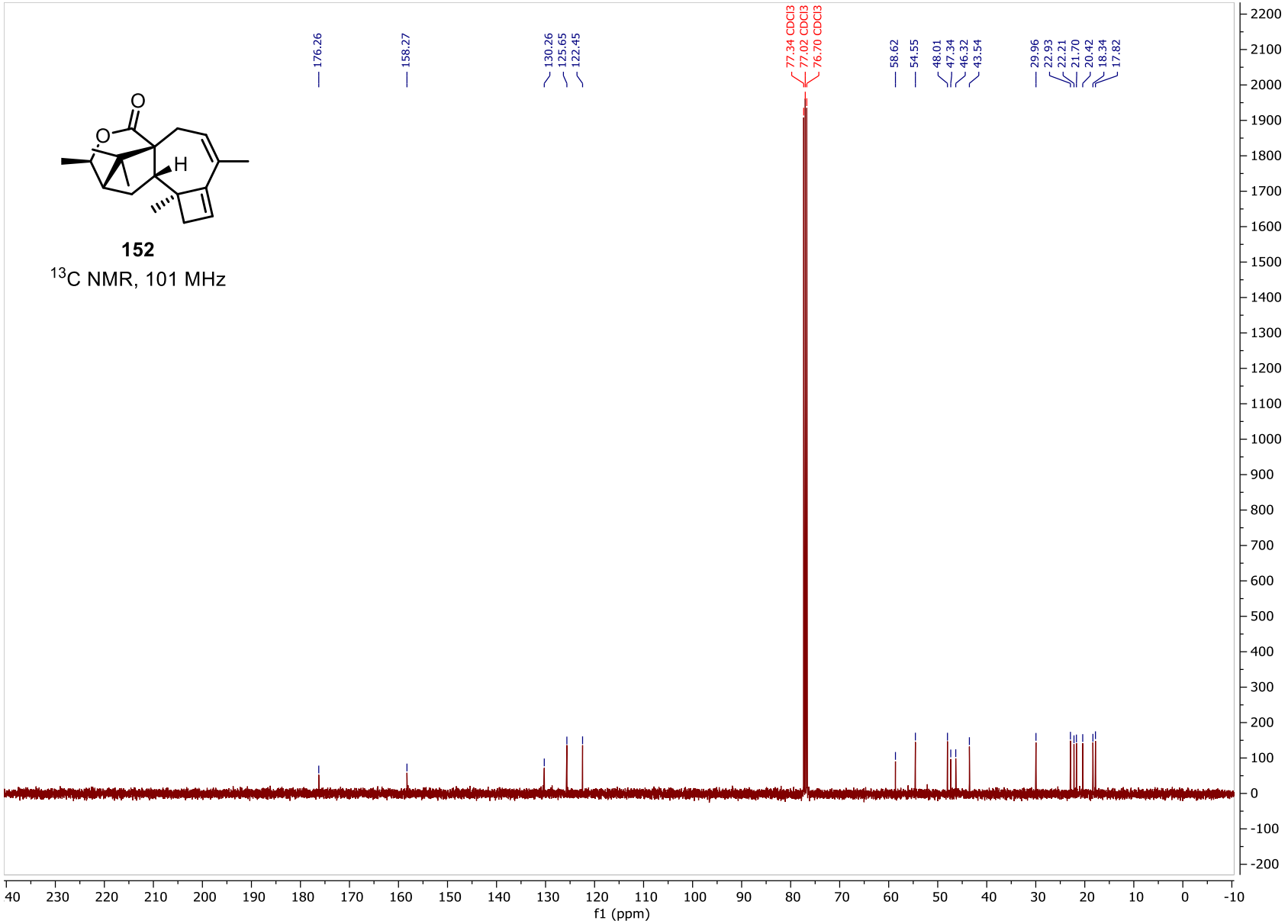
176.26
158.27
130.26
125.65
122.45
77.34 CDCl3
77.02 CDCl3
76.70 CDCl3
58.62
54.55
48.01
47.34
46.32
43.54
29.96
22.93
22.21
21.70
20.42
18.34
17.82
O
O
H
152
13C NMR, 101 MHz
f1 (ppm)

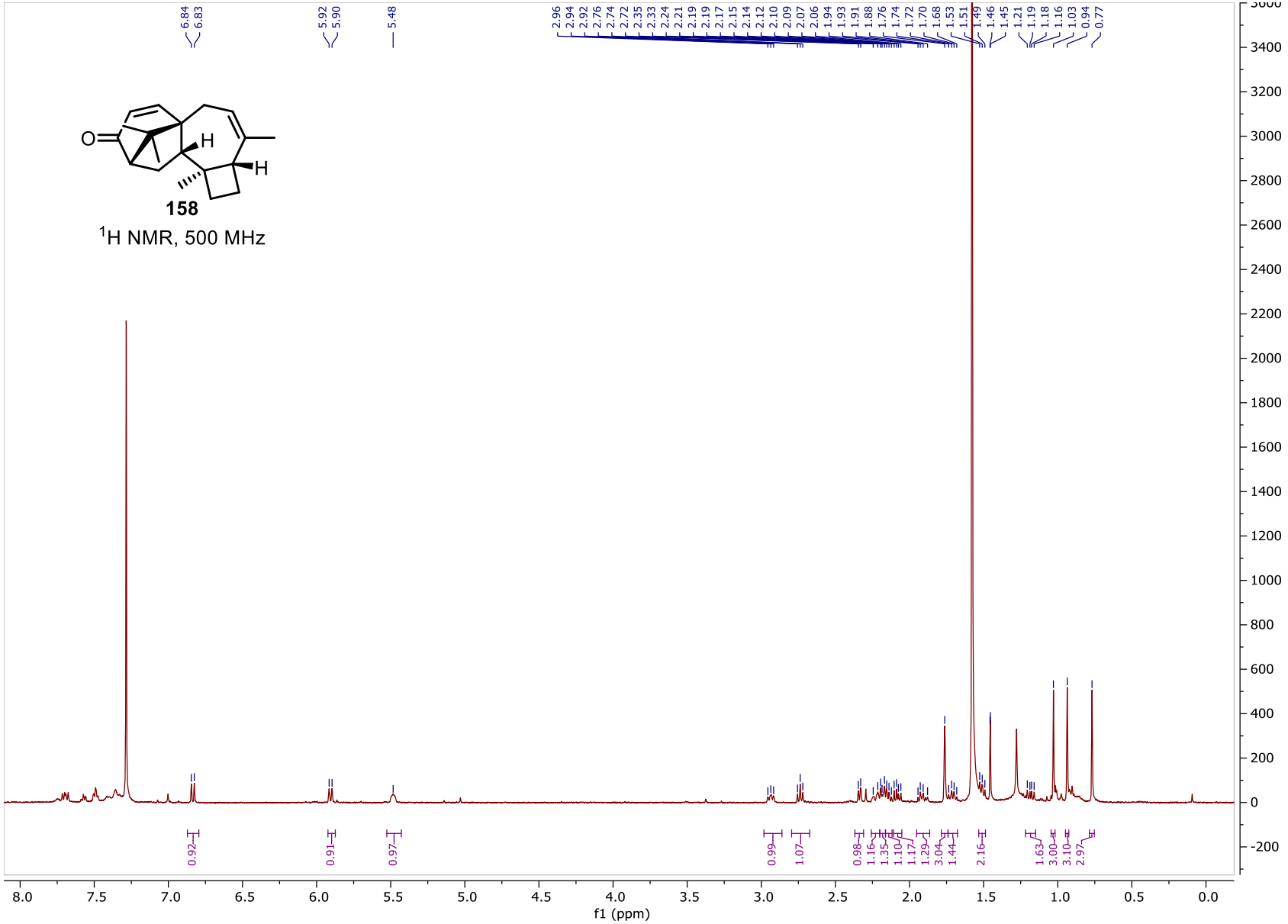
158
1H NMR, 500 MHz
f1 (ppm)

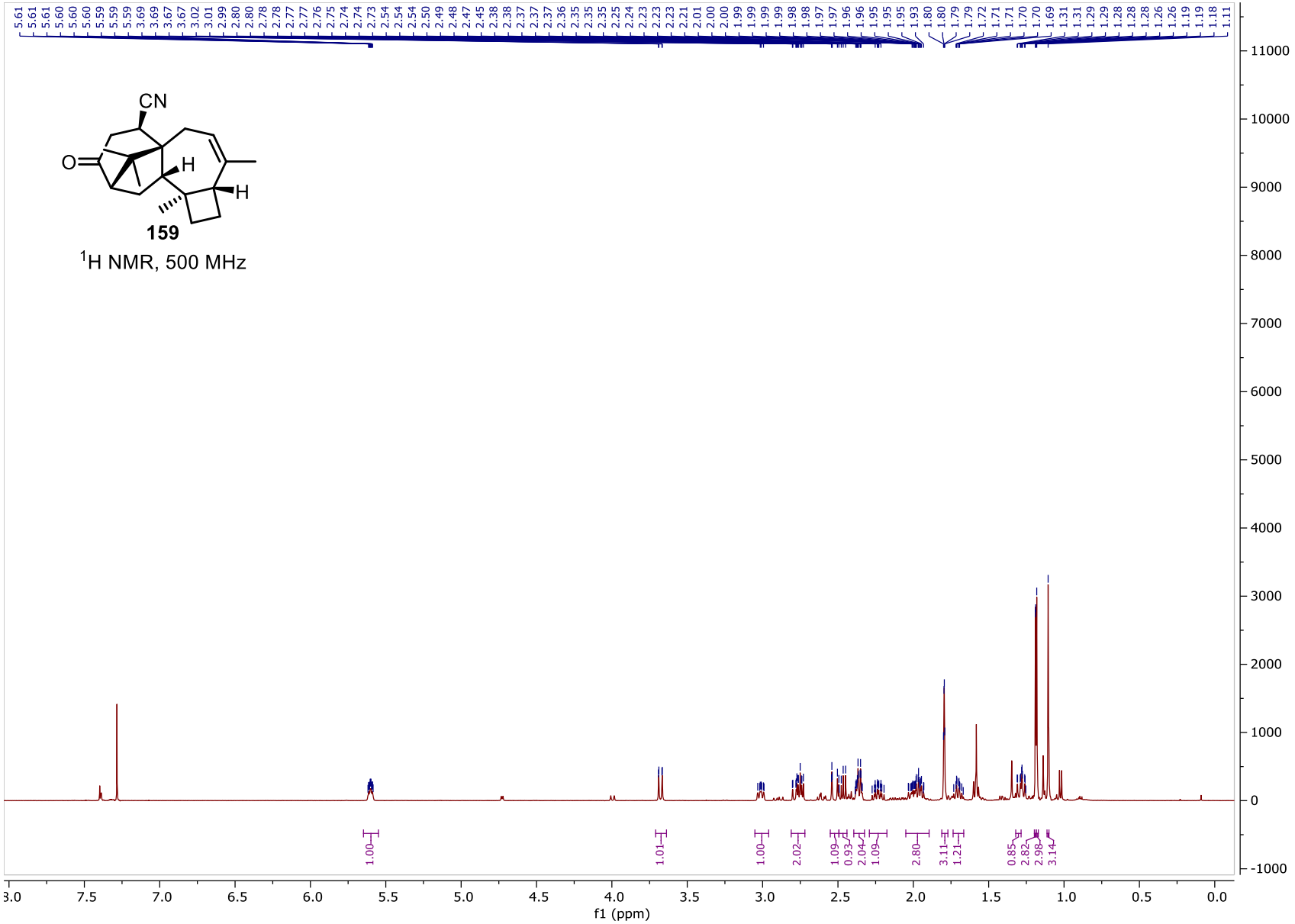
CN
O
H
H
159
1H NMR, 500 MHz
f1 (ppm)

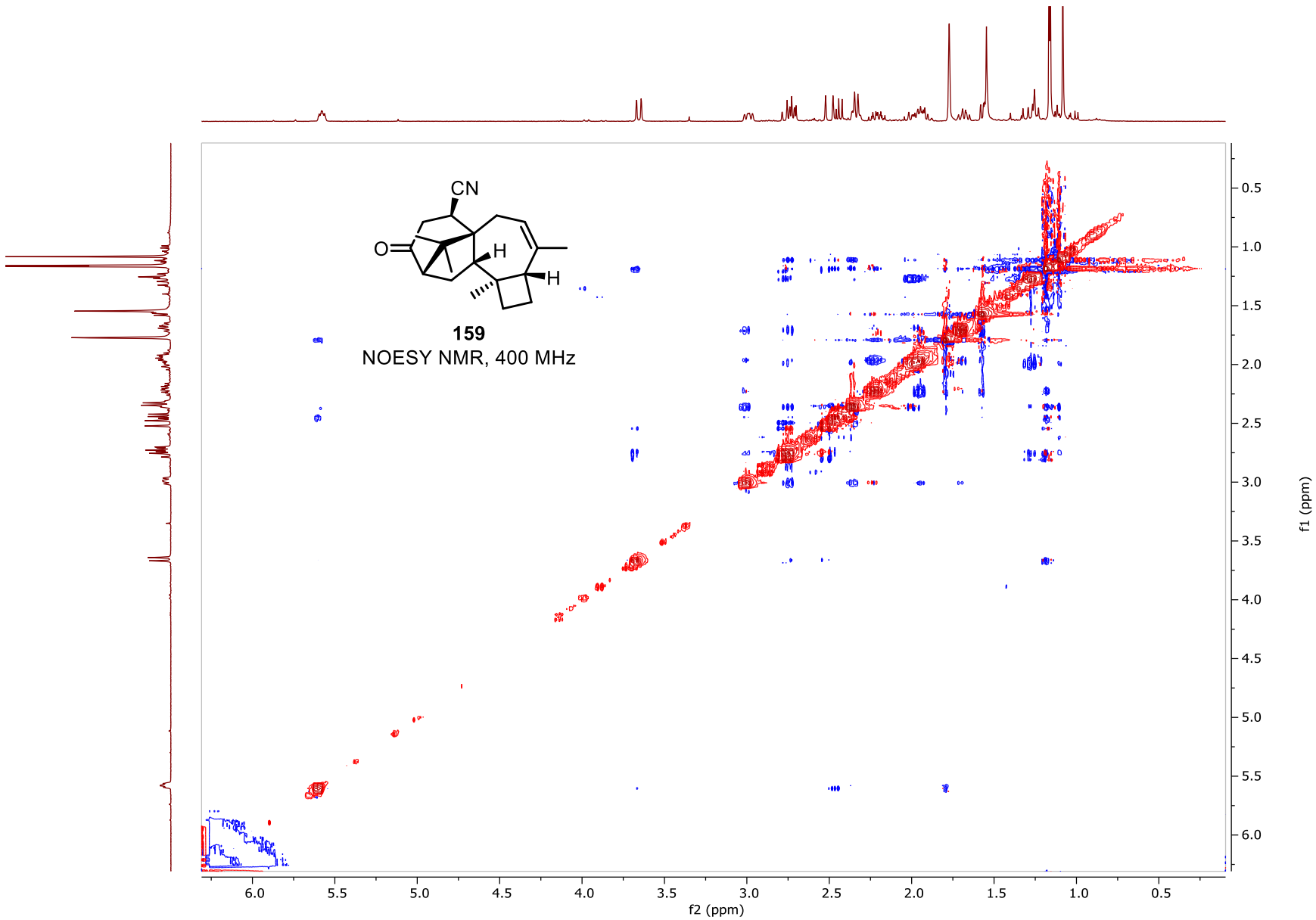
CN
O
H
H
159
NOESY NMR, 400 MHz
f2 (ppm)
f1 (ppm)

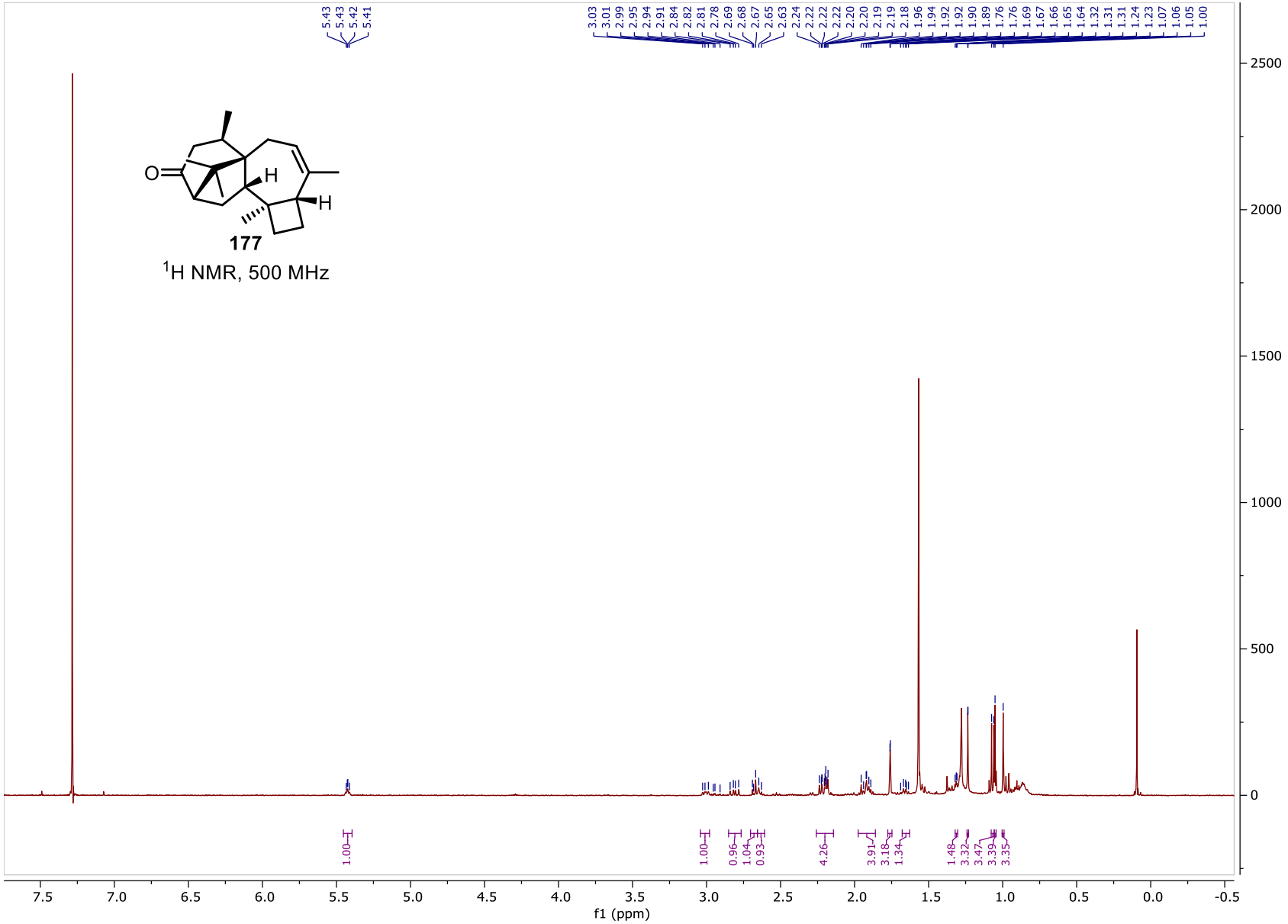
O
H
H
177
1H NMR, 500 MHz
f1 (ppm)

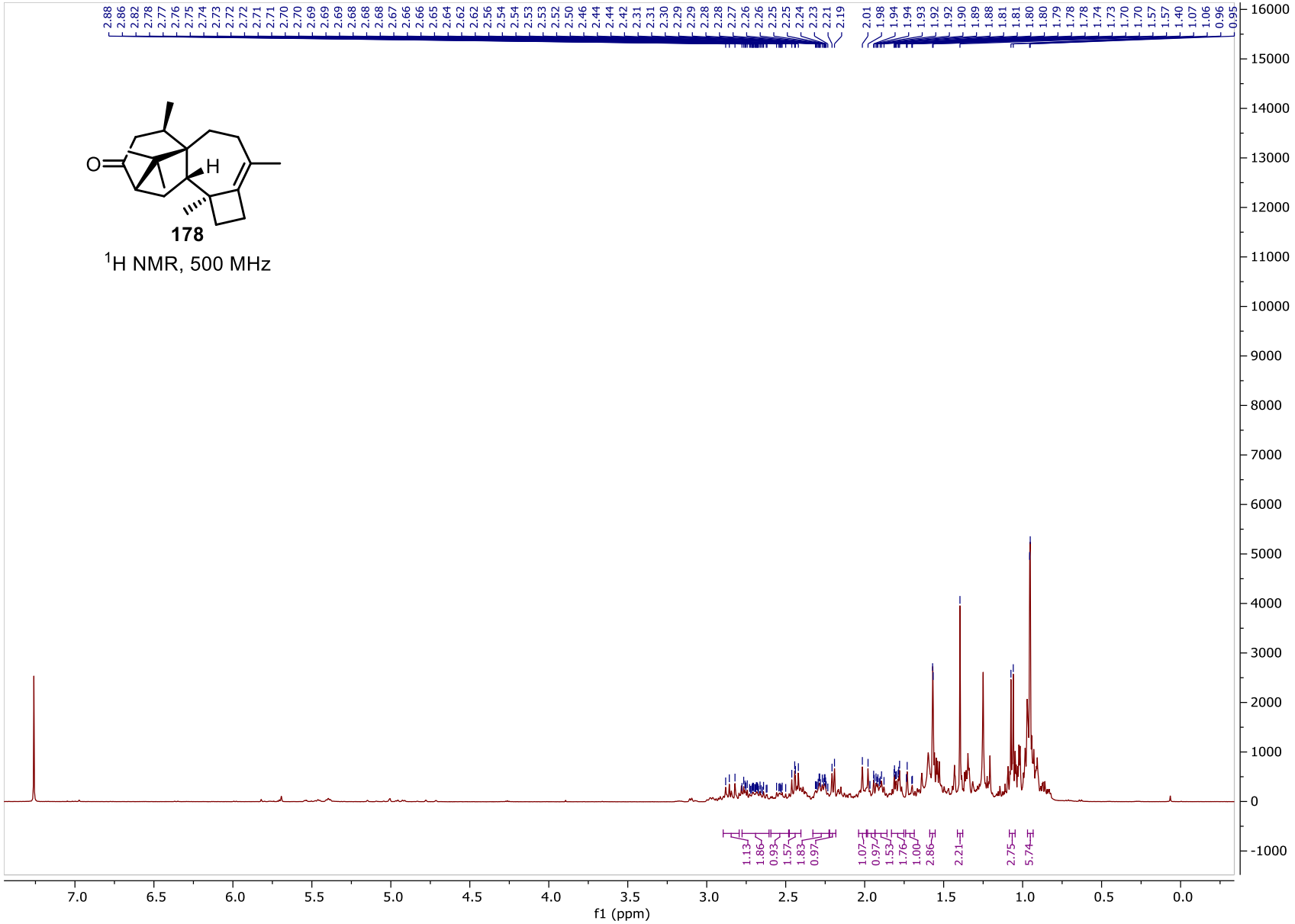
O
H
178
1H NMR, 500 MHz
f1 (ppm)

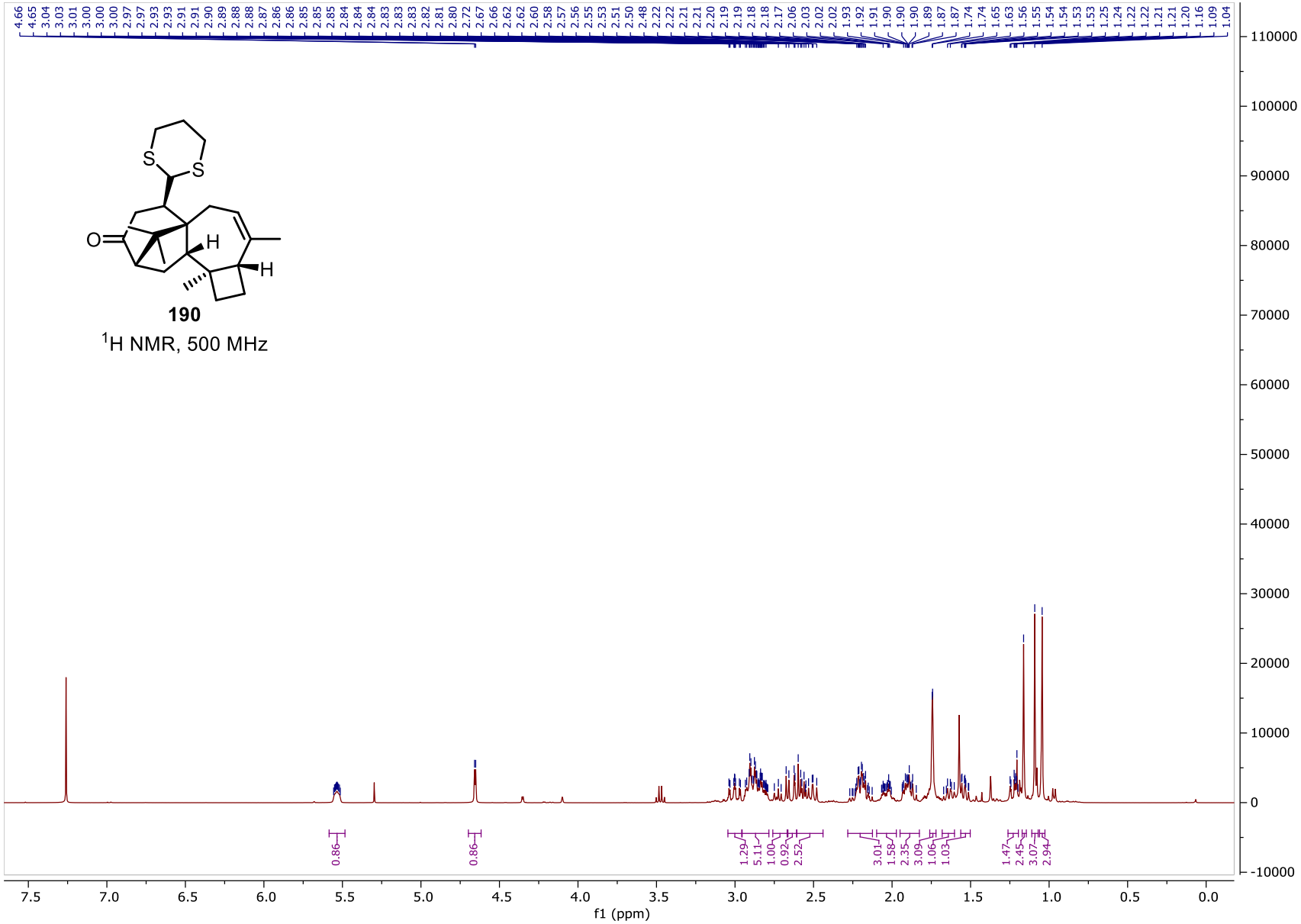
S
S
O
H
H
190
1H NMR, 500 MHz
f1 (ppm)

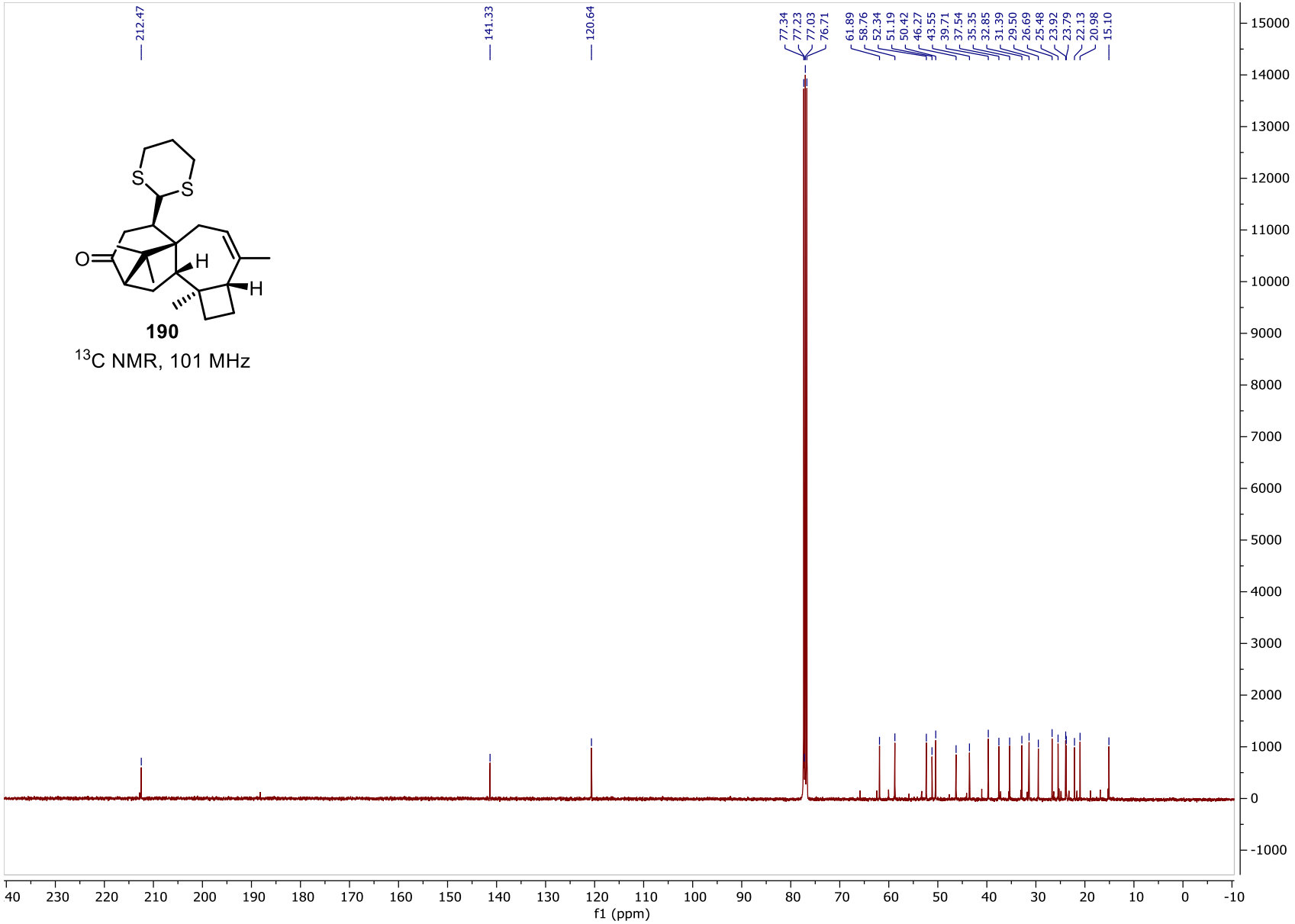
212.47
141.33
120.64
77.34
77.23
77.03
76.71
61.89
58.76
52.34
51.19
50.42
46.27
43.55
39.71
37.54
35.35
32.85
31.39
29.50
26.69
25.48
23.92
23.79
22.13
20.98
15.10
S
S
O
H
H
190
13C NMR, 101 MHz
f1 (ppm)

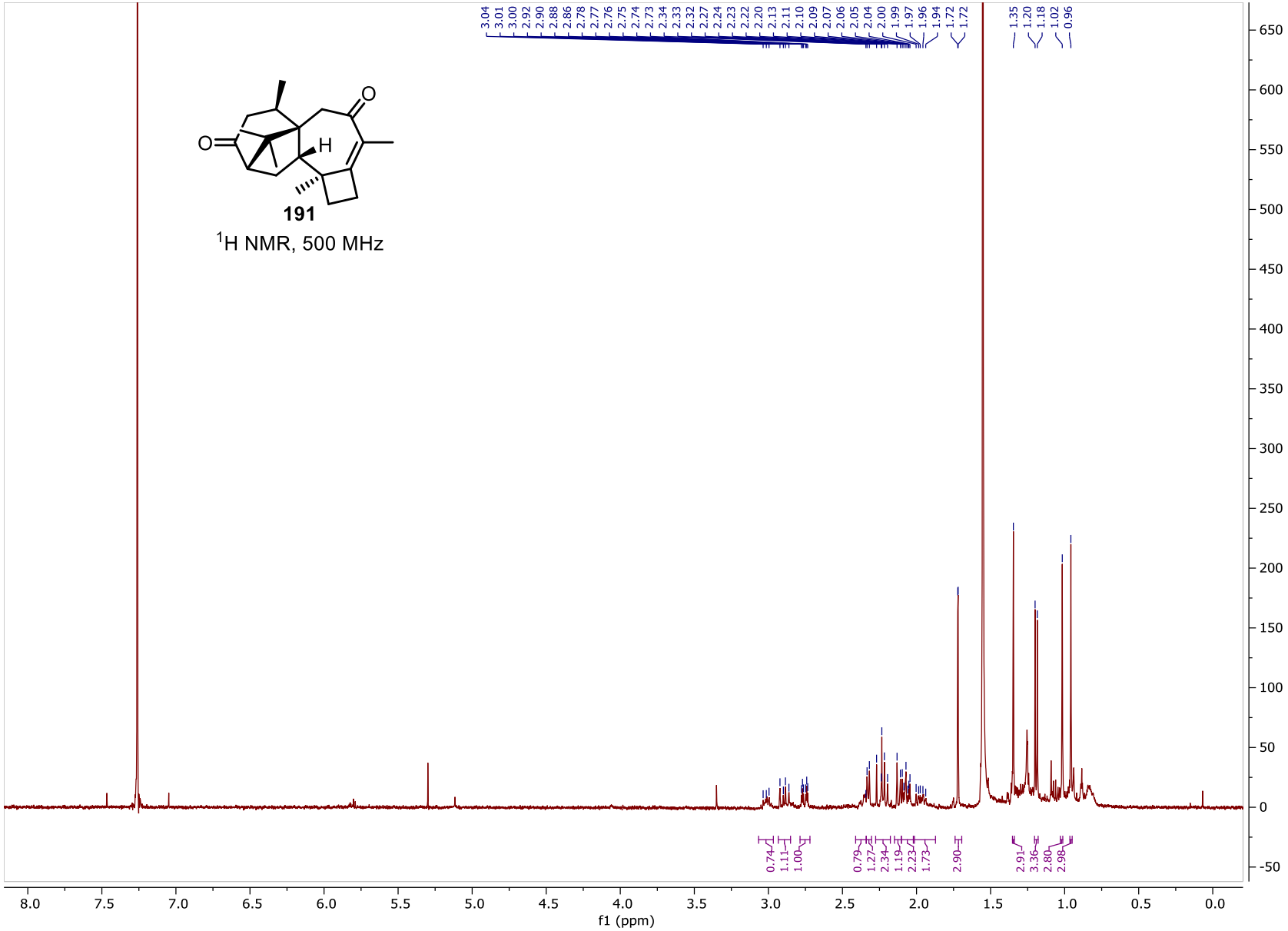
191
^{1}H NMR, 500 MHz
f1 (ppm)

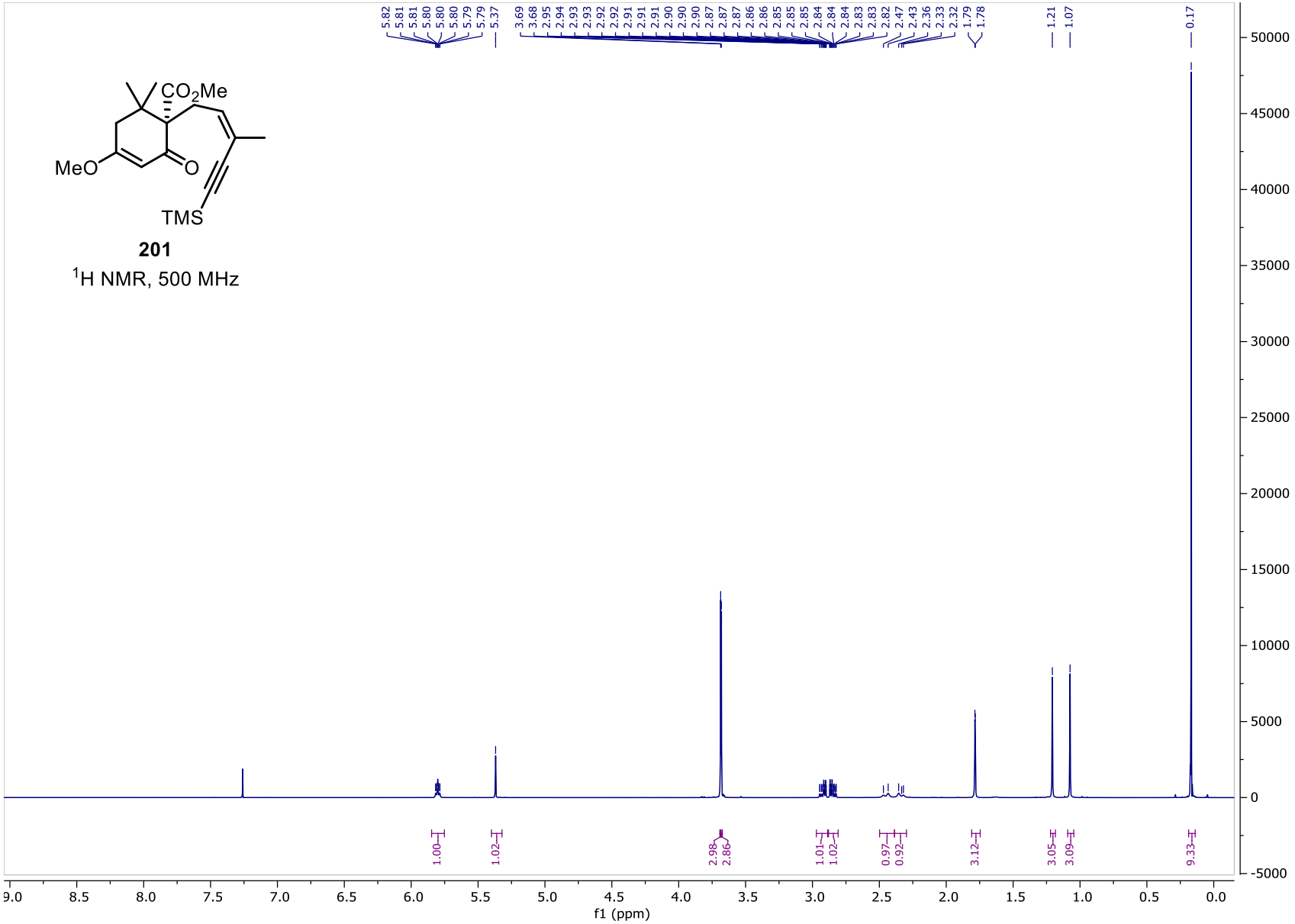
CO2Me
MeO
O
TMS
201
1H NMR, 500 MHz
f1 (ppm)

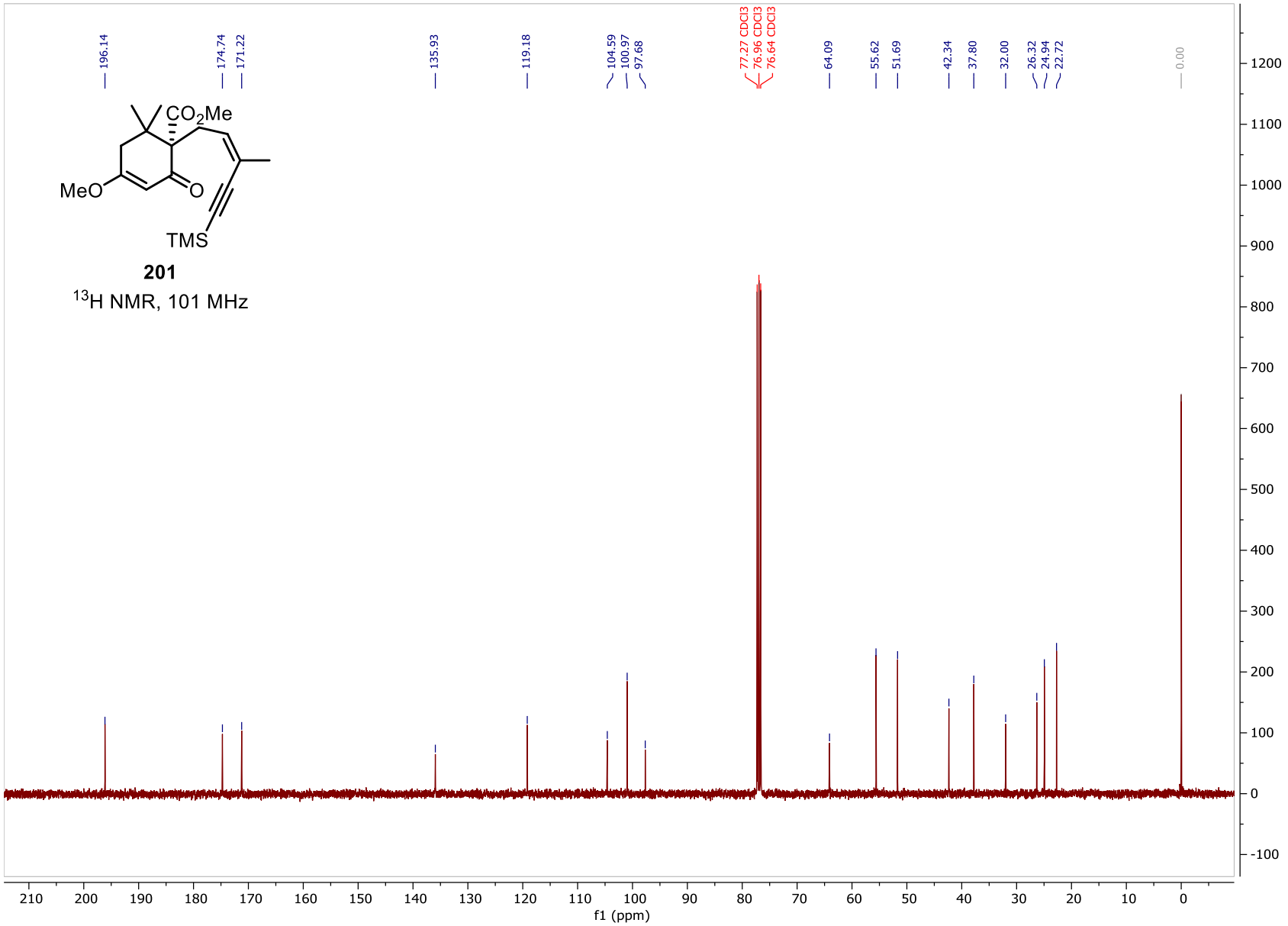
196.14
174.74
171.22
135.93
119.18
104.59
100.97
97.68
77.27 CDCl3
76.96 CDCl3
76.64 CDCl3
64.09
55.62
51.69
42.34
37.80
32.00
26.32
24.94
22.72
0.00
CO2Me
MeO
O
TMS
201
13H NMR, 101 MHz
f1 (ppm)